

**Strategies and analytical procedures for
a sustainable plastic waste management.**
An application to poly (ethylene terephthalate) and
polylactide in the packaging sector

JOSÉ DAVID BADÍA VALIENTE

EDITORIAL
UNIVERSITAT POLITÈCNICA DE VALÈNCIA



Strategies and analytical procedures for a sustainable plastic waste management

An application to poly (ethylene terephthalate)
and polylactide in the packaging sector

Memòria per optar al grau de doctor

José David Badía Valiente

Direcció

Amparo Ribes Greus

Institut Tecnològic de Materials
Universitat Politècnica de València

València, 2011



UNIVERSITAT
POLITÈCNICA
DE VALÈNCIA



This editorial is member of the UNE, which guarantees the diffusion and commercialization of its publications at national and international level.

First Edition, 2013

© José David Badia Valiente

© of the present edition:

Editorial Universitat Politècnica de València
www.editorial.upv.es

ISBN: 978-84-9048-055-7 (printed version)

Publishing reference: 5633

Any unauthorized copying, distribution, marketing, editing, and in general any other exploitation, for whatever reason, of this piece of work or any part thereof, is strictly prohibited without the authors' expressed and written permission.



UNIVERSITAT
POLITÈCNICA
DE VALÈNCIA



Na Amparo Ribes Greus, Catedràtica d' Universitat del Departament de Màquines i Motors Tèrmics de la Universitat Politècnica de València, investigadora de l' Institut de Tecnologia dels Materials de dita Universitat,

CERTIFIQUE:

Que el treball "*Strategies and analytical procedures for a sustainable plastic waste management. An application to poly(ethylene terephthalate) and polylactide in the packaging sector*", que ha dut a terme i que presenta En José David Badia Valiente per a l' obtenció del Grau de Doctor en Enginyeria i Producció Industrial amb menció europea, ha estat desenvolupat baix la meua supervisió i direcció als laboratoris del Grup de Degradació i Reciclatge de Materials Polimèrics de l' Institut de Tecnologia de Materials, així com als laboratoris del Departament de Tecnologia de Fibres i Polimers de l' Escola d' Enginyeria i Ciències Químiques de la Kungliga Tekniska Högskolan (KTH), Estocolm, Suècia. I per a que així conste, signe el present document, a València, 30 de Juny de 2011.

**Strategies and analytical procedures for a sustainable plastic waste management.
An application to poly (ethylene terephthalate) and polylactide in the packaging
sector.**

Abstract

The purpose of this Ph.D. Thesis was to assess the influence of different waste management processes such as material, energetic and biological valorisations on two key polyesters of the packaging industry, the current non-renewable poly (ethylene terephthalate) (PET) and the potential candidate to replace it in a near future, the bio-based polylactide (PLA). For that reason, several pilot plants were used to simulate the degradation conditions undergone by PET and PLA under mechanical recycling, pyrolysis, combustion and burial in soil. The changes were monitored by Differential Scanning Calorimetry (DSC), Dynamic-Mechanical-Thermal Analysis (DMTA), Thermogravimetric analysis (TGA), Fourier-Transform Infrared Spectrometry (FTIR), 2D-IR correlation spectroscopy for Evolved Gas Analysis (EGA), MALDI-TOF Mass Spectrometry, Scanning Electron Microscopy (SEM), Melt-Flow Rate (MFR), Tensile and Charpy testing, and Viscosimetry. Some strategies and analytical procedures were proposed, developed and applied to establish reliable specific parameters to be used as indicators of degradation and thus monitor the influence of each valorisation process on the quality of the material. The behaviour of mechanically recycled PET and PLA was assessed in terms of chemical, microstructural, thermal and mechanical properties. A general loss of performance was shown for PET and PLA reprocessed once and twice respectively. Afterwards, the properties of PLA recyclates were better in relative terms than those of PET recyclates. The thermal and thermo-oxidative decompositions caused by pyrolysis and combustion processes were evaluated concerning the thermal stability, evolved gases and kinetics of decomposition. The use of controlled combustion was stressed for both polymers since less energy was necessary to trigger the decomposition, and the mixture of evolved gases was more homogeneous. Finally, the use of combined thermal analysis techniques was proven as a reliable procedure to monitor the degradation subjected by PLA under burial in soil. The replacement of PET by PLA remains therefore as a suitable option from the point of view of the plastic waste management, since PLA offers better performance after reprocessing than PET, and its energetic valorisation - provided the biological valorisation cannot fulfil the demand - is possible and effective.

Estrategias y procedimientos analíticos para una gestión sostenible de residuos plásticos. Una aplicación en el caso del poli(tereftalato de etileno) y la polilactida en el sector del envase y embalaje.

Resumen

El propósito de esta tesis doctoral fue evaluar la influencia de los diferentes procesos de gestión de residuos, tales como la valorización material, energética y biológica de dos poliésteres clave de la industria del embalaje: el actual no-renovable poli (tereftalato de etileno) (PET) y el potencial candidato para sustituirlo en un futuro próximo, la polilactida (PLA) de base renovable. Se utilizaron diversas plantas piloto para simular las condiciones de la degradación sufrida por PET y PLA en el reciclado mecánico, la pirólisis, la combustión y el enterramiento en suelo. Los cambios fueron monitorizados por calorimetría diferencial de barrido (DSC), análisis dinámico-mecánico-térmico (DMTA), análisis termogravimétrico (TGA), espectrometría infrarroja con transformada de Fourier (FTIR), espectroscopia de correlación 2D-IR para el análisis de gases (EGA), espectrometría de masas MALDI-TOF, microscopía electrónica de barrido (SEM), índice de fluidez de masa fundida (MFR), ensayos de tracción e impacto Charpy y viscosimetría. Se han propuesto, desarrollado y aplicado diversas estrategias y procedimientos analíticos para establecer parámetros fiables para ser utilizados como indicadores de la degradación y por tanto controlar la influencia de cada proceso de valorización en la calidad del material. El comportamiento de PET y PLA reciclados mecánicamente se evaluó en base a sus propiedades químicas, microestructurales, mecánicas y térmicas. Se observó una pérdida general de prestaciones de PET y PLA reprocesado una vez y dos veces, respectivamente. Además, las propiedades de los materiales reciclados de PLA fueron mejores en términos relativos a los productos reciclados de PET. Las descomposiciones térmica y termo-oxidativa causadas por los procesos de pirólisis y combustión se evaluaron sobre la estabilidad térmica, gases emitidos y cinéticas de descomposición. Se destaca el uso de la combustión controlada para ambos polímeros, ya que se necesita menos energía para iniciar la descomposición, y la mezcla de gases que se desprenden es más homogénea. Por último, el uso combinado de técnicas de análisis térmico se demostró como un procedimiento fiable para monitorizar la degradación sufrida por el PLA en condiciones de enterramiento en suelo. La sustitución de PET por PLA, por tanto, se establece como una opción adecuada desde el punto de vista de la gestión de los residuos plásticos, ya que el PLA ofrece mejores prestaciones después del reprocesamiento que el PET, y su valorización energética - siempre que la valorización biológica no puede satisfacer la demanda - es factible y eficaz.

**Estratègies i procediments analítics per a una gestió sostenible dels residus plàstics.
Una aplicació en el cas del poli (tereftalat d'etilè) i la polilactida al sector de l'envàs i l'embalatge.**

Resum

El propòsit d'aquesta tesi doctoral va ser avaluar la influència dels diferents processos de gestió de residus, com ara la valorització material, energètica i biològica de dos polièsters clau a la indústria de l'embalatge: l'actual no-renovable poli (tereftalat d'etilè) (PET) i el potencial candidat per substituir-lo en un futur proper, la polilactida (PLA), de base renovable. Es van utilitzar diverses plantes pilot per simular les condicions de la degradació patida per PET i PLA en el reciclatge mecànic, la piròlisi, la combustió i l'enterrament. Els canvis van ser monitoritzats per calorimetria diferencial de rastreig (DSC), anàlisi dinàmic-mecànic-tèrmic (DMTA), anàlisi termogravimètric (TGA), espectrometria infrarroja amb transformada de Fourier (FTIR), espectroscòpia de correlació 2D-IR per a l'anàlisi de gasos (EGA), espectrometria de masses MALDI-TOF, microscòpia electrònica de rastreig (SEM), índex de fluïdesa de massa fosa (MFR), assaigs de tracció i impacte Charpy i viscosimetria. S'han proposat, desenvolupat i aplicat diverses estratègies i procediments analítics per establir paràmetres fiables per ser utilitzats com a indicadors de la degradació i per tant controlar la influència de cada procés de valorització en la qualitat del material. El comportament de PET i PLA reciclats mecànicament es va avaluar en base a les seves propietats químiques, microestructurals, mecàniques i tèrmiques. Es va observar una pèrdua general de prestacions de PET i PLA reprocessat una i dues vegades, respectivament. A més, les propietats dels materials reciclats de PLA van ser millors en termes relatius als productes reciclats de PET. La descomposició tèrmica i termo-oxidativa causades pels processos de piròlisi i combustió es van avaluar sobre l'estabilitat tèrmica, gasos emesos i cinètiques de descomposició. Es destaca l'ús de la combustió controlada per ambdós polímers, ja que es necessita menys energia per provocar la descomposició, i la barreja de gasos que es desprèn és més homogènia. Finalment, l'ús combinat de tècniques d'anàlisi tèrmic es va demostrar com un procediment fiable per monitoritzar la degradació patida pel PLA en condicions d'enterrament. La substitució de PET per PLA, per tant, s'estableix com una opció adequada des del punt de vista de la gestió dels residus plàstics, ja que el PLA ofereix millors prestacions després del reprocessament que el PET, i la seua valorització energètica - sempre que la valoració biològica no pugui satisfer la demanda - és factible i eficaç.

Strategier och analysförfaranden för en hållbar avfallshantering av plast. En tillämpning av polyetentereftalat och polylaktid i förpackningssektorn.

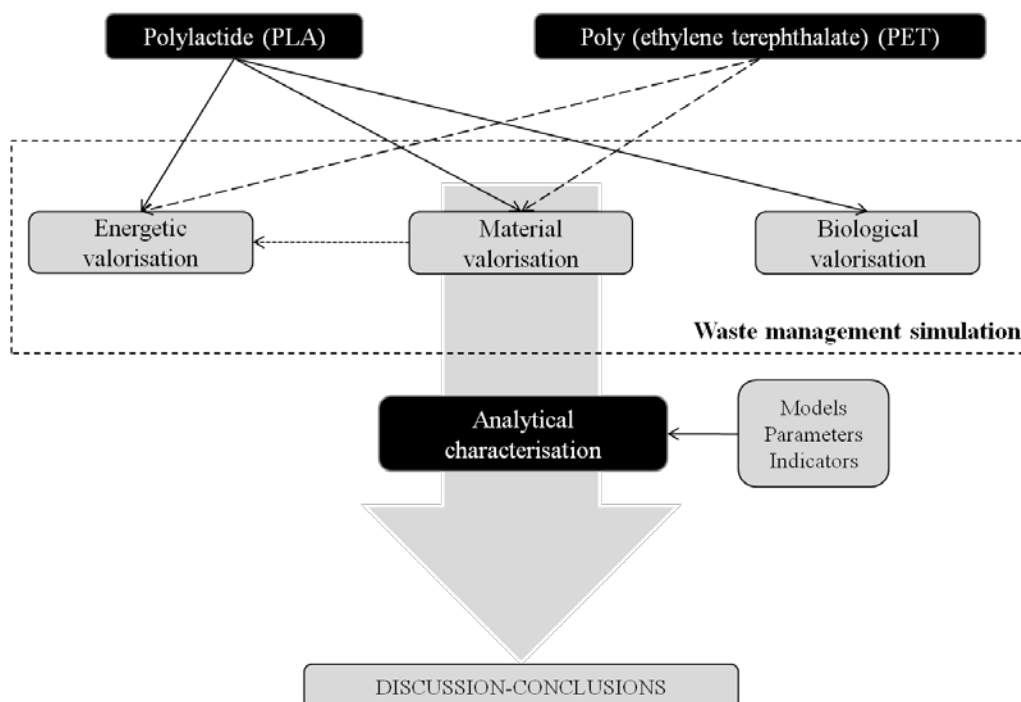
Sammanfattning

Syftet med denna avhandling var att bedöma inverkan av olika processer för avfallshantering såsom materiella, energirika och biologiska värderingar på två viktiga polyestrar inom förpackningsindustrin. Den nuvarande icke-förnybara Polyetentereftalat (PET) samt, den potentiella kandidaten att ersätta den inom en snar framtid, den biobaserade polylaktid (PLA). Av den anledningen användes flera pilotanläggningar för att simulera de nedbrytningsvillkor som PET och PLA genomgår under mekanisk återvinning, pyrolys, förbränning och nedgrävning i jord. Strategier och analysmetoder har föreslagits, utvecklats och tillämpats för att fastställa tillförlitliga, specifika parametrar att använda som indikatorer för nedbrytning och därmed övervaka inverkan av varje valorisationsprocess på materialets kvalitet. Den termo-mekaniska nedbrytningen, framkallad av mekanisk återvinning bedömdes för PET och PLA i form av mikrostrukturella förändringar och korrelerades med deras termiska och mekaniska prestanda. En generell förlust av egenskaper visades för både PET och PLA som upparbetats en respektive två gånger. Efteråt var egenskaperna hos återvunnet PLA-material relativt sett bättre än de hos återvunnet PET-material. Det termiska och termo-oxidativa sönderfall som orsakades av pyrolys och förbränningsprocesser utvärderades avseende termisk stabilitet, utvecklade gaser och nedbrytningens kinetik. Användningen av kontrollerad förbränning betonades för båda polymererna eftersom denna krävde mindre energi för att sätta igång nedbrytningen, samt att blandningen av avgivna gaser var mer homogen. Slutligen visade sig användningen av kombinerade termiska analysmetoder vara ett tillförlitligt förfarande för att övervaka nedbrytning av PLA-material som begravts i jord. Avseende plastavfallshantering är det därför fortfarande ett lämpligt alternativ att byta ut PET mot PLA, eftersom PLA ger bättre egenskaper efter återanvändning än PET, och för att dess energiska värden - förutsatt att det biologiska värdet inte kan uppfylla efterfrågan - är möjliga och effektiva.

Aim of the study

The aim of this doctoral thesis was to contribute to the study of the influence of different plastic waste management valorisation processes on the chemical and physical properties of two key polyesters in the packaging industry, the current widely used synthetic one, poly (ethylene terephthalate) (PET) and the bio-based polylactide (PLA), likely candidate to replace PET in the packaging sector.

The procedure followed to achieve this purpose is shown in the Figure below. In a first step, several pilot plants were used for simulation of the degradation suffered by both polymers under several waste management procedures, and their combinations thereof. Material valorisation was simulated by mechanical recycling, energetic valorisation by pyrolysis and combustion, and biological valorisation by burial in soil tests. To achieve the purpose, several models and analytical strategies were proposed to apply a suitable quality assessment of the materials, highlighting specific parameters reliable to be used as indicators of degradation and thus for monitoring the quality of the material in each case. Finally, the performance of both polymers facing the proposed valorisations was assessed.



Structure of the thesis

The text is structured under the following topics:

Firstly, two background chapters are focused on the materials and the analytical strategies followed in the study:

Chapter I. Plastics for packaging.

Chapter II. Experimental procedures and analytical methods

Afterwards, three chapters gathering the results of the application of each valorisation process and the subsequent discussion are shown. Each chapter is structured according to the following scheme: (1) short introduction specially addressing the state of the art of the valorisation process and its application on the polymers under consideration; (2) contributions of this thesis; and (3) a summary of the remarkable results in the field. These chapters are:

Chapter III. Material valorisation. Studies of mechanical recycling on PET and PLA.

Chapter IV. Energetic valorisation. Modelling the thermal behaviour of PET and PLA for pyrolysis and combustion systems.

Chapter V. Biological valorisation. Performance of Thermal Analysis Techniques for monitoring the biodegradation in soil process on PLA.

Finally, the conclusions are gathered and rephrased in the last chapter where the main results are highlighted. As well, several future lines of study are suggested.

Chapter VI. Conclusions

Contributions of this thesis

The most remarkable results of this thesis are gathered in the following contributions, shown along the text for the different fields:

Material valorisation (Chapter III)

CONTRIBUTION III-A: *Thermal analysis as a quality tool for assessing the influence of thermo-mechanical degradation on recycled poly(ethylene terephthalate)*

CONTRIBUTION III-B: *A statistical design of experiments for optimizing the MALDI-TOF-MS sample preparation of polymers. An application in the assessment of the thermo-mechanical degradation mechanisms of poly (ethylene terephthalate).*

CONTRIBUTION III-C: *The role of crystalline, mobile amorphous and rigid amorphous fractions on the performance of recycled poly (ethylene terephthalate) (PET)*

CONTRIBUTION III-D: *Assessing the MALDI-TOF MS sample preparation procedure to analyze the influence of thermo-oxidative ageing and thermo-mechanical degradation on poly (lactide).*

CONTRIBUTION III-E: *Material valorisation of amorphous polylactide. Influence of thermo-mechanical degradation on the morphology, segmental dynamics, thermal and mechanical performance*

Energetic valorisation (Chapter IV)

CONTRIBUTION IV-A: *Detailed methodology to assess the thermal stability and kinetics of thermal and thermo-oxidative decomposition behaviours of reprocessed poly (ethylene terephthalate)*

CONTRIBUTION IV-B: *Assessing the thermal stability and kinetics of thermal and thermo-oxidative decompositions of reprocessed polylactide*

Biological valorisation (Chapter V)

CONTRIBUTION V-A: *Thermal analysis applied to the characterization of degradation in soil of polylactide: I. Calorimetric and viscoelastic analyses*

CONTRIBUTION V-B: *Thermal analysis applied to the characterization of degradation in soil of polylactide: II. On the thermal stability and thermal decomposition kinetics*

Table of contents

Summary	11
Resumen	13
Resum	15
Sammanfattning	17
Aim of the study	19
Table of contents	23

CHAPTER I. PLASTICS FOR PACKAGING

1. Features of packaging	37
2. Bio-based polymers	41
2.1. Figures and perspectives	43
2.2. Classification and properties of biodegradable plastics	46
3. Plastic waste management	49
3.1. Plastic residues and prevention	49
3.2. Recovering procedures	51
3.3. Recycling figures in Europe	53
3.4. Bio-plastics: a new source of waste	55
4. Polymers under study	57
4.1. Poly (ethylene terephthalate)	57
4.1.1. <i>Synthesis and properties of PET</i>	57
4.1.2. <i>Applications and market of PET</i>	60
4.2. Polylactide	62
4.2.1. <i>Synthesis and properties of PLA</i>	63
4.2.2. <i>Applications and market of PLA</i>	68
5. References in this chapter	71

CHAPTER II. EXPERIMENTAL PROCEDURES AND ANALYTICAL METHODS

1. Materials and reagents	79
1.1. Polymers	79
1.2. MALDI reagents	79
1.3. Solvents	80
2. Pilot plants for degradation	81
2.1. Processing facilities	82
2.1.1. <i>Multiple extrusions</i>	82
2.1.2. <i>Multiple injections</i>	82
2.2. Compression moulding	84
2.3. Reactor for energetic valorisation	84
2.4. Biodegradation chambers	84
3. Analytical techniques and calculation methods	87
3.1. Capillary viscosimetry	88
3.1.1. <i>Fundamentals</i>	88
3.1.2. <i>Calculation methods</i>	92
3.1.3. <i>Experimental parameters</i>	95
3.2. Mass spectrometry	96
3.2.1. <i>Fundamentals</i>	96
3.2.2. <i>Fundamentals of the statistical design of experiments</i>	102
3.2.3. <i>Experimental parameters</i>	104
3.2.4. <i>Calculation methods</i>	105
3.3. Fourier transform infrared analysis	106
3.3.1. <i>Fundamentals</i>	106
3.3.2. <i>Calculation methods</i>	110
3.3.3. <i>Experimental procedure</i>	110
3.4. Scanning electron microscopy	111
3.4.1. <i>Fundamentals</i>	111
3.4.2. <i>Experimental parameters</i>	114
3.5. Melt-mass flow rate	115
3.5.1. <i>Fundamentals</i>	115
3.5.2. <i>Experimental procedure</i>	115

3.6. Tensile testing	116
3.6.1. <i>Fundamentals</i>	116
3.6.2. <i>Experimental parameters</i>	118
3.7. Impact testing	119
3.7.1. <i>Fundamentals</i>	119
3.7.2. <i>Experimental parameters</i>	120
3.8. Thermogravimetry	121
3.8.1. <i>Fundamentals</i>	121
3.8.2. <i>Kinetic analysis of thermal decompositions</i>	123
3.8.3. <i>Experimental parameters</i>	131
3.9. Evolved-gas analysis: 2D-correlation IR	132
3.9.1. <i>Fundamentals</i>	132
3.9.2. <i>Synchronous and asynchronous spectra</i>	135
3.9.3. <i>Analysis of 2D-IR spectra</i>	137
3.9.4. <i>Experimental procedure</i>	138
3.10. Differential Scanning Calorimetry	140
3.10.1. <i>Fundamentals</i>	140
3.10.2. <i>Calculation methods</i>	141
3.10.3. <i>Experimental procedure</i>	144
3.11. Dynamical – mechanical - thermal analysis	145
3.11.1. <i>Fundamentals</i>	145
3.11.2. <i>Dynamic viscoelastic moduli of a polymer</i>	149
3.11.3. <i>DMTA instrumentation</i>	150
3.11.4. <i>The glass-rubber relaxation</i>	151
3.11.5. <i>Experimental parameters</i>	154
4. References in this chapter	155

CHAPTER III. MATERIAL VALORISATION

1. Introduction	165
2. Reusing and primary recycling	167
3. Mechanical recycling	169
3.1. Types of plastic solid waste fractions	171
3.2. Mechanical recycling process	173
4. Mechanical recycling of PET	177
4.1. Contamination of recycled PET	178
4.2. Specific super-clean decontamination processes for PET	182
4.3. Use and sustainability of recycled PET	184
4.4. Use of recycled PET in food applications	187
4.5. The PET recycling system in Spain	188
4.6. The thermo-mechanical degradation of PET	191
5. Mechanical recycling of PLA	195
6. References in this chapter	199
7. Contributions in this thesis	203
CONTRIBUTION III-A: <i>Thermal analysis as a quality tool for assessing the influence of thermo-mechanical degradation on recycled poly(ethylene terephthalate)</i>	207
CONTRIBUTION III-B: <i>A statistical design of experiments for optimizing the MALDI-TOF-MS sample preparation of polymers. An application in the assessment of the thermo-mechanical degradation mechanisms of poly (ethylene terephthalate)</i>	217
CONTRIBUTION III-C: <i>The role of crystalline, mobile amorphous and rigid amorphous fractions on the performance of recycled poly (ethylene terephthalate) (PET)</i>	231
CONTRIBUTION III-D: <i>Assessing the MALDI-TOF MS sample preparation procedure to analyze the influence of thermo-oxidative ageing and thermo-mechanical degradation on poly (lactide)</i>	255

CONTRIBUTION III-E: <i>Material valorisation of amorphous polylactide. Influence of thermo-mechanical degradation on the morphology, segmental dynamics, thermal and mechanical performance.</i>	271
8. Remarkable results	289

CHAPTER IV. ENERGETIC VALORISATION

1. Chemical recycling with energetic valorisation	297
1.1. Pyrolysis	303
1.2. Gasification	305
1.3. Incineration	307
2. Thermolysis of PET and PLA	313
2.1. Thermal and thermo-oxidative decomposition mechanisms of PET	313
2.2. Thermal and thermo-oxidative decomposition mechanisms of PLA	319
2.3. Approaching pyrolysis and gasification of plastics by TGA.	321
3. References in this chapter	323
4. Contributions in this thesis	329
CONTRIBUTION IV-A: <i>Detailed methodology to assess the thermal stability and kinetics of thermal and thermo-oxidative decomposition behaviours of reprocessed poly(ethylene terephthalate)</i>	331
CONTRIBUTION IV-B: <i>Assessing the thermal stability, thermal and thermo-oxidative decomposition behaviours of reprocessed polylactide for the packaging industry</i>	369
5. Remarkable results	399

CHAPTER V. BIOLOGICAL VALORISATION

1. Biodegradation: general aspects	405
1.1. Degradation after service life	406
1.2. Biodegradation processes	408
1.2.1. <i>Biodeterioration</i>	408
1.2.2. <i>Biofragmentation</i>	409
1.2.3. <i>Bioassimilation</i>	412
2. Testing procedures for assessing biodegradation	415
2.1. Analytical strategies	415
2.2. Relevant ISO standards for the measurement of biodegradation	417
2.3. Standardisation and certification	418
3. Biodegradation of PLA	421
4. References in this chapter	425
5. Contributions in this thesis	429
CONTRIBUTION V-A: <i>Thermal analysis applied to the characterization of degradation in soil of polylactide: I. Calorimetric and viscoelastic analyses</i>	431
CONTRIBUTION V-B: <i>Thermal analysis applied to the characterization of degradation in soil of polylactide: II. On the thermal stability and thermal decomposition kinetics</i>	441
6. Remarkable results	451

CHAPTER VI. CONCLUSIONS

1. Conclusions	457
2. Conclusiones	465
3. Future research lines	475

GLOSSARIES

List of tables	479
----------------	-----

List of figures	483
Glossary of terms	495
Main symbology	499

EPILOGUE

Pensaments, agraiments, dedicatòries	503
--------------------------------------	-------	-----

CHAPTER I: PLASTICS FOR PACKAGING

CONTENTS

1. Features of packaging	37
2. Bio-based polymers	41
2.1. Figures and perspectives	43
2.2. Classification and properties of biodegradable plastics	46
3. Plastic waste management	49
3.1. Plastic residues and prevention	49
3.2. Recovering procedures	51
3.3. Recycling figures in Europe	53
3.4. Bio-plastics: a new source of waste	55
4. Polymers under study	57
4.1. Poly (ethylene terephthalate)	57
4.1.1. <i>Synthesis and properties of PET</i>	57
4.1.2. <i>Applications and market of PET</i>	60
4.2. Polylactide	62
4.2.1. <i>Synthesis and properties of PLA</i>	63
4.2.2. <i>Applications and market of PLA</i>	68
5. References in this chapter	71

CHAPTER I

PLASTICS FOR PACKAGING

1. FEATURES OF PACKAGING

The polymer industry is normally made up of a large number of companies and agents that operate plastics during their service lives and further disposal. The activities or functions of these companies are not mutually exclusive; indeed, they frequently overlap. In any case, the **structure of the polymer industry** can be divided essentially into the following categories ⁽¹⁾: manufacturers (of monomers, chemicals, additives, modifiers...), compounders, processors, fabricators and finishers. After the conversion of the polymer into a plastic, other agents like distributors, sellers, customers, waste recoverers and waste managers, are involved.

The world of polymers thus represents a key sector in the global economy. Actually, only the European plastics industry produces 55 million tonnes (Mt) of polymeric materials per year, representing 24% of the global plastics production, according to data from *PlasticsEurope* ⁽²⁾. However, global plastics production fell back from 245 Mt in 2008 to 230 Mt in 2009 as a consequence of the continued economic slowdown.

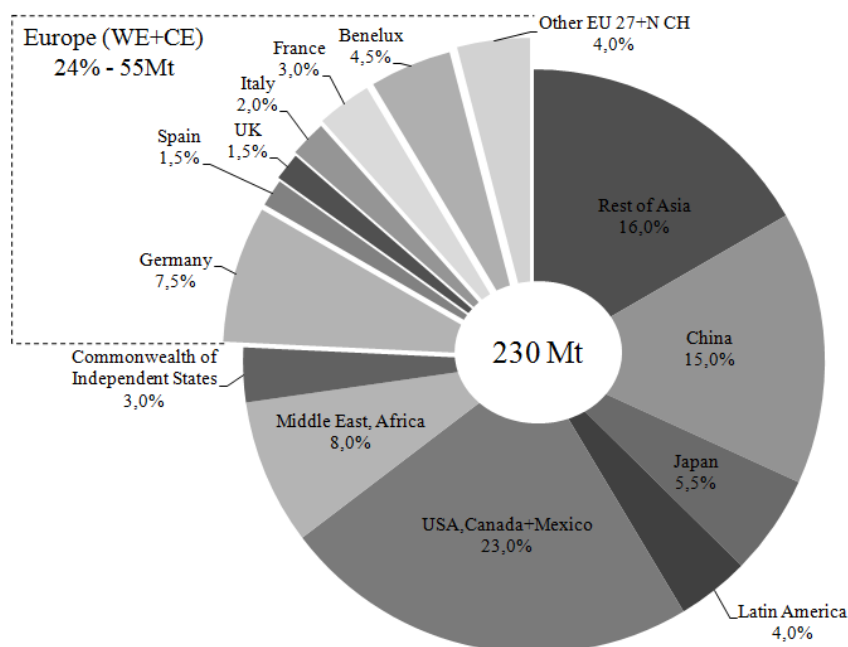


Figure 1. 1. World plastics production in 2009. Adapted from *PlasticsEurope* – report 2010 ⁽²⁾

Plastic production facilities are well placed across Europe. Germany is the major producer, accounting for 7,5% of global production, followed by the Benelux (4.5%), France (3%), Italy (2%), and the UK and Spain (1.5%), as shown in Figure 1. 1. Concerning the demand of plastics by converters in Europe, it was 48,5 Mt in 2008, which fell to 40,5 Mt in 2009. The major countries are Germany and Italy, together accounting for around 40% of the European conversion to plastic products.

In a general view, **packaging** is the science, art and technology of enclosing or protecting products for distribution, storage, sale, and use. It also refers to the process of design, evaluation, and production of packages ⁽³⁾.

The different types of packages can be classified according to different features ⁽⁴⁾:

- **intended customer:** for example, a transport package or distribution package can be the shipping container used to ship, store, and handle the product or inner packages. Some identify a consumer package as one which is directed toward a consumer or household.
- **type of product** being packaged: medical, chemical , food ...
- **by layer or function:**
 - Primary packaging is the material that first envelops the product and holds it. This usually is the smallest unit of distribution or use and is the package which is in direct contact with the contents.
 - Secondary packaging is outside the primary packaging used to group primary packages together.
 - Tertiary packaging is used for bulk handling, warehouse storage and transport shipping.

Packaging , as well as package labeling have several **objectives** ⁽⁵⁾:

- **Physical protection** - The objects enclosed in the package may require protection from, among other things, mechanical shock, vibration, electrostatic discharge, compression or temperature.
- **Barrier protection** - Permeation is a critical factor in design. A barrier from oxygen, water vapor, dust, etc., is often required in order to keep the contents clean, fresh, sterile and safe for the intended service life.

- **Containment or agglomeration** - Small objects are typically grouped together in one package for reasons of efficiency. It is the case of liquids, powders, and granular materials. As well, single serving or single dosage packaging has a precise amount of contents to control usage.
- **Information transmission** - Packages and labels communicate how to use, transport, recycle, or dispose of the package or product.
- **Marketing** - Marketing communications and graphic design are applied to the surface of the package.

As shown in Fig 1.2, packaging is the **largest end use market segment** with a 40.1% of share. This is followed by building and construction (20.4%), automotive (7.0%) and electrical and electronic equipment (5.6%). Others include different small segments like sport, leisure, agriculture or machinery engineering ⁽²⁾. The most common used polymers are low and high density polyethylene (LDPE, and HDPE, respectively), polypropylene (PP), **poly (ethylene terephthalate) (PET)**, polystyrene (PS) and poly (vinyl chloride) (PVC). LDPE and HDPE are used as bottles for milk, water, juice, cosmetics, shampoo, dish and laundry detergents, and household cleaners, bags for groceries and retail purchases, cereal box liners, or reusable shipping containers. PP may be used as container for yogurt, margarine, take-out meals, and deli foods, medicine bottles, bottle caps and closures and bottles for catsup and syrup. PET is used for plastic bottles for soft drinks, water, juice, sports drinks, beer, mouthwash, catsup and salad dressing, food jars for peanut butter, jelly, jam and pickles, as well as ovenable film and microwavable food container. PS products are food service items, such as cups, plates, bowls, cutlery, meat and poultry trays, and rigid food containers such as for yoghourts. It is also used as protective foam packaging for furniture, electronics and other delicate items. In addition, compact disc cases and aspirin bottles can also be produced. PVC is used in rigid packaging applications including blister packs and clamshells. Flexible packaging uses include bags for bedding and medical or shrink wrap.

It can be seen that the use of poly (ethylene terephthalate) (PET) is significantly directed to the packaging sector and thus was chosen as model synthetic polymer in this thesis. However, the use of petroleum-based plastics is being reduced for environmental and economical reasons. In this sense, the current introduction of bio-based polymers is

winning market share and thus opens new alternatives to current applications. In the following lines, a short overview of bio-based polymers is given, in order to introduce the polymer used in this thesis: polylactide.

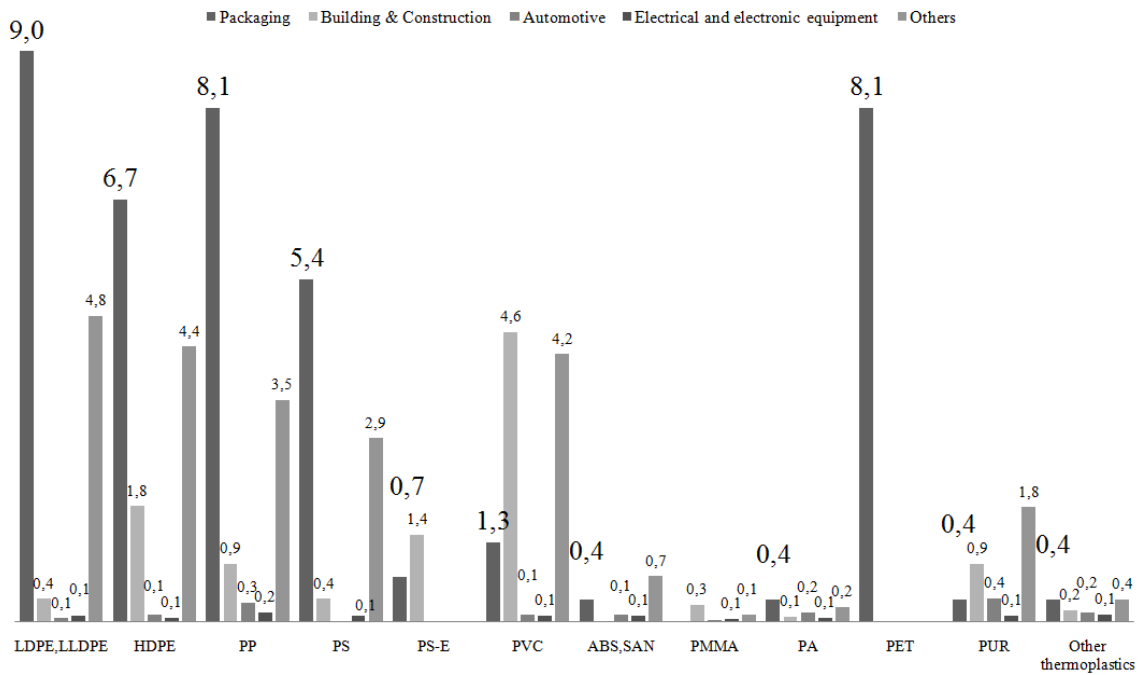


Figure 1. 2. Percentages of European plastic demand in 2009 by segments (commodities + technical polymers). Total demand: 45 Mt. Adapted from *PlasticsEurope* – report 2010⁽²⁾

2. BIO-BASED POLYMERS

The interest in environmentally degradable polymers began more than thirty years ago, when it was first recognized that the commonly used commodity packaging plastics were accumulating in the environments in which they were discarded after use, since these polymers were developed for their resistance properties, being unmanageable in landfills and as litter when disposed of in a negligent manner. More recently, the problem of polymer accumulation in the environment has been recognized as more general than packaging plastics, extending to recalcitrant water-soluble and other specialty polymers and plastics such as poly(acrylic acid), poly(vinyl alcohol), poly(acryl amide), poly(alkylene oxides), and even some modified natural polymers, such as celluloses. These polymers are widely used in applications like permanent and temporary coatings, pigment dispersants, mining, detergents or water treatment; and all are potential contributors to environmental problems and, therefore, targets for replacement with environmentally degradable substitutes⁽⁶⁾. With growing concerns for the environment and limited fossil reserves, the investigation on biodegradable polymers becomes a global priority⁽⁷⁾. The use of long-lasting polymers as packaging materials for short application is not further justified, also because mechanical recycling of these materials is often impractical due to food contamination⁽⁸⁾.

Bio-based polymers abound in nature. Wood, leaves, fruits, seeds and animal furs all contain natural polymers. Bio-based polymers have been used for food, furniture and clothing for thousands of years. Every year about $170 \cdot 10^3$ Mt of biomass are produced by nature, of which only 3,5% ($6 \cdot 10^3$ Mt) are utilised by mankind, as shown in Fig. 1.3. Most of these are used for food, about 1/3 is used for energy, paper, furniture and construction, and only 5% (300 million tonnes) are consumed for other non-food purposes such as chemicals and clothing⁽⁹⁾. Research and development in the field of bio-based plastics is making significant advancements towards creating compounds that represent an economically viable and environmentally friendly alternative to traditional petroleum-based plastics⁽⁷⁾.

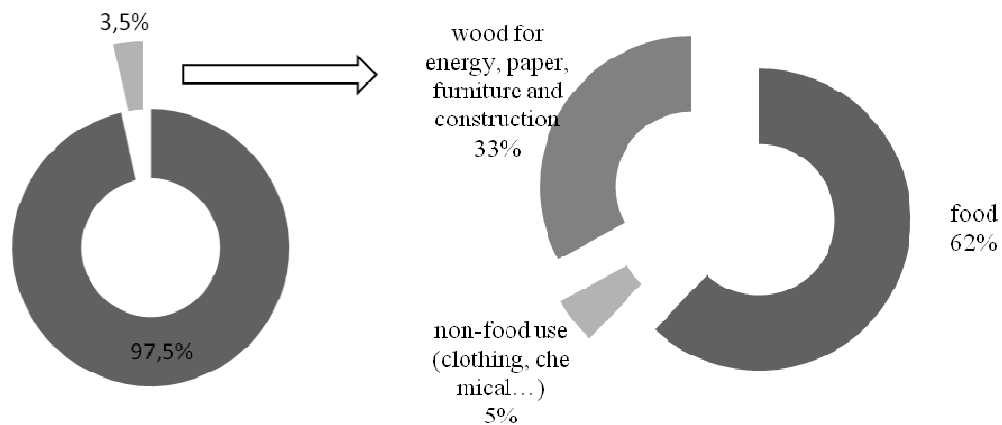


Figure 1. 3. Worldwide production of biomass (left) and use of mankind (right). Adapted from report PRO-BIP 2009 ⁽¹⁰⁾

Benefits of conversion to this **green generation of plastics** are numerous and warrant continued research into synthesizing novel degradable polymers, developing more efficient production systems, and utilizing bio-based, renewable feedstocks for sustainable production systems ⁽⁷⁾. The commercialization of biodegradable polymers should continue increasing, especially in markets where plastic products have very short, single-use applications. According to *Keenan et al* ⁽⁷⁾, the general attitude in society has come to value environmentally green products, and consumers are slowly becoming to accept paying relatively higher prices for these novel products. This eco-conscious, biodegradable plastic market should continue expanding, as bio-based resin prices are made more competitive with conventional commodity plastics and consumer misconceptions regarding the instability of degradable plastics are being clarified.

The presence of bio-based polymers in industrial processes is not new. Artificial bio-based plastics have a history of approximately 150 years. The first artificial thermoplastic, celluloid, was invented in the 1860s. Since then, numerous new compounds derived from renewable resources have been developed. For instance, the protein casein was used for paints and glues and later on, in formulations with formaldehyde, as plastic used for products like buttons, knives and letter openers. Soy protein was reacted with formaldehyde and co-condensed with phenol or urea, used by the Ford Company to produce numerous automotive parts such as steering wheels, glove-box doors and interior trim. However, many of these inventions in the 1930s and 1940s stayed in laboratory scale mainly due to the discovery of crude oil and its large-scale industrial use for synthetic

polymers since the 1950s. Due to the shocking of prices of oil price during the 1970s, the interest in the possibilities offered by non-petrochemical feedstock was renewed. Based on some first attempts in the 1980s, interest rose again in the 1990s and broad attention was paid to bio-based chemistry in general and bio-based and biodegradable plastics in particular since the early 2000s. One of the main drivers especially in the 1990s was the goal to provide the market with plastics that are biodegradable, in order to solve the problem of rapidly increasing amounts of waste and limited landfill capacities⁽¹⁰⁾. A short description of the technical potential for the market of bio-based polymers is given hereafter.

2.1. FIGURES AND PERSPECTIVES

As shortly introduced above, the development of plastics depends on many factors, among them world **economic growth** and the affordability and **supply security** of resources. For fossil fuels and feedstock, the affordability and supply clearly depend on geopolitical developments, oil production and processing capacities or the demand in developing countries. These factors are reflected in the price levels of crude oil and natural gas, which are likely to strongly influence the further development of fossil fuel-based polymers⁽¹⁰⁾.

Another potentially important determining factor for the future of the polymer industry is the **climate policy**. In the last few years, an increasing apparent coupling of the prices of fossil fuels and agricultural products has been observed⁽¹⁰⁾. There are different views about whether this is primarily a consequence of the use of biomass for energy purposes (primarily biofuels) or whether other reasons are equally or even more important⁽¹¹⁾. Among the other reasons quoted are droughts, increased prices of energy and fertilizers, declining global stocks due to changed policies or the increased demand from the developing world and speculation. Until recently, the Organisation for Economic Co-operation and Development (OECD) and other organizations assigned a modest influence to biofuels⁽¹²⁾. However, a World Bank report concluded that the large increase in biofuels production in Europe and the USA is indeed the most important reason for the rising food grain prices⁽¹³⁾.

Today, public environmental concern, climate change and limited fossil fuel resources are important drivers for governments, companies and scientists to find alternatives to crude oil. Bio-based plastics may offer important contributions by reducing the dependence on fossil fuels and the related environmental impacts. Bio-based plastics will in addition be able to substantially reduce the chemical industry's environmental footprint only if bio-based plastics manage to overcome a meaningful share of standard plastics. Bio-based plastics have a higher product value than biofuels (e.g. ethanol) but their product value is lower than for special and fine chemicals and pharmaceuticals. Also the value added created by bulk bio-based plastics will take an intermediate position. While the replacement by conventional bulk plastics may be a long-term goal, plastics applied for higher value applications are nevertheless of interest today because they could pave the way for bio-based bulk products.

Fig 1.4. illustrates the **stage of development for the various bio-based plastics**. It is remarkable that each technology development stage is represented by several important products. Moreover, both fully and partly bio-based plastics are present in each technology development stage. Not surprisingly, more materials are in the R&D and pilot plant stage than in large-scale commercial production ⁽¹⁰⁾.

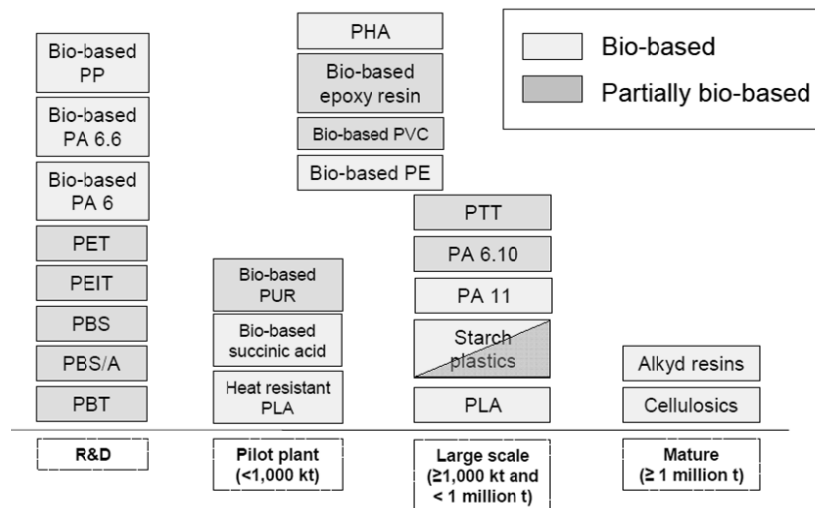


Figure 1. 4. Development stage of main emerging bio-based material types. Reproduced from report PRO-BIP 2009 ⁽¹⁰⁾

According to calculations published in *PRO-BIP2009* ⁽¹⁰⁾, for all plastics including fibres in Western Europe, the maximum technical substitution potential of bio-based plastics

(including fibres) in place of petrochemical plastics is thus estimated at 48 Mt, or 82% of total plastics. Worldwide, the total maximum technical substitution potential of bio-based plastics and fibres replacing their petrochemical counterparts is estimated at 240 Mt, or 90% of the total consumption of plastics and fibres (data from 2007).

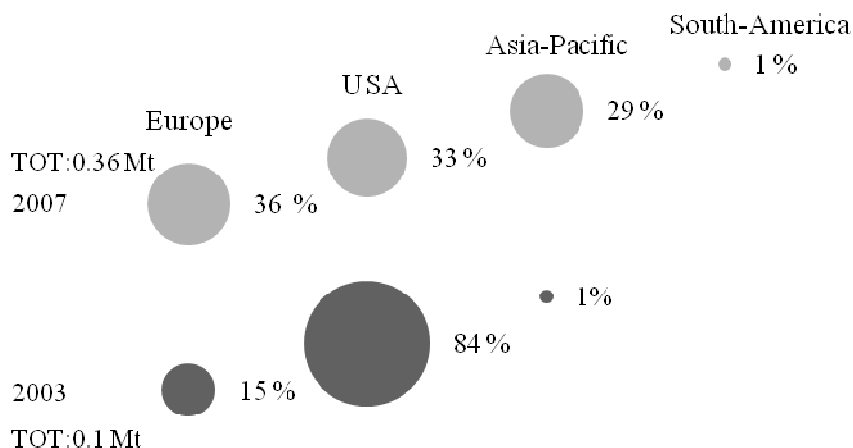


Figure 1. 5. Capacity of emerging bio-based plastics by regions, 2003 and 2007. Adapted from report PRO-BIP 2009⁽¹⁰⁾

From a geographic perspective, the leading position of the USA and Europe in the year 2003 changed to a more balanced regional distribution in 2007. The USA still had the leading position in the emerging bio-based plastics industry. However, the USA share of production capacity of bio-based plastics in the world decreased from 84% in 2003 to 33% in 2007, as shown in Fig 1.5. Europe, the second most important region for bio-based plastics, increased its share from 15% in 2003 to 36% in 2007. On the other hand, the Asia Pacific region became the third leading region over this 5-year period.

There are still several factors determining whether the **speed of implementation of bio-based polymers** will be high or low in the subsequent years. A selection of important success factors is listed below.

Financial

- Prices of fossil fuels, especially oil.
- Price level of biofeedstocks (agricultural products) such as starch, sugar and vegetable oils.

- Investment risks.
- Fiscal policy measures (e.g. to support processes with minimal greenhouse gas emissions).
- Economic competitiveness compared to other locations.
- Availability of capital, interest rate.

Technology

- Reliability of new technology, acceptable downtimes.
- Speed of technology development.
- Patent situation.
- Availability of trained personnel.

Interaction with other sectors and other plants

- Collaboration with companies from the agroindustry chain.
- Availability of raw materials.
- Usefulness of co-products, integration into site.

Regulation

- Non-fiscal policy measures (e.g., voluntary agreements or labelling).
- Public procurement.

Market pull

- Demand for bio-based products by retailers and producers of consumer goods.
- Attitude of final consumers and other stakeholders (acceptance or rejection).
- Existence of operational old plants versus growth of the chemical industry.

2.2. CLASSIFICATION AND PROPERTIES OF BIODEGRADABLE PLASTICS

Biodegradable polymers can be classified according to different criteria. They can be sorted according to their chemical composition, synthesis method, processing method,

economic importance, application, etc. Each of these classifications provides different and useful information⁽¹⁴⁾.

According to their origin two groups can be considered:

- **natural polymers**, coming from natural resources, which include six sub-groups:
 - polysaccharides (starch, cellulose, lignin, chitin).
 - proteins (gelatine, casein, wheat gluten, silk and wool).
 - lipids (plant oils including castor oil and animal fats).
 - polyesters produced by micro-organism or by plants (polyhydroxy-alcanoates, poly-3-hydroxybutyrate).
 - polyesters synthesised from bio-derived monomers (poly(lactic acid) or **polylactide**).
 - miscellaneous (natural rubbers, composites).

- **synthetic polymers**, synthesised from crude oil, where the following sub-groups can be found:
 - aliphatic polyesters (polyglycolic acid, polybutylene succinate, polycaprolactone).
 - aromatic polyesters or blends of the two types (polybutylene succinate terephthalate).
 - polyvinylalcohols.
 - modified polyolefins (polyethylene or polypropylene with specific agents sensitive to temperature or light).

Concerning the **biodegradability**, a very broad range of plastics can be produced fully or partially from biomass and that these plastics can be tailored to be fully or partially biodegradable, as shown in Fig 1.6.

Table 1. 1 gives a comparison of the **typical properties of biodegradable polymers** with those of commodities. Their mechanical properties can be comparable with those of conventional polymers in specific applications with different features⁽¹⁵⁾. There are flexible materials with medium service temperature like PE, relatively stiff materials with medium service temperature like PS and stiff materials with a high service temperature like PET. The performance expected from bio-based plastic materials used in **food packaging ap-**

plications is containing the food and protecting it from the environment and maintaining food quality ⁽¹⁶⁾. To perform these functions it is important to control and modify their mechanical and barrier properties that consequently depend on the structure of the polymeric packaging material.

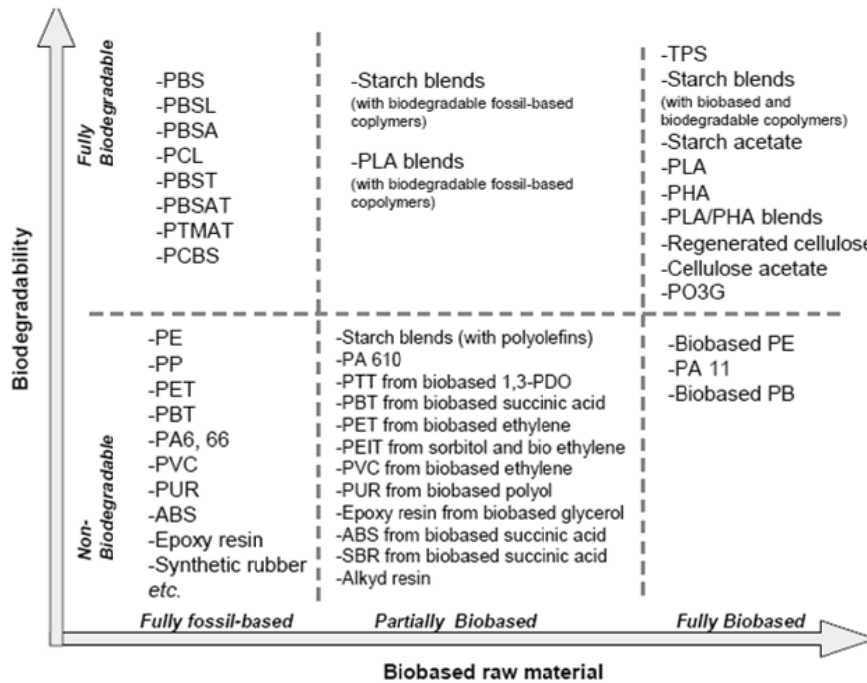


Figure 1. 6. Current and emerging (partially) bio-based plastics and their biodegradability. Reproduced from report PRO-BIP 2009 ⁽¹⁰⁾

Table 1. 1. Comparison of typical biodegradable polymer properties with commodities. Adapted from ref (14). Note that properties depend on the grade of each polymer.

	Glass transition temperature (°C)	Melting temperature (°C)	Tensile strength (MPa)	Tensile modulus (MPa)	Elongation at break (%)
LDPE	-100	98-115	8-20	300-50	100-1000
PCL	-60	59-64	4-28	390-470	700-1000
PS	70-115	100	34-50	2300-3300	1.2-2.5
Starch	---	110-115	35-80	600-850	580-820
PET	73-80	245-265	48-72	2800-4100	30-300
PLA	40-70	130-180	48-53	3500	30-240

3. PLASTIC WASTE MANAGEMENT

The **sustainable development** (SD) is defined as “development that meets the needs of the present generation without compromising the ability of future generations to meet their own needs”, which is adopted in many confederations and countries, as well as it has also become a central notion for many companies, business councils, political parties, NGOs, etc. In general, the field of SD is subdivided into three areas: economic, environmental, and social. These so-called pillars or dimensions of sustainability need to be addressed in assessing the sustainability of a project, policy, etc. A popular way of expressing the three pillars of SD is known as People, Planet, Profit (or PPP or P3), where People represents the social pillar, Planet the environmental pillar, and Profit the economic pillar. At the World Summit on Sustainable Development in Johannesburg, 2002, this was modified into People, Planet, Prosperity, where the change of Profit into Prosperity was supposed to reflect the fact that the economic dimension covers more than company profit⁽¹⁷⁾. Policy principles require that a sustainability analysis may be part of the justification for actions like adopting a policy, implementing a particular technology or purchasing a specific product.

One of the factors that determine the sustainability of a country is the **prevention** procedures and **waste management processes** of its residues. In the context referred in this thesis, a short review of the managing options for plastic waste is addressed.

3.1. PLASTIC RESIDUES AND PREVENTION

The general waste and packaging waste in particular, have significantly grown in recent decades, so that different stakeholders have directed their efforts to identify the most appropriate mechanisms to reduce their impact on the environment. In this context, prevention is a priority as far as helps reduce waste generation and involves a saving of raw materials and energy⁽¹⁸⁾.

In preventing the increase in packaging waste, an overall approach must be adopted, trying to act on the different aspects that minimize their impact throughout its life cycle. This requires analyzing the different areas to work on prevention, from identifying opportunities for improvement in the packaging and production processes to the effective management of packaging waste. At the same time, it should be noted that the container is not an element that exists in isolation but is part of the product offered to the consumer.

The causes of the increase in the generation of packaging waste respond to numerous economic, social and cultural reasons. **Changes in economic and social model** are reflected in many ways such as increased purchasing power of households, increased consumption, increased life expectancy or families with few members. According to a report by *Ecoembes*⁽¹⁸⁾, the profile of the average consumer of the XXI century is that of a person who has little free time, therefore, places a high value and preferably dedicated to leisure activities. This situation has a negative impact on the time citizens spend on household tasks, going shopping or cooking. The main reflection of the changes in our society are on the shopping cart: shopping frequency has decreased dramatically and just packaged products are purchased as one of the main values that provides the package is that it ensures sanitary conditions of products over time. Another phenomenon that also results in increased waste generation is the demand for packaged products tailored to consumer needs. Single-person households demand products fractionated into smaller portions to avoid waste of resources (expired products) and minimize the space required for storage. The clearest examples of this reduction in size of packaging formats are given in the fields of nutrition, hygiene and beauty. This division requires proportionally more packaging than larger formats. Consequently, the consumption *per capita* of packaging in small households is higher than in households with more members. This trend has resulted in a growing generation of waste, thus requiring the implementation of measures to minimize their environmental impact.

Prevention requires the active involvement of all actors from government, the manufacturers for raw material, packers and distributors to consumers of the product packaging. Thus, only through a set of measures that combine quantitative and qualitative prevention systems which are designed to recover the value of the waste, the objective will be achieved. In this context, the industry is undergoing a process of continuous improvement affecting the packaged goods and manufacturing processes, while ensuring that the containers meet its core functions.

Prevention must take into account the packaging system as a whole, comprising the primary container, the grouping and transport. Current prevention measures aimed at reducing the weight of the container are especially representative of those related to the improvement of containers by design changes and technological improvements of the materials. Additionally, other preventive measures implemented have been the elimination of elements of packaging and the use of containers of greater capacity, especially in the industrial field. With regard to preventive measures aimed at increasing the reuse of packaging, include the replacement of single-use containers for reusable, and the second use of packaging from suppliers that otherwise would have resulted in waste. These actions are common practice in industry. Regarding preventive measures to minimize the environmental impact of packaging waste generated, the trend is the reduction of printed surfaces, with the use of containers made of compatible elements for recycling.

3.2. RECOVERING PROCEDURES

Increasing cost and decreasing space of landfills are forcing considerations of alternative options for plastics solid waste (PSW) disposal ⁽¹⁹⁾. Years of research, study and testing have resulted in a number of treatment and recovery methods for PSW that can be economically and environmentally viable ⁽²⁰⁾.

Different classifications can be found in literature for the recovery procedures ^(21- 22). For example, PSW treatment and recycling processes could be allocated to four major categories: re-extrusion (primary), mechanical (secondary), chemical (tertiary) and energy recovery (quarternary). Each method provides a unique set of advantages that make it particularly beneficial for specific locations, applications or requirements. Mechanical recycling (i.e. secondary or material recycling) involves physical treatment as shown in Chapter IV, while chemical recycling and treatment (i.e. tertiary encompassing feedstock recycling) produces feedstock chemicals for the chemical industry. Energy recovery involves complete or partial oxidation of the material, producing heat, power and/or gaseous fuels, oils and chars besides by-products that must be disposed of, such as ash. This classification does not consider the biological assimilation of biodegradable polymers, since the industry of bio-based polymers was not established a decade ago. In order to offer a complete view of the treatment processes, the scheme shown in Fig. 1.7. has been arranged.

The subjacent idea is to recover and valorise the plastic goods, as much as possible. Thus, once fulfilled their *intended / designed service lives*, which do not necessarily coincide with their *performance lives* (those respectively are, the durability period designed, and the period the good could really offer good properties), the items should be recovered, not disposed. As well, the combination of processes should be intensively stressed, adapting to each case.

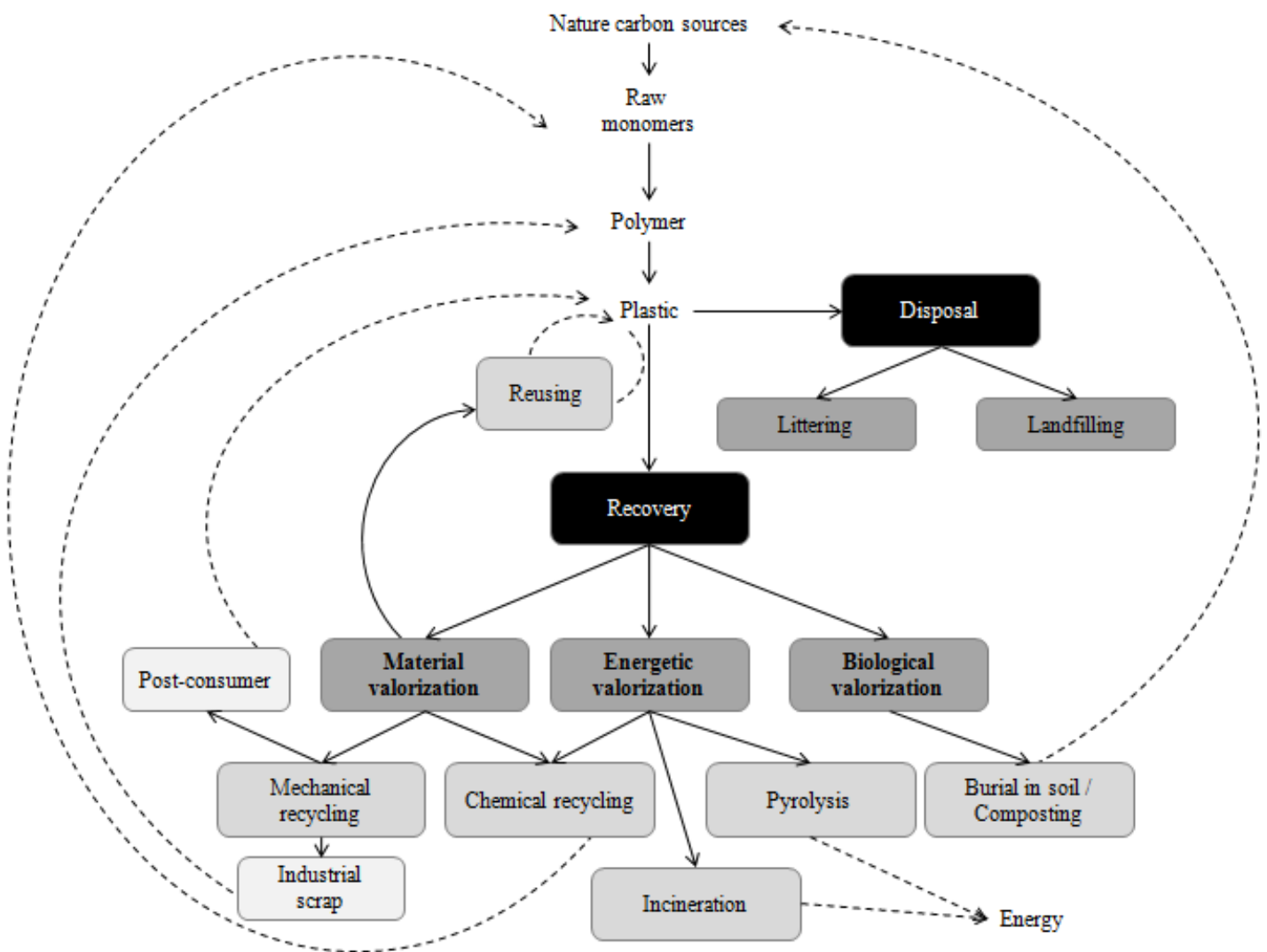


Figure 1. 7. General scheme of plastics life-recover-disposal cycle

The continued development of recovery technologies, investment in infrastructure, the establishment of viable markets and participation by industry, government and consumers

are all considered priorities of the highest order ⁽²³⁾. A life cycle assessment (LCA) approach to Municipal Solid Waste (MSW) technologies will assist in identifying environmental impacts associated with the alternatives in a ‘cradle to grave’ fashion identifying the most sustainable options. It is essential to **integrate waste management (IWM)** schemes in the production cycle of plastics and treatment schemes of PSW. LCA schemes aid in the selection, application of suitable techniques, technologies and management programs to achieve specific waste management objectives and goals. IWM target is to control the waste generation from processes to meet the needs of a society at minimal environmental impact and at an efficient resource usage by activating the potentials of waste prevention, re-use and recycling ⁽²¹⁾. The IWM cycle can be grouped into six categories, namely:

- waste generation.
- waste handling, sorting and processing at the source.
- collection.
- separation and processing.
- transfer station handling and waste transport.
- disposal.

3.3. RECYCLING FIGURES IN EUROPE

According to the 2010 report of *PlasticsEurope* ⁽²⁾, the European plastic converters used 55 Mt of plastics in 2009. Of all plastics used by consumers, 24.3 Mt ended up as post-consumer waste. Of this, 11.2 Mt were disposed of and 13.1 Mt were recovered. Overall this represents an increase of 2.5% in total recovered quantity over 2008, which was 21,3%. Mechanical recycling quantity increased by 3.1% because of stronger activities of some packaging collecting and recycling systems as well as through stronger exports outside of Europe for recycling purposes. Energy recovery quantity increased 2.2% mainly because of stronger usage of post consumer plastic waste as alternative fuel in special power plants and cement kilns.

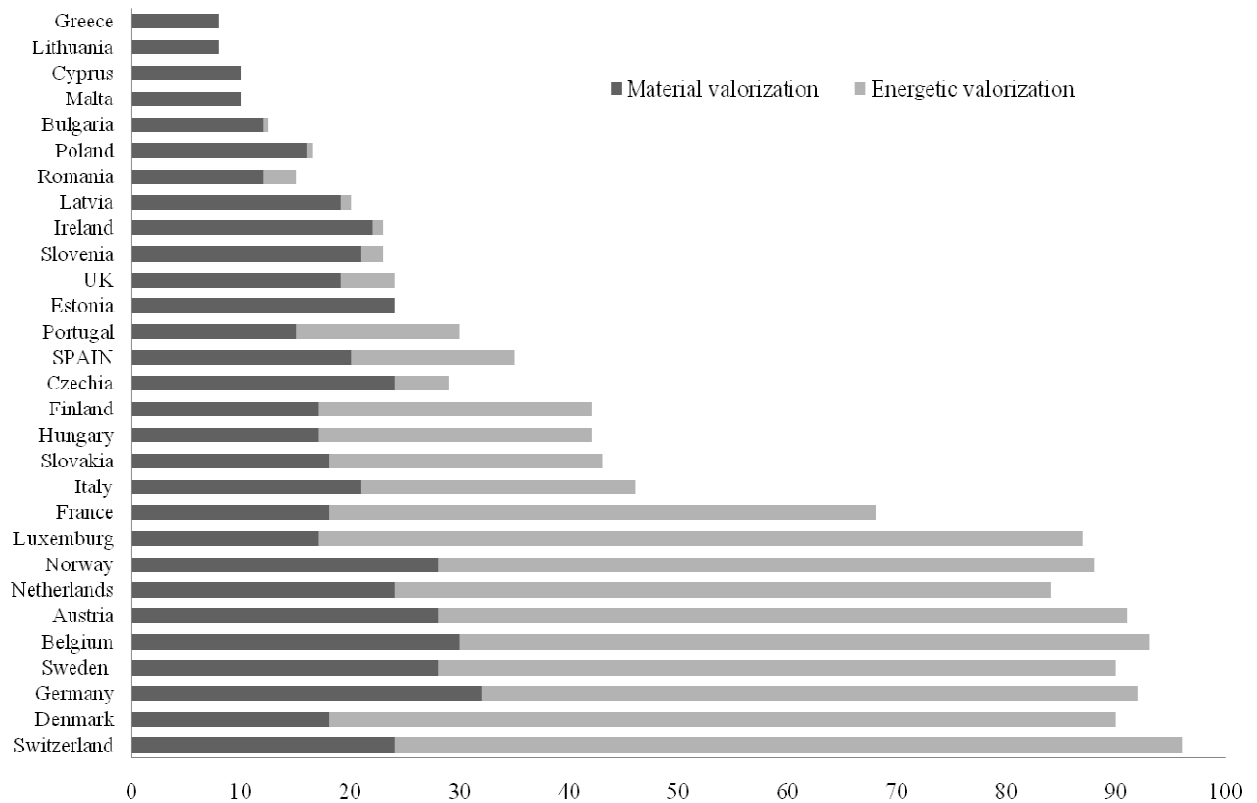


Figure 1. 8. Total recovery ratio of post-consumer plastic waste in Europe in 2009. Adapted from *Plastics Europe – report 2010* ⁽²⁾

Material recycling and energy recovery of post-consumer plastics waste are very different by country. In Switzerland, Germany, Sweden and Denmark there is very little landfill, which highlights that these countries have almost completed their diversion-from-landfill strategy. Fig 1.8 shows that countries with high recovery rates score highly on both recycling and energy recovery. This means that a strategy which includes energy recovery is not contradictory to achieving good recycling results. A complete resource management strategy, therefore, needs to address both areas. Fig 1.8 also shows that though recycling performance is similar across most European countries, there are big differences in the utilisation of energy recovery.

3.4. BIO-PLASTICS: A NEW SOURCE OF WASTE

With the incoming appearance of bio-based polymers into the plastic market, several considerations should be taken into account in order to prevent the management of this new source of waste. Indeed, biodegradable polymers broaden the range of waste management treatment options over traditional plastics. Biodegradable packaging is most suitable for domestic and/or municipal composting and should be separated from and other non-biodegradable packaging and collected with organic waste at household level for composting⁽²⁴⁾.

Biodegradable packaging is generally inappropriate for landfill because of their propensity to release methane under anaerobic conditions. By using local or regional composting facilities, the total waste to landfill could be reduced, in addition to the reduction of transport cost and associated emissions. To facilitate composting, infrastructure must be established to certify biodegradable packaging materials and to collect biodegradable packaging with organic waste. According to *Davies and Song*⁽²⁴⁾ there is no reason why biodegradable packaging materials cannot be collected with other plastic packaging for incineration, since generally no hazardous compounds may be released.

As a drawback, the growth in biodegradable plastics could weaken the already stressed plastics recycling industry by complicating the identification and sorting processes. To ensure that this does not become the case, strong clear labelling is required so that such products can be easily identified and separated.

Despite widespread public awareness of the material and effective infrastructure for rigorous control of certification, collection, separation and compositing are crucial to materialize the fully benefits⁽²⁴⁾, biodegradable polymers can make significant contributions to material recovery, reduction of landfill and utilisation of renewable resources.

4. POLYMERS UNDER STUDY

In this section, poly(ethylene terephthalate) (PET), synthetic polyester coming from non-renewable petroleum-based sources, and polylactide (PLA), bio-based polyester coming from renewable resources, are shortly introduced.

4.1. POLY (ETHYLENE TEREPHTHALATE)

Polyethylene terephthalate (PET) was first patented by *J. Fiber R. Whinfield* and *J.T. Dickson* in 1941, by means of transesterification of DMT (dimethyl terephthalate) and glycol in a 1:2:4 ratio, distilling the methanol released in the reaction mixture as the synthesis took place in the presence of a catalyst SbO_3 . Later, the contribution of *W.K. W. Birtwhistle* and *C.G. Ritchie* led them to launch the first commercial fibre: the **terylene**, which became the first production of the Imperial Chemical Industries. The second was the polyester fibre from DuPont **Dacron**. Since then, the PET has presented a continuous technological development to achieve a high level of sophistication based on growth in demand for the product worldwide and diversification of its potential use. From 1976, PET has been used to manufacture light packaging, transparent and tough mainly for drink storage. Over the 20 years on the market, PET has diversified into many sectors replacing traditional materials implanted or raising new packaging alternatives which have resulted in a tremendous growth in consumption. Presently, it remains the packaging material which currently offers the best prospects for growth worldwide⁽²⁵⁾.

4.1.1. SYNTHESIS AND PROPERTIES OF PET

The process of synthesis follows a condensation polymerization, which involves a condensation reaction in which two functional groups of the initial monomers react with each other to remove a small neutral molecule, usually water (methanol molecules can also condense in this case). The polyethylene terephthalate (PET) is a polyester that can be obtained based on the schedule shown in Fig 1.9. Obtaining is driven by three reactions.

The first two reactions are an esterification and a transesterification. The esterification reaction is between ethylene glycol (EG) and terephthalic acid (TPA) and the transesterification is between dimethyl terephthalate (DMT) and ethylene glycol. The third reaction is the polycondensation process⁽²⁵⁾.

The PET process is usually transformed by **injection-stretch blowing** in order to produce hollow bodies or by **thermoforming** processes if foils are prepared. To a lesser extent, PET can also be subjected to extrusion and injection in these cases requiring pure varieties usually chemically modified PET. During these processes, the polymer molecules bi-orient in two different directions. In the case of packaging, orientation takes place according to a longitudinal direction parallel to the axis of the container, and in a direction transverse to it. It is precisely this property, known as **bi-orientation**, which confers high mechanical strength PET, which together with its transparency, makes it an ideal material for packaging liquid products. In the case of containers obtained by thermoforming, the film presents an almost perfect lattice structure in addition to its strength and low permeability, and provides the package of a highly transparency. In fact, carbonated soft drinks can generate pressure inside the bottle reaching 6 bar⁽²⁵⁾.

The characteristics of the materials are intimately linked to the process of transformation to which they have been submitted. PET belongs to the thermoplastic family. The polymer may exist as an amorphous (transparent - bottle grade) and semicrystalline (opaque and white). Crystalline region in semicrystalline PET is developed during the crystallization process where the crystalline regions become in their equilibrium state. During the process, the crystallite size and shape can be changed with the moulding process⁽²⁶⁾. Amorphous PET, A-PET, is quenched from its melt and becomes in a non-equilibrium state, where the chains have not aligned among themselves⁽²⁷⁾. Semicrystalline, S-PET, is very sensitive towards physical aging when it is stored below its glass transition temperature. Furthermore, A-PET can become S-PET, through drawing and annealing⁽²⁶⁾.

The annealing processes allow the chains to rearrange among themselves into more equilibrium states in which they become crystalline. Depending on the end-use of the plastic it is good to have the option to choose between A-PET and S-PET.

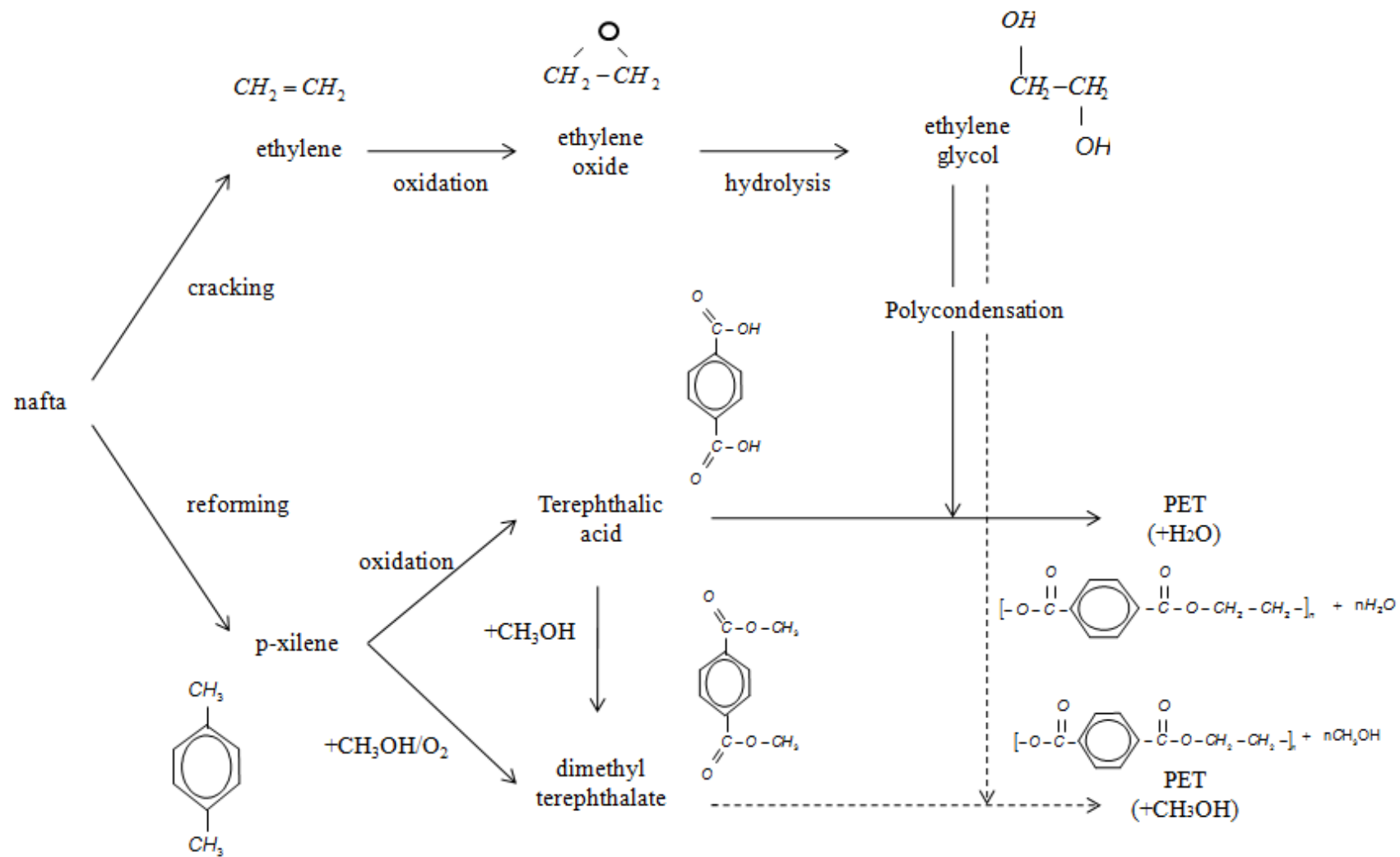


Figure 1. 9. Chemical routes for the polymerization of PET

PET has a wide variety of properties which makes it very **versatile**. PET has **good mechanical, chemical and barrier properties**⁽²⁶⁾. Due to its gloss, transparency, low permeability to gases, PET is used in bottles, electronic application, sports, and household tools and also as isolator⁽²⁸⁾.

Nevertheless, PET has some drawbacks to overcome, such as its sensitivity towards the chemical and mechanical degradation occurring during reprocessing and humidity. Therefore, it is unavoidable that the process must be performed with caution⁽²⁸⁾. PET is most sensitive to moisture at temperature near its glass transition. Moisture affects the amorphous region to mobilize and realign, not the crystalline region due to they are in its equilibrium and is permeable⁽²⁸⁾. This phenomenon is called **chemi-crystallization** in which the crystallinity of the polymer will rise. Another phenomenon which can be caused by the moisture content is the **chain-scission** where a degradation of mainly the ester-bond occurs. Chain-scission usually degrades the ester-bonds into a **hydroxyl group** and a **carboxyl group**. Due to chain-scission, it is mostly certain that the end-groups rearrange and form new structures. Depending on the formation the composition becomes more or less amorphous or crystalline. The change in composition affects PET properties⁽²⁸⁾ and therefore it is essential to dry PET during the process to achieve the best results and properties. As well, PET storage must be controlled in order to prevent that moisture penetrate into its surface.

4.1.2. APPLICATIONS AND MARKET OF PET

The production of PET is continuously increasing. In Fig 1.10, the market data on the supply and demands of PET both in Europe (Western Europe) and in the world are gathered, according to available facts published by *PlasticsEurope*⁽²⁾. The PET produced in Europe does not accomplish the demand from manufacturers, which is completed by the importations from the rest of the countries in the World. The application market of PET is large. The largest area is the fibre sector, which can be further produced as clothes, bags or toys which can be seen in Fig 1.11. The areas for sheets, strapping and bottle are nearby equally.

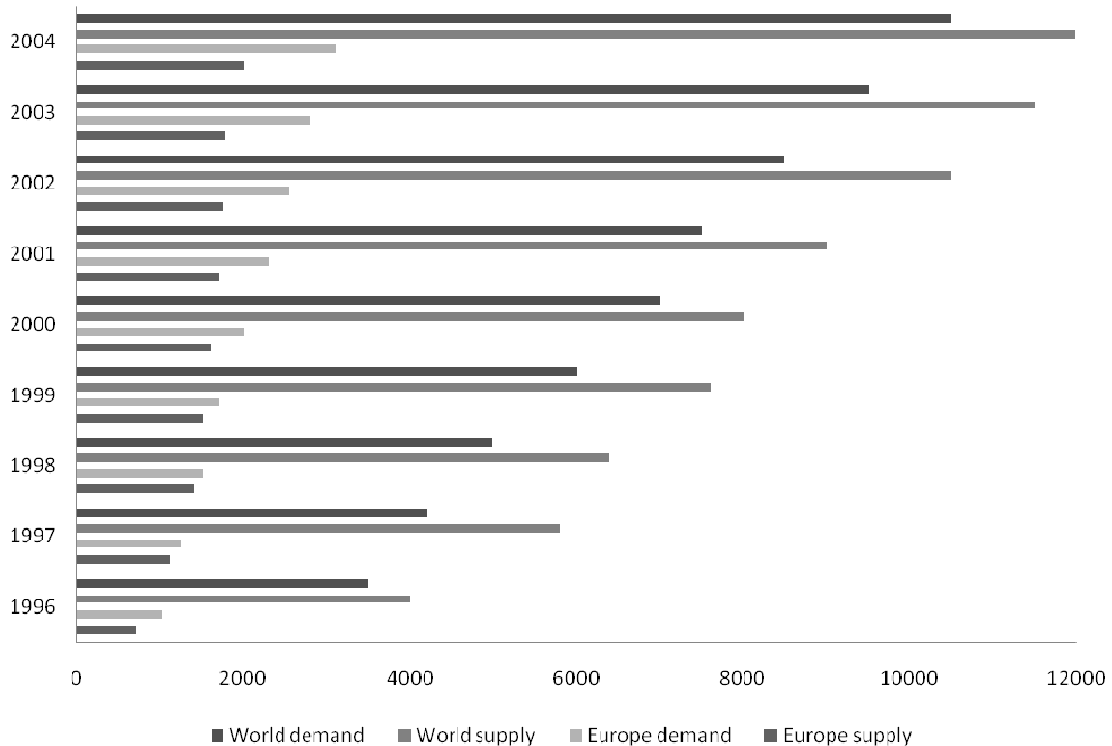


Figure 1. 10. World and European supplies and demands of PET, in kilotonnes. Adapted from data in *PlasticsEurope* webpage ⁽²⁹⁾

Due to its versatility and good properties, PET is a desirable material at the bottles-films and packaging industry and has become one of the most used thermoplastic. High molecular weight PET is most desirable due to it can store liquid without any hazardous interference by the surroundings. Typical packaging applications of PET include:

- Bottles for beverages such as soft drinks, fruit juices, mineral waters. It is especially suitable for carbonated drinks, cooking and salad oils, sauces and dressings and detergents.
- Wide mouth jars and tubs for jams, preserves, fruits & dried foods.
- Trays for pre-cooked meals that can be re-heated in either microwave or conventional ovens. Pasta dishes, meats and vegetables.
- Foils for 'boil-in-the-bag' pre-cooked meals, snack foods, nuts, sweets, long life confectionery.

- Other PET products with an extra oxygen barrier are ideal for containing beer, vacuum packed dairy products e.g., cheese, processed meats, 'Bag in Box' wines, condiments, coffee, cakes, syrups.

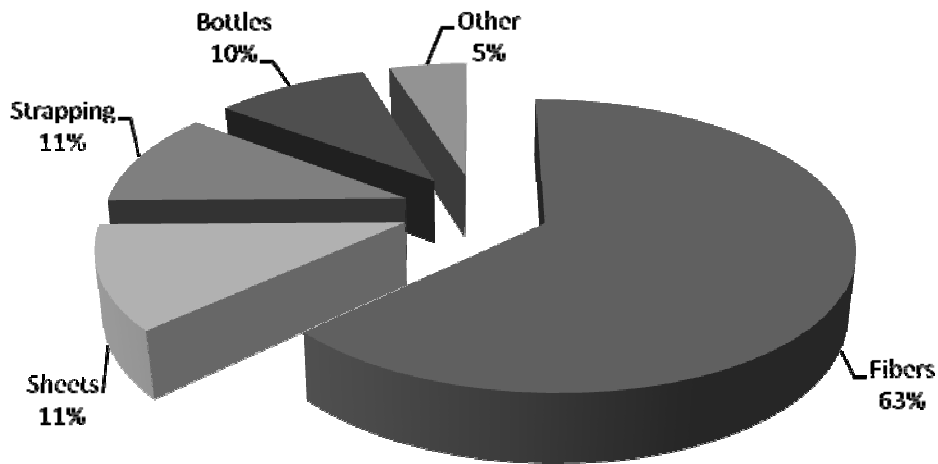


Figure 1. 11. Worldwide applications of PET in 2004. Adapted from ref (28)

4.2. POLYLACTIDE

PLA is at present one of the most promising bio-based polymer, and thus has been the subject of profuse literature with several reviews and book chapters during the last years^{(30) (31)}. PLA belongs to the family of aliphatic polyesters commonly made from α -hydroxy acids such as polyglycolic acid (PGA). As long as the basic monomers (lactic acid, lactide) can be produced from renewable resources (carbohydrates) by fermentation, PLA complies with the rising worldwide concept of sustainable development and is classified as an environmentally friendly material⁽³¹⁾.

4.2.1. SYNTHESIS AND PROPERTIES OF PLA

A. The monomers

Lactic acid is a compound that plays a key role in several biochemical processes. For instance, lactate is constantly produced and eliminated during normal metabolism and physical exercise. Lactic acid has been produced on an industrial scale in the food industry as an acidity regulator, or in cosmetics, pharmaceuticals and animal feed. It can be obtained either by carbohydrate fermentation or by common chemical synthesis. The lactic acid is the simplest hydroxyl acid with an asymmetric carbon atom and two optically active configurations, namely the L- and D- isomers (Fig 1.12), which can be produced in bacterial systems, whereas mammalian organisms only produce the L- isomer, which is easily assimilated during metabolism⁽³¹⁾.

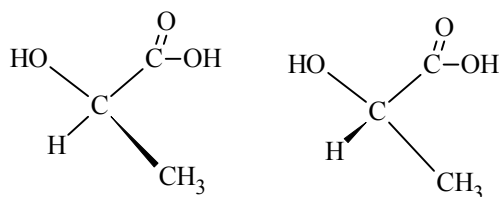


Figure 1. 12. Stereoisomers of lactic acid. (left): L(+), (right): D(-)

Lactic acid is mainly prepared in large quantities (around 200 kt per year) by the bacterial fermentation of carbohydrates, which can be classified according to the type of bacteria used:

Hetero-fermentative method

It produces less than 1.8 mol of lactic acid per mole of hexose, with other metabolites in significant quantities, such as acetic acid, ethanol, glycerol, mannitol and carbon dioxide.

Homo-fermentative method

It leads to larger yields of lactic acid and lower levels of by-products, and is mainly used in industrial processes⁽³²⁾. The conversion yield from glucose to lactic acid is higher than 90 %. The majority of the fermentation processes use species of *Lactobacilli* which give high yields of lactic acid. Some organisms predominantly produce the L- isomer, such as

Lactobacilli amylophilus , *L. bavaricus* , *L. casei* and *L. maltaromicus* , whereas, *L. delbrueckii* , *L. jensenii* or *L. acidophilus* produce the D- isomer or a mixture of L- and D-^{(30) (32)} . These different bacteria are homo-fermentative.

In general, the sources of basic sugars are glucose and maltose from corn or potato, sucrose from cane or beet sugar, etc. In addition to carbohydrates, other products, such as B vitamins, amino acids and different nucleotides, are formed. The **processing conditions** are an acid pH ~ 6, a temperature ~ 40°C and a low oxygen concentration. The major method of separation (Fig 1.13) consists in adding CaCO₃ , Ca(OH)₂ , Mg(OH)₂ , NaOH, or NH₄OH to neutralize the fermentation acid and to give soluble lactate solutions, which are subsequently filtered to remove both the cells (biomass) and the insoluble products. The product follows then evaporation, crystallization, and acidification with H₂SO₄ to obtain the crude lactic acid. Before polymerization, it is purified by separation techniques including ultra-filtration, nano-filtration, electro-dialysis and ion-exchange processes.

The cyclic dimer of lactic acid combines two of its molecules and gives rise to L -lactide or LL -lactide, D -lactide or DD -lactide, and meso-lactide or LD -lactide (a molecule of L -lactic acid associated with another one of D -lactic acid). A mixture of L- and D- lactides is a racemic lactide (rac-lactide). Lactide is usually obtained by the depolymerization of low molecular weight PLA under reduced pressure to give a mixture of L-, D- and meso-lactides.

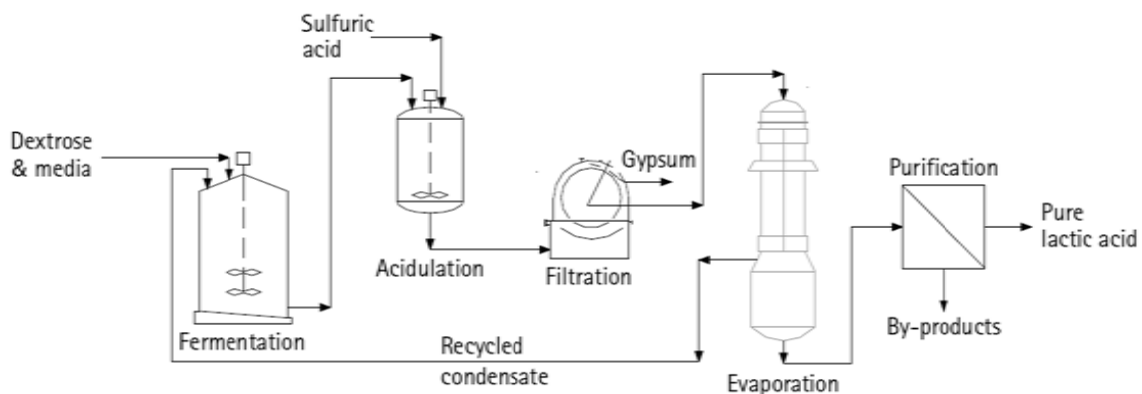


Figure 1. 13. Industrial obtaining of lactic acid, as reproduced from ref (33)

Fig 1.14 shows the different stereofoms of lactide. The different percentages of the lactide isomers formed depend on the lactic acid isomer feedstock, temperature and the na-

ture and content of catalyst ⁽³²⁾. A key point in most of the processes is the separation between each stereoisomer to control the final PLA structure (such as vacuum distillation) which is based on the boiling point differences between the meso- and the L- or D- lactide.

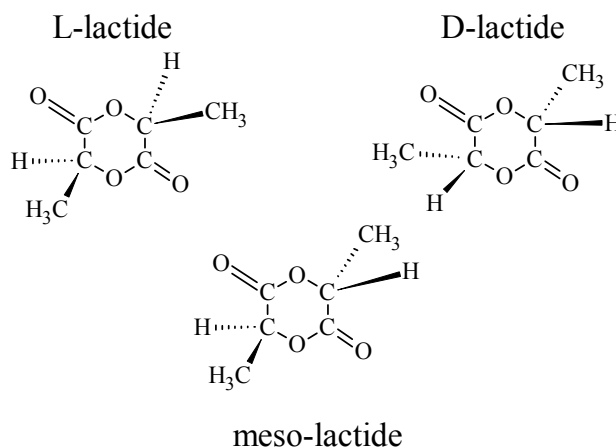


Figure 1. 14. Different structures of lactide

B. Polymerization processes

The synthesis of PLA is a multistep process which starts from the production of lactic acid and ends with its polymerization ⁽³²⁾. An intermediate step is often the formation of the lactide. Fig 1.15 shows that the synthesis of PLA can be driven by three main routes:

- Lactic acid is polymerized by condensation to yield a low molecular weight, brittle polymer, which, for the most part, is unusable, unless external coupling agents are employed to increase its chains length.
- Second route is the azeotropic dehydrative condensation of lactic acid. It can yield high molecular weight PLA without the use of chain extenders or special adjuvants
- The third and main process is **ring-opening polymerization** (ROP) of lactide to obtain high molecular weight PLA, patented by Cargill (US) in 1992 ⁽³⁴⁾.

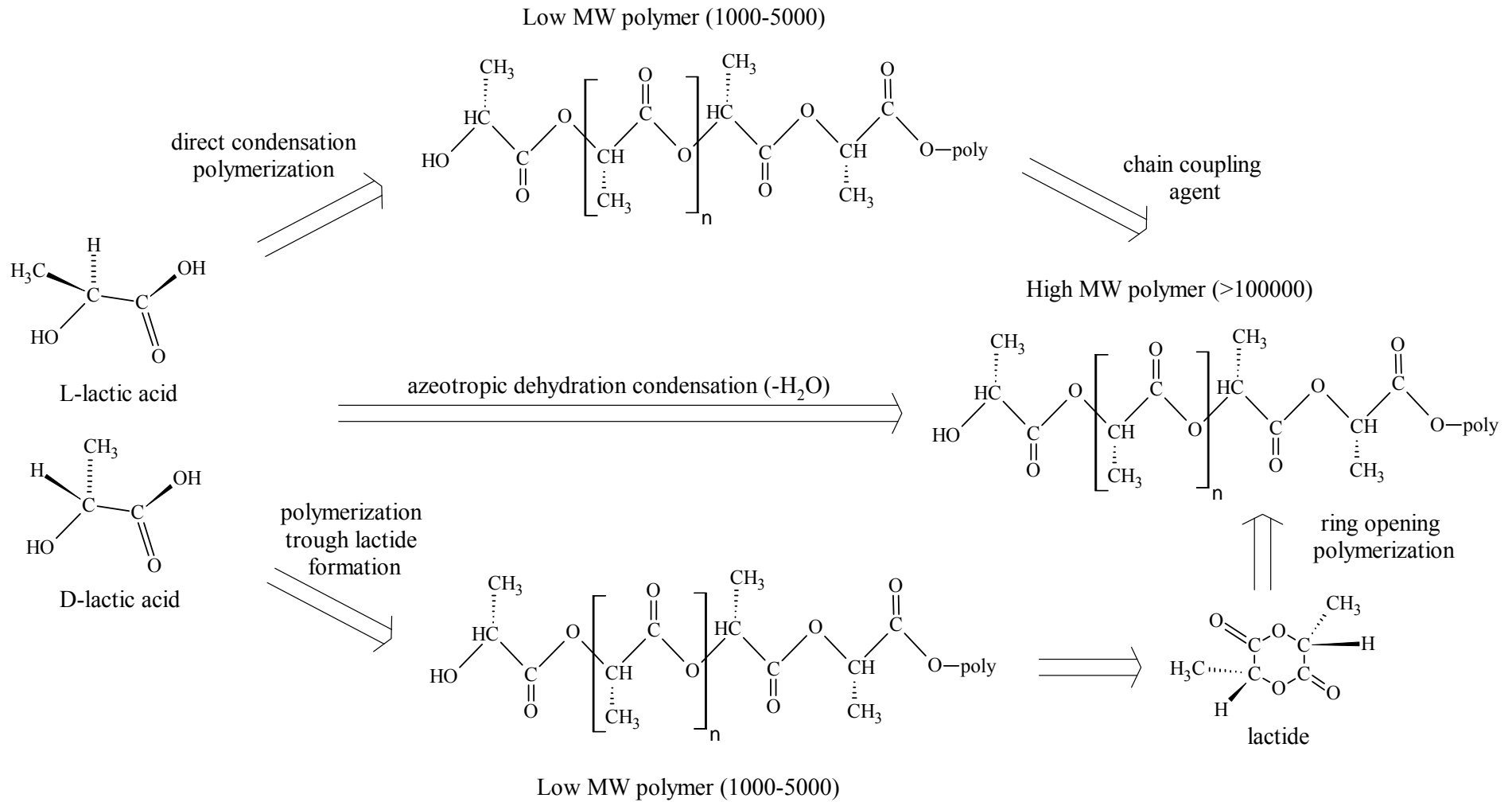


Figure 1. 15. Synthesis methods for obtaining high molecular weight PLA, reproduced from *Hartmann*⁽³²⁾

In general, a polymer prepared by ROP and built of L-stereoisomer elements is referred to as poly(L-lactide) (PLLA), and, accordingly, a polymer containing both D- and L-stereoisomer elements is referred to as poly(DL-lactide) (PDLLA). The two different stereoisomers provide a tool for varying the polymer properties to a certain extent without using additives or comonomers ⁽³⁵⁾. The L-stereoisomer constitutes the main fraction of PLA derived from renewable sources since the majority of lactic acid from biological sources exists in this form. Depending on the composition of the optically active enantiomers, PLA can crystallize in three forms (α , β and γ), which affects the structural, thermal, barrier and mechanical properties of the polymer ⁽³⁶⁾. In general terms, PLA polymers with a L-content greater than 90% tend to be crystalline while those with lower optical purity are amorphous. Note that the general term polylactide (PLA) is used when the type of isomer is not specified. For polylactides prepared by polycondensation the name poly(lactic acid) is preferred ⁽³⁵⁾.

The **lactide method** is the only procedure for producing pure high molecular weight PLA ($M_w \sim 100000$ Da). The ROP of lactide was first demonstrated by Carothers in 1932, but high molecular weights were not obtained until improved lactide purification techniques were developed by DuPont in 1954. This polymerization has been successfully carried out calling upon various methods, such as solution, bulk, melt or suspension process. The mechanism involved in ROP can be ionic (anionic or cationic) or coordination–insertion, depending on the catalytic system ⁽³¹⁾.

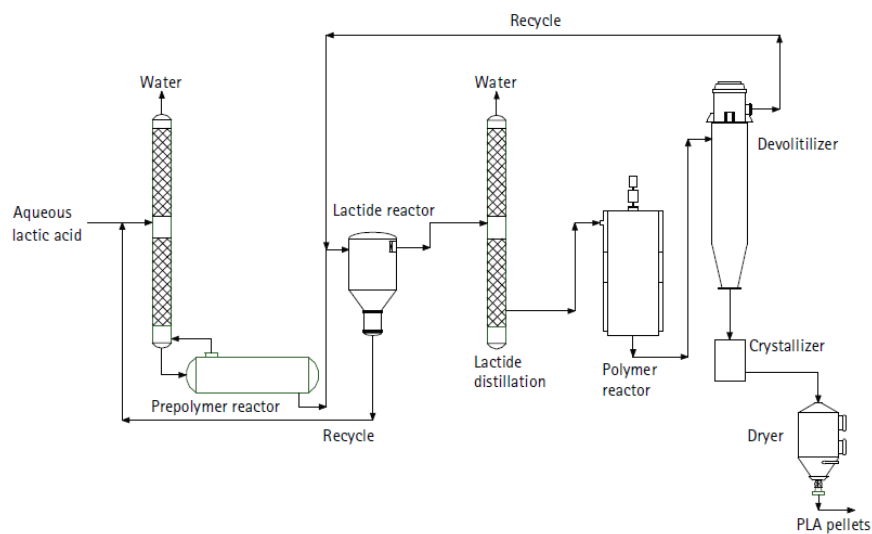


Figure 1. 16. Industrial production of PLA by Natureworks™ as reproduced from ref (33)

The role of the racemization and the extent of transesterification in the homo or copolymerization, are also decisive for the enantiomeric purity and chain architecture of the resulting macromolecules, conforming the different available PLA grades⁽³¹⁾. Each grade is optimized for both processing and end use performance in its intended application. Therefore, the related properties may vary from one grade to another.

4.2.2. APPLICATIONS AND MARKET OF PLA

PLA is commercially and available in large-scale production for a wide range of grades. It has a reasonable price and some remarkable properties to fulfil different applications. For instance, the PLA production capacity of Cargill (USA) in 2006 was $1,4 \cdot 10^5$ t per year at 2–5 €/kg⁽³⁷⁾, which has currently decreased to nearly 1,6 €/kg. The main concern of PLA is the price of this polymer. On an industrial scale, the manufacturing cost of lactic acid monomer will be targeted to less than 0,6 €/kg because the selling price of PLA should decrease roughly by half from its present price. There are several issues that need to be addressed for the biotechnological production of lactic acid, such as the development of high-performance lactic acid-producing microorganisms and the lowering of the costs of raw materials and fermentation processes⁽³⁸⁾. According to different sources, the consumption of PLA in 2006 was only about $6 \cdot 10^5$ t per year and nowadays only ~30 % of lactic acid is used for PLA production⁽³¹⁾. To date, PLA is relatively more expensive than most of the petroleum based polymers. Nonetheless, increasing oil prices and the implementation of environmental policies from the government, such as “green taxes” in countries like Germany or Japan, and mandatory use of compostable polymers for packaging by some large corporations, will create a push to expand the use of PLA⁽³⁶⁾. As the uses for PLA continue to increase, the demand for the agricultural feedstock for PLA production (mainly corn today), will increase as well. To overcome the potential competitive issues of raw materials with human and livestock food supply chains, innovations involving the use of alternative starch and sugar sources, including biomass and other low value by-product wastes are expected to take place.

At present, PLA-based materials are mainly found in three different markets, namely, the biomedical (initial market), agricultural and the packaging (mainly food-contact applications). In order to arrive to a larger market, some PLA drawbacks must be overcome, such

as its limited mechanical and barrier properties and heat resistance, and, in order to meet market expectations, the world production of PLA must be substantially increased.

Biomedical applications

PLA has been widely studied for use in medical applications because of its bioresorbability and biocompatibility properties in the human body. The literature reports examples on medical or biomedical products are fracture fixation devices like screws, sutures, delivery systems and micro-titration plates⁽³⁴⁾.

Agricultural applications

Since PLA is an environmentally friendly polymer that can be designed to controllably biodegrade, it is ideally suited for many applications in the environment where recovery of the product is not practical, such as agricultural mulch films and bags.

Packaging applications

Commercially available PLA packaging can provide better mechanical properties than polystyrene and have properties more or less comparable to those of PET^{(30) (34)}. Market studies show that PLA is an economically feasible material for packaging. With its current consumption, it is at the present the most important market in volume for biodegradable packaging^{(30) (34)}. For instance, reported types of manufactured products are blow-moulded bottles, injection-moulded cups, spoons and forks, thermoformed cups and trays, paper coatings, fibres for textile industry or sutures, films and various moulded articles⁽³⁴⁾.

5. REFERENCES IN THIS CHAPTER

1. Frados J, Ed., *The Society of the Plastics Industry*, 13th ed. Society of the Plastics Industry, New York (1977)
2. PlasticsEurope. *Plastics-The facts 2010. An analysis of European plastics production, demand and recovery from 2009* (2010)
3. Sokora W. *Fundamentals of Packaging Technology*, Institute of Packaging Professionals (2002)
4. Brody A L, Marsh K S. *Encyclopedia of Packaging Technology* (1997)
5. Bix L, Rifon N, Lockhart H, De la Fuente J. *The Packaging Matrix: Linking Package Design Criteria to the Marketing Mix*. IDS Packaging. (2003).
6. Swift G. *Environmentally degradable polymers*. In: Bastioli C. *Handbook of biodegradable polymers*. Smithers Rapra Technology (2005).
7. Keenan T M, Tantebaum S W, Nakas J P. *Biodegradable polymers from renewable forest resources*. In: Smith R. *Biodegradable polymers for industrial applications*. Woodhead publishing limited (2005).
8. Kale G, Auras R, Singh S P. *Degradation of commercial biodegradable packages under real composting and ambient exposure conditions*. *Journal of polymers and the environment* 14, 317-334 (2006)
9. Thoen J, Bush R. *Industrial chemicals from biomass - industrial concepts*. In: Kamm B, Gruber P R, Kamm M. *Biorefineries - industrial processes and products: Status Quo and future directions*. Vol 2. Wiley-VCH, Weinheim (2006)
10. Shen L, Haufe J, Patel M K. *Product overview and market projection of emerging bio-based plastics PRO-BIP 2009*. University of Utrech. Commissioned by European Polysaccharide Network of Excellence and European Bioplastics (2009)
11. Banse M, Nowicki P, Van Mejlil, H. *Why are current world food prices so high*. Wageningen UR (2008)
12. Legg W. *Is the promotion of biofuels contributing towards the sustainable use of resources?* Pune, India Conference on Biotechnology for Sustainable Development - Green chemicals and materials, biorefinery, bioenergy, clean water. Hosted by the National Chemical Laboratory (NCL) (2008)
13. World Bank. G8 Hokkaido-Toyako Summit – *Double Jeopardy: Responding to high food and fuel prices* (2008) <http://siteresources.worldbank.org/NEWS/MiscContent/21828409/G8-HLsummit-paper.pdf> (checked:2011/03/22).
14. Clarinval A M, Crif J H. *Classification of biodegradable polymers*. In: Smith R. *Biodegradable polymers for industrial applications*. Woodhead publishing limited (2005)

15. Clarinval A L. *Classification and comparison of thermal and mechanical properties of commercialized polymers*. International Congress & Trade Show, The Industrial Applications of Bioplastics (2002)
16. I.S. Arvanitoyannis. *Totally and partially biodegradable polymer blends based on natural synthetic macromolecules: preparation, physical properties, and potential as food packaging materials*. Journal of Macromolecular Science, Reviews in Macromolecular Chemistry and Physics 39, 205-271 (1999)
17. Heijungs R, Huppes G, Guinée J B. *Life cycle assessment and sustainability analysis of products, materials and technologies. Toward a scientific framework for sustainability life cycle analysis*. Polymer Degradation and Stability 95, 422-428 (2010)
18. Ecoembes S.A (Ecoembalajes España S.A.). *Plan empresarial de prevención de los residuos de envases 2006-2008*. (2006)
19. Zia K M, Bhatti H N, Bhatti I A. *Methods for polyurethane and polyurethane composites, recycling and recovery: a review*. Reactive and functional polymers 67, 675-692 (2007)
20. Howard G T. *Biodegradation of polyurethane: a review*. International Biodeterioration and Biodegradation 49, 245–252 (2002)
21. Al-Salem S M, Lettieri P, Baeyens J. *Recycling and recovery routes of plastic solid waste (PSW): A review*. Waste management 29, 2625-2643 (2009)
22. Al-Salem S M, Lettieri P, Baeyens J. *The valorization of plastic solid waste (PSW) by primary to quaternary routes: from re-use to energy and chemicals*. Progress in Energy and Combustion Science 36, 103-129 (2010)
23. Scheirs J. *Polymer recycling. Science, technology and applications*. Wiley series in polymer sciences (1998)
24. Davis G, Song J H. *Biodegradable packaging based on raw materials from crops and their impact on waste management*. Industrial Crops and Products 23, 147–161 (2006)
25. Agencia Nacional de Evaluación y Prospectiva (ANEP). *PET: Un producto tecnológico*. (2006)
26. Sun N, Yang J, Shen D. *The effect of water absorption on the physical ageing of amorphous poly(ethylene terephthalate) film*. Polymer Communication 40, 6619-6622 (1999)
27. Tan S, Su A, Li W, Zhou E. *New Insight into Melting and Crystallization Behavior in Semicrystalline Poly(ethylene terephthalate)*. Polymer Science 38: 53-60 (2000)
28. Awaja F, Pavel D. *Recycling of PET*. European Polymer Journal 41, 1453-1477 (2005)
29. PlasticsEurope. <http://www.plasticseurope.org/what-is-plastic/types-of-plastics/pet.aspx>. Checked: 2011/03/23.
30. Auras R, Harte S, Selke S. *An overview of polylactides as packaging materials*. Macromolecular Bioscience 4, 835-864 (2004)

31. Averous L. *Polylactic Acid: Synthesis, Properties and Applications*. In: Belgacem M, Gandini A. *Monomers, Polymers and Composites from Renewable Resources*. Elsevier (2008)
32. Hartmann H. *High molecular weight polylactic acid polymers*. In: Kaplan D L. *Biopolymers from Renewable Resources*. Springer-Verlag (1998)
33. Vink E. *The eco-profile for current Ingeo^(R) polylactide production*. *Industrial Biotechnology* 6, 212-224 (2010)
34. Doi Y, Steinbüchel A. *Biopolymers, Applications and Commercial Products – Polyesters III*. Wiley-VCH, Weinheim (2002)
35. Södergård A, Plackett D. *Poly lactide-Based Biocomposites*. In: Misra M, Drzal L T, Mohanty A K. *Natural Fibers, Biopolymers, and Biocomposites*, CRC Press (2005)
36. Lim L T, Auras R, Rubino M. *Processing technologies for poly(lactic acid)*. *Progress in Polymer Science* 33, 820–852 (2008)
37. Natureworks. <http://www.natureworksllc.com>. Checked: 2011/03/23
38. Häkkinen T, Vares S. *Environmental impacts of disposable cups with special focus on the effect of material choices and end of life*. *Journal of Cleaner Production* 101, 1458-1463 (2010)

CHAPTER II

EXPERIMENTAL PROCEDURES AND ANALYTICAL METHODS

CHAPTER II: EXPERIMENTAL PROCEDURES AND ANALYTICAL METHODS

CONTENTS

1. Materials and reagents	79
1.1. Polymers	79
1.2. MALDI reagents	79
1.3. Solvents	80
2. Pilot plants for degradation	81
2.1. Processing facilities	82
2.1.1. <i>Multiple extrusions</i>	82
2.1.2. <i>Multiple injections</i>	82
2.2. Compression moulding	84
2.3. Reactor for energetic valorisation	84
2.4. Biodegradation chambers	84
3. Analytical techniques and calculation methods	87
3.1. Capillary viscosimetry	88
3.1.1. <i>Fundamentals</i>	88
3.1.2. <i>Calculation methods</i>	92
3.1.3. <i>Experimental parameters</i>	95
3.2. Mass spectrometry	96
3.2.1. <i>Fundamentals</i>	96
3.2.2. <i>Fundamentals of the statistical design of experiments</i>	102
3.2.3. <i>Experimental parameters</i>	104
3.2.4. <i>Calculation methods</i>	105
3.3. Fourier transform infrared analysis	106
3.3.1. <i>Fundamentals</i>	106
3.3.2. <i>Calculation methods</i>	110
3.3.3. <i>Experimental procedure</i>	110
3.4. Scanning electron microscopy	111

3.4.1. <i>Fundamentals</i>	111
3.4.2. <i>Experimental parameters</i>	114
3.5. Melt-mass flow rate	115
3.5.1 <i>Fundamentals</i>	115
3.5.2. <i>Experimental procedure</i>	115
3.6. Tensile testing	116
3.6.1. <i>Fundamentals</i>	116
3.6.2. <i>Experimental parameters</i>	118
3.7. Impact testing	119
3.7.1. <i>Fundamentals</i>	119
3.7.2. <i>Experimental parameters</i>	120
3.8. Thermogravimetry	121
3.8.1. <i>Fundamentals</i>	121
3.8.2. <i>Kinetic analysis of thermal decompositions</i>	123
3.8.3. <i>Experimental parameters</i>	131
3.9. Evolved-gas analysis: 2D-correlation IR	132
3.9.1. <i>Fundamentals</i>	132
3.9.2. <i>Synchronous and asynchronous spectra</i>	135
3.9.3. <i>Analysis of 2D-IR spectra</i>	137
3.9.4. <i>Experimental procedure</i>	138
3.10. Differential Scanning Calorimetry	140
3.10.1. <i>Fundamentals</i>	140
3.10.2. <i>Calculation methods</i>	141
3.10.3. <i>Experimental procedure</i>	144
3.11. Dynamical – mechanical - thermal analysis	145
3.11.1. <i>Fundamentals</i>	145
3.11.2. <i>Dynamic viscoelastic moduli of a polymer</i>	149
3.11.3. <i>DMTA instrumentation</i>	150
3.11.4. <i>The glass-rubber relaxation</i>	151
3.11.5. <i>Experimental parameters</i>	154
4. References in this chapter	155

1. MATERIALS AND REAGENTS

1.1. POLYMERS

Virgin poly(ethylene terephthalate) (PET), commercially labelled as Laser⁺ Melinar⁽¹⁾, AdvanSa Limited (United Kingdom) and virgin poly(ethylene terephthalate) (PET) SEDAPET SP04⁽²⁾ obtained from Catalana de Polimers S.A., Grup LaSeda (Barcelona, Spain) in the form of pellets were bottle-grade resins used to simulate thermo-mechanical degradation due to successive extrusion and injection cycles, respectively.

Virgin polylactide (PLA) 2002D was a thermo-forming grade PLA⁽³⁾ obtained from Natureworks LLC (Minnetonka, MN) in the form of pellets, and submitted to multiple injection cycles and biodegradation tests.



Figure 2. 1. Raw pellets of PET (left) and PLA (right)

1.2. MALDI REAGENTS

MALDI matrixes, namely 1,8,9-anthracenetriol (dithranol), 2-(4-hydroxyphenylazo) benzoic acid (HABA), trans-3-indoleacrylic acid (IAA), 2,4,6-trihydroxy acetophenone (THA), ferulic acid (FA), 2,5-dihydroxybenzoic acid (DHB) were purchased from Sigma-Aldrich (Stockholm, Sweden).

The cationization agent, sodium trifluoroacetate (NaTFA), was also purchased from Sigma-Aldrich (Stockholm, Sweden).

1.3. SOLVENTS

1,1,1,3,3,3-hexafluoro-2-propanol (HFIP) and dichloromethane (CH_2Cl_2) were purchased from VWR (Sweden), and tetrahydrofuran (THF) was purchased from VWR (Sweden) for MALDI sample preparation of PLA.

Tetrahydrofuran, phenol and 1,1,2,2-tetrachloroethane were purchased from Sigma-Aldrich Química SA (Spain) for viscosimetric analysis.

2. PILOT PLANTS FOR DEGRADATION

In order to understand the influence of each type of valorisation procedure, in terms of polymeric degradation, several pilot plants were used in this study, as summarized in Fig 2.2. For the purpose of studying thermo-mechanical degradation induced by material valorisation techniques, two processing facilities, namely extrusion and injection moulding, were used. In addition, with the aim of analyzing the effect of thermal and thermo-oxidative degradations provoked by energetic valorisations such as pyrolysis and combustion, the thermal reactor of a thermogravimetric analyzer was chosen. Finally, to study the biodegradation due to biological valorisation a burial chamber was employed.

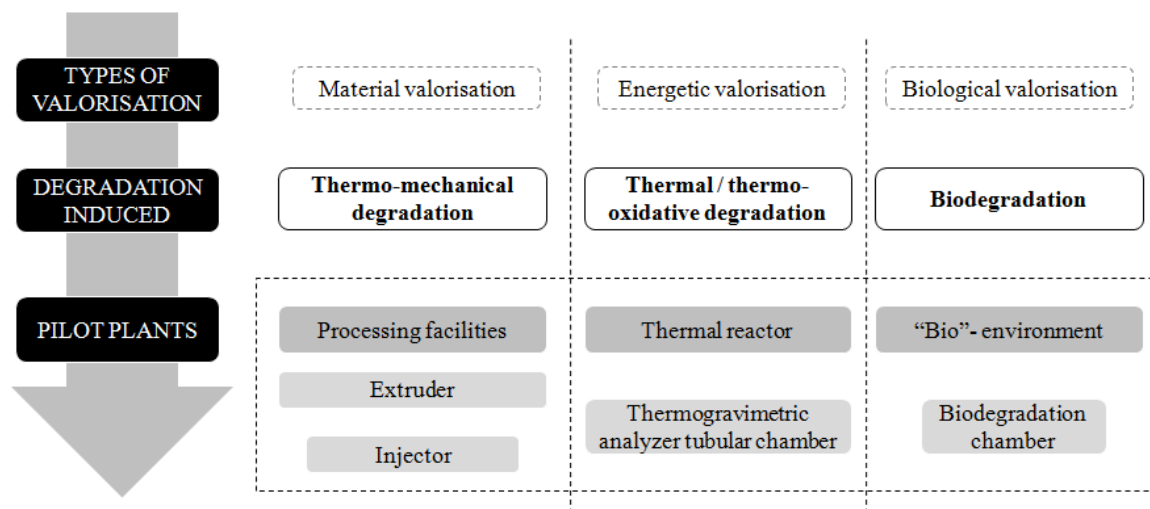


Figure 2. 2. Schematic relation between valorisation techniques, degradation induced and pilot plants needed and applied for simulation.

In this section, the experimental conditions of the different degradation techniques are given, along with specific sample preparation procedures.

2.1. PROCESSING FACILITIES

2.1.1. MULTIPLE EXTRUSIONS

Preliminary studies on virgin PET were performed in Kungliga Tekniska Högskolan KTH (Royal Institute of technology), Stockholm, Sweden. Mechanical recycling was simulated by multiple extrusion up to six times employing a Brabender Plasticorder PL2000 co-rotating twin-screw (see Fig 2.3.) extruder with 2.2 cm diameter and a L/D ratio of 16 (C.W. Brabender Instruments, Inc., NJ). The temperature profile at the extruder was 250-260-270 °C from the feeder to the mouth of the extruder. After each reprocessing step, the material was cooled by air, ground, and sieved by means of a Moretto ML 18110 C Animex Plant granulator. Some material was sorted as sample and kept again in a desiccator to prevent it from hydrolysis caused by environmental humidity until further analysis; the rest was reintroduced at the mechanical recycling simulation process.

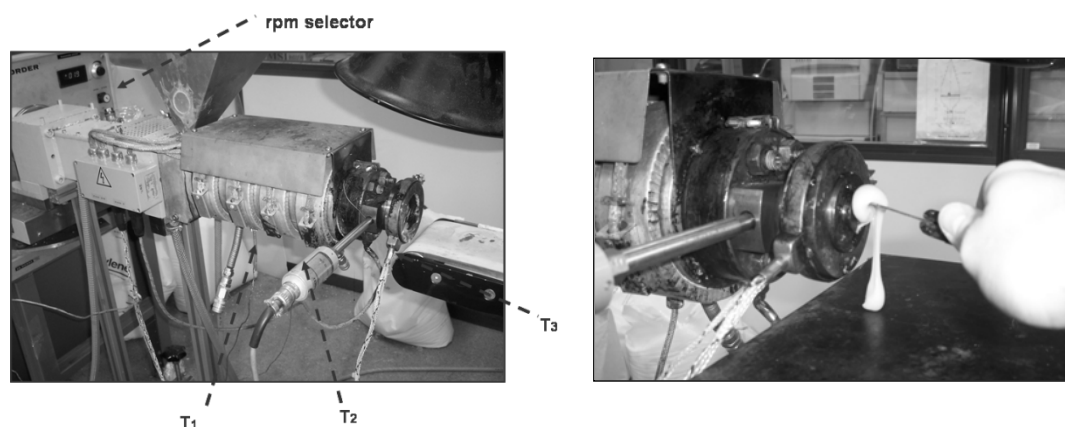


Figure 2. 3. Extrusion machine and detail of die, respectively

2.1.2. MULTIPLE INJECTIONS

Pellets were processed by technicians of AIMPLAS (Technological Institute of Plastic), in Paterna, Valencia, Spain. The reprocessing procedure, to which samples were subjected, is shown in the chart-flow depicted in Fig 2.4 by means of the machinery shown in Fig 2.5. Prior to processing, virgin materials (VPET and VPLA) pellets were dried in a dehumidifier Conair Micro-D FCO 1500/3 (UK), in order to remove as much

humidity⁽⁴⁾ as possible from the flakes (during 5 h at 160 °C for PET and during 2 h at 80 °C in the case of PLA) . Afterwards, samples were processed by means of injection moulding through an Arburg 420 C 1000-350 (Germany) injector, single-screw model (diameter $\Phi=35$ mm, length/ $\Phi=23$).

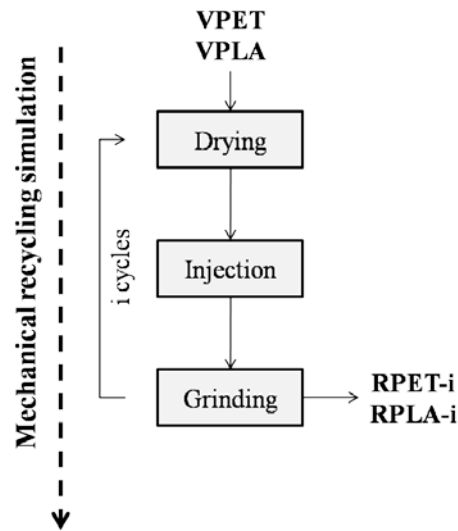


Figure 2. 4. Schematic reprocessing simulation cycle

Successive processing steps were applied under the same conditions, obtaining dumbbell samples following ISO 527-2 (type 1A)⁽⁵⁾. Temperature gradient set from hopper to die was 270, 275, 280, 285 and 280°C for PET; and 160, 170, 190, 200 and 190°C in the case of PLA. Moulds were set at 15 °C. Cooling time residence was 40 s and total residence time ca. 60s. Samples were dried before each processing cycle. After injection, a fraction of the samples was kept as test specimen and the rest was ground by means of a cutting mill Retsch SM2000 (UK), which provided pellets of size $d < 20$ mm to feed into the recirculation process. Up to five processing cycles were applied to obtain the different testing specimens of reprocessed PET (RPET-i or RPLA-i, with i : 1-5).



Figure 2. 5. Machinery employed for simulation of reprocessing for both PET and PLA. From left to right: dehumidifier, injector, cutting mill.

2.2. COMPRESSION MOULDING

Rectangular plates of 1mm thick of VPET and RPET-i were arranged by melt compression in a Collin PCS-GA Type Press 800 (GA, USA) preset at 260 °C by technicians of AIMPLAS. Five pressure steps were performed as follows :5 minutes at 4 bar, 3 minutes at 100 bar, 1 minutes at 80 bar, 5 minutes at 180 bar, and 15 minutes at 75 bar.

In the case of VPLA and RPLA-i, similar plates were prepared by melt compression in the same press at an initial temperature of the hot plates of 195°C and final temperature of 60°C. Five pressure steps were performed as follows: 5 minutes at 6 bar, 8 minutes at 75 bar, 8 minutes at 155 bar, 4 minutes at 215 bar, and 11 minutes at 45 bar.

These samples were used for viscoelastic characterization by Dynamical Thermal Mechanical Analysis, as explained afterwards.

2.3. REACTOR FOR ENERGETIC VALORIZATION

Energetic valorisation through pyrolysis and combustion processes was carried out by means of the tubular reactor (Fig 2.6) of a Thermogravimetric analyzer Mettler-Toledo TGA/SDTA 851 (Columbus, OH). An inert Ar atmosphere was used for assessing the thermal decomposition behaviour, whereas an O₂ reactive atmosphere was applied for characterizing the thermo-oxidative decomposition processes of PET and PLA and their recyclates.

2.4. BIODEGRADATION CHAMBERS

Specimens of 145 x 10 x 1 mm³ were cut from the melt-pressed plates for the degradation in soil tests. PLA plates were subjected to a controlled degradation in soil test under controlled conditions (temperature, water content and pH), following the ISO 846-1997⁽⁶⁾. Shortly, the specimens were buried in biologically active soil and kept in a Heraeus B12 (Hanau, Germany) culture oven at 28 °C, as shown in Fig 2.7. To ensure the oxygenation of the soil, a protocol of periodical air oxygen supply was followed. Test

specimens were extracted at 0, 30, 150, 300 and 450 days, cleaned and kept in a desiccator during 4 days in order to ensure water desorption before being analyzed.

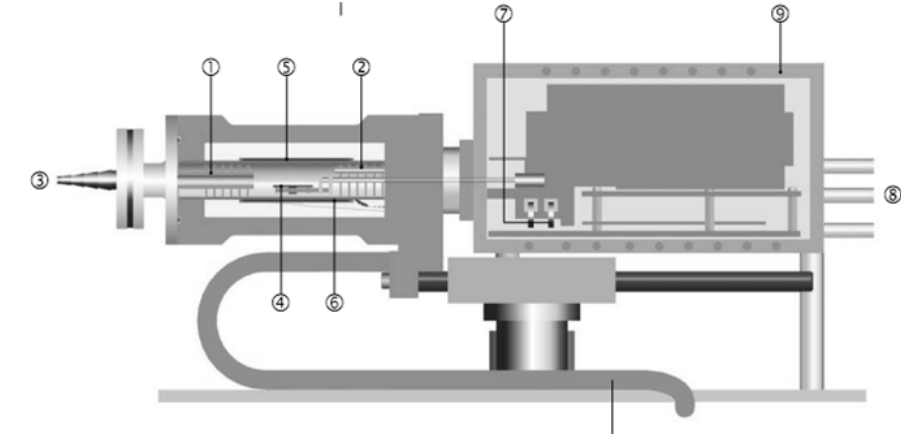


Figure 2. 6. Tubular reactor of the thermogravimetric analyzer⁽⁷⁾. Legend: 1) baffles, 2) reactive gas capillarity, 3) gas outlet , 4) temperature sensor, 5) furnace header, 6) furnace temperature sensor, 7) adjustment ring weights, 8) protective and purge gas connector, 9) thermostated balance chamber



Figure 2. 7. Bio-degradation in soil test. (left): oven; (centre): chamber; (right): detail of buried specimens

3. ANALYTICAL TECHNIQUES AND CALCULATION METHODS

A short description of the basics of each analytical technique, along with the experimental parameters and calculation methods is given. The analytical techniques used respond to the query of offering a complete analysis of the degradation effects in terms of morphological, structural, mechanical, thermal and viscoelastic properties, as shown in Fig 2.8.

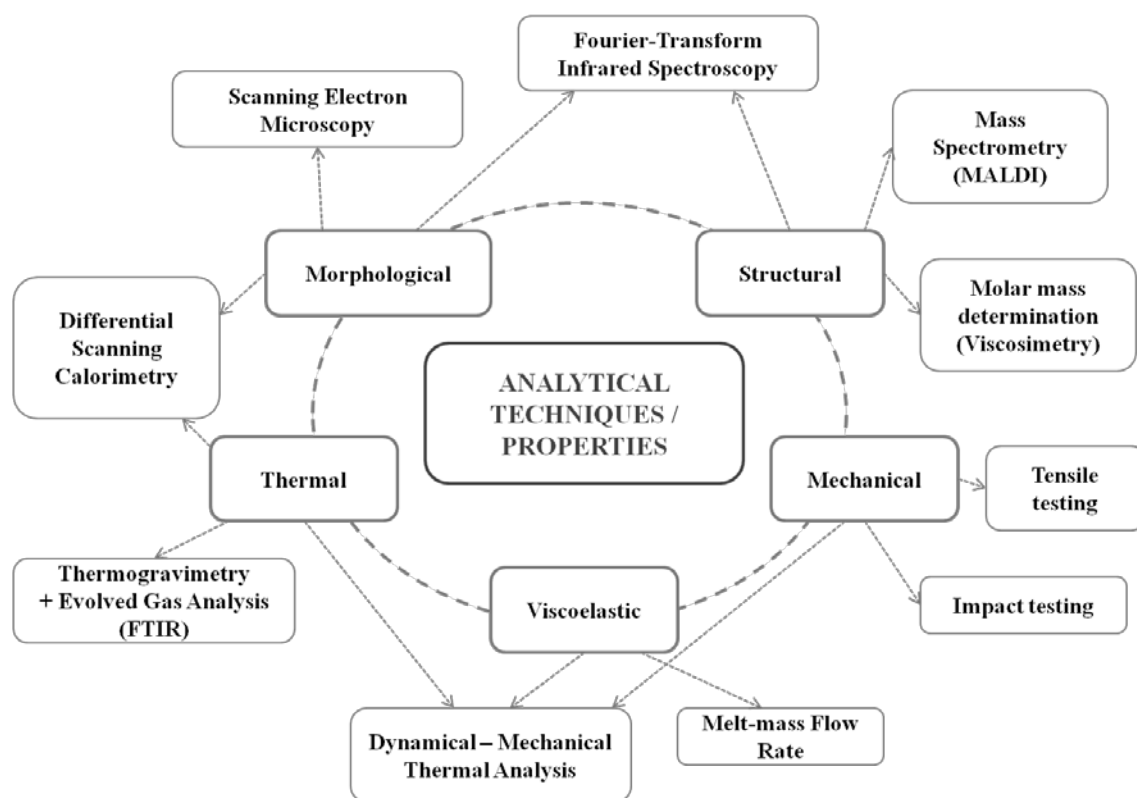


Figure 2. 8. Summary of techniques applied, in connection with the analyzed properties

The experiments were carried out at the Laboratories of the Research Group of Degradation and recycling of Polymeric Materials of the Technological Institute of Materials of the Polytechnic University of Valencia, and the Polymer and Fibre Technology Department of the School of Chemical Science and Engineering of the Royal Institute of Technology of Stockholm, Sweden.

3.1. CAPILLARY VISCOSIMETRY

3.1.1. FUNDAMENTALS ⁽⁸⁾

The viscosity of a polymer solution depends on concentration and size (i.e., molar mass) of the dissolved polymer, and thus both features are correlated. Viscosity techniques are very useful because they are experimentally simple. However, they are less accurate and the determined viscosity average molar mass M_V is less precise than those obtained by other techniques like Steric Exclusion Chromatography (SEC). For example, M_V depends on a parameter which depends on the solvent used to measure the viscosity. Therefore the measured molar mass is influenced by the solvent used. Despite these drawbacks, viscosity techniques are very valuable. Fig 2.9 shows a piece of a liquid moving at a strain rate $\dot{\gamma}$ under an applied shear stress of $\tau = F \cdot A^{-1}$.

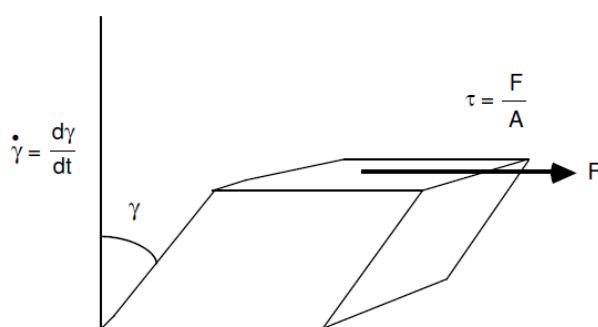


Figure 2. 9. A liquid moving at shear rate under an applied stress τ

The **viscosity** of a liquid is the ratio η of the applied shear stress τ to the resulting strain rate $\dot{\gamma}$ (or equivalently, the ratio of the shear stress required to move the solution at a fixed strain rate to that shear strain):

$$\eta = \frac{\tau}{\dot{\gamma}} \quad (2. 1)$$

, where u is the displacement in the direction of the flowing. The **strain rate** can be therefore drawn from:

$$\dot{\gamma} = \frac{d}{dt} \frac{du}{dy} = \frac{d}{dy} \frac{du}{dt} = \frac{dv_x}{dy} \quad (2. 2)$$

, where v_x represents the longitudinal speed of flowing. Then, the relationship between the experimental variables is:

$$\eta = \frac{\tau}{\dot{\gamma}} \quad (2.3)$$

A **Newtonian fluid** is one in which the viscosity is independent of the shear rate, that is, in a plot of shear stress versus shear strain rate is linear with slope η . In Newtonian fluids all the energy goes into sliding molecules by each other. In **non-Newtonian fluids**, the shear stress/strain rate relation is not linear. Typically the viscosity drops at high shear rates. Plots of shear force vs. shear rate for Newtonian and non-Newtonian fluids are given in Fig 2. 10.

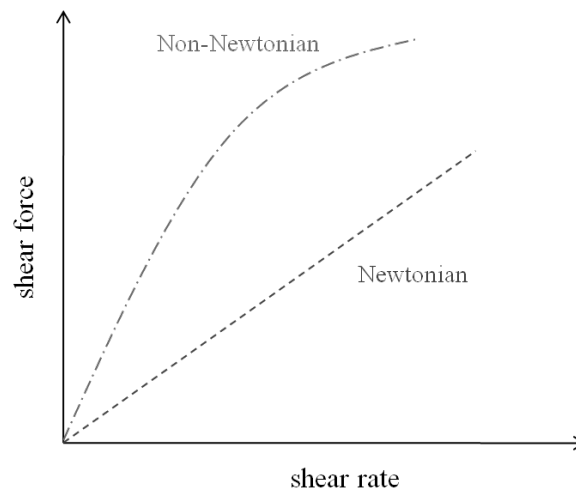


Figure 2. 10. Schematic plots of Newtonian and Non-Newtonian behaviours

Considering η_0 as the viscosity of the pure solvent and η the viscosity of a solution using that solvent, several methods exist for characterizing the solution viscosity, or more specifically, the capacity of the solute to increase the viscosity of the solution. That capacity is quantified by using one of several different measures of solution viscosity corresponding to solutions at different concentrations c . The most common solution viscosity terms are:

Relative viscosity

$$\eta_R = \frac{\eta_0}{\eta} \quad (2.4)$$

Specific viscosity

The specific viscosity expresses the incremental viscosity due to the presence of the polymer in the solution.

$$\eta_{SP} = \frac{\eta - \eta_0}{\eta} = \eta_R - 1 \quad (2.5)$$

Inherent viscosity

The inherent viscosity expresses the capacity of a polymer to cause the solution viscosity to increase; that is, the incremental viscosity per unit concentration of polymer. As with other polymer solution properties, the solutions used for viscosity measurements will be non-ideal and therefore η_{INH} will depend on c .

$$\eta_{INH} = \frac{\ln \eta_R}{c} \quad (2.6)$$

Intrinsic viscosity

$$[\eta] = \lim_{c \rightarrow 0} \frac{\eta_{SP}}{c} \quad (2.7)$$

$[\eta]$ will be shown to be a unique function of molar mass (for a given polymer-solvent-temperature). The remaining form for the viscosity is the inherent viscosity. In the limit of zero concentration, η_{INH} extrapolates the same as $\frac{\eta_{SP}}{c}$ and becomes equal to the intrinsic viscosity, as shown as follows:

$$\lim_{c \rightarrow 0} \frac{\ln \eta_R}{c} = \lim_{c \rightarrow 0} \frac{\ln(\eta_{SP} + 1)}{c} = \lim_{c \rightarrow 0} \frac{\eta_{SP}}{c} = [\eta] \quad (2.8)$$

Accordingly, the intrinsic viscosity can be found either extrapolating $\frac{\eta_{SP}}{c}$ or η_{INH} to zero concentration, as shown afterwards.

The **molar mass** can be obtained by applying the **Mark-Houwink relationship**, considering K and α are polymer-solvent-temperature dependent parameters:

$$[\eta] = K \cdot M_V^\alpha \quad (2.9)$$

The approaches from the fundamentals of viscosity of fluids towards the viscosity of polymers can be found in literature ⁽⁸⁾. Considering polydisperse polymers, the following

assumptions are made: first, the total specific viscosity is the sum of the specific viscosities for each component (i.e., each molar mass of the polymer). Secondly, the specific mass of each component can be calculated from the intrinsic viscosity due to that component. Finally, the relation between intrinsic viscosity and molar mass is independent of molar mass; that is, K and α are independent on the molar mass.

$$\eta_{SP} = \sum_i (\eta_{SP})_i \quad , \quad (\eta_{SP})_i = [\eta]_i \cdot c_i \quad , \quad [\eta]_i = K \cdot M_i^\alpha \quad (2.10)$$

Consequently, from derivation of above equations, it can be derived:

$$\frac{\eta_{SP}}{c} = \frac{\sum_i (\eta_{SP})_i}{c} = \frac{\sum_i K \cdot c \cdot M_i^\alpha}{c} = \frac{\sum_i K \cdot \frac{N_i \cdot M_i}{V} M_i^\alpha}{\sum_i \frac{N_i \cdot M_i}{V}} = \frac{\sum_i K \cdot N_i \cdot M_i \cdot M_i^\alpha}{\sum_i N_i \cdot M_i} = K \cdot \frac{\sum_i N_i \cdot M_i^{\alpha+1}}{\sum_i N_i \cdot M_i} \quad (2.11)$$

, and considering that

$$\lim_{c \rightarrow 0} \frac{\eta_{SP}}{c} = K \cdot M_V^\alpha \quad (2.12)$$

, the viscosity average molar mass is defined as:

$$M_V = \left(\frac{\sum_i N_i \cdot M_i^{\alpha+1}}{\sum_i N_i \cdot M_i} \right)^{\frac{1}{\alpha}} \quad (2.13)$$

In comparison to common number-average molar mass M_n and weight-average M_w molar masses, when $\alpha=1$, $M_V = M_w$, and actually $M_n \leq M_V \leq M_w$ (Fig 2.11). For typical α (\in 0.5-0.8) M_V is closer to M_w , since the viscosity properties are expected to be a function of the size and not just the number of polymer chains. Note that:

$$M_n = \left(\frac{\sum_i N_i \cdot M_i}{\sum_i c \cdot N_i} \right) \quad (2.14)$$

$$M_w = \left(\frac{\sum_i N_i \cdot M_i^2}{\sum_i N_i \cdot M_i} \right) \quad (2.15)$$

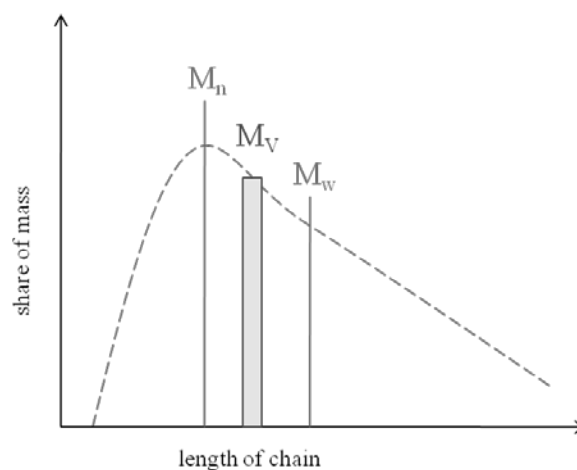


Figure 2. 11. Comparison of molar masses.

3.1.2. CALCULATION METHODS⁽⁹⁾

Because of the **height difference between bulbs** in the Cannon-Fenske (Fig 2.12) viscosimeter, there is a hydrostatic head or driving pressure to cause the liquid to flow through the capillary or narrow diameter section of the viscometer. Details can be found in ISO 1628-1⁽⁹⁾. Shortly, the experiment consists in measuring the time the liquid takes to flow through the capillary between marks.

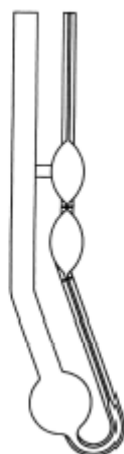


Figure 2. 12. Cannon-Fenske type capillary viscosimeter

During the flow of a Newtonian fluid through a capillary, in kinetic energy terms, the time is proportional to the solution viscosity through the following relation:

$$\eta = \frac{\pi \cdot r_c^4 \cdot \Delta P}{8 \cdot V_f \cdot L} \cdot t = A \cdot \rho \cdot t \quad (2.16)$$

, where r_c is the radius of the capillary, V_f the volume of liquid, ΔP the pressure difference and L the length of the capillary. When flowing due to gravity only in the tube of length h , $\Delta P = \rho \cdot g \cdot h$ where ρ is the solution density. The physical constants of the viscosimeter can be then lumped into a single constant denoted above as A . If A is known for a particular viscosimeter, the measurement of flow time and solution density can be used to determine solution viscosity.

A more accurate calculation of solution viscosity in terms of flow time would account for **kinetic energy of the moving liquid**. The result with kinetic energy is:

$$\eta = A \cdot \rho \cdot \left(t - \frac{B}{A \cdot t} \right) \quad (2.17)$$

, where B is a constant. If the flow occurs rapidly ($t \downarrow$), the liquid is moving fast and there can be significant kinetic energy. In this case it is important to correct for kinetic energy. On the contrary, for slow flows ($t \uparrow$) the kinetic energy term, which is proportional to $1/t$, gets small. Physically, the liquid is moving slowly and has little kinetic energy. In practice, it is simplest to use long flow times and ignore the kinetic energy term. For most accurate results, there are several **important working considerations**:

- The viscometer must be clean. Any contamination from previous solutions might add to the current solution and change its viscosity. A clean tube also means a tube that is free from dust particles. Dust particles can add to the solution as hard spheres with a large hydrodynamic volume that might increase the solution viscosity and affect the results, especially when working with very dilute solutions.
- It is best to choose a viscometer such that the flow time is greater than 100 seconds. When $t > 100$ seconds, it is permissible to ignore the kinetic energy terms. It is then a simple matter to calculate relative viscosity and specific viscosity by comparing the flow time of the solution, t , to the flow time of the pure solvent, t_0 .

- To adjust flow times, viscometers are available with different radius capillaries. The smaller the capillary, the longer the flow time. Then the viscometer must be selected to give good flow times in the expected viscosity range for the solutions.

A. Huggins and Kraemer extrapolations

According to the aforementioned definitions of the different viscosimetric parameters, the extrapolations of the inherent and specific viscosities to concentrations near to zero, the intrinsic viscosity can be obtained from the intersection of both curves in the ordinate, as shown in Fig 2.13.

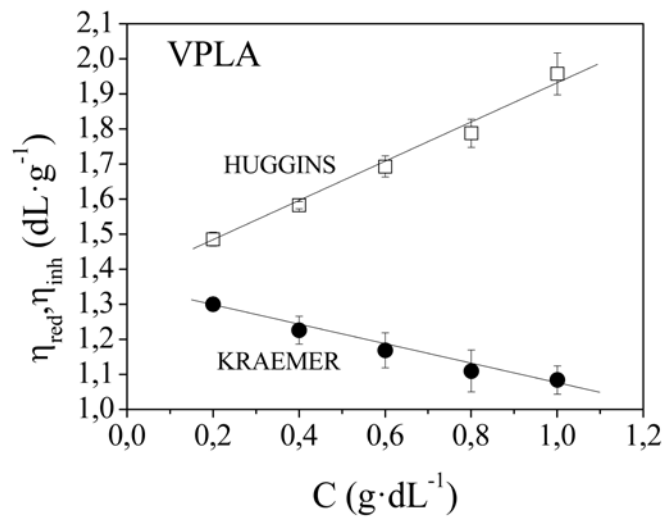


Figure 2. 13. Experimental results of viscosimetric experiments for virgin PLA

The used expressions are shown as follows:

Huggins equation

$$\frac{\eta_{SP}}{c} = [\eta] + k' \cdot [\eta]^2 \cdot c \quad (2.18)$$

Kraemer equation

$$\frac{\eta_{INH}}{c} \approx [\eta] + k'' \cdot [\eta]^2 \cdot c \quad (2.19)$$

3.1.3. EXPERIMENTAL PARAMETERS

The intrinsic viscosity $[\eta]$ was measured according to the standard ISO 1628-1⁽⁹⁾ by means of a Cannon-Fenske capillary viscosimeter type at 25 °C, with the use of 60/40 wt% phenol/1,1,2,2-tetracholoethane as solvent in the case of PET and at 30 °C in tetrahydrofurane (THF) in the case of PLA. Dissolutions of pellets ranged from 0.2 to 1 g·dL⁻¹. Measurements were performed by quintuplicate for each concentration c and $[\eta]$ was obtained from extrapolation to $c \rightarrow 0$ of Huggins and Kraemer plots.

In the case of PET, the number and weight average molar mass values (M_n , M_w g·mol⁻¹) were calculated with the Mark-Houwink equation $[\eta]=K \cdot M_v^\alpha$, with constants $K=3.72 \cdot 10^{-4}$ dL·g⁻¹ and $\alpha=0.73$ for M_n ⁽¹⁰⁾, and $K=4.68 \cdot 10^{-4}$ dL·g⁻¹ and $\alpha=0.68$ for M_w ⁽¹¹⁾. The polydispersity index was consecutively calculated as $PDI=M_w \cdot M_n^{-1}$.

In the case of PLA, the viscous molar mass values (M_v , g·mol⁻¹) were calculated, with constants $K=6.4 \cdot 10^{-4}$ dL·g⁻¹ and $\alpha=0.68$ ⁽¹²⁾.



Figure 2. 14. Pictures of experimental test for measuring capillary viscosimetry

3.2. MASS SPECTROMETRY

3.2.1. FUNDAMENTALS

Polymers may display a wide variety of **structures**, including linear, cyclic and branched chains, copolymers in which different repeat units are aligned along the chain in different manners, and star polymers with different numbers of arms. The identification of the molecular structure is the first step in the analysis of a polymeric material. Many synthetic polymers are heterogeneous within themselves in many aspects. Homopolymers may exhibit both molar mass distribution (MMD) and end-groups distribution (EGD). Copolymers may also show chemical composition distribution (CCD) and functionality distribution (FTD) in addition to the MMD. Therefore, different kinds of heterogeneity need to be investigated in order to proceed to the structural and molecular characterization of polymeric materials⁽¹³⁾.

The estimation of molar masses (MM) and of **molar-mass distributions** is of a primary interest in polymer characterization work, and much effort has been dedicated directly to develop suitable methods for their determination. **End-groups analysis** provides more important structural information, concerning the estimation of the different end-groups present for the same molecular structure, since it can happen due to different synthetic and degradation routes or to end capping. Determining the composition and sequence of the functional repeating units in the polymeric backbone is essential, since the physical and chemical properties of these materials may be influenced⁽¹³⁾. Among the techniques developed for polymer characterization, **Mass Spectrometry** (MS) is one of the most powerful. Mass spectra analysis involves the formation of gaseous ions from a specific analyte (M) and the subsequent measurement of the mass-to-charge ratio (m/z) of these ions. Molecular ions are generally formed by the removal of an electron from M (M^+), whereas quasi-molecular ions appear when adding an ion to the analyte: $[M+H]^+$, $[M+Na]^+$, $[M+Cl]^+$. The exact m/z value of molecular or quasi-molecular ions reveals the elemental composition of the ion and thus allows for the compositional analysis of the sample under study⁽¹⁴⁾.

A. Matrix-assisted laser desorption/ionization mass spectrometry (MALDI MS)

MALDI MS is a soft ionization technique introduced in the early 90s for the characterization of biopolymers. The development of the technique during recent years

has allowed for the characterization of high molecular weight polymers, offering the possibility of resolve polymeric chain distributions. MALDI makes use of short pulses of laser light to induce the formation of intact gaseous ions. Analyte molecules are not directly exposed to laser light, but are homogeneously embedded in a large excess of ‘**matrix**’, which consists of small organic molecules (see Fig 2. 15). The matrix molecules strongly absorb the laser light to allow for very efficient energy transfer to the analyte. The high energy density obtained in the solid or liquid matrices (even at moderate laser irradiance) induces instantaneous vaporization of a microvolume (called a *plume*), and a mixture of ionized matrix and analyte molecules is released into the vacuum of the ion-source. The laser pulse must not be too long, otherwise analyte molecules will not all desorb at the same time. On the other hand, there is no advantage in using ultra-short pulses (fractions of picoseconds) and there are many disadvantages (for instance, a laser which generates ultra-short pulses is expensive and bulky). The nitrogen laser, operating at a wavelength of 337 nm, has a very compact design, it is pulsed and its shots last about 3 ns, which is perfect for the scope of MALDI.

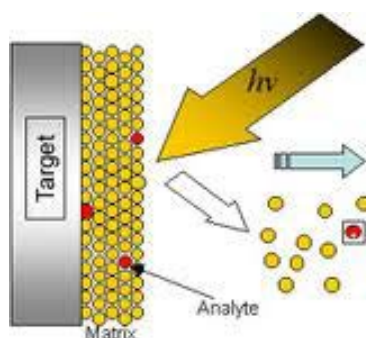


Figure 2. 15. Desorption/ionization process induced by laser to an analyte embedded in a matrix.

The **Time-Of-Flight (TOF)** analyzers are non-scanning-mass type analyzers. For m/z separation with a TOF analyzer, the ions produced in the ion source are initially accelerated through a potential V to acquire kinetic energies in the keV range (Eq 2.20). Then, ions traverse (“fly”) a distance d to reach a detector after a time t , which is measured⁽¹⁵⁻¹⁷⁾. The flight time depends on the ion velocity v (Eq. 2. 21), which is in turn dependent on m/z (Eq. 2. 22). The time taken by an ion to reach the detector is proportional to the square root of the ion’s m/z value.

$$E_k = z \cdot eV = m \cdot \frac{v^2}{2} \quad (2.20)$$

$$t = \frac{d}{v} \quad (2.21)$$

$$t = \frac{\left(\frac{m}{z}\right)^{1/2}}{\left(\frac{d}{2 \cdot eV}\right)^{1/2}} \quad (2.22)$$

Based on these relationships, the higher masses (therefore, larger ions) take longer times to arrive to the detector. Thus, in order to avoid overlaps with simultaneously arriving smaller ions produced later during the ionization process, the ion source must be pulsed, which is achieved by the use of a laser. In addition, a simple TOF analyzer offers poor resolution due to this spread in velocity of ions of the same mass, due to kinetic energy, spatial and temporal distributions of the ions, and can be minimized by time-lag focusing (delayed extraction) and the use of a reflectron. This device is an ion mirror with an electric field which retards and reflects the entering ions. Fig 2.16 shows the scheme of a reflectron MALDI-TOF mass spectrometer. When the electrodes are turned off, the MALDI spectrum is recorded in the linear mode, whereas if they are turned on, the spectrum is recorded in the reflectron (or reflected) mode. When faster ions (those with higher energies) penetrate deeper into the reflector take more time to turn around, and therefore they reach the reflectron detector at the same time as the slower ions with the same mass, which spend less time inside the **reflectron**⁽¹⁸⁾.

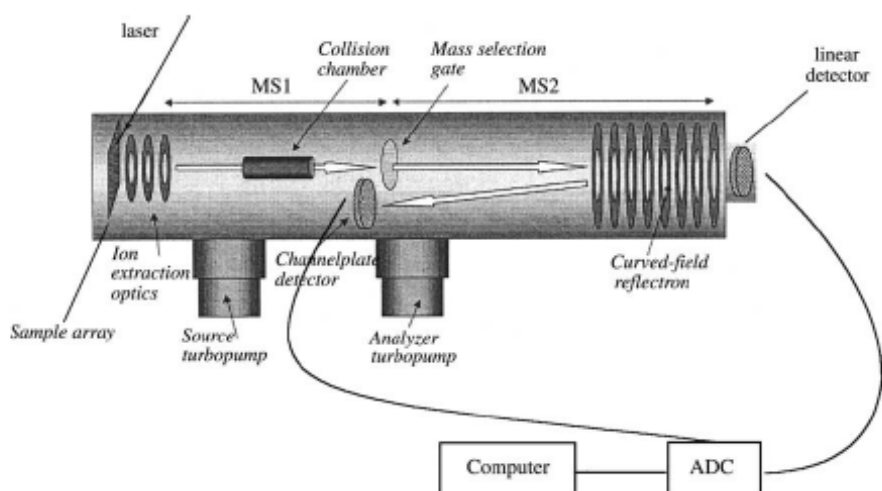


Figure 2. 16. Schematic representation of a MALDI equipment with reflector (as adapted from *Montaudo et al.* (19))

With Mass Spectrometry (MS), due to the variety of structures that can be found, the process of analyzing a polymer has to be proceeded by steps⁽¹³⁾:

- **Determination of the chemical structure of the backbone:** The polymer structure determination consists in finding out the chemical units that constitute the backbone and the type of chemical bonds linking the monomers together. MS can be applied to structure analysis and polymer identification, since the mass spectrum of polymer possesses characteristic peaks, peculiar to a polymer structure⁽²⁰⁻²¹⁾. Such is the case of the spacing between peaks. For example, poly(ethylene terephthalate) (PET) has a spacing of 192,168 m/z , which can be used for identification.
- **End-group determination:** Taking into account that the general structure of the ions detected by MS is of the type: $G1\text{-}n\text{A}\text{-}G2\text{ C}^+$, where G1 and G2 stand for end-groups, A is the repeating unit and C is a proton or a cation, the end-group determination is performed as follows: One considers the mass number of one of the MS peaks, subtracts the mass of C, then subtracts many times the mass of a repeat unit until one obtains the sum of masses of G1+G2 (residual of the calculation).
- **Relative abundance:** Synthetic polymers are often made of a mixture of chains with different end-groups, and it is of high interest to establish the relative abundance of each species.

B. Sample preparation

Despite the remarkable development of this technique, there are still some lacking concepts regarding the optimization of the MALDI signal that have to be considered. These issues are related to both sample preparation factors and instrumental settings during sample analysis, as it is shown in Fig 2.17.

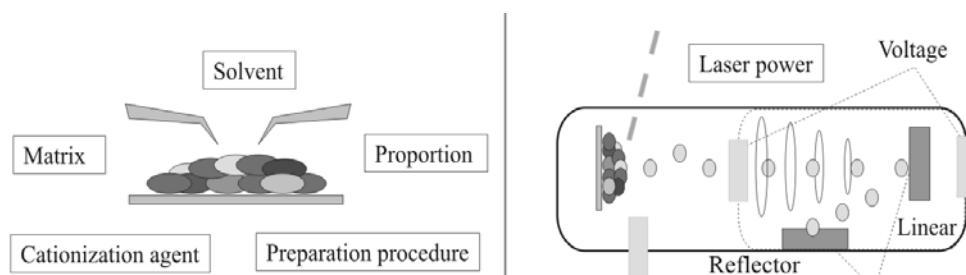


Figure 2. 17. MALDI analysis. Left: sample preparation. Right: Instrumental settings

- **Sample preparation** takes into account factors such as the choice of matrix, the solvent, the cationization agent or the proportion used of each one for the sample preparation. The final goal is to achieve a homogeneous co-crystallization of sample and matrix molecules. In MALDI of synthetic polymers, typically rather inhomogeneous sample preparations are obtained and often one has to search not only for the sweet spots offering good resolution and signal intensity, but also in cases those spots which give any polymer signal ⁽²²⁾.
- Dealing with the **matrix selection**, it is generally considerable to match the polarity of the matrix with that of the polymer under investigation. Nevertheless, matrix selection is still a trial and error procedure. As suggestions, *Nielen* tabulated many combinations of polymer-matrix-solvents sample preparation conditions in a review ⁽²²⁾. An ideal matrix should have the following properties: high electronic absorption at the employed wavelength, good vacuum stability, low vapour pressure, and good miscibility with the analyte in the solid-state ⁽²³⁾. Exhaustive list of useful matrices are available in the literature ⁽²⁴⁾. 1,8,9-anthracenetriol (dithranol), 2-(4-hydroxyphenylazo) benzoic acid (HABA), trans-3-indoleacrylic acid (IAA), 2,4,6-trihydroxy acetophenone (THA), ferulic acid (FA) and 2,5-dihydroxybenzoic acid (DHB) have been successfully used in other studies with PLA, PET and other polyesters ⁽²⁵⁾. Chemical structures of used matrixes are depicted in Fig 2.18.
- Concerning the **selection of the correct solvent**, the goal was to avoid segregation during the evaporation/crystallization of the MALDI target. If actually a mixture of solvents is used in the sample preparation then the solvent

composition will change during the solvent evaporation process because of differences in volatility. As a consequence, the solubility of the polymer changes as well, thus when some less volatile non-solvent is present in the preparation, the polymer might precipitate before matrix crystal formation⁽²²⁾. For the case of PLA, the finding was straightforward, and **tetrahydrofuran** (THF) was used. Nevertheless, to find a good solvent that could dissolve PET at room temperature lead to the use of the **azeotropic mixture of dichloromethane (CH₂Cl₂) and 1,1,1,3,3,3-hexafluoro-2-propanol (HFIP) (70:30, V:V)**⁽²⁵⁾. In that sense, when the choice of a suitable matrix was addressed, it was extremely important that the mixture behaved as one during the evaporation process of the solvent, avoiding therefore sample segregation, which could thus impoverish the quality of the signal⁽²⁵⁾.

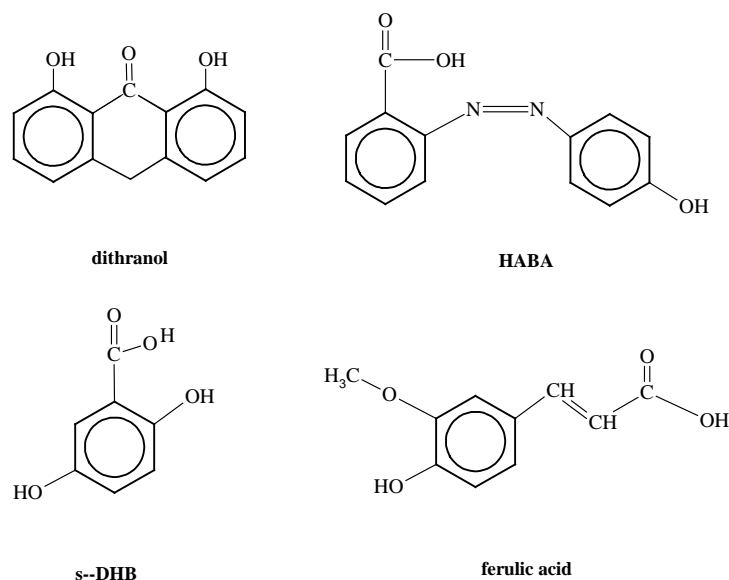


Figure 2. 18. MALDI matrixes used in this thesis

- **Suitability of a cationization agent:** The ionization process of MALDI can be aided by the addition of a sodium (Na) or potassium (K) salt. Since polyesters are relatively polar polymers, Na⁺ and K⁺ are observed in the MALDI spectra, even if they are not deliberately added to the matrix/analyte mixture⁽²⁶⁻²⁸⁾. It is known that these cations are present as impurities in matrixes, reagents, solvents or glassware among other sources, and therefore polymers with high cation affinity do not necessarily need a high amount of extra salt in the MAC sample⁽²³⁾. The

presence of specific functional groups in the polymers, such as carboxyl and hydroxyl is very important in the cationization process ⁽²⁹⁾. In addition, matrixes such as HABA and dithranol are particularly insensitive to impurities ⁽³⁰⁾ and therefore the study of the addition of a cationization agent for these MALDI experiments is justified. Sodium Trifluoroacetate (NaTFA) was chosen as a source of ions. The quantity of NaTFA to be added to the *MAC* was also investigated, in order to explore its influence on the quality of the MALDI response.

- **Instrumental settings during sample analysis** covers all the experimental conditions during desorption/ionization, transmission and detection. Extended information regarding the instrumental factors can be found elsewhere ^(22; 23).

The individual and synergic influence of MALDI sample preparation factors such as the choice of the matrix and solvent, the use of cationization agent and the proportion of these components in the sample mixture were investigated in this study. In this sense, a mathematical procedure was preferred, “blind” to physico-chemical interactions and correlations. A statistical **Design of Experiments (DoE)** was used, since this methodology is capable of covering any kind of scientific or industrial problem, by optimizing the value of a specific effect; in this case, the enhancement of the MALDI signal was thus intended. Thus, a short introduction is addressed hereafter.

3.2.2. *FUNDAMENTALS OF THE STATISTICAL DESIGN OF EXPERIMENTS (DoE)*

Design of experiments (DoE) plays a fundamental role in the optimization of scientific and industrial problems ⁽³¹⁾. These problems involve the study of the effects of multiple input variables on the experimental outcome, i.e., the response. These input variables are called **factors (F)** and the experiments are called factorial experiments. *F* can be either quantitative (categorical variable) or qualitative (based on a continuous variable but only use a few controlled values in the experiment). Each factor must have two or more settings so that the effect of change in factor setting on the response can be explored. These settings are called **levels (L)** of the factor. Any combination of levels of factors (*F/L*) corresponds to a **run** in practical experimentation. **Factorial design** concerns the

selection and arrangement of combinations F/L in a factorial experiment. Investigators select F to systematically vary during an experiment in order to determine their effect on the **response** variable. After screening the factors to determine which are important for explaining process variation, DoE is useful to understand how F interact and drive the measurement and consequently helps select the F/L that produce optimal process performance. Further information can be found in general literature ^{(32) (33) (34)}.

Experimenting one factor at a time (OFT) maintaining the rest of factors constant was considered the correct procedure to perform experiments at the beginning. Nevertheless, this method only provided the estimation of the effect of a unique factor under selected and fixed conditions of the other factors. In order to consider this estimation generally relevant it would be necessary to assume that the effect should be the same in all conditions for the rest of factors and thus that the factors affect the response in an additive manner. **DoE can remarkably improve the characteristics of the study:** whether the F really act in an additive way, DoE permits the estimation with higher precision; on the contrary, if F do not act in an additive way, DoE is capable, unlike OFT, of detecting and estimating the interactions of F and measuring this no-additivity ⁽³⁵⁾.

Reproducibility of the experiments must also be taken into account. **Repeat and replicate** measurements are both multiple response measurements taken at the same F/L combination; but repeat measurements are taken during the same experimental run or consecutive runs, while replicate measurements are taken during identical but distinct experimental runs, which are often randomized. Whether repeats or replicates are used, it depends on the sources of variability interesting to explore and the resource constraints of the experiment. Designs with both repeats and replicates enable to examine multiple sources of variability. Because replicates are from distinct experimental runs, usually spread over a longer period of time, they can include sources of variability that are not included in repeat measurements. For example, replicates can include variability from changing equipment settings between runs or variability from other environmental factors that may change over time. Replicate measurements can be more expensive and time-consuming to collect ⁽³⁵⁾.

DoE analysis is performed by the use of the General Linear Model (GLM) ⁽³⁵⁾, which comprises the univariate analysis of variance with balanced and unbalanced designs, analysis of covariance, and regression, for each response variable. Interpretation of results

is drawn from **main effects plots (MEP)** and **interaction plots (IEP)**. MEP show the direct effect of each F on the response, evaluated along the different L considered. IEP are useful for the study of interactions between F by means of the comparison of the relative strength of the effects across factors. An interaction between factors occurs when the change in response from the low level to the high level of one factor is not the same as the change in response at the same two levels of a second factor. That is, the effect of one factor is dependent upon a second factor ⁽³⁵⁾.

The application of DoE is therefore very valuable, not only for the determination of the optimal settings of an experiment, but also for the understanding of the effect of each factor, individually or in combination, to the final response. Thus, a DoE was applied for the improvement of the MALDI sample preparation, taking into account matrix, proportion analyte-to-matrix and amount of cationization agent. Further details are extended in the Discussion of Results of Chapter III.

3.2.3. EXPERIMENTAL PARAMETERS

MALDI-TOF/MS experiments were conducted on a Bruker UltraFlex MALDI-TOF mass spectrometer with a SCOUT-MTP ion source (Bruker Daltonics, USA) equipped with a nitrogen laser (337 nm), a gridless ion source and a reflector (Fig 2.19). All spectra were acquired in the reflector positive ion mode with an acceleration voltage of 25 kV and a reflector voltage of 26.3 kV. The detector m/z range was 1600–10000 Da in the case of PET and 200–6000 Da for PLA analysis in order to exclude high intensity signals arising from the low mass ions and to cover the whole mass spectrum. The laser intensity was set to the maximum value possible, taking care for not burning the *MAC* in order to avoid the appearance of high-intensity background peaks, which could decrease the signal-to-noise ratio and the resolution. Spectra were gathered by irradiating 40-50 different positions at the centre area on the sample spot, with a total of 2500 shots per sample. Time-to-mass conversion of the time-of-flight mass spectra was achieved using a self-calibration method ⁽³⁶⁾.

All spectra were treated using FlexAnalysis 2.4 (Bruker Daltonics, USA) software. Interpretation of data was done taking into account all decimals of the atomic masses composing the oligomers, but note that m/z values are given with only one decimal.



Figure 2. 19. MALDI-TOF-MS Bruker Daltonics

3.2.4. CALCULATION METHODS

Signal-to-Noise ratio (S/N) and **Resolution** (RES) stand out as suitable quality indicators in many different spectrometric studies, and therefore were chosen for the analysis. Peaks corresponding to the species that provide with higher intensities were analyzed. Besides, in order to perform a representative description of the oligomeric distribution in both polymers, the peaks of up to seven repeating units were considered for calculations. Absolute and relative E (being $E = S/N$ or RES) were analyzed as well. Effects are listed as follows:

$$E = \sum_i \left(E_i \cdot \frac{I_i}{I_{max}} \right) \quad (2.23)$$

$$E_{rel} = \sum_i \left(\frac{E_i}{E_{max}} \cdot \frac{I_i}{I_{max}} \right) \quad (2.24)$$

where I is the intensity of the peak, I_{max} the maximum intensity, E_{max} the maximum effect (S/N or RES) and i is the counter of the studied peaks.

3.3. FOURIER TRANSFORM INFRARED ANALYSIS

3.3.1. FUNDAMENTALS ⁽³⁷⁾

As one of the few techniques that can provide information about the chemical bonding in a material, it is particularly useful for the **non-destructive analysis** of solids and thin films, for which there are few alternative methods. Liquids and gases are also commonly studied, more often in conjunction with other techniques. Chemical bonds vary widely in their sensitivity to probing by infrared techniques.

Infrared refers to that part of the **electromagnetic spectrum** between the visible and microwave regions. Electromagnetic spectrum refers to the seemingly diverse collection of radiant energy, from cosmic rays to X-rays to visible light to microwaves, each of which can be considered as a wave or particle travelling at the speed of light, as it is shown in Fig 2.20.

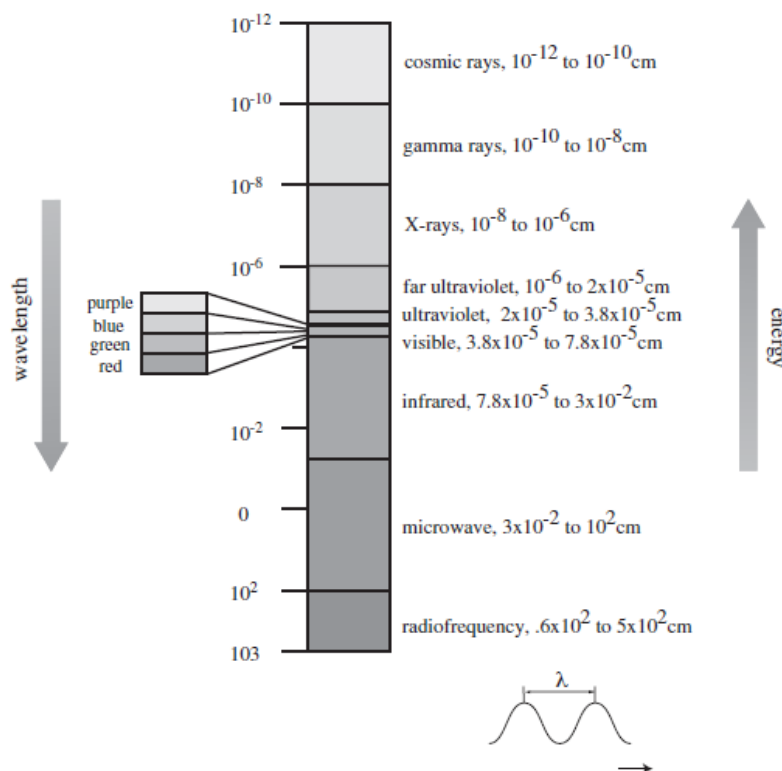


Figure 2. 20. The electromagnetic spectrum, as adapted from ref (38)

These waves differ from each other in the length λ (cm) and frequency ν ($\text{Hz} = \text{s}^{-1}$), which are inversely related between them, and connected to the energy by means of:

$$\nu = c \cdot \lambda^{-1} \quad , \quad E = h \cdot \nu \quad (2.25)$$

, where h is the Planck's constant ($6.6 \cdot 10^{-34} \text{ J} \cdot \text{s}^{-1}$).

In wavenumbers, the mid IR range is $4000\text{--}400 \text{ cm}^{-1}$ (Fig 2.21). An increase in wavenumber corresponds to an increase in energy. Infrared radiation is absorbed by organic molecules and converted into energy of **molecular vibration**. In IR spectroscopy, an organic molecule is exposed to infrared radiation. When the radiant energy matches the energy of a specific molecular vibration, absorption occurs. Therefore the **wavenumbers** (sometimes referred to as *frequencies*) at which an organic molecule absorbs radiation give information on **functional groups** present in the molecule. Certain groups of atoms absorb energy and therefore, give rise to bands at approximately the same frequencies. The potential utility of IR is that it is a function of the chemical bond of interest, rather than being applicable as a generic probe. The limitations arise from sample-to-sample variations that modify the optical quality of the material.

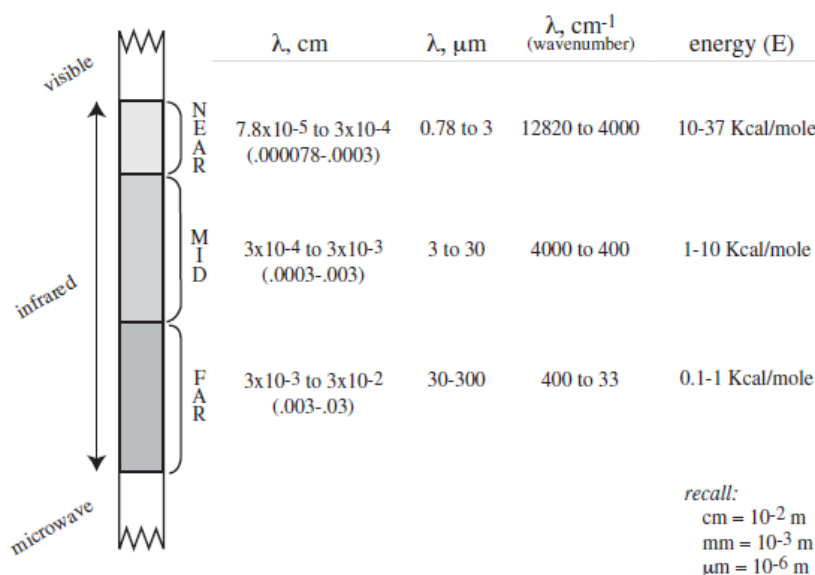


Figure 2. 21. The IR regions in the electromagnetic spectrum, as adapted from ref (38)

Defining I_0 to be the intensity of the light incident upon the sample and I the intensity of the beam after it has interacted with the sample, the goal of the basic **infrared experiment** is to determine the intensity ratio I/I_0 as a function of the frequency of the light (ν). A plot of this ratio versus the frequency is the infrared spectrum. The infrared spectrum is commonly plotted in one of three formats: as transmittance, reflectance, or absorbance. If one is measuring the fraction of light transmitted through the sample, this ratio is defined as:

$$T_\nu = \frac{I_T}{I_0} \Big|_\nu \quad (2.26)$$

,where T_ν is the transmittance of the sample at frequency ν , and I_T is the intensity of the transmitted light. Similarly, if one is measuring the light reflected from the surface of the sample, then the ratio is equated to R_ν , or the reflectance of the spectrum, with I_T being replaced with the intensity of the reflected light I_R . The third format, absorbance, is related to transmittance by the Beer-Lambert Law:

$$A_\nu = -\log(T_\nu) = \varepsilon_\nu \cdot b \cdot c \quad (2.27)$$

, being c the concentration of chemical bonds responsible for the absorption of infrared radiation, b is the sample thickness (optical path), and ε_ν is the frequency-dependent absorptivity, a proportionality constant that must be experimentally determined at each ν by measuring the absorbance of samples with known values of $b \cdot c$.

There exist different technical aids to allow the measurement of different geometries of samples. When an **Attenuated Total Reflection (ATR)** crystal is used, as shown in Fig 2.22, the infrared beam is directed into the crystal. Exploiting the principles of a waveguide, the change in refractive index at the crystal surface causes the beam to be back-reflected several times as it propagates down the length of the crystal before it finally exits to the detector. If the sample is put in contact with the crystal surface, the beam will interact weakly with the sample at several points. For extremely thin samples, this is a means of increasing the effective path length. Since the propagating beam in the crystal barely penetrates through the surface of the sample adjacent to the crystal, signals at a sample surface can be enhanced, as well. This also helps in the study of opaque samples. Approximately fivefold amplification in signals is typical over a direct

transmission experiment. The quality of the crystal-sample interface is critical, and variability in that interface can make ATR results very difficult to quantify.

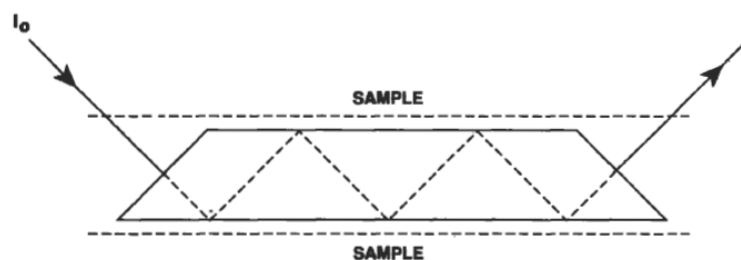


Figure 2. 22. Typical beam path configuration of FTIR-ATR, adapted from ⁽³⁷⁾

Different crystals can be used in ATR, such as diamond, germanium or an alloy of zinc and selenium. In addition, it should be note that the interface is critical, and variability in that interface can make ATR results very difficult to quantify.

There are two types of **molecular vibrations**, stretching and bending, as shown as follows for a simple molecule like water:



Figure 2. 23. Stretching modes of vibration: (left) symmetrical, (right) anti symmetrical

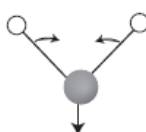


Figure 2. 24. Bending mode of vibration of water (scissoring)

The vibration modes depend on the linearity and the surrounding, and thus the in-plane and out-of plane alternatives take place. See for example stretching and bending vibrations for the important organic group, $-\text{CH}_2-$, in Fig 2. 25

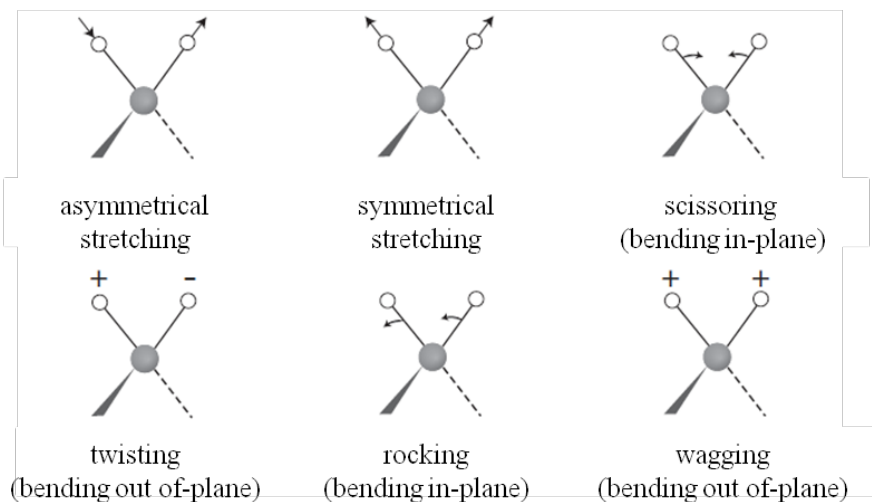


Figure 2. 25. Vibrations of the group $-\text{CH}_2-$

3.3.2. CALCULATION METHODS

The identification of functional groups was performed by the position of the peak corresponding to the characteristic wavenumber of vibration. Semi-quantitative analysis was performed by calculating functional indexes:

$$I_v = \frac{P_v}{P_{ref}} \quad (2. 28)$$

, being P the parameter of analysis considered, taking into account the area under the curve in case a single peak was defined, or the intensity (height) of the peak in case overlapped phenomena were encountered. In the latter case, a deconvolution procedure was performed taking into account Gaussians and Lorentzians for fitting to skewed curves. P_{ref} corresponds to the same parameter for a reference peak, which is supposed not to vary with the degradation process and to be independent of the conformational arrangement of the sample, as specifically explained for each polymer.

3.3.3. EXPERIMENTAL PROCEDURE

FT-IR spectra were collected by a NEXUS Thermo Nicolet 5700 FT-IR Spectrometer (MA, USA), previously calibrated, and equipped with a single-reflection Smart Performer accessory for attenuated total reflection (ATR) measurements, with diamond crystal (Fig

2.26) . 32 co-added spectra were recorded for each specimen at a resolution of 4 cm^{-1} with a spacing of 1 cm^{-1} , from 4000 to 600 cm^{-1} of wavenumber. In the case of PET, the spectra were normalized to the 1410 cm^{-1} peak ⁽³⁹⁾ before any data processing, corresponding to the benzene ring in-plane deformation, which is usually used as internal standard due to it is not sensitive to effects of orientation or conformation ⁽⁴⁰⁾, and it is useful to correct possible variations arisen from defects in surface quality or sample positioning. In the case of PLA, the spectra were normalized to the 1454 cm^{-1} peak ⁽⁴¹⁾.



Figure 2. 26. Picture of used IR spectrometer with ATR accessory

A background was performed before the analysis of the samples. The effect of water and atmospheric CO_2 was corrected and subtracted from the spectra. Further corrections such as baselines, refractive indexes and incident angles were also applied. At least 8 measurements per material were performed at different locations of the sample, in order to obtain representative results.

FTIR was also used for the determination of the gases evolved from the energetic valorisation of PET and PLA, as shown afterwards.

3.4. SCANNING ELECTRON MICROSCOPY

3.4.1. FUNDAMENTALS⁽⁴²⁾

The basic principle of the scanning electron microscope (SEM) is to scan the specimen with a finely focused electron beam of keV energy. An image is formed by scanning a cathode-ray tube (CRT) in synchronism with the beam (Fig 2.27) and by modulating the brightness of this tube with beam-excited signals. In this way, an image is built up point-by-point that shows the variations in the generation and collection efficiency of the chosen signal at different points on the specimen. Unlike with transmission electron microscopy (TEM), there is no need to refocus the signal-carrying particles generated in the specimen. This makes it possible to examine rough, solid specimens with a minimum of specimen preparation. By using different conditions and specimens, it is possible to obtain images showing the surface topography, average atomic number, surface potential distribution, magnetic domains, crystal orientation, and crystal defects in a solid specimen.

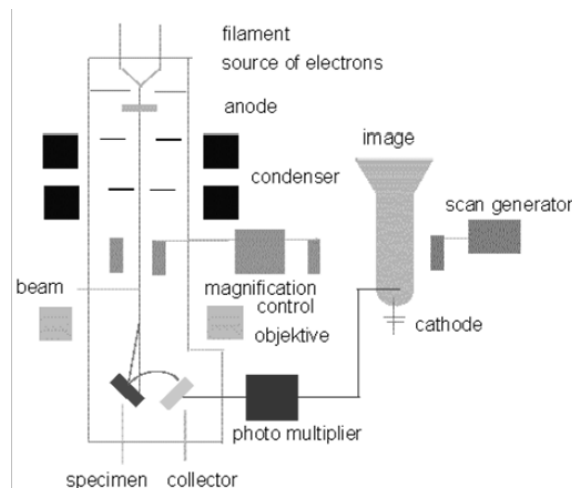


Figure 2. 27. Schematic diagram of a scanning electron microscope

Computers have been used in the SEM to control system setup, to scan the incident electron beam, move the specimen, collect data, for image processing and analysis, replay, and to provide for remote operation by an operator at a different location. Generally, the image resolution of an SEM is about an order of magnitude poorer than that of a TEM. However, because the SEM image relies on surface processes rather than

transmission, it is able to image bulk samples up to many centimetres in size and (depending on instrument design and settings) has a great depth of field, and so can produce images that are good representations of the three-dimensional shape of the sample.

A. *Main types of electrons*

The signals from the specimen mainly include:

- **Secondary electrons (SE)**, which leave the specimen with an energy of typically 1 to 10eV with 50eV being specified as the upper energy limit. In fact, many hundreds of secondary electrons can be excited within the specimen by a single primary electron, but only those which are excited within ~ 10 nm of the surface can escape into the vacuum and be detected. Thus, secondary electrons can be subdivided into:
 - those that escape at the point where the primary enters the specimen (SE-I), and
 - those that are excited at the exit point if there is one (SE-II). In most cases, the primary excited secondary electrons are capable of higher resolution than the others.

- **Backscattered electrons (BSE)**, which leave the specimen with an appreciable fraction of the primary beam energy. (For the purpose of a definition, a backscattered electron has energy greater than 50eV.) In order to be backscattered from a thin film or from a solid target, a primary electron must experience one or more close encounters with the nuclei of the target atoms (Rutherford scattering events). The terms *rediffused electrons* and *reflected electrons* are synonymous with backscattered electrons.

- **Elastically scattered electrons**, which have an energy loss, from a solid target, of typically less than ~ 1 eV. In some cases, electrons with characteristic energy losses can also be detected.

B. Sample preparation for SEM analysis

In order to enhance the SEM signal, the sample preparation is of high importance. By the use of a **Conductive Coating**, an ultra-thin coating of electrically conducting material, deposited either by high vacuum evaporation or by low vacuum sputter coating of the sample. This is done to prevent the accumulation of static electric fields at the specimen due to the electron irradiation required during imaging. Such coatings include **gold**, gold/palladium, platinum, tungsten, graphite etc. and are especially important for the study of specimens with the scanning electron microscope. Another reason for coating, even when there is more than enough conductivity, is to improve contrast, a situation more common with the operation of a Field Emission SEM.

3.4.2. EXPERIMENTAL PARAMETERS

The morphology of the specimens was analyzed by means of a Hitachi S-4800 Field Emission Scanning Electron Microscope (Tokyo, Japan), as shown in Fig. 2.28. The samples from each material were prepared by cutting square pieces from a randomly chosen part of the processed specimen. The pieces were mounted on metal studs and sputter-coated with a 2 nm gold layer using a Cressington 208HR high resolution sputter coater (Watford, UK), equipped with a Cressington thickness monitor controller.



Figure 2. 28. SEM (left) and sputter coater (right) used for analysis in this thesis

3.5. MELT-MASS FLOW RATE

3.5.1 .FUNDAMENTALS

Melt-mass flow rate (MFR) or index (MFI) is a measurement of the ease of flow of the melt of a thermoplastic polymer. It is defined as the mass of polymer, in grams, flowing in ten minutes through a capillary of a specific diameter and length by a pressure (applied via prescribed alternative gravimetric weights for alternative prescribed temperatures). The method is described in the standard ISO-1133⁽⁴³⁾.

In the industry, the MFR is an indirect measure of molecular weight, with high melt flow rate corresponding to low molecular weight. At the same time, melt flow rate is a measure of the ability of the material's melt to flow under pressure. MFR is inversely proportional to viscosity of the melt at the conditions of the test, though it should be kept in mind that the viscosity for any such material depends on the applied force. The technologists should choose a material with a melt index so high that he can easily form the polymer in the molten state into the article intended, but on the other hand so low that the mechanical strength of the final article will be sufficient for its use.

3.5.2. EXPERIMENTAL PROCEDURE

Melt mass-flow rate (MFR) measurements of virgin and multi-extruded PET material were carried out by a Melt Indexer CFR-91 (Campana Srl., Italy) according to the standard ISO-1133. The test temperature was set at 270 °C and the nominal load was 1,2 kg. Measurements on each sample were repeated six times and the average was considered as the characteristic value.



Figure 2. 29. Picture of MFR indexer used

3.6. TENSILE TESTING

3.6.1. FUNDAMENTALS ⁽⁴⁴⁻⁴⁵⁾

In materials science, the strength of a material is its ability to withstand an applied stress without failure. The applied stress may be tensile, compressive, or shear. Strength of materials is a subject which deals with loads, deformations and the forces acting on the material. A load applied to a mechanical member will induce internal forces (stresses) that cause deformations (strain) of the material. The strength of any material relies on three different type of analytical method: **strength**, **stiffness** and **stability**, where strength refers to the load carrying capacity, stiffness refers to the deformation or elongation, and stability means refers to the ability to maintain its initial configuration. The method is thoroughly explained in the ISO 527-1 ⁽⁴⁶⁾.

Material yield strength refers to the point on the engineering **stress-strain curve** (Fig 2.30) beyond which the material experiences deformations that will not be completely reversed upon removal of the loading.

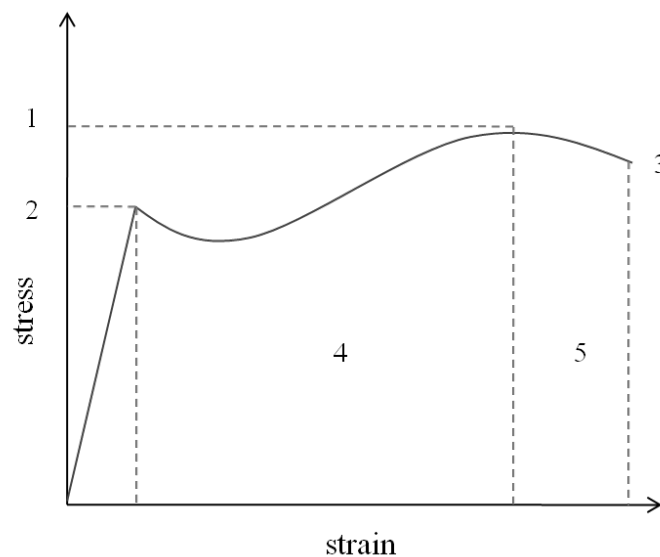


Figure 2. 30. Stress-strain curve. 1. Ultimate Strength 2. Yield Strength 3. Rupture 4. Strain hardening region 5. Necking region.

A material's strength is dependent on its **microstructure**. Strength is considered in terms of compressive strength, tensile strength, and shear strength, namely the limit states of

compressive stress, **tensile stress** and shear stress, respectively. The effects of **dynamic loading** are probably the most important practical part of the strength of materials, especially the problem of fatigue. Repeated loading often initiates brittle cracks, which grow slowly until failure occurs. **Tensile testing**, also known as **tension testing** ⁽⁴⁵⁾, is a fundamental materials science test in which a sample is subjected to uniaxial tension until failure. The results from the test are commonly used to select a material for an application, for quality control, and to predict how a material will react under other types of forces. Main properties that are directly measured via a tensile test are **Young modulus, stress and strain at break** ⁽⁴⁵⁾. The knowledge of the elastic properties describing the reversible deformation behaviour is a fundamental requirement for the design of statically and dynamically loaded components.

A. The tensile test

The most common testing machine used in tensile testing is the **universal testing machine**. This type of machine has two crossheads; one is adjusted for the length of the specimen and the other is driven to apply tension to the test specimen. There are two types: hydraulic powered and electromagnetically powered machines. The **alignment** of the test specimen in the testing machine is critical, because if the specimen is misaligned, either at an angle or offset to one side, the machine will exert a bending force on the specimen. This is especially bad for brittle materials, because it will dramatically skew the results. The test process involves placing the test specimen in the testing machine and applying tension to it until it fractures. During the application of tension, the elongation of the gage section is recorded against the applied force. The data is manipulated so that it is not specific to the geometry of the test sample. The elongation measurement is used to calculate the engineering strain ε , using the following equation:

$$\varepsilon = \frac{\Delta L}{L_0} = \frac{L - L_0}{L_0} \quad (2. 29)$$

where ΔL is the change in gage length, L_0 is the initial gauge length, and L is the final length. The force measurement is used to calculate the engineering stress σ , using the following equation:

$$\sigma = \frac{F}{A} \quad (2. 30)$$

, where F is the force and A is the cross-section of the gauge section.

3.6.2. EXPERIMENTAL PARAMETERS

Tensile testing was carried out at laboratory conditions according to ISO 291, atmosphere 23/50, class 1⁽⁴⁷⁾. Tensile tests were performed on virgin and reprocessed materials in order to investigate the changes in macroscopic mechanical properties, on dumbbell samples following ISO 527-2 (type 1A)⁽⁵⁾, by means of an Instron 5566 universal electromechanical testing instrument (Instron Corp, MA, USA), at a crosshead speed of 10 mm·min⁻¹ for PET and of 5 mm·min⁻¹ for PLA, a 10 kN load cell and gauge length of 50 mm (Fig 2.31). Analyses were repeated at least 6 times per material, and the average of elastic modulus, elongation at break and stress at break were used as representative values.



Figure 2. 31. Universal testing machine used for analysis

3.7. IMPACT TESTING

3.7.1. FUNDAMENTALS⁽⁴⁸⁾

In mechanics, an **impact** is a high force or shock applied over a short time period when two or more bodies collide. Such a force or acceleration usually has a greater effect than a lower force applied over a proportionally longer time period of time. The effect depends critically on the relative velocity of the bodies to one another. At normal speeds, during a perfectly **inelastic collision**, an object struck by a projectile will deform, and this deformation will absorb most, or even all, of the force of the collision. Viewed from the conservation of energy perspective, the kinetic energy of the projectile is changed into heat and sound energy, as a result of the deformations and vibrations induced in the struck object. However, these deformations and vibrations cannot occur instantaneously. A high-velocity collision (an impact) does not provide sufficient time for these deformations and vibrations to occur. Thus, the struck material behaves as if it was more brittle than it is, and the majority of the applied force goes into fracturing the material. The materials actually are more brittle on short time scales than on long time scales.

The **Charpy impact test** is a standardized high strain-rate test which determines the amount of energy absorbed by a material during fracture. This absorbed energy is a measurement of a given material's **toughness** and acts as a tool to study temperature-dependent brittle-ductile transition. It is widely applied in industry, since it is easy to prepare and conduct and the results can be obtained quickly and cheaply. But a major disadvantage is that all results are only comparative, as well as its destructive featuring. The **instrument** consists of a pendulum axe swinging at a notched sample of material. The energy transferred to the material can be inferred by comparing the difference in the height of the hammer before and after a big fracture. The notch in the sample affects the results of the impact test, thus it is necessary for the notch to be of regular dimensions and geometry. The size of the sample can also affect results, since the dimensions determine whether or not the material is in plane strain. Details can be found in ISO 179⁽⁴⁹⁾.

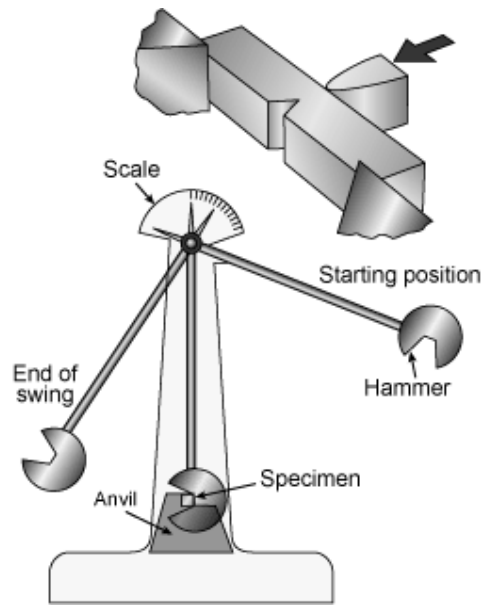


Figure 2. 32. Schematic impact test

3.7.2. EXPERIMENTAL PARAMETERS

Charpy impact experiments were carried out following ISO 179⁽⁴⁹⁾, with a hammer of 1 J and a notch size radius of 1,5 mm, under the same laboratory conditions than tensile tests. Analyses were repeated at least 5 times per material, and the averages were taken as representative values.

The Impact experiments were carried out in the University of Miskolc (Hungary), by staff of the Fibre and Polymer Technology department of the School of Chemical Science and Engineering at Kungliga Tekniska Högskolan (Royal Institute of Technology), Stockholm, Sweden.

3.8. THERMOGRAVIMETRY

3.8.1. FUNDAMENTALS

Thermogravimetry or Thermogravimetric Analysis is, by definition of the International Conference of Thermal Analysis, a technique in which the **mass** of a substance is measured as a function of **temperature**, while the substance is subjected to a controlled temperature program. The analysis can be done dynamically, through a program of heating at constant speed, or in isothermal conditions, as a time function. In both cases, it determines weight loss or weight loss rate for each temperature or time, either directly related to the elimination of volatile or through a chemical process.

The key elements are controlling the weight of a sample subjected to rigorous testing and temperature control. The result of thermogravimetric analysis is presented using a thermogravimetric curve (TG) or **thermogram**. It consists of a sigmoidal curve with one or more stages, depending on the chemical nature of the components, composition of the sample or the analytical gas. Thermogravimetric analysis can be also interpreted by inspection of the differential thermogravimetric curve DTG which is the first derivative of the thermogravimetric curve, in which case the maximum falling slope of the thermogravimetric curve corresponds to a peak in the differential curve DTG.

The use of **gas** determines the thermal stability as only effect of temperature if an inert environment is used, such as Ar; as well, more realistic approaches can be performed by using a reactive gas such as O₂ for testing the thermo-oxidative decomposition behaviours of the sample under consideration. In this sense, the TGA can be used as reactor for simulating pyrolytic and combustion reactions, as **energetic valorisation tools** for a sustainable waste management of polymeric materials.

Generally, the evolution of the thermal decomposition process of a polymeric material in the thermo-balance as a function of temperature can be described schematically as follows:

- A weight loss of low to moderate temperatures ($T < 150\text{ }^{\circ}\text{C}$) corresponds to the loss of volatile components in the system as water, organic solvents or low molecular weight gases absorbed.

- For $T \in 150\text{-}250\text{ }^{\circ}\text{C}$, the loss of low molecular weight components such as additives, water of crystallization, plasticizers or even first products of decomposition at low temperatures can be detected.
- At temperatures above $225\text{-}250\text{ }^{\circ}\text{C}$ thermal degradation is normally initiated, which evolution depends on the type of atmosphere used during the test, so that when the thermogravimetric analysis is performed in the presence of oxygen or air is called the thermo-oxidative degradation.
- At $T > 500\text{ }^{\circ}\text{C}$ charring occurs for hydrocarbon compounds which thermal degradation does not lead to the formation of volatile fragments, leaving these compounds as waste along with inorganic fillers or additives which are not degradable. If the test is performed in an oxidizing atmosphere, the charred residue is gasified by transformation into carbon dioxide and inorganic waste and ash are metal oxides or salts are not oxidized.

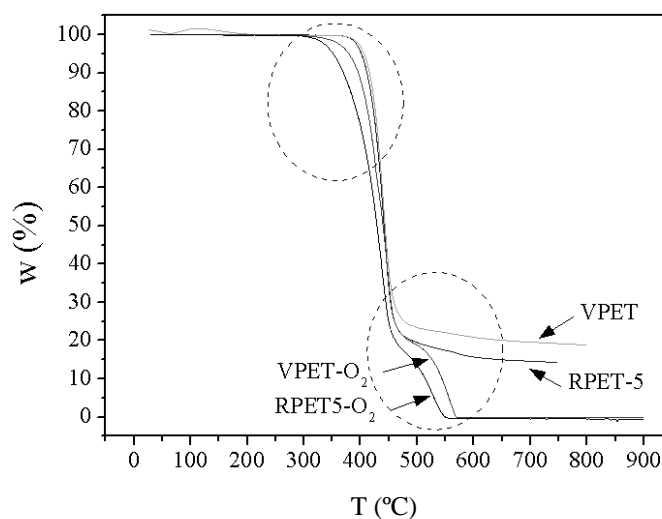


Figure 2. 33. TG curves of virgin PET and its fifth recyclate under inert and oxidative conditions. Highlighted regions point to the induction and deceleration of the thermal decompositions.

When the Thermogravimetry technique is hyphenated to other technique for **evolved gas analysis**, supplementary information concerning the nature of change in mass in connection to the underlying degradation mechanisms can be obtained, as it is shown in the next section.

3.8.2. KINETIC ANALYSIS OF THERMAL DECOMPOSITIONS

In the attempt to develop a model for plastic thermal and thermo-oxidative decompositions in full-scale systems, the main purpose is to describe the behaviour of polymers in terms of an intrinsic kinetics, in which heat and mass transfer limitations are not included. General kinetic models are proposed in literature for plastics and biomasses. These models do not take into account the rigorous and exhaustive description of the chemistry of thermal decomposition of polymers and describe the process by means of a simplified reaction pathway. It is widely known that each single reaction step considered is representative of a complex network of reactions⁽⁵⁰⁾.

Khawan and *Flanagan*⁽⁵¹⁾ reviewed the relationship between the theoretical decomposition mechanisms and their mathematical models, the so-called kinetic functions $f(\alpha)$. Kinetic analysis of non-isothermal experiments is generally performed by using a single step kinetic equation:

$$\frac{d\alpha}{dt} \equiv \beta \cdot \frac{d\alpha}{dT} = A \cdot f(\alpha) \cdot k(T) = A \cdot f(\alpha) \cdot e^{-\frac{Ea}{R \cdot T}} \quad (2.31)$$

, where t is the time (s), T the temperature (K), α is the conversion degree, β is the heating rate used in the thermogravimetric experiment ($\text{K} \cdot \text{s}^{-1}$), R is the ideal gas constant ($8.31 \text{ J} \cdot \text{mol}^{-1} \cdot \text{K}^{-1}$), A a pre-exponential factor (s^{-1}), $f(\alpha)$ the kinetic function (see Table 2.1.) and Ea is the activation energy ($\text{J} \cdot \text{mol}^{-1}$). For thermogravimetric experiments, $\alpha = (m_0 - m_t)/(m_0 - m_\infty)$, where m stands for mass (g), and subscripts 0 , ∞ and t respond to initial, final and actual thermogravimetric values. The obtaining of the so-called kinetic triplet ($f(\alpha)$ -model, Ea , A) may provide new knowledge regarding the kinetic model of thermal and thermo-oxidative decomposition for virgin polyesters and their recyclates, and offer new insights in further energetic valorisation processes for this polymer.

The integration of Eq. (2.31) after rearranging, leads to:

$$g(\alpha) = \int_0^\alpha \frac{d\alpha}{f(\alpha)} = \frac{A \cdot Ea}{\beta \cdot R} \cdot \int_0^\infty \frac{e^{-x}}{x^2} = \frac{A \cdot Ea}{R \cdot T} \cdot p(x) \quad , \quad x = \frac{Ea}{R \cdot T} \quad (2.32)$$

Under linear heating rate program, Eq. (2. 32) does not have an exact analytical solution to the temperature integral $p(x)$ and therefore some studies have reported different equations to approach the best values within lower error margin ⁽⁵²⁾ . In this thesis, the *Senum-Yang* ⁽⁵³⁾ approximation (Eq 2. 33) truncated at its fifth term was used, since it gives deviations from the exact value of the temperature integral lower than 10^{-8} % for $x > 10$ ⁽⁵⁴⁾, which permits its application in solid-state decomposition reactions, where x is usually higher.

$$p(x) = \frac{e^{-x}}{x^2} \cdot \sum_n \frac{n \cdot (1 - n)}{x + 2 \cdot (n + 1)} \quad (2. 33)$$

A. Determination of activation energy – isoconversional methods

Solid-state kinetics were developed from reaction kinetics in homogeneous systems (i.e gases and liquids), and it has been generally assumed that the activation energy and the pre-exponential factor remain constant. However, it has been proved that these kinetic parameters may vary with the progress of the decomposition. This variation can be detected by isoconversional methods, which use data from different multi-linear non-isothermal experiments and do not take modelistic assumptions for the analysis, main source of error of model-fitting methods. The most broadly used isoconversional methods which were applied in this thesis are:

- **Linear integral methods**, which give rise to linear functions from which slopes the Ea at a fixed α is obtained.
 - **Flynn-Wall-Ozawa (FWO)** ⁽⁵⁵⁻⁵⁶⁾ (supported on *Doyle's* integral approximation ⁽⁵⁷⁾)

$$[\log(\beta)]_y = \log\left(\frac{A_\alpha \cdot Ea_\alpha}{R \cdot g(\alpha)}\right) - 2,315 - \frac{0,457 \cdot Ea_\alpha}{R} \cdot \left[\frac{1}{T_\alpha}\right]_x \quad (2. 34)$$

- **Kissinger-Akahira-Sunose (KAS)** ⁽⁵⁸⁻⁵⁹⁾

$$\left[\ln\left(\frac{\beta}{T^2}\right)\right]_y = \ln\left(\frac{A_\alpha \cdot R}{Ea_\alpha \cdot g(\alpha)}\right) - \frac{Ea_\alpha}{R} \cdot \left[\frac{1}{T_\alpha}\right]_x \quad (2. 35)$$

, where $g(\alpha)$ is the inverse integral kinetic model $g(\alpha) = \int_0^\alpha (f(\alpha))^{-1} \cdot d\alpha$

- **Linear differential methods**, which also give rise to linear functions from which slopes the Ea at a fixed α is obtained.

- **Friedman** ⁽⁶⁰⁾

$$\left[\ln \left(\frac{d\alpha}{dt} \right)_{\alpha} \right]_y = \ln(A_{\alpha} \cdot f(\alpha)) - \frac{Ea_{\alpha}}{R} \cdot \left[\frac{1}{T_{\alpha}} \right]_x \quad (2.36)$$

- **Kissinger** ⁽⁵⁸⁾ (Not isoconversional, yields the activation energy from the information at the peak of the DTG curve).

$$\left[\ln \left(\frac{\beta}{T_p^2} \right) \right]_y = \ln \left(\frac{f'(\alpha) \cdot A \cdot R}{Ea} \right) - \frac{Ea}{R} \cdot \left[\frac{1}{T_p} \right]_x \quad (2.37)$$

- **Non-Linear integral methods**, where the activation energy (Ea_{α}) is the value that minimizes Ω in Eq (2.38) for a particular α .

- **Vyazovkin and Dollimore (VYZ)** ⁽⁶¹⁾

$$\Omega = \left| \sum_{i=1}^h \sum_{j \neq i}^h \frac{\beta_j \cdot I(Ea_{\alpha}, T_{\alpha}^i)}{\beta_i \cdot I(Ea_{\alpha}, T_{\alpha}^j)} \right|, \quad I(Ea_{\alpha}, T_{\alpha}^{i,j}) = p_{i,j} \left(\frac{Ea_{\alpha}}{R \cdot T_{\alpha}} \right) \quad (2.38)$$

, where i and j are counters through the h experiments performed at different heating rates.

- **Advanced Isoconversional (AIC)** also developed by Vyazovkin ⁽⁶²⁾, accounts for variable heating rates and systematic errors in the activation energy

$$\Omega = \left| \sum_{i=1}^h \sum_{j \neq i}^h \frac{J(Ea_{\omega}, T_i(t_{\alpha}))}{J(Ea_{\omega}, T_j(t_{\alpha}))} \right|, \quad J(Ea_{\omega}, T(t)) = \int_{t_{\alpha}-\Delta\alpha}^{t_{\alpha}} e^{-\frac{Ea_{\omega}}{R \cdot T(t)}} \cdot dt \quad (2.39)$$

, where i and j are counters through the h experiments performed at different heating rates β . $T(t)=T_0+\beta\cdot t$, where T_0 is the initial temperature. $\Delta\alpha = (m^{-1})$, with m being the number of α segments chosen for integration. The integral $J(Ea_\alpha, T(t))$ can be numerically evaluated by the Simpson 1/3 method.

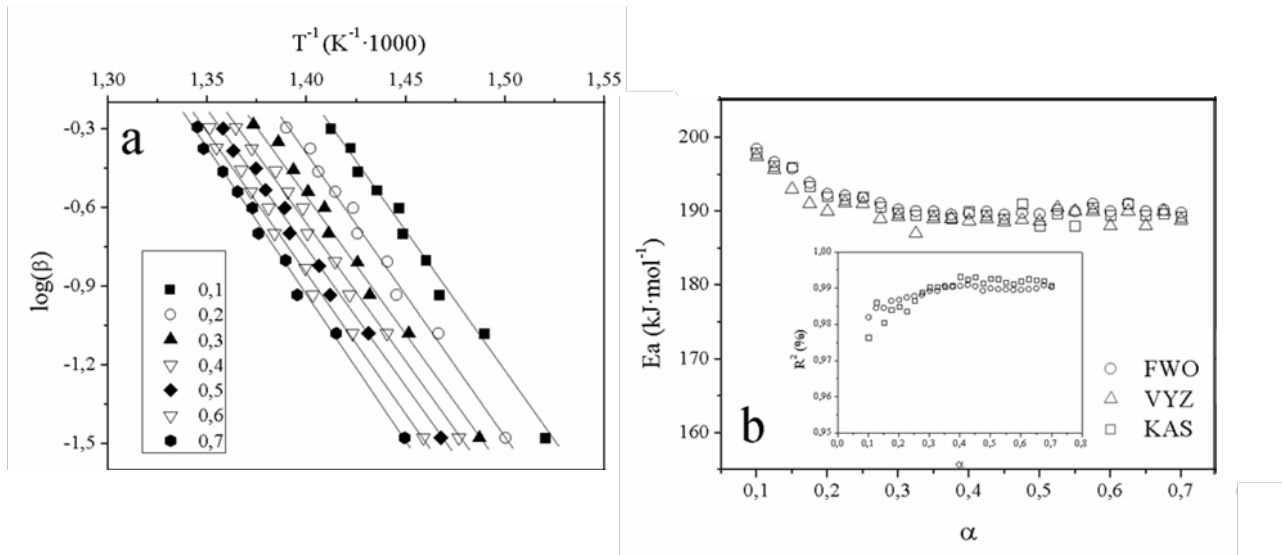


Figure 2. 34. Application of isoconversional methods to virgin PET. (a) An example of FWO method for experiments under Ar; (b) Ea evolution with the conversion degree evaluated by FWO, KAS and VYZ methods (inset: regression coefficients of fittings)

B. The use of Master-Plots

The reaction model may adopt various expressions, based on nucleation and nuclei growth, phase boundary reactions, diffusion or chemical reactions. The environmental gases, inert or reactive, have important roles regarding the selection of the decomposition models. A list of the most common $f(\alpha)$ applied to polymers is given in Table 2.1.

Master Plots ($M-P$) are reference theoretical curves ($M-P_t$) depending on the kinetic model, but generally independent of the kinetic parameters of the process. Due to, in many cases, the experimental kinetic data can easily be transformed into experimental curves $M-P_e$, a comparison with the $M-P_t$ allows the selection of the appropriate kinetic model of the process under investigation or, at least, reducing the span of suitable kinetic models⁽⁶³⁾.

Table 2. 1. Summary of main kinetic models for the analysis of thermal decompositions

model	differential form $f(\alpha)=1/k \cdot d\alpha/dt$	integral form $g(\alpha)=k \cdot t$
NUCLEATION MODELS		
Avrami-Erofeyev (A2)	$2 \cdot (1 - \alpha) \cdot [-\ln(1 - \alpha)]^{1/2}$	$[-\ln(1 - \alpha)]^{1/2}$
Avrami-Erofeyev (A3)	$3 \cdot (1 - \alpha) \cdot [-\ln(1 - \alpha)]^{2/3}$	$[-\ln(1 - \alpha)]^{1/3}$
Avrami-Erofeyev (A4)	$4 \cdot (1 - \alpha) \cdot [-\ln(1 - \alpha)]^{3/4}$	$[-\ln(1 - \alpha)]^{1/4}$
GEOMETRICAL CONTRACTION MODELS		
Contracting area (R2)	$2 \cdot (1 - \alpha)^{1/2}$	$1 - (1 - \alpha)^{1/2}$
Contracting volume (R3)	$3 \cdot (1 - \alpha)^{1/3}$	$1 - (1 - \alpha)^{1/3}$
REACTION-ORDER MODELS		
Zero-order (F0/R1,n=0)	1	α
First-order (F1,n=1)	$(1 - \alpha)$	$-\ln(1 - \alpha)$
Second-order (F2,n=2)	$(1 - \alpha)^2$	$\frac{1}{1 - \alpha} - 1$
Third-order (F3,n=3)	$(1 - \alpha)^3$	$\frac{1}{2} \cdot \left[\frac{1}{(1 - \alpha)^2} - 1 \right]$

There exist three main types of $M-P_t$, those based on the differential form ($M-P_f$) of the generalized kinetic equation Eq. (2.31) ; those based on the integral form ($M-P_g$), according to Eq. (2.32); and the most common one that combines both differential and integral forms ($M-P_{fg}$), that are usually reduced at $\alpha=0.5$ for better visualization. The mathematical description of each curve can be found elsewhere⁽⁶³⁾. They are described after the introduction of the so-called generalized time θ , which denotes the reaction time taken at a particular α at infinite temperature, defined as⁽⁶⁴⁻⁶⁵⁾

$$\theta = \int_0^t e^{-\frac{Ea}{R \cdot T}} \cdot dt \quad (2.40)$$

, which differentiation in combination with Eq. (2.31), one obtains:

$$\frac{d\alpha}{d\theta} = A \cdot f(\alpha) = \frac{d\alpha}{dt} \cdot \frac{Ea}{R \cdot T} \quad (2.41)$$

Therefore, assuming A and Ea constant, due to interdependence of kinetic parameters, and using a reference point at $\alpha=0.5$, the theoretical $M-P_t$ and the expression for the reduced form of the experimental data can be drawn from Eq. (2.40) and Eq. (2.41) obtaining Eq. (2.42) and Eq. (2.43) for $M-P_f$ and $M-P_g$, respectively:

$$\frac{\frac{d\alpha}{d\theta}}{\frac{d\alpha}{d\theta}|_{0.5}} = \frac{f(\alpha)}{f(0.5)} = M-P_t \equiv M-P_e = \frac{\frac{d\alpha}{dt} \cdot e^{\frac{Ea}{R \cdot T}}}{\frac{d\alpha}{dt}|_{0.5} \cdot e^{\frac{Ea}{R \cdot T}|_{0.5}}} \quad (2.42)$$

$$\frac{\theta}{\theta_{0.5}} = \frac{g(\alpha)}{g(0.5)} = M-P_t \equiv M-P_e = \frac{p(x)}{p(x_{0.5})} \quad (2.43)$$

To enhance the study given in this work, instead of using a constant Ea for all the process, the varying Ea_α obtained in the previous section was applied, calculating the $M-P_e$ points at each specific α . The advantage of using $M-P_f$ and $M-P_g$ in contrast to $M-P_{fg}$ is that the formers disperse clearly among different models in the ranges $\alpha < 0.5$ and $\alpha > 0.5$ respectively, therefore permitting a straightforward identification, whereas the latter tends to produce confusion due to the coincidence of lines from different kinetic models.

C. Independence of heating rate

In order to complete the kinetic triplet, the pre-exponential factor A has to be found. As well, the ***Perez-Maqueda et al*** criterion ⁽⁶⁶⁾ ($P-Mc$) has to be accomplished; that is, the independence of the activation parameters Ea , A on the heating rate β . This criterion is usually employed with Ea and A invariable with the aid of the ***Coats-Redfern*** ⁽⁶⁷⁾ equation written in the form:

$$\left[\ln \frac{\beta \cdot g(\alpha)}{T^2} \right]_y = \ln \frac{A \cdot R}{Ea} + \frac{Ea}{R} \cdot \left[\frac{1}{T} \right]_x \quad (2.44)$$

, the points {x, y} should lie on the same straight line for all heating rates. In this work, the variation of A along the decomposition reaction A_α was evaluated along with the effective variation of Ea_α obtained by the isoconversional methods.

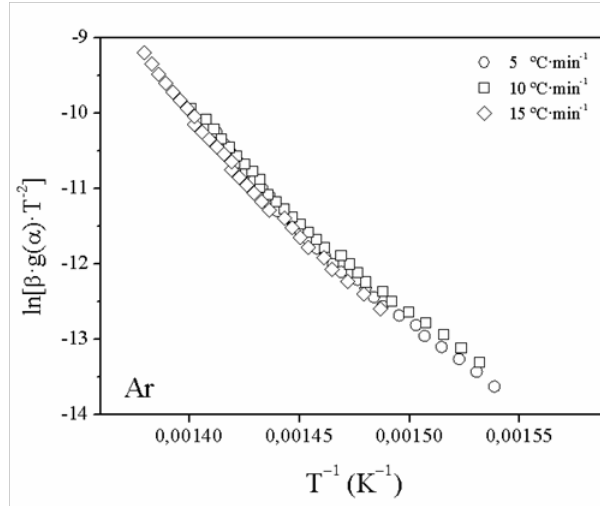


Figure 2. 35. Application of Pérez-Maqueda et al. criterion for thermal decomposition of PET.

D. Summary-kinetic methodology

A schematic overview of the kinetic methodologies carried out in this thesis is finally shown in Figs 2.36 and 2.37.

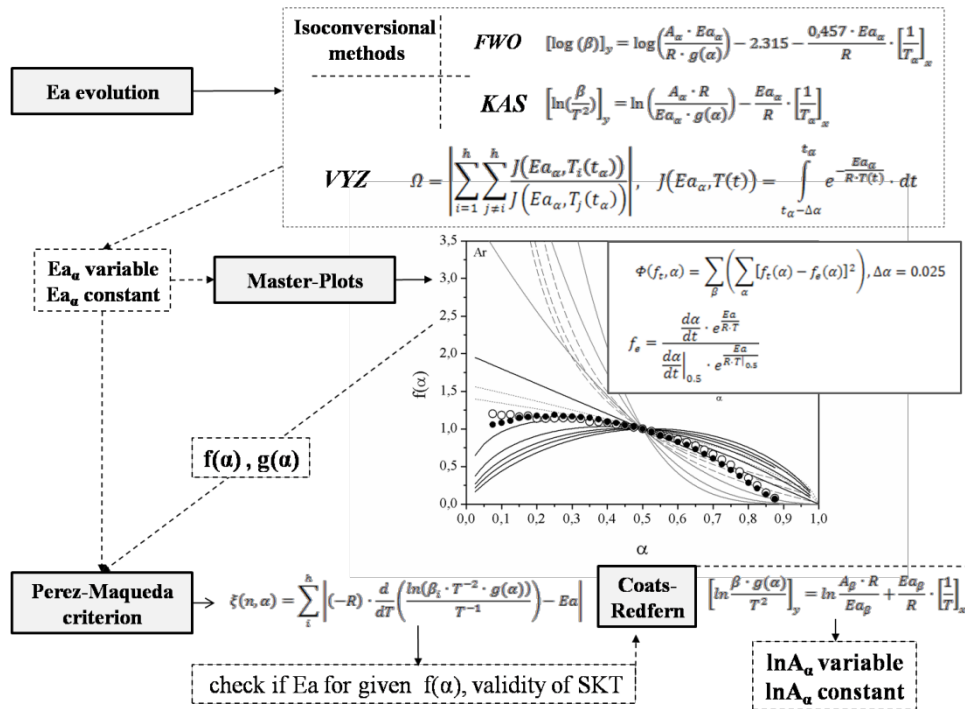


Figure 2. 36. Kinetic methodology applied for recycled PET and PLA

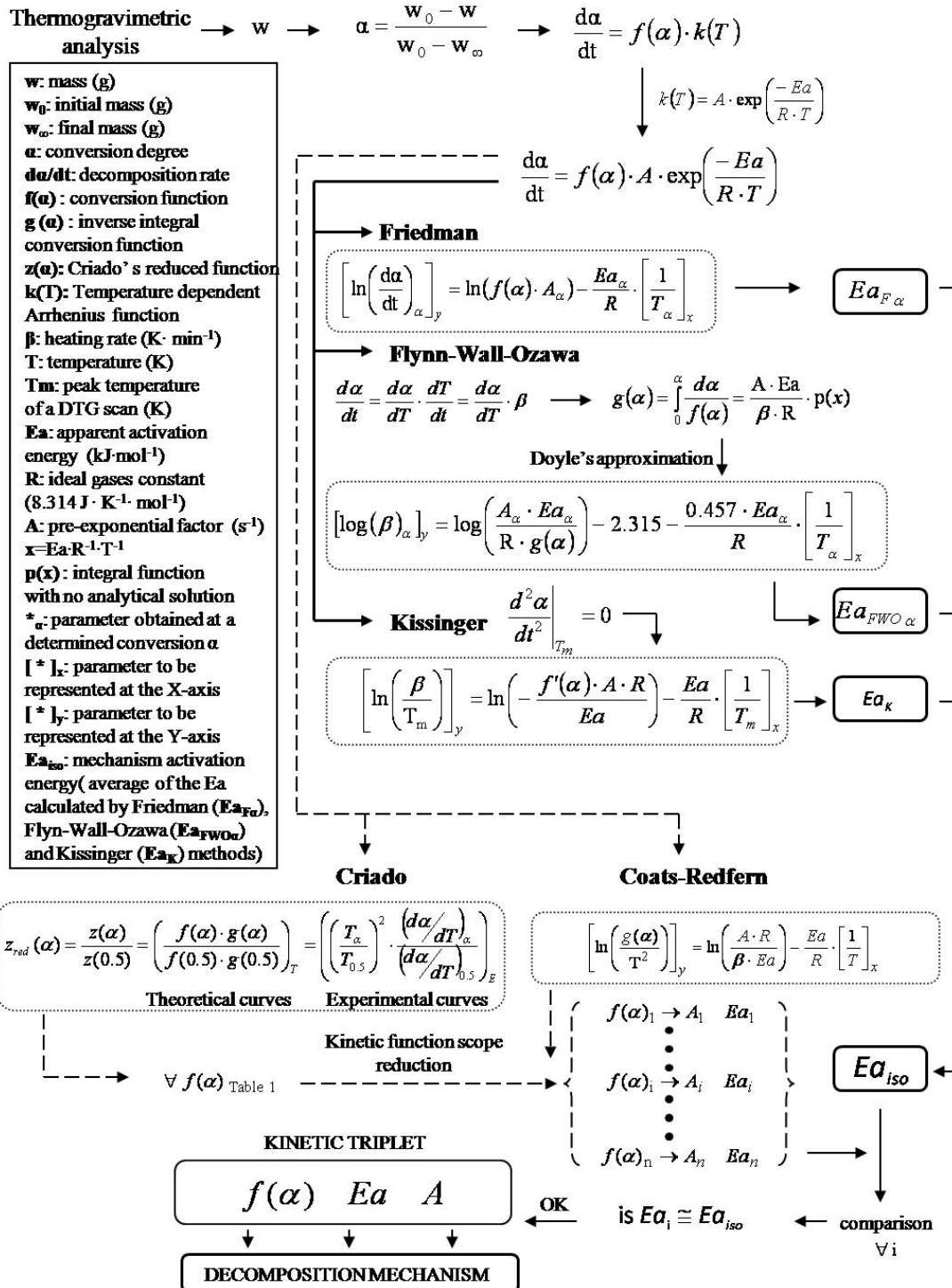


Figure 2. 37. Kinetic methodology applied for bio-degraded PLA

3.8.3. EXPERIMENTAL PARAMETERS

Multi-linear non-isothermal thermogravimetric experiments were carried out in a Mettler-Toledo TGA/SDTA 851 (Columbus, OH). Samples weighing ca. 5 mg were heated in an alumina holder with capacity for 70 μL . Experiments were performed from 25 to 900 $^{\circ}\text{C}$ at different heating rates ($\beta = 2, 5, 7, 10, 12, 15, 17, 20, 25, 30$ $^{\circ}\text{C}\cdot\text{min}^{-1}$) for PET and from 25 to 750 $^{\circ}\text{C}$ at $\beta = 2, 5, 7, 10, 12, 15$ $^{\circ}\text{C}\cdot\text{min}^{-1}$ for recycled PLA and $\beta = 5, 10, 15, 20, 25, 30$ $^{\circ}\text{C}\cdot\text{min}^{-1}$ for buried-in-soil PLA, under constant flow of 50 $\text{mL}\cdot\text{min}^{-1}$ of gas of analysis. An inert Ar atmosphere was used for assessing the thermal decomposition behaviour, whereas an O_2 reactive atmosphere was applied for characterizing the thermo-oxidative decomposition processes of virgin materials and their recyclates. Experiments were repeated at least three times, and the averages were considered as representative values.



Figure 2. 38. Picture of TGA used in this thesis

3.9. EVOLVED-GAS ANALYSIS: 2D-CORRELATION IR

3.9.1. FUNDAMENTALS⁽⁶⁸⁻⁷¹⁾

A. Evolved-Gas analysis

The IUPAC Compendium of chemical terminology defines the evolved gas analysis (EGA) as “a technique in which the nature and/or amount of volatile products released by a substance subjected to a controlled temperature program are determined”. The possibility to detect the nature of the released gases or vapours on-line is fundamental to prove a supposed reaction, either under isothermal or under dynamic temperature conditions.

Among the different possibilities, thermo-analytical instruments, such as pyrolysers, thermo-balances, differential thermal analyzers or calorimeters (but sometimes even simply temperature-controlled reactors), are the most commonly used tools to heat a sample under investigation. Thermogravimetry, in addition, is very useful for the quantification of each single gaseous evolution process as the result of an increasing thermal ramp or a defined isothermal temperature. These techniques have been successfully on-line coupled to perform evolved gas analysis. To obtain the IR spectra of the gases evolved during the programmed analysis, the thermo-analytical instrument is coupled with a FTIR spectrometer by means of a heated transfer line; the released vapours or gases are so transferred to the heated gas cell of the FTIR instrument, the temperatures of the cell and the transfer line being independently selected. A complete review of the application of EGA coupled to FTIR can be found in literature⁽⁷²⁾.

B. 2D-Correlation IR Spectroscopy

2D-Correlation IR Spectroscopy (hereafter 2D-IR) has gained much attention since its introduction⁽⁶⁸⁾. Basically, in 2D-IR, a spectrum is obtained as a function of two independent IR wavenumbers, due to the application of an external perturbation, such as temperature, and provides information that cannot be drawn from conventional one-dimensional IR spectra. Although a deep description of this analytical procedure can be found elsewhere⁽⁶⁸⁻⁷¹⁾, a short description with the basics to understand the discussion of results, is given hereafter.

In a generalized 2D correlation spectroscopy study, the underlying similarity or dissimilarity among systematic variations in spectroscopic signals is examined. The pattern of intensity variations is systematically analyzed by a simple **cross-correlation** technique. The correlation intensities thus obtained are displayed in the form of a 2D map defined by two independent spectral axes for further analysis. Such a 2D map is referred to as a 2D correlation spectrum, even though many of today's 2D correlation studies include applications in the field outside of spectroscopy, such as chromatography and microscopy. Fig 2. 39 shows a typical 2D correlation spectrum, displayed in a pseudo 3D representation mode or a so-called fishnet plot. Peaks appearing over the 2D spectral plane provide detailed information about the complex dynamics of the phase transition process.

It is noted that 2D correlation peaks can take either positive or negative intensities and signs **of correlation** peaks play an important role in the interpretation of 2D correlation spectra. More detailed discussion on this particular 2D correlation spectrum will be given later.

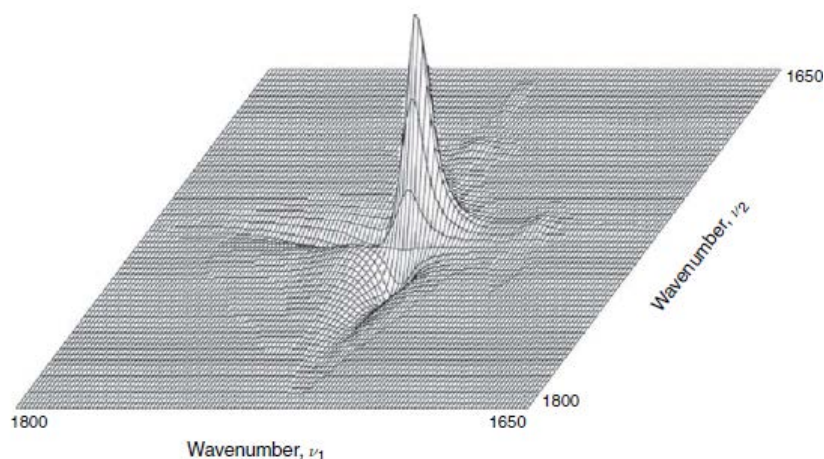


Figure 2. 39. 3D-IR fishnet representation, as reproduced from ref (70)

Fig 2.40. shows the basic scheme used for a generalized 2D correlation spectroscopy experiment. In a typical (1D) optical spectroscopy measurement, a selected electromagnetic probe, such as an IR or UV beam, is used to study the system of interest. Characteristic interactions between the probe and the system constituents are displayed in the form of a spectrum, which in turn is used for further examination of the state of the system. In a generalized 2D correlation experiment, an additional factor comes into play,

which is the external perturbation applied to the system to somehow stimulate its constituents. The response of the system to the applied perturbation often manifests as measurable variations in spectral signals of the system. The portions of the spectral signals influenced by the given perturbation to undergo some intensity variations are by convention referred to as dynamic spectra. In a typical generalized 2D correlation spectroscopy experiment, a series of perturbation-induced dynamic spectra are collected in a sequential order in an alignment with the applied external perturbation. Dynamic spectra for a 2D correlation experiment may be collected, for example, as a function of time.

Time-dependent evolution of transient spectral signals, arising from various constituents of the system affected by the perturbation, is thus monitored. It is common to collect dynamic spectra as a direct function of the essentially static measure of the imposed physical effect itself, such as **temperature**, pressure, concentration, stress, electrical field, and so on. The conceptual scheme described in Fig 2.40 to induce dynamic spectra obviously is a very general one, as it does not even specify the physical nature or mechanisms with which the applied perturbation affects the system constituents.

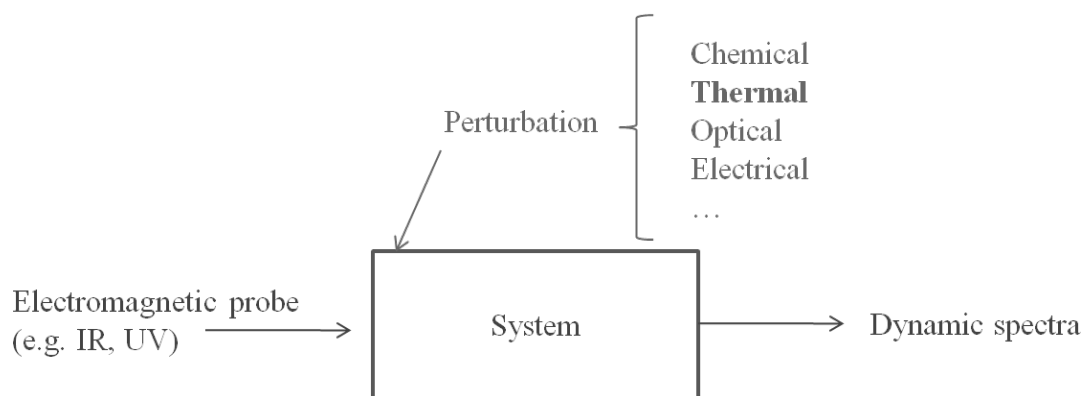


Figure 2. 40. Schematic representation of external dynamic perturbation for 2D-IR correlation analysis, as adapted from ref (70)

3.9.2. SYNCHRONOUS AND ASYNCHRONOUS SPECTRA ⁽⁶⁸⁻⁷¹⁾

Fig 2.41 shows a schematic example of a typical synchronous 2D correlation spectrum plotted as a contour map. The contour map representation of a 2D spectrum is much easier to navigate through for detailed analysis of fine features, compared with the pseudo 3D fishnet plot. On the other hand, a fishnet plot provides much better visual sense for the relative intensities of correlation peaks. It can be easily seen that a synchronous 2D spectrum is a symmetric spectrum with respect to the main diagonal line corresponding to coordinates $\nu_1 = \nu_2$.

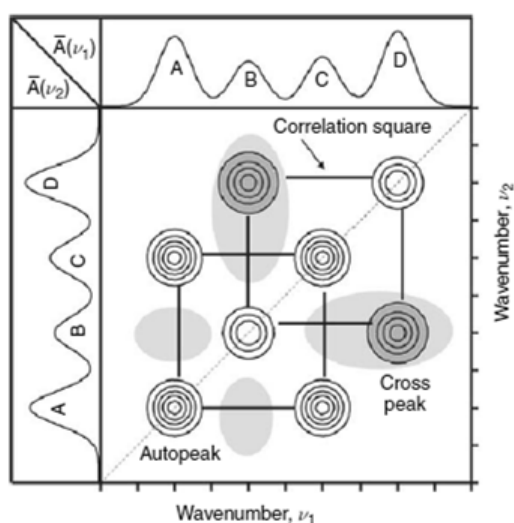


Figure 2. 41. Synchronous 2D-IR correlation spectrum, as reproduced from ref (70)

Correlation peaks appear at both diagonal and off-diagonal positions. The intensity of peaks located at diagonal positions corresponds mathematically to the autocorrelation function (equivalent to the continuous form of statistical variance) of spectral signal intensity variations. Diagonal peaks are therefore often referred to as **autopeaks**. In the spectrum shown in Fig 2. 42 as example, there are four distinct autopeaks located at the coordinates of the spectrum: A, B, C, and D. The magnitude of an autopeak intensity, which is always positive, represents the overall extent of spectral intensity variation observed at the specific wavenumber coordinate ν . Thus, a region of the spectrum which changes intensity to a greater extent under a given perturbation will show a stronger autopeak, while those remaining near constant develop little or do not form autopeak. Summing up, an autopeak represents the overall susceptibility of the spectral signal intensity to change, when an external perturbation is applied to the system.

A **cross peak** located at an off-diagonal position of a synchronous 2D spectrum represents simultaneous or coincidental intensity changes of two different signals observed at coordinates ν_1 and ν_2 . Such a synchronized change, in turn, suggests the possible existence of a coupled or closely related origin of the signal variations. It is often useful to construct a correlation square, joining the pair of cross peaks located at opposite sides of the main diagonal line drawn through the corresponding autopeaks, to show the existence of coherent variations of signal intensities at these coordinates. In the example spectrum, bands A and C are synchronously correlated, as well as bands B and D. Two separate synchronous correlation squares could, therefore, be constructed. While the sign of an autopeak is always positive, the sign of a cross peak can be either positive or negative. For convenience, negative peaks (depressions in 3D) are indicated by shading.

The sign of a synchronous cross peak becomes positive if the two spectral signals, measured at the wavenumbers ν_1 and ν_2 corresponding to the coordinates of the cross peak, are either increasing or decreasing together as functions of the external variable. On the other hand, the appearance of a negative cross peak indicates that one of the signals is increasing while the other is decreasing. In the example spectrum of Fig 2. 43. the signs of cross peaks at the coordinate (A, C) and (C, A) are positive, indicating that both intensities at A and C are either increasing or decreasing together. By contrast, the cross peak signs at the coordinate (B, D) and (D, B) are negative, indicating that intensity at one band is increasing, while the other is decreasing. The correlation intensity between band A and B is very small, suggesting that the patterns of intensity changes of these two bands are substantially different. The appearance of slightly negative correlation intensity indicates that the intensities at bands A and B are probably changing in the opposite direction.

Fig 2. 36. shows an example of an **asynchronous 2D correlation spectrum**. The intensity of an asynchronous spectrum represents the non-simultaneous changes of signal intensities at ν_1 and ν_2 , occurring instead in a sequential or successive manner. The asynchronous spectrum has no autopeaks, consisting exclusively of cross peaks located at off-diagonal positions. In Fig 2. 37, asynchronous correlations are observed for band pairs A and B, A and D, B and C, as well as C and D. Unlike a synchronous 2D spectrum, an asynchronous spectrum is anti-symmetric with respect to the main diagonal line. Thus, the sign of the asynchronous peak at (A, B) is opposite to the peak sign at (B, A). By extending lines from the spectral coordinates of the pair of cross peaks to corresponding

diagonal positions, one can construct the asynchronous correlation square. An asynchronous cross peak develops only if the intensities of two signals measured at ν_1 and ν_2 change out of phase (i.e., delayed or accelerated) with each other. This feature is especially useful in differentiating overlapped bands arising from signals of different physical origins. For example, different signal contributions from individual components of a complex mixture, chemical functional groups experiencing different effects from some external field, or inhomogeneous materials comprised of multiple phases may all be effectively discriminated. Even if features are located close to each other, as long as the signatures or the pattern of signal intensity variations along the external variable are substantially different, asynchronous cross peaks will develop between their corresponding coordinates. The sign of an asynchronous cross peak can also be either positive or negative and can be used to determine the sequential order of signal changes.

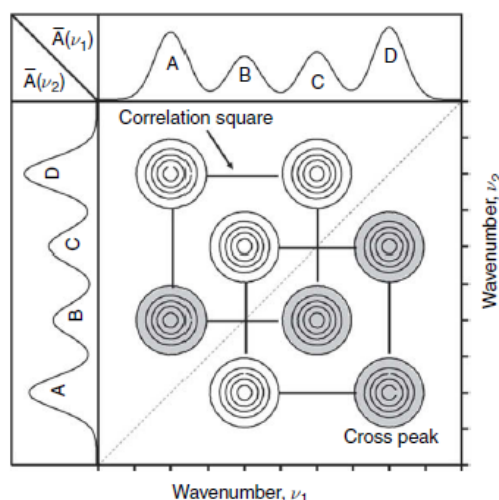


Figure 2.42. Asynchronous 2D-IR correlation spectrum, as reproduced from ref (70)

3.9.3. ANALYSIS OF 2D-IR SPECTRA ⁽⁶⁸⁻⁷¹⁾

By applying the Hilbert transform method, the synchronous and asynchronous correlation spectra of two signals 1 and 2 at different wavenumbers ν can be described by:

$$\varphi(\nu_1, \nu_2) = (T_{max} - T_{min})^{-1} \cdot \int_{T_{min}}^{T_{max}} \tilde{y}(\nu_1, t) \cdot \tilde{y}(\nu_2, t) \cdot dt \quad (2.45)$$

$$\Psi(\nu_1, \nu_2) = (T_{max} - T_{min})^{-1} \cdot \int_{T_{min}}^{T_{max}} \tilde{y}(\nu_1, t) \cdot \tilde{z}(\nu_2, t) \cdot dt \quad (2.46)$$

, where T_{min} and T_{max} are the limit temperatures of the TGA experiment, ν is the spectral variable (wavenumber in IR spectroscopy), \tilde{y} is the dynamic spectra and \tilde{z} its Hilbert transform, which expressions are shown as follows:

$$\tilde{y}(\nu, t) = \begin{cases} y(\nu, t) - \bar{y}(\nu), & t \in [T_{min}, T_{max}] \\ 0, & else \end{cases} \quad (2.47)$$

$$\tilde{z}(\nu, t) = \frac{1}{\pi} \cdot \int_{T_{min}}^{T_{max}} \tilde{y}(\nu, t') \cdot (t' - t)^{-1} \cdot dt' \quad (2.48)$$

, being \bar{y} the reference spectrum usually time-averaged as:

$$\bar{y}(\nu, t) = \int_{T_{min}}^{T_{max}} y(\nu, t') \cdot dt \quad (2.49)$$

The **rules** for determination of the sequence of spectral intensity changes are listed hereafter:

1) If the intensity in the synchronous spectrum is positive: $\varphi(\nu_1, \nu_2) > 0$

1.1.) A positive cross-peak in the asynchronous spectrum $\Psi(\nu_1, \nu_2) > 0$ states that the change in intensity of ν_1 occurs before the change in ν_2 .

1.2.) A negative cross-peak in the asynchronous spectrum $\Psi(\nu_1, \nu_2) < 0$ states that the change in intensity of ν_2 occurs before the change in ν_1 .

2) If the intensity in the synchronous spectrum is negative: $\varphi(\nu_1, \nu_2) < 0$, the rules above are reversed.

3.9.4. EXPERIMENTAL PROCEDURE

Evolved Gas Analysis (EGA) was applied to fumes released by both thermal and thermo-oxidative processes by means of coupled TGA/FT-IR. In this case, the TGA analysis was focused on a temperature range in which the main decomposition range of PET and PLA

occurred by means of a heating rate of $1\text{ }^{\circ}\text{C}\cdot\text{min}^{-1}$, according to the equipment specifications. Samples weighing $\sim 40\text{ mg}$ were heated in an alumina holder with capacity for $900\text{ }\mu\text{L}$. The flow rate of the carrier gas was set to $25\text{ mL}\cdot\text{min}^{-1}$, according to technical specifications. FT-IR gas-phase spectra were collected by a previously calibrated Thermo Nicolet 5700 FT-IR Spectrometer (MA, USA), from 4000 to 600 cm^{-1} of wavenumber, at a resolution of 4 cm^{-1} . Both transfer line and gas cell were kept at $250\text{ }^{\circ}\text{C}$ to prevent gas condensation. 16 coadded spectra were recorded every 30 s to assure accuracy of the temperature scanning. The Gram-Schmidt plots as well as its corresponding 3D and individual spectra at different constant temperatures were analyzed.



Figure 2. 43. FTIR spectrometer coupled to thermo-balance for analysis of fumes

3.10. DIFFERENTIAL SCANNING CALORIMETRY

3.10.1. FUNDAMENTALS

The Differential Scanning Calorimetry (DSC) is an analytical tool for characterizing the physical properties of a polymer, enabling the determination of melting, crystallization, and mesomorphic transition temperatures, as well as their respective enthalpy changes, and characterization of the glass transition and other effects which show either changes in heat capacity or a latent heat ⁽⁷³⁾. DSC also enables the study of the kinetics of transitions in a wide dynamic range. Because of its simplicity and ease of use DSC is widely applied in polymer science.

The essential feature of the DSC is the record of **differential measurements**, which can be registered from both isothermal and dynamic modes, by heating or cooling ramps. DSC commonly has two sample positions, one for the **sample** under investigation and the other for a **reference** sample, which is often an empty crucible or one filled with an inert material (Fig 2.44).

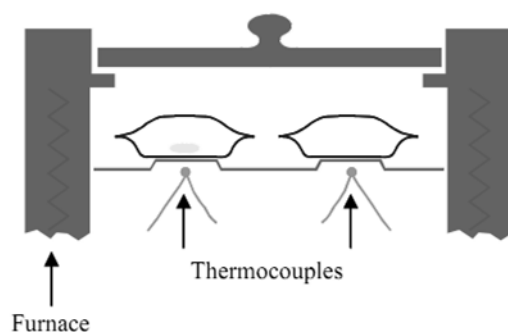


Figure 2. 44. Geometrical disposition of sample and reference holders in the DSC, as shown in ⁽⁷³⁾.

Two main **types of DSC** are distinguished: “Heat-flow” and “**Power compensation**”. In the former, the flow of heat exchange of the sample with the medium through a thermal resistance is measured. The measurement signal is a temperature difference. In the latter, more commonly used, during heating the same power is supplied to both microfurnaces through the control circuit. If there is thermal symmetry, the temperature in both microfurnaces is equal (thus there is null balance). But when an asymmetry occurs (i.e. a chemical or physical transition involves the release or absorption of heat), a temperature difference is registered between both microfurnaces containing sample and reference.

Then, this temperature difference is compensated electronically by proportional control, either increasing or decreasing the heat flow.

Thus, the differential measures, in both types of calorimeter, will be proportional to heat flow. The heat power measured in a DSC test can be related to the heat capacity C_p of a material as follows:

$$C_p = \frac{dh}{dT} \quad (2.50)$$

3.10.2. CALCULATION METHODS

Fig 2.45 shows as example the DSC curves for virgin PLA of the different spectra corresponding to first and second heatings and intermediate cooling:

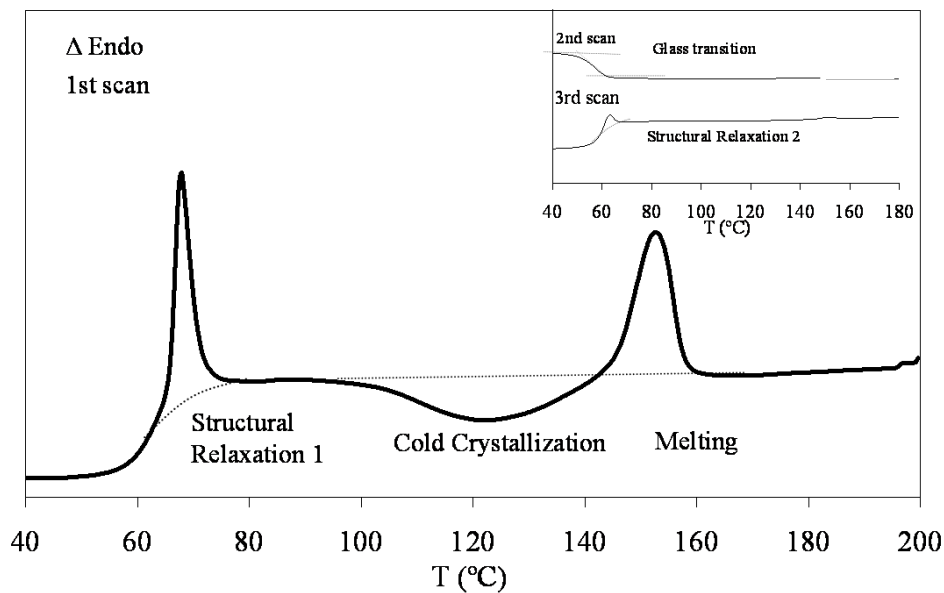


Figure 2. 45. DSC of virgin PLA

The characterization of DSC curves depends on which phenomenon is analyzed:

A. Direct parameters

- The **glass transition** is usually assessed in terms of glass transition temperature, corresponding to the midpoint of the jump in change of

capacity. Different methodologies can be found in literature, but in this work, the ISO 11357-2⁽⁷⁴⁾ was followed.

- The **crystallization** (exothermal) and **melting** (endothermal) were characterized by the induction (also named onset) and peak temperatures, as well as by the area under the thermal phenomenon, in relation to a baseline. If crystallization was produced during the heating ramp, it is known as glass- or cold- crystallization.
- The **structural relaxation** was studied on the basis of changes in the enthalpy of the endothermic phenomenon superimposed to the glass transition. Thus, the relative structural relaxation enthalpy was obtained by the subtraction of the structural relaxation enthalpy of the first scan to the one related obtained in the second heating scan

B. Amorphous and crystalline fractions

According to a three-fraction model, the relative percentages of the crystalline (X_C), mobile amorphous fraction (X_{MAF}) and rigid amorphous fraction (X_{RAF}), were calculated as follows:

$$X_C = \frac{\Delta h_m - \sum \Delta h_{CC}}{\Delta h_m^0} \quad (2.51)$$

$$X_{MAF} = \frac{\Delta C_p}{\Delta C_p^0} \quad (2.52)$$

$$X_{RAF} = 1 - X_{MAF} - X_C \quad (2.53)$$

, being Δh_m and Δh_{CC} the specific melting and cold-crystallization enthalpies ($\text{J}\cdot\text{g}^{-1}$), Δh_m^0 the melting enthalpy of the fully crystalline polymer, and ΔC_p^0 the heat capacity increment of a fully amorphous polymer

C. Lamellar thickness distribution

When a crystalline sample has finite size crystals, the melting temperature T_m is always far below the theoretical equilibrium temperature T_m^0 , the temperature at which a polymer is in its most stable energy state, forming a single crystal:

$$\Delta G_C = \Delta H_m - T \cdot \Delta S_m \rightarrow \{\Delta G_C = 0, \text{equilibrium}\} \rightarrow T_m^0 = \frac{\Delta H_m}{\Delta S_m} \quad (2.54)$$

Thus, the melting temperature T_m depends on the thickness of crystalline lamellae l_C , according to the Gibbs-Thomson equation, which is derived from free energy change given by:

$$T_m = T_m^0 \cdot \left[1 - \left(\frac{2 \cdot \sigma_e}{\Delta h_{mV} \cdot l_C} \right) \right] \quad (2.55)$$

, where T_m^0 means the equilibrium melting temperature of an infinite crystal, σ_e is the surface free energy of the basal plane where the chains fold and Δh_{mV} the melting enthalpy per volume unit.

D. Polymorphism: deconvolution of multi-peak transitions

In many cases, there are transitions that are not attributable to a single peak, which may be related to populations that have different crystal conformations. It is therefore necessary to characterize the distribution of lamellar thickness for each of the populations. Thus, several deconvolutions were applied, as shown in Fig 2.46.

The partial crystallinities of each population X_C^i were then calculated as $\Delta h_m^i / \Delta h_m$ (for i =number of populations) and the contributions of each partial crystallinity to the overall crystallinity were obtained as:

$$X_C^i = \frac{X_C^i}{X_C} \quad (2.56)$$

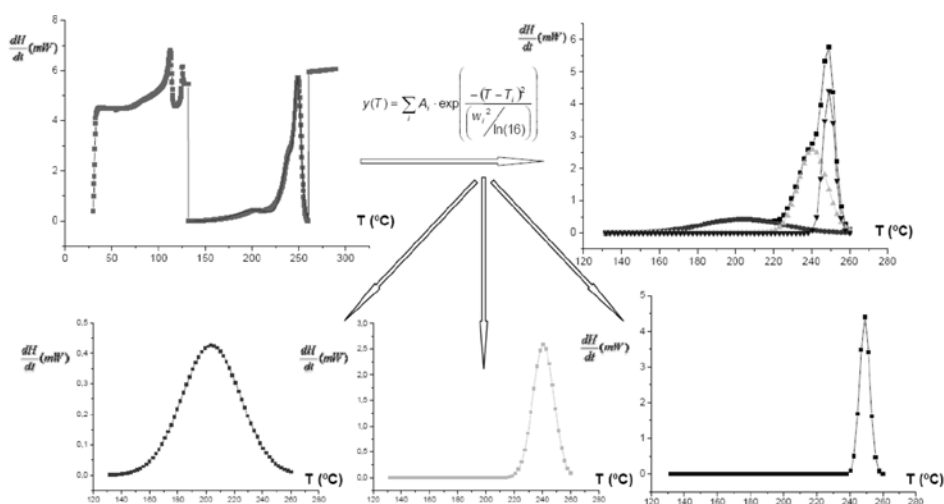


Figure 2. 46. Example of deconvolution applied to melting endotherms of multi-extruded PET

3.10.3. EXPERIMENTAL PROCEDURE

DSC analyses were carried out by a Mettler Toledo DSC 820 instrument (Columbus, OH) calibrated with indium and zinc standards. Approximately 5 mg of pellets were placed in 40 μL aluminum pans, which were sealed and pierced to allow the N_2 gas flow (50 $\text{ml}\cdot\text{min}^{-1}$). A heating/cooling/heating program with a $\pm 2^\circ\text{C}\cdot\text{min}^{-1}$ rate was employed in the temperature range between 25°C and 290°C for PET and between 0 and 200 °C for PLA. The samples were characterized at least by triplicate and the averages were taken as representative values.

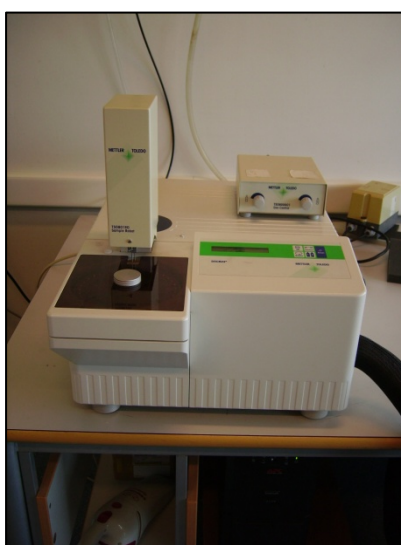


Figure 2. 47 Picture of DSC analyzer used in this thesis

3.11. DYNAMICAL – MECHANICAL - THERMAL ANALYSIS

3.11.1. FUNDAMENTALS

Dynamic Mechanical Thermal Analysis (abbreviated as DMTA, also known as Dynamic Mechanical Spectroscopy) is a technique used to study and characterize the viscoelastic behaviour of polymers. A sinusoidal stress σ is applied and the strain ε in the material is measured, allowing one to determine the complex modulus E^* . The temperature of the sample or the frequency of the stress are often varied, leading to variations in the complex modulus; this approach can be used to locate the glass-rubber relaxation of the material, as well as to identify transitions corresponding to other molecular motions. The apparent activation energy, the free volume or the fragility are other parameters that can be obtained by DMTA very valuable to assess the cooperative movement of the macromolecular chains.

A. Viscoelasticity of polymers

Polymers composed of long molecular chains have unique viscoelastic properties, which combine the characteristics of elastic solids and Newtonian fluids. The classical theory of elasticity describes the mechanical properties of **elastic solids** where stress is proportional to strain in small deformations. Such response of stress is independent of strain rate, and can be modelled by a spring.

$$\sigma = E \cdot \varepsilon \quad (2.57)$$

On the other hand, the classical theory of hydrodynamics describes the properties of **viscous fluid**, for which the response of stress is dependent on strain rate, where the constant of proportionality is known as **viscosity**, which may be modelled by a dashpot.

$$\sigma = \eta \cdot \frac{d\varepsilon}{dt} \quad (2.58)$$

The polymers, when subjected to an external action (thermal, mechanical, magnetic...), react developing processes in its structure that have the property of not adapting instantly

to a new equilibrium. These processes spend characteristic times, which are known as relaxation spectra. In addition, it has to be noticed that the response of a polymer depends on both time and temperature of application.

Specifically, the **viscoelasticity** is a molecular rearrangement. When a stress is applied to a viscoelastic material such as a polymer, parts of the long polymer chain change position. This movement or rearrangement is called creep. Polymers remain a solid material even when these parts of their chains are rearranging in order to accompany the stress, and as this occurs, it creates a back stress in the material. When the back stress has the same magnitude as the applied stress, the material no longer creeps. When the original stress is taken away, the accumulated back stresses will cause the polymer to return to its original form. The material creeps, which gives the prefix *visco-*, and the material fully recovers, which gives the suffix *-elasticity*.

B. Constitutive models of linear viscosity

Viscoelastic materials, such as amorphous or semicrystalline polymers, can be modelled in order to determine their stress or strain interactions as well as their temporal dependencies. These models, which include the Maxwell model, the Kelvin-Voigt model, and the Standard Linear Solid Model, are used to predict a material's response under different loading conditions. As introduced above, the viscoelastic behaviour has elastic and viscous components modelled as linear combinations of springs and dashpots, respectively. Each model differs in the arrangement of these elements, and all of these viscoelastic models can be equivalently modelled as electrical circuits. In an equivalent electrical circuit, stress is represented by voltage and the derivative of strain (velocity) by current. The elastic modulus of a spring is analogous to a circuit's *capacitance* (due to it stores energy) and the viscosity of a dashpot to a circuit's *resistance* (since it dissipates energy).

The simpler combinations are arranging a spring and a dashpot both in series (Maxwell model) or in parallel (Voigt-Kelvin), but further models can be also considered.

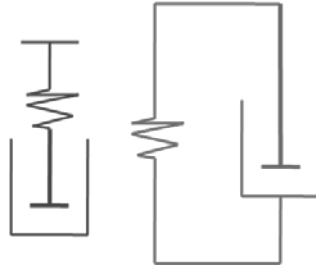


Figure 2. 48. Electric-like schemes of Maxwell (left) and Voigt-Kelvin (right) models for viscoelasticity of polymers

Maxwell model

The Maxwell model can be represented by a purely viscous dashpot (D) and a purely elastic spring (S) connected in series. The model can be represented by the following equation:

$$\frac{d\varepsilon}{dt} = \frac{d\varepsilon_S}{dt} + \frac{d\varepsilon_D}{dt} = \frac{\sigma}{\eta} + \frac{1}{E} \cdot \frac{d\sigma}{dt} \quad (2. 59)$$

Under this model, if the material is put under a constant strain, the stresses gradually relax. When a material is put under a constant stress, the strain has two components. First, an elastic component occurs instantaneously, corresponding to the spring, and relaxes immediately upon release of the stress. The second is a viscous component that grows with time as long as the stress is applied. As the total deformation is constant during the experiment, the strain rate is zero. Then from Eq. 2.59, defining the relaxation time as $\tau = \eta \cdot E^{-1}$, the Maxwell model predicts that stress decays exponentially with time, which is accurate for most polymers.

$$\sigma(t) = \sigma_0 \cdot \exp(-t/\tau) \quad (2. 60)$$

One limitation of this model is that it does not predict creep accurately. The Maxwell model for creep or constant-stress conditions postulates that strain will increase linearly with time. However, polymers for the most part show the strain rate to be decreasing with time. Application to soft solids: thermoplastic polymers in the vicinity of their melting

temperature, fresh concrete (neglecting its ageing), numerous metals at a temperature close to their melting point.

Kelvin–Voigt model

The Kelvin–Voigt model, also known as the Voigt model, consists of a Newtonian damper and Hookean elastic spring connected in parallel. It is used to explain the creep behaviour of polymers. The constitutive relation is expressed as a linear first-order differential equation:

$$\sigma(t) = E \cdot \varepsilon(t) + \eta \cdot \frac{d\varepsilon(t)}{dt} \quad (2. 61)$$

This model represents a solid undergoing reversible, viscoelastic strain. Upon application of a constant stress, the material deforms at a decreasing rate, asymptotically approaching the steady-state strain. When the stress is released, the material gradually relaxes to its undeformed state. At constant stress (creep), the model is quite realistic as it predicts strain to tend to σ/E as time continues to infinity. When the stress disappears in a recovery test, a viscoelastic expression is obtained:

$$\varepsilon(t) = \varepsilon_0 \cdot \left(1 - \exp(-t/\tau)\right) \quad (2. 62)$$

Similar to the Maxwell model, the Kelvin–Voigt model also has limitations. The model is extremely good with modelling creep in materials, but with regards to relaxation the model is much less accurate. Applications: organic polymers, rubber, wood when the load is not too high.

Generalized Maxwell Model

The Generalized Maxwell, also known as the Maxwell-Weichert model is the most general form of the models described above. It takes into account that relaxation does not occur at a single time, but at a **distribution of times**. Due to molecular segments of different lengths with shorter ones contributing less than longer ones, there is a varying time distribution. The Weichert model shows this by having as many spring-dashpot Maxwell elements as are necessary to accurately represent the distribution.

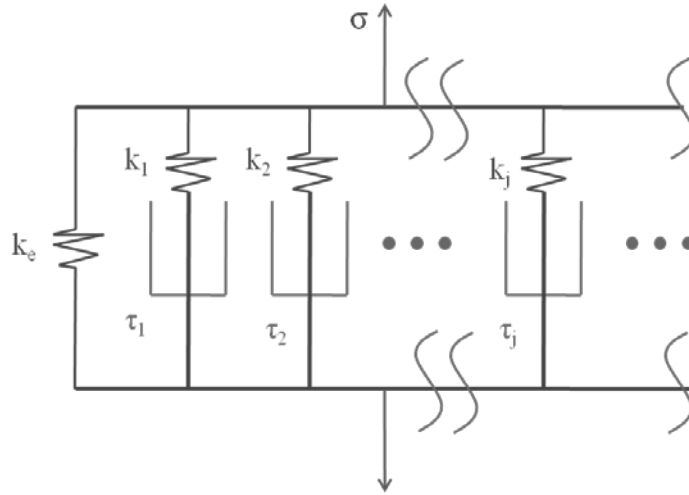


Figure 2. 49. Electric-like scheme to approach the real viscoelastic behaviour of a polymer

3.11.2. DINAMIC VISCOELASTIC MODULI OF A POLYMER

The viscoelastic property of polymer is studied by dynamic mechanical analysis where a sinusoidal force (stress σ) is applied to a material and the resulting displacement (strain ε) is measured. For a perfectly elastic solid, the resulting strain and the stress will be perfectly in phase. For a purely viscous fluid, there will be a 90 degree phase lag of strain with respect to stress. Viscoelastic polymers have the characteristics in between, where some phase lag will occur during DMA tests. Defining:

Stress $\sigma(t) = \sigma_0 \cdot \cos(\omega \cdot t + \delta)$ (2. 63)

Strain $\varepsilon(t) = \varepsilon_0 \cdot \cos(\omega \cdot t)$ (2. 64)

, where ω is frequency of strain oscillation, t is time, and δ is the phase lag between stress and strain.

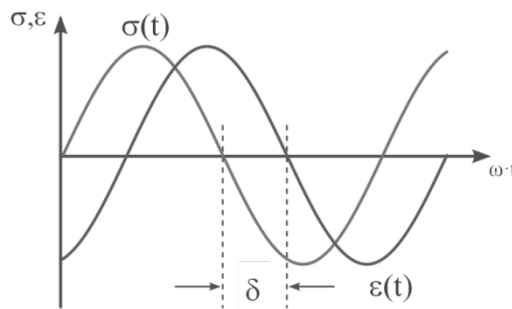


Figure 2. 50. Phase-lag between stress and strain

Combining trigonometrically both definitions, dividing by the deformation amplitude ε_0 , one arrives to:

$$\sigma(t) = \varepsilon_0 \cdot E' \cdot \cos(\omega \cdot t) + \varepsilon_0 \cdot E'' \cdot \sin(\omega \cdot t) \quad (2. 65)$$

, where the following terms are defined:

Storage modulus, which measures the stored energy, representing the elastic portion.

$$E' = \frac{\sigma_0}{\varepsilon_0} \cos(\delta) \quad (2. 66)$$

Loss modulus, which measures the energy dissipated as heat, representing the viscous portion.

$$E'' = \frac{\sigma_0}{\varepsilon_0} \sin(\delta) \quad (2. 67)$$

Loss tangent, which relates both moduli:

$$\tan(\delta) = \frac{E''}{E'} \quad (2. 68)$$

3.11.3. DMTA INSTRUMENTATION

The instrumentation of a DMTA consists of a displacement sensor such as a linear variable differential transformer, or LVDT, which measures a change in voltage as a result of the instrument probe moving through a magnetic core, a temperature control system or furnace, a drive motor (a linear motor for probe loading which provides load for the applied force), a drive shaft support and guidance system to act as a guide for the force from the motor to the sample, and sample clamps in order to hold the sample being tested. A general schematic of the primary components of a DMA instrument is shown in Fig 2.51.

Analyzers are made for both stress (force) and strain (displacement) control.

- In **strain control**, the probe is displaced and the resulting stress of the sample is measured by implementing a force balance transducer, which utilizes different shafts. The advantages of strain control include a better short time response for materials of low viscosity and experiments of stress relaxation are done with relative ease.
- In **stress control**, a set force is applied to the same and several other experimental conditions (temperature, frequency, or time) can be varied. Stress control is typically less expensive than strain control because only one shaft is needed, but this also makes it harder to use. Some advantages of stress control include the fact that the structure of the sample is less likely to be destroyed and longer relaxation times/ longer creep studies can be done with much more ease.

Two major kinds of test modes can be used to probe the viscoelastic properties of polymers: temperature sweep and **frequency sweep** tests. A third, less commonly studied test mode is dynamic stress-strain testing.

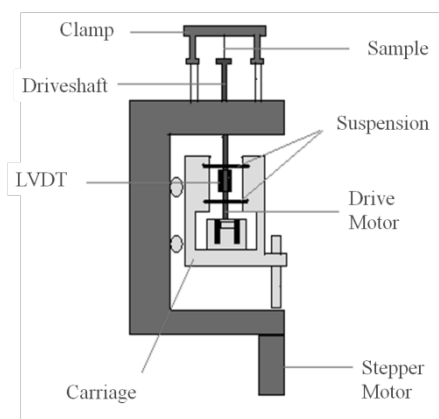


Figure 2. 51. Schematic representation of a DMTA instrument

3.11.4. THE GLASS-RUBBER RELAXATION

The study of the loss modulus (E'') by means of DMTA provides important information regarding the dynamics involved throughout the glass transition of the materials. The

strong-fragile glass former concept proposed by Angell ⁽⁷⁵⁾ was used in this work, in which the variation of the viscosity with temperature could be explained under two border limits. On the one hand, the $\tau(T)$ of a strong glass-forming behaviour can be expressed by an Arrhenius law, which reveals a strong resistance against structural changes.

$$\tau(T) = \tau_0 \cdot \exp\left(\frac{E_a}{R \cdot T}\right) \quad (2.69)$$

, where τ_0 is a time reference scale (s), R is the ideal gas constant ($8.31 \text{ J} \cdot \text{K}^{-1} \cdot \text{mol}^{-1}$) and E_a is the Arrhenius apparent activation energy obtained as:

$$E_a = R \cdot \frac{d \ln \tau}{d(1/T)} \quad (2.70)$$

On the other hand, a fragile glass-forming polymer would deviate from the thermally-activated Arrhenius behaviour, as usually happens to linear polymeric materials ⁽⁷⁶⁻⁷⁷⁾. For this reason, the temperature dependence of the relaxation times $\tau = \omega^{-1} = (2 \cdot \pi \cdot f)^{-1}$ of E'' spectra obtained during the glass transition relaxation at different angular/linear frequencies ω / f was fitted to the Vogel-Fulcher-Tamman-Hesse ⁽⁷⁸⁻⁸⁰⁾ model:

$$\tau(T) = \tau_0 \cdot \exp\left(\frac{B}{T - T_{VFTH}}\right) = \tau_0 \cdot \exp\left(\frac{D \cdot T_{VFTH}}{T - T_{VFTH}}\right) \quad (2.71)$$

, where B (K) and T_{VFTH} (K) are positive parameters specific to the material. It has been shown that T_{VFTH} is identified to the Kauzmann ⁽⁸¹⁻⁸²⁾ temperature T_K , which represents the configurational ground state temperature, at which the viscosity diverges and the excess configurational entropy vanishes ⁽⁸¹⁻⁸²⁾. It typically appears 40-60 K below the T_g . It is common to rewrite the parameter B into $B = D \cdot T_{VFTH}$, where D is an adimensional factor termed as fragility or strength parameter. Qualitatively, D is related to the topology of the theoretical potential energy surface of the system, where fragile systems ($D \leq 6$) present high density of energy minima, contrarily to strong systems ($D \geq 15$) which present lower density. As well, the so-called fragility index m permits an assessment of the deviation of $\tau(T)$ from the Arrhenius behaviour of polymers. It is defined as the characteristic slope of the fragility plot $\log \tau$ vs $T_g \cdot T^{-1}$ and varies between two limiting values of 16 and ≥ 200 for strong and fragile glass-formers, respectively ⁽⁸¹⁾⁽⁸³⁾:

$$m = \left. \frac{d \log(\tau)}{d(T_g/T)} \right|_{T=T_g} = \frac{B \cdot T}{\ln(10) \cdot (T_g - T_{VFTH})^2} \quad (2.72)$$

, considering the T_g corresponding to the experiments at $\tau \sim 100\text{-}200$ s. In this work, the peak temperature of the E'' maximum at the experiment at lower f (0.01 Hz) was considered, which were very similar to those obtained by DSC. m can be associated to the average height of the energy barrier than conformers may overcome to reach their energy minima. Shortly, a fragile glass-former experiences a dramatic loss of properties (rheological, mechanical...) throughout a specific short temperature interval, such as the glass-rubber relaxation, while a strong glass-former maintains its properties without any significant change. The influence of the chemistry of the backbone and of the side-groups on the fragility of polymers were thoroughly discussed by *Kunal et al* ⁽⁸⁴⁾, stating that fragility depended upon the relative size balance between backbone and side groups. PET, due to its characteristic rigid backbone involving aromatic rings, is inherently fragile, associated to inefficient packing of rigid chains. The apparent activation energy in this case was defined in comparison to the Arrhenius activation energy, combining Eqs. 2.69 and 2.70.

$$E_a = R \cdot \frac{d \ln \tau}{d(1/T)} = \frac{R \cdot B}{\left(1 - \frac{T_{VFTH}}{T}\right)^2} \quad (2.73)$$

As well, the free volume coefficient could be drawn from the analysis of E'' spectra, taking into account the empirical expression formulated by Doolittle ⁽⁸⁵⁾, where the relaxation times of the viscoelastic mechanism were found to behave as follows:

$$\tau(T) = CT_1 \cdot \exp\left(\frac{CT_2}{\phi \cdot T}\right) \quad (2.74)$$

, where ϕ is the free-volume coefficient given by $\phi = (v - v_0) \cdot v^{-1}$, being v and v_0 the total and occupied specific volumes, respectively; and CT_1 and CT_2 constant parameters, where the latter is close to the unity, which in comparison with VFTH equation, it gave out:

$$\phi = \frac{(T - T_{VFTH})}{B} \quad (2.75)$$

3.11.5. EXPERIMENTAL PARAMETERS

The mechanical and viscoelastic properties of neat and buried-in-soil PLA were assessed by means of a Rheometric Scientifics Dynamic-Mechanical-Thermal Analyser Mark IV (USA). On the other hand, the DMTA test were conducted in dual cantilever clamping with 15 mm of effective length between clamps, with the three point bending mode, by means of a DMA/SDTA861^e Dynamic Mechanical Analyzer, from Mettler-Toledo (OH, USA) for virgin and reprocessed PET and PLA. Experiments were carried out from 25 °C to 175°C (PET) or 130 °C (PLA) with isothermal steps of 2°C, measuring 24 frequencies (8 per decade) between 0.1 and 100 Hz. The sample was placed over a 20-mm bending platform and a 10-mm knife-edge probe tip provided the mechanical excitation. Analyses were performed at least thrice per sample and the average was taken as representative values.



Figure 2. 52. DMTA devices used in this thesis: (left) MarK IV, (right) DMA/SDTA861^e

4. REFERENCES OF THIS CHAPTER

1. Advansa. Laser + Melinar (R). Technical datasheet.
2. Catalana de Polimers, S.A. SEDAPET SP04 Technical datasheet. 2004.
3. NatureWorks®. PLA Polymer 2002D. Technical datasheet. 2005.
4. Fann DM, Huang S K, Lee J Y. *Kinetics and thermal crystallinity of recycled PET. II. Topographic study on thermal crystallinity of injection molded recycled PET.* Journal of Applied Polymer Science 61, 261-271 (1996)
5. ISO 527-2: Plastics -- Determination of tensile properties -- Part 2: Test conditions for moulding and extrusion plastics. 1993.
6. ISO 846, 1997. Plastics--determination of behaviour under the action of microorganisms. Evaluation by visual examination or measurement of changes in mass or physical properties.
7. Mettler-Toledo. Thermal analysis excellence-Brochure: Thermogravimetry for unmatched performance. 2007.
8. Stuart B H. *Polymer analysis.* John Wiley & Sons (2002)
9. ISO 1628-1. Plastics -- Determination of the viscosity of polymers in dilute solution using capillary viscometers -- Part 1: General principles.
10. Fakirov S. *Polyethylene terephthalate.* In: Olabisi O. Handbook of thermoplastics. New York : Marcel Dekker (1994)
11. Jabarin S A. *Crystallization kinetics of polyethylene terephthalate, I. Isothermal crystallization from the melt.* Journal of Applied Polymer Science 34, 85-96 (1987)
12. Spinu M, Jackson C, Keating M Y, Gardner K H. *Material Design in Poly(Lactic Acid) Systems: Block Copolymers, Star Homo- and Copolymers, and Stereocomplexes.* Journal of Macromolecular Science – Pure and Applied Chemistry 33, 1497–1530 (1996)
13. Montaudo G, Montaudo MS, Samperi F. *Matrix-Assisted Laser desorption Ionization/Mass Spectrometry of Polymers (MALDI-MS).* In: Lattimer RP, Montaudo G. Mass Spectrometry of Polymers. Boca Raton, Florida : CRC Press LLC, 2001
14. Mc Lafferty F W, Turecek F. *Interpretation of Mass Spectra.* 4th ed. Mill Valley : University Science Books (1993)
15. Johnstone R A, Malcolm E R. *Mass spectrometry for chemists and Biochemists.* 2nd. Cambridge : Cambridge University Press (1996)
16. Hoffmann E, de Charette J, Stroobant V. *Mass spectrometry: Principles and Applications.* Chichester: Wiley (1996)
17. Cottter R J. *Time-of-flight mass spectrometry.* Washignton DC : ACS Professional Reference Books (1997)

18. Polce M, Wesdemiotis C *Introduction to Mass Spectrometry of Polymers*. In: Montaudo G, Lattimer RP. *Mass Spectrometry of Polymers*. Boca Raton, Florida : CRC Press LLC (2002)
19. Montaudo G, Samperi F, Montaudo MS. *Characterization of synthetic polymers by MALDI-MS*. *Progress in Polymer Science* 31, 277-357 (2006)
20. Statheropoulos M, Georgakopoulos K, Giorgio G. *The Interpretation of Mass Spectra of Polymers using a Hybrid Software System based on Library Searching and Euristic*. *Journal of Analytical and Applied Pyrolysis* 5, 1 (1985)
21. Garozzo D, Montaudo G. *Identification of Polymers by Library Search of Pyrolysis Mass Spectra and Pattern Recognition Analysis*. *Journal of Analytical and Applied Pyrolysis* 6, 1 (1985)
22. Nielen MWF. *MALDI Time-Of-Flight Mass Spectrometry of Synthetic Polymers* *Mass Spectrometry Reviews* 18, 309-344 (1999)
23. Montaudo G, Montaudo MS, Samperi F. *Matrix-Assisted Laser Desorption Ionization/Mass Spectrometry of Polymers (MALDI-MS)*. In: Lattimer RP, Montaudo G. *Mass Spectrometry of Polymers*. Boca Raton, Florida : CRC Press LLC (2001)
24. Rader H I, Schrepp W. *MALDI-TOF mass spectrometry in the Analysis of Synthetic Polymers*. 1998, *Acta Polymerica* 49, 272 (1998)
25. Hoteling AJ, Mourey TH, Owens KG. *Importance of solubility in the Sample Preparation of Poly(ethylene terephthalate) for MALDI-TOF-MS* *Analytical Chemistry* 76, 750-756 (2005)
26. Danis PO, Karr DE. *A facile sample preparation for the analysis of synthetic organic polymers by Matrix-Assisted Laser Desorption/Ionization*. *Organic Mass Spectrometry* 28, 923-925 (1993)
27. Lloyd PM, Scrivener E, Maloney DR, Haddleton DM, Derrick PJ. *Cation Attachment to Synthetic Polymers in Matrix-assisted Laser Desorption/Ionization Mass Spectrometry*. *Polymer preprint* 37, 847-848 (1996)
28. King RC, Goldschmidt R, Xiong Y, Owens KG, Atlanta GA. *Mechanistic studies of the Cationization of Synthetic Polymers by Alkali Metals in the Matrix-Assisted Laser Desorption/Ionization experiment*. 43rd ASMS Conference in Mass Spectrometry. 1237 (1995)
29. Xu N, Huang ZW, Throck-Watson J, Gage DA. *Mercaptobenzothiazoles: a new class of matrices for Laser Desorption Ionization Mass Spectrometry*. *Journal of the American Society of Mass Spectrometry* 8, 116 (1997)
30. Montaudo G, Samperi F, Montaudo MS. *Characterization of synthetic polymers by MALDI-MS*. *Progress in Polymer Science* 31, 277-357 (2006)
31. Mukerjee R, Jeff-Wu, CF. *A modern theory of factorial design*. New York : Springer Science+Bussines Media Inc. (2006)
32. Weber D , Skillings J H. *A first course in the design of experiments*. Boca Ratón, Florida : CRC Press LLC (2000)

33. Pukelsheim H. *Optimal Design of experiments*. Philadelphia (PA) : Society for Industrial and applied Mathematics (2006)
34. Antony J. *Design of Experiments for engineers and scientists*. Oxford : Butterworth-Heinemann publications (2003)
35. Box G E, Hunter J S , Hunter W G. *Statistics for experimenters. Design, innovation and discovery*. New Jersey : John Wiley & sons (2005)
36. Montaudo G. *Mass spectrometry of synthetic polymers: mere advances or revolution?* Trends in Polymer Science 4, 81-86 (1996)
37. Cox J N. *FTIR: Fourier Transform Infrared Spectroscopy*. In: Brundle C R, Evans A y S Wilson S. Encyclopaedia of materials characterization: surfaces, interfaces, thin films. Greenwich : Gulf Professional Publishing (1992)
38. Department of chemistry and biochemistry. University of Colorado. *Infrared Spectroscopy: Theory*. Online edition for organic chemistry lab courses (2002)
39. Cole K C, Guèvremont J, Ajji A, Dumoulin M M, *Characterization of Surface Orientation in Poly(ethylene terephthalate) by Front-Surface Reflection Infrared Spectroscopy* Applied. Spectroscopy 48, 1513-1521 (1994)
40. Walls D J. *Application of ATR-IR to the Analysis of Surface Structure and Orientation in Uniaxially Drawn Poly(ethylene terephthalate)*, Journal of Applied Spectroscopy 45, 1193-1198 (1991).
41. Kister G, Cassanas G, Vert M. *Effects of morphology, conformation and configuration on the IR and Raman spectra of various poly(lactic acid)s* , Polymer 39, 267-272 (1998)
42. Wells O C. *Scanning Electron Microscopy*. Encyclopaedia of Materials: Science and Technology. Elsevier Science Ltd. (2001)
43. ISO 1133. *Plastics -- Determination of the melt mass-flow rate (MFR) and the melt volume-flow rate (MVR) of thermoplastic*. 2005.
44. Beer & Johnston, *Mechanics of Materials*. McGraw Hill. (2006)
45. Davis J R, *Tensile testing* , ASM International, (2004)
46. ISO 527-1. *Plastics -- Determination of tensile properties -- Part 1: General principles*. (1993)
47. ISO 291. *Plastics - standard atmospheres for conditioning and testing* (1997)
48. Meyers M A, Kumar C K. *Mechanical Behaviours of Materials*. Prentice Hall (1998)
49. ISO 179. *Plastics -- Determination of Charpy impact properties* (1996).
50. Wunderlich, B. *Thermal analysis of polymeric materials*. Berlin : Springer (2005)
51. Khawan A, Flanagan D R. *Solid-State Kinetic Models: Basics and Mathematical Fundamentals*. Journal of Physical Chemistry B 110, 17315-17328 (2006)

52. Pérez-Maqueda L A, Sánchez-Jiménez P E, Criado J M. *Kinetic analysis of solid-state reactions: precision of the activation of the activation energy calculated by integral methods.* International Journal of Chemical Kinetics 37, 658-666 (2005)
53. Senum G I, Yang R T. *Rational approximations of the integral of the Arrhenius function.* Journal of Thermal Analysis and Calorimetry 11, 446 (1977)
54. Pérez-Maqueda L A, Criado J M. *The accuracy of Senum and Yang's approximations to the Arrhenius Integral.* Journal of Thermal Analysis and Calorimetry 60, 909-915 (2000)
55. Flynn J H, Wall L A. *A quick, direct method for the determination of activation energy from thermogravimetric data.* Journal of Polymer Science 4, 323-342 (1966)
56. Ozawa T. *Kinetic analysis of derivative curves in thermal analysis.* Journal of Thermal Analysis 2, 301 (1970)
57. Doyle C D. *Series approximations to the equation of thermogravimetric data.* Nature, 207, 209 (1965)
58. Kissinger H E. *Reaction kinetics in differential thermal analysis.* Analytical Chemistry 29, 1702-1706 (1957)
59. Akahira T, Sunose T. Res. Rep. Chiba Inst. Technol., 16, 22-31 (1971)
60. Friedman H L, *Kinetics and gaseous products of thermal decomposition of polymers.* Journal of Macromolecular Science Part A 1,57-79 (1967)
61. Vyazovkin S , Dollimore D. *Linear and non-linear procedures in isoconversional computations of the activation energy of non-isothermal reactions in solids.* Journal of Chemical Information and Modelling 36, 42-45 (1996)
62. Vyazovkin S. *Advanced Isoconversional Method.* Journal of Thermal Analysis 49, 1493-1499 (1997)
63. Gotor F J, Criado J M, Malek J, Koga N. *Kinetic Analysis of Solid-State Reactions: The Universality of Master Plots for Analyzing Isothermal and Nonisothermal Experiments.* The Journal of Physical Chemistry A 104 , 10777-10782 (2000)
64. Ozawa T. *A New Method of Analyzing Thermogravimetric Data.* Bulletin of the Chemical Society of Japan, 38, 1881 (1965)
65. Ozawa T. *Non-isothermal kinetics and generalized time.* Thermochemica Acta, 100, 109. (1986)
66. Pérez-Maqueda L A, Criado J M, Gotor F. J, Málek J. *Advantages of combined kinetic analysis of experimental data obtained under any heating profile.* The Journal of Physical Chemistry A 106 , 2862-2868 (2002)
67. Coats A W, Redfern J P. *Kinetic analysis from thermogravimetric data.* Nature 68, 4914 (1964)
68. Noda I. *Two-Dimensional Infrared (2D IR) Spectroscopy: Theory and Applications.* Applied Spectroscopy 44, 550-561 (1990)

69. Noda I. *Generalized Two-Dimensional Correlation Method applicable to Infrared, Raman, and other types of Spectroscopy*, Applied Spectroscopy 47, 1329-1336 (1993)
70. Noda I. *Recent developments in two-dimensional infrared (2D IR) correlation spectroscopy*. Applied Spectroscopy 47, 1317-1323 (1993)
71. Xiaoming D, Bo Y, Haiying Z, Guangzhong Y, Ozaki Y. *Generalized two-dimensional correlation spectroscopy - Theory and applications in analytical field*. Science in China Serie B: Chemistry 47, 257-266 (2004)
72. Materazzi S, Gentili A, Curini R. *Applications of evolved gas analysis: Part 1: EGA by infrared spectroscopy*. Talanta 68, 489-496 (2006)
73. Schick C, *Differential Scanning Calorimetry (DSC) of semicrystalline polymers*. Analytical and Bioanalytical Chemistry 395, 1589-1611 (2009)
74. ISO 11357-2 Plastics. *Differential Scanning Calorimetry. Part 2- Determination of the glass transition*. (1999)
75. Angell C A. *Relaxation in liquids, polymers and plastic crystals - strong/fragile patterns and problems*. Journal of Non-Crystalline Solids 131-133, 13 (1991)
76. Godard M.E., Saiter J.M. *Fragility and non-linearity in polymethyl(α -n-alkyl) acrylates*. Journal of Non-Crystalline Solids 235, 635-639 (1998)
77. Saiter A, Hess M, D'Souza N. A, Saiter J. M. *Entropy and fragility in vitreous polymers*. Polymer 43, 7497 (2002)
78. Vogel H, *The temperature dependence law of the viscosity of fluids*. Phys Z 22, 645-646. (1921)
79. Fulcher G.S. *Analysis of recent measurements of the viscosity of glasses*. Journal of the American Ceramic Society 8, 339-355 (1925)
80. Tammann G, Hesse G. *The dependence of viscosity upon temperature of supercooled liquids*. Z Anorg Allg Chem. 156, 245-257 (1926)
81. Bohmer R, Angell C.A. In: Richert R, Blumen A, *Disorder effects on relaxational processes*, Springer, Berlin (1994)
82. Scherer G W. *Theories of relaxation*. Journal of Non-Crystalline Solids 123, 75-89 (1990)
83. Vilgis T.A. *Strong and fragile glasses: A powerful classification and its consequences*. Physical Review B 47, 2882-2885 (1993)
84. Kunal K, Robertson C. G, Pawlus S, Hahn S. F, Sokolov A. P. *Role of Chemical Structure in Fragility of Polymers: A Qualitative Picture*. Macromolecules 41, 7232-7238 (2008)
85. Doolittle A.K. *Studies in Newtonian flow. II. The dependence of the viscosity of liquids on free-space*. Journal of Applied Physics 22, 1471-1475 (1951)

CHAPTER III

MATERIAL VALORISATION

Studies of mechanical recycling on PET and
PLA

CHAPTER III: MATERIAL VALORISATION

CONTENTS

1. Introduction	165
2. Reusing and primary recycling	167
3. Mechanical recycling	169
3.1. Types of plastic solid waste fractions	171
3.2. Mechanical recycling process	173
4. Mechanical recycling of PET	177
4.1. Contamination of recycled PET	178
4.2. Specific super-clean decontamination processes for PET	182
4.3. Use and sustainability of recycled PET	184
4.4. Use of recycled PET in food applications	187
4.5. The PET recycling system in Spain	188
4.6. The thermo-mechanical degradation of PET	191
5. Mechanical recycling of PLA	195
6. References in this chapter	199
7. Contributions in this thesis	203
CONTRIBUTION III-A: <i>Thermal analysis as a quality tool for assessing the influence of thermo-mechanical degradation on recycled poly(ethylene terephthalate)</i>	207
CONTRIBUTION III-B: <i>A statistical design of experiments for optimizing the MALDI-TOF-MS sample preparation of polymers. An application in the assessment of the thermo-mechanical degradation mechanisms of poly (ethylene terephthalate)</i>	217

CONTRIBUTION III-C: <i>The role of crystalline, mobile amorphous and rigid amorphous fractions on the performance of recycled poly (ethylene terephthalate) (PET)</i>	231
CONTRIBUTION III-D: <i>Assessing the MALDI-TOF MS sample preparation procedure to analyze the influence of thermo-oxidative ageing and thermo-mechanical degradation on poly (lactide)</i>	255
CONTRIBUTION III-E: <i>Material valorisation of amorphous polylactide. Influence of thermo-mechanical degradation on the morphology, segmental dynamics, thermal and mechanical performance</i>	271
8. Remarkable results	289

1. INTRODUCTION

The **material valorisation** involves the management of plastic solid waste (PSW) by means of any of the procedures commonly known as R-options: Reuse and Recycle (the third R, Recover would actually be the general concept behind all valorisation options: biological, material and/or energetic).

The **reuse** of materials is the most effective recovering option; since there would be no collecting, processing and/or redistribution involved in the management of goods that could be just extend their service lives. This would be the case in durable and resistant applications such as boxes or pallets in the distribution sector. As well, another R to add to the valorisation philosophy would be the **reduction** in origin, which means the design of goods with less amount and variety of plastics without losing performance. Once all the efforts have been driven towards the reduction and further reuse of polymers is not feasible, the goods have to be considered as waste. In this moment, the **recycling** of the material takes place. Note that the terms *recovering*, *recycling* and *material valorisation* merge in this case to the same idea (“from a material, obtaining another material”) and are indiscriminately used in literature. Even more, the material valorisation would not only comprise the obtaining of a material with similar properties than the used one by means of mechanical procedures; it would also involve the obtaining of the raw components of the plastic by means of chemical processes, which is also known as *chemical recycling*.

Figure 3.1 shows a schematic overview of the material valorisation options for the waste management of plastics. In this chapter, since the recovering of materials is performed by means of mechanical procedures, the term used is **mechanical recycling**. Thus, a short description of the current technologies for the mechanical recycling is given hereafter. As well, a review of the most important studies on the thermo-mechanical degradation of PET and PLA is addressed. Finally, the contributions of this thesis related to the mechanical recycling of both polymers are discussed in detail.

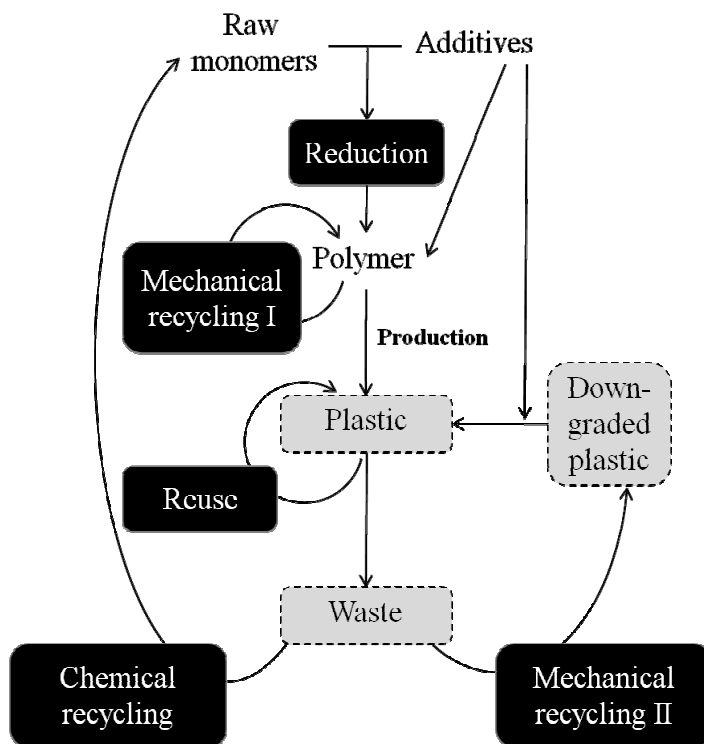


Figure 3.1. General scheme of material valorisation

2. REUSING AND PRIMARY RECYCLING

Plastics are used in a large number of applications on a daily basis and thus some items end up in the waste stream after a single use (single-life or cycle) or a short time after purchase, such as food packaging. Reusing plastic is preferable to recycling as it uses less energy and fewer resources⁽¹⁾. Generally, reusing has some advantages:

- Conservation of fossil fuels since plastic production uses 4–8% of global oil production, i.e. 4% as feedstock and 4% during conversion⁽²⁾
- Reduction of Plastic Solid Waste (PSW).
- Reduction of energy in comparison to other recycling processes.
- Reduction of carbon-dioxide (CO₂), nitrogen-oxides (NO_x) and sulphur-dioxide (SO₂) emissions.

Primary mechanical recycling (shown in Fig 3.1 as *Mechanical Recycling I*), better known as re-extrusion, is the re-introduction of scrap, industrial or single-polymer plastic edges and parts to the extrusion cycle in order to produce products of the similar material. This process utilizes scrap plastics that have similar features to the original products⁽³⁾. Primary mechanical recycling is only feasible with semi-clean scrap, therefore making it an unpopular choice within recyclers. Materials that do not meet the specifications are palletised and reintroduced into the recycling loop or at the final stages of the manufacturing. According to *Al Salem et al*⁽¹⁾, most of the PSW being recycled is of process scrap from industry recycled via primary recycling techniques.

3. MECHANICAL RECYCLING

Mechanical recycling, also known as secondary recycling (shown in Fig 3.1. as *Mechanical Recycling II*), is the process of recovering plastic solid waste (PSW) for the re-use in manufacturing plastic products via mechanical means⁽⁴⁾. Its promotion was mainly taken worldly during the 1970s. Potential mechanical recycling of PSW can only be performed on single-polymer plastics streams, namely PE, PP, PS, PET etc. The more complex and contaminated the waste, the more difficult it is to recycle it mechanically.

The removal of plastic waste flow of urban waste depends largely on the profit from sale. Consecutively, the supply of material for recycling should be granted at zero costs, taking into account ⁽⁵⁾ both the economic benefit of saving by not going to landfill, and the environmental benefit to exploit the material or the energy contained in these materials. As pointed out in Chapter I, a successful mechanical recycling will be achieved only if a commitment between administrations, waste managers and householders is assured (Fig3.2.)



Figure 3.2. Material cycle of a plastic package, as adapted from ref (6)

Mechanical recycling opens an economic and viable route for PSW recovery, especially for the case of foams and rigid plastics⁽⁷⁾. A number of products found in our daily lives come from mechanical recycling processes, such as grocery bags, pipes, gutters, window and door profiles, shutters and blinds, etc. The quality is the main issue when dealing with mechanically recycled products. The industrial PSW generated in manufacturing, processing, and distribution of plastic products is well suited for the use as a raw material for mechanical recycling due to the clear separation of different types of resins, the low level of dirt and impurities present, and their availability in large quantities ⁽¹⁾. Mechanical recycling of PSW has also become an important issue in R&D, where numerous researchers have devoted their efforts to⁽¹⁾.

The **demand for recycled materials** is increasing largely⁽⁸⁾ due to the packers want to use an environmentally more attractive package, with the inclusion of recycled content in their formulations. Besides this, there are other incentives that may encourage recycling, such as a higher landfill fees, legislation requiring recycled content, increased market demand for products with recycled material or a possible increase of the price of oil, bringing the price of the virgin material to higher values than those of the recycled material.

Despite the potential of recycling, there exist several **obstacles and drawbacks** for its correct implementation, as for example ⁽⁵⁾:

- Lack of social awareness.
- The low price of oil makes the virgin material is much cheaper than the recycled material, which is not conducive to recycling.
- The plastic container is never returnable and as low density increases the cost, as they have a high volume, previous grinding for transport to recycling centres is necessary.
- Plastic waste usually cannot be recycled directly, as they tend to be mixed and / or contaminated. This requires an absolute separation, complicating their collection, in addition to washing and use of additives to obtain high-quality waste.
- The majority of plastic waste is present in the film type, very difficult to recover.

- The recycled material cannot be totally re-used in the manufacture of new packaging for food for health reasons and should be used for other items.
- Poor quality products are obtained, which limits their applications. Gama of grades reduced.
- The volume of recycled material cannot be ensured to the supplier, in contrast to virgin material.

These drawbacks have to be overcome in order to achieve higher rates of mechanical recycling, as in European countries such as Germany, as shown in Fig 3.3., with the aim of reducing considerably the rate of landfilling still used in Spain.

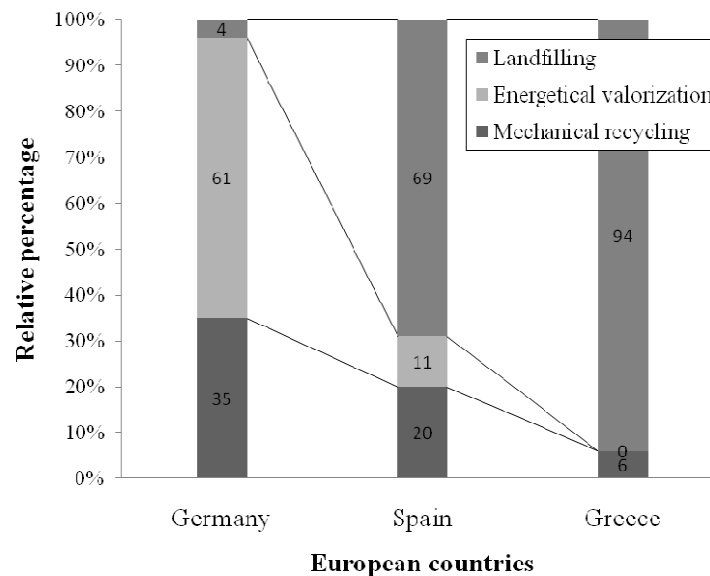


Figure 3.3. PSW management options in Spain in comparison with the European countries with highest and lowest mechanical recycling percentages. Adapted from PlasticsEurope report (9).

3.1. TYPES OF PLASTIC SOLID WASTE FRACTIONS

Separation, washing and preparation of PSW are all essential to produce high quality, clear, clean and homogenous end-products⁽¹⁾. Each source of plastic waste has its own characteristics, and therefore they should be perfectly identified before reintroduction into a processing system. Different groups can be distinguished⁽⁵⁾:

Industrial waste (scrap)

In all transformation processes there is inevitably a generation of waste originating from cuts, quality control rejection, off-spec material, etc. Most transformers return its industrial plastic waste in the production line, being a clean and homogeneous material. The only process that is required is to regrind these wastes. With no waste generated is a "clean technology."

Post-consumer waste

This is waste of plastic products that have been used for a particular application, have completed their life cycle and can be recovered for additional employment. One can distinguish three types:

- ***industrial waste / commercial***

They are plastics that have been used by industry or commerce to the tasks of distribution and transportation of items such as plastic film used as a cover to wrap pallets or other packaging systems. These wastes are usually clean and essentially homogeneous nature which facilitates the further work of recycling. These wastes are bags, cans and containers for the chemical and food packaging foils, obsolete industrial equipment, boxes, etc. The main plastics used are PE, PP, PS and PVC. This sector produces large quantities of plastic waste that are only inferior to those that appear in the RSU.

- ***agricultural residues***

Among the products with an intermediate lifetime one may include the irrigation pipes and valves, containers, drums and tanks. They are highly contaminated by land, so that the washing operation in the recycling stage is crucial for success in the final pellet. Among the short-lived products include plastic sheet to cover greenhouses and bags for fertilizers.

- ***household waste or municipal solid waste (MSW)***

They are usually food packaging, cleaning products, perfumes and household products in general. They go into household waste with food waste and other containers of paper, cardboard, glass, metal, etc. The mixture and diversity of material affects the recovery of plastic materials present more complex than in previous cases. Selective collection

favours the optimization of recycling, from the beginning to get a degree of separation. Municipal solid waste (MSW) has a plastic content of only about 8%. Plastics which are among the MSW are estimated at 65% to PE, 15% to PS / EPS, 10% PVC and 5% for PET⁽⁵⁾. They are usually difficult to identify.

3.2. MECHANICAL RECYCLING PROCESS

Recycling PSW via mechanical means involves a number of treatments and preparation steps to be considered. The most general scheme was described by *Aznar et al.*⁽¹⁰⁾ and is illustrated in Fig 3.4.

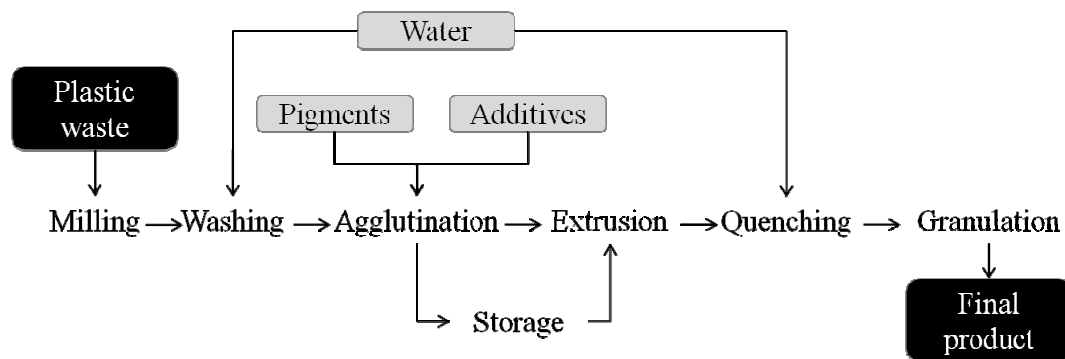


Figure3.4. Mechanical recycling steps as described by *Aznar et al.*⁽¹⁰⁾

The steps involved are usually the following⁽¹⁰⁾:

- 1) **Cutting/shredding:** Large plastic parts are cut by shear or saw for further processing into chopped small pellets, powder or flakes. This is usually achieved by milling, grinding or shredding⁽⁷⁾.
- 2) **Contaminant separation:** Paper, dust and other forms of impurities are separated from plastic usually in a cyclone.
- 3) **Floating:** Different types of plastic flakes are separated in a floating tank according to their density.

4) **Milling:** Separate, single-polymer plastics are milled together. This step is usually taken as a first step with many recyclers around the world.

5) **Washing and drying:** This step refers to the pre-washing stage (beginning of the washing line). The actual plastic washing process occurs afterwards if further treatment is required. Both washing stages are executed with water. Chemical washing is also used in certain cases (mainly for glue removal from plastic), where caustic soda and surfactants are used.

6) **Agglutination:** The product is gathered and collected either to be stored and sold later on after the addition of pigments and additives, or sent for further processing.

7) **Extrusion:** The plastic is extruded to strands and then pelletised to produce a single- polymer plastic.

8) **Quenching:** Involves water-cooling the plastic by water to be granulated and sold as a final product.

Further reading on the procedures of sorting and pre-treatments of PSW is recommended (1,11).

The applications of recycled polymers are usually driven to less-demanding performances. A valid example of utilizing PSW is the recycling of PET. For example, about three-quarters of reclaimed PET in the UK and USA are then sent to textile and sheet-making plants, where they are again molten to produce textile and sheet products by resin moulding techniques well established for PET and other plastics conversion. These techniques could be summarized as follows⁽¹⁾:

- **Extrusion moulding:** the resin or PSW flakes are molten and extruded through a mould by single or twin screws to form a moulded product. Products from this process include pipes, sheets, film and wire covering.
- **Injection moulding:** heated molten resin is injected into a mould to solidify and form the product desired. Products made this way range from washbowls, buckets and plastic models to larger products such as bumpers and pallets.

- **Blow moulding:** a *parison* (hollow plastic melt) obtained by extrusion or injection moulding is clamped in a mould, and inflated with air to make bottles for all kinds of uses, such as shampoo bottles. PET bottles are made by means of stretch blow moulding so as to make them less likely to rupture.
- **Vacuum moulding:** a heat-softened sheet is sandwiched in a mould, and the space between the sheet and mould sealed and evacuated to form products such as cups and trays.
- **Inflation moulding:** extrusion moulding where a molten resin is inflated into a cylinder to form a film. This method is used to make products such as shopping bags.

4. MECHANICAL RECYCLING OF PET

The first reported PET bottle recycling process was established by a company named St. Jude Polymers in 1976, that began recycling PET bottles into plastic strapping and paint brush bristles. The next year, St. Jude became the first to “re-pelletise” post-consumer PET plastic, which moved PET remanufacturing companies relying on plastic in pelletised form for their processes, thus increasing the variety of products that could be made from recycled, post-consumer PET plastic ⁽¹²⁾.

A major push in the development of both the demand and the capacity for post-consumer PET recycling occurred when a major plastic fibre manufacturer named Wellman, Inc. entered the picture in 1978, and began recycling PET bottles into a fibre product that was suitable for both carpet and fibrefill applications. Wellman continued to increase its use of recycled PET and throughout the 1980s and early 1990s increased their processing capacity and consequently the market demand for post-consumer PET. An important factor in Wellman’s development of post-consumer PET processing capacity was the integration of the recycled PET processed into its own product lines. Another was the development of the first textile fibre manufactured from 100% recycled PET in 1993, called “Eco Spun,” which is now a familiar fabric material particularly in sportswear where it was first used. Today, St. Jude and Wellman are joined by more than a dozen other companies, whose combined PET recycling processing capacity produces over 1/4million tones of recycled PET resin annually ⁽¹²⁾.

With recent **advances in PET recycling technology**, it is now possible to close the material loop, by recycling bottles and containers back into bottles and containers, even in some food-contact packaging applications. In the USA, the federal Food and Drug Administration (FDA) issued “letters of non-objection (NOL)” for the use of post-consumer PET in a number of food-contact packaging applications, which greatly increased the demand for recycled PET plastic and the ability to produce new PET packages from 100%, post-consumer recycled PET plastic. In this way, there are three generic types of food-contact packaging applications/processes for which the use of post-consumer recycled PET were issued NOL ⁽¹²⁾:

- depolymerization processes which chemically break down PET plastic into its component chemicals, to be used as raw monomers;
- multi-layer, or laminated food-contact containers where post-consumer PET is combined with a virgin PET food-contact layer;
- full-contact food packaging containers where 100% post-consumer PET is used.

Food-contact packaging applications are one of the largest uses of PET plastic resin. The ability to recycle these food-contact packages back into new PET food-contact packages will help ensure the long-term viability of PET plastics recycling and the ability to avoid the use of virgin PET in food contact package manufacturing.

The value of the post-consumer PET plastic and its ability to be economically remanufactured into new products is dependent on the quality of the material as it passes through the recycling process

4.1. CONTAMINATION OF RECYCLED PET

In general, plastics intermediate processors receive plastic containers (primarily in baled form, but in some cases loose) that have been separated from other recyclable materials at Municipal Reclamation Facilities (MRFs), buy-back or drop-off centres, and then granulate them for sale as dirty regrind to reclaimers and end-users. In most cases, plastic intermediate processors take in loose plastic bottles and produce baled plastics for sale to Plastic Reclamation Facilities (PRFs), reclaimers or end-users. Most PRFs are designed to separate plastics into their individual resin categories, and then further separate each plastic resin type by colour or other market specification parameters. These colour segregated plastic resins are then fed into granulators at PRFs or reclaimers to produce dirty regrind. Another major function of the plastics intermediate processor is the **sorting and removal of contaminants** from the plastic resin streams they process.

Contamination limits the ultimate marketability of the full range of PET plastic containers collected by local recycling programs. Contamination reduces the value of recyclable PET, since it hinders processing and causes unproductive downtime and clean-up expenses for PET processors, reclaimers and end-users; and thus results in unnecessary

manufacturing waste from the PET recycling process. Actually, PET containers can be confused with food and liquid containers that are made from other plastic resins that pose major contamination problems for the PET recycling process. In addition, some PET containers are manufactured with barrier resins, closures, labels, safety seals, or contain product residues which can introduce incompatible materials that contaminate the PET recycling process. The increase in recycling collection programs that commingle different kinds of recyclable materials can also introduce non-plastic contaminants, like broken glass, or dirt.

Packaging manufacturers are establishing to adopt **design for recycling** criteria that aim to limit the package's impact on the overall recycling process. Many materials that cause contamination troubles for PET recycling are contained in the PET bottle itself. As a general rule, the best practice for reducing the incidence of these contaminants is to design PET bottles and containers that do not contain materials that contaminate the PET recycling process.

However, even after applying good practices in design for recycling, several contaminants can affect the quality of recycled PET. A short list is considered hereafter:

A. Polyvinyl chloride (PVC)

The primary contaminant to the PET recycling process is any source of polyvinyl chloride (PVC) plastic resin, since during reprocessing and remanufacturing post-consumer PET resin, even at very low concentrations, PVC can form acids. These acids break down the physical and chemical structure of PET, causing it to turn yellow and brittle, which would render the PET material unacceptable for many high-value end-use applications. In addition, the presence of PVC may result in out gassing of chlorine vapours during certain stages of PET reprocessing that may increase the cost of control systems or regulatory compliance for the facility operator.

B. Other Resins

The presence of plastic resins other than PET may also pose problems in the processing and remanufacture of PET. While some of these are acceptable to the PET recycling industry, many are not. The presence of **caps** may introduce plastics other than PVC that may contaminate the PET recycling process or add separation costs. In addition, some

are made of aluminium, which can introduce problems for some PET reclaimers and end-users or increase cleaning costs.

C. Distinct PET grades

There are a growing number of PET containers and other PET packaging materials which are marked with the SPI (Society of Plastic Industry) #1 resin identification code that pose a number of specific problems to PET reclaimers.



Figure 3.5. SPI identification code for PET.

In some cases these containers are manufactured with modified PET plastic resins or in laminated forms that contain barrier resins that are either incompatible with the recycling of bottle-grade PET plastic resin, or are difficult to distinguish from acceptable materials with current sorting technology. These modified PET resins may have physical or chemical properties that make them incompatible with bottle-grade PET resin during the recycling process. A brief description of the most common incompatible items is listed as follows:

- **PET Microwave Trays**, which are manufactured from crystallized PET, known as C-PET, and are incompatible with bottle-grade PET resin and must be excluded. These C-PET trays are often solidly pigmented (opaque), adding to their incompatibility.
- **PET Drinking glasses**, “Clamshells,” and “Blister-pack” which are manufactured from A-PET (amorphous PET).
- **PET salad/food take-out trays**, the clear plastic thermoformed cover affixed to a cardboard placard containing a product. While some of these materials are

technically compatible with the recycling of bottle-grade PET, there are “look-alike” packaging items that are made from incompatible resins, such as oriented polystyrene, that current sorting technology cannot distinguish from PET, and must be excluded.

- **PET Laundry Scoops** - plastic laundry scoops with the SPI #1 (PETE) recycling code should also be excluded from the PET mixture. While technically it is possible to recycle laundry scoops with PET bottles if they are clear or transparent green, it is best to exclude them as many laundry scoops are opaque and may introduce contaminants due to pigmentation.
- **Glycol-modified PET (PET-G)**. PET-G containers are manufactured differently than other PET containers and are generically known as extrusion-blown containers (referred to as E-PET containers). PET-G and other E-PET containers have a lower melting point than bottle-grade PET resin and can cause a number of technical and operating problems to PET reclaimers. Many of these PET-G and other E-PET containers are marked with the SPI #1 resin identification code and are difficult to distinguish from PET bottles that are acceptable for recycling, even with automated sorting technology.
- **Multi-layer PET containers** - an increasing number of PET containers on the market are manufactured with a multi-layer construction. Some of these containers are manufactured with a barrier resin known as ethyl vinyl alcohol (EVOH). The presence of EVOH is a problem for some reclaimers as it affects the clarity of the finished product or can cause a change in the intrinsic viscosity (IV) of the recycled PET that renders it unacceptable for certain end-use applications. Like PET-G, however, it is very difficult to distinguish a multi-layer PET container from a single-layer PET container. Once again, it is important to determine whether a particular purchaser has any specific restrictions on the presence of these materials.
- **Coloured PET**. While PET containers are manufactured in many different colours, PET reclaimers and end-users are generally only interested in clear and

transparent green containers, as they have the best end-use applicability. While there are a growing number of transparent blue PET bottles and containers entering the marketplace, some reclaimers have restrictions as to the presence of blue containers, while other reclaimers are able to blend them off into certain end-use applications. The presence of any pigmentation other than transparent green is unacceptable to most PET reclaimers and no other colours of PET bottles or containers should be included for recycling. These restrictions include any opaque coloured PET containers as well as transparent amber (brown) or blue PET bottles or containers.

- **Labels.** While most paper and plastic labels used on custom-PET containers and the glues used to affix them can be removed from granulated PET during the cleaning process, certain PET containers, including coffee containers, liquor bottles and mustard jars, may contain metalized labels that pose problems for some reclaimers.

4.2. SPECIFIC SUPER-CLEAN DECONTAMINATION PROCESSES FOR PET

For those materials obtained by conventional mechanical recycling processes, in order to achieve the necessary characteristics for being used in contact with food, a subsequent treatment processes called **super-clean** is required. These processes remove the contaminants that can be adsorbed on the surface of the plastic. Presently, it is possible to distinguish three types of processes depending on the super-clean treatment used for decontamination:

A. Decontamination by heat treatment

This process is carried out by introducing the ground in an extruder at 280 ° C. Infusible and insoluble impurities that may still contain the material in the filter will be removed. The current temperature can cause a rupture of chains and an overall drop in viscosity, thus a polycondensation is provoked to increase the molar mass by weight and

number and therefore maintain the properties. During the polycondensation it is necessary to remove the water released by the esterification by vacuum or by gas flow throughout the reaction. Polycondensation removes pollutants mainly by diffusion, due to exposure of the PET flakes at high temperatures with long residence times.

B. Decontamination by physic-chemical treatments

This type of decontamination is essentially a chemicaletching of the surface and top layers of PET, where pollutants can be located (by penetration, adsorption or absorption phenomena). It is usually performed by washing the PET in a soda bath in a rotary mixer at high temperatures, which causes ester hydrolysis of the surface. This type of polycondensation erases contaminants by diffusion, due to the exposure of PET flakes at high temperatures during high residence times.

C. Decontamination by solvent extraction

This system is based on the dissolution / precipitation selective solvent for plastics and the removal of any other substance. It is a process that has not been really developed yet at an industrial scale, although smaller lab-scale experiments have been successfully carried out.

D. Solid state polymerization processes

There are different techniques or PET recycling processes globally recognized as to their effectiveness in decontamination. They usually maintain or increase the intrinsic viscosity of the waste, due to the chemical reactions occurring in elongate the polymer chains, remarkably improving the final properties of the material. This process usually called *solid state polymerization* (SSP). The material is introduced into a pre-crystallizer, where the flakes are cleaned and warmed up, and subsequently introduced into a heat exchanger fluidized bed under nitrogen, to avoid the formation of acetaldehyde. The crystalline material is fed, usually by gravity, to a polycondensation reactor where the intrinsic viscosity is increased to the desired level.

A summary of the patented and available technologies for PET super-clean decontamination processes can be found in literature⁽¹³⁾.

4.3. USE AND SUSTAINABILITY OF RECYCLED PET

A successful recycling programme does not only depend on post-consumer waste collection. Whether the products made out of collected, reclaimed and recycled material respond to the needs of consumers, in other words, if recycled products are actually bought, points out the feasibility of the recycling industry of PET. Several applications are devoted for R-PET as shown in the next figure⁽¹⁴⁾:

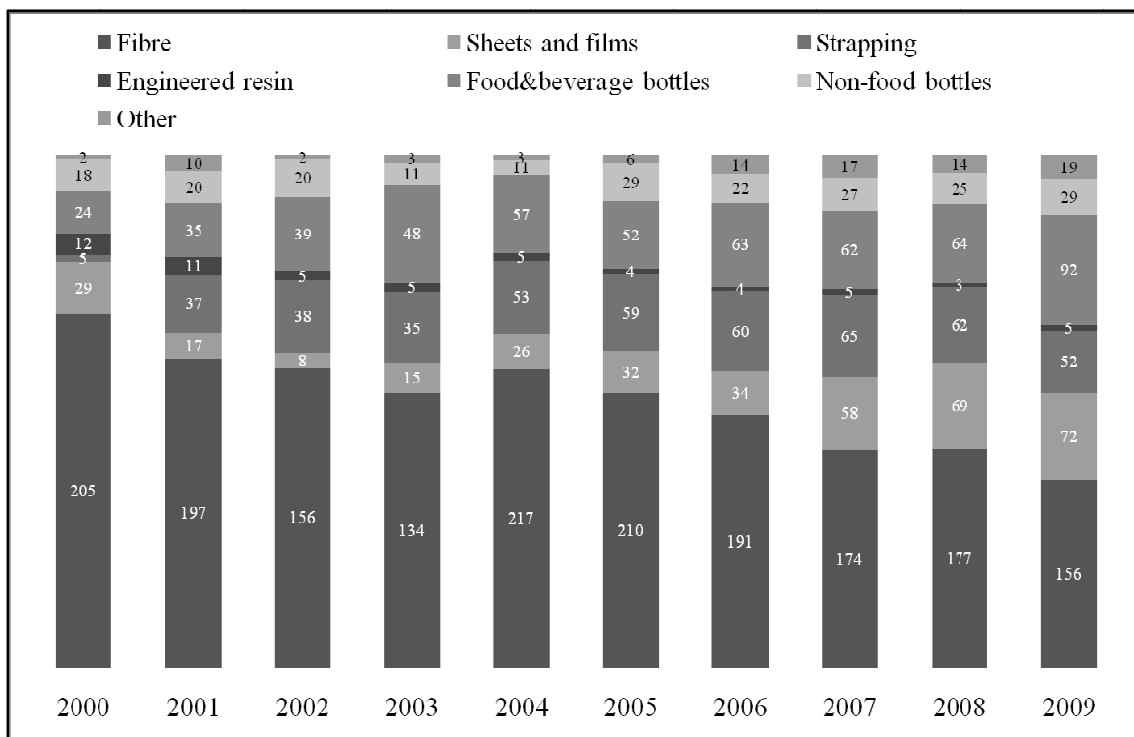


Figure 3.6. Usage of recycled PET in USA (MMkgs/year), as reported by Napcor⁽¹⁴⁾

Among the applications of recycled PET which are being developed nowadays, the most significant facts⁽⁹⁾ are given for:

Fibres

In 2009, 40% of all recovered European PET was used to produce polyester fibres. Reprocessed flakes are melted and spun into strands. It is the length and the thickness of

the resulting fibre to determine which product the reclaimed material will be turned into. Fibres from 5 to 150mm large (staple grades) are the ones most sought after. For example, larger diameter fibres are used to stuff anoraks, sleeping bags and soft toys. Recycled PET is also used to spin fibres of smaller diameter. These are woven into polar fleece fabric used for sweatshirts, jackets and scarves. Such fabrics can contain up to 100% of recycled material. As an example, a polar fleece jacket uses 25 recycled PET bottles.

Packaging

As examples, egg containers and other preformed plastic boxes (such as fruit boxes) account for about 27% of total recycled PET usage.

Other recycled PET packaging applications include containers for water, soft drinks, juices, toiletries and household products. These are said to "close the recycling loop" as they allow a container to be recycled into a new container. 22% of European RPET was used to make containers (food and non-food) in 2009.

All recycled containers are claimed to remain recyclable.

New Applications

The PET industry is in constant search for new applications for reclaimed material. There are many developing markets for recovered PET:

- Polyurethane foams can be made by thanks to polyester polyols developed from PET flakes
- Engineered resins made from recovered PET can be injection moulded to manufacture computer and automotive parts
- Other alternative production processes use "spun-bonded" PET in the manufacture of shoe liners, webbing, and geo-textiles (shoes, backpacks).

The **sustainability** of using recycled PET has been evaluated. A LCI Report⁽¹⁵⁾ shows that for every kg of recycled PET flake used, the energy used is reduced by 84% and greenhouse gas emissions by 71%, as shown in Figs 3.7 and 3.8, from the studies reported by NAPCOR (National Association for PET Container Resources)⁽¹⁴⁾.

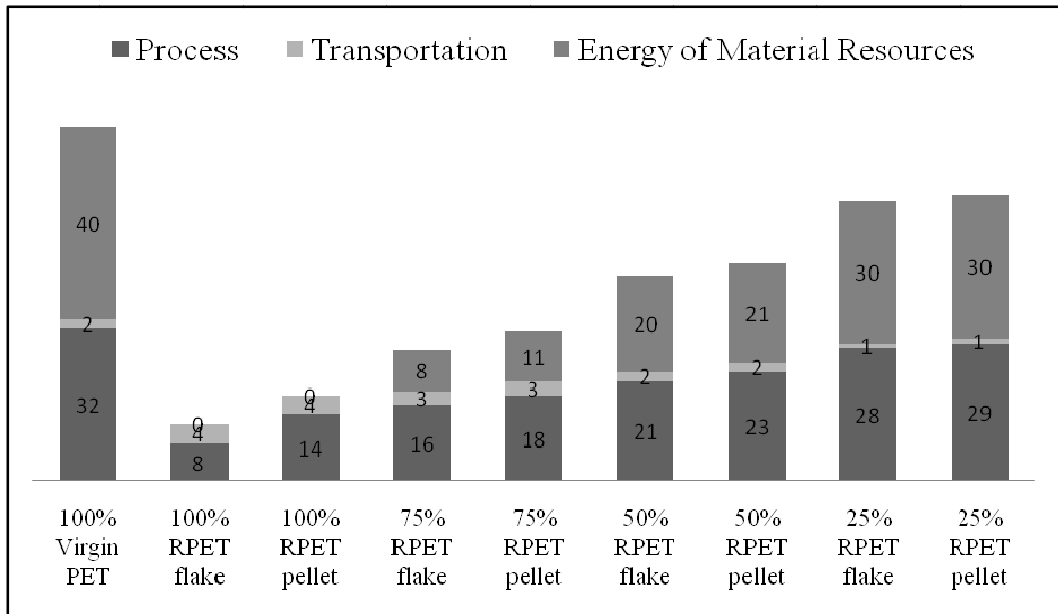


Figure 3.7. Comparison of Energy used for producing Virgin PET to Varying Levels of Recycled PET, as reported by NAPCOR(15)

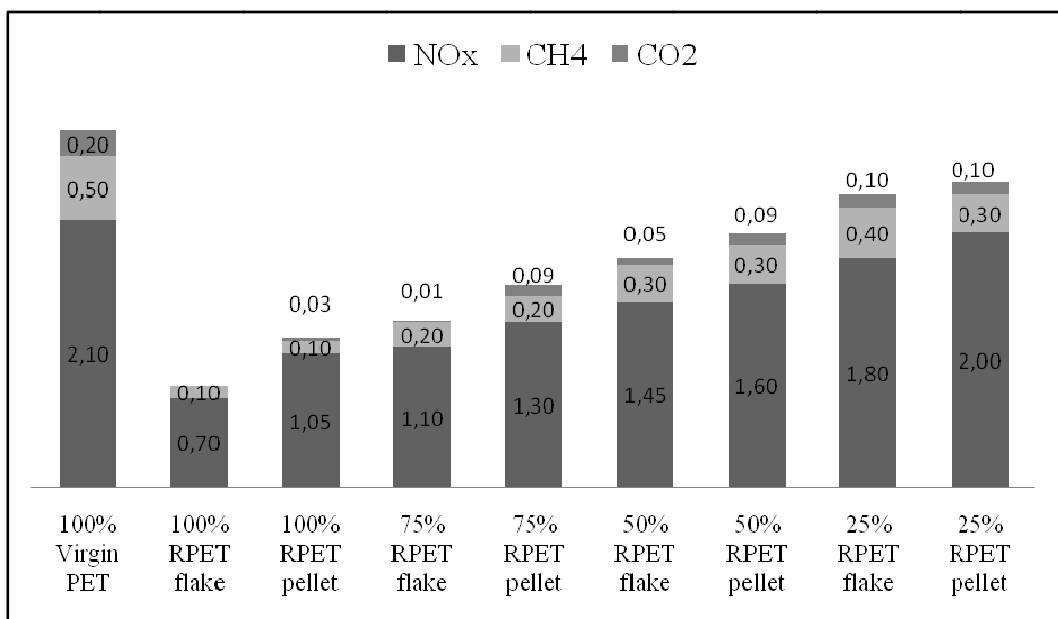


Figure 3.8. Comparison of gases released during production of Virgin PET to Varying Levels of Recycled PET, as reported by NAPCOR (15)

4.4. USE OF RECYCLED PET IN FOOD APPLICATIONS

The use of recycled materials in food contact applications ensuring their use harmless to human health is a topic of interest for many years to the administration, industries and the scientific community, which has lead to a large number of studies that have given out guidelines and recommendations, influencing the body of law on the subject in some countries.

The first country to start working on this matter was the United States of America (USA), during the 80s; it was considered important for development to establish the possibility of using recycled plastic in food contact. These specifications are reflected in the first regulation on recycled plastic food contact was made in 1992, Points to Consider for the Use of Recycled Plastics in Food Packaging: Chemistry Considerations, by the FDA ⁽¹⁶⁾. This document was the starting point and referenced for most subsequent studies on this subject. It was a description of the types of recycling available, the acceptable limits of chemical contaminants in the recycled material to ensure public health and suggested a protocol to assess whether the recycling process was designed to remove chemical contaminants. It also established the concept of **functional barrier multilayer products**. This document was reviewed, updated and replaced in 2006 by another entitled "Use of Recycled Plastics in Food Packaging: Chemistry Considerations" ⁽¹⁷⁾ which established new standards for food security, limiting some points such as: no need to assess heavy metal contamination in the case of recycled PET, the establishment of source controls, or limitations on the use of material.

The European Commission published a new document which is an implementation guide for the specific case of PET, entitled "Guidance and Criteria for Safe Recycling of Post Consumer Terephthalate Polyethylene (PET) Into New Food Packaging Applications"⁽¹⁸⁾, where PET was established as the plastic material with best performance in direct contact with food. This guide gives an overview on the PET recycling, separate collection and special treatments for decontamination. It also establishes some basic points of control at source, process efficiency, and quality assurance.

All these documents reflect the aspects of the phenomena that occur in the container and between the container and food in food safety such as:

- adsorption properties is the polymer.
- diffusion component of the package itself.
- migration of packaging components to food.
- the different behaviour of the adsorption, diffusion and migration based on several factors: the polymer, food, weather conditions and temperature of contact bottle-feed.

In addition to these aspects of food security, these documents contain other aspects of raw material and manufacturing process itself, including:

- origin of the waste
- possible misuse (misuse) of packaging waste generated
- control of the process.
- quality assurance.
- traceability

4.5. THE PET RECYCLING SYSTEM IN SPAIN

A. Type of collection

There are different observed types of collection with respect to PET. The main ones are: systems of deposit, return and collection systems. There is a difference in the figures collected from various European countries. There are three dominant countries in the collection of PET: Germany, France and Italy, representing 56.7% of the total collection, which is consistent with the fact that countries with a more established collection systems. Spain currently has 4.8% of the PET bottle collection in Europe, almost the same level as Belgium is 4.5%, although the Spanish population is 4 times larger than Belgium.

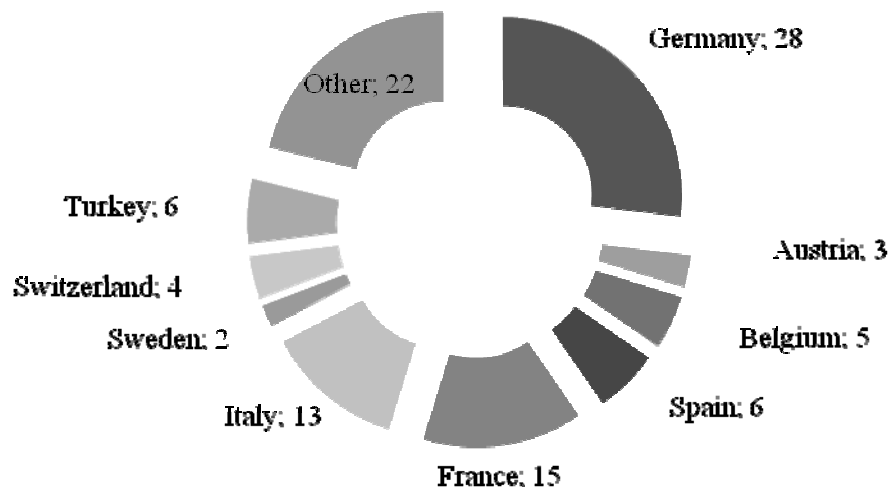


Figure 3.9. Percentages of PET collection of European countries in 2006, as adapted from PCI-PETCORE report ⁽¹⁹⁾

C. Containers involved

In general there are two types of containers in terms of composition, which reflect only PET bottles and containers that collect different materials at once (which can be only plastic containers or plastic containers with metal containers and drink cartons). In the first case it involves a very selective collection, focusing on drink bottles and therefore restricted to a food source. In the second case, in addition to be different materials, there is also a double origin (food and non-food). The type of container collected by multi-material is given both in Spain and in France, Belgium, Italy and Portugal.

D. Figures and facts

In Spain, almost $1 \cdot 10^5$ tones are recycled each year ⁽²⁰⁾. In particular, the total volume of production rose in 2007 up to 141.600,900 tones. The mechanical processes to recycle PET are very varied, adjusting to the type of residue obtained and to the quality of the recyclate that is aimed. Accordingly, different companies placed in Spain recycle post-consumer packaging goods, homologated by Ecoembalajes España S.A. (ECOEMBES), which is the company in charge of the Integrated Management of Residues System in Spain ⁽²¹⁾. Most of these companies (Table 3.1) are distributed along the Mediterranean coast, as can be seen in Fig 3.10. The distribution of recycled PET is mainly directed to national companies, as shown in Fig3.11.

Table 3.1 .Collection figures of Spanish companies, as reported by AIMPLAS-ECOEMBES ⁽²¹⁾

Company	(tones/year)
PET, Compañía para su reciclado	62700
Extremadura Torre PET	25500
Riberpet	16600
Iparpet recycling	12200
Recuperaciones de plásticos de Barcelona	9600
Recuprod	9500
Reciclatjes del Lluçanes	3300
Reciclajes FELMA	2200

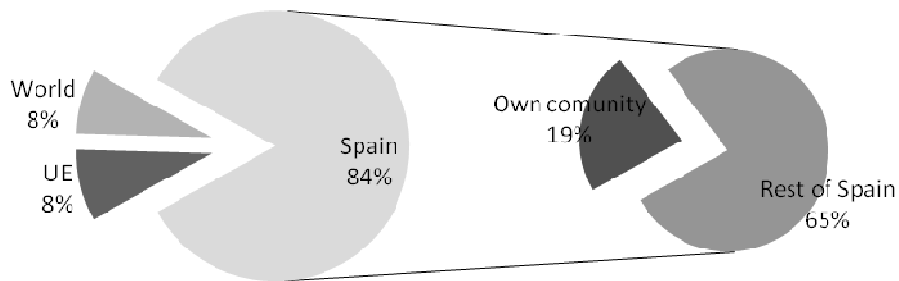


Figure 3.10. Distribution of Spanish recycled PET, as reported by AIMPLAS-ECOEMBES ⁽²¹⁾

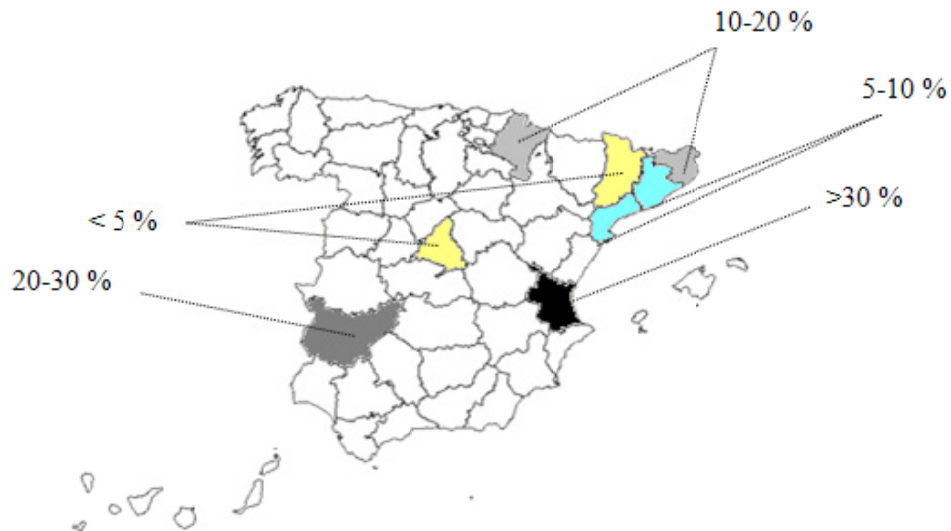


Figure 3.11. PET production capabilities, as reported by AIMPLAS-ECOEMBES ⁽²¹⁾

4.6. THE THERMO-MECHANICAL DEGRADATION OF PET

During its life cycle (synthesis - processing - service life - discarding - recovery), PET is subjected to the influence of degradative agents such as oxygen, light, mechanical stresses, temperature and water, which, separately or in combination, give rise to chemical and physical changes which alter the stabilization mechanism. Individually or synergically, these agents may provoke the breakage of the macromolecules and diminish the final properties and productivity during processing. Therefore these degradation processes modify the structure and composition of the polymer and consequently change the thermal, rheological and mechanical properties of recycled PET. The assessment of the degradation state is necessary to determine the quality of recycled PET and guarantee their further performance in second-market applications. PET degradation reactions generally follow the postulated mechanistic routes of polyesters:

- Hydrolysis, which leads to the formation of hydroxyl and carboxyl linear oligomers with shorter chain length.
- Esterification.
- Intramolecular transesterification, both from the end of the chain (backbiting) or in the middle of the chain, which lead to the formation of cyclic oligomers and linear species with shorter length.
- Intermolecular transesterifications, which interchange ester units between different chains, which lead to an increase in the heterogeneity of the polymer.
- Chain scissions inherent to thermo-mechanical reactions may produce random chain cleavage, leading to the formation of mainly linear hydroxyl and carboxyl terminated species.

Hydrolysis

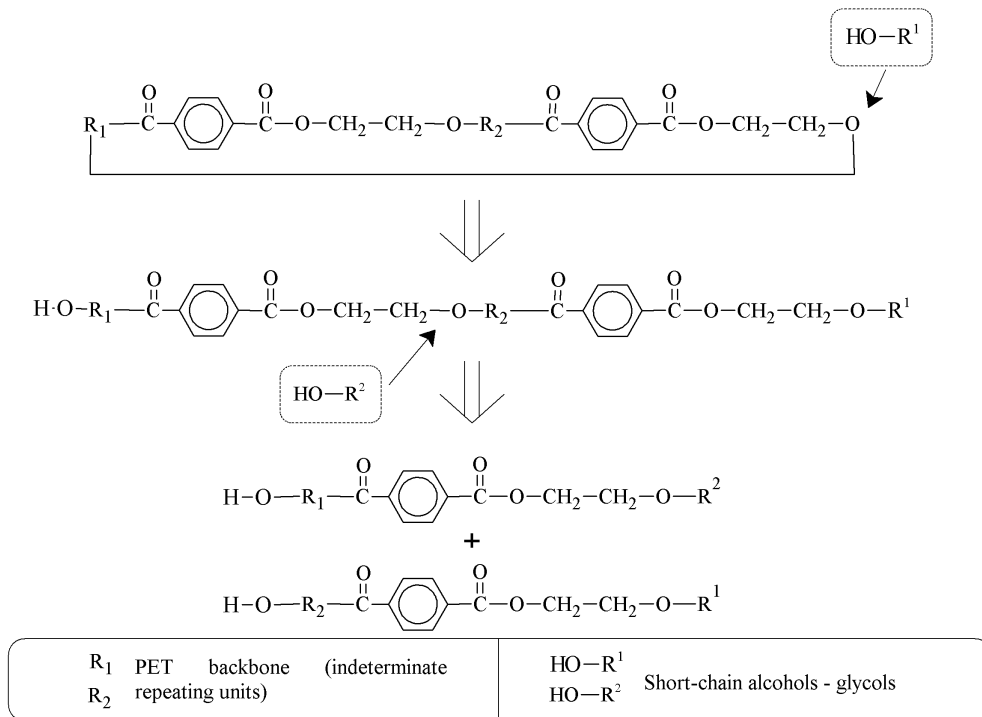


Figure 3.12. Scheme of hydrolysis of PET.

Esterification

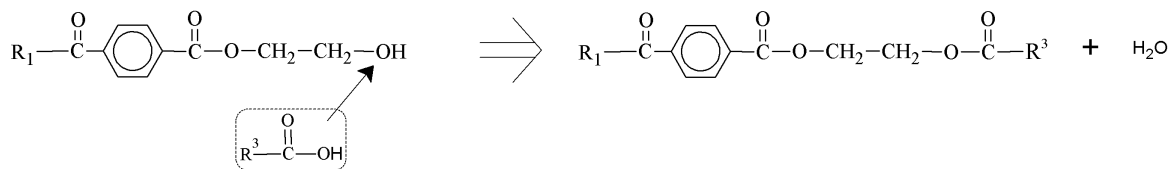


Figure 3.13. Scheme of esterification of PET.

Intramolecular transesterification

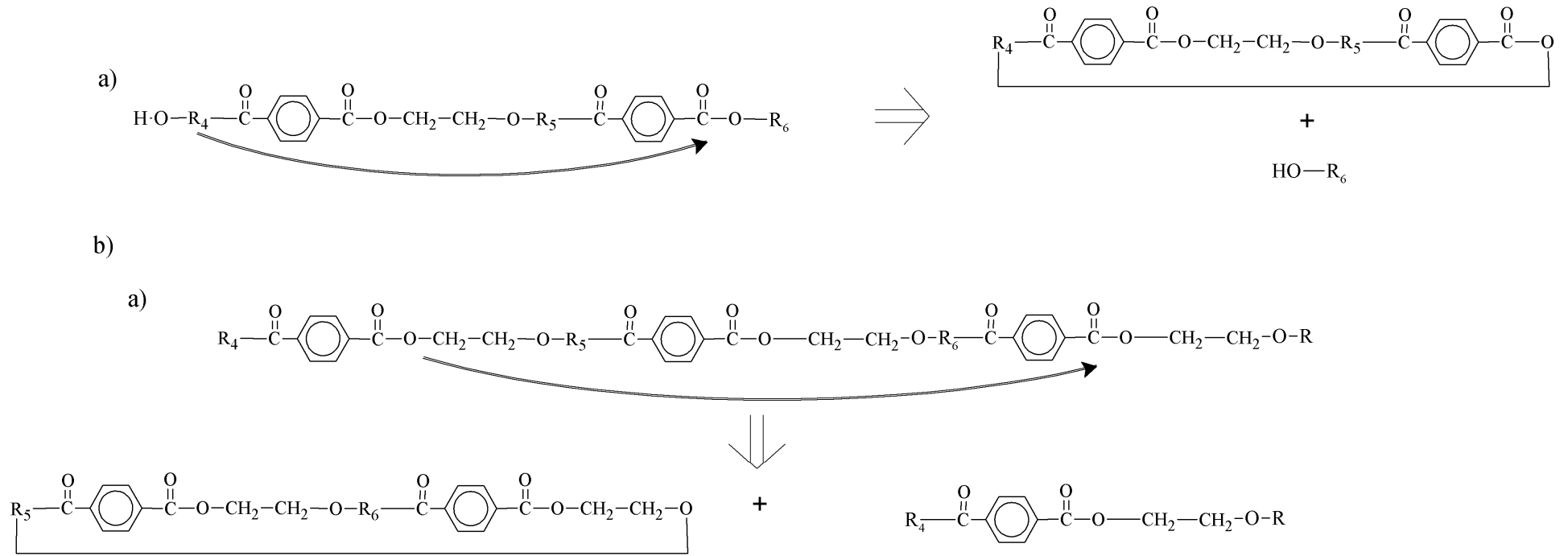


Figure 3.14. Scheme of intramolecular transesterification of PET. a: from the end of the chain (backbiting); b: in the middle of the chain

Intermolecular transesterifications

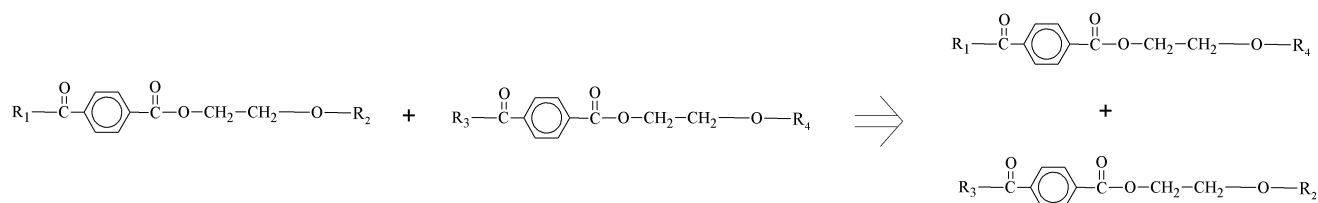


Figure 3.15. Scheme of intermolecular transesterification of PET.

Chain scissions

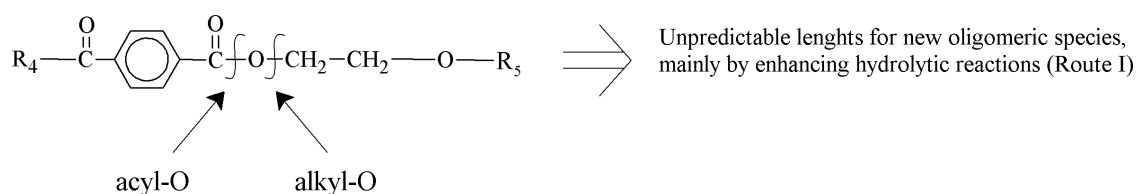


Figure 3.16. Scheme of chain scission reactions of PET.

An extended analysis of the thermo-mechanical degradation reactions leading to variations in the oligomeric distribution of PET due to mechanical recycling is given in the **Contribution III.B**. As will be shown for each contribution, the properties of recyclates differ in some extent from those of virgin PET. Several studies have characterized the changes of performance of PET due to recycling in terms of:

- morphology and conformation⁽²²⁻²⁵⁾
- molar mass and molar mass distribution⁽²⁶⁻²⁹⁾
- mechanical properties^(24-28,30-31)
- rheological^(24,28-30)
- thermal properties⁽²⁶⁻³³⁾

Contributions III.A and **III.C** show the effects of mechanical recycling by multiple extrusions and multiple injections to the structural and morphological properties of PET, in connection to the influence on its thermal, mechanical and viscoelastic performance.

5. MECHANICAL RECYCLING OF PLA

Though biodegradable and therefore thought for a composting end-of-life, the possibility of recycling to enlarge the service of bio-based materials remains a positive challenge of current interest. Thus, there is a debate and concern about the impact of bio-based plastics on the current plastics recycling infrastructure and contamination of the recycling stream.

In contrast to the widely spread and largely established PET industry and market, the development of commercial PLA is currently growing from the R&D stage to the implementation at local levels by a reduced group of companies. Thus, only the information of recent advances of separation of PLA in waste streams and few scientific papers on recycled PLA for packaging can be found (without considering the PLA used in biomedical applications).

Considering the **sorting technologies for PLA waste**, while current waste reduction systems are evolving, companies like Natureworks are committed to responsibly introduce their PLA products into the market. As can be deduced from the previous sections, the first step is to evaluate several different sorting technologies to identify PLA goods from other plastics. *Near-Infrared (NIR)* sorting is the industry's preferred plastics sorting technology because it can accurately identify the many different polymers already in use today (different polymers reflect an identifiable light spectrum). According to Natureworks⁽³⁴⁾, testing on widely-used present-day technology proved that PLA can be identified in the mixed waste plastics stream with very high accuracy. Analytical testing laboratories of companies like Titech and Unisenor have demonstrated the ability of its near-infrared sorting systems to eject concentrated amounts of PLA in a PET sorting operation. A sorting efficiency in a single pass was found to be a minimum of 96-99% accuracy, which is consistent with other plastics considered contaminants using the PET flake sorting technology.

With regards to the recovering of PLA waste, it can be effectively recycled by hydrolysis, in order to obtain lactic acid (feedstock/chemical recycling). However, the alternative of **mechanical recycling** has been scarcely addressed in literature and thus becomes an interesting field of knowledge which was addressed in this thesis. The occurrence of chain

cleavage will modify the performance of PLA for service after mechanical recycling. The studies in literature are few, and report the degradation of reprocessed PLA by multiple extrusion ⁽³⁵⁾ or injection cycles ⁽³⁶⁾, as well as different sets of combined individual cycles of extrusion, injection and annealing ⁽³⁷⁻³⁸⁾ on the chemical structure, oligomeric distribution, morphology, thermal, rheological, mechanical or permeability properties. As introductory facts, the likely reactions of thermo-mechanical degradation leading to chain scissions of PLA, chemically equivalent to those shown by PET, are shown:

Hydrolysis

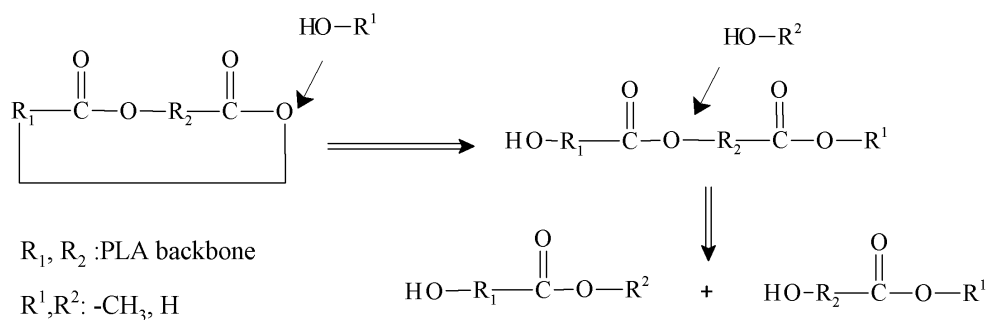


Figure 3.17. Scheme of hydrolysis of PLA.

Esterification

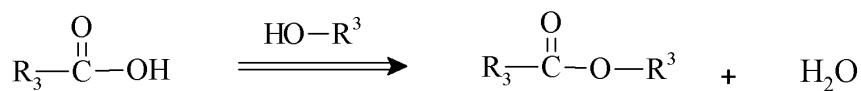


Figure 3.18. Scheme of esterification of PLA.

Intramolecular transesterifications

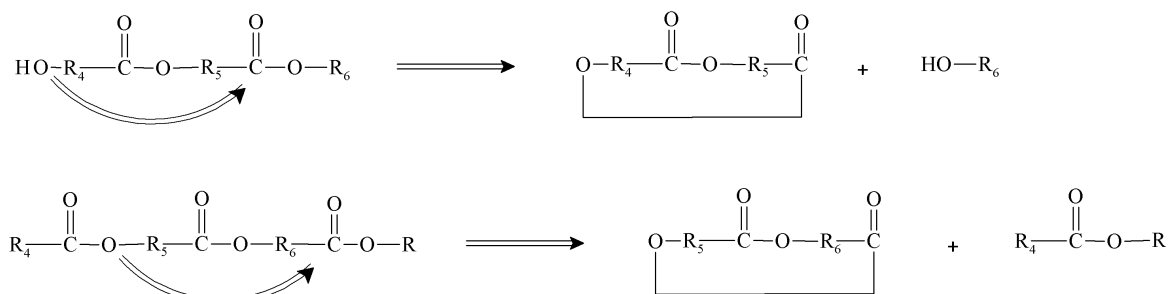


Figure 3.19. Scheme of intramolecular transesterifications of PLA.

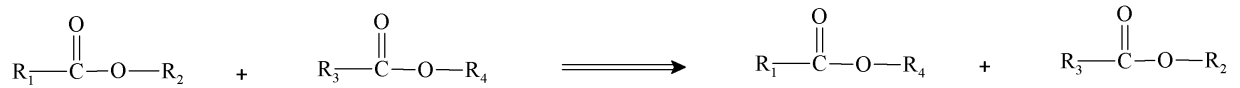
Intermolecular transesterifications

Figure 3.20. Scheme of intermolecular transesterifications of PLA.

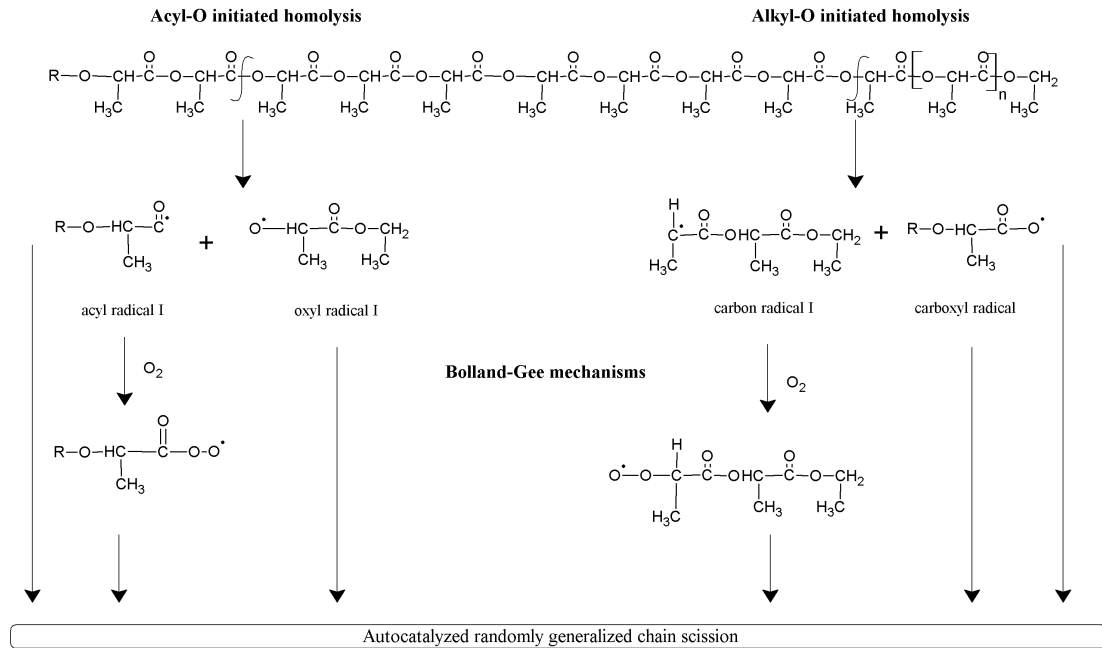
Chain scission

Figure 3.21. Scheme of chain scission of PLA.

An extended analysis of the thermo-mechanical degradation reactions, induced by successive injection cycles, leading to variations in the oligomeric distribution of PLA due to mechanical recycling is given in the **Contribution III.D**, while in **Contribution III.E** the influence on the thermal, mechanical and viscoelastic performance is assessed.

6. REFERENCES IN THIS CHAPTER

1. Al-Salem S M, Lettieri P, Baeyens, J. *Recycling and recovery routes of plastic solid waste (PSW): A review*. Waste management, 29, 2625-2643(2009)
2. Perdon S, *Sustainable development in practice: case studies for engineers and scientists*. In: Azapagic A, Perdon S, Clift R, Editors, *Introduction to Sustainable Development (first ed.)*, Wiley (2004)
3. Al-Salem S M, *Establishing an integrated databank for plastic manufacturers and converters in Kuwait*, Waste Management 29, 479–484 (2009)
4. Mastellone M.L, *Thermal treatments of plastic wastes by means of fluidized bed reactors*. Ph.D. Thesis, Department of Chemical Engineering, Second University of Naples, Italy. (1999)
5. Ribes Greus A, Vilaplana F, Contat L Cuadernos Guía. Universidad Politécnica de Valencia. 2008.
6. ECOEMBES. Catálogo para la prevención de residuos de envases 2003-2006.
7. Zia K.M, Bhatti H.N , Bhatti I.A, *Methods for polyurethane and polyurethane composites, recycling and recovery: a review*. Reactive & Functional Polymers 67, 675–692 (2007)
8. López J. Apuntes Master en Ingeniería Mecánica y Materiales. 2007.
9. PlasticsEurope, EuPC, EPRO, EuPR. Consolidated data. *The compelling facts about plastics. An analysis of European plastics production, demand and recovery for 2008*. (2009)
10. Aznar M.P, Caballero M.A, Sancho J.A, Francs E, *Plastic waste elimination by co-gasification with coal and biomass in fluidized bed with air in pilot plant*, Fuel Processing Technology 87,409–420(2006)
11. Scheirs, J. Sorting and separation techniques. Polymer recycling. Science, technology and applications. Chichester : John Wiley & sons, (1998)
13. AIMPLAS. *Uso de PET reciclado para envase alimentario. Informe de novedades tecnológicas*. (2011)
14. NAPCOR. *Report on post consumer PET container recycling activity*. (2009)
15. PDACC, APR, NAPCOR, PETRA. *Life cycle inventory of 100% postconsumer HDPE and PET recycled resin from postconsumer containers and packaging*. (2010)
16. FDA. *Points to consider for the use of recycled plastics in food packaging: chemistry considerations*. (1992)
17. FDA. *Use of Recycled Plastics in Food Packaging: Chemistry Considerations* (2006)

18. Roland F, Bayer F, Welle F. *Guidance and Criteria for Safe Recycling of Post Consumer Terephthalate Polyethylene (PET) Into New Food Packaging Applications*. European Commission(2004)
19. PETCORE-PCI. *Post Consumer PET recycling in Europe 2006 and Prospects to 2011*.(2006)
20. Verdejo, E. *Informe de vigilancia tecnológica: PET reciclado*. AIMPLAS (2010)
21. AIMPLAS-ECOEMBES. *Situación actual y perspectivas del uso de PET para envases en contacto con alimentos*(2008)
22. Romao W, Franco M F, Corilo Y E, Eberlin M N, Spinacé M A S, De Paoli M A . *Poly(ethylene terephthalate) thermo-mechanical and thermo-oxidative degradation mechanisms*. Polymer Degradation and Stability 94, 1849-1859 (2009)
23. Romao W Franco M. F., Iglesias A H, Sanvido G B, Maretto D A. Gozzo F C, Poppi RJ, Eberlin MN, De Paoli MA. *Fingerprinting of bottle-grade poly(ethylene terephthalate) via matrix-assisted laser desorption/ionization mass spectrometry*. Polymer Degradation and Stability 95, 667-671 (2009)
24. Pawlak A, Pluta M, Morawiec J, Galeski A, Pracella M. *Characterization of scrap poly(ethylene terephthalate)*, European Polymer Journal 36, 1875-1884 (2000)
25. Lusinchi JM, Pietrasanta Y, Robin JJ Boutevin B; *Recycling of PET and PVC wastes*, Journal of applied Polymer Science 69, 657-665(1998)
26. Torres N, Robin J J, Boutevin B. *Study of thermal and mechanical properties of virgin and recycled poly(ethylene terephthalate) before and after injection molding*. European Polymer Journal 36, 2075-2080 (2000)
27. Oromiehie A, Mamizadeh A. *Recycling PET beverage bottles and improving properties* Polymer International 53, 728-732 (2004)
28. La Mantia F, Vinci M. *Recycling poly(ethylene terephthalate)*. Polymer Degradation and Stability, 45, 121-125(1994)
29. Assadi R, Colin X, Verdu J, *Irreversible structural changes during PET recycling by extrusion*; Polymer 45 4403-4412(2004)
30. Awaja F, Pavel D, *Injection stretch blow moulding process of reactive extruded recycled PET and virgin PET blends*. European Polymer Journal 41, 2614-2634(2005).
31. Mancini SD, Zanin M. *Consecutive steps of PET recycling by injection: Evaluation of the procedure and of the Mechanical properties*. Journal of Applied Polymer Science, 76 266-275(2000).
32. Badía JD, Vilaplana F, Karlsson S, Ribes-Greus A, *Thermal analysis as a quality tool for assessing the influence of thermo-mechanical degradation on recycled poly(ethylene terephthalate)*. Polymer Testing 28, 169-175 (2009)

-
33. Romao W, Franco MF, Bueno MI, De Paoli M-A. *Distinguishing between virgin and post-consumption bottle-grade poly(ethylene terephthalate) using thermal properties*. *Polymer Testing* 29, 879-885 (2010)
34. Natureworks. *A case study. Using Near-Infrared Sorting to Recycle PLA Bottles*. (2009)
35. Zenkiewicz M, Richert J, Rytlewsky P, Moraczewski K, Stepczynska M, Karasiewicz T. *Characterisation of multi-extruded poly(lactic acid)*. *Polymer Testing* 28, 412-418 (2009)
36. Badia J D , Ribes-Greus A. *Assessing the thermal stability and kinetics of thermal and thermal-oxidative decompositions of reprocessed poly(lactide)*. Manuscript.
37. Carrasco F; Pagès P; Gámez-Pérez J; Santana OO, MasPOCH ML. *Processing of poly(lactic acid): Characterization of chemical structure, thermal stability and mechanical properties*. *Polymer Degradation and Stability* 95, 116-125 (2010)
38. Carrasco F, Pagès P, Gámez-Pérez J, Santana OO, MasPOCH ML. *Kinetics of the thermal decomposition of processed poly(lactic acid)*. *Polymer Degradation and Stability* 95, 2508-2514 (2010)

7. CONTRIBUTIONS IN THIS THESIS

The material valorisation by successive mechanical recycling on both poly(ethylene terephthalate) (PET) and polylactide (PLA) was assessed. The effects of the thermo-mechanical degradation inherent to the processing conditions were evaluated in terms of structural and morphological changes, and its consequent influence on the thermal and mechanical performance was characterised. Fig. 3.22 summarises the focus of these studies, along with the analytical techniques used for the purpose.

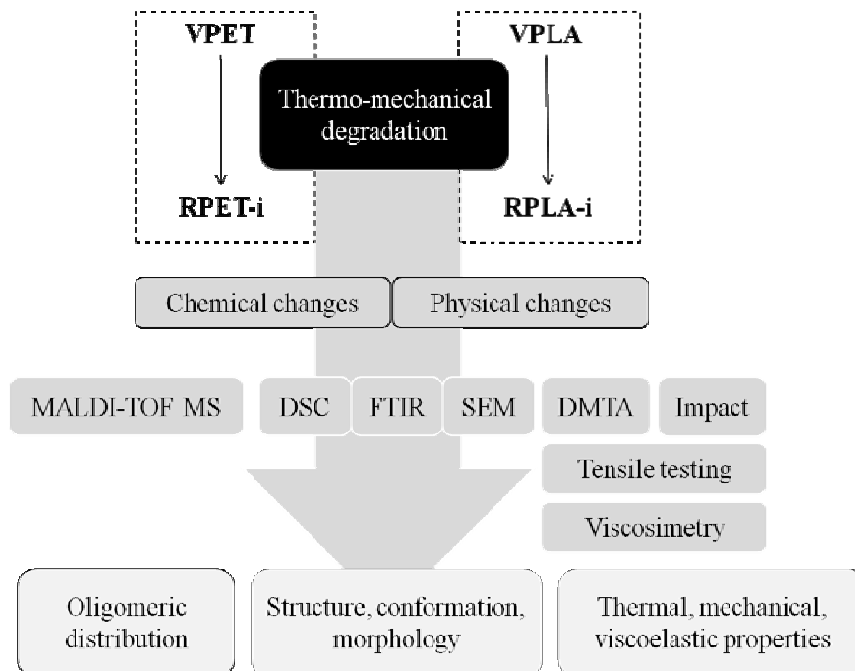


Figure 3.22. Schematic description of the contributions of this thesis in the field of material valorisation of plastic materials

The most remarkable highlights of these works are:

- The application of two specific procedures by means of successive extrusions and injections for modelling mechanical recycling.
- The comparison between commonly-used industrial quality parameters and the degradation indicators proposed by thermal analysis.

- The development of a statistical Design of Experiments to improve the MALDI-TOF-MS sample preparation of PET and PLA.
- The proposal of the mechanistic pathways followed by reprocessed PET and PLA during thermo-mechanical degradation.
- The application of a three-fraction model to understand the influence of the rigid and mobile amorphous fractions and the rigid crystalline fraction on the performance of PET.
- The monitoring of the cold-crystallization of reprocessed PLA, as well as the use of a deconvolution process and a partial areas method to study the evolution of the melting endotherm of both PET and PLA.
- The analysis of the segmental dynamics throughout the glass-rubber relaxation of both PET and PLA, to assess the effects of reprocessing in terms of dynamic fragility, chain mobility and free volume.

The results of the studies were reported in five contributions, which are shown as follows:

CONTRIBUTION III-A: J.D. Badía, Francisco Vilaplana, Sigbritt Karlsson, A. Ribes-Greus. Thermal analysis as a quality tool for assessing the influence of thermo-mechanical degradation on recycled poly(ethylene terephthalate). *Polymer Testing* 2009, 28; 169-175.

CONTRIBUTION III-B: J.D. Badía, E. Strömberg, A. Ribes-Greus, S. Karlsson. A statistical design of experiments for optimizing the MALDI-TOF-MS sample preparation of polymers. An application in the assessment of the thermo-mechanical degradation mechanisms of poly (ethylene terephthalate). *Analytica Chimica Acta* 2011, 692; 85-95

CONTRIBUTION IV-C: J.D. Badía, E. Strömberg, S. Karlsson, A. Ribes-Greus. The role of crystalline, mobile amorphous and rigid amorphous fractions on the performance of recycled poly (ethylene terephthalate) (PET). Manuscript.

CONTRIBUTION III-D: J.D. Badía, E. Strömberg, A. Ribes-Greus, S. Karlsson. Assessing the MALDI-TOF MS sample preparation procedure to analyze the influence of thermo-oxidative ageing and thermo-mechanical degradation on poly (lactide). *European Polymer Journal*. 2011, 47; 1416-1428

CONTRIBUTION III-E:J.D. Badía, E. Strömberg, S. Karlsson, A. Ribes-Greus. Material valorisation of amorphous polylactide. Influence of thermo-mechanical degradation on the morphology, segmental dynamics, thermal and mechanical performance. Manuscript.

CONTRIBUTION III-A

Thermal analysis as a quality tool for assessing the influence of thermo-mechanical degradation on recycled poly(ethylene terephthalate)

J.D. Badia, Francisco Vilaplana, S. Karlsson, A. Ribes-Greus

Polymer Testing 2009, 28; 169-175



ELSEVIER

Contents lists available at ScienceDirect

Polymer Testing

journal homepage: www.elsevier.com/locate/polytestPOLYMER
TESTING

ROGER BROWN

Test Method

Thermal analysis as a quality tool for assessing the influence of thermo-mechanical degradation on recycled poly(ethylene terephthalate)

J.D. Badía^a, Francisco Vilaplana^{a,b}, Sigbritt Karlsson^b, A. Ribes-Greus^{a,*}

^aInstituto de Tecnología de Materiales (ITM), Escuela Técnica Superior de Ingeniería del Diseño, Universidad Politécnica de Valencia, Camino de Vera s/n, E-46022 Valencia, Spain

^bSchool of Chemical Science and Engineering, Fibre and Polymer Technology, KTH - Royal Institute of Technology, Teknikringen 56-58, SE-10044 Stockholm, Sweden

ARTICLE INFO

Article history:

Received 6 October 2008

Accepted 18 November 2008

Keywords:

Thermal analysis

Recycling

Poly(ethylene terephthalate) (PET)

Quality assessment

Degradation

ABSTRACT

Mechanical recycling of poly(ethylene terephthalate) (PET) was simulated by multiple processing to assess the effects of thermo-mechanical degradation, and characterized using rheological and thermal analysis techniques. Thermo-mechanical degradation under repeated extrusion induces chain scission reactions in PET, which result in a dramatic loss in the deformation capabilities and an increase in the fluidity of the polymer under reprocessing, reducing its recycling possibilities after four extrusion cycles. Multiple reprocessing severely affects the storage modulus and the microstructure of recycled PET, both in the amorphous and crystalline regions. Multimodal melting behavior is observed for reprocessed PET, indicating heterogeneous and segregated crystalline regions. A deconvolution procedure has been applied to individually characterize each crystalline population in terms of lamellar thickness distribution and partial crystallinity. Thermal analysis techniques such as differential scanning calorimetry (DSC) and dynamic-mechanical analysis (DMA) have proved to be suitable techniques for the quality assessment of recycled PET, giving unequivocal information about its degree of degradation compared to the common technological measurements of melt-mass flow rate (MFR) or oxidative stability (T_{Ox}).

© 2008 Elsevier Ltd. All rights reserved.

1. Introduction

Poly(ethylene terephthalate) (PET) is a well established engineering and commodity polymer which has registered an important increasing production trend during recent years [1,2]. The associated problem related to PET waste disposal is, however, not satisfactorily solved yet; according to recent statistics [3], only 35% of all PET bottles in Europe were recovered in 2005 through re-using, mechanical recycling, feedstock recycling or energy recovery. Among all recovery methods, mechanical recycling represents one of the most successful processes and has received

considerable attention due to its main advantages, since it is environmentally friendly, relatively simple, requires low investment and its technological parameters are controlled [4]. Moreover, recent life cycle assessment studies have pointed out that mechanical recycling is the most preferable recovery route for relatively clean and homogeneous waste streams in terms of energy saving and emission of gases contributing to global warming [5].

However, mechanical recycling is still far away from being fully deployed; in general, recycling industries are characterized by a low degree of knowledge about plastic products and their properties. Recycled plastics usually come from unknown origins, they may be subjected to degradation processes and they may have been contaminated during previous usage [6]. Polymers are subjected

* Corresponding author. Tel.: +34 96 387 98 17; fax: +34 96 387 71 89.
E-mail address: aribes@ter.upv.es (A. Ribes-Greus).

to the influence of degradative agents such as oxygen, light, mechanical stress, temperature and water from which, separately or in combination during its life cycle (synthesis - processing - service life - discarding - recovery), arise chemical and physical changes that alter its stabilization mechanisms and long-term properties [7]. These degradation processes may modify the structure and composition of PET and, consequently, change the thermal, rheological and mechanical properties of recyclates [8–14]. The assessment of the degradation state is therefore necessary to determine the quality of recycled PET and to guarantee its further performance in second-market applications. Simulation of mechanical recycling by multiple processing has been widely employed to mimic the effects of thermo-mechanical degradation on polymers [15–18].

Traditionally, the evaluation of the melt flow rate (MFR) and the mechanical properties of the recyclates have been the only properties that are determined in the specification sheets of the final recycled material, but such analyses may give misleading information about the properties and long-term performance of recycled products in new applications [6]. Fast, cost-effective and reliable characterization procedures for plastic recyclates should be developed and implemented in the recycling facilities to guarantee their quality properties. Thermal analysis techniques have been successfully used in our group to monitor and control the degradative effects on the macroscopic properties of polymers submitted to different environments, including degradation in soil, photo-oxidation, hydrolysis and thermo-oxidation [19,20].

The aim of this work is to mimic the microstructural changes that PET suffers through thermo-mechanical degradation during mechanical recycling using thermal analysis techniques and compare the obtained analytical results with those given by the technological quality properties usually measured in large-scale mechanical recycling facilities. Semicrystalline PET was subjected to multiple processing up to six cycles and the changes in melt-mass flow rate, oxidative stability, morphology and mechanical properties were correlated with reprocessing cycles to model the degradation influence on recycled PET.

2. Experimental

2.1. Materials and sample preparation

Virgin poly(ethylene terephthalate) (PET), commercially labeled as Laser+ Melinar (AdvanSa Limited, United Kingdom) was employed as reference material in this study. Previous to the mechanical recycling simulation process, it was put in a forced ventilation oven, Heraeus D-6450 (Heraeus GmbH, Germany), at 160 °C for 4 h, and afterwards kept in a desiccator to avoid hydrolysis reactions that can produce molecular weight reduction [21].

Mechanical recycling was simulated following the scheme shown at Fig 1. Multiple reprocessing up to six times was performed by using a Brabender Plasticorder PL2000 co-rotating twin-screw extruder with 2.2 cm diameter and a L/D ratio of 16 (C.W. Brabender Instruments, NJ, USA). The temperature profile at the extruder

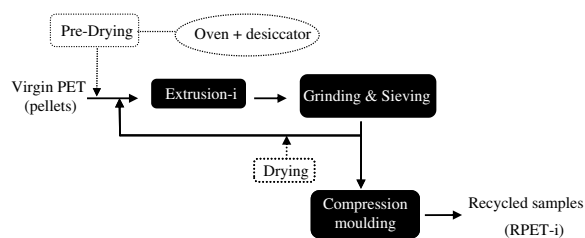


Fig. 1. Schematic representation of the mechanical recycling simulation procedure by multiple processing and analysis techniques employed (RPET-i: PET reprocessed “i” times).

was 250–260–270 °C from the feeder to the mouth of the extruder. After each reprocessing step, the material was cooled by air, ground and sieved. Some material was taken as a sample and placed again in a desiccator to prevent it from hydrolysis caused by environmental humidity until further analysis; the rest was reintroduced into the mechanical recycling simulation process. Rectangular sheets with dimensions 72 mm × 72 mm × 0.5 mm were obtained from the extracted samples by compression molding at 270 °C and 180 bar employing a hot-plate press (0230H Press, Pasadena Hydraulics Inc., CA, USA).

2.2. Melt-mass flow rate (MFR)

Melt-mass flow rate (MFR) measurements of virgin and reprocessed PET material were carried out on a Melt Indexer CFR-91 (Campana Srl., Italy) according to ISO 1133:1999 standard. The test temperature was set at 270 °C and the nominal load was 1,2 kg. Measurements on each sample were repeated six times and the average was considered as the characteristic value.

2.3. Differential scanning calorimetry (DSC)

Differential scanning calorimetry (DSC) was employed to evaluate the influence of reprocessing on the crystallinity, the melting behavior and the oxidative stability of virgin and reprocessed PET samples. Analyses were carried on a Mettler Toledo DSC 820^e instrument (Columbus, OH) calibrated with indium. All experiments were carried out with a common heating rate of 10 K min⁻¹. Approximately 10 mg of sample was weighed and placed in 40 μL aluminum pans, which were sealed and pierced to allow the gas flow (of 50 mL min⁻¹).

In order to assess the oxidation temperature (T_{Ox}), samples were heated from 25 °C up to 400 °C under an oxygen atmosphere. T_{Ox} was obtained from the onset point of the oxidation curve shown by the calorimetric analysis. Each sample was run three times and the average was assumed as the characteristic value.

The crystallinity and the melting behavior were studied by means of calorimetric scans under a nitrogen atmosphere. A heating/cooling/heating program was performed in a temperature range between 25 °C and 290 °C. The samples were analyzed by triplicate and the glass transition (T_g), melting (T_m) and crystallization (T_c) temperatures, as well as melting (ΔH_m) and crystallization (ΔH_c) enthalpies, were calculated and averaged to obtain the representative values.

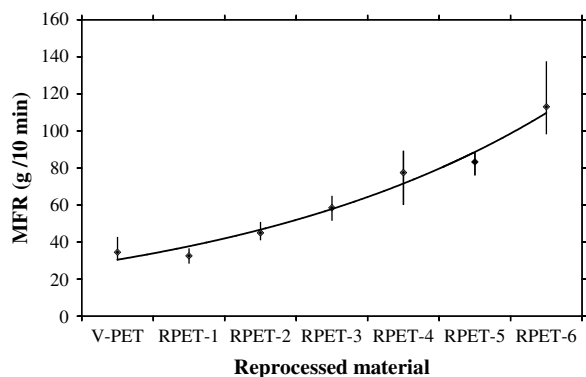


Fig. 2. Evolution of melt-mass flow rate (MFR) through reprocessing simulation.

2.4. Differential mechanical thermal analysis (DMTA)

Rectangular strips (35 mm × 1 mm × 0.5 mm) were cut from the pressed sheets and employed as test specimens. Samples were tested in a DMA Q800 (TA Instruments, DL, USA), employing a single-cantilever clamping geometry with a load of 0.001 N and 1 Hz frequency. Samples were stabilized at 35 °C for 5 min and then heated to 180 °C. Storage modulus and loss modulus were recorded as a function of temperature and time. Only samples up to the fourth recyclate could offer complete DMTA scans, due to the brittleness caused by the recycling procedure on the samples from the fifth and the sixth recyclates.

3. Results and discussion

3.1. Melt-mass flow rate (MFR)

The processability of polymer recyclates in large-scale mechanical recycling facilities is usually assessed using melt-mass flow rate (MFR) experiments. Fig. 2 shows the evolution of MFR with reprocessing steps; a continuous and exponential increase of the MFR parameter can be observed with consecutive reprocessing cycles, which is almost fourfold after the sixth recycling step. This increase in the fluidity of reprocessed PET may be related to progressive diminution of the molecular weight through

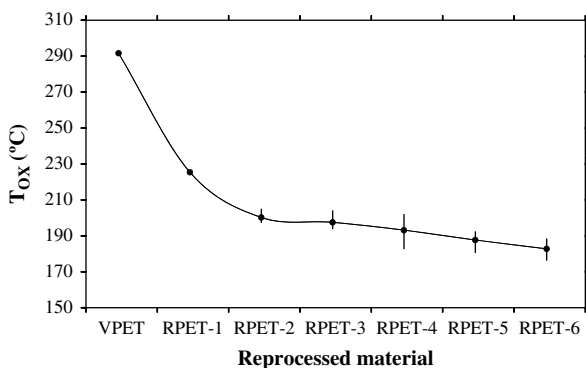


Fig. 3. Effect of reprocessing on the oxidation temperature (T_{Ox}) of PET.

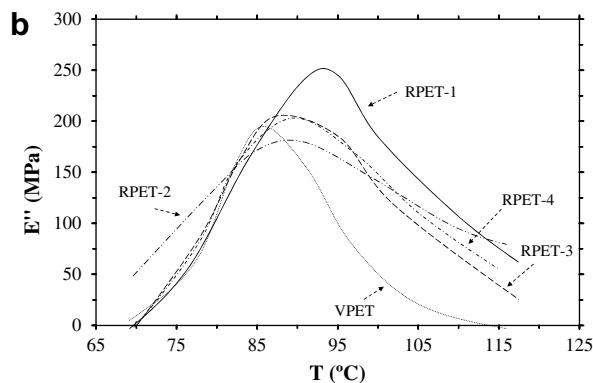
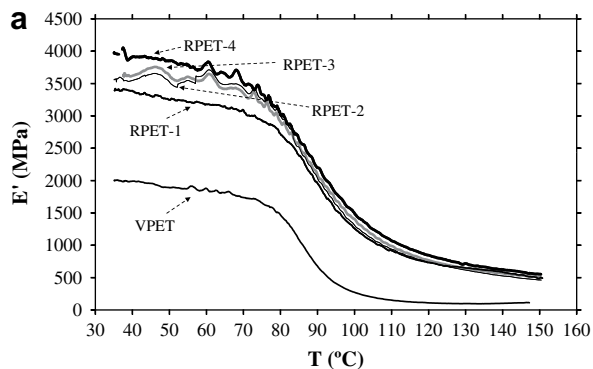


Fig. 4. Reprocessing influence on the dynamic-mechanical behavior of PET: a) storage modulus; b) loss modulus.

multiple processing; thermo-mechanical degradation at the extruder may induce chain scission reactions within the polymeric chain that contribute to this reduction [13].

3.2. Oxidative stability

The oxidation temperature (T_{Ox}) as calculated using differential scanning calorimetry is a standardized parameter, employed to assess the oxidative stability of

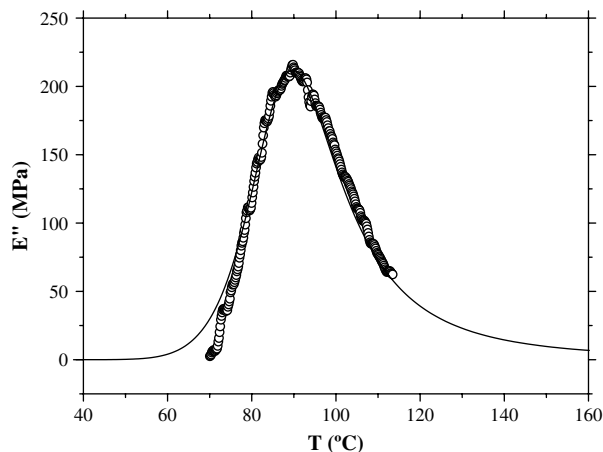


Fig. 5. Loss modulus experimental data fitting to Fuoss–Kirkwood model for virgin PET (○: experimental data; —: fitted function).

Table 1

Fuoss–Kirkwood parameters for virgin and reprocessed PET after loss modulus fitting as a function of temperature.

Material	E''_{\max} (MPa)	T_{\max} (°C)	$m_{\text{FK}} \cdot E_a \cdot R^{-1}$ (K)	R^2 (fitting coefficient)
VPET	202.8	86.4	1310.6	0.994
RPET-1	254.3	92.4	1045.3	0.983
RPET-2	190.2	89.2	616.9	0.987
RPET-3	212.0	89.7	843.9	0.967
RPET-4	213.1	89.7	881.6	0.973

commercial polymeric materials. The initial extrusion steps are responsible for dramatic decrease of the T_{Ox} parameter, with a reduction of approximately 30% of the initial value after 2 processing steps (Fig. 3). From the third reprocessing step on, no significant differences are noticed, since the parameter reaches an almost constant value. It is supposed that the oxidative stability is mainly affected by thermo-mechanical degradation only during the first steps of extrusion and further reprocessing cycles would not alter that trend. Contradictory information is therefore shown: on the one hand, MFR increases almost exponentially with increasing reprocessing cycles; on the other hand, the oxidative stability is mainly affected during the first processing step, but subsequent reprocessing steps slightly modify the stabilization properties. Further analyses are therefore required to evaluate the degradation effects and the quality of in-plant recycled PET.

3.3. Dynamic-mechanical-thermal analysis (DMTA)

The influence of multiple processing on the dynamic-mechanical properties of PET was evaluated using DMTA tests. The storage (E') and loss modulus (E'') were recorded

for PET reprocessed samples and their evolution as a function of temperature is displayed in Fig. 4. Reprocessing induces a progressive increase of the storage modulus of PET up to four extrusion cycles, both below and above the glass transition region (Fig. 4a). No spectra could be obtained for PET samples submitted to more than four reprocessing cycles, due to the brittleness induced by reprocessing and the loss of its plastic properties. The mechanical and plastic performance of in-plant recycled PET in second-market application may be therefore only guaranteed up to four processing cycles. The higher storage modulus of PET through repeated extrusion may be caused by chain scission reactions induced by thermo-mechanical degradation, which produce progressively shorter polymeric chains that have the ability to crystallize more freely during cooling after each extrusion, leading to the embrittlement of the material and the decrease of its deformation capacity [9,22].

A prominent viscoelastic relaxation in the loss modulus can be observed for virgin and reprocessed PET between 70 and 100 °C, which is assigned to the glass transition of PET chains (Fig. 4b). In general, reprocessed samples exhibit a broader loss modulus peak displaced to higher temperatures, compared to virgin PET. A deeper analysis on the influence of multiple processing on the glass transition relaxation was performed by fitting the experimental loss modulus values as a function of temperature to the empirical Fuoss–Kirkwood model (Fig. 5), as reported in previous studies [16].

$$E''(T) = \frac{E''_{\max}}{\cos h \left(m_{\text{FK}} \frac{E_a}{R} \left(\frac{1}{T} - \frac{1}{T_{\max}} \right) \right)}$$

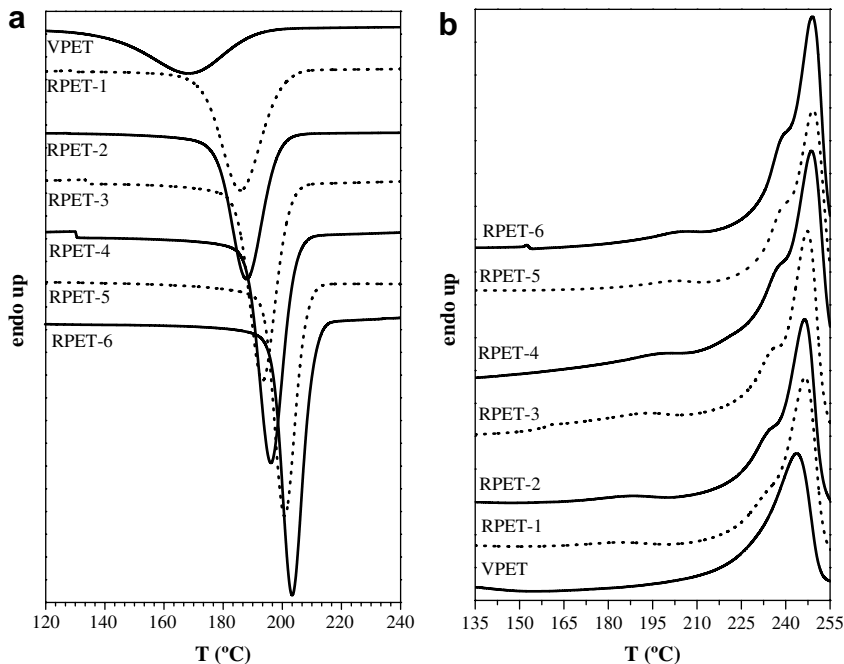


Fig. 6. DSC thermograms for virgin and reprocessed PET: a) crystallization scan; b) second melting scan.

E''_{\max} is the maximum of the loss modulus; m_{FK} is the Fuoss–Kirkwood parameter; E_a is the activation energy of the relaxation process; R is the ideal gas constant; T is the temperature; T_{\max} is the temperature of the maximum of the loss modulus, which is related to the glass transition temperature at a frequency of 1 Hz. The fitted values of T_{\max} and the dispersion parameter $m_{FK} \cdot E_a \cdot R^{-1}$, which is inversely related to the width of the viscoelastic relaxation, are presented in Table 1 for virgin and reprocessed PET samples. The value of T_{\max} is higher for reprocessed PET compared to that of virgin PET, while the dispersion parameter decreases with consecutive extrusion cycles. The broadening and the shift of the relaxation curves towards higher temperatures with multiple processing may be explained as due to thermo-mechanical degradation effects on PET chains. Random scission of PET chain linkages caused by mechanical and thermal stress in the extruder may lead to a diverse distribution of polymeric chain lengths, which may crystallize forming heterogeneous crystalline domains. These more abundant and heterogeneously distributed crystalline regions may hinder the mobility of the amorphous regions within the glass transition relaxation, causing broader and less regular loss modulus curves through the temperature range, and displacement of the relaxation peak to higher temperatures.

3.4. Melting and crystalline behavior

The study of the melting and crystallization behavior using differential scanning calorimetry was performed to prove the hypotheses established in the discussion of the dynamical-mechanical analyses and to get a deeper insight into the microstructural changes caused by multiple processing. Parameters such as melting and crystallization temperatures and enthalpies, as well as the crystallinity degree, the lamellar thickness distribution and the glass transition temperature were the main focuses of the study.

The influence of reprocessing on the crystallization behavior has been studied from the cooling thermograms (Fig. 6a); the crystallization temperatures (T_C) and crystallization enthalpies (ΔH_C) could be recorded and are displayed in Table 2. Once the previous thermal history of the materials has been erased by the first heating scan, the chains are free to rearrange into a new crystalline stage. Cooling thermograms appear sharper and shifted to higher

Table 2

Calorimetric parameters for virgin and reprocessed PET: crystallization temperature (T_C), crystallization enthalpy (ΔH_C), glass transition temperature (T_g), melting temperature (T_m), melting enthalpy (ΔH_m), and degree of crystallinity (X_C).

Material	Cooling scan		Heating scan			
	T_C (°C)	ΔH_C (J/g)	T_g (°C)	T_m (°C)	ΔH_m (J/g)	X_C (%)
VPET	170.3	−44.0	79.0	243.7	43.9	31.4
RPET-1	183.9	−57.5	79.1	246.1	57.7	41.2
RPET-2	188.2	−59.5	78.5	245.5	56.2	40.2
RPET-3	193.7	−66.8	78.3	247.0	67.6	48.3
RPET-4	196.5	−77.4	82.9	247.7	71.9	51.3
RPET-5	201.1	−67.4	84.9	248.7	59.6	42.6
RPET-6	202.9	−78.4	85.3	248.0	67.4	48.2

temperatures with every reprocessing cycle, indicating that the crystallization process occurs earlier and faster for samples subjected increased number of extrusion cycles.

Fig. 6b displays the curves of the second heating scan for the study of the effects of reprocessing on the melting behavior. The melting temperatures (T_m), the melting enthalpies (ΔH_m) and the glass transition temperatures (T_g), have been directly calculated from the thermograms; the degree of crystallinity (X_C) could equally be calculated as:

$$X_C = \frac{\Delta H_m}{\Delta H_m^0}$$

where ΔH_m is the melting enthalpy and ΔH_m^0 the theoretical melting enthalpy of the fully crystalline PET, assumed to be 140 J/g [23]. These results are fully presented in Table 2. In all cases, the degree of crystallinity (X_C) is higher for the reprocessed samples than for virgin PET, and also progressively increases with every reprocessing step. These results are in agreement with the dynamic-mechanical

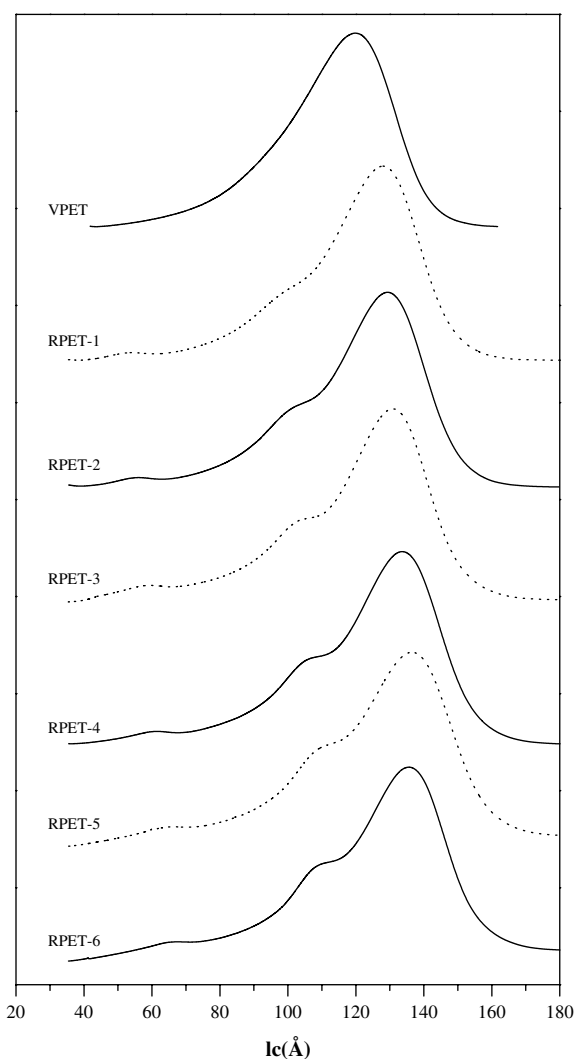


Fig. 7. Lamellar thickness distribution evolution for virgin and reprocessed PET.

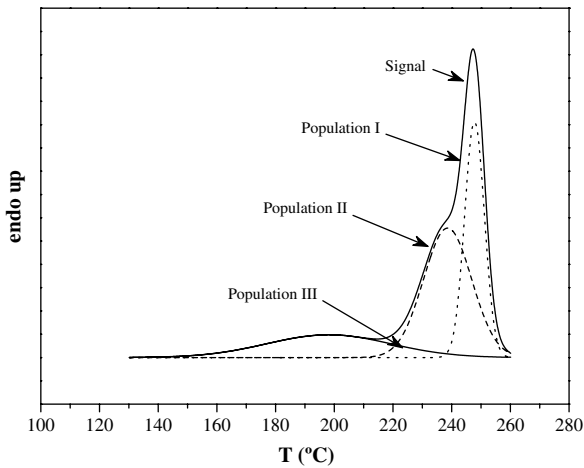


Fig. 8. Deconvolution of the melting calorimetric thermogram into crystalline populations I, II, and III for PET reprocessed 4 times.

behavior and prove the hypotheses presented; chain scission caused by thermo-mechanical degradation at the extruder may produce an increase in crystallinity and, as a result, a loss of mechanical and plastic properties.

On the other hand, the melting curves increasingly spread out through the temperature region with every reprocessing step, which may suggest the modification of the crystalline population under repeated extrusion. The lamellar thickness (l_c) distribution was therefore studied applying the Hoffman–Lauritzen nucleation theory [24–26] to relate the evolution of the l_c distribution with the reprocessing simulation. The Thomson–Gibbs equation was employed to assess the evolution of the lamellar thickness distribution:

$$l_c = \left[\left(1 - \frac{T_m}{T_m^0} \right) \frac{\Delta h_{mV}}{2\sigma_e} \right]^{-1}$$

where T_m is the melting temperature; T_m^0 is the equilibrium melting temperature of an infinite crystal (564 K); σ_e is the surface free energy of the basal plane where the chains fold (0.106 J m^{-2}); Δh_{mV} is the melting enthalpy per volume unit ($2.1 \times 10^8 \text{ J m}^{-3}$), both values obtained from Lu and Hay [27]. Fig. 7 represents the l_c distribution for virgin PET and each reprocessed sample. In this figure, a prominent distribution related to the most probable lamellar size can

be seen. The plots shift to higher l_c values with every reprocessing step, showing the continuous formation of crystalline zones with higher lamellae size. However, a closer inspection of the lamellar distribution curve revealed the presence of various small shoulders overlapped to the principal distribution which are more prominent with each reprocessing step. The chain scissions may enhance the crystallization and segregation of crystals with different crystalline sizes, highlighting the heterogeneity of this material.

In order to better understand the effects of the degradation process on the crystalline phase, the endothermic peaks of the second heating scan were carefully studied. A multimodal endothermic behavior, attributed to a segregation of the initial crystalline distribution into three main populations can be observed. A deconvolution procedure was applied to the melting thermograms in order to individually characterize the behavior of each population and their contribution to the overall effect using a partial areas study. The following expression was employed as deconvolution model:

$$l_c(T) = \sum_i A_i \exp\left(\frac{-(T - T_i)^2}{\frac{w_i^2}{\ln(16)}}\right)$$

where T_i represents the average value of the temperatures range considered; A_i is the maximum intensity of the curve; w_i acts as a dispersion parameter. Fig. 8 gives an example of the deconvolution model fitting to the experimental response. Populations have been labeled as I, II and III, from the higher to the lower peak temperature, and their melting enthalpies and temperatures are shown at Table 3. A shift of the T_m of approximately 5°C for populations I and II and 20°C for population III can be observed. The partial crystallinity of each population X_C^i has been calculated as $\Delta H_m^i / \Delta H_m^0$ (for $i = \text{I, II, III}$). Population III seems to be more affected by reprocessing operations, as X_C^{III} reached doubled values from the third recycle on. Furthermore, in order to analyze the contribution of each partial crystallinity to the overall crystallinity, a new parameter (relative partial crystallinity) is calculated as $X^i = X_C^i / X_C$. This parameter clearly demonstrates that population I diminishes, population II does not show a specific variation trend, and for population III an overall increase of X^{III} is seen through the reprocessing cycles.

As it was discussed from the results of DMA, the increase in the degree of crystallinity may influence the values of glass transition temperature (T_g) calculated from

Table 3

Individual melting parameters and partial crystallinity for each population after deconvolution of the melting calorimetric thermograms for virgin and reprocessed PET.

Material	Population I				Population II				Population III			
	T_m^{I} ($^\circ\text{C}$)	ΔH_m^{I} (J/g)	X_C^{I} (%)	X^{I} (%)	T_m^{II} ($^\circ\text{C}$)	ΔH_m^{II} (J/g)	X_C^{II} (%)	X^{II} (%)	T_m^{III} ($^\circ\text{C}$)	ΔH_m^{III} (J/g)	X_C^{III} (%)	X^{III} (%)
VPET	243.7	43.9	31.4	–	–	–	–	–	–	–	–	–
RPET-1	246.1	23.3	16.6	40.3	235.9	27.8	19.8	48.1	184.3	6.7	4.8	11.6
RPET-2	245.5	21.4	15.3	38.0	236.7	28.0	20.0	49.8	189.4	6.9	4.9	12.2
RPET-3	247.0	22.6	16.1	33.2	236.9	28.9	20.6	42.6	195.4	16.4	11.7	24.2
RPET-4	247.7	25.0	17.9	34.6	238.2	33.9	24.2	46.9	197.3	13.3	9.5	18.5
RPET-5	248.7	19.6	14.0	32.8	240.7	27.7	19.8	46.6	204.3	12.3	8.8	20.7
RPET-6	248.0	22.3	15.9	34.1	240.7	29.7	21.2	45.4	205.3	13.4	9.6	20.6

the calorimetric scans (Table 2). The T_g values show small variations until the fourth reprocessing cycle, and continuously increases up to 6 °C. As the amount of free chains induced by thermo-mechanical degradation is rising, the tendency of the smaller chains to fit among the larger ones facilitates the packing of these chains in crystalline domains, decreasing the amount of amorphous areas. Hence, more energy would be required to increase the mobility of the amorphous regions and to achieve the glass transition [28].

4. Conclusions

Multiple processing has been proposed to mimic the thermo-mechanical degradation effects on the microstructure and properties of poly(ethylene terephthalate) (PET) under mechanical recycling. The results of commonly-employed technological parameters, such as the melt-mass flow rate (MFR) and the oxidation temperature (T_{Ox}), have been compared with the structural information provided by thermal analysis techniques such as dynamic-mechanical analysis (DMA) and differential scanning calorimetry (DSC). It was demonstrated that the employment of MFR and T_{Ox} parameters alone may induce misleading information when the degradation state and the quality of recycled PET is assessed.

Thermo-mechanical degradation causes deep changes in the microstructure and properties of PET under recycling. A dramatic increase in the degree of crystallinity is observed during consecutive extrusion cycles, leading to significant embrittlement of the recycled material and the complete loss of its plastic deformation properties after 4 reprocessing cycles. Chain scission reactions induced under thermo-mechanical degradation may result in a heterogeneous distribution of polymeric chain lengths in the melt state, altering the subsequent amorphous and crystalline microstructure in recycled PET after chain rearrangement during cooling. The existence of a multimodal melting distribution in reprocessed PET could be verified using DSC; the enhanced crystallization and segregation of these populations could be studied in detail employing a deconvolution procedure in terms of their partial degree of crystallinity and their lamellar thickness distribution.

Acknowledgements

The authors would like to acknowledge the Spanish Ministry for Environment (Project 555/2006/3-6.1) for financial support. F.V. and J.D.B. want to thank the Spanish Ministry for Education and Science for the concession of a predoctoral research position through the FPU programme. AdvanSa is acknowledged for providing the material. Royal Institute of Technology (KTH) and Universidad Politécnica de Valencia (UPV) are thanked for additional economical support.

References

- [1] O. Olabisi (Ed.), Handbook of Thermoplastics, Marcel Dekker Inc., New York, 1997.
- [2] Plastics Europe (Ed.), The Compelling Facts About Plastics. An Analysis of Plastics Production, Demand and Recovery for 2005 in Europe (2007).
- [3] Petcore, PET collection statistics (2005).
- [4] F. Awaja, D. Pavel, Recycling of PET, European Polymer Journal 41 (7) (2005) 1453–1477.
- [5] G. Finnveden, J. Johansson, P. Lind, Å. Moberg, Life cycle assessment of energy from solid waste—part 1: general methodology and results, Journal of Cleaner Production 13 (3) (2005) 213–229.
- [6] F. Vilaplana, S. Karlsson, Quality concepts for the improved use of recycled polymeric materials: a review, Macromolecular Materials and Engineering 293 (4) (2008) 274–297.
- [7] S. Karlsson, Recycled polyolefins. Material properties and means for quality determination, Advances in Polymer Science 169 (2004) 201–230.
- [8] M. Day, D.-M. Wiles, Photochemical degradation of poly(ethylene terephthalate). III. Determination of decomposition products and reaction mechanism, Journal of Applied Polymer Science 16 (1972) 191.
- [9] N. Torres, J.-J. Robin, B. Boutevin, Study of thermal and mechanical properties of virgin and recycled poly(ethylene terephthalate) before and after injection molding, European Polymer Journal 36 (10) (2000) 2075–2080.
- [10] R.-J. Ehrig (Ed.), Plastics Recycling: Products and Processes, Hanser Publishers, New York, 1992.
- [11] L. Reigh, S. Stivala (Eds.), Elements of Polymer Degradation, McGraw-Hill, New York, 1971.
- [12] X. Colin, J. Verdu, Polymer degradation during processing, Comptes Rendus Chimie 9 (2006) 1380–1395.
- [13] M.-A. Silva-Spinace, M.-A. De Paoli, Characterization of poly(ethylene terephthalate) after multiple processing cycles, Journal of Applied Polymer Science 80 (2001) 20–25.
- [14] S. Karlsson, Advances in Polymer Science 169 (2004) 201–229.
- [15] A. Pawlak, M. Pluta, J. Morawiec, A. Galeski, M. Pracella, Characterization of scrap poly(ethylene terephthalate), European Polymer Journal 36 (9) (2000) 1875–1884.
- [16] F. Vilaplana, A. Ribes-Greus, S. Karlsson, Degradation of recycled high-impact polystyrene. Simulation by reprocessing and thermo-oxidation, Polymer Degradation and Stability 91 (9) (2006) 2163–2170.
- [17] A. Oromiehie, A. Mamizadeh, Recycling PET beverage bottles and improving properties, Polymer International 53 (2004) 728–732.
- [18] R. Assadi, X. Colin, J. Verdu, Irreversible structural changes during PET recycling by extrusion, Polymer 45 (2004) 4403–4412.
- [19] L. Santonja-Blasco, L. Contat-Rodrigo, R. Moriana-Torró, Ribes-Greus, Thermal characterization of polyethylene blends with a biodegradable masterbatch subjected to thermo-oxidative treatment and subsequent soil burial test, Journal of Applied Polymer Science 106 (2007) 2218–2230.
- [20] R. Moriana-Torró, L. Contat-Rodrigo, L. Santonja-Blasco, A. Ribes-Greus, Thermal characterisation of photo-oxidized HDPE/Mater-BI and LDPE/Mater-BI blends buried in soil, Journal of Applied Polymer Science 109 (2008) 1177–1188.
- [21] S.-S. Hosseini, S. Taheri, A. Zadhoush, A. Mehrabani-Zeinabad, Hydrolytic degradation of poly(ethylene terephthalate), Journal of Applied Polymer Science 103 (2007) 2304–2309.
- [22] D. Fann, S.-K. Huang, J.-Y. Lee, Kinetics and thermal crystallinity of recycled PET.I. Dynamic cooling crystallization studies on blends recycled with engineering PET, Journal of Applied Polymer Science 61 (1996) 1375–1385.
- [23] B. Wunderlich (Ed.), Macromolecular Physics, vol. 1, A Press, New York and London, 1973 p. 389.
- [24] J.-L. Lauritzen, J.-D. Hoffman, Theory of formation of polymer crystals with folded chains in dilute solution, Journal of Research of the National Bureau of Standards 64 (A) (1960) 73–102.
- [25] J.-L. Lauritzen, J.-D. Hoffman, Crystallization of bulk polymers with chain folding: theory of growth of lamellar spherulites, Journal of Research of the National Bureau of Standards 65 (A) (1961) 297–336.
- [26] J.-D. Hoffman, G.-T. Davis, J. Lauritzen, The rate of crystallization of linear polymers with chain folding. Treatise on solid state chemistry, in: N.B. Hannay (Ed.), Crystalline and noncrystalline solids, vol. 3, Plenum Press, New York, 1976, pp. 497–614 (Chapter 7).
- [27] X.-F. Lu, J.-N. Hay, Isothermal crystallization kinetics and melting behaviour of poly(ethylene terephthalate), Polymer 42 (2001) 9423–9431.
- [28] S.-D. Mancini, M. Zanin, Consecutive steps of PET recycling by injection: evaluation of the produce and of the mechanical properties, Journal of Applied Polymer Science 76 (2000) 266–275.

CONTRIBUTION III-B

A statistical design of experiments for optimizing the MALDI-TOF-MS
sample preparation of polymers.

An application in the assessment of the thermo-mechanical degradation
mechanisms of poly (ethylene terephthalate)

J.D. Badia, E. Strömberg, A. Ribes-Greus, S. Karlsson

Analytica Chimica Acta 2011, 692; 85-95



A statistical design of experiments for optimizing the MALDI-TOF-MS sample preparation of polymers. An application in the assessment of the thermo-mechanical degradation mechanisms of poly (ethylene terephthalate)

J.D. Badía^a, E. Strömberg^b, A. Ribes-Greus^a, S. Karlsson^{b,*}

^a Instituto de Tecnología de Materiales (ITM), Universidad Politécnica de Valencia Camino de Vera s/n, E-46022 Valencia, Spain

^b School of Chemical Science and Engineering, Fibre and Polymer Technology, KTH – Royal Institute of Technology, Teknikringen 56-58, SE-10044 Stockholm, Sweden

ARTICLE INFO

Article history:

Received 22 January 2011

Received in revised form 21 February 2011

Accepted 27 February 2011

Available online 5 March 2011

Keywords:

Matrix-assisted laser desorption/ionization

time-of-flight

Mass spectrometry

Design of Experiments

Poly (ethylene terephthalate)

Recycling

Thermo-mechanical degradation

ABSTRACT

The sample preparation procedure for MALDI-TOF MS of polymers is addressed in this study by the application of a statistical Design of Experiments (DoE). Industrial poly (ethylene terephthalate) (PET) was chosen as model polymer. Different experimental settings (levels) for matrixes, analyte/matrix proportions and concentrations of cationization agent were considered. The quality parameters used for the analysis were signal-to-noise ratio and resolution. A closer inspection of the statistical results provided the study not only with the best combination of factors for the MALDI sample preparation, but also with a better understanding of the influence of the different factors, individually or in combination, to the signal. The application of DoE for the improvement of the MALDI measure of PET stated that the best combination of factors and levels was the following: matrix (dithranol), proportion analyte/matrix/cationization agent (1/15/1, V/V/V), and concentration of cationization agent (2 g L^{-1}). In a second part, multiple processing by means of successive injection cycles was used to simulate the thermo-mechanical degradation effects on the oligomeric distribution of PET under mechanical recycling. The application of MALDI-TOF-MS showed that thermo-mechanical degradation primarily affected initially predominant cyclic species. Several degradation mechanisms were proposed, remarking intramolecular transesterification and hydrolysis. The ether links of the glycol unit in PET were shown to act as potential reaction sites, driving the main reactions of degradation.

© 2011 Elsevier B.V. All rights reserved.

1. Introduction

Matrix-assisted laser desorption/ionization time-of-flight mass spectrometry (MALDI-TOF-MS) has gained attention during the last years as a potential technique for the analysis of the compositions,

end groups and, in some cases, molecular weight distributions of intact synthetic polymers [1]. Characteristics and main applications of MALDI can be found in several reviews [2,3]. Poly(ethylene terephthalate) (PET) has been extensively used over the last two decades, mainly in the food packaging sector, due to its excellent mechanical, chemical, processing and thermal properties [4], and therefore was taken as model polymer in this work.

The difficulty of performing good-quality and reliable MALDI measurements depend on many factors such as the molar mass of the polymer, the choice of solvent, the choice of matrix, the ratio analyte/matrix/cationization agent, the laser energy or the mode of detection (linear or reflector), among others [5]. Especially for the case of PET, the importance of the solubility in the sample preparation process has been discussed, and it was demonstrated that the use of the azeotropic mixture of dichloromethane (CH_2Cl_2) and 1,1,1,3,3,3-hexafluoro-2-propanol (commonly referred to as HFIP) 70:30 (V/V) could dissolve PET at room temperature as well as increase the solubility of different matrixes [6], which would enhance the homogeneity of the MALDI sample. Other studies have addressed the complexity of analyzing polymers with high molar mass [7,8] due to factors such as: the uncertainty in the choice of

Abbreviations: ϕ , diameter screw (injection machine); d, diameter pellet; DEG, diethyleneglycol; DHB, 2,5-dihydroxybenzoic acid; DoE, Design of Experiments; EG, ethylene glycol; F, factor (for the DoE); FA, ferulic acid; G, glycol unit (EG); GLM, general linear model; HABA, hydroxyphenylazo benzoic acid; IAA, trans-3-indoleacrylic acid; IP, interaction plot; m , number of GT repeating units ($m > n$); m/z , mass-to-charge ratio; MALDI, matrix-assisted laser desorption/ionization; MAC, combination of matrix/analyte/cationization agent; MEP, main effects plot; MMD, molar mass distribution; MS, mass spectrometry; n , number of GT repeating units; NaTFA, sodium trifluoroacetate; P , also p -value, statistic (for the DOE); PET, poly(ethylene terephthalate); pc-PET, post-consumed PET; RES, resolution; RPET- i , PET reprocessed i cycles; SA, sample analysis; SP, sample preparation; S/N , signal-to-noise ratio; T, terephthalate unit; THA, 2,4,6-trihydroxy acetophenone; TOF, time of flight; V, volume; VPET, virgin PET.

* Corresponding author. Present address: Skövde University, SE-541 28 Skövde, Sweden. Tel.: +46 87908581; fax: +46 810075.

E-mail addresses: sigbritt.karlsson@his.se, sigbritt@polymer.kth.se (S. Karlsson).

the optimal matrix to perform the measurement; the selection of the proportion analyte/matrix; or the suitability of adding a cationization agent. The decision usually is stated as a result of a trial and error empirical procedure [5,9–11]. Despite some studies report issues such as the selection of the best matrix [6] or the correlation of the laser energy with the obtained MALDI response [12], novel fast and cost-effective methodologies should be implemented, in order to optimize the performance of the MALDI measurement.

Design of Experiments (DoE) [13] stands as a useful, reliable and immediate procedure that can provide us not only with the best combination of factors for the preparation of the MALDI sample, as shown in literature [14–16], but also help understand the influence of each factor individually or in combination on the quality of the response.

MALDI studies of polyesters are of great interest [17–19], especially the studies of poly(ethylene terephthalate) (PET) under different degradation environments [7,8,20–25]. Degradation is usually explained as the formation and disappearance of linear and cyclic oligomeric species $[GT_L]_n$ and $[GT_C]_n$, where G is a glycol unit, T a terephthalate unit, n the number of repeating units forming the oligomers, and L and C stand for linear and cyclic, respectively. Degradation of PET under hydrolytic [7] conditions revealed the apparition of chain-scission processes generating carboxyl terminated oligomers $(H-[GT_L]_m-OH$ and $T-[GT_L]_m-OH)$ and ethylene glycol terminated oligomers $H-[GT_L]_m-GH$ (m : number of repeating units being $m < n$). Plasma-oxidative and chemical treatment [21] induced ester scission processes that yield $H-[GT_L]_n-OH$ species, decreased the presence of $[GT_C]_n$ and showed an increase of $[GT_C]_n-G$ species. Thermal degradation, at the common processing temperature close to 280°C [22] showed the formation of cyclic and linear anhydride oligomers, which auto-catalyzed hydrolytic reactions with the consequent increase of carboxyl terminated polyester chains $H-[GT_L]_n-OH$. When this degradation was experienced in oxidizing atmosphere [24,25], the study of the discoloration mechanisms was achieved, also demonstrating that formation of cyclic and carboxyl terminated species formed via chain scission in the ether link of PET are indicative of degradation. Most of the aforementioned studies [17–25] were applied to PET samples synthesized at the labs, and not to industrially obtained specimens. In addition, these studies were performed after dissolution–concentration–separation–dissolution or to filtered extracts after PET dissolution [8,25] which can offer good spectra, but also inadvertently discard the apparition of species which might be important for the elucidation of the degradation mechanisms. However, studies performed directly on polymeric pellets have been scarcely reported [24]. In contrast, the present study was performed on neat PET which is totally dissolved along with the matrix and a cationization agent and directly spotted on the MALDI plate, being the sample preparation procedure widely discussed.

The amount of post-consumer PET (pc-PET) present in urban solid waste is high and has to be managed. During its life cycle (synthesis, processing, use, discarding, cleaning, recycling), PET is subjected to the interaction of degradation agents such as oxygen, light, mechanical stresses, temperature or water. Individually or synergically, these agents may provoke the breakage of the macromolecules and diminish the final properties and productivity during processing [26–29]. Major applications of recycled pc-PET are in the textile industry, but new mechanical recycling technologies such as superclean[®] and bottle-to-bottle[®] point out the legal possibility of using certain fraction of pc-PET in new food-contact packages [30,31]. Therefore, the influence of recycling on the PET structure and the consequent presence of low molecular weight compounds (LMWC) must be assessed in order to prevent the consumer from the ingestion of hazardous substances. With the purpose of facing this problem, the application of protocols

to simulate the degradation subjected during the recycling process by polymers has been successfully performed for commodities [32–38] such as polyethylene (PE) [32], polypropylene (PP) [32], polystyrene (PS) [33,34], poly(vinyl chloride) (PVC) [35] or PET [36–38]. However, the studies on the application of MALDI to characterize the effect of multiple processing on the PET structure are still few [8,25], and based on the analysis of low-molecular weight PET oligomers. Latest publications study the influence of thermo-mechanical degradation applied by successive extrusion cycles on industrial PET samples. Authors propose an oligomer degradation model in which the most indicative fact is the loss of $[GT_C]_n-G$ species for the formation of $H-[GT_L]_n-OH$ and $[GT_C]_n$ species via degradation mainly occurring in the ether link of the dyethylene glycol (DEG) unit. In the present work, the influence of successive injection molding operations is addressed.

Summing up, this work is devoted to a double purpose: in the first part of the study, a statistical Design of Experiments (DoE) is used to find the appropriate settings for the sample preparation of MALDI for polymers, taking poly(ethylene terephthalate) (PET) as model; in the second part, a simulation of mechanical reprocessing was carried out by multiple injection molding cycles on commercial PET and the influence of thermo-mechanical degradation was monitored by the use of MALDI.

2. Statistical Design of Experiments (DoE)

Design of Experiments (DoE) can remarkably improve the characteristics of the study: if the variables really act in an additive way, DoE permits the estimation with higher precision; but if variables do not act additively, DoE is capable of detecting and estimating the interactions of variables and measuring this non-additivity [13]. DoE plays a fundamental role in the resolution of scientific and industrial problems [39] which involve the study of the influence (Effect, E) of multiple input variables (Factors, F) on the experimental outcome, i.e. the response. F can be either quantitative (categorical variable) or qualitative (based on a continuous variable but only use a few controlled values in the experiment). Each factor must have two or more settings (Levels, L) so that the E of change in L can be assessed on the response. Any combination of factors and levels (F/L) corresponds to a run in practical experimentation. Factorial design concerns the selection and arrangement of F/L combination, where investigators select F to systematically vary along different L during an experiment in order to determine their E on the response. After screening the F to determine which are important for explaining process variation, DoE is useful to understand how F interact and drive the measurement and consequently helps select the F/L that produce optimal process performance.

DoE is performed by the use of the General Linear Model (GLM) [13], which comprises the univariate analysis of variance with balanced and unbalanced designs, analysis of covariance, and regression, for each response variable. Interpretation of results is drawn from main effects plots (MEP) and interaction plots (IP). MEP show the direct E of each F on the response, evaluated along the different L considered. IP are useful for the study of interactions between F by means of the comparison of the relative strength of the E across F . An interaction between F occurs when the change in response from the low- L to the high- L of one F is not the same as the change in response at the same two L of a second F . That is, the E of one F is dependent upon a second F [13]. It is also worth mentioning that the reproducibility of the experiments must be carefully taken into account. Repeated and replicated measurements are both multiple response measurements taken at the same F/L combination; but repeated measurements are taken during the same experimental run or consecutive runs, while replicated measurements are taken during identical but distinct experimental runs, which are often randomized. Whether repeats or replicates are used, it

Table 1
Summary of factors, levels and general characteristics of the design of experiments applied in this study.

Factor	Type	Number of levels	Levels			Effects	
Matrix	Qualitative	3	Dithranol	HABA	FA	S/N	S/N_{rel}
Proportion of analyte/matrix (V:V)	Quantitative	3	1/5	1/10	1/15	RES	RES_{rel}
C_{NaTFA} (g L ⁻¹)	Quantitative	4	0	0.5	1	2	
Replicates	3	Total blocks	3				
Base runs	36 (3 ² ·4 ¹)	Total runs	108				

depends on the sources of variability interesting to explore and the resource constraints of the experiment. Designs with both repeats and replicates enable to examine multiple sources of variability from experimental handling of tests. Further details can be found in literature [13].

The application of DoE is therefore very valuable, not only for the determination of the optimal settings of an experiment, but also for the understanding of the effect of each factor at different levels, individually or in combination, to the final response.

3. Experimental procedure

3.1. Materials and reagents

Poly (ethylene terephthalate) (PET) SEDAPET SP04 was a bottle-grade PET obtained from Catalana de Polimers S.A. [40], Grup LaSeda (Barcelona, Spain) in the form of pellets. MALDI matrixes, namely 1,8,9-anthracenetriol (dithranol), 2-(4-hydroxyphenylazo)benzoic acid (HABA), trans-3-indoleacrylic acid (IAA), 2,4,6-trihydroxy acetophenone (THA), ferulic acid (FA), 2,5-dihydroxybenzoic acid (DHB), as well as the cationization agent, sodium trifluoroacetate (NaTFA), were purchased from Sigma-Aldrich (Stockholm, Sweden). 1,1,1,3,3,3-Hexafluoro-2-propanol (HFIP) and dichloromethane (CH₂Cl₂) were purchased from VWR (Sweden).

3.2. Reprocessing simulation

Prior to processing, virgin PET (VPET) pellets were dried during 5 h at 160 °C in a dehumidifier Conair Micro-D FCO 1500/3 (UK), in order to remove as much humidity as possible from the PET flakes [26]. Afterwards, samples were processed by means of injection molding employing an Arburg 420 C 1000-350 (Germany) injector, single-screw model (diameter $\Phi = 35$ mm, length/ $\Phi = 23$). Successive processing steps were applied under the same conditions. Temperature gradient set from hopper to die was 270, 275, 280, 285 and 280 °C. Moulds were set at 15 °C. Cooling time residence was 40 s and total residence time ca. 60 s. Samples were dried before each processing cycle. After injection, a fraction of the samples was kept as test specimen and the rest was ground by means of a cutting mill Retsch SM2000 (UK), which provided pellets of size $\Phi < 20$ mm to be fed back into the recirculation process. Up to five processing cycles were applied to obtain the different testing specimens of reprocessed PET (RPET-*i*, with *i*: 1–5).

3.3. MALDI sample preparation and analysis

MALDI sample mixtures (matrix (*M*) + analyte (*A*) + cationization agent (*C*), *MAC*) were prepared in laboratory conditions according to ISO 291, atmosphere 23/50, class 1 [41]. Individual solutions of *M* and *A* in HFIP/CH₂Cl₂ (30:70, V:V) were arranged at a concentration of 10 g L⁻¹. According to the Design of Experiments (see Section 4.1), different volumetric proportions of *M/A* were applied. As well, the solutions of *C* at different concentrations were added to the *MAC* in the same volumetric amount as the *A*. More details are given

in Table 1. The mixtures were then vortexed using a Vortex Genie (Scientific Industries, Bohemia, NY, USA). Approximately 0.5 μ L of the sample mixture were added on the target plate and the spots were allowed to dry at ambient temperature before insertion into the instrument.

MALDI-TOF-MS experiments were conducted by means of a Bruker UltraFlex MALDI-TOF mass spectrometer with a SCOUT-MTP ion source (Bruker Daltonics, USA) equipped with a nitrogen laser (337 nm), a gridless ion source and a reflector. All spectra were acquired in the reflector positive ion mode with an acceleration voltage of 25 kV and a reflector voltage of 26.3 kV. The detector *m/z* range was 1600–10,000 Da in order to exclude high intensity signals arising from the low mass ions and to cover the whole PET mass spectrum. The laser intensity was set to the maximum value possible to acquire high resolution spectra, which were gathered by irradiating 40–50 different positions at the center area on the sample spot, with a total of 2500 shots per sample. Time-to-mass conversion of time-of-flight mass spectra was achieved using a self-calibration method [42]. All spectra were treated using FlexAnalysis 2.4 (Bruker Daltonics, USA) software. Interpretation of data was performed taking into account all decimals of the atomic masses composing the oligomers, but note that *m/z* values are given with only one decimal along the document. Statistical Design of Experiments was aided by Minitab® 15.1.0.0 software (Minitab Inc., USA).

4. Results and discussion

4.1. Determination of the experimental factors and levels considered for DoE analysis of MALDI sample preparation

In order to optimize the MALDI measurement, the identification of the experimental factors (and levels) susceptible of being tailored is a critical step. Generally speaking, in a MALDI experiment, two main stages can be distinguished: sample preparation (*SP*) and sample analysis (*SA*). Wetzel et al. [14] considered experimental parameters in the *SA* stage for different mixtures of polystyrene with dithranol and retinoic acid focusing on those mixtures which gave better quality signal. On the other hand, Brandt et al. [16] investigated the effect of the molar mixing ratio for several synthetic polymers, stating that the optimal value depended on the studied combination of matrix, polymer and solvent used in the *SP* stage, setting in this case the experimental settings for the *SA*.

Given that each variable (factor *F*) is assessed at different settings (levels *L*), it is therefore a huge amount of *F/L* combinations and thus considering a Design of Experiments to study the interaction of all of them shall not be operative, since this fact would imply the necessity of performing a large number of runs [16]. Different variables were therefore identified, since a *SP* of good quality must consider the interaction matrix-analyte, which mainly means the choice of a suitable matrix, the selection of the best solvent for the mixture matrix/analyte/cationization agent (*MAC*), the proportion between all the components of the *MAC* and the role of adding salt. On the other hand, an appropriate *SA* takes into account parameters such as the power of the laser employed or the detection mode (linear-reflector, positive-negative). Preliminary experiments and

Table 2
Results of analysis of variance in terms of p -value ($\alpha/\text{symbol} = 0.05$) after application of the design of experiments to MALDI-TOF-MS spectra of virgin PET.

Factors	Effect			
	S/N	RES	S/N_{rel}	RES_{rel}
Blocks	0.414	0.009	0.357	0.183
Main				
Matrix	0	0	0	0
Proportion	0	0	0.021	0.059
C_{NaTFA}	0	0	0.067	0.107
Interactions				
Matrix and proportion	0	0	0.014	0.013
Matrix and C_{NaTFA}	0	0	0	0
Proportion and C_{NaTFA}	0	0	0.005	0.033
Matrix and proportion and C_{NaTFA}	0	0	0.129	0.001
R^2 (%)	96.21	91.31	69.88	76.67

some considerations were thus performed to decrease this amount of F/L .

Actions on the Sample Analysis stage are stated as follows: After a screening, the power of the laser was set to the maximum possible (70% according to technical settings), in order to avoid burning the MAC during the flight of ions and therefore reduce the appearance of high-intensity background peaks, which could decrease the signal-to-noise ratio and the resolution of the measurement [43]. According to Montaudo et al. [5], the linear mode is essentially used for the determination of the molar mass distribution (MMD) of polymers, whereas the reflector mode allows for the identification of oligomers or side-products, as well as the characterization of end-groups. Since this work was focused on the effects of reprocessing on PET structure and thus the apparition of new oligomers, and the correlation between the MMD of polymers drawn by MALDI and other techniques, i.e. size exclusion chromatography (SEC), is not clear yet [44], the reflector mode was preferred. In addition, the MALDI measurements were performed in the <10,000 Da mass range, in which the highest mass resolution and the best conditions for the formation of molecular ions were encountered. Polycondensation polymers usually present cyclic low molar mass oligomers that may affect the physical properties of polyesters, causing problems in their processing steps [25]. In this range, the study of the degradation reactions taking place during the processing of polymers can be achieved. Finally, the use of cationization agents preferably promotes positive ions to the flying adducts, so therefore the positive detection mode was more suitable.

On the other hand, actions taken to reduce the span of F/L at the sample preparation stage required special attention, due to the strong influence on the quality of the MALDI spectra [5]: Firstly, an ideal matrix should have the following properties: high electronic absorption at the employed wavelength, good vacuum stability, low vapor pressure, and good miscibility with the analyte in the solid-state [5]. Exhaustive list of useful matrices are available in the literature [45]. Dithranol, HABA, FA, IAA, THA and s-DHB have been successfully used in other studies with PET or polyesters [6], and therefore were considered for sample preparation. Secondly, a very important factor taken into account was the selection of an appropriate solvent that could dissolve PET at room temperature. For this reason, the use of the azeotropic mixture of dichloromethane (CH_2Cl_2) and 1,1,1,3,3,3-hexafluoro-2-propanol (HFIP) (70:30, V:V) was chosen [6]. In this sense, when the choice of a suitable matrix was addressed, it was extremely important that the mixture behaved as one during the evaporation process of the solvent, avoiding therefore sample segregation, which could thus impoverish the quality of the signal [6]. When the aforementioned matrices were tested at 10 g L^{-1} in the azeotrope, only the three first resulted soluble. Finally, the ionization process of MALDI can be aided by the addition of a sodium (Na) or potassium (K) salt. Since polyesters are relatively polar polymers, Na^+ and K^+ charged species

can be observed in the MALDI spectra, even if they are not deliberately added to the matrix/analyte mixture [46–48]. It is known that these cations are present as impurities in matrices, reagents, solvents or glassware among other sources, and therefore polymers with high cation affinity do not necessarily need a high amount of extra salt in the MAC sample [5]. The presence of specific functional groups in the polymer, such as carboxyl and hydroxyl is very important in the cationization process [49]. In addition, matrices such as HABA and dithranol are particularly insensitive to impurities [2] and therefore the study of the addition of a cationization agent for this MALDI experiment of poly(ethylene terephthalate) is justified. Sodium Trifluoroacetate (NaTFA) was chosen as a source of ions. The quantity of NaTFA to be added to the MAC was also investigated, in order to explore its influence on the quality of the MALDI response.

4.2. Design of experiments applied to MALDI spectra of PET

In the previous section, the span of MALDI key factors F was reduced to three: selection of a suitable matrix, proportion of analyte/matrix and the concentration of the cationization agent (NaTFA). A general factorial design [13] was performed, taking into account the levels L at which each F were analyzed summarized in Table 1.

In order to perform the Design of Experiments, a significant step is the correct choice of parameters to be considered as reliable effects E . Some authors considered the signal-to-noise ratio S/N for assessing the quality of MALDI in DoE studies [14,15]. Others also used the Resolution RES as suitable quality indicator [16]. Both responses were chosen in this study as Effects for the DoE. After a first screening, the adducts which provided with the signal of highest intensity were the sodium adducts corresponding to cyclic oligomers $[\text{GT}_C]_n$ (see structure in Table 3), and thus were chosen for the analysis. Wetzel et al. [14] studied the S/N of three selected peaks in the low, center and high m/z range. Brandt et al. [16] applied their study focused on the peak at the maximum of the distribution. With the aim of improving the validity of this analysis, a span of 1500 m/z between 2000 and 3500 m/z in which up to seven $[\text{GT}_C]_n \text{ Na}^+$ peaks (2136.8, 2329.0, 2521.2, 2713.2, 2905.5, 3097.6, 3289.8 and 3482.0 m/z), with a separation of a $[\text{GT}]$ repeating unit (192.168 m/z) was chosen for characterization. This region was preferred in order to avoid the interaction with the decomposition range of the matrix at lower m/z , covering the m/z range where the MALDI signal of PET is significant. Absolute and relative E (being $E = S/N$ or RES) were analyzed as follows:

$$E = \sum_i \left(E_i \cdot \frac{I_i}{I_{\text{max}}} \right) \quad (1)$$

$$E_{\text{rel}} = \sum_i \left(\frac{E_i}{E_{\text{max}}} \cdot \frac{I_i}{I_{\text{max}}} \right) \quad (2)$$

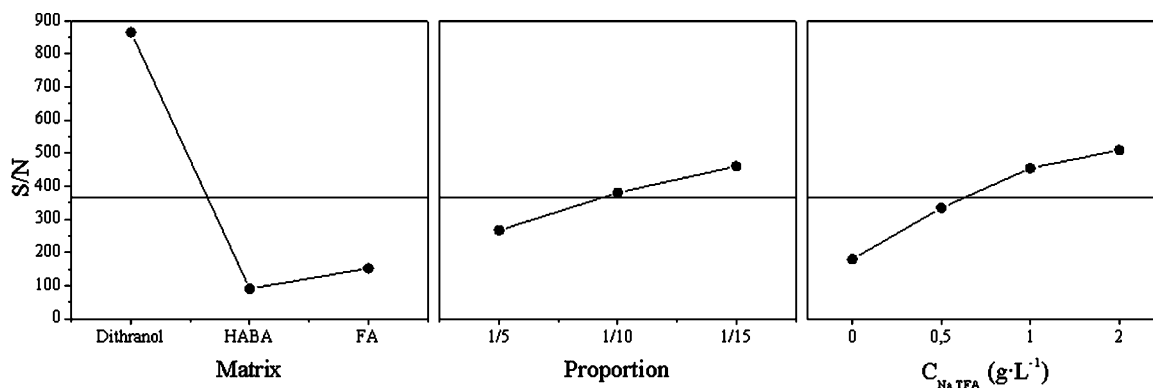


Fig. 1. Main effects plot for the analysis of the signal-to-noise (S/N) ratio.

where I is the intensity of the peak, I_{max} the maximum intensity, E_{max} the maximum effect and i is the counter of the seven studied peaks. Table 2 shows the results of the analysis of variance in terms of p -value (P) and adjusted regression coefficient (R^2) for each E according to the General Linear Model (GLM) [13] applied for the evaluation of the quality of the DoE. The statistic P measures the significance of a change in level of a factor, individual or in combination with other factors (interaction), to the effect. If P is lower than or equal to a confidence value (α), then the factor or the interaction is significant, and its assessment is worth. It can be seen how for the absolute effects (S/N and RES), all factors and interactions have to be considered, since $P < \alpha$ (the common $\alpha = 5\%$ has been chosen). The use of relative effects (S/N_{rel} and RES_{rel}) might reduce the number of experimental runs to study, since some factors and interactions seem to be not significant ($P > \alpha$). It is also important to state that the experimental procedure followed for the sample preparation was reproduced under the same conditions to assure the good performance of the DoE [13]. In this sense, the fact of carrying out the experiments by triplicate added a new factor to the DoE analysis ("Blocks" in Minitab), but no relationship between this factor and both effects (S/N and RES) was found, which confirms that there was no significant experimental error related to the sample preparation affecting the quality of the results. Apart from P , R^2 measures the suitability of the GLM to explain the variability of data. The closer R^2 is to 1, the better is the selection of the effect to characterize the experiment under consideration. Therefore, absolute effects were chosen, since the relative parameters offered a confidence value far below 95%. All experiments for the combination of the three factors at all levels were therefore applied.

Main effects plots (MEP) and interaction plots (IP) are intuitive tools very useful to estimate the influence of factors through the different levels, both in general or in combination, respectively, to the considered effect. Figs. 1 and 2 show the MEP of the DoE results for both S/N and RES effects respectively, in which the comparison of the changes in the level means provided information

concerning the factors that may influence the response the most. The horizontal line crossing these graphs is the *grand mean*, which is the average of all data for a specific effect (S/N or RES), and is a valuable reference for the data interpretation. The following interpretations can be drawn: Firstly, it is clearly seen how, considering all experiments, those performed with dithranol provided a MALDI signal with higher S/N and higher RES , far from those given by HABA and FA. In addition, regarding the influence of the proportion analyte/matrix, the variation was different for both effects: whereas an increase of the percentage of matrix increased the S/N of the MALDI spectra, it came together with a reduction of the RES . Finally, an increase of the concentration of NaTFA enhanced the S/N of the signals, being the results in the case of the RES higher in this fashion: $0.0 > 2.0 > 0.5 > 1.0 \text{ g L}^{-1}$, being the RES when 2 g L^{-1} representative, since it is close to the *grand mean*.

Interaction plots (IP) will help elucidate the best conditions for the analysis. Figs. 3 and 4 show the IP for the three factors to S/N and RES , respectively. These plots are useful to observe the general influence of all factors in combinations. The following facts were stressed: Initially, it can be observed how for the three matrices, increasing the proportion of analyte/matrix in the MALDI sample represented a general increase in the S/N (Fig. 3a and c) and a decrease in the RES (Fig. 4a and c), being this effect more appreciable for dithranol > FA > HABA, and the latter completely insensitive. On the other hand, an increase in the concentration of the cationization agent was not relevant for the S/N results in the case of using HABA and FA, whereas it was remarkably positive when using dithranol (Fig. 3b and e), as previously suggested. However, for the examination of the influence of the salt on the RES , it is seen how it was negatively affected when HABA and FA were considered, while for the case of employing dithranol, the RES increased to higher values as more salt was added to the MALDI sample (Fig. 4b and e). Finally, the interaction between proportion of analyte/matrix used and concentration of NaTFA showed a general increase in the S/N when both factors were increased (Fig. 3d and f), whereas no clear

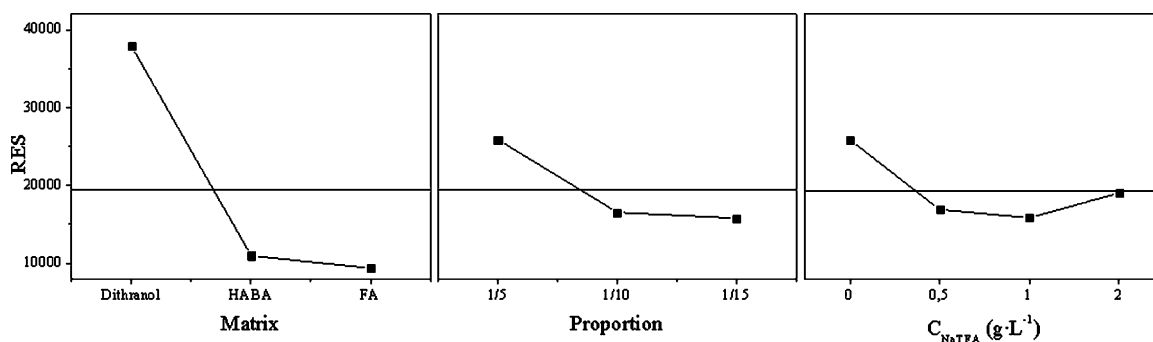


Fig. 2. Main effects plot for the analysis of the resolution (RES).

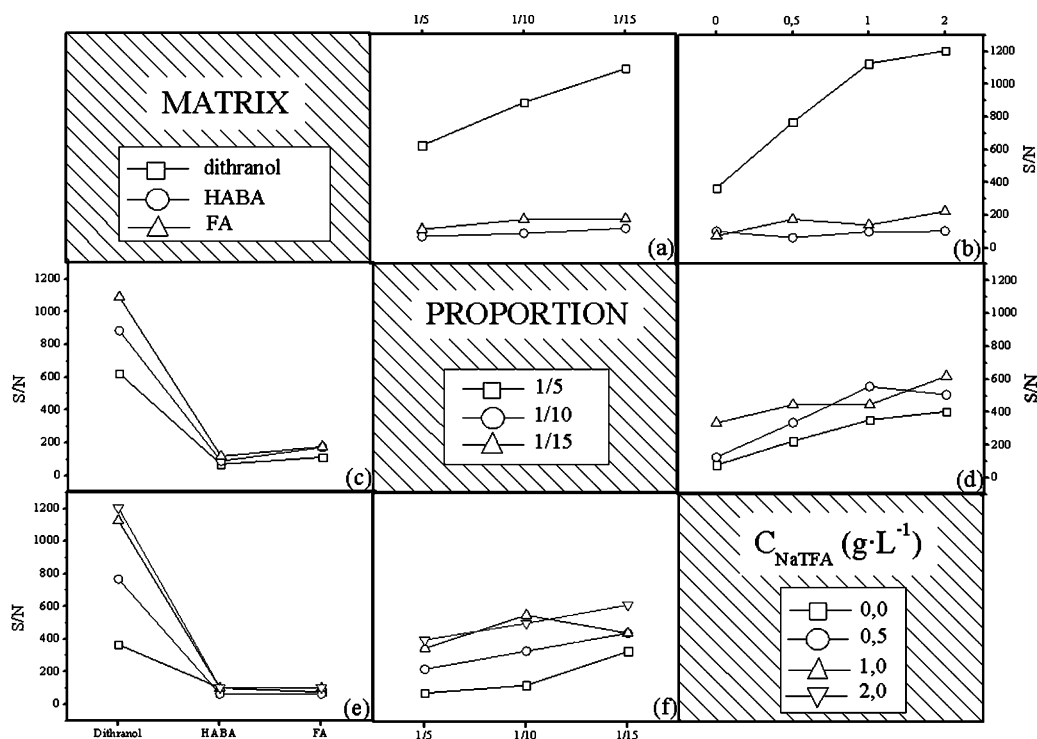


Fig. 3. Interaction plot for the analysis of the signal-to-noise (S/N) ratio.

tendency was found for the study of the RES , as it is shown in Fig. 4d and f.

Discussion was stated in association with the MALDI spectra. For a better comparison, a selection of the MALDI spectra is shown in Fig. 5, focused on a unique adduct centered at $2329.0\ m/z$, corresponding to the cyclic predominant adduct $([GT_c]_n Na)^+$, for 12 repeating units, which intensity for all spectra was remarkable. The following conclusions were remarked: Firstly, the effect of the

matrix used was the key quality factor for the analysis, since both S/N and RES considerably increased with the use of dithranol, to the detriment of HABA and FA, even though FA behaved better than HABA. This fact can be checked by the observation of the spectra depicted in Fig. 5d–e–f. Furthermore, the discussion about which proportion resulted best for the analysis had to be decided in terms of which parameter is more decisive for the analysis. It is shown that the higher amount of matrix was used, the better S/N was obtained,

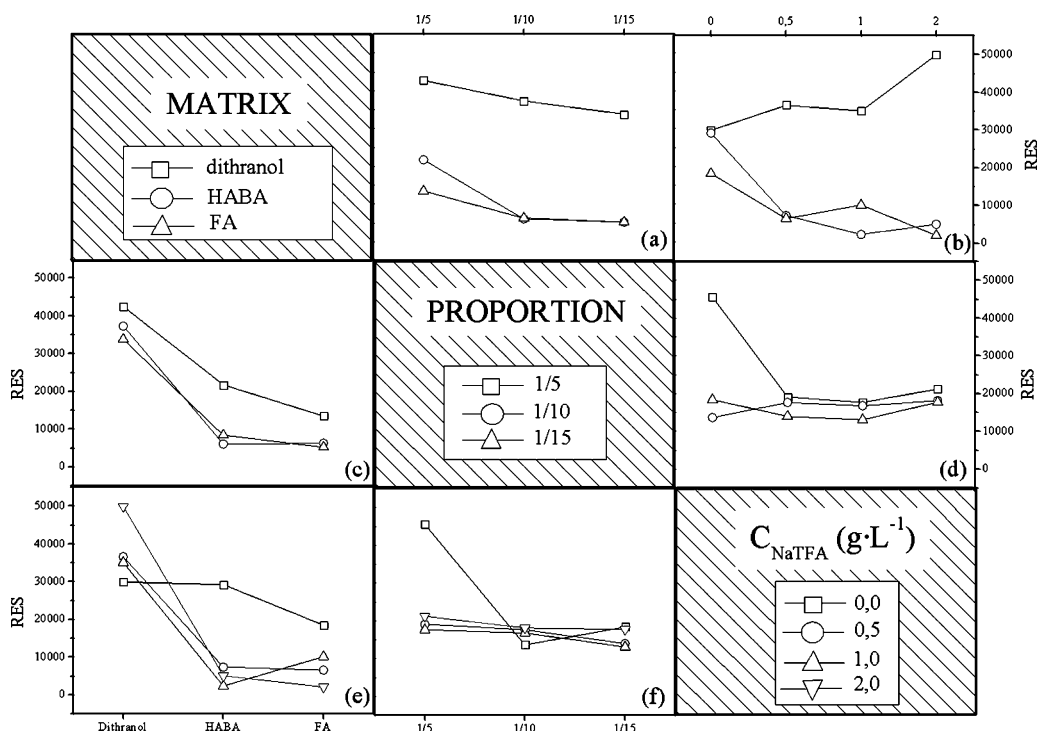


Fig. 4. Interaction plot for the analysis of the resolution (RES).

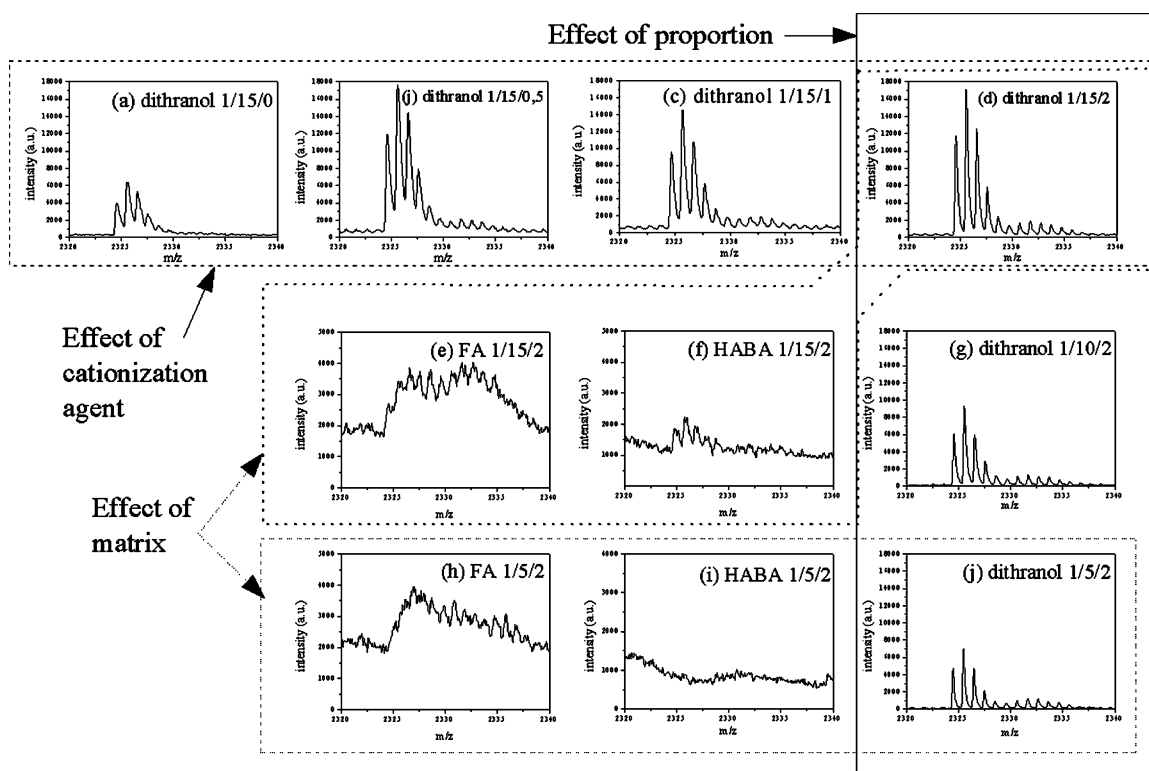


Fig. 5. MALDI-TOF MS spectra in the m/z 2300–2400 range to check the applicability of the design of experiments applied (note that scales have been modified for better visualization).

but the lower *RES* was achieved. In terms of spectra, the analysis of Fig. 5d–g–j clearly shows what was hypothesized by the DoE analysis. Especially for the case of using dithranol, it can be seen how the increase of *S/N* was more substantial than the small decrease experienced by the *RES*. Even more, the statistical analysis of the response (Table 2) gave a higher regression value, which strengthens the choice of the *S/N* as key parameter in this study. Thus, it was decided to prepare MALDI samples with the analyte/matrix proportion 1/15 (V/V), which in the MAC means 1/15/1 (V/V/V). Finally, the study of the influence of the cationization agent was considered. The main effects plot (Fig. 1) stated that the higher the addition of salt was employed, the higher the *S/N* obtained was. Concerning the *RES* (Fig. 2), it was higher in this fashion: $0.0 > 2.0 > 0.5 > 1.0 \text{ g L}^{-1}$, being the *RES* representative when 2 g L^{-1} were used, since it was close to the *grand mean*. Interaction plots can be used as reduced DoE for a specific factor. In other terms, once decided dithranol as established matrix, the observation of the influence of the other variables could be followed by the IP. Fig. 3b and e showed that the higher the amount of NaTFA was used, the higher the *S/N* value was obtained for dithranol, which was clear up to now. The influence of NaTFA on the *RES* (Fig. 4b and e) was surprisingly remarkable, because only in the case of applying dithranol, the increment in concentration of NaTFA increased the *RES*, unlikely pointed out by MEP. Deep observation of Fig. 5a–b–c–d clearly showed that the best spectrum was given for the highest concentration of salt.

Taking into account all these considerations, the application of the DOE for the improvement of the MALDI measure of PET stated that the best combination of levels and factors was the following: matrix (dithranol), proportion (1/15/1), and concentration of cationization agent (2 g L^{-1}).

4.3. Study of PET thermo-mechanical degradation

The second part of the study was devoted to the characterization of the thermo-mechanical degradation mechanisms of PET sub-

jected to multiple injection molding cycles, as a good example for the application of the previous analysis. PET degradation reactions generally follow the postulated mechanistic routes of polyesters: Route I: Hydrolysis, which leads to the formation of hydroxyl and carboxyl linear oligomers with shorter chain length. Route II: Esterification. Route III: Intramolecular transesterification, both from the end of the chain (backbiting) or in the middle of the chain, which lead to the formation of cyclic oligomers and linear species with shorter length. Route IV: Intermolecular transesterifications, which interchange ester units between different chains, which lead to an increase in the heterogeneity of the polymer. Route V: Chain scissions inherent to thermo-mechanical reactions may produce random chain cleavage, leading to the formation of mainly linear hydroxyl and carboxyl terminated species. Route VI: Oxidation processes, giving rise to glycol-aldehyde terminated units. In addition, MALDI experiments in which the use of NaTFA is used as catalyst, shows acetylation reactions, which are considered as Route VII.

The MALDI spectrum of VPET is shown in Fig. 6. In the inset, the zoomed area corresponding to two repeating $[\text{GT}]_n$ units ($n = 10, 11$), in the m/z 1900–2300 range is given as an example for identifi-

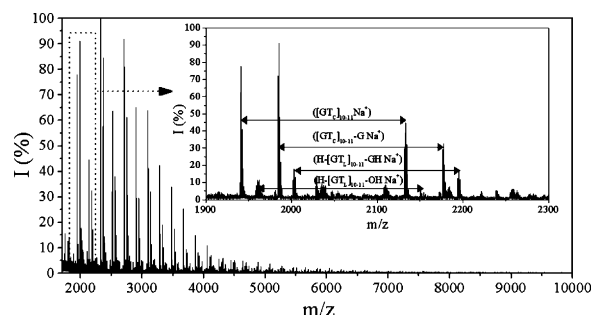


Fig. 6. MALDI-TOF MS spectrum of virgin PET. Inset: zoomed area in the m/z range 1900–2300 for identification of predominant oligomers.

Table 3
Structures and m/z values for cyclic oligomeric species assigned in the MALDI-TOF MS spectra of virgin and reprocessed PET (for $n = 10, 11$).

Species	Structures	$[M+Na]^+$
$[GT_C]_n$		1944.7/2136.9
$[GT_C]_n-G$		1988.8/2180.9
$[GT_C]_n-G_2$		2032.8/2225.0
T- $[GT_C]_n$		2092.8/2285.0

cation of main cyclic and linear oligomeric species, which structures are depicted in Tables 3 and 4, respectively. Note that species appeared at more m/z than those presented, but only values for $n = 10, 11$ are presented for better visualization. The predominant oligomeric species are cyclic oligomers, $[GT_C]_n$, mainly detected as Na^+ adducts ($[M+Na]^+ : m/z$ 1944.7, 2136.9), as well as cyclic oligomers with an extra glycol linkage in the backbone $[GT_C]_n-G$, found as $[M+Na]^+ : m/z$ 1988.8, 2180.9. Linear oligomers present in VPET were assigned as those bearing two glycol units H- $[GT_L]_n$ -GH (found at $[M+Na]^+ : m/z$ 2006.8, 2198.9), and those having glycol and carboxyl end groups H- $[GT_L]_n$ -OH (found at $[M+Na]^+ : m/z$ 1962.7, 2154.9).

Thermo-mechanical degradation subjected by multiple reprocessing induced modifications in the oligomeric distribution of the

PET sample. Fig. 7 shows the influence of degradation on the mass spectra corresponding to each reprocessed material, in comparison with the virgin one, where the m/z range has been reduced to one repeating unit $[GT]_n$ ($n = 10$) for better visualization. New cyclic and linear oligomeric species were detected, as shown in Tables 3 and 4, respectively. Even though it is known that ion abundances in MALDI experiments can considerably vary, the increase of oligomers gained by the reprocessed materials, in comparison with the virgin PET, was prominent and reproducible.

Low abundant ions of the linear oligomers found were H- $[GT_L]_n$ -G₂H (or HG- $[GT_L]_n$ -GH), which bear a glycol and a diethylene glycol (DEG) unit ($[M+Na]^+ : m/z$ 2050.8); HT- $[GT_L]_n$ -OH, having two terephthalate units ($[M+Na]^+ : m/z$ 2210.8); H- $[GT_L]_n$ -GA, bearing a glycol and a glycol-aldehyde unit ($[M+Na]^+ : m/z$ 2034.7);

Table 4
Structures and m/z values for linear oligomeric species assigned in the MALDI-TOF MS spectra of virgin and reprocessed PET (for $n = 10, 11$).

Species	Structures	$[M+Na]^+$
H- $[GT_L]_n$ -OH		1962.7/2154.9
H- $[GT_L]_n$ -GH		2006.8/2198.9
H- $[GT_L]_n$ -G ₂ H		2050.8/2242.9
H- $[GT_L]_n$ -GA		2034.75/2226.9
HT- $[GT_L]_n$ -OH		2210.8/2303.0
TFA- $[GT_L]_n$ -OH		2058.7/2250.9

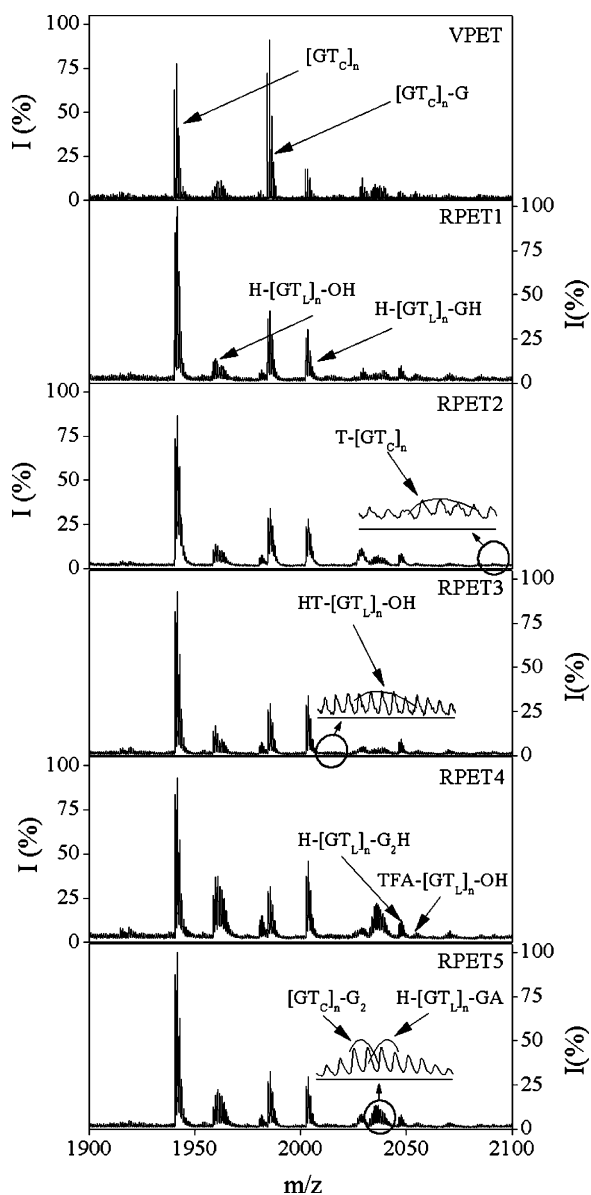


Fig. 7. MALDI-TOF MS spectra in the m/z 1900–2100 range to characterize the appearance of oligomeric species due to thermo-mechanical degradation. Zoomed areas represent low abundant oligomeric species.

and TFA- $[\text{GT}_L]_n\text{-OH}$, which has carboxyl and trifluoroacetate (TFA) end groups ($[\text{M}+\text{Na}]^+ : m/z$ 2058.7). Minor cyclic oligomeric adducts were T- $[\text{GT}_C]_n$, which presents an extra terephthalate unit in the backbone, found as $[\text{M}+\text{Na}]^+ : m/z$ 2092.8; and $[\text{GT}_C]_n\text{-G}_2$ ($[\text{M}+\text{Na}]^+ : m/z$ 2032.8), which has an extra DEG unit in the backbone. The evolution of their relative ion abundances, taking into account intensities and areas for calculations, is depicted in Fig. 8.

Fig. 9 shows a proposal of mechanisms of polymer degradation. In order to follow the discussion, the nomenclature $\text{R}^I_a\text{R}^{II}_b$ has been used, where R^I stands for *Reaction* and a for the specific reaction shown at the degradation map in Fig. 9, and R^{II} stands for *Route*, being b , the likely mechanism for this reaction, according to the aforementioned general chemical routes. The most remarkable changes were those experienced by the cyclic species $[\text{GT}_C]_n$ and $[\text{GT}_C]_n\text{-G}$ and, with less presence, by linear species H- $[\text{GT}_L]_n\text{-GH}$ and H- $[\text{GT}_L]_n\text{-OH}$. The relative abundance of the $[\text{GT}_C]_n$ oligomers increased with further reprocessing cycles, which can be explained by intramolecular cyclization reactions of $[\text{GT}_C]_n\text{-G}$ species (R_1R_{III} ($m < n$)). Intermolecular reactions between esters and ethers groups [R_2R_{IV} ($\neq n$)] or by linear oligomer cyclization reactions, from H- $[\text{GT}_L]_n\text{-GH}$ and H- $[\text{GT}_L]_n\text{-OH}$ ($\text{R}_{3,4}\text{R}_{III}$ ($m < n$)), releasing ethylene glycol and water as by-products [50], can also occur, but general increasing tendency of these latter species suggests that it was the loss of ethylene glycol from cyclic $[\text{GT}_C]_n\text{-G}$ the main reaction after the first reprocessing. Actually, the strong decrease of relative abundance of $[\text{GT}_C]_n\text{-G}$ throughout the entire reprocessing cycles reveals these were the most reactive species. Both mainly produced H- $[\text{GT}_L]_n\text{-OH}$ by cleavage of the ester bond, giving rise to a vinyl-ester terminated PET which hydrolyzed yielding a vinyl alcohol which rearranged into acetaldehyde, thus leaving carboxyl end groups (R_5R_I) [21,22,51]; and with minor intensity, H- $[\text{GT}_L]_n\text{-GH}$, by hydrolysis (R_6R_I) and by intermolecular reactions involving a water molecule [50] (R_6R_{IV} ($\neq n$)). These last species could interact between them by interchanging glycol and water units, being the production of H- $[\text{GT}_L]_n\text{-OH}$ more remarkable (R_7R_{IV} ($\neq n$)). In addition, alternative H- $[\text{GT}_L]_m\text{-OH}$ ($m = n - 1$) could be formed as a result of chain scission reactions of the ester groups of H- $[\text{GT}_L]_n\text{-GH}$ (R_7R_I , ($m < n$)), by the loss of the transformed vinyl-ester group [21], which might be enhanced by the shear induced by thermo-mechanical processing. Likewise, the occurrence of lighter H- $[\text{GT}_L]_m\text{-OH}$ groups is reported as an effect of intramolecular cyclization reactions [21], releasing a sub-product of R_3R_{III} , with $m < n$. The carboxyl end groups are mainly attributed to thermal degradation reactions during reprocessing [52] and therefore are a good indicator of chain scission processes. These results are in agreement with those reported in other studies, where the presence of carboxyl groups was monitored by techniques such as

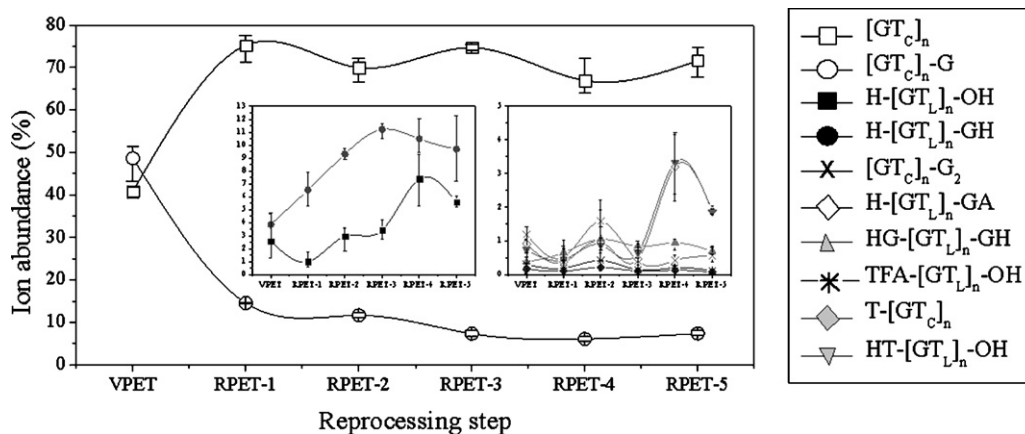


Fig. 8. Normalized ion abundances of PET oligomeric species through the multiple reprocessing cycle.

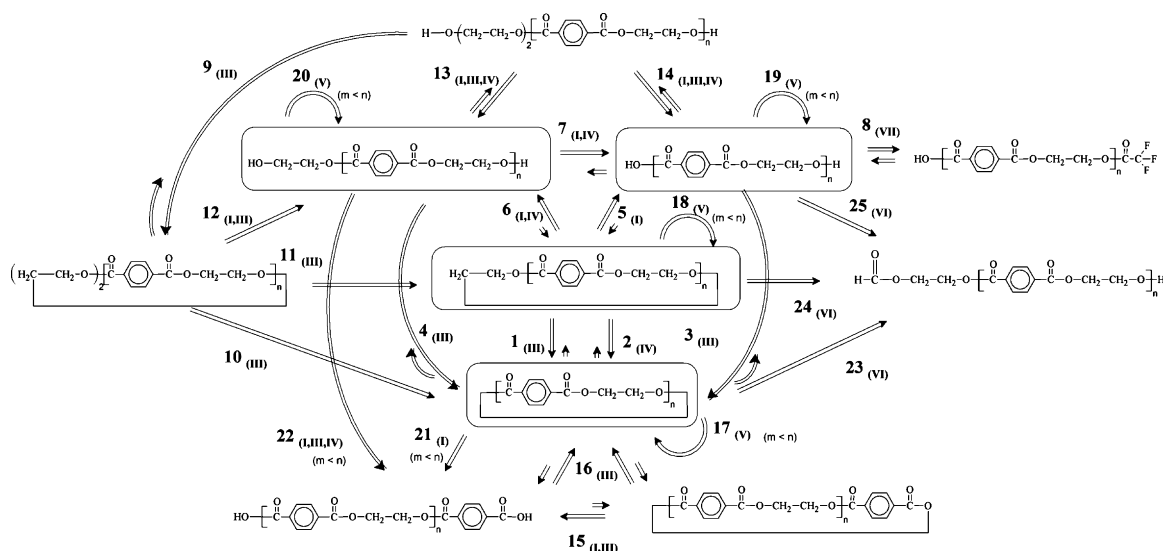


Fig. 9. Proposed mechanisms of thermo-mechanical degradation of PET.

titration or Fourier transform infrared spectrometry (FTIR) [29]. It is worth mentioning that, besides indicating the degradation already undergone by the polymer, the role of carboxyl end groups is indicative of further degradation, since they can act as hydrolysis catalyzers [26–28].

Low abundant species slightly interacted in the general oligomers degradation mechanism, since its presence was maintained at low abundance levels during the thermo-mechanical degradation. TFA- $[\text{GT}_L]_n\text{-OH}$ is formed after an acetylating reaction between the TFA and the hydroxyl end groups [25] (R_8R_{VII}). Species such as HG- $[\text{GT}_L]_n\text{-GH}$ and $[\text{GT}_C]_n\text{-G}_2$, which formation/elimination is driven by intramolecular transesterifications and hydrolytic processes (R_9R_{III} ($m < n$)), played a role in the formation of $[\text{GT}_C]_n$ ($R_{10}R_{I,III}$ ($m < n$)), $[\text{GT}_C]_n\text{-G}$ ($R_{11}R_{I,III}$ ($m < n$)), H- $[\text{GT}_L]_n\text{-GH}$ and H- $[\text{GT}_L]_n\text{-OH}$ ($R_{12}R_{I,III}$ ($m < n$), $R_{13,14}R_{I,III}$ ($m < n$), IV ($\neq n$)), by means of the mechanisms explained above, involving ethylene glycol units. Other minor species such as HT- $[\text{GT}_L]_n\text{-OH}$ and T- $[\text{GT}_C]_n$, which equilibrium might be guided by hydrolytic or intramolecular reactions [50]. ($R_{15}R_{I,III}$ ($m < n$)), interacted with the formation of $[\text{GT}_C]_n$, with the loss of terephthalic units ($R_{16}R_{III}$). Thermo-mechanical degradation inducing chain scission to PET can be explained through reactions $R_{17-20}R_V$ ($m < n$), which gives rise to similar species to the original but with less repeating units in its backbone. Chain scissions leading to species different to the original might also occur, but were not considered in the oligomers degradation mechanism for the sake of clarity. It can be seen how the formation of HT- $[\text{GT}_L]_n\text{-OH}$ through reactions $R_{21}R_I$ and $R_{22}R_{I,III}$ ($m < n$), IV ($\neq n$), was more remarkable along the reprocessing cycles, in agreement with other studies [25]. This oligomer could also be produced as a result of β -scission reactions from decomposition of $[\text{GT}_C]_n$ at high temperatures $R_{21}R_{V(m < n)}$ [50]. Likewise, oxidation processes led to the formation of H- $[\text{GT}_L]_n\text{-GA}$, as suggested by other authors [25] ($R_{23-25}R_{VI}$). Finally, intermolecular transesterifications have to be also considered to occur during the whole processing, leading to a more heterogeneous chain distribution which may affect the polydispersity index of PET [53].

5. Conclusions

The sample preparation procedure for the analysis of poly(ethylene terephthalate) (PET) samples by means of MALDI-TOF MS was assessed. A statistical Design of Experiments (DoE) taking into account the following factors (levels): choice of the cor-

rect matrix (dithranol, HABA, FA), the proportion analyte/matrix (1/5, 1/10, 1/15 V/V), and the amount of cationization agent ($C_{\text{NaTFA}} = 0, 0.5, 1, 2 \text{ g L}^{-1}$ in the same volumetric amount as the analyte) were considered. The study was performed analyzing the effect of changing the aforementioned factors among their different levels on quality parameters such as signal-to-noise ratio (S/N) and resolution (RES), both in absolute and relative terms. Main effects plots and interaction plots permitted to understand the influence of each factor to the quality of the MALDI spectra. The application of DoE for the improvement of the MALDI measure of commercial PET stated that the best combination of levels and factors was the following: matrix (dithranol), proportion analyte/matrix (1/15, V/V), and concentration of NaTFA (2 g L^{-1}).

Multiple processing by means of successive injection cycles was used to simulate the thermo-mechanical degradation effects on the oligomeric distribution of PET under mechanical recycling. Several degradation mechanistic routes were proposed. Degradation primarily affected to initially predominant cyclic species, by dramatically decreasing the abundance of $[\text{GT}_C]_n\text{-G}$, which was mainly transformed into $[\text{GT}_C]_n$, H- $[\text{GT}_L]_n\text{-GH}$ and H- $[\text{GT}_L]_n\text{-OH}$, among other low abundant oligomeric species, that played an important role in the formation-disappearance reactions occurred due to multiple reprocessing. Such is the case of cyclic oligomers like T- $[\text{GT}_C]_n$ and $[\text{GT}_C]_n\text{-G}_2$; or linear oligomers like HG- $[\text{GT}_L]_n\text{-GH}$, HT- $[\text{GT}_L]_n\text{-OH}$, H- $[\text{GT}_L]_n\text{-GA}$, or TFA- $[\text{GT}_L]_n\text{-OH}$.

Acknowledgements

The authors would like to acknowledge the Spanish Ministry of Science and Innovation for the financial support through the Research Project UPOVCE-3E-013. The Spanish Ministry for Education is acknowledged for the concession of a predoctoral research position to J.D. Badía by means of the FPU program. Catalana de Polimers, S.A. and AIMPLAS are acknowledged for providing and processing the material, respectively. Royal Institute of Technology (KTH, Sweden) and Universitat Politècnica de València (UPV, Spain) are also thanked for additional economical support.

Appendix A. Supplementary data

Supplementary data associated with this article can be found, in the online version, at doi:10.1016/j.aca.2011.02.063.

References

- [1] M. Polce, C. Wesdemiotis, Introduction to mass spectrometry of polymers, in: G. Montaudo, R.P. Lattimer (Eds.), *Mass Spectrometry of Polymers*, CRC Press LLC, Boca Raton, FL, 2002.
- [2] G. Montaudo, F. Samperi, M.S. Montaudo, Characterization of synthetic polymers by MALDI-MS, *Progress in Polymer Science* 31 (2006) 277–357.
- [3] S.M. Weidner, S. Trimpin, Mass spectrometry of synthetic polymers, *Analytical Chemistry* 80 (2008) 4349–4361.
- [4] F. Awaja, D. Pavel, Recycling of PET, *European Polymer Journal* 41 (7) (2005) 1453–1477.
- [5] G. Montaudo, M.S. Montaudo, F. Samperi, Matrix-assisted laser desorption ionization/mass spectrometry of polymers (MALDI-MS), in: R.P. Lattimer, G. Montaudo (Eds.), *Mass Spectrometry of Polymers*, CRC Press LLC, Boca Raton, FL, 2001.
- [6] A.J. Hoteling, T.H. Mourey, K.G. Owens, Importance of solubility in the sample preparation of poly(ethylene terephthalate) for MALDI-TOF-MS, *Analytical Chemistry* 76 (2005) 750–756.
- [7] S. Weidner, G. Kühn, B. Wethmann, H. Schroeder, U. Just, R. Borowski, R. Decker, B. Schwarz, I. Schmucking, I. Seifert, A new approach of characterizing the hydrolytic degradation of poly(ethylene terephthalate) by MALDI-MS, *Journal of Polymer Science. Part A: Polymer Chemistry* 35 (1997) 2183.
- [8] W. Romao, M.F. Franco, A.H. Iglesias, G.B. Sanvido, D.A. Maretto, F.C. Gozzo, R.J. Poppi, M.N. Eberlin, M.A. De Paoli, Fingerprinting of bottle-grade poly(ethylene terephthalate) via matrix-assisted laser desorption/ionization mass spectrometry, *Polymer Degradation and Stability* 95 (4) (2010) 1–6.
- [9] P. Juhasz, C.E. Costello, K. Biemann, Matrix-assisted laser desorption mass spectrometry with 2-(4-hydroxyphenylazo) benzoic acid matrix, *Journal of the American Association of Mass Spectrometry* 4 (1992) 399.
- [10] M.C. Fitzgerald, R.G. Parr, L.M. Smith, Basic matrices for the matrix-assisted laser/desorption mass spectrometry of proteins and oligonucleotides, *Analytical Chemistry* 65 (22) (1993) 3204–3211.
- [11] X. Tang, P.A. Dreifuss, A. Vertes, New matrices and accelerating voltage effects in matrix-assisted laser desorption/ionization of synthetic polymers, *Rapid Communications in Mass Spectrometry* 9 (1995) 1141.
- [12] S.J. Wetzel, C.M. Guttman, J.E. Girard, The influence of matrix and laser energy on the molecular mass distribution of synthetic polymers obtained by MALDI-TOF-MS, *International Journal of Mass Spectrometry* 238 (2004) 215–225.
- [13] G.E. Box, J.S. Hunter, W.G. Hunter, *Statistics for Experimenters. Design, Innovation and Discovery*, John Wiley & Sons, New Jersey, 2005.
- [14] S.J. Wetzel, C.M. Guttman, K.M. Flynn, Filliben, Significant parameters in the optimization of MALDI-TOF-MS for synthetic polymers, *Journal of the American Society for Mass Spectrometry* 17 (2006) 246–252.
- [15] K.H. Liland, B.-H. Mevik, E.-O. Rukke, T. Almøy, M. Skaugen, Isaksson, Quantitative whole spectrum analysis with MALDI-TOF M, Part 1: measurement optimization, *Chemometrics and Intelligent Laboratory Systems* 96 (2009) 210–218.
- [16] H. Brandt, T. Ehmann, M. Otto, Investigating the effect of mixing ratio on molar mass distribution of synthetic polymers determined by MALDI-TOF mass spectrometry using design of experiments, *Journal of the American Society for Mass Spectrometry* 21 (2010) 1870–1875.
- [17] J. Guittard, M. Tessier, J.C. Blais, G. Bolbach, L. Rozes, E. Maréchal, J.C. Tabet, Electropray and matrix-assisted laser desorption/ionization mass spectrometry, *Journal of Mass Spectrometry* 31 (1996) 1409.
- [18] J.B. Williams, A.I. Gusev, D.M. Hercules, Characterization of polyesters by matrix-assisted laser desorption/ionization mass spectrometry, *Macromolecules* 30 (1996) 3781.
- [19] S. Carroccio, P. Rizzarelli, G. Scaltrò, C. Puglisi, Comparative investigation of photo- and thermal-oxidation processes in poly(butylene terephthalate), *Polymer* 49 (2008) 3371–3381.
- [20] S. Weidner, G. Kühn, U. Just, Characterization of oligomers in poly(ethylene terephthalate) by matrix-assisted laser desorption/ionization mass spectrometry, *Rapid Communications in Mass Spectrometry* 9 (1995) 697.
- [21] S. Weidner, G. Kühn, J. Friedrich, H. Schröder, Plasmaoxidative and chemical degradation of poly(ethylene terephthalate) studied by matrix-assisted laser desorption/ionization mass spectrometry, *Rapid Communications in Mass Spectrometry* 10 (1996) 40–46.
- [22] F. Samperi, C. Puglisi, R. Alicata, G. Montaudo, Thermal degradation of poly(ethylene terephthalate) at the processing temperature, *Polymer Degradation and Stability* 83 (2004) 3–10.
- [23] G. Colomines, J.J. Robin, G. Tersac, Study of the glycolysis of PET by oligoesters, *Polymer* 46 (2005) 3230–3247.
- [24] F.C.L. Ciolacu, N.M. Choudhury, N. Dutta, N.H. Voelcker, MALDI-TOF MS and DIOS-MS investigation of the degradation and discoloration of poly(ethylene terephthalate), *Macromolecules* 36 (2006) 7872–7881.
- [25] W. Romao, M.F. Franco, Y.E. Corilo, M.N. Eberlin, M.A.S. Spinacé, M.A. De Paoli, Poly(ethylene terephthalate) thermo-mechanical and thermo-oxidative degradation mechanisms, *Polymer Degradation and Stability* 94 (2009) 1849–1859.
- [26] D.M. Fann, S.K. Huang, J.Y. Lee, Kinetics and thermal crystallinity of recycled PET. II. Topographic study on thermal crystallinity of the injection-molded recycled PET, *Journal of Applied Polymer Science* 61 (2) (1996) 261–271.
- [27] R.J. Ehrig, *Plastics Recycling: Products and Processes*, Hanser Publishers, New York, 1992.
- [28] P.P. Klemchuck, *Polymer Stabilization and Degradation*, ACS, Washington, 1985.
- [29] S.D. Mancini, M. Zanin, Consecutive steps of PET recycling by injection: evaluation of the procedure and of the mechanical properties, *Journal of Applied Polymer Science* 76 (2) (2000) 266–275.
- [30] R. Franz, A. Mauer, F. Welle, European survey on post-consumer poly(ethylene terephthalate) (PET) materials to determine contamination levels and maximum consumer exposure from food packages made from recycled PET, *Food Additives & Contaminants: Part A* 21 (3) (2004) 265–286.
- [31] F. Welle, Post-consumer contamination in high-density polyethylene (HDPE) milk bottles and the design of a bottle-to-bottle recycling process, *Food Additives Contaminants* 22 (2005) 999–1011.
- [32] E. Strömberg, S. Karlsson, The design of a test protocol to model the degradation of polyolefins during recycling and service life, *Journal of Applied Polymer Science* 112 (2009) 1835–1844.
- [33] F. Vilaplana, A. Ribes-Greus, S. Karlsson, Degradation of recycled high-impact polystyrene. Simulation by reprocessing and thermo-oxidation, *Polymer Degradation and Stability* 91 (2006) 2163–2170.
- [34] F. Vilaplana, S. Karlsson, A. Ribes-Greus, Changes in the micro-structure and morphology of high-impact polystyrene subjected to multiple processing and thermo-oxidative degradation, *European Polymer Journal* 43 (2007) 4371–4381.
- [35] N. Yarahmadi, I. Jakubowicz, T. Gevert, Effects of repeated extrusion on the properties and durability of rigid PVC scrap, *Polymer Degradation and Stability* 73 (1) (2001) 93–99.
- [36] J.D. Badía, F. Vilaplana, S. Karlsson, A. Ribes-Greus, Thermal analysis as a quality tool for assessing the influence of thermo-mechanical degradation on recycled poly(ethylene terephthalate), *Polymer Testing* 28 (2009) 169–175.
- [37] F. La Mantia, M. Vinci, Recycling poly(ethylene terephthalate), *Polymer Degradation and Stability* 45 (1994) 121–125.
- [38] N. Torres, J.J. Robin, B. Boutevinn, Study of thermal and mechanical properties of virgin and recycled poly(ethylene terephthalate) before and after injection molding, *European Polymer Journal* 36 (2000) 2075–2080.
- [39] R. Mukerjee, C.F. Jeff-Wu, *A Modern Theory of Factorial Design*, Springer Science+Business Media Inc., New York, 2006.
- [40] Catalana de Polimers, S.A. SEDAPET SP04 Technical datasheet, 2004.
- [41] ISO 291:1997, *Plastics—standard atmospheres for conditioning and testing*.
- [42] G. Montaudo, M.S. Montaudo, C. Puglisi, F. Samperi, Determination of absolute mass values in MALDI-TOF of polymeric materials by a method of self-calibration of the spectra, *Analytical Chemistry* 66 (1994) 4366–4369.
- [43] W. Ens, Y. Mao, F. Mayer, K.G. Standing, Properties of matrix-assisted laser desorption measurements with a time-to-digital converter, *Rapid Communications in Mass Spectrometry* 5 (3) (1997) 117–123.
- [44] G. Montaudo, M.S. Montaudo, Polymer characterization methods, in: G. Montaudo, R.P. Lattimer (Eds.), *Mass Spectrometry of Polymers*, CRC Press LLC, Boca Raton, 2002.
- [45] H.I. Rader, W. Schrepp, MALDI-TOF mass spectrometry in the analysis of synthetic polymers, *Acta Polymerica* 49 (1998) 272.
- [46] P.O. Danis, D.E. Karr, A facile sample preparation for the analysis of synthetic organic polymers by matrix-assisted laser desorption/ionization, *Organic Mass Spectrometry* 28 (8) (1993) 923–925.
- [47] P.M. Lloyd, E. Scrivener, D.R. Maloney, D.M. Haddleton, P.J. Derrick, Cation attachment to synthetic polymers in matrix-assisted laser desorption/ionization mass spectrometry, *Polymer Preprint* 37 (1) (1996) 847–848.
- [48] R.C. King, R. Goldschmidt, Y. Xiong, K.G. Owens, G.A. Atlanta, Mechanistic studies of the cationization of synthetic polymers by alkali metals in the matrix-assisted laser desorption/ionization experiment, 3rd ASMS Conference in Mass Spectrometry (1995) 1237.
- [49] N. Xu, Z.W. Huang, J. Throck-Watson, D.A. Gage, Mercaptobenzothiazoles: a new class of matrices for laser desorption ionization mass spectrometry, *Journal of the American Society of Mass Spectrometry* 8 (2) (1997) 116, 997.
- [50] I. Goodman, B.F. Nesbitt, The structures and reversible polymerization of cyclic oligomers from poly(ethylene terephthalate), *Polymer* 1 (1960) 384–386.
- [51] K.C. Khemani, A novel approach for studying the thermal degradation, and for estimating the rate of acetaldehyde generation by the chain scission mechanisms in ethylene glycol based polyesters and copolyesters, *Polymer Degradation and Stability* 67 (2000) 91–99.
- [52] D.N. Bikiaris, G.P. Karayannidis, Effect of carboxylic end groups on the thermooxidative stability of PET and PBT, *Polymer Degradation and Stability* 63 (1999) 213–218.
- [53] G. Montaudo, M.S. Montaudo, C. Puglisi, S. Samperi, Evidence for ester-exchange reactions and cyclic oligomer formation in the ring-opening polymerization of lactide with aluminum complex initiators, *Macromolecules* 29 (20) (1996) 6461–6465.

CONTRIBUTION III-C

The role of crystalline, mobile amorphous and rigid amorphous fractions on
the performance of recycled poly (ethylene terephthalate) (PET)

J.D. Badia, E. Strömberg, S. Karlsson, A. Ribes-Greus

Manuscript

**THE ROLE OF CRYSTALLINE, MOBILE AMORPHOUS AND RIGID AMORPHOUS
FRACTIONS ON THE PERFORMANCE OF RECYCLED POLY (ETHYLENE
TEREPHTHALATE) (PET)**

J.D. Badia¹, E. Strömberg², S. Karlsson², A. Ribes-Greus^{1,*}

¹ Instituto de Tecnología de Materiales (ITM),

Universitat Politècnica de València

Camino de Vera s/n, E-46022 Valencia, Spain

² School of Chemical Science and Engineering,

Fibre and Polymer Technology,

KTH - Royal Institute of Technology,

Teknikringen 56-58, SE-10044 Stockholm, Sweden

*corresponding author: aribes@ter.upv.es

Keywords: poly(ethylene terephthalate) (PET), mechanical recycling, mobile amorphous fraction (MAF), rigid amorphous fraction (RAF), glass-rubber relaxation, dynamic fragility

Abstract:

The action of thermo-mechanical degradation induced by mechanical recycling on poly (ethylene terephthalate) was simulated by successive injection moulding cycles. Degradation reactions were mainly driven by the reduction of diethyleneglycol to ethylene glycol units in the flexible domain of the PET backbone, and the formation of –OH terminated species with shorter chain length. Chain scission processes induced by degradation reduced the molar mass and modified the conformational arrangement of chains. The results were assessed in terms of microstructural modifications, taking into account a three-fraction model involving crystalline, mobile amorphous (MAF) and rigid amorphous fractions (RAF). A remarkable increase of RAF, to a detriment of MAF was observed, while the percentage of crystalline fraction remained nearly constant. Deeper analysis of the melting behaviour and the segmental dynamics around the glass-rubber relaxation showed the role of each fraction leading to a loss of thermal, viscoelastic and mechanical performance, particularly remarkable after the first processing cycle.

1. Introduction

The extended use of poly(ethylene terephthalate) (PET) over the last two decades, mainly in the food packaging sector, is due to its excellent mechanical, chemical, processing and thermal properties. Consequently, the amount of post-consumer PET present in urban solid waste is high and has to be managed. Among all recovery methods, mechanical recycling represents one of the most successful processes and has received considerable attention due to its main advantages. During its life cycle (synthesis, processing, use, discarding, cleaning, recycling), PET is subjected to the interaction of degradation agents such as oxygen, light, mechanical stresses, temperature or water. Individually or synergically, these agents may provoke the breakage of the macromolecules and diminish the final properties and productivity during processing [1-3]. In this sense, the application of protocols to simulate the degradation subjected by polymers during recycling has been effectively performed for commodities such as polyethylene (PE) [4], polypropylene (PP) [4], polystyrene (PS) [5-6], poly (vinyl chloride) (PVC) [7] or PET [8-14].

Reported analyses for PET generally showed a loss of mechanical [10-11, 14-15] thermal [8, 14-15] or rheological [11, 15] properties. Further information can be found in the review by *Awaja* and *Pavel* [16]. The majority of studies explained the effects of reprocessing taking into account a two-fraction model, in which only amorphous and crystalline domains were present, and thus related the changes in properties to the relative balance between both fractions [10]. Nevertheless, different studies performed by means of techniques such as X-ray scattering techniques

[17-19], Fourier-Transform Infra-Red Analysis (FTIR) [20], Temperature-Modulated Differential Scanning Calorimetry (TMDSC) [21-22], Thermo-Mechanical Analysis (TMA) [23] or micro-indentation [19] showed the suitability of a three-fraction model to describe the microstructure of PET. With this model, mobile (composed by the mobile amorphous fraction *MAF*) and rigid (formed by a crystalline *C* and a rigid amorphous fraction *RAF*) domains are defined [24-25]. The *RAF* is normally assigned to both the amorphous-crystalline interface in basal lamellar planes [26-28], in connection to the bulk amorphous fraction *MAF*, as well as to the inter-spherulitic domains constrained between crystalline lamellae stacks [25]. On the other hand, the *MAF*, which normally behaves contributing to the heat capacity jump throughout the glass transition, is associated to the freely interstack regions [29]. This model has not been discussed yet to understand the effects of reprocessing on PET. However, its application permits to define accurately the changes on the microstructure of PET and control the quality of the recycled material.

The aim of this work was firstly focused on testing the structural groups affected by chain scission induced by thermo-mechanical degradation. Afterwards, the evolution of the microstructure throughout the reprocessing stages was assessed by thermal analysis, according to a three-fraction model. Finally, the performance of recycled PET was correlated with the crystalline, mobile amorphous and rigid amorphous fractions.

2. Experimental procedure and calculations

2.1. Material, reprocessing simulation and sample preparation

Poly (ethylene terephthalate) (PET) SEDAPET SP04 was a bottle-grade PET obtained from Catalana de Polimers S.A., Grup LaSeda (Barcelona, Spain) in the form of pellets. Prior to processing, virgin PET (VPET) pellets were dried during 5 h at 160 °C in a dehumidifier Conair Micro-D FCO 1500/3 (UK), in order to remove as much humidity as possible from the PET flakes. Afterwards, the samples were processed by means of injection moulding employing an Arburg 420 C 1000-350 (Germany) injector, single-screw model (diameter $\Phi=35$ mm, length/ $\Phi=23$). Successive processing steps were applied under the same conditions, being the samples carefully dried before each processing cycle. Temperature gradient set from hopper to die was 270, 275, 280, 285 and 280 °C. Moulds were set at 15 °C. Cooling time residence was 40 s and total residence time nearly 60 s. After injection, a fraction of the samples was kept as test specimen and the rest was ground by means of a cutting mill Retsch SM2000 (UK), which provided pellets of size $\Phi < 20$ mm to be fed back into the recirculation process. Up to five processing cycles were applied to obtain the different testing specimens of reprocessed PET (RPET-i, with i: 1-5).

Prismatic probes of 1 mm of thickness were prepared for DMTA characterization by melt compression in a Collin PCS-GA Type Press 800 (GA, USA) preset at 260 °C. Five pressure steps were performed with the program: 5 minutes at 4 bar, 3 minutes at 100 bar, 1 minutes at 80 bar, 5 minutes at 180 bar, and 15 minutes at 75 bar.

2.2. Mechanical performance

Tensile testing was carried out at laboratory conditions 23/50, according to ISO 291, atmosphere 23/50, class 1 [30]. Tensile tests were performed on reprocessed PET in order to investigate the changes in macroscopic mechanical properties, on dumbbell samples following ISO 527-2 (type 1A) [31], by means of an Instron 5566 universal electromechanical testing instrument (Instron Corp, MA, USA), at a crosshead speed of 10 mm·min⁻¹, a 10 kN load cell and gauge length of 50 mm. Analyses were repeated at least 6 times per material, and the average of elastic modulus, elongation at break and stress at break were used as representative values.

Charpy impact experiments were carried out following ISO 179 [32], with a hammer of 1 J and a notch size radius of 1,5 mm, under the same laboratory conditions than tensile tests. Analyses were repeated at least 5 times per material, and the averages were taken as representative values.

2.3. Scanning Electron Microscopy (SEM)

The morphology of the specimens was analysed by means of a Hitachi S-4800 Field Emission Scanning Electron Microscope (Tokyo, Japan). The samples from each material were prepared by cutting squared pieces from a randomly chosen part of the processed specimen. The pieces were mounted on metal studs and sputter-coated with a 2 nm gold layer using a Cressington 208HR high resolution sputter coater (Watford, UK), equipped with a Cressington thickness monitor controller.

2.4. Fourier-Transform Infrared (FT-IR) Analysis

FT-IR spectra were collected by a NEXUS Thermo Nicolet 5700 FT-IR Spectrometer (MA, USA), previously calibrated, and equipped with a single-reflection Smart Performer accessory for attenuated total reflection (ATR) measurements, with diamond crystal. 32 co-added spectra were recorded for each specimen at a resolution of 4 cm^{-1} with a spacing of 1 cm^{-1} , from 4000 to 600 cm^{-1} of wavenumber. IR spectra were analyzed with the help of OMNIC 7.0 software from Thermo Scientific. The peak at 1410 cm^{-1} was used for normalization [33] before any data processing, corresponding to the benzene ring in-plane deformation, which is usually used as internal standard due to it is not sensitive to effects of orientation or conformation [34], and it is useful to correct possible variations arisen from defects in surface quality or sample positioning. At least 8 measurements per material were performed at different locations of the plate, in order to obtain representative results. Presented spectra correspond to the average of each individual analysis.

2.5. Molar mass determination

The intrinsic viscosity $[\eta]$ was measured according to the standard ISO 1628-1 [35], by means of a Cannon-Fenske capillary viscosimeter type at 25 °C, with the use of 60/40 wt% phenol/1,1,2,2-tetrachloroethane as solvent. Dissolutions of pellets ranged from 0.1 to 0.5 $\text{g}\cdot\text{dL}^{-1}$. Measurements were performed by quintuplicate for each concentration c and $[\eta]$ was obtained from extrapolation to $c \rightarrow 0$ of Huggins and Kraemer plots [36], which respectively account for the variation of reduced η_{red} and inherent η_{inh} viscosities with the concentration, being $\eta_{red} = c^{-1} \cdot \eta_{sp}$, $\eta_{inh} = c^{-1} \cdot \ln$

η_{rel} , $\eta_{sp} = \eta_{rel} - 1$ and $\eta_{rel} = t \cdot t_0^{-1}$, where t and t_0 were the times (s) of flowing of the dissolution and solvent, respectively. The number and weight average molar mass values (M_n , M_w , $\text{g}\cdot\text{mol}^{-1}$) were calculated with the Mark-Houwink equation $[\eta] = K \cdot M_v^\alpha$, with constants $K = 3.72 \cdot 10^{-4} \text{ dL}\cdot\text{g}^{-1}$ and $\alpha = 0.73$ for M_n , and $K = 4.68 \cdot 10^{-4} \text{ dL}\cdot\text{g}^{-1}$ and $\alpha = 0.68$ for M_w [37-38]. The polydispersity index was consecutively calculated as $PDI = M_w \cdot M_n^{-1}$. Note that the values do not necessarily correspond to those that could be obtained by Gel Permeation Chromatography, but it has been shown [39] that are suitable for monitoring degradation processes.

2.6. Differential Scanning Calorimetry (DSC)

DSC analyses were carried out by a Mettler Toledo DSC 820 instrument (Columbus, OH) calibrated with indium and zinc standards. Approximately 5 mg of pellets were placed in 40 μL aluminium pans, which were sealed and pierced to allow the N_2 gas flow (50 $\text{mL}\cdot\text{min}^{-1}$). A heating/cooling/heating program with a $\pm 2^\circ\text{C}\cdot\text{min}^{-1}$ rate was employed in the temperature range between 25 °C and 290 °C. The samples were characterized with the aid of the software STAR^e 9.10, at least by triplicate, and the averages were taken as representative values.

The glass transition was characterized according to ISO 11357-2 [40] and the temperature in its inflection point (T_g) and the jump in heat capacity (ΔC_p) were recorded. Crystallization and melting phenomena were assessed in terms of their onset and peak temperatures, along with the enthalpies related to their areas to common baselines.

According to a three-fraction model, the relative values of the crystalline (X_c), mobile amorphous

fraction (X_{MAF}) and rigid amorphous fraction (X_{RAF}), were calculated as follows:

$$X_C = \frac{\Delta h_m - \sum \Delta h_{CC}}{\Delta h_m^0} \quad (1)$$

$$X_{MAF} = \frac{\Delta C_p}{\Delta C_p^0} \quad (2)$$

$$X_{RAF} = 1 - X_{MAF} - X_C \quad (3)$$

, being Δh_m and Δh_C the specific melting and cold-crystallization enthalpies ($\text{J}\cdot\text{g}^{-1}$), Δh_m^0 the melting enthalpy of a fully crystalline PET (140 $\text{J}\cdot\text{g}^{-1}$ [41]), and ΔC_p^0 the heat capacity increment of a fully amorphous PET (0.405 $\text{J}\cdot\text{g}^{-1}\cdot\text{K}^{-1}$ [42]).

2.7. Dynamical-Mechanical Thermal Analysis (DMTA)

DMTA test were conducted in dual cantilever clamping with 10 mm of effective length between clamps, in bending mode, by means of a DMA/SDTA861^e Dynamic Mechanical Analyzer, from Mettler-Toledo (OH, USA). Experiments were carried out from 25 °C to 175 °C with isothermal steps of 2°C, measuring 8 frequencies per decade between 0.1 and 100 Hz.

3. Results and discussion

3.1. Structural changes induced by thermo-mechanical degradation

The absorbance spectra of virgin poly (ethylene terephthalate) (VPET) and its successive recyclates (RPET-i, i: 1-5) were recorded by Fourier-Transform Infrared Spectroscopy (FT-IR). Typical PET spectra were obtained for all samples. Assignments of IR bands can be found

elsewhere [43-44]. Interesting structural changes could be deduced by inspection of **Figure 1** and **Figure 2**, which respectively show the evolution of the absorption of the stretching vibration bands of the ethylene group associated to the glycol units of PET, and the development of a polymeric-bonded -OH end-group. Different studies [45-46], in which combinations of PET with poly(ethylene glycol) were assessed, showed that bands situated near 2962 cm^{-1} and 2903 cm^{-1} may be assigned to the asymmetrical $\nu_{as}(\text{CH}_2)$ and symmetrical $\nu_s(\text{CH}_2)$ stretching vibrations of the ethylene glycol (EG) group of PET, while the bands around 2918 cm^{-1} and 2854 cm^{-1} can be assigned to the same vibrations in case diethylene glycol domains (DEG) were present in PET backbone. It is shown in **Figure 1** that both VPET and RPET-1 absorbed at these latter wavenumbers, which bands vanished for the rest of recyclates. This effect is in agreement with the mechanisms described in a previous study [9] in which the degradation of VPET was explained by the loss of EG units via mainly intramolecular transesterifications or homolytic reactions, such as chain scission by hydrolysis. On the other hand, the increase of the band centred around 3548 cm^{-1} (**Figure 2**) suggested the promotion of -OH terminated species with more reprocessing cycles, also in agreement with our previous results [9]. The increase of these species may explain the increased yellowed appearance of PET recyclates with each processing step, due to they can act as precursors of discoloration reactions, as shown by *Choudhury et al.* [47]. This feature impoverishes RPET possibilities to be employed in food-packaging goods.

The nature of the -OH terminated species, mainly hydroxyl and carboxyl species, to act as auto-catalysers during thermo-mechanical degradation may be an evidence of reduction of molar mass. Thus, the evolution of the molar

tendency was attenuated and the variations showed an asymptotic profile towards slightly inferior values for further recyclates. Consequently, the polydispersity index showed a similar value after the second recycle, related to

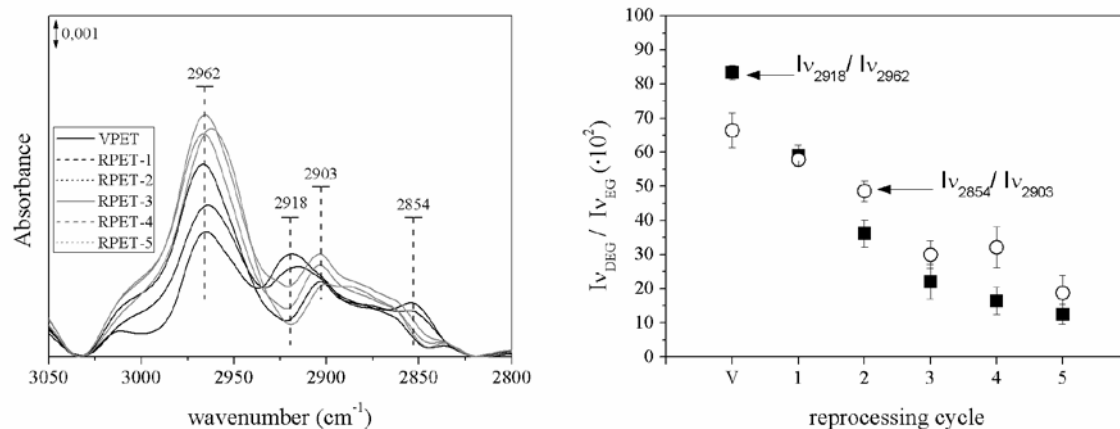


Figure 1. FT-IR analysis of the C-H stretching region: (left) FT-IR spectra evolution; (right) semi-quantitative analysis.

masses was correlated to the number of recyclates, as shown in **Figure 3**. Satisfactory linear correlation values were obtained for both Huggins and Kraemer plots for all materials ($R^2 > 0.925$). An exponential profile for the overall molar mass decay was found, where two different stages were distinguished. Both M_w and M_n decreased steeply with each reprocessing step during the two first processing cycles, with marginal drops of ~ 35 % from VPET to RPET-1 and ~ 32 % from RPET-1 to RPET-2 in the case of M_w . From the second recycle on, the

likely similar distributions of chains.

The significant decrease in molar mass may affect the processability and homogeneity of PET recyclates. Surface characterization of reprocessed PET by SEM shown at **Figure 4** exhibited typical morphologies of industrially-processed polymers. The micrographs of RPET-5 presented a loss of the orientation of the processing lines shown by VPET. In addition, the surface seemed to be less smooth and more liable to mechanical scratches. This effect has been found for other recycled commodities such as

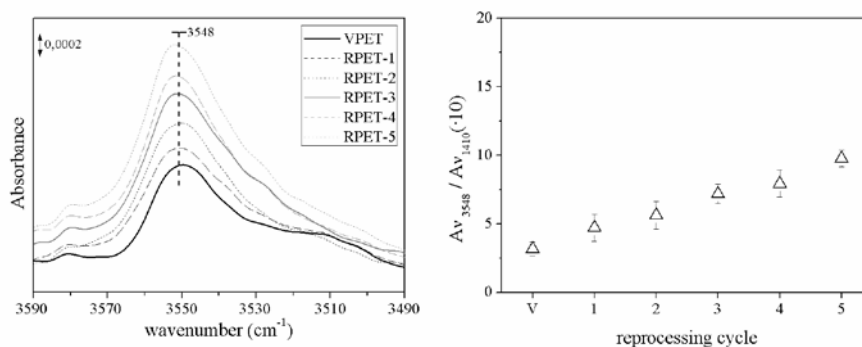


Figure 2. O-H stretching vibration study: (left) FT-IR spectra evolution; (right) semi-quantitative analysis

PE, PP or PS [4, 6]. As well, inefficiently melted pellets were adhered to the surface, thus indicating a loss of processability of RPET-5 under the same experimental conditions of VPET. The morphological defects may arise as a result of new structural and conformational arrangements between the amorphous and crystalline regions of PET and thus a deep characterization is given afterwards.

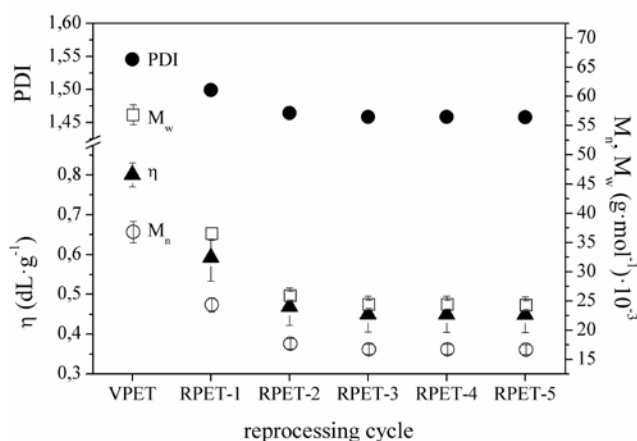


Figure 3. Evolution of intrinsic viscosity, molar masses and polydispersity index.

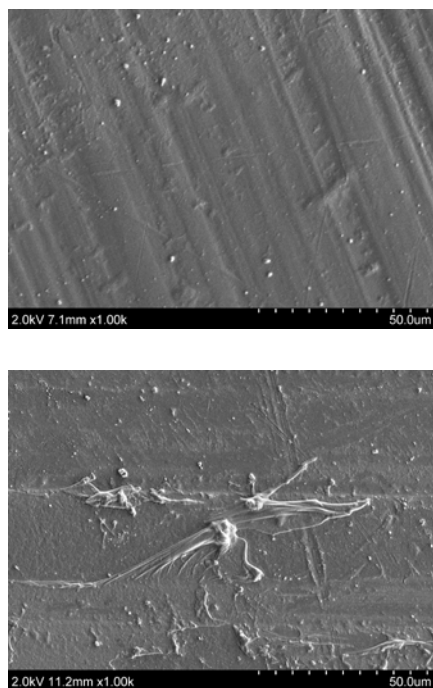


Figure 4. Surface analysis by SEM. (upper: VPET, lower: RPET-5)

3.2. Influence of reprocessing on the conformational morphology of PET

Differential Scanning Calorimetric (DSC) and FT-IR analysis were applied to assess the conformational changes induced by successive reprocessing to PET. On the one hand, the results of the use of the three-fraction model to explain the evolution of the ratios of crystalline (X_C), mobile amorphous (X_{MAF}) and rigid amorphous (X_{RAF}) fractions is shown in **Figure 5**. An initial (X_C , X_{MAF} , X_{RAF}) distribution of $\sim (29/53/18)$ % was found for VPET, similar to that reported in other studies [48]. The crystalline fraction showed a slight overall increase ($\sim 5\%$), whereas *MAF* and *RAF* suffered the main effects of reprocessing, differing at RPET-5 around a 25 % from their original proportion in VPET. Interestingly, the major change happened from the first to the second recycle, involving a marginal modification close to a 10 % for both X_{MAF} and X_{RAF} . The results suggested that the *MAF* was principally attacked due to thermo-mechanical degradation, releasing shorter chains that might fold among themselves and rearrange into inter-crystalline domains, that is, *RAF*, with each reprocessing cycle. On the other hand, the FT-IR analysis of specific *gauche/trans* pairs was also useful to characterize the changes in morphology of PET. The vibrations of the ethylene group of the glycol unit of PET exist in two forms, a *gauche* or relaxed form, present in the amorphous phase of PET; and a *trans*, or extended form, which is more present in the crystalline fraction of PET. The bands at 1471 cm^{-1} and 1466 cm^{-1} form the *gauche/trans* pair of the C-H bending vibration of the glycol unit in PET, whereas the bands at 899 cm^{-1} and 846 cm^{-1} form the respective for the rocking vibration of the same group. The study of the relative ratio of the absorbance areas for both vibration bands is

shown in **Figure 6**. In a two-fraction model, where only amorphous and crystalline domains were considered, the variation between *gauche* and *trans* conformers might be directly related. On the contrary, in a three-fraction model, the decrease of the ratios could then not necessarily related to an increase of the relative absorbance of the *trans* conformers of PET, responsible of chain packing in crystalline domains. As confirmed by DSC, since the increment of the crystalline fraction was not significantly prominent, the *gauche/trans* ratio indicated a decrease of the amorphous domains due to reprocessing. This change was especially remarkable after the second recyclate, fact that may be related to the reduction from diethylene glycol to ethylene glycol in the PET backbone, as explained above. After reprocessing, the new structures with shorter backbones and less flexible glycol units may rearrange into more packed structures.

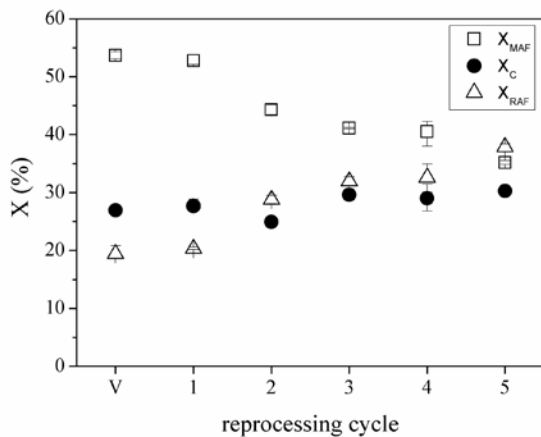


Figure 5. Evolution of the balance between crystalline and mobile and rigid amorphous fractions

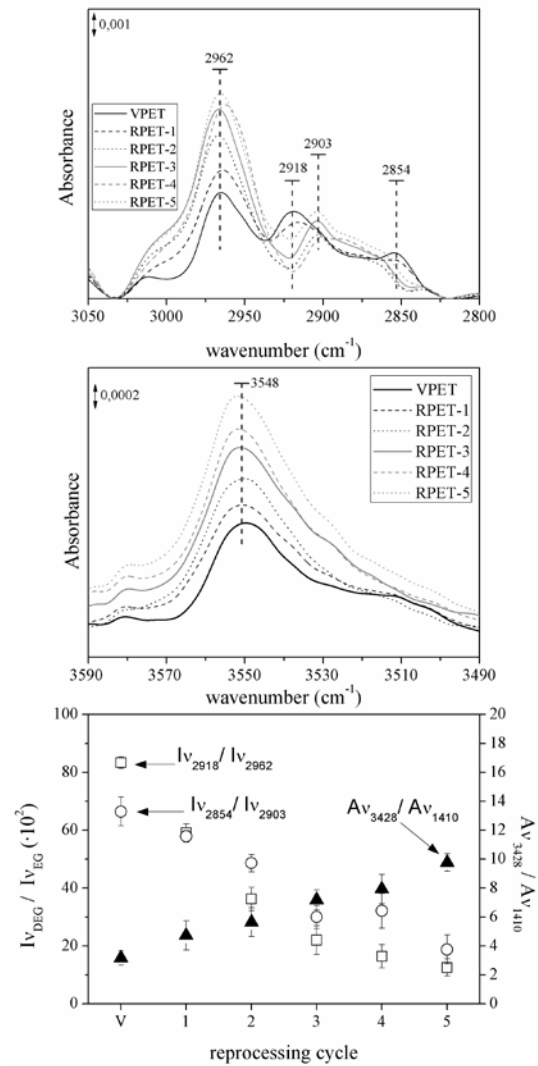


Figure 6. C-H vibrations study: (upper) FT-IR spectra evolution of C-H bending band; (middle) FT-IR spectra evolution of C-H rocking band; (lower) semiquantitative analysis.

3.3. An extended study of the crystalline fraction

Further analysis evidenced that the morphological changes underwent by PET facing successive injection-moulding operations gave rise to different crystalline domains, as shown in previous reports [8]. The influence of reprocessing on the crystallization behaviour was studied from the cooling thermograms (**Figure 7**); considering onset (T_{CO}) and peak

Table 1. Calorimetric parameters

Material	T_g (°C)	T_{C0} (°C)	ΔT_C (°C)	T_C (°C)	Δh_C (J·g ⁻¹)	Δh_m (J·g ⁻¹)
VPET	77.6 ± 0.5	146.3 ± 0.5	54.2 ± 0.4	171.6 ± 2.6	-35.8 ± 2.1	37.7 ± 1.1
RPET-1	77.1 ± 0.3	165.5 ± 0.5	37.1 ± 0.8	189.0 ± 0.6	-36.4 ± 0.2	38.7 ± 1.3
RPET-2	76.4 ± 0.1	185.3 ± 2.3	32.2 ± 1.7	204.7 ± 3.1	-38.1 ± 1.4	35.2 ± 0.4
RPET-3	76.2 ± 0.1	189.2 ± 0.8	29.1 ± 1.1	208.3 ± 1.3	-40.2 ± 0.9	41.4 ± 0.5
RPET-4	76.3 ± 0.7	188.1 ± 0.3	28.3 ± 2.1	211.7 ± 2.5	-39.3 ± 1.8	40.6 ± 3.2
RPET-5	76.2 ± 0.7	184.3 ± 0.6	30.2 ± 1.7	211.1 ± 0.8	-41.8 ± 1.4	42.3 ± 0.4

crystallization temperatures (T_C), crystallization temperature range (ΔT_C) and specific crystallization enthalpy (Δh_C) for the assessment, which values are gathered at **Table 1**. The low cooling rate used in the DSC analysis promoted the formation of nuclei for the crystallization, and it was therefore useful for the comparison between the formation of crystalline domains of virgin and reprocessed PET. The cooling thermograms appeared sharper and steeper at the beginning of the crystallization, as well as involving bigger enthalpies with each reprocessing cycle, being particularly remarkable the change from RPET-1 to RPET-2. As well, the crystallization started at higher temperatures and thus earlier, and it was produced in a shorter temperature range. The T_C was appointed as a quality parameter to distinguish between virgin and reprocessed PET in previous reports [8, 49], and therefore its reduction pointed out the presence of shorter chains with each reprocessing cycle. The whole crystalline fraction formed during cooling was melted during subsequent

DSC heating, as shown in **Table 1** by the values of specific melting enthalpy Δh_m similar to those of crystallization Δh_C , which also remarkably increased until the second recycle.

In order to characterize the crystalline fraction of PET and its further recyclates, an approach by applying the *Hoffman-Lauritzen* nucleation theory [50-52] to relate the evolution of the lamellar thickness (l_C) distribution with the reprocessing cycle was performed. The *Thomson-Gibbs* equation (Eq. 4) was used to assess the evolution of the lamellar thickness distribution:

$$l_C(T_m) = \left[\left(1 - \frac{T_m}{T_m^0} \right) \cdot \frac{\Delta h_{mV}}{2 \cdot \sigma_e} \right]^{-1} \quad (4)$$

, where T_m is the melting temperature; T_m^0 is the equilibrium melting temperature of an infinite crystal (564 K); σ_e is the surface free energy of the basal plane where the chains fold (0.106 J·m⁻²); Δh_{mV} is the melting enthalpy per volume unit

($2.1 \cdot 10^8 \text{ J} \cdot \text{m}^{-3}$), both values obtained from studies by *Lu and Hay* [53].

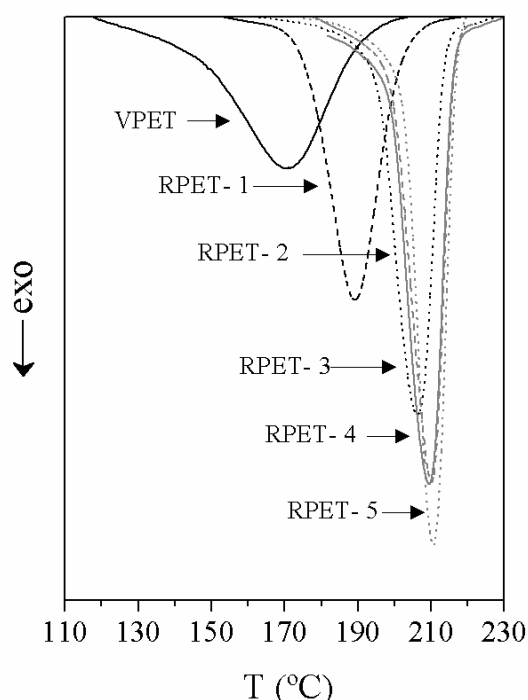


Figure 7. Evolution of DSC cooling thermograms

Figure 8 represents the l_c distribution for virgin and reprocessed PETs. In this figure, a prominent distribution related to the most probable lamellar size can be seen. A bimodal melting behaviour is displayed, which is still on debate [54-60]. Under isothermal DSC crystallization conditions, multiple melting behaviour of PET can be associated to a superposed melting-crystallization-remelting process [54-56], to the enthalpy recovery connected to the mobilization of the constrained *RAF* [57] and/or the melting of two distinct crystal populations [58-60]. In any case, the effects of degradation could be monitored by the analysis of the melting endotherm at lower temperatures. It was assumed that the thermo-mechanical degradation enhanced the crystallization and segregation of crystals with different crystalline sizes,

highlighting the heterogeneity suffered by PET during in-plant recycling.

In order to better explain the effect of the degradation process on the crystalline fraction, a deconvolution procedure [61] was applied to the melting thermograms with the aim of individually characterizing the behaviour of each i population and its contribution to the overall effect using a partial areas study, as early proposed [8].

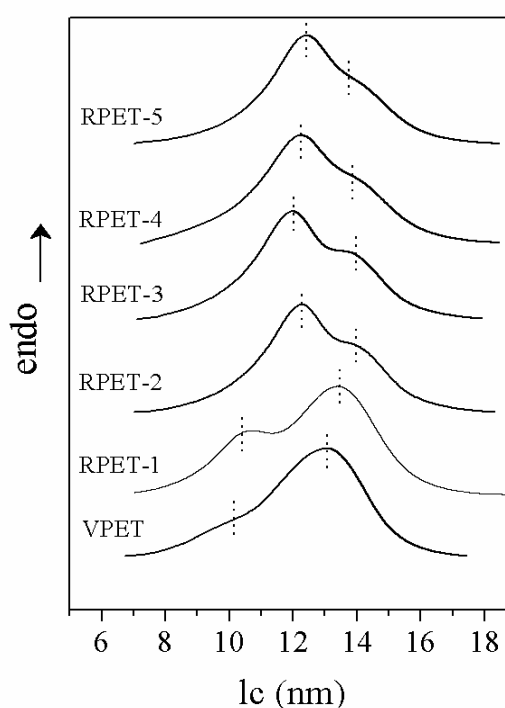


Figure 8. Lamellar thickness distributions of virgin and reprocessed PETs.

Fitting DSC procedures were performed by means of OriginLab OriginPro 8.0, which uses the Levenberg-Marquardt algorithm [62-63] to adjust the parameter of the fitting values in the iterative procedure. Populations were labelled as I and II from the lowest to the highest peak temperature (T_m^i), which are registered at **Table 2**, along with their melting onset temperatures (T_{m0}^i), melting range temperatures (ΔT_m^i) and

average lamellar thicknesses (l_c^i). As well, the so-called relative partial crystallinity of each population [8] was calculated by means of $X^i = X_C^i / X_C = \Delta h_m^i / \Delta h_m$, where Δh_m^i is the partial melting enthalpy of each population i , and compared to the full crystallinity degree (X_C) in **Figure 9**. Despite X_C was not sensitive to changes induced by reprocessing, the use of X^i provided new insights on the formation of new crystals. The plots showed a continuous development of crystalline zones with lower lamellar size, especially from the first to the second recyclate. In connection with the result from the cooling DSC scan, the formation of shorter chains might act as nuclei upon crystallization, which promoted the growth of more crystalline domains. The melting processes of both populations were also sharpened during reprocessing, with an overall ΔT_m^i change of $\sim 8^\circ\text{C}$ for population I, and $\sim 17^\circ\text{C}$ for population II. As well, the onsets of melting of populations I and II were displaced $\sim 8^\circ\text{C}$ and $\sim 20^\circ\text{C}$ to higher temperatures, respectively. Contrarily, the peak temperatures and their corresponding lamellar thicknesses did not follow the same trend for both populations.

Whereas T_m^{II} remained around 250°C for an average lamellar thickness of 13-14 nm, population I underwent an important increase of $\sim 8^\circ\text{C}$ in its T_m^I , from 207 to 215°C , related to the increase in l_c^I from 9.8 nm in VPET to 12.7 nm in RPET-5. Considering the variation of X^I respect to X^{II} , the distribution balance of populations I/II (%), which was $\sim 10/90$ for VPET, decayed down to $\sim 60/40$ after the second reprocessing cycle, and then smoothly decreased until a $\sim 55/45$ for RPET-5.

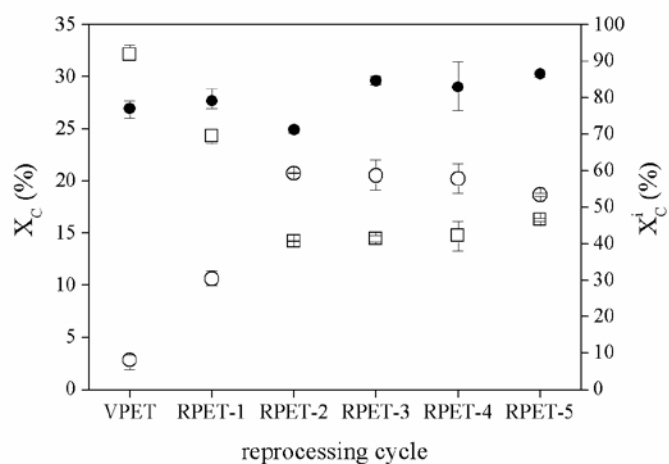


Figure 9. Evolution of relative partial crystallinity degrees

Table 2. Calorimetric parameters after deconvolution

Material	T_{m0}^I ($^\circ\text{C}$)	ΔT_m^I ($^\circ\text{C}$)	T_m^I ($^\circ\text{C}$)	l_c^I (\AA)	T_{m0}^{II} ($^\circ\text{C}$)	ΔT_m^{II} ($^\circ\text{C}$)	T_m^{II} ($^\circ\text{C}$)	l_c^{II} (\AA)
VPET	207.7 ± 1.7	39.1 ± 1.4	233.2 ± 0.6	9.8 ± 0.12	212.3 ± 1.8	47.4 ± 2.1	249.8 ± 0.3	13.8 ± 0.13
RPET-1	207.6 ± 1.6	41.7 ± 2.5	238.4 ± 0.1	10.8 ± 0.02	220.6 ± 1.4	39.4 ± 1.8	250.2 ± 0.1	14.0 ± 0.05
RPET-2	210.6 ± 0.1	41.8 ± 2.2	241.7 ± 0.1	11.6 ± 0.01	228.1 ± 1.3	35.4 ± 0.2	248.8 ± 0.1	13.5 ± 0.01
RPET-3	214.8 ± 0.7	35.6 ± 0.4	245.1 ± 0.5	12.4 ± 0.14	230.4 ± 1.1	29.6 ± 1.1	250.3 ± 0.2	14.1 ± 0.08
RPET-4	216.8 ± 2.5	34.7 ± 0.7	245.4 ± 0.2	12.6 ± 0.06	229.2 ± 2.0	30.8 ± 2.8	250.5 ± 1.1	14.1 ± 0.31
RPET-5	215.3 ± 0.1	35.0 ± 0.3	245.9 ± 0.1	12.7 ± 0.02	231.3 ± 0.1	29.4 ± 0.6	249.7 ± 0.15	13.8 ± 0.04

The rearrangement of new crystalline domains after each reprocessing cycle was promoted towards populations with smaller average sizes, being the tendency changed from RPET-1 to RPET-2. These variations in crystallinity, along with the relative variation between mobile and rigid amorphous fractions might role the performance of PET recyclates in applications that service at sub- T_g temperatures.

3.4. Segmental dynamics around the glass transition. The influence of multiple processing on the viscoelastic response of PET and its successive recyclates throughout the glass transition relaxation was evaluated by means of multi-frequency DMTA tests. The loss (E'') moduli were recorded for PET reprocessed samples and their evolution as a function of temperature are displayed in **Figure 10**, respectively, for the analysis performed at a frequency of 1 Hz. Results at the rest of applied frequencies showed similar tendencies.

A prominent viscoelastic relaxation was displayed by virgin and reprocessed PETs, along a wide α -relaxation that corresponds to the glass-rubber transition which extended from 60 °C to near 140 °C. This relaxation is associated to the long-range segmental motions of the amorphous regions, and is highly dependent on the interaction with the rigid domains, comprised by both *RAF* and crystalline fractions. In connection with FT-IR results, it was shown by NMR studies that the molecular motions of the α -relaxations are driven by the *trans/gauche* isomerism of the ethylene groups of the glycol units of PET backbone [64]. In general, reprocessed samples present a broader E'' peak, as shown by the evolution of their Full Widths at Medium High (*FWMH*), in conjunction with a displacement to lower values of the peak

temperature T_p , which is more sensitive to morphological changes at the amorphous fraction than the T_g obtained by DSC experiments. According to other reports in literature [22, 65-66], for PET samples that accounted for X_C of about 30 %, this decrease of T_p is indicative of dual amorphous fractions, having unlike mobility, thus it would also demonstrate the presence of *RAF*. As suggested in previous studies for multiple extrusions of PET [8] and in accordance to DSC results, random scission induced by thermo-mechanical degradation of the PET backbone produced shorter polymer chains that may explain the diverse distribution of lengths. The heterogeneity of the crystalline region may affect the mobility of the already decreased *MAF*, being hindered within the glass transition relaxation. As well, the increase of *RAF* which remained vitrified during glass-rubber transition might also constrain the cooperative movement of the *MAF*.

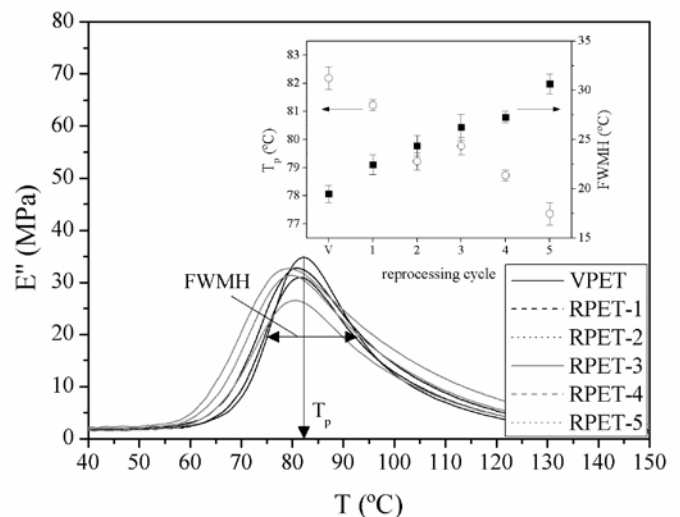


Figure 10. Evolution of loss moduli. Inset: variation of the peak temperatures and the full widths at medium height.

A deeper assessment of the influence of reprocessing to the glass-forming behaviour of PET provided more information regarding the molecular mobility of PET chains throughout the glass transition. The strong-fragile glass former concept proposed by Angell [67] was used, in which the variation of the viscosity with temperature could be explained under two border limits. On the one hand, the relationship between relaxation times and temperature $\tau(T)$ of a strong glass-forming behaviour can be expressed by an Arrhenius law, which reveals a strong resistance against structural changes. On the other hand, a fragile glass-forming polymer would deviate from the thermally-activated Arrhenius behaviour, as usually happens to linear polymeric materials [68-69]. Therefore, a fragile glass-former experiences a dramatic loss of properties (rheological, mechanical...) throughout a specific short temperature interval, such as the glass-rubber relaxation, while a strong glass-former maintains its properties without significant changes. For this reason, the temperature dependence of the relaxation times $\tau = \omega^{-1} = (2 \cdot \pi \cdot f)^{-1}$ of E'' spectra obtained during the glass transition relaxation at different angular/linear frequencies ω / f was fitted to the Vogel-Fulcher-Tamman-Hesse [70-72] model. The so-called fragility index m permitted an assessment of the deviation of $\tau(T)$ from the Arrhenius behaviour of polymers. It is defined as the characteristic slope of the fragility plot $\log \tau$ vs $T_g \cdot T^{-1}$ and varies between two limiting values of 16 and ≥ 200 for strong and fragile glass-formers, respectively [73-74]:

$$m = \left. \frac{d \log(\tau)}{d(T_g/T)} \right|_{T=T_g} = \frac{B \cdot T}{\ln(10) \cdot (T_g - T_{VFTH})^2} \quad (5)$$

, where B (K) and T_{VFTH} (K) are positive parameters specific for the material. Qualitatively, B can be related to the topology of the theoretical potential energy surface of the system, where fragile systems ($B \downarrow$) present high density of energy minima, contrarily to strong systems ($B \uparrow$) which present lower density. Consequently, m can be associated to the average height of the energy barrier that conformers may overcome to reach their energy minima. The evolution of B and T_{VFTH} is gathered in **Table 3**. Excellent linear correlation values (R^2) were obtained for the VFTH fitting. In addition, the Angell's diagram is shown at **Figure 11**. The fragility index, obtained from the slope of the curves at $T=T_g$, decreased with each reprocessing cycle, as also given in **Table 3**. The influence of the chemistry of the backbone and of the side-groups on the fragility of polymers were thoroughly discussed by Kunal *et al* [75], stating that fragility depended upon the relative size balance between backbone and side groups. PET, due to its characteristic rigid backbone involving aromatic rings, is inherently fragile, associated to inefficient packing of rigid chains. In polymers with rigid backbones, studies in literature indicate that an increase in chain length lead to an increase in dynamic fragility due to inefficient packing [76-77]. On the contrary, a cutback in chain length due to chain scission processes may allow the rearrangement of shorter chains in the MAF, promoted by the availability of more free volume. However, if the free chains were primordially arranged into rigid fractions, the cooperative movement would be reduced, thus diminishing the dynamic fragility of the polymer, as shown by the fragility parameters B and m .

The subsequent calculation of the activation energies related to the glass-rubber relaxation Ea_{GT} , along with the free volume

Table 3. Results from the assessment of the segmental dynamics

Material	VFTH fitting				Calculated parameters			
	T _g (°C)*	T _K ** (°C)	D	R ²	B (K)	Φ (%)	Ea (kJ·mol ⁻¹)	m
VPET	77.6 ± 2.1	42.0 ± 1.7	2.87 ± 0.81	0.998	905.5	3.92	732	109
RPET-1	77.1 ± 1.1	41.5 ± 1.2	2.58 ± 0.52	0.996	813.1	4.37	653	97
RPET-2	76.4 ± 0.8	39.9 ± 0.5	2.55 ± 0.06	0.988	798.3	4.56	609	91
RPET-3	76.2 ± 0.8	39.9 ± 0.3	2.52 ± 0.03	0.998	789.4	4.58	610	91
RPET-4	76.3 ± 0.6	38.9 ± 0.6	2.44 ± 0.04	0.994	762.5	4.89	555	83
RPET-5	76.2 ± 0.8	37.9 ± 0.1	2.46 ± 0.05	0.993	765.7	4.99	531	79

* T_g=T_p taken at the experiment at frequency 0.01 Hz
 **T_{VFTH}=T_K (Kauzman temperature)

coefficient ϕ obtained by means of Eqs. (6) and (7), pictured the change in cooperative movement due to thermo-mechanical degradation, as shown in **Table 3**.

$$Ea_{GT} = R \cdot \frac{d \ln \tau}{d(1/T)} = \frac{R \cdot B}{\left(1 - \frac{T_{VFTH}}{T}\right)^2} \quad (6)$$

$$\phi = \frac{(T - T_{VFTH})}{B} \quad (7)$$

The free volume is usually ascribed to the packing defects in the structure due to inhibition of the segmental mobility below T_g , and thus, due to reprocessing, the rearrangement of the chains may provoke molecular-size cavities. This effect might promote the liability of gases to permeate through the polymer in packaging applications [25], therefore reducing the second-life performance of PET for similar purposes. On the other hand, the high apparent activation energies (Ea_{GT}) found for virgin PET, as observed for other studies [78-79], progressively decreased for

each PET recyclate. Taking into account that the constraints induced by the crystalline fraction may remain similarly, due to no significant increase in X_C was obtained, the decrease of dynamic fragility found for reprocessed PET may be explained by the remarkable formation of *RAF* and connected reduction of *MAF*.

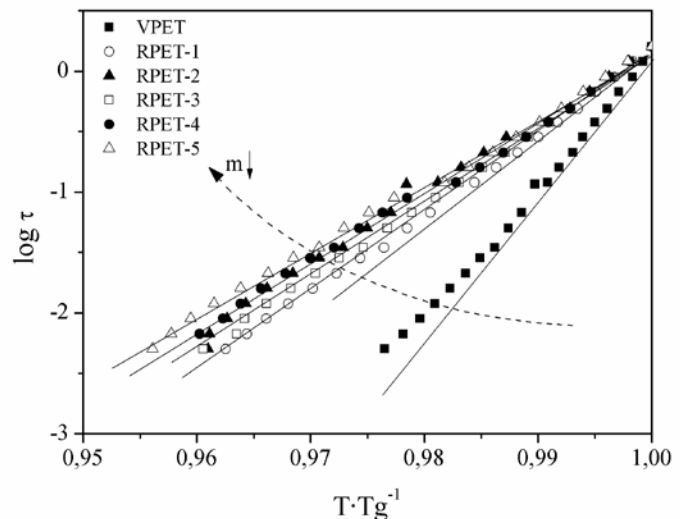


Figure 11. Angell's plot. Evolution of the fragility index m.

3.5. The role of MAF and RAF on the mechanical performance PET

The influence of the microstructural conformation of reprocessed PET was finally assessed on the mechanical performance by tensile and impact testing, and the study of the storage modulus (E') spectra by DMTA. **Figure 12** shows the results obtained by traditionally used tensile and impact tests. On the one hand, a slight overall variation in the Young modulus ($\sim 14\%$) was registered for RPET-3,4,5 in comparison to that of VPET. On the other hand, the stress and elongation at break were clearly influenced by the reprocessing cycles, showing a critical drop from RPET-1 to RPET-2. The chemical and morphological changes induced by reprocessing gave out more brittle materials with lower ductility, as drawn from the variation of the impact strength value, which was halved for the second recycle. These results were in agreement with those given by other authors for PET [12], PS [5] or PE [4] who did not observed significant changes in the elastic modulus due to reprocessing, though the elongation at break strongly diminished.

The thermo-mechanical degradation effects on the macroscopic mechanical properties could be explained by the role of the increasing *RAF* throughout the processing cycles. A Strain-Induced Crystallinity (SIC) phenomenon may have occurred upon tensile testing below T_g , where part of the newly formed *RAF* due to reprocessing may enhance interactions and entanglements between chains, as well as act as precursor of new nucleation sites, enhancing the growth of the crystalline phase during tensile testing, as supported by X-ray Diffraction studies [80-82]. Furthermore, *Schick et al* suggested that the *RAF* itself may vitrify [21], thus increasing the rigidity of PET upon drawing, acting as topological constraints against deformation transforming the initial ductile behaviour of PET, breaking the probe by means of a brittle fracture with lower applied stress.

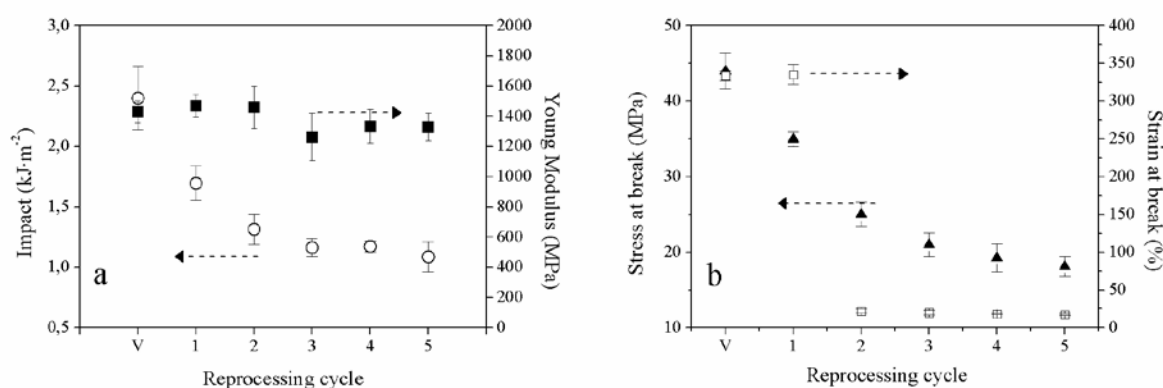


Figure 12. Variation of mechanical properties as analyzed by tensile and impact testing.

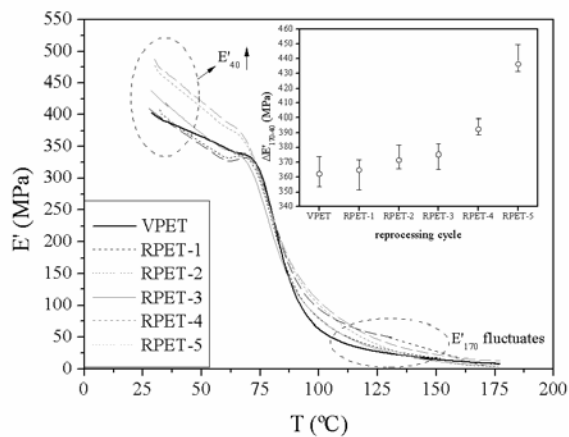


Figure 13. Evolution of storage moduli at 1 Hz.
Inset: variation of mechanical stresses through the reprocessing cycles

Concerning the role of *MAF*, its diminution was more significant upon glass-rubber relaxation. **Figure 13** represents the viscoelastic storage modulus (E') of virgin PET and its five successive recyclates obtained by DMTA performed at 1 Hz. Experiments performed at the rest of frequencies showed similar behaviours. The mechanical strength $\Delta E'$, calculated as the difference between the E' values at 40 and 170 °C, was evaluated. Taking into account that the crystalline fraction remained scarcely changed along the reprocessed materials, the role of *MAF* drove the increase of $\Delta E'$. In connection with DSC results, the significant loss of *MAF* negatively affected the elastic behaviour of PET, since less non-constrained amorphous chains were subjected to the tension of the experiment, therefore increasing E' and subsequently $\Delta E'$ showed an overall increase of ~20 % from VPET to RPET-5.

4. Conclusions

Thermo-mechanical degradation induced by successive injection moulding cycles affected PET structure by mainly reducing initial

diethylene glycol domains to ethylene glycol units in the flexible part of the PET backbone.

Besides, chain scission processes produced –OH terminated species with shorter chain length, which increased the yellowish aspect of PET recyclates and reduced its molar mass.

The effects on the microstructure were assessed taking into account a three-fraction model involving crystalline (C), mobile amorphous fraction (MAF) and rigid amorphous fraction (RAF). The initial (X_C , X_{MAF} , X_{RAF}) distribution of ~ (29/53/18) % changed to ~ (27/44/29) % after the second injection and to ~ (32/36/35) % after the fifth injection, thus showing that degradation mainly drove the cleavage of *MAF* and the tendency of shortened PET chains to reorganize into *RAF*. However, the study of the crystalline fraction was also significant. After each reprocessing step, the crystalline fraction was formed earlier and steeper during cooling, thus altering PET processability. Despite the overall crystallinity fraction scarcely changed, a deep characterization of the bimodal melting behaviour indicated the formation of crystalline populations with smaller lamellar thickness.

The rearrangement after reprocessing affected to the viscoelastic and mechanical performance. The reduction of the *MAF* mainly converted into *RAF*, and the shortening of chain lengths in the *MAF* increased the free volume and produced new conformations in which the change from a glassy to a rubbery state was overcome easier and involving less activation energy, due to a loss in cooperative movement. The role of *RAF* was relevant in the behaviour at break during macroscopic mechanical testing, due to it might act as precursor of crystallinity and/or vitrify, thus promoting a strain-induced crystallization

during tensile drawing and subsequently enhance the embrittlement of PET.

The study of all properties showed a significant loss after the application of the first reprocessing step, thus showing a sort of threshold for PET to be recovered by further mechanical recycling.

References

1. D.M. Fann, S. K. Huang, J.Y. Lee. Kinetics and thermal crystallinity of recycled PET. II. Topographic study on thermal crystallinity of injection molded recycled PET. *Journal of Applied Polymer Science* 1996; 61; 261-271
2. R. J. Ehrig. *Plastics Recycling: Products and Processes*. New York : Hanser Publishers, 1992.
3. P. P. Klemchuck. *Polymer Stabilization and Degradation*. Washington : ACS, 1985.
4. E. Strömberg, S. Karlsson. The design of a test protocol to model the degradation of polyolefins during recycling and service life. *Journal of Applied Polymer Science* 2009; 112: 1835-1844.
5. F. Vilaplana, A. Ribes-Greus, S. Karlsson. Degradation of recycled high-impact polystyrene .Simulation by reprocessing and thermo-oxidation. *Polymer Degradation and Stability* 2006; 91: 2163-2170.
6. F. Vilaplana, S. Karlsson. A. Ribes-Greus. Changes in the micro-structure and morphology of high-impact polystyrene subjected to multiple processing and thermo-oxidative degradation. *European Polymer Journal* 2007; 43: 4371-4381.
7. N. Yarahmadi, I. Jakubowicz, T. Gevert. Effects of repeated extrusion on the properties and durability of rigid PVC scrap. *Polymer Degradation and Stability* 2001; 73: 93-99.
8. J.D. Badía, F. Vilaplana, S. Karlsson, A. Ribes-Greus. Thermal analysis as a quality tool for assessing the influence of thermo-mechanical degradation on recycled poly(ethylene terephthalate). *Polymer Testing* 2009; 28: 169-175.
9. J.D. Badía, E. Strömberg, A. Ribes-Greus, S. Karlsson. A statistical design of experiments for optimizing the MALDI-TOF-MS sample preparation of polymers. An application in the assessment of the thermo-mechanical degradation mechanisms of poly (ethylene terephthalate). *Analytica Chimica Acta* 2011; 692: 85-95
10. S.D.Mancini, M. Zanin. Consecutive Steps of PET Recycling by Injection: Evaluation of the Procedure and of the Mechanical Properties. *Journal of Applied Polymer Science* 2000; 76: 266-275.
11. F. La Mantia, M. Vinci. Recycling poly(ethylene terephthalate). *Polymer Degradation and Stability* 1994; 45: 121-125.
12. N. Torres, J.J. Robin, B. Boutevin. Study of thermal and mechanical properties of virgin and recycled poly(ethylene terephthalate) before and after injection molding. *European Polymer Journal* 2000; 36: 2075-2080.
13. W. Romao, M. F. Franco, Y. E. Corilo, M.N. Eberlin, M.A.S, Spinacé, M.A. De Paoli. Poly(ethylene terephthalate) thermo-mechanical and thermo-oxidative degradation mechanisms. *Polymer Degradation and Stability* 2009; 94: 1849-1859.
14. A. Oromiehie, A. Mamizadeh. Recycling PET beverage bottles and improving properties. *Polymer International* 2004; 53: 728-732.
15. A. Pawlak, M. Pluta, J. Morawiec, A. Galeski, M. Pracella. Characterization of scrap poly(ethylene terephthalate). *European Polymer Journal* 2000; 36: 1875-1884.
16. F. Awaja, D. Pavel. Recycling of PET. *European Polymer Journal* 2005; 41: 1453-1477.
17. Y. Fu, B. Annis, A. Boller, Y. Jin, B. Wunderlich. Analysis of structure and properties of poly(ethylene terephthalate). *Journal of Polymer Science: Polymer Physics* 1994; 32: 2289-2306.
18. Y. fu, W. R. Busing, Y. Jin, K. A. Affholter, B. Wunderlich. Structure analysis of the non-crystalline material in poly(ethylene terephthalate) fibers. *Macromolecular Chemistry Physics* 1994; 195: 803-822.

19. A. Flores, M. Pieruccini, N. Stribeck, S.S. Funari, E. Bosch F.J. Baltá-Calleja. Structure formation in poly (ethylene terephthalate) upon annealing as revealed by microindentation hardness and X-ray scattering. *Polymer* 2005; 24: 9404-9410.
20. K.C. Cole, A. Aiji, E. Pellerin. New insights into the development of ordered structure in poly(ethylene terephthalate). Results from external reflection infrared spectroscopy. *Macromolecules* 2002; 32: 770-784.
21. C. Schick, A. Wurm, A. Mohamed. Vitrification of the rigid amorphous phase in semicrystalline polymers revealed from frequency-dependent heat capacity. *Colloid Polymer Science* 2001; 279: 800-806.
22. B. Wunderlich. Reversible crystallization and the rigid amorphous phase in semicrystalline polymers. *Polymer Science* 2003; 28: 383-450.
23. P. G. Karagiannidis, A. C. Stergiou, G. P. Karayannidis. Study of crystallinity and thermomechanical analysis of annealed poly(ethylene terephthalate) films. *European Polymer Journal* 2008; 44: 1475-1486.
24. R. Rastogi, W. P. Vellinga, S. Rastogi, C. Schick, H.E.H. Meijer. The three-phase structure and mechanical properties of poly(ethylene terephthalate). *Journal of Polymer Science: Part B: Polymer Physics* 2004; 42: 2092-2106.
25. J. Lin, S. Shenogin, S. Nazarenko. Oxygen solubility and specific volume of rigid amorphous fraction in semicrystalline poly(ethylene terephthalate). *Polymer* 2002; 43: 4733-4743.
26. Z. Xia, H.J. Sue, Z. Wang, C. A. Avila-Orta, B. S. Hsiao. Determination of crystalline lamellar thickness in poly(ethylene terephthalate) using small-angle x-ray scattering and transmission electron microscopy. *Journal of Macromolecular Science, Part B: Physics* 2001; 40: 625-638.
27. H. G. Haubruge, A.M. Jonas, R. Legras. Morphological Study of Melt-Crystallized Poly(ethylene terephthalate). A. Comparison of Transmission Electron Microscopy and Small-Angle X-ray Scattering of Bulk Samples. *Macromolecules* 2004; 37: 126-134.
28. A. Bartolotta, G. Di Marco, F. Farsaci, M. Lanza, M. Pieruccini. DSC and DMTA study of annealed cold-drawn PET: a three phase model interpretation. *Polymer* 2003; 44: 5771-5777.
29. B. B. Sauer, B.S. Hsiao, B S. Effect of the heterogeneous distribution of lamellar stacks on amorphous relaxations in semicrystalline polymers *Polymer* 1995; 36: 2553-2558.
30. ISO 291:1997. Plastics - standard atmospheres for conditioning and testing.
31. ISO 527-2: Plastics -- Determination of tensile properties -- Part 2: Test conditions for moulding and extrusion plastics. 1993.
32. ISO 179-1 Plastics -- Determination of Charpy impact properties -- Part 1: Non-instrumented impact test. 2010.
33. K. C. Cole, J. Guèvremont, A. Aiji, M.M. Dumoulin. Characterization of surface orientation in poly(ethylene terephthalate) by front-surface reflection infrared spectroscopy. *Applied Spectroscopy* 1994; 48: 1513-1521.
34. D.J. Walls. Application of ATR-IR to the analysis of surface structure and orientation in uniaxially drawn poly(ethyleneterephthalate). *Applied Spectroscopy* 1991; 45: 1193-1198
35. ISO 1628-1: 2009. Plastics -- Determination of the viscosity of polymers in dilute solution using capillary viscometers -- Part 1: General principles.
36. L. H. Sperling. Introduction to physical polymer science. 4th. Hoboken : John Wiley & Sons, 2006.
37. S. Fakirov. Polyethylene terephthalate. In: O Olabisi. Handbook of thermoplastics. New York : Marcel Dekker, 1994, p. 451.
38. S. A. Jabarin. Crystallization kinetics of polyethylene terephthalate, I. Isothermal crystallization from the melt. *Journal of Applied Polymer Science* 1987; 34: 85-96.
39. N. B. Sanches, M. L. Dias, E. B. Pacheco. Comparative techniques for molecular weight evaluation of poly(ethylene terephthalate) (PET). *Polymer testing* 2005; 24: 688-693.

40. ISO 11357-2 Plastics. Differential Scanning Calorimetry. Part 2- Determination of the glass transition. 1999.
41. B. Wunderlich. *Macromolecular Physics*. A Press New York and London : 1973, Vol. 1, p. 389.
42. B. Wunderlich, *The Athas Data Base on Heat Capacities of Polymers*. Pure and Applied Chemistry 1995; 67, 1019-1026 . <http://web.utk.edu/athas/databank/>.
43. F.J. Boerio, S.K. Bahl, G.E. McGraw. Vibrational analysis of polyethylene terephthalate and its deuterated derivatives. *Journal of Polymer Science, Polymer Physics* 1976; 14: 1029–1046.
44. A. Miyake. The infrared spectrum of polyethylene terephthalate. I The effect of crystallization. *Journal of Polymer Science* 1959; 38: 479–495.
45. B. J. Holland, J. N. Hay. Analysis of comonomer content and cyclic oligomers of poly(ethylene terephthalate). *Polymer* 2002; 43: 1797-1804.
46. B. García-Gaitán, M. D. P. Pérez-González, A. Martínez-Richa, G. Luna-Bárceñas, S. M. Nuño-Donlucas, Segmented block copolymers of poly(ethylene glycol) and poly(ethylene terephthalate). *Journal of Polymer Science Part A: Polymer Chemistry* 2004, 42: 4448–4457.
47. C. F. Ciolacu, N. R. Choudhury, N. K. Dutta. Colour formation in poly(ethylene terephthalate) during melt processing. *Polymer Degradation and Stability* 2006; 91: 875-885.
48. J. D. Menczel, M. Jaffe. How did we find the rigid amorphous phase? *Journal of Thermal Analysis and Calorimetry* 2007; 89: 357-362.
49. W. Romao, M. F. Franco, M. I. M.S. Bueno, M. A. De Paoli, Distinguishing between virgin and post-consumption bottle-grade poly(ethylene terephthalate) using thermal properties, *Polymer Testing* 2010; 29: 879-885-
50. J.L. Lauritzen and J.D. Hoffman. Theory of formation of polymer crystals with folded chains in dilute solution. *Journal of Research of the National Bureau of Standards* 1960; 64: 73–102.
51. J.L. Lauritzen and J.D. Hoffman. Crystallization of bulk polymers with chain folding: theory of growth of lamellar spherulites. *Journal of Research of the National Bureau of Standards* 1961; 65: 297–336.
52. J.D. Hoffman, G.T. Davis, J. L. Lauritzen, The rate of crystallization of linear polymers with chain folding. *Treatise on solid state chemistry*. In: N.B. Hannay, *Crystalline and noncrystalline solids vol. 3*, Plenum Press, New York (1976). Hoffman. pp. 497-614.
53. X.F. Lu, J.N. Hay, Isothermal crystallization kinetics and melting behaviour of poly(ethylene terephthalate). *Polymer* 2001; 42; 9423–9431.
54. Z. G.Wang, B. S. Hsiao, B. B. Sauer, W.G. Kampert. The nature of secondary crystallization in poly(ethylene terephthalate). *Polymer* 1999; 40: 4615-4627.
55. A. A. Minakov, D. A. Mordvintsev, C. Schick. Melting and reorganization of poly(ethylene terephthalate) on fast heating (1000 K/s). *Polymer* 2004; 45: 3755-3763.
56. V. H. G. Zachmann, H. A. Stuart. Schmelz- und kristallisationserscheinungen bei makromolekularen substanzen. V. Partielles schmelzen und neukristallisieren von terylen. *Die Makromolekulare Chemie* 1960; 41: 148–173.
57. M. Song. Rigid amorphous phase and low temperature melting endotherm of poly(ethylene terephthalate) studied by modulated differential scanning calorimetry. *Journal of Applied Polymer Science* 2001; 81: 2779-2785.
58. G. E. Sweet, J. P. Bell. Multiple endotherm melting behavior in relation to polymer morphology. *Journal of Polymer Science. Part A-2: Polymer physics* 1969, 10: 1273-1283.
59. R. C. Roberts. Poly(ethylene terephthalate) II—Morphological changes on annealing. *Polymer* 1969; 10: 117-125.
60. S. Tan, A. Su, W. Li, E. Zhou. New insight into melting and crystallization behavior in semicrystalline poly(ethylene terephthalate). *Journal of Polymer Science: Part B: Polymer physics* 2000; 38: 53-60.

61. L. Santonja-Blasco, R. Moriana, J. D. Badía, A. Ribes-Greus. Thermal analysis applied to the characterization of degradation in soil of polylactide: I. Calorimetric and viscoelastic analyses. *Polymer Degradation and Stability* 2010; 95: 2185-2191.
62. K. Levenberg. A method for solution of certain non-linear problems in least squares. *Quarterly of Applied Mathematics* 1944; 2: 164-168.
63. D. W. Marquardt. An algorithm for the least-squares estimation of non-linear parameters. *SIAM Journal of Applied Mathematics* 1963; 11: 431-441.
64. A. D. English. Macromolecular dynamics in solid poly(ethylene terephthalate): ^1H and ^{13}C solid-state NMR. *Macromolecules* 1984; 17: 2182-2192.
65. J. Zhao, J. Wang, C. Li, Q. Fan. Study of the amorphous phase in semicrystalline poly(ethylene terephthalate) via physical aging. *Macromolecules* 2002; 35: 3097-3103.
66. J. Zhao, R. Song, Z. Zhang, X. Linghu, Z. Zheng, Q. Fan, A study of the physical aging in semicrystalline poly(ethylene terephthalate) via differential scanning Calorimetry. *Macromolecules* 2001; 34: 343-345.
67. C.A. Angell. Relaxation in liquids, polymers and plastic crystals - strong/fragile patterns and problems. *Journal of Non-Crystalline Solids* 1991; 13: 131-133.
68. M.E. Godard, J.M. Saiter. Fragility and non-linearity in polymethyl(α -n-alkyl) acrylates. *Journal of Non-Crystalline Solids* 1998; 235: 635-639..
69. A. Saiter, M. Hess, N. A. D'Souza, J. M. Saiter. Entropy and fragility in vitreous polymers. *Polymer* 2002; 43: 7497
70. H. Vogel, The temperature dependence law of the viscosity of fluids. *Phys Z* 1921; 22: 645-646.
71. G.S. Fulcher. Analysis of recent measurements of the viscosity of glasses. *Journal of the American Ceramic Society* 1925; 8: 339-355.
72. G. Tammann and G. Hesse. The dependence of viscosity upon temperature of supercooled liquids. *Z Anorg Allg Chem.* 1926; 156: 245-257.
73. R. Bohmer, C.A. Angell in: R. Richert , A. Blumen, *Disorder effects on relaxational processes*, Springer, Berlin, 1994.
74. T.A. Vilgis. Strong and fragile glasses: A powerful classification and its consequences. *Physical Review B* 1993; 47 2882-2885.
75. K. Kunal, C. G. Robertson, S. Pawlus, S. F. Hahn, A. P. Sokolov. Role of Chemical Structure in Fragility of Polymers: A Qualitative Picture. *Macromolecules* 2008; 41: 7232-7238.
76. P.G. Santangelo, C. M. Roland. Molecular weight dependence of fragility in polystyrene. *Macromolecules* 1998; 31: 4581 4585.
77. M. L. Williams, R. F. Landel, J. D. Ferry. The temperature dependence of relaxation mechanisms in amorphous polymers and other glass-forming liquids. *Journal of the American Chemistry Society* 1955; 77: 3701-3707.
78. N. M. Alves, J. F. Mano, J. L. Gómez-Ribelles. Molecular mobility in polymers studied with thermally stimulated recovery. II. Study of the glass transition of a semicrystalline PET and comparison with DSC and DMA results. *Polymer* 2002; 43: 3627-3633.
79. M. Cristea, D. Ionita, B. C. Simionescu. A new insight in the dynamo-mechanical behavior of poly(ethylene terephthalate). *European Polymer Journal* 2010; 46: 2005-2012.
80. G. E. Welsh, D. J. Blundell, A. H. Windle. A Transient Liquid Crystalline Phase as a Precursor for the Crystallization in Random Co-polyesters Fibers. *Macromolecules* 1998; 31: 7562-7565.
81. A. Mahendrasingam, C. Martin, W. Fuller, D. J. Blundell, R. J. Oldman, D. H. MacKerron, J. L. Harvie, C. Riekel. Observation of a transient structure prior to strain-induced crystallization in poly(ethylene terephthalate). *Polymer* 2000; 41: 1217-1221.
82. S. Ran, Z. Whang, C. Burger, B. Chu, B. H. Hsiao. Mesophase as the precursor for Strain-Induced Crystallization in Amorphous

Poly(Ethylene Terephthalate) Film.
Macromolecules 2002; 35: 10102-10107.

CONTRIBUTION III-D

Assessing the MALDI-TOF MS sample preparation procedure to analyze the influence of thermo-oxidative ageing and thermo-mechanical degradation on poly (lactide)

J.D. Badia, E. Strömberg, S. Karlsson, A. Ribes-Greus

European Polymer Journal 2011, 47; 1416-1428



Assessing the MALDI-TOF MS sample preparation procedure to analyze the influence of thermo-oxidative ageing and thermo-mechanical degradation on poly (Lactide)

J.D. Badía^a, E. Strömberg^b, A. Ribes-Greus^a, S. Karlsson^{b,*}

^a Instituto de Tecnología de Materiales (ITM), Universitat Politècnica de València, Camino de Vera s/n, E-46022 Valencia, Spain

^b School of Chemical Science and Engineering, Fibre and Polymer Technology, KTH – Royal Institute of Technology, Teknikringen 56-58, SE-10044 Stockholm, Sweden

ARTICLE INFO

Article history:

Received 25 October 2010

Received in revised form 4 March 2011

Accepted 1 May 2011

Available online 10 May 2011

Keywords:

Matrix-Assisted Laser Desorption/Ionization
Time-of-Flight Mass Spectrometry (MALDI-TOF MS)

Design of Experiments (DoE)

Poly(lactide) (PLA)

Thermo-mechanical degradation

Thermo-oxidative ageing

ABSTRACT

Multiple processing by means of successive injection cycles was used to simulate the thermo-mechanical degradation effects on the oligomeric distribution of PLA under mechanical recycling. Likewise, an accelerated thermal ageing over PLA glass transition was performed in order to simulate its service life. MALDI-TOF MS was used for the analysis and the sample preparation procedure was assessed by means of a statistical Design of Experiments (DoE). The quality effects in use for the analysis were signal-to-noise ratio and Resolution. Different matrixes, analyte/matrix proportions and the use of NaTFA as cationization agent were considered. A deep inspection of the statistical results provided a better understanding of the influence of the different factors, individually or in combination, to the signal. The application of DoE for the improvement of the MALDI measurement of PLA stated that the best combination of factors (levels) was the following: matrix (s-DHB), proportion analyte/matrix (1/5 V/V), and no use of cationization agent. Degradation primarily affected the initially predominant cyclic $[LA_C]_n$ and linear $H-[LA_L]_n-OH$ species, where LA stands for a PLA repeating unit. Intramolecular and intermolecular transesterifications as well as hydrolytic and homolytic reactions took place during the formation and disappearance of oligomeric species. In both degradation mechanisms induced by thermal ageing and thermo-mechanical degradation, the formation of $H-[LA_L]_n-O-CH_3$ by intermolecular transesterifications was highlighted.

© 2011 Elsevier Ltd. All rights reserved.

Abbreviations: ϕ , diameter screw (injection machine); C, cyclic; d, diameter pellet; DHB, 2,5-dihydroxybenzoic acid; DOE, Design Of Experiments; E, effect; F, factor (for the DOE); GLM, General Linear Mode; HABA, hydroxyphenylazo benzoic acid; IP, Interaction Plot; L, level/subscript; linear; LA, lactic acid unit; LMWC, low molecular weight compounds; m , number of LA repeating units ($m > n$); m/z , mass-to-charge ratio; MALDI, Matrix-Assisted Laser Desorption/Ionization; MAC, combination of matrix (M)/analyte(A)/cationization agent(C); MEP, main effects plot; MS, Mass Spectrometry; n , number of LA repeating units; NaTFA, sodium trifluoroacetate; P , also p -value, statistic (for the DOE); PE, poly(ethylene); PET, poly(ethylene terephthalate); PLA, polylactide; PP, poly(propylene); PS, poly(styrene); PVC, poly(vinyl chloride); RES, resolution; SP, sample preparation; S/N, signal-to-noise ratio; TOF, time of flight; V, volume; VPLA, virgin PLA.

* Corresponding author. Present address: Skövde University, Högskolan i Skövde, Box 408, 541 28 Skövde, Sweden. Tel.: +46 0500 44 81 43.

E-mail addresses: sigbritt@polymer.kth.se, sigbritt.karlsson@his.se (S. Karlsson).

1. Introduction

The packaging industry is a highly important economic sector that involves big quantities of plastic materials. One-use applications critically reduce the service life of these products, being rapidly drawn to the disposal step with all their properties almost intact. Packages made of commodities such as polyethylene (PE), polypropylene (PP), polystyrene (PS) or poly(ethylene terephthalate) (PET) are usually immediately discarded after the first use, and their elimination and reintegration into the carbon cycle can require hundreds or even thousands of years. Therefore, the interest on plastic materials that accomplish the twofold benefit of being biodegradable and come from renewable resources has gained much attention. The most

popular biodegradable polymers are poly (lactic acid) or polylactides (PLA), polycaprolactone (PCL), poly (butylene adipate terephthalate) (PBAT) and polyhydroxybutyrate (PHB) [1].

Polylactides are thermoplastic polyesters obtained from the ring-opening polymerization of lactide, which may be derived from the fermentation of sugar feedstocks at competitive prices compared to that previously achievable from petrochemical-derived products [2]. PLAs have numerous interesting properties including good processability, mechanical properties, thermal stability and low environmental impact [2–3], which enhance their performance as suitable candidates for replacing commodities at the packaging sector. This solution will therefore imply the increase of a new source of polymeric waste, which would have to be managed. Moreover, with the aim of extending the service life of PLA goods, before finally discarding them, it would be advisable to explore the possibilities of recovering the material. Among all recovery methods, mechanical recycling represents one of the most successful processes and has received considerable attention due to its main advantages, since it is relatively simple, requires low investment, and its technological parameters are controlled [4]. Moreover, life cycle assessment studies have pointed out that mechanical recycling is the most preferable recovery route for relatively clean and homogeneous waste streams in terms of energy saving and emission of gases contributing to global warming [5]. Nevertheless, polymers are subjected to the influence of degradative agents such as oxygen, UV-light, mechanical stresses, temperature and water, which, separately or in combination, during its material loop (synthesis – processing – service life – discarding – recovery), results in chemical and physical changes that alter their stabilization mechanisms and long-term properties [6]. These degradation processes may modify the structure and composition of PLA and consequently change the thermal, rheological and mechanical properties of the recyclates [7–8]. The assessment of the degradation mechanism is therefore necessary to determine the quality of recycled PLA and guarantee its further performance in second-market applications. Simulation of mechanical recycling by multiple processing and service life by accelerated thermal ageing to assess the effects of thermal and thermo-mechanical degradation has been previously performed for commodities [9–15] such as PE [9], PP [9], PS [10–11], poly (vinyl chloride) (PVC) [12] or PET [13–16].

Matrix-Assisted Laser Desorption/Ionization Time-Of-Flight Mass Spectrometry (MALDI-TOF-MS) has gained attention during the last years as a potential technique for the analysis of the compositions, end groups and, in some cases, molecular weight distributions of intact synthetic polymers [17]. Characteristics and main applications of MALDI can be found in several reviews [18–19]. Studies on polyesters is an issue of interest among researchers [20–21], but studies of polylactides are still few [22–29], and mainly applied to low molecular weight PLA synthesized under laboratory conditions. As far as we are concerned, studies on the application of MALDI to characterize the effect of multiple-processing and accelerated thermal ageing on specifically commercial PLA have

not been published and therefore this is an area of interest for future work.

The difficulty of performing good-quality and reliable MALDI measurements depends on many factors such as the molar mass of the polymer, the choice of solvent, the choice of matrix [30–32], the ratio analyte/matrix, the use of cationization agent, the laser energy or the mode of detection (linear or reflector), among others [30]. Some research groups have reported these difficulties and have found correlations between the crystal and/or molecular structure of matrices and the MALDI spectral data [31]. Advances and contributions in issues such as the choice of the correct solvent for sample crystallization [32], matrix functional groups arrangement [33], improvement of signal-to-noise ratio [33], or the influence of crystallinity of polymers on the measurement [34] have been performed. However, there are still no clear criteria enabling the prediction of the optimal conditions for the matrix-polymer sample preparation. Cost-effective methodologies should be therefore implemented, in order to optimize the performance of the MALDI measurement. Despite its straightforward applicability, speediness and ease, statistical methods such as the Design of Experiments (DoE) are not widely applied yet. DoE plays a fundamental role in the optimization of scientific and industrial problems [35], which involves the study of the influence of multiple input variables (factors) analyzed at different scenarios (levels) on the experimental outcomes (effects). DoE [36] stands as a useful, reliable and immediate procedure that can provide us not only with the best combination of settings for the preparation of the MALDI sample, but also help understand the influence of each factor individually or in combination on the quality of the response. In previous works, the suitability of DoE to understand the influence of matrix, analyte/matrix proportion and amount of cationization agent was reported for the study of poly(ethylene terephthalate) [16].

In the present study, simulation of reprocessing and service life was performed by successive injection moulding cycles and accelerated thermo-oxidative ageing respectively on commercial PLA. In the first part of the study, DoE was applied for determining the best conditions of the MALDI sample preparation for PLA in order to enhance the quality of the signal, taking into account matrix, proportion analyte/matrix and use of cationization agent. In the main analysis, the oligomeric degradation mechanisms that may explain the influence of degradation occurring in PLA during both thermo-mechanical and thermo-oxidative ageing were studied.

2. Experimental procedure

Fig. 1 schematically shows the procedure followed to simulate degradation induced by multiple processing and service life. Materials, reagents, simulation conditions and MALDI analytical features are stated as follows:

2.1. Materials and reagents

Polylactide (PLA) 2002D is a thermo-forming grade PLA obtained from Natureworks LLC (Minnetonka, MN) as

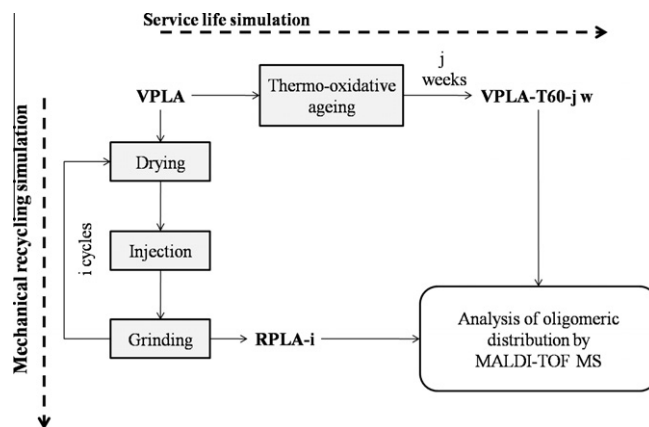


Fig. 1. Experimental procedure followed for the simulation of degradation induced by PLA due to mechanical recycling and service life.

pellets, provided by AIMPLAS (Paterna, Spain). MALDI matrixes, namely 1,8,9-anthracenetriol (dithranol), 2-(4-hydroxyphenylazo) benzoic acid (HABA), 2,5-dihydroxybenzoic acid (s-DHB), as well as the cationization agent, sodium trifluoroacetate (NaTFA), were purchased from Sigma–Aldrich (Stockholm, Sweden). Tetrahydrofurane was purchased from VWR (Sweden).

2.2. Reprocessing simulation

Prior to processing, virgin PLA pellets were dried during 2 h at 80 °C in a dehumidifier Conair Micro-D FCO 1500/3 (UK), in order to remove as much humidity as possible from PLA flakes. Afterwards, samples were processed by means of injection moulding by means of an Arburg 420 C 1000–350 (Germany) injector, single-screw model (diameter $\Phi = 35$ mm, length/ $\Phi = 23$). Successive processing steps were applied under the same conditions. Temperature gradient set from hopper to die was 160, 170, 190, 200 and 190 °C. Moulds were set at 15 °C. Cooling time residence was ca. 40 s and total residence time ca. 60 s. Samples were dried before each processing cycle. After injection, a fraction of the samples was kept as test specimens and the rest was ground by means of a cutting mill Retsch SM2000 (UK), which provided pellets of size $d < 20$ mm to be fed back into the process. Up to five processing cycles were applied to obtain the different testing specimens of reprocessed PLA (RPLA-i, with i: 1–5).

2.3. Service life simulation

Thermo-oxidative aging was performed on dehumidified virgin PLA by means of a Heraeus UT 6060 (Hanau,

Germany) forced-ventilation oven under air atmosphere at 60 °C. Samples were removed for analysis after the exposure times of 1, 3, 6, 10 and 12 weeks.

2.4. MALDI sample preparation and analysis

MALDI sample mixtures (matrix (M) + analyte (A) + cationization agent (C), MAC) were prepared in laboratory conditions according to ISO 291, atmosphere 23/50, class 1 [37]. Individual solutions of M, A and C in THF were prepared at a concentration of 10 g L⁻¹. Different proportions (Table 1) of M/A, according to the Design of Experiments (section 3.2) were applied. In case C was added to the MAC, it was in the same volumetric ratio as the A. The mixtures were then vortexed using a Vortex Genie (Scientific Industries, Bohemia, NY). Approximately 0.5 μ L of the sample mixture were added on the target plate and the spots were allowed to dry at ambient temperature before insertion into the instrument.

MALDI-TOF/MS experiments were conducted on a Bruker UltraFlex MALDI-TOF mass spectrometer with a SCOUT-MTP ion source (Bruker Daltonics, USA), a gridless ion source and a reflector. All spectra were acquired in the reflector positive ion mode with an acceleration voltage of 25 kV and a reflector voltage of 26.3 kV. The detector m/z range was 200–6000 Da in order to exclude high intensity signals arising from the low mass ions and to cover the whole PLA mass spectrum. Ions below 100 m/z were removed with pulsed deflection. The laser intensity was set to the maximum value possible, taking care not to burn the MAC in order to avoid the appearance of high-intensity background peaks, which could decrease the signal-to-noise ratio and the resolution. Spectra were gathered by

Table 1

Summary of factors, levels and general characteristics of the Design of Experiments applied in this study.

Factor	Type	Number of levels	Levels	Effects
Matrix	Qualitative	3	s-DHB Dithranol HABA	S/N S/N _{rel}
Proportion of analyte/matrix (V/V)	Quantitative	3	1/5 1/10 1/20	RES RES _{rel}
NaTFA	Qualitative	2	YES NO	
Replicates	3	Total blocks	3	
Base runs	18 (3 ² ·2 ¹)	Total runs	54	

irradiating 40–50 different positions at the centre area on the sample spot, with a total of 2500 (5×500) shots per sample. Time-to-mass conversion of the time-of-flight mass spectra was achieved using a self-calibration method [38]. All MALDI spectra were treated using FlexAnalysis 2.4 (Bruker Daltonics, USA) software. Interpretation of data was carried out taking into account all decimals of the atomic masses composing the oligomers, but note that m/z values are given with only one decimal. Statistical Design of Experiments (DoE) was aided by Minitab® 15.1.0.0 software (Minitab Inc., USA). Measurements were performed by triplicate and the average values were considered as representative.

3. Results and discussion

The present work is divided into two different sections. In the first part of the study, the design of experiments, DoE, was applied for determining the best conditions of the MALDI sample preparation for PLA in order to enhance the quality of the spectra. Thereafter, the MALDI analysis of the influence of thermo-oxidative and thermo-mechanical degradation on the oligomeric distribution of polylactide was assessed.

3.1. Determination of the experimental factors and levels considered for DoE analysis of MALDI sample preparation

With the aim of performing a reliable MALDI measurement with good-quality signals, some considerations regarding the sample preparation (SP) were taken into account. The followed procedure is explained with more detail in a previous work [16]. Some variables were defined as Factors (F) for the DoE: suitable matrix, reasonable proportion analyte/matrix and necessity of cationization agent. Given that each factor could be analyzed for a wide span of levels (L), the study of the interaction of all of them shall not be operative, and thus a preliminary screening was performed in order to reduce this quantity of F/L situations: Firstly, S-DHB, Dithranol and HABA were chosen (Fig. 2) as proper [30] matrixes from an exhaustive list in literature [39]. Tetrahydrofuran (THF) was taken as solvent for all components since it was extremely important that the mixture behaved as one during the evaporation process of the solvent, avoiding thus sample segregation, which could impoverish the quality of the signal [40]. On the other hand, since polyesters are relatively polar poly-

mers, Na^+ and K^+ adducts could be observed in the MALDI spectra, even if they were not deliberately added to the mixture [41–43]. It is known that these cations are present as impurities in matrixes, reagents, solvents or glassware among other sources, and therefore polymers with high cation affinity do not necessarily need a high amount of extra salt in the sample [30]. The presence of specific functional groups such as carboxyl and hydroxyl is very important in the cationization process [44]. On the other hand, the fact that matrixes such as HABA and dithranol are particularly insensitive to impurities [18] justified the study of the addition of a cationization agent. Sodium Trifluoroacetate (NaTFA) was chosen as a source of ions.

3.2. The Design of Experiments applied to MALDI-VPLA

The levels L at which each F was analyzed are summarized in Table 1. In order to perform the DoE, a significant step is the correct choice of parameters to be considered as reliable effects (E). signal-to-noise ratio (S/N) and resolution (RES) stand out as suitable quality indicators in many different spectrometric studies [35], and therefore were chosen for this study. A schematic summary of the combination of DoE and MALDI is depicted in Fig. 3.

After a first screening, the adducts which provided the signal of highest intensity were cyclic $([\text{LA}_n \text{Na}]^+)$, and thus were chosen for the analysis. With the aim of assuring the reliability of this study, instead of focusing the discussion on the results obtained from the study of an individual peak, a span of 500 m/z between 1500 and 2000 m/z in which up to seven $([\text{LA}_n \text{Na}]^+)$ peaks (1536.3, 1608.3, 1680.4, 1752.5, 1824.5, 1896.6, and 1968.6 m/z), with a separation of a LA repeating unit (72.062 m/z) were chosen for characterization. Absolute and relative effects E (being $E = S/N$ or RES) were analyzed according to the following expressions:

$$E = \sum_i \left(E_i \cdot \frac{I_i}{I_{\max}} \right) \quad (1)$$

$$E_{\text{rel}} = \sum_i \left(\frac{E_i}{E_{\max}} \cdot \frac{I_i}{I_{\max}} \right) \quad (2)$$

where I is the intensity of the peak, I_{\max} the maximum intensity, E_{\max} the maximum of the effect and i is the counter of the seven studied peaks. Table 2 shows the results of the analysis of variance in terms of p -value (P) and adjusted regression coefficient (R^2) for each E according to

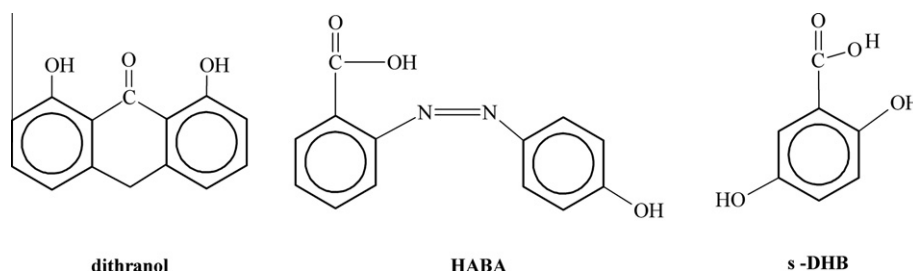


Fig. 2. Chemical structures of the matrixes used for the MALDI analysis.

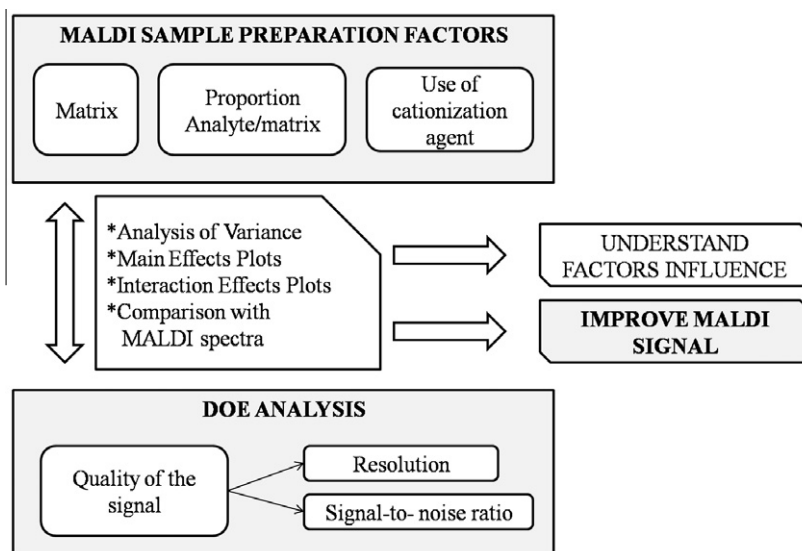


Fig. 3. Schematic summary of the purpose of combining DOE with MALDI analysis.

Table 2

Results of Analysis of Variance after application of the Design of Experiments to MALDI-TOF MS spectra of virgin PLA.

Factors	Effect			
	S/N	RES	S/N_{rel}	RES_{rel}
	P -value ($\alpha = 0.05$)			
Blocks	0.779	0.315	0.064	0.210
<i>Main</i>				
Matrix	0	0	0.024	0.016
Proportion	0	0	0.937	0.575
NaTFA	0	0.055	0	0
<i>Interactions</i>				
Matrix and Proportion	0	0	0	0
Matrix and NaTFA	0	0	0	0
Proportion and NaTFA	0.111	0	0.319	0.048
Matrix and Proportion and NaTFA	0	0	0	0
R^2 (%)	99.00	98.56	86.48	90.87

the General Linear Model (GLM) [36] applied for the evaluation of the DoE. The statistic P measures the significance

of a change in level L of a factor F , individual or in combination with other F (interaction), to the E . If P is lower than or equal to a confidence value (α), then this F (or interaction of F) is significant, and its assessment is thus worthy. On the other hand, R^2 measures the suitability of the GLM to explain the variability of data. The closer R^2 is to 1, the better is the selection of the E to characterize the experiment under consideration. Some conclusions could be drawn from this analysis: Absolute effects were chosen, since those relative offered R^2 far below 95%. In addition, the fact of carrying out the experiments by triplicate added a new factor to the DoE analysis (*Blocks*), but no relationship between this factor and both effects (S/N and RES) was found, which means that there was no significant experimental error related to the sample preparation affecting the quality of the results. Finally, all F influenced both the S/N and RES of the MALDI signal and therefore were considered for analysis, since $P < \alpha$ being α the commonly chosen 5%. Note that in the case of the study of the RES by modifying the addition of NaTFA, $P = 5.5\%$,

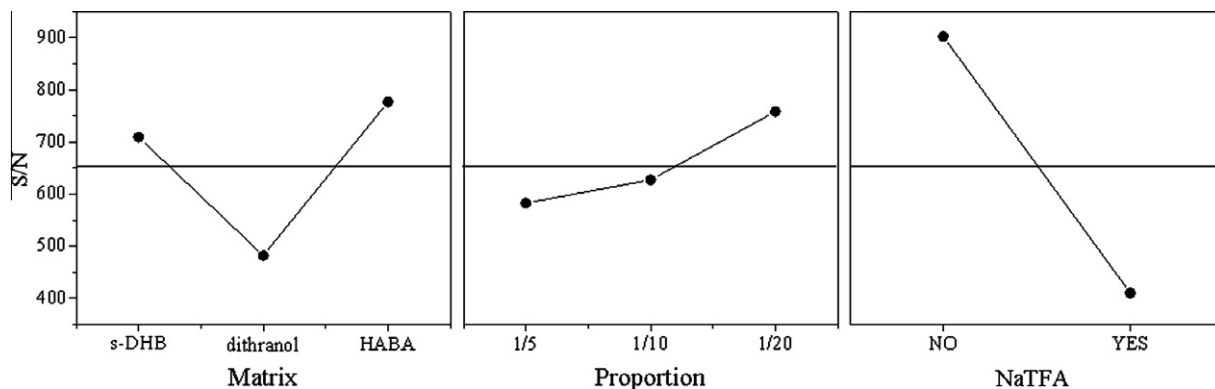


Fig. 4. Main effects plot for the analysis of the signal-to-noise ratio (S/N).

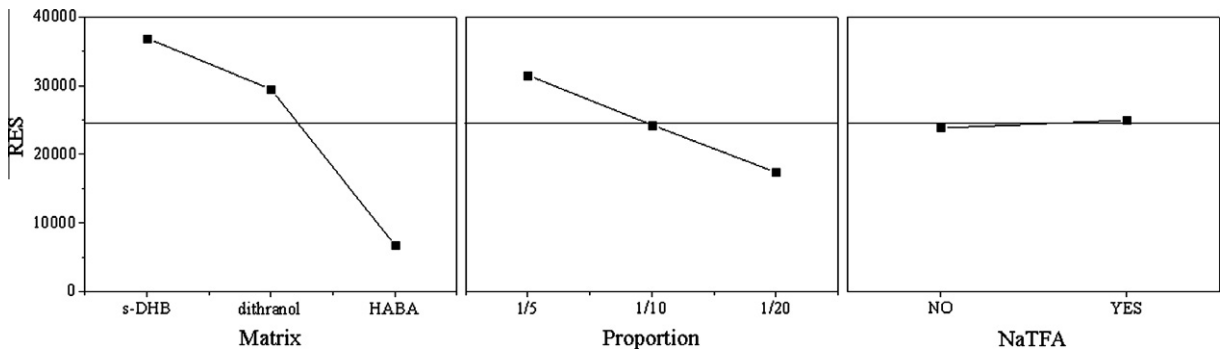


Fig. 5. Main effects plot for the analysis of the Resolution (RES).

which is not far from α . Concerning the interaction of NaTFA and proportion analyte/matrix, $P = 0.111$, which indi-

cates that its interpretation was not necessarily trustable and thus was not considered.

Table 3

Relative variations in S/N and RES means taking as reference run (s-DHB, 1/5, NO).

	Main effects				
	Matrix		Proportion		Salt
	Dithranol	HABA	1/10	1/15	YES
S/N	-32.0%	9.5%	7.6%	30.1%	-54.52%
RES	-20.1%	-81.6%	-23.0%	-45.0%	4.5%

Main effects plots (MEP) and Interaction Plots (IP) are intuitive tools very useful to estimate the influence of factors though the different levels, both in general or in combination, respectively, to the considered E . The study of these plots was assessed as follows: Fig. 4 and Fig. 5 show the main effects plot (MEP) for both S/N and RES, respectively. The overall influence of all factors on the quality parameters chosen for the assessment of the signal could be drawn from these plots. The horizontal line crossing these graphs is the so-called *grand mean*, which is the averaged sum of all data for a specific effect (S/N or RES). Values above this line can be considered significant, whereas

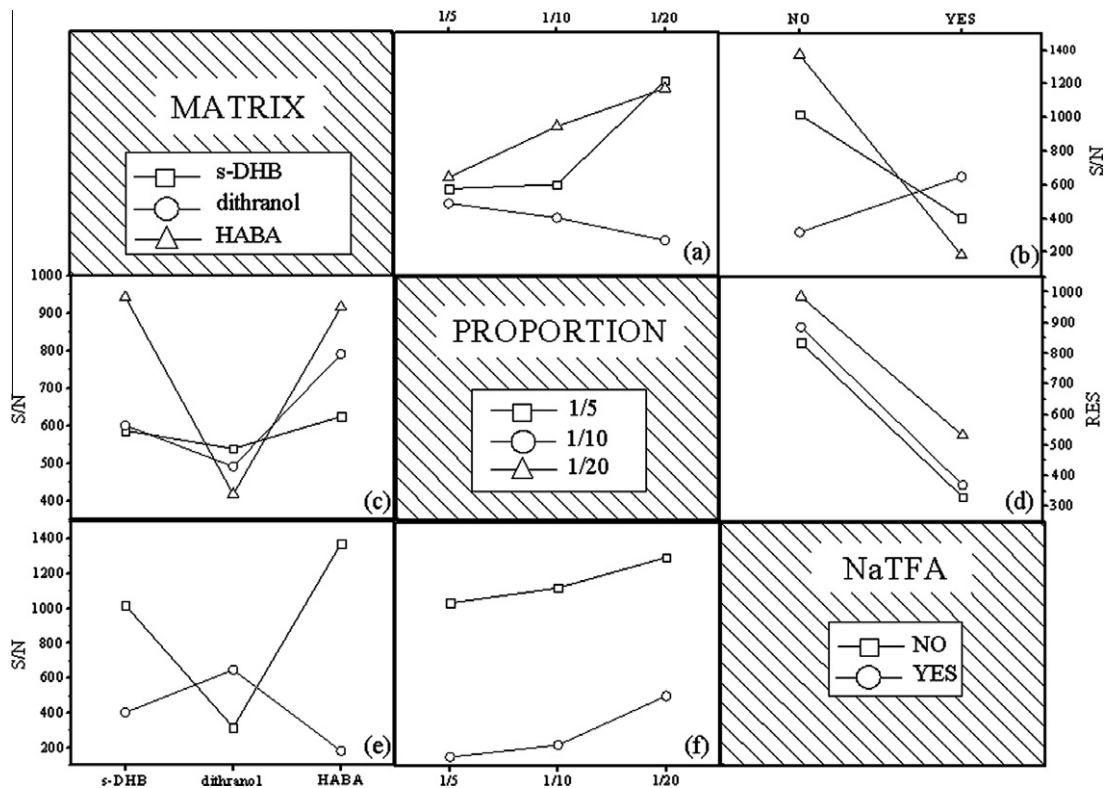


Fig. 6. Interaction Plot for the analysis of the signal-to-noise ratio (S/N).

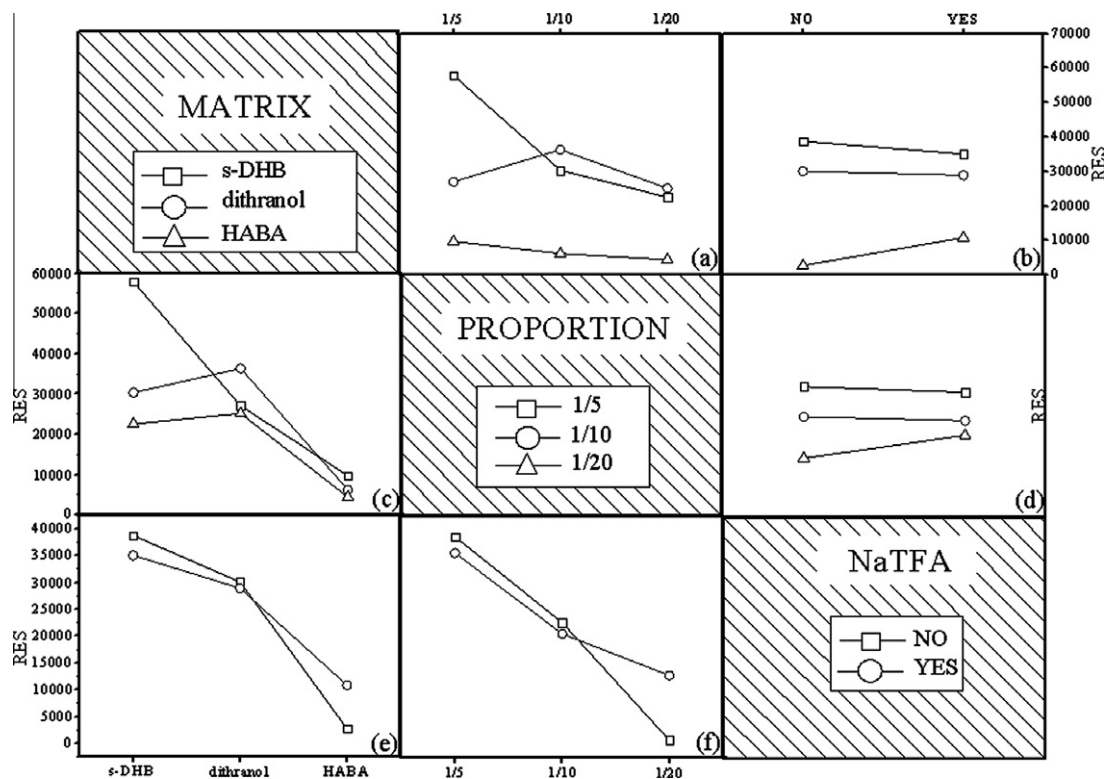


Fig. 7. Interaction Plot for the analysis of the Resolution (*RES*).

values below demonstrate the little influence of a specific factor on the E under study. In order to numerically interpret their results, Table 3 shows the changes among levels for a determined factor which were calculated for the data means of each effect $\overline{E}(\Delta L|_F)(\%)$ by the following expression:

$$\overline{E}(\Delta L|_F)(\%) = \frac{\overline{E}(L) - \overline{E}(L_{REF})}{\overline{E}(L_{REF})} \times 100 \quad (3)$$

The selection of the reference level (L_{REF}) for each factor is arbitrary and for convenience the choices were stated as follows: *s-DHB* for the factor *Matrix*, $1/5$ for the factor *Proportion* and *NO* for the factor *NaTFA*. The following conclusions were drawn: Firstly, experiments with dithranol provided the lowest *S/N* values. On the other hand, despite the *S/N* was generally higher when using HABA instead of *s-DHB* (+9.5%), the loss of *RES* was dramatically high (-81.6%), and therefore the use of *s-DHB* seemed to be more adequate. Furthermore, the influence of the analyte/matrix proportion was opposite for both effects; while increasing the amount of matrix generally increased the *S/N* (+30.1% from $1/5$ to $1/20$), the *RES* was contrarily negatively affected (-45.0% for the same conditions). In this case, since the overall variations were quite similar, the decision of which proportion was satisfactory for the analysis will be tackled later, when studying the Interaction Plots, specifically for the chosen matrix. Finally, the addition of NaTFA generally favoured the *RES* means (+4.5%), but the high

reduction in the *S/N* means (-54.5%) advised not to use cationization agent in this study.

Further interpretation of the Interaction Plots for both *S/N* and *RES* shown at Figs. 6 and 7 respectively, offered more information regarding the synergetic influence of a couple of factors at all studied L for a specific F . For better understanding, discussion was focused on sub-plots *a* and *c* in both figures, in order to evaluate the interaction matrix/proportion, specifically for the use of *s-DHB*. Similar interpretation could be drawn in case the joint influence of two F was intended for the rest of matrices. By means of applying Eq. (3) for the variation of proportion when *s-DHB* was used, increasing it from $1/5$ to $1/20$ led to an increase of 60.6% in *S/N* means, accompanied by a decrease of 61.1% in *RES* means. The dilemma therefore was to settle on which of both effects was more decisive for the analysis. Fig. 8 shows the MALDI spectra of PLA analyzed with *s-DHB*, for better correlation between the DoE results and the quality of the signal. As pointed out by DoE, the addition of NaTFA strongly reduced the *S/N*. Likewise, the higher amount of matrix was used for the sample preparation, the less accurate could the peaks be isolated from the rest, because of a reduction in resolution. In addition, it was noticeable that even when the signal-to-noise ratio was enhanced when more amount of matrix was used, the relative intensity peaks were contrarily decreased. In conclusion, the chosen criterion was taken according to the parameters aimed in this analysis: first, identification (improved by the resolution) and afterwards,

semi-quantification (enhanced by the signal-to-noise ratio) of oligomers. Therefore, selecting *RES* as the key parameter in this case, it was concluded that the application of a DoE for the improvement of the MALDI measure of PLA would be superior with the following combination of factors and levels: matrix (*s*-DHB), proportion analyte/matrix (1/5, V/V), and use of NaTFA (NO). The following sections thus show the MALDI analysis of the degradation subjected by both accelerated thermo-oxidative ageing and multiple reprocessing cycles.

3.3. Identification of oligomeric species

Fig. 9 shows the MALDI spectra for virgin PLA corresponding to 22 LA units, as an example for identification of cyclic and linear oligomeric species, indicated for VPLA, and summarized at Table 4. Note that species appeared at more m/z than those presented, but only values for $n = 22$ are shown for clarity. Full symbols were used for Na^+ adducts and hollow symbols for H^+ adducts. Predominant species found for virgin PLA were, in order of abundance: (i) cyclic $[\text{LA}_n]_n$, mainly present as Na^+ adducts ($[\text{M}+\text{Na}]^+$: m/z 1608.3) and in less quantities, H^+ adducts ($[\text{M}+\text{H}]^+$: 1585.3 m/z); (ii) linear $\text{H}-[\text{LA}_n]_n-\text{OH}$, which bears a hydroxyl and a carbonyl end groups ($[\text{M}+\text{Na}]^+$: m/z 1626.3 and $[\text{M}+\text{H}]^+$: m/z 1604.3); and, (iii) linear $\text{H}-[\text{LA}_n]_n-\text{O}-\text{CH}_3$, which has a methoxyl group and a hydroxyl group bearing ($[\text{M}+\text{Na}]^+$: m/z 1640.3 and $[\text{M}+\text{H}]^+$: m/z 1618.3), commonly found at PLAs obtained by ring opening polymerization (ROP) due to the use of alkoxydic initiators, which remain in the terminal units [28]. Other low predominant species found that might be formed as by-products at the processing temperature were: (iv) linear $\text{CH}_3-\text{O}-[\text{LA}_n]_n-\text{CH}_3$, bearing two methoxyl groups ($[\text{M}+\text{Na}]^+$: m/z 1654.4 and $[\text{M}+\text{H}]^+$: m/z 1632.4); and (v) linear $\text{CH}_3-\text{CO}-\text{O}-[\text{LA}_n]_n-\text{H}$, which has a hydroxyl and a carboxylic methyl ester groups as ending units ($[\text{M}+\text{Na}]^+$: m/z 1668.4 and $[\text{M}+\text{H}]^+$: m/z 1646.4), that might appear due to esterification reactions from different chain capping routes during polymerization. In addition, the MALDI spectra show that both even-membered and odd-membered oligomeric species appeared for virgin PLA. Since the presence of odd-membered oligomers may not be explained by reason of PLA ROP, it may be admitted that intermolecular transesterifications took place in parallel to the polymerization process, thus causing a random cleavage of the polylactide backbone, as suggested by Montaudo et al. [28].

3.4. Degradation studies

Fig. 10 shows the proposed degradation mechanisms map for polylactide degradation, which involves the reactions of formation and disappearance of the aforementioned main oligomeric species. Low abundant species (linear $\text{CH}_3-\text{O}-[\text{LA}_n]_n-\text{CH}_3$, and linear $\text{CH}_3-\text{CO}-\text{O}-[\text{LA}_n]_n-\text{H}$) were not included since their abundance was not significant during the process and their reactivity can be explained under the same conditions as the methoxyl ester species $\text{CH}_3-\text{O}-[\text{LA}_n]_n-\text{H}$. Thermo-oxidative ageing and thermo-mechanical degradation influenced the oligomeric distribution of polylactide differently and

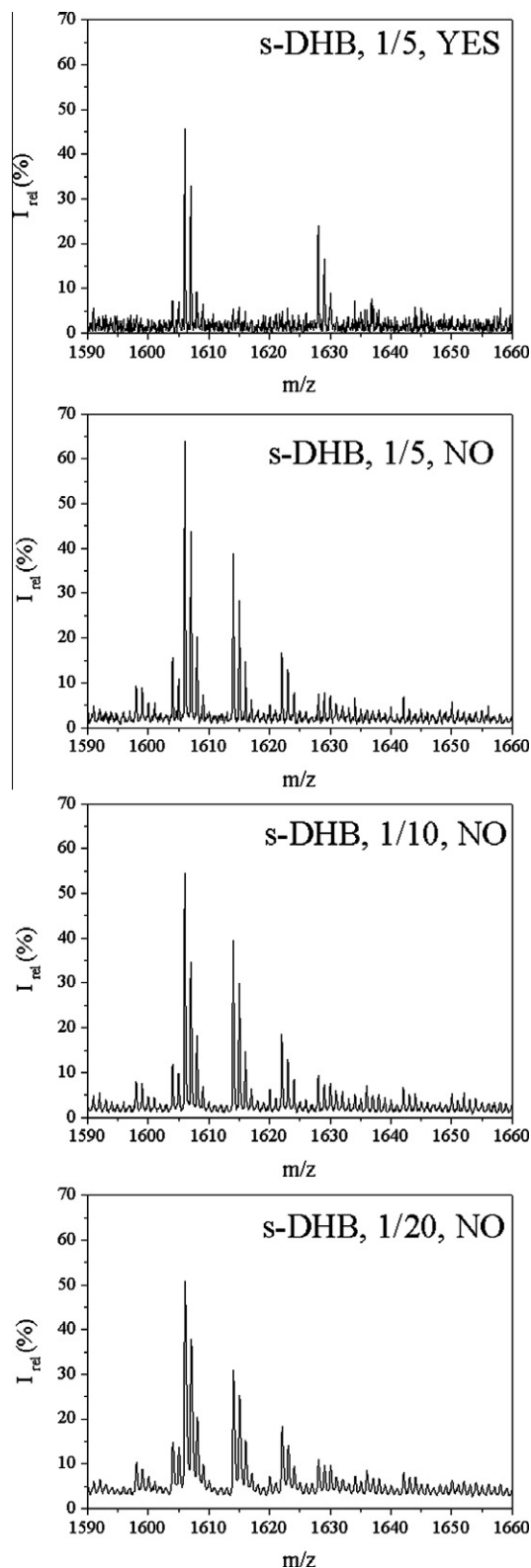


Fig. 8. MALDI-TOF MS spectra of PLA at different MALDI sample preparations to check the applicability of the Design of Experiments applied.

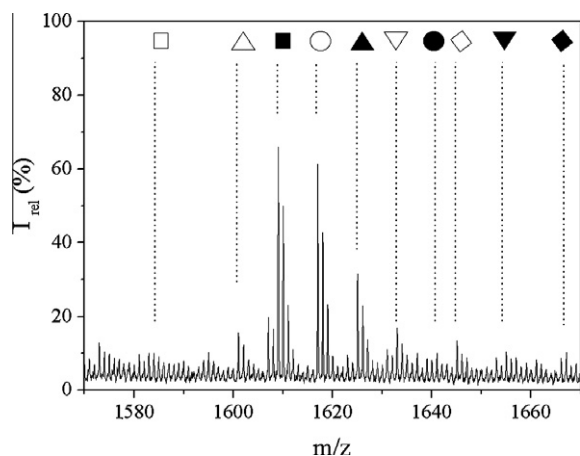


Fig. 9. Identification of oligomeric species that compose PLA (see Table 4 for symbology).

therefore the discussion is stated in the next paragraphs according to the studied type of degradation.

The reactions of PLA degradation generally followed the postulated mechanistic routes of polyesters which are shown as follows for the case of PLA¹: Route I: Hydrolysis, which leads to the formation of hydroxyl and carboxyl linear oligomers with shorter chain length. Route II: Esterification. Route III: Intramolecular transesterification, *a*: from the end of the chain (backbiting); *b*: in the middle of the chain, which leads to the formation of cyclic oligomers and linear species with shorter length. Route IV: Intermolecular transesterifications, which interchange ester units between different chains, leading to an increase in the heterogeneity of the polymer. Routes V: Chain scission reactions, acyl-O and alkyl-O β-C initiated homolytic chain-scissions at temperatures above melting; and radical reactions induced by oxygen, which may produce random chain cleavage, leading to the formation of mainly linear hydroxyl and carboxyl terminated species.

It is known that the physical and chemical features of polylactide are directly connected to its stereochemistry. Indeed, the Molar Mass Distribution (MMD) of PLA would vary if the D/L ratio was different [45]. However, The PLA used in this work is eminently amorphous (>95% L-lactide), and its morphological configuration remains nearly equal along the degradation processes [46], without showing a hint of crystallinity that might influence the MALDI signal due to different interactions with the matrix or condition the degradation mechanisms. According to Montaudo et al. [5], the linear mode is essentially used for the determination of the MMD of polymers, whereas the reflector mode allows for the identification of oligomers or side-products, as well as the characterization of end-groups. Since this work was focused on the effects of reprocessing and thermo-oxidative aging on PLA structure and thus the apparition of new oligomers, and the correlation between the MMD of polymers drawn by MALDI and other techniques, i.e. Size Exclusion Chromatography (SEC), is not

clear yet [47], the reflector mode was preferred. Since degradation starts primarily at the amorphous part of PLA backbone, the nature of the newly formed oligomers would be essentially the same.

3.5. Thermo-oxidative ageing

Fig. 11 shows the evolution of the relative ion abundances of the oligomeric species along the accelerated thermo-oxidative ageing carried out at 60 °C. Note that both intensities and areas under curves for both Na⁺ and H⁺ ions were considered for calculations. Ageing at temperatures above the glass transition temperature of PLA (ca. 55 °C [48]) enhances the molecular mobility of the chains and therefore might increment the possibilities of reaction. The variation of ion abundances showed a two-stage tendency: during the first step, up to 3 weeks, there was an increasing tendency of formation of cyclic [LA_C]_n, along with a decrease of linear H-[LA_L]_n-OH, which suggested the dominance of middle-chain intramolecular transesterifications (Route III), aided by temperature. Besides, there was a first increase of linear H-[LA_L]_n-O-CH₃, that might be mainly produced by esterification (Route II) of H-[LA_L]_n-OH. In addition, minor species might rapidly react to very low proportions along the rest of the thermo-oxidative ageing.

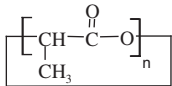
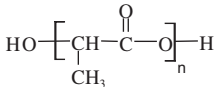
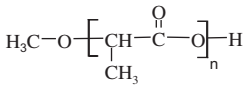
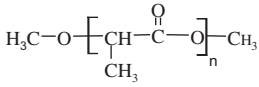
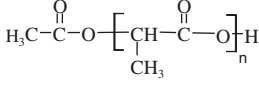
In a second stage, from 3 weeks up to 12 weeks, the tendency described for the main oligomeric species changed. There was a strong reduction of cyclic [LA_C]_n species to proportions below the values present in neat VPLA. On the other hand, the increasing tendency of H-[LA_L]_n-O-CH₃ species was slightly maintained, occurring along with a remarkable increment of H-[LA_L]_n-OH species, which may be explained by hydrolytic reactions mainly affecting the [LA_C]_n induced by present water and methanol traces (Route I) that could easily attack a more liable structure, excited by temperature. As well, the auto-oxidation reactions [49] may be promoted at long exposition times at this second stage, auto-catalyzed by radical species, which may induce homolytic reactions in the polymeric structure (Routes V). Likewise, the apparition of new hydroxyl and carboxyl terminated groups might auto-catalyze these reactions. Intermolecular transesterifications (Route IV) would take place favouring ester-exchange through chain cleavage along the polymer chain, as drawn from the odd-membered species found in the MALDI spectra [28].

3.6. Thermo-mechanical degradation

Fig. 12 shows the evolution of the relative ion abundances of polylactide oligomeric species along the multiple reprocessing steps. Thermo-mechanical degradation induced by means of multiple reprocessing underwent modifications in the oligomeric distribution of the PLA sample, in a different fashion than that shown by the study of the influence of the accelerated thermo-oxidative ageing. Thermo-mechanical degradation followed a single step, in which the apparition or disappearance of species occurred gradually. Degradation agents associated to reprocessing were more aggressive for the polymeric distribution, since chains were submitted to temperatures

¹ Schemes available at the on-line additional information.

Table 4
Oligomeric species found for PLA by means of MALDI analysis.

Species	Structures	m/z $[M+H]^+$	m/z $[M+Na]^+$		
$[LA_C]_n$		□	■	1586,4	1608,4
$HO-[LA_L]_n-H$		△	▲	1604,4	1626,4
$CH_3-O-[LA_L]_n-H$		○	●	1618,4	1640,4
$CH_3-O-[LA_L]_n-CH_3$		▽	▼	1632,4	1654,4
$CH_3-CO-O-[LA_L]_n-H$		◇	◆	1646,4	1668,4

above PLA melting temperature, in which the reactions among end-groups are enhanced. As well, the susceptibility of recycles to both O-acyl and O-alkyl homolysis via β -C scission [50–52] at higher temperatures might increase due to a remarked weakness of the structure throughout the reprocessing cycles. Even more, short melting and cooling stressing cycles applied during the injection procedure might increase the possibilities of changes in the morphol-

ogy. Undesirable components such as presence of water moieties and methanol traces from the initiation process could also affect the materials, by subjecting PLA chains to scission reactions that may decrease the molecular weight of the polymer [46]. Although care was taken when processing the samples in order to avoid the presence of humidity prior to the process, PLA is very hygroscopic, and after some cycles, the efficiency of water removal

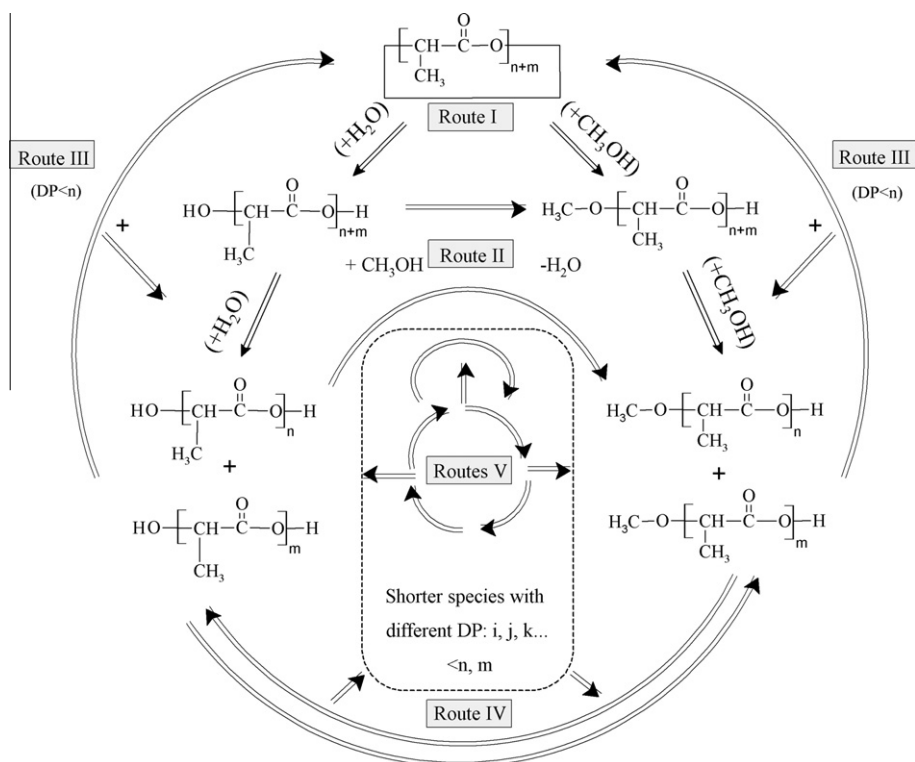


Fig. 10. Proposed degradation mechanism map for polylactide.

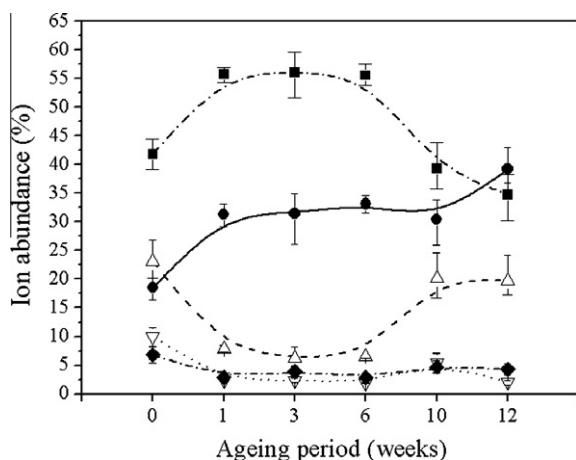


Fig. 11. Influence of thermo-oxidative ageing on the relative abundances of PLA oligomeric species.

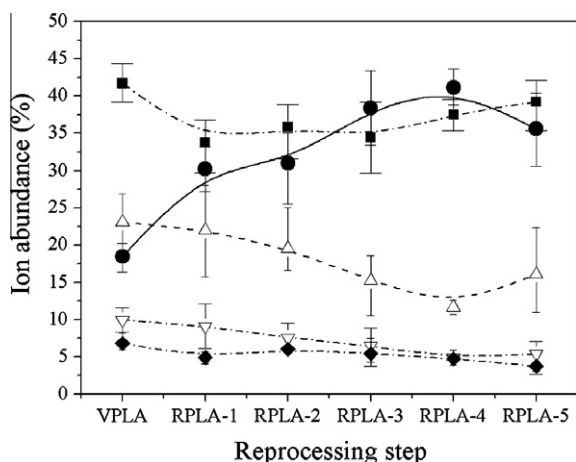


Fig. 12. Influence of thermo-mechanical cycles on the relative abundances of PLA oligomeric species.

could be diminished, thus enhancing the occurrence of hydrolytic reactions. Finally, shear mechanical forces taking place during the injection and the grinding processes induce degradation in a larger extent and therefore would, inherently to reprocessing, break the polymeric chains, leading to smaller species that may vary the oligomeric distribution of polylactide. Main differences were stated as follows:

On the one hand, cyclic $[LA_C]_n$ species showed a gradual decrease to abundance values close to 35% up to the third recyclate and recovered its presence at the fifth recyclate. Likewise, linear $HO-[LA_L]_n-H$ presented a similar behaviour, ranging its variation from 25% to a 15%. The most remarkable changes were those occurring for linear $CH_3-O-[LA_L]_n-H$ species, which presented a noticeable increase, being the most predominant species after three processing cycles, and achieving a proportion of up to 40% for the fourth recyclate. This fact, together with the reduction of linear $HO-[LA_L]_n-H$ and cyclic $[LA_C]_n$ sug-

gested that the prime reactions taking place during thermo-mechanical degradation of PLA followed a two-step behaviour: (i) hydrolysis (Route I) or intramolecular transesterification (Route III) to mainly release $HO-[LA_L]_n-H$, and (ii) immediate esterification of $HO-[LA_L]_n-H$ into $CH_3-O-[LA_L]_n-H$ (Route II), due to the high reactivity of $HO-[LA_L]_n-H$ at the processing conditions.

On the other hand, the abundance of $CH_3-O-[LA_L]_n-H$ would be also generally aided by intermolecular transesterifications (Route IV) of ester-terminated species, such as low abundant species (linear $CH_3-CO-O-[LA_L]_n-H$ and $CH_3-O-[LA_L]_n-CH_3$), which might be incorporated into the main oligomeric degradation cycle. Note that the ion abundances of these species were above 5% for all recyclates, in contrast to the abundances found for thermally-aged PLA. Their presence can be explained as side-products/impurities after the grinding-melting-injection process, which induced a more heterogeneous degradation effect than that presented by thermo-oxidative ageing, since more degrading agents were present and therefore a new oligomeric distribution appeared after each reprocessing step. Finally, the homolytic chain-scission reactions induced by reprocessing would randomly attack the polymeric backbones, releasing shorter chains with different ending units which contributed to increase the heterogeneity and polydispersion of the material [28].

4. Conclusions

The sample preparation procedure for the analysis of polylactide (PLA) samples by means of MALDI-TOF MS was assessed. A statistical Design of Experiments (DoE) taking into account the following factors (levels): choice of the correct matrix (*s*-DHB, dithranol, HABA), the proportion analyte/matrix (1/5, 1/10, 1/20 V/V), and the use of cationization agent (YES, NO) was considered. The study was performed by means of analyzing the effect of changing the aforementioned factors among their different levels on spectroscopic signals taking into account quality parameters such as signal-to-noise ratio (*S/N*) and Resolution (*RES*). Main effects plots and interaction plots permitted to understand the influence of each factor to the quality of the MALDI spectra. The application of DoE for the improvement of the MALDI analysis of PLA stated that the best spectra were obtained with mixtures prepared with *s*-DHB as matrix, in a proportion analyte/matrix (V/V 1/5), without cationization agent, considering that *RES* was the key effect for the analysis.

Multiple processing by means of successive injection cycles was used to simulate the thermo-mechanical degradation effects on the oligomeric distribution of PLA under mechanical recycling. Likewise, an accelerated thermo-oxidative ageing over the glass transition was executed in order to simulate service life. Degradation primarily affected the initially predominant cyclic $[LA_C]_n$ and linear $H-[LA_L]_n-OH$ species. Intramolecular and intermolecular transesterifications as well as hydrolytic reactions occurred during the formation and disappearance of oligomeric species. In both mechanisms induced by thermo-oxidative and thermo-mechanical degradation, the formation of $H-[LA_L]_n$

—O—CH₃ was highlighted, although a different behaviour was observed. Thermo-oxidative ageing presented a two-stage performance, governed by intramolecular transesterifications during the first stage and chain-scission reactions during the second stage, when over-exposure to temperature conditions triggered the depolymerization of cyclic species. On the other hand, thermo-mechanical degradation seemed to occur mainly via hydrolytic, homolytic and intermolecular transesterifications, giving rise to a noticeable major abundance of H—[LA]_n—O—CH₃ groups, especially after the third recycle.

Acknowledgements

The authors would like to acknowledge the Spanish Ministry of Science and Innovation for the financial support through the Research Project UPOVCE-3E-013. The Spanish Ministry for Education is acknowledged for the concession of a predoctoral research position to J.D. Badía by means of the FPU program. AIMPLAS is acknowledged for providing and processing the material, respectively. Royal Institute of Technology (KTH, Sweden) and Universitat Politècnica de València (UPV, Spain) are also thanked for additional economical support.

Appendix A. Supplementary data

Supplementary data associated with this article can be found, in the online version, at doi:10.1016/j.eurpolymj.2011.05.001.

References

- Mohanty AK, Misra M, Hinrichsen G. Biofibres, biodegradable polymers and biocomposites: an overview. *Macromol Mater Eng* 2000;276(277):1–24.
- Auras R, Harte B, Selke S. An overview of polylactides as packaging materials. *Macromol Biosci* 2004;4:835–65.
- Tsuji H, Doi Y. Polyesters III. Applications and commercial Products. In: Steinbüchel A, editor. *Biopolymers*. Weinheim: Wiley-VCH, Verlag GmbH; 2002.
- Awaja F, Pavel D. Recycling of PET. *Eur Polymer J* 2005;41:1453–77.
- Finnveden G, Johansson J, Lind P, Moberg A. Life cycle assessment of energy from soild waste-Part1: general methodology and results. *J Cleaner Prod* 2005;13(3):213–29.
- Karlsson S. Recycled polyolefins. Material properties and means for quality determination. *Adv Polym Sci* 2004;169:201–30.
- Ehrig RJ. *Plastics Recycling: Products and Processes*. New York: Hanser Publishers; 1992.
- Klemchuck PP. *Polymer Stabilization and Degradation*. Washington: ACS; 1985.
- Strömberg E, Karlsson S. The design of a test protocol to model the degradation of polyolefins during recycling and service life. *J Appl Polym Sci* 2009;112:1835–44.
- Vilaplana F, Ribes-Greus A, Karlsson S. Degradation of recycled high-impact polystyrene. Simulation by reprocessing and thermo-oxidation. *Polym Degrad Stab* 2006;91:2163–70.
- Vilaplana F, Karlsson S, Ribes-Greus A. Changes in the micro-structure and morphology of high-impact polystyrene subjected to multiple processing and thermo-oxidative degradation. *Eur Polymer J* 2007;43:4371–81.
- Yarahmadi N, Jakubowicz I, Gevert T. Effects of repeated extrusion on the properties and durability of rigid PVC scrap. *Polym Degrad Stab* 2001;73(1):93–9.
- Badía JD, Vilaplana F, Karlsson S, Ribes-Greus A. Thermal analysis as a quality tool for assessing the influence of thermo-mechanical degradation on recycled poly(ethylene terephthalate). *Polym Test* 2009;28:169–75.
- La-Mantia F, Vinci M. Recycling poly(ethylene terephthalate). *Polym Degrad Stab* 1994;45:121–5.
- Torres N, Robin JJ, Boutevin B. Study of thermal and mechanical properties of virgin and recycled poly(ethylene terephthalate) before and after injection molding. *Eur Polymer J* 2000;36:2075–80.
- Badía JD, Strömberg E, Ribes-Greus A, Karlsson S. A statistical design of experiments for optimizing the MALDI-TOF-MS sample preparation of polymers. An application in the assessment of the thermo-mechanical degradation mechanisms of poly(ethylene terephthalate). *Analytica Chimica Acta* 2011;692(1–2):85–95.
- Polce Michael J, Wesdemiotis Chrys. Introduction to Mass Spectrometry of Polymers. In: Montaudo Giorgio, Lattimer Robert P, editors. *Mass Spectrometry of Polymers*. Boca Raton, Florida: CRC Press LLC; 2002.
- Montaudo G, Samperi F, Montaudo M-S. Characterization of synthetic polymers by MALDI-MS. *Prog Polym Sci* 2006;31:277–357.
- Weidner SM, Trimpin S. Mass spectrometry of synthetic polymers. *Anal Chem* 2008;80:4349–61.
- Williams JB, Gusev AI, Hercules D, Characterization M. Characterization of polyesters by matrix-assisted laser desorption/ionization mass spectrometry. *Macromolecules* 1996;30:3781.
- Carroccio S, Rizzarelli P, Scaltro G, Puglisi C. Comparative investigation of photo- and thermal-oxidation processes in poly(butylene terephthalate). *Polymer* 2008;49:3371–81.
- Spassky N, Simic V, Montaudo MS, Hubert-Pfalzgraf LG. Inter- and intramolecular ester exchange reactions in the ring-opening polymerization of (D, L)-lactide using lanthanide alkoxide initiators. *Macromol chem phys* 2000;201(17):2432–40.
- Shyamroy S, Garnaik B, Sivaram S. Structure of poly(L-lactic acid) prepared by the dehydrocondensation of L-lactic acid with organotin catalyst. *J Polym Sci, Part A: Polym Chem*. 2005;43(10):2164–77.
- Jalabert M, Frascini C, Prud'Homme R. Synthesis and characterization of poly(L-lactide)s and poly(D-lactide)s of controlled Molecular Weight. *J Polym Sci, Part A: Polym Chem* 2007;45:1944–55.
- Nagahata R, Sano D, Suzuki H, Takeuchi K. Microwave-assited single-step synthesis of poly(lactic acid) by direct polycondensation of lactic acid. *Macromol Rapid Commun* 2007;28(4):437–42.
- Kowalski A, Libiszowski J, Duda A, Penczek S. Polymerization of L, L-Dilactide initiated by Tin(II) butoxide. *Macromolecules* 2000;33(6):1964–71.
- Takizawa K, Nulwala H, Hu J, Yoshinaga K, Hawker CJ. Molecularly defined (L)-lactic acid oligomers and polymers: synthesis and Characterization. *J Polym Sci, Part A: Polym Chem* 2008;46(18):5977–90.
- Montaudo G, Montaudo MS, Puglisi C, Samperi F. Evidence for ester-exchange reactions and cyclic oligomer formation in the ring-opening polymerization of lactide with aluminium complex initiators. *Macromolecules* 1996;29(20):6461–5.
- Waschen O, Reichert KH. Thermal decomposition of biodegradable polyesters-III. Studies on the mechanisms of thermal degradation of oligo-L-lactide using SEC, LACC and MALDI-TOF MS. *Polym Degrad Stab* 1997;55:225–31.
- Montaudo G, Montaudo MS, Samperi F. Matrix-Assisted Laser desorption Ionization/Mass Spectrometry of Polymers (MALDI-MS). In: Lattimer RP, Montaudo G, editors. *Mass Spectrometry of Polymers*. Boca Raton, Florida: CRC Press LLC; 2001. p. 422.
- Hotelling AJ, Kawaoka K, Goodberlet MC, Yu WM, Owens KG. Optimization of matrix-assisted laser desorption/ionization Time-of-flight collision-induced dissociation using Poly(ethylene glycol). *Rapid Commun Mass Spectrom* 2003;17:1671–6.
- Meier M, Schubert U. Evaluation of a new multilayer spotting technique for MALDI-TOF-MS for synthetic polymers. *Rapid Commun Mass Spectrom* 2003;17:713–6.
- Hotelling AJ, Nichols WF, Giesen DJ, Lenhard JR, Knochenmuss R. Electron transfer reactions in laser desorption/ionization and matrix-assisted laser desorption/ionization: factors influencing matrix and analyte ion intensities. *Eur J Mass Spectrom* 2006;12:345–58.
- Sroka-Bartnik A, Olejniczak S, Sochaki M, Biela T, Potrzebowski MJ. Solid-State NMR Spectroscopy as a Tool supporting Optimization of MALDI-TOF MS analysis of Polylactides. *J Am Soc Mass Spectrom* 2009;20:67–72.
- Mukerjee R, Jeff-Wu CF. *A Modern Theory of Factorial Design*. New York: Springer Science+Business Media Inc.; 2006.
- Box GE, Hunter JS, Hunter WG. *Statistics for experimenters. Design, innovation and discovery*. New Jersey: John Wiley and sons; 2005.

- [37] ISO 291:1997. Plastics – standard atmospheres for conditioning and testing.
- [38] Montaudo G. Mass spectrometry of synthetic polymers: mere advances or revolution? *Trans Polym Sci* 1996;4(3):81–6.
- [39] Rader HI, Schrepp W. MALDI-TOF mass spectrometry in the Analysis of Synthetic Polymer. *Acta Polymerica* 1998;49:272.
- [40] Hoteling AJ, Mourey TH, Owens KG. Importance of solubility in the Sample Preparation of Poly(ethylene terephthalate) for MALDI-TOF-MS. *Anal Chem* 2005;77:750–6.
- [41] Danis PO, Karr DEA. A facile sample preparation for the analysis of synthetic organic polymers by matrix-assisted laser desorption/ionization. *Org Mass Spectro* 1993;28:923.
- [42] Lloyd PM, Scrivener E, Maloney DR, Haddleton DM, Derrick PJ. Cation attachment to synthetic polymers in matrix-assisted laser desorption/ionization mass spectrometry. *Polymer preprint* 1996;37(1):847–8.
- [43] King R C, Goldschmidt R, Xiong Y, Owens K G. *Mechanistic studies of the Cationization of Synthetic Polymers by Alkali Metals in the matrix-assisted laser desorption/ionization experiment*. 43rd ASMS Conference in Mass Spectrometry: 1237. Atlanta, GA, 1995.
- [44] Xu N, Huang ZW, Watson JT, Dage DA. Mercaptobenzothiazoles: a new class of matrices for Laser Desorption Ionization Mass Spectrometry. *J Am Soc Mass Spectrom* 1997;8:116.
- [45] Södergard A, Stolt M. Properties of lactic acid based polymers and their correlation with composition. *Prog Polym Sci* 2002;27(6):1123–63.
- [46] Badía J D, Strömberg E, Karlsson S, Ribes-Greus A. *Influence of mechanical recycling to the structural, morphological, mechanical, thermal and viscoelastic properties of polylactide*. Manuscript in preparation.
- [47] Montaudo G, Montaudo MS. *Polymer Characterization methods*. In: Montaudo G, Lattimer RP, editors. *Mass Spectrometry of Polymers*. Boca Raton, Florida: CRC Press LLC; 2002.
- [48] Santonja-Blasco L, Moriana R, Badía JD, Ribes-Greus A. Thermal analysis applied to the characterization of degradation in soil of polylactide: I. Calorimetric and viscoelastic analyses. *Polym Degrad Stab* 2010;95:2185–91.
- [49] Bolland JL, Gee G. Kinetic studies in the chemistry of rubber and related materials. II. The kinetics of oxidation of unconjugated olefins. *Trans Faraday Soc* 1946;42:236–43.
- [50] Kopinke FD, Mackenzie K. Mechanistic aspects of the thermal degradation of poly(lactic acid) and poly(beta-hydroxybutyric acid). *J Anal Appl Pyrol* 1997;40:43–53.
- [51] Kopinke FD, Remmler M, Mackenzie K, Möder M, Wachsen O. Thermal decomposition of biodegradable polyesters – II: poly(lactic acid). *Polym Degrad Stab* 1996;53:329–42.
- [52] Mc Neill IC, Leiper HA. Degradation studies of some polyesters and polycarbonates – 2: polylactide: degradation under isothermal conditions, thermal degradation mechanisms and photolysis of the polymer. *Polym Degrad Stab* 1985;11:309–26.

CONTRIBUTION III-E

Material valorisation of amorphous polylactide. Influence of thermo-mechanical degradation on the morphology, segmental dynamics, thermal and mechanical performance

J.D. Badia, E. Strömberg, S. Karlsson, A. Ribes-Greus

Manuscript

MATERIAL VALORISATION OF AMORPHOUS POLYLACTIDE. INFLUENCE OF THERMO-MECHANICAL DEGRADATION ON THE MORPHOLOGY, SEGMENTAL DYNAMICS, THERMAL AND MECHANICAL PERFORMANCE

J.D. Badia¹, E. Strömberg², S. Karlsson², A. Ribes-Greus^{1,*}

¹ Instituto de Tecnología de Materiales (ITM),

Universitat Politècnica de València

Camino de Vera s/n, E-46022 Valencia, Spain

² School of Chemical Science and Engineering,

Fibre and Polymer Technology,

KTH - Royal Institute of Technology,

Teknikringen 56-58, SE-10044 Stockholm, Sweden

*corresponding author: aribes@ter.upv.es

Keywords: poly(lactide) (PLA), mechanical recycling, cold-crystallization, glass-rubber relaxation, cooperative movement

Abstract:

The effects of thermo-mechanical degradation on polylactide (PLA) subjected to mechanical recycling by means of five successive injection cycles were initially addressed in terms of macroscopic mechanical properties and surface modification. A deeper inspection on the structure and morphology of PLA was associated to the thermal properties and viscoelastic behaviour. Despite the FTIR analysis did not show significant changes in functional groups, a remarkable reduction in molar mass was found by viscosimetric analysis. PLA remained amorphous throughout the reprocessing cycles, but the occurrence of a cold-crystallization during DSC and DMTA measurements, which enthalpy increased with each reprocessing step, suggested chain scission due to thermo-mechanical degradation. The effect of chain shortening studied on the glass-rubber relaxation by DMTA showed an increase in free-volume affecting the segmental dynamics of PLA, particularly after the application of the second reprocessing step, in connection to the overall loss of performance showed by the rest of properties.

1. Introduction

The interest on plastic materials such as poly(lactic acid)s or polylactides (PLA) that accomplish the two-fold benefit of being biodegradable and come from renewable resources has gained much attention. Polylactides are thermoplastic polyesters obtained from the ring-opening polymerization of lactide, which may be derived from the fermentation of sugar feedstocks at competitive prices compared to that previously achievable from petrochemical-derived products [1]. PLAs have numerous interesting properties including good processability, mechanical properties, thermal stability and low environmental impact [2-3], which enhance their performance as suitable candidates for replacing commodities at the packaging sector. However, the increase of a new source of polymeric waste is implied, which would have to be managed. Moreover, with the aim of enhance the material valorisation of PLA goods, it would be advisable to explore the possibilities of extending their service lives before finally discarding them to bio-disposal facilities, such as composting plants. Among all material recovery methods [4], mechanical recycling represents one of the most successful processes and has received considerable attention due to its main advantages, since it is relatively simple, requires low investment, and its technological parameters are controlled. Nevertheless, polymers are subjected to the influence of degrading agents such as oxygen, UV-light, mechanical stresses, temperature and water, which, separately or in combination, during its material loop (synthesis - processing - service life - discarding - recovery), results in chemical and physical changes that alter their stabilization mechanisms and long-term properties. These degradation processes may

modify the structure and composition of PLA and consequently change the thermal, viscoelastic and mechanical properties of the recyclates [5].

On the one hand, the simulation of mechanical recycling by multiple processing and service life by accelerated thermal ageing to assess the effects of thermal and thermo-mechanical degradation has been previously performed for commodities [6-13]. The scarce studies on the degradation of reprocessed PLA [14-17] reported the loss of mechanical performance of recycled PLA in terms of decoupling between amorphous and crystalline phases. However, no studies were found reporting the performance of reprocessed PLA which remains amorphous regardless the number of processing cycles, as in the case of this study. On the other hand, the assessment of the glass-rubber transition and the segmental dynamics of PLA have been reported in several studies [18-20] for different PLA grades, but not reported for the case of reprocessed PLA.

In order to model mechanical recycling as a suitable valorisation option for recovering PLA prior to bio-disposal, the purpose of this work was to characterize the influence of multiple processing on PLA microstructure and segmental dynamics, and its subsequent influence on its thermal and mechanical performance.

2. Experimental procedure and calculations

2.1. Material and reprocessing simulation

Polylactide (PLA) 2002D was a thermo-forming grade PLA obtained from Natureworks LLC (Minnetonka, MN) as pellets, provided by AIMPLAS (Paterna, Spain). Prior to processing, virgin PLA pellets were dried during 2 h at 80 °C

in a dehumidifier Conair Micro-D FCO 1500/3 (UK), in order to remove as much humidity as possible from PLA flakes. Afterwards, the samples were processed by means of injection moulding by means of an Arburg420 C 1000-350 (Germany) injector, single-screw model (diameter $\Phi=35$ mm, length/ $\Phi=23$). Temperature gradient set from hopper to nozzle was 160, 170, 190, 200 and 190°C. Moulds were set at 15 °C. Cooling time residence was ca. 40 s and total residence time ca. 60s. Samples were dried before each processing cycle. After injection, a fraction of the samples was kept as test specimens and the rest was ground by means of a cutting mill Retsch SM2000 (UK), which provided pellets of size $d < 20$ mm to be fed back into the process. Up to five processing cycles were applied under the same conditions to obtain the different testing specimens of reprocessed PLA (RPLA-i, with i: 1-5). Dumbbell probes for tensile and impact testing were obtained according to ISO 527-2 (type 1A) [21]. 1 mm thick prismatic probes for SEM and DMTA were obtained from compression moulding, as described elsewhere [22].

2.2. Mechanical properties

Tensile testing and impact testing were carried out at laboratory conditions 23/50, according to ISO 291, atmosphere 23/50, class 1 [23]. Tensile tests were performed on reprocessed PLA in order to investigate the changes in macroscopic mechanical properties, by means of an Instron 5566 universal electromechanical testing instrument (Instron Corp, MA, USA), at a crosshead speed of $5 \text{ mm} \cdot \text{min}^{-1}$, a 10 kN load cell and gauge length of 50 mm. Analyses were repeated at least 6 times per material, and the average of elastic modulus, elongation at break

and stress at break were used as representative values.

Charpy impact experiments were carried out following ISO 179 [24], with a hammer of 1 J and a notch size radius of 1,5mm. The samples were characterized at least by triplicate and the averages were taken as representative values.

2.3. Scanning Electron Microscopy (SEM)

The morphology of the specimens was analysed by means of a Hitachi S-4800 Field Emission Scanning Electron Microscope (Tokyo, Japan). The samples from each material were prepared by cutting square pieces from a randomly chosen part of the processed specimen. The pieces were mounted on metal studs and sputter-coated with a 2 nm gold layer using a Cressington 208HR high resolution sputter coater (Watford, UK), equipped with a Cressington thickness monitor controller.

2.4. Differential Scanning Calorimetry (DSC)

DSC analyses were carried out by a Mettler Toledo DSC 820 instrument (Columbus, OH) calibrated with indium and zinc standards. Approximately 5 mg of pellets were placed in 40 μL aluminium pans, which were sealed and pierced to allow the N_2 gas flow ($50 \text{ ml} \cdot \text{min}^{-1}$). A heating/cooling/heating program with a $\pm 2^\circ\text{C} \cdot \text{min}^{-1}$ rate was employed in the temperature range between 0 °C and 200 °C. The samples were characterized at least by triplicate and the averages were taken as representative values.

2.5. Fourier-Transform Infrared (FT-IR) Analysis

FT-IR spectra were collected by a NEXUS Thermo Nicolet 5700 FT-IR Spectrometer (MA, USA), previously calibrated, and equipped with a

single-reflection Smart Performer accessory for attenuated total reflection (ATR) measurements, with diamond crystal. 32 co-added spectra were recorded for each specimen at a resolution of 4 cm^{-1} with a spacing of 1 cm^{-1} , from 4000 to 600 cm^{-1} of wavenumber. Spectra were normalized to the 1454 cm^{-1} peak [25] before any data processing which is usually used as internal standard and it is useful to correct possible variations arisen from defects in surface quality or sample positioning. At least 8 measurements per material were performed, in order to obtain representative results. Presented spectra correspond to the average of each individual analysis.

2.6. Molar mass determination

The intrinsic viscosity $[\eta]$ was measured according to the standard ISO 1628-1 [26], by means of a Cannon-Fleske capillary viscosimeter type at 30 °C, with the use of analytical grade tetrahydrofurane (THF) supplied by Fluka as solvent. Dissolutions of pellets ranged from 0.1 to 1 $\text{g}\cdot\text{dL}^{-1}$. Measurements were performed by quintuplicate for each concentration c and $[\eta]$ was obtained from extrapolation to $c \rightarrow 0$ of Huggins and Kraemer plots, which respectively account for the variation of reduced η_{red} and inherent η_{inh} viscosities with the concentration, being $\eta_{\text{red}} = c^{-1} \cdot \eta_{\text{sp}}$, $\eta_{\text{inh}} = c^{-1} \cdot \ln \eta_{\text{rel}}$, $\eta_{\text{sp}} = \eta_{\text{rel}} - 1$ and $\eta_{\text{rel}} = t \cdot t_0^{-1}$, where t and t_0 were the times (s) of flowing of the dissolution and solvent, respectively. The viscous molar mass values (M_V , $\text{g}\cdot\text{mol}^{-1}$) was calculated with the Mark-Houwink equation $[\eta] = K \cdot M_V^\alpha$, with constants $K = 6.4 \cdot 10^{-4} \text{ dL}\cdot\text{g}^{-1}$ and $\alpha = 0.68$ [27].

2.7. Dynamical-Mechanical Thermal Analysis (DMTA)

DMTA test were conducted in dual cantilever clamping with 15 mm of effective length between clamps, with the three point bending mode, by means of a DMA/SDTA861^e Dynamic Mechanical Analyzer, from Mettler-Toledo (OH, USA). Experiments were carried out from 25 °C to 130 °C with isothermal steps of 2°C, measuring 24 frequencies (8 per decade) between 0.1 and 100 Hz. Analyses were performed at least thrice per sample and the average was taken as representative values.

2.8. Analytical software and computational assumptions.

FT-IR spectra were characterized by OMNIC 7.0 from Thermo Scientific. DSC and DMTA analyses were performed with the aid of the software STAR^e 9.10 from Mettler-Toledo. Fitting procedures were performed by means of OriginLab OriginPro 8.0, which uses the Levenberg-Marquardt algorithm [28-29] to adjust the parameter of the fitting values in the iterative procedure.

Values are plotted in terms of {average, dev_{max} , dev_{min} }, where $\text{dev}_{\text{max}} = \max(\text{data}) - \text{average}(\text{data})$, and $\text{dev}_{\text{min}} = \text{average}(\text{data}) - \min(\text{data})$. Tabulated errors correspond to the standard deviation of data.

3. Results and discussion

3.1. Surface characterization and mechanical performance

The surface characterization of reprocessed PLA by SEM, shown at **Figure 1** exhibited typical topologies of industrially-processed polymers [6,8]. After 5 reprocessing cycles, the micrographs presented a rough and heterogeneous surface where inefficiently melted particles arose, in comparison to that of VPLA, anticipating modifications in the performance of the material. The effects of reprocessing on the macroscopic mechanical properties are shown at **Figure 2**, in terms of Young modulus, stress and strain at break and impact value. The Young modulus remained almost unaltered during the 2 first reprocessing cycles, which was in agreement with previous reports in which this PLA grade showed similar performance [16]. However, from the third injection cycle on, the Young modulus decreased showing a significant drop ($\sim 28\%$) for the fifth recycle. On the other hand, the impact resistance was decreased by $\sim 10\%$ after the first cycle, maintaining its value nearly invariant throughout the rest of injections, as comparable with the behaviour shown by multi-extruded PLA [14]. Regarding the performance at break, despite all samples gave short strains, an overall increasing fashion within a narrow range was found, as the $\sim 21\%$ which was registered from VPLA to RPLA-5, in agreement with other studies [16]. On the other hand, a small and gradual drop in the stress values ($\sim 6,6\%$) was also presented. These results differ significantly to those reported elsewhere for PLA with higher D- content [15], which showed higher reductions in strain and stress at break. Indeed, the diminution of mechanical performance along the reprocessing cycles could

be attributed to the inherent chain scission processes [30]. Further analytical techniques helped confirm these assumptions.

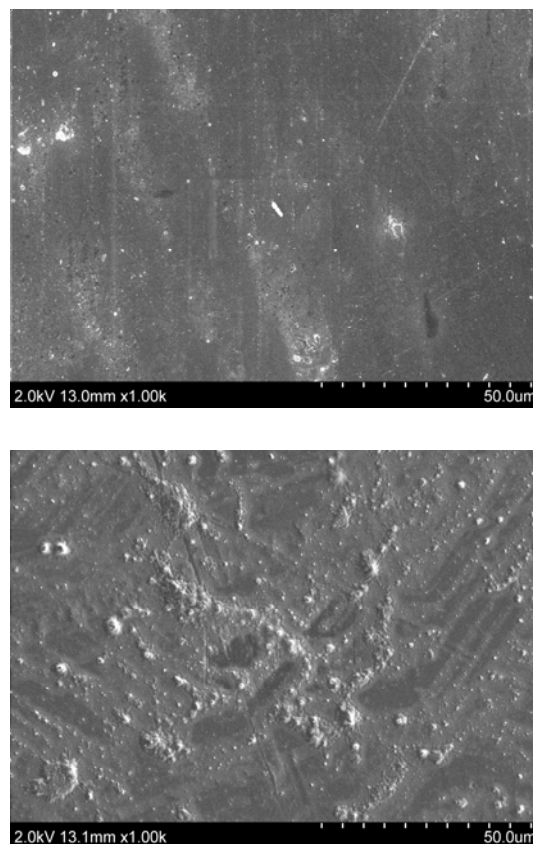


Figure 1. SEM pictures of (upper) VPLA and (lower) RPLA-5.

3.2. Structural changes

The absorbance spectra of virgin polylactide (VPLA) and its successive recyclates were recorded by Fourier-Transform Infrared Spectroscopy (FT-IR), as shown in **Figure 3a** for the case of VPLA and RPLA-5. The spectra of intermediate RPLA-i were similar. Complete description of the bands can be found in literature [25]. In a previous study carried out by means of MALDI-TOF MS analyses [30], the presence of new carboxy-methyl and carboxyl terminated species underwent by reprocessing was reported. In order to ascertain a semi-quantitative picture

of the structural changes caused by reprocessing, the relative absorbance ratios of the areas corresponding to the maximum peaks of the C-H stretching region (3100-2800 cm^{-1} , **Figure 3c**), and the maxima of the C=O stretching region (1800-1700 cm^{-1} , **Figure 3b**) were determined related to the area of the reference peak at 1454 cm^{-1} which is assigned to the C-H asymmetric bending mode and known to be suitable as internal standard [25], to obtain comparable results without experimental influence of the dimensions of the probes. Both functional indexes (**Figure 3d**) showed an increasing tendency, more significant for the carbonyl group, along with a displacement to higher wavenumbers of the peak, which may be indicative of the appearance of new carbonyl-linked species both in the middle and at the end as carboxyl groups, and may be a symptom of reduction of molar mass.

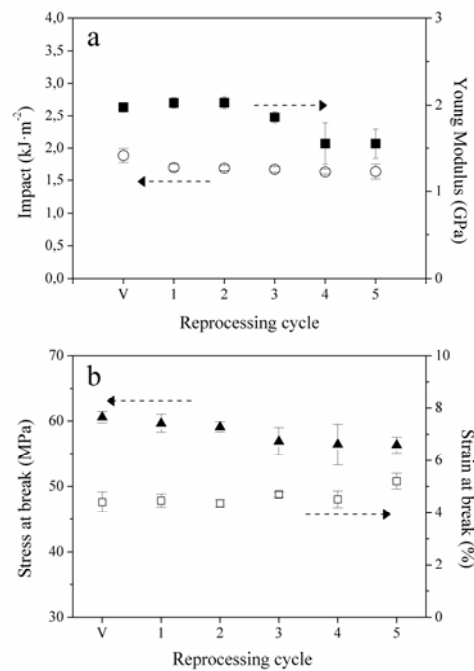


Figure 2. Results from tensile and impact testing: (a) Young Modulus and Impact value; (b) Stress and strain at break.

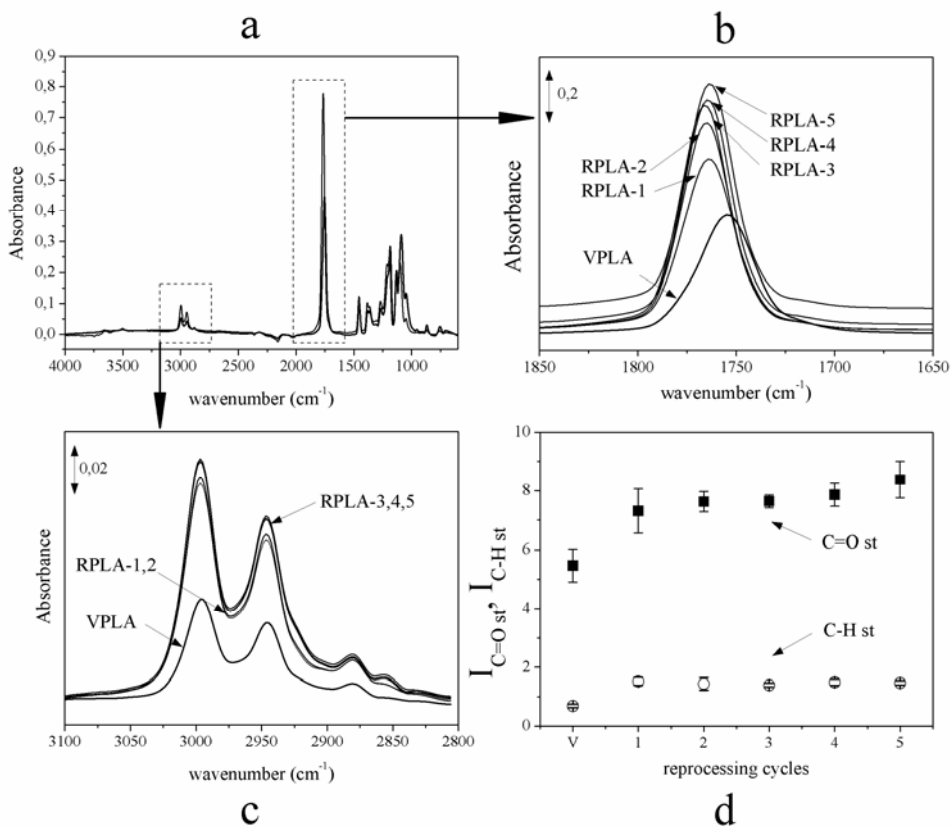


Figure 3. FT-IR analysis: (a) FT-IR spectra of virgin and fifth reprocessed PLA; (b) evolution of the carbonyl region; (c) variation of the hydroxyl region; (d) changes in functional indexes (ref: 1454 cm^{-1} [28])

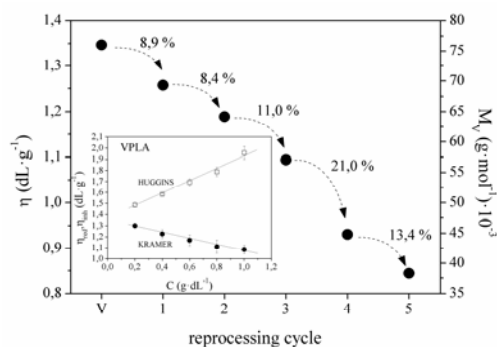


Figure 4. Variation of intrinsic viscosity and molar mass throughout the injection steps.

Insert: Detail of calculation of Huggins and Kraemer plots for the case of VPLA.

Consequently, the viscous molar mass (M_V) was assessed and its evolution correlated to the number of reprocessing cycles, as shown in **Figure 4**. The linear regression values obtained for both Huggins and Kraemer plots for all materials were higher than 0.975. The inset in **Figure 4** shows an example of both plots for the case of VPLA. The M_V decreased steeply with each reprocessing step, with marginal drops around 10 % until the third recyclate and bigger ones afterwards. After 5 reprocessing cycles, a 50 % decrease of M_V ranged from VPLA to RPLA-5. These results indicated a sort of threshold for the structure to resist further thermo-mechanical degradation until 2 reprocessing cycles. Consequently, the macroscopic mechanical performance might be affected, as previously observed. In the next sections, these changes were studied in terms of calorimetric parameters and segmental dynamics.

3.3. The study of the amorphous and crystalline phases of reprocessed PLA.

The cooling scans of VPLA and its further recyclates uniquely showed a glass transition, thus suggesting that reprocessing did not

promoted the apparition of a crystalline phase. This was confirmed by FT-IR analysis, which showed that there was no generation of new bands at 687, 739, 921 and 1293 cm^{-1} , representative of crystalline regions along the reprocessing cycles.

However, the heating scans displayed, besides the glass transition, a cold-crystallization and a subsequent melting, as shown in **Figure 5** for all materials. The calorimetric thermograms were characterized by the key indicators in each region:

- (i) the glass transition temperature (T_G) was calculated as the temperature at the midpoint, according to ISO 11357-2 [31];
- (ii) the cold-crystallization induced by the DSC temperature program was characterised by the induction and peak temperatures (T_{CC0} and T_{CC} , respectively), and the specific cold-crystallization enthalpy (Δh_{CC}), which represents the area between the baseline and the exothermic curve;
- (iii) the melting of the cold-crystallized domains was assessed by the peak temperature (T_M) and the area between baseline and the endotherm, from which the specific melting enthalpy (Δh_M) was obtained.

The variation of these parameters can be seen at **Table 1**. A low reduction of T_G was observed. According to the Fox-Flory relationship [32], this could indicate that the decrease of molar mass induced by reprocessing was not significant enough to reduce dramatically the T_G . Concerning the evolution of T_{CC0} and T_{CC} , a progressive diminution was shown along the successive reprocessing cycles. In addition, a significant increment in Δh_{CC} was found from

VPLA to the first recyclate, to nearly equal values until the last injection cycle. The same trend was found for Δh_M . Quantitatively, it was proved that $\Delta h_M \sim \Delta h_{CC}$ for both virgin and reprocessed PLAs, which meant that all the crystalline domains produced during the cold-crystallization were completely melted. The chain scission due to thermo-mechanical degradation may lead to shorter chains acting as nucleation centres, thus increasing the Δh_{CC} and then modifying the crystallization kinetics and consequently the processability of PLA [33]. All these results were in contrast to those reported in other studies with a PLA with a 8% of D- content and $22 \cdot 10^4 \text{ g} \cdot \text{mol}^{-1}$, which showed a drop of T_G of about $10 \text{ }^\circ\text{C}$ and the presence of crystalline phases in the glassy state, which appeared during cooling. Interestingly, this formation of crystalline domains was reported after the second injection cycle [15].

A deep characterisation of the melting behaviour of these newly formed crystallites was necessary to shed light on the influence of thermo-mechanical degradation. The shape of the endotherms showed a change from a uni-modal to a bi-modal distribution, which is attributed to a superimposed melting-crystallization-melting process, dependant on the kinetics of the temperature program [34-35]. A deconvolution procedure [22] was thus applied to describe both processes with correlation values R^2 higher than 0.952. A partial areas study [9] allowed monitoring the evolution of both crystalline domains as given at **Figure 6**, in terms of peak temperatures (T_M^i) and relative partial areas (A_M^i), where $i=I$ or II were used as labels for the lowest and highest peak temperatures, respectively. It could be seen how both parameters behaved likewise in pairs, describing similar decreasing or increasing profiles. The

peaks were separated progressively until the second recyclate, where the position of the endotherms, characterized by its peak temperature, held unmovable for the rest of recyclates. Simultaneously, the melting of A_M^I decreased progressively reaching almost equal proportions than that of A_M^{II} . The effect of the thermo-mechanical degradation could be ascribed to the variation of the first area A_M^I , which would be indicative of the promoted tendency of crystals to melt, and thus for molten shorter chains to recrystallize. Both overall decreases of $\sim 5 \text{ }^\circ\text{C}$ in T_M^I and $\sim 47 \%$ in A_M^I suggested the presence of weaker cold-crystallized domains along the injection cycles.

Table 1. Results from DSC characterization

Material	T_G ($^\circ\text{C}$)	T_{CC0} ($^\circ\text{C}$)	T_{CC} ($^\circ\text{C}$)	Δh_{CC} ($\text{J} \cdot \text{g}^{-1}$)	Δh_M ($\text{J} \cdot \text{g}^{-1}$)
VPLA	57,2 $\pm 0,1$	106,2 $\pm 1,7$	123,5 $\pm 0,2$	2,21 \pm 0,01	2,19 \pm 0,04
RPLA-1	56,7 $\pm 0,1$	105,6 $\pm 0,3$	117,3 $\pm 0,3$	23,37 $\pm 0,14$	23,83 $\pm 0,67$
RPLA-2	56,5 $\pm 0,2$	102,0 $\pm 0,1$	110,2 $\pm 0,4$	28,52 $\pm 0,34$	29,77 $\pm 1,70$
RPLA-3	56,7 $\pm 0,3$	101,2 $\pm 0,6$	109,1 $\pm 1,0$	28,32 $\pm 0,60$	27,33 $\pm 0,97$
RPLA-4	56,8 $\pm 0,1$	100,1 $\pm 0,3$	107,3 $\pm 0,5$	27,41 $\pm 0,51$	26,94 $\pm 0,52$
RPLA-5	56,6 $\pm 0,1$	99,6 \pm 0,2	106,4 $\pm 0,1$	28,53 $\pm 0,73$	28,31 $\pm 1,04$

The arrangement of these shorter backbones in terms of chain mobility might be the indicators for the variations in the mechanical properties shown at the beginning of the study. Hence, the cooperative movement of PLA chains was investigated by DMTA.

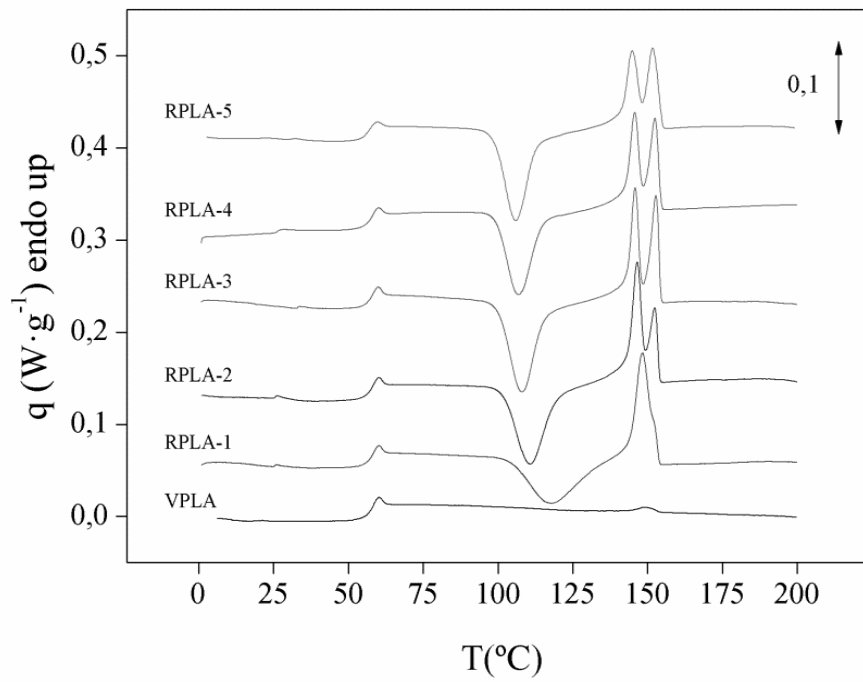


Figure 5. Evolution of the heating DSC thermograms for VPLA and RPLA-i (i:1-5)

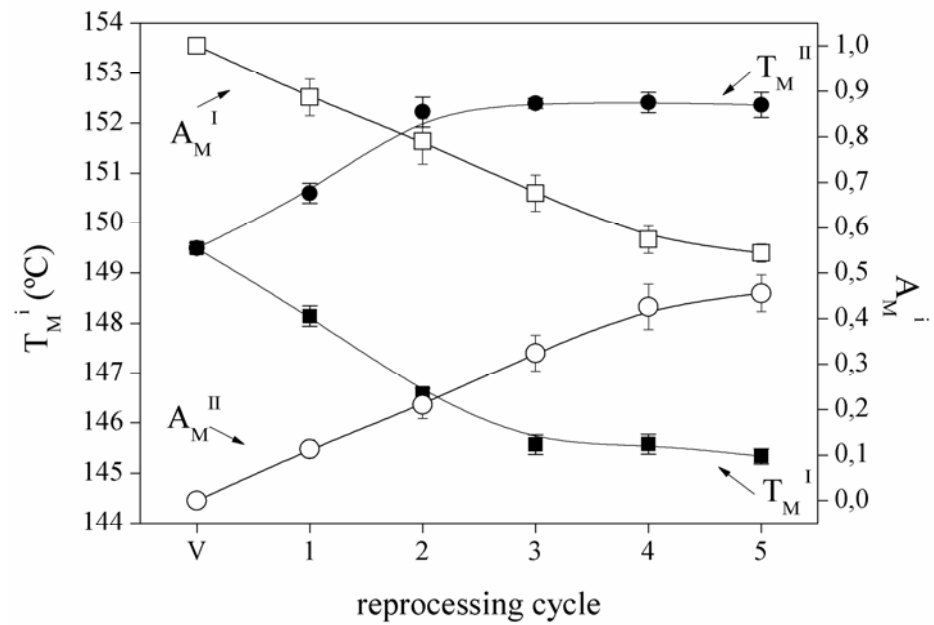


Figure 6. Results of partial area study after deconvolution of the melting region of the DSC scans.

3.4. Viscoelastic behaviour and segmental dynamics

The viscoelastic behaviour of the studied PLA was investigated by DMTA experiments within the glass-rubber relaxation. **Figure 7** shows the isochronal plots of the storage (E') and loss (E'') moduli versus temperature for virgin PLA at the commonly used frequency of 1 Hz. Similar curves were obtained for all the other frequencies, but they are not displayed to avoid visualization matters.

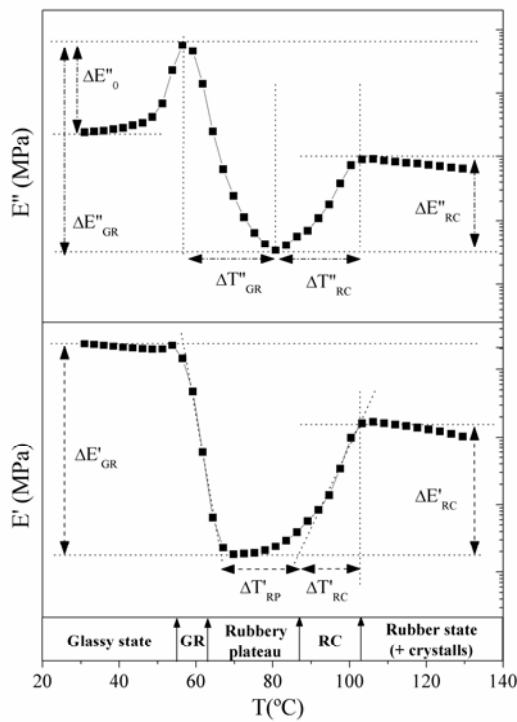


Figure 7. DMTA spectra of VPLA at 1Hz: (upper) loss modulus; (lower) storage modulus

The viscoelastic spectra showed different relaxation zones which were related to the calorimetric transitions along the increasing temperature-axis. At temperatures reaching the glass-rubber relaxation, the PLAs showed a drop in the storage modulus of nearly 99% of the initial value that after a rubbery plateau increased until 5-8 % of the modulus was recovered by the

formation of crystalline phases in the rubber state, regardless the reprocessing cycle or frequency analyzed. The influence of reprocessing can be observed in **Figure 8**, where the DMTA scans of recyclates are shown in comparison with those of VPLA. The parameters used for characterisation were temperature gradients ($\Delta T'_{RP}$, $\Delta T'_{RC}$, $\Delta T''_{GR}$, and $\Delta T''_{RC}$) and mechanical stresses ($\Delta E'_{GR}$, $\Delta E'_{RC}$, $\Delta E''_0$, $\Delta E''_{GR}$, and $\Delta E''_{RC}$) where the subscripts 0, GR, RP and RC stand for initial, glass-rubber transition, rubbery plateau, and recrystallization, respectively. The values averaged from the experiments at all frequencies are given in **Table 2**.

All the temperature gradients showed a decreasing profile. Concerning the evolution of $\Delta T'_{RP}$, a widening of the rubbery plateau due to the addition of chemical crosslinkers to PLA was reported elsewhere [36]. Conversely, the shortening of the rubbery plateau registered in **Table 2** might be indicative of chain cleavage. Likewise, the decrease in $\Delta T'_{RC}$ was related to the presence of shorter chains after each reprocessing cycle, which would speed up the nucleation inducing a cold-crystallization at lower temperatures, as also shown by the DSC results (T_{CC0}). Regarding the evolution of the mechanical stresses, an initial increase up to the second recyclate was shown, and afterwards the values decreased to nearly equal values for RPLA-3,4,5. The origin of these results can be understood in terms of cooperative movement within the amorphous phase throughout the glass-rubber relaxation and thus a deeper inspection into the influence of reprocessing into the glass-forming behaviour of PLA was performed.

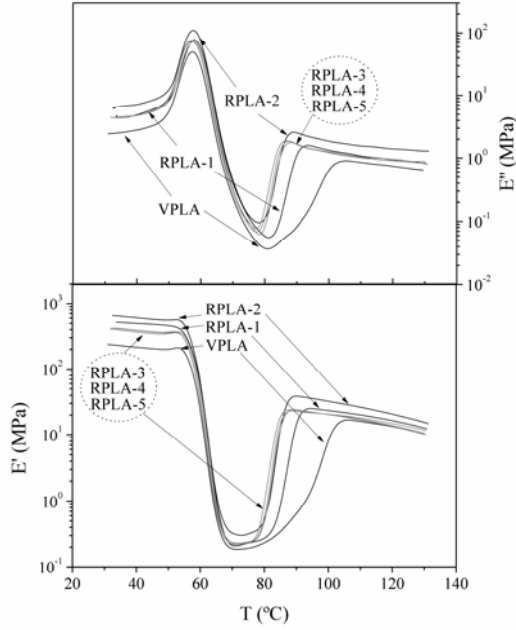


Figure 8. Evolution of storage (lower) and loss (upper) moduli at 1 Hz.

Shortly, a fragile glass-former experiences a dramatic loss of properties (rheological, mechanical...) throughout a specific short temperature interval, such as the glass-rubber relaxation, while a strong glass-former maintains its properties without any significant change. The relaxation of strong systems is generally found to be Arrhenius-like, whereas for fragile systems, it is remarkably non-Arrhenius [37-38] and describable by a Vogel-Fulcher-Tamman-Hesse (VFTH) behaviour [39-41], as shown in Eq. (1)

$$\begin{aligned} \tau(T) &= \tau_0 \cdot \exp\left(\frac{B}{T - T_{VFTH}}\right) \\ &= \tau_0 \\ &\cdot \exp\left(\frac{D \cdot T_{VFTH}}{T - T_{VFTH}}\right) \quad (1) \end{aligned}$$

, where τ are the relaxation times (s), that is $(2\pi f)^{-1}$, and f is the linear frequency of the DMTA tests, τ_0 is a time reference scale, and B (K) and T_{VFTH} (K) are positive parameters specific to the material. T_{VFTH} typically appears 40-60 K below the T_G . It is common to rewrite the

parameter B into $B = D \cdot T_{VFTH}$, where D is an adimensional factor termed as fragility or strength parameter. Qualitatively, D is related to the topology of the theoretical potential energy surface of the system, where fragile systems ($D \leq 6$) present high density of energy minima, contrarily to strong systems ($D \geq 15$) which present lower density. As well, the so-called fragility index m permits an assessment of the deviation of $\tau(T)$ from the Arrhenius behavior of polymers. It varies between two limiting values of 16 and ≥ 200 for strong and fragile glass-formers, respectively [42], and can be obtained by the following expression:

$$\begin{aligned} m &= \left. \frac{d \log(\tau)}{d(T_G/T)} \right|_{T=T_G} \\ &= \frac{B \cdot T}{\ln(10) \cdot (T_G - T_{VFTH})^2} \quad (2) \end{aligned}$$

In order to study the effects of reprocessing on the dynamic fragility of PLA, the relationship of τ with the T_p from the different loss tangentspectra were fitted to the VFTH model, which results with linear correlation R^2 coefficients higher than 0,950 are gathered in **Table 3**, along with the fragility parameters D , B and m . VPLA showed fragile glass-former performance, in agreement with other studies performed on fully amorphous PLA [43]. Up to the second recycle, PLA became more fragile. Afterwards, there was a change in the variation trend. These results were in agreement with the evolution shown by the mechanical stresses, as can be seen in **Table 2**.

The influence of the chemical structure of polymers on their fragility was discussed with detail by *Sokolov et al.* [44]. The changes can be

Table 2. Evolution of parameters drawn from DMTA characterization

Material	Storage modulus				Loss modulus				
	$\Delta E'_{GR}$ (Mpa)	$\Delta E'_{RC}$ (Mpa)	$\Delta T'_{RP}$ (°C)	$\Delta T'_{RC}$ (°C)	$\Delta E''_0$ (Mpa)	$\Delta E''_{GR}$ (Mpa)	$\Delta E''_{RC}$ (Mpa)	$\Delta T''_{GR}$ (°C)	$\Delta T''_{RC}$ (°C)
VPLA	235,49 ± 3,50	19,23 ± 1,44	20,5 ± 3,9	13,5 ± 1,4	62,12 ± 4,99	64,33 ± 4,61	1,30 ± 1,33	24,7 ± 1,5	18,4 ± 2,6
RPLA-1	496,67 ± 4,40	28,82 ± 3,02	14,0 ± 3,4	7,7 ± 0,9	89,85 ± 3,23	94,52 ± 3,29	1,99 ± 1,55	21,9 ± 0,9	9,7 ± 1,5
RPLA-2	612,05 ± 5,89	46,96 ± 6,81	11,2 ± 3,4	6,7 ± 0,9	131,00±8, 16	137,29 ± 7,06	2,68 ± 1,77	19,4 ± 1,0	8,9 ± 2,2
RPLA-3	397,65 ± 5,19	28,84 ± 4,19	11,1 ± 2,8	6,1 ± 0,9	85,33±5,7 9	89,43 ± 5,37	1,61 ± 2,30	18,3 ± 1,2	7,9 ± 1,3
RPLA-4	381,57 ± 4,29	28,33 ± 5,39	10,2 ± 3,6	5,8 ± 1,0	84,00±3,5 0	88,17 ± 2,90	1,92 ± 1,28	19,1 ± 1,5	7,5 ± 1,6
RPLA-5	400,03 ± 9,10	30,16 ± 5,33	9,9 ± 3,7	6,0 ± 0,7	86,57±4,0 2	90,57 ± 3,47	1,77 ± 2,64	18,8 ± 1,5	7,3 ± 1,2

ascribed to the mobility of chains, both physically or chemically, which in turn will affect the cooperative movement and the packing efficiency. An increase in fragility implies higher chain cooperativity and vice versa. Thus, the subsequent calculation of the activation energies related to the glass-rubber relaxation Ea_{GT} , or the free volume coefficient ϕ obtained by means of Eqs. (3) and (4) could picture the change in cooperative movement due to thermo-mechanical degradation.

$$Ea_{GT} = R \cdot \frac{d \ln \tau}{d(1/T)} = \frac{R \cdot B}{\left(1 - \frac{T_{VFTH}}{T}\right)^2} \quad (3)$$

$$\phi = \frac{(T - T_{VFTH})}{B} \quad (4)$$

As can be seen in **Figure 9**, both Ea_{GT} and ϕ displayed a logical contrary behaviour. After the second recyclate, the free volume available

considerably increased (~20 %) which may promote the liability of gases to permeate through the packing defects of the polymer in packaging applications therefore reducing the second-life performance of PLA for similar purposes. The results were in agreement with those from DSC characterization, where a change of tendency in the melting endotherm towards a major presence of weaker crystalline domains was shown from the second to the third recyclate, which may strengthen the idea of a threshold of performance of PLA facing successive reprocessing cycles. As well, the less efficient packing of PLA reprocessed more than 2 times could explain the reduction of the Young Modulus and stress at break found in the study of the macroscopic mechanical properties.

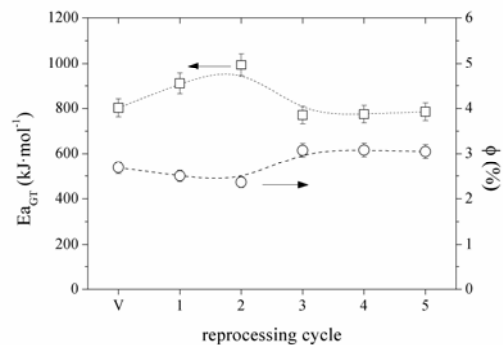


Figure 9. Evolution of apparent activation energy associated to the glass-rubber relaxation and coefficient of free volume

Table 1. Results of fitting the viscoelastic behaviour to VFTH model. Fragility parameters: D, B, m.

Material	VFTH				
	R ²	T _{VFTH} (°C)	D	B (K)	m
VPLA	0,994	15,8 ± 0,4	5,47 ± 0.10	1581	127
RPLA-1	0,972	19,3 ± 2,1	5,55 ± 0,31	1622	143
RPLA-2	0,973	22,0 ± 2,1	5,65 ± 0,92	1655	156
RPLA-3	0,961	25,1 ± 0,9	4,36 ± 0,53	1292	120
RPLA-4	0,964	26,0 ± 1,7	4,32 ± 0,42	1284	120
RPLA-5	0,953	26,1 ± 2,0	4,33 ± 0,31	1283	122

4. Conclusions

Poly lactide (PLA) submitted to in-plant recycling simulation underwent thermo-mechanical degradation which modified its structure and morphology and induced consequences on its thermal and mechanical properties.

Despite non significant changes were drawn from the observation of the functional groups of PLA, a remarkable reduction in molar mass was found. After 5 reprocessing steps, PLA remained amorphous in the glassy state. However, the study of the calorimetric thermograms showed the apparition of a cold-crystallization, which was favoured by the presence of shorter PLA chains due to chain scission processes, particularly after the second reprocessing cycle. In connection, the material offered more free volume favouring the mobility of chains throughout the glass-rubber relaxation, which in macroscopic terms was related to a loss in elastic modulus and stress at break, as indicator of chain scission that also affected the heterogeneity

during processing as shown by the analysis of the surface.

All assessed properties showed a significant loss of PLA performance after the application of the second reprocessing step, thus suggesting a sort of threshold to be recovered by further mechanical recycling.

References

1. Mohanty AK, Misra M, Hinrichsen G. Biofibres, biodegradable polymers and biocomposites: an overview. *Macromolecular Materials and Engineering* 2000; 276: 1-24
2. Tsuji H, Doi Y. *Biopolymers. Polyesters III. Applications and commercial Products*. In: Steinbüchel A, editor. *Biopolymers*. Weinheim : Wiley-VCH Verlag GmbH, 2002.

3. Auras R, Harte S, Selke S. An overview of polylactides as packaging materials. *Macromolecular Bioscience* 2004; 4: 835-865.
4. Al-Salem S M, Lettieri P, Baeyens J. Recycling and recovery routes of plastic solid waste (PSW): A review. *Waste management* 2009;29: 2625-2643.
5. Vilaplana F, Karlsson S. Quality concepts for the improved use of recycled polymeric materials: a review. *Macromolecular Materials and Engineering* 2008; 293: 274-297.
- 6.. The design of a test protocol to model the degradation of polyolefins during recycling and service life. *Journal of Applied Polymer Science* 2009; 112: 1835-1844.
7. Vilaplana F, Ribes-Greus A, Karlsson S. Degradation of recycled high-impact polystyrene .Simulation by reprocessing and thermo-oxidation. *Polymer Degradation and Stability* 2006; 91: 2163-2170.
8. Vilaplana F, Karlsson S, Ribes-Greus A. Changes in the micro-structure and morphology of high-impact polystyrene subjected to multiple processing and thermo-oxidative degradation. *European Polymer Journal* 2007; 43: 4371-4381.
9. Badía JD, Vilaplana F, Karlsson S, Ribes-Greus A. Thermal analysis as a quality tool for assessing the influence of thermo-mechanical degradation on recycled poly(ethylene terephthalate). *Polymer Testing* 2009; 28: 169-175.
10. La Mantia F, Vinci M. Recycling poly(ethylene terephthalate). *Polymer Degradation and Stability* 1994; 45: 121-125.
11. Torres N, Robin JJ, Boutevin B. Study of thermal and mechanical properties of virgin and recycled poly(ethylene terephthalate) before and after injection molding. *European Polymer Journal* 2000;36: 2075-2080.
12. Badía JD, Strömberg E, Ribes-Greus A, Karlsson S. A statistical design of experiments for optimizing the MALDI-TOF-MS sample preparation of polymers. An application in the assessment of the thermo-mechanical degradation mechanisms of poly(ethylene terephthalate). *Analytica Chimica Acta* 2011; 692: 85-95.
13. Badía JD, Strömberg E, Karlsson S, Ribes-Greus A. The role of crystalline, mobile amorphous and rigid amorphous fractions on the performance of recycled poly(ethylene terephthalate) (PET). Manuscript in preparation
14. Zenkiewicz M, Richert J, Rytlewski P, Moraczewski K, Stepczynska M, Karasiewicz T. Characterisation of multi-extruded poly(lactic acid). *Polymer Testing* 2009; 28: 412-418.
15. Pillin I, Montrelay N, Bourmaud A, Grohens Y. Effect of thermo-mechanical cycles on the physico-chemical properties of poly(lactic acid). *Polymer Degradation and Stability* 2008; 93: 321-328.
16. Carrasco F; Pagès P; Gámez-Pérez J; Santana OO, MasPOCH ML. Processing of poly(lactic acid): Characterization of chemical structure, thermal stability and mechanical properties. *Polymer Degradation and Stability* 2010; 95: 116-125.
17. Carrasco F, Pagès P, Gámez-Pérez J, Santana OO, MasPOCH ML. Kinetics of the thermal decomposition of processed poly(lactic acid).

Polymer Degradation and Stability 2010;95:2508-2514

18. Alves NM, Mano JF, Gómez-Ribelles JL. Molecular mobility in polymers studied with thermally stimulated recovery. II. Study of the glass transition of a semicrystalline PET and comparison with DSC and DMA results. *Polymer* 2002;43: 3627-3633.

19. Zuza E, Ugartemendia JM, López A, Meaurio E, Lejardi A, Sarasua JR. Glass transition behavior and dynamic fragility in polylactides containing mobile and rigid amorphous fractions. *Polymer* 2008; 49: 4427-4432.

20. Arnoult M, Dargent E, Mano JF. Mobile amorphous phase fragility in semi-crystalline polymers: comparison of PET and PLLA. *Polymer* 2007;48: 1012-1019.

21. ISO 527-2: Plastics -- Determination of tensile properties -- Part 2: Test conditions for moulding and extrusion plastics. 1993.

22. Santonja-Blasco L, Moriana R, Badía JD, Ribes-Greus A. Thermal analysis applied to the characterization of degradation in soil of polylactide: I. Calorimetric and viscoelastic analyses. *Polymer Degradation and Stability* 2010; 95: 2185-2191.

23. ISO 291. Plastics - standard atmospheres for conditioning and testing. 1997

24. ISO 179-1 Plastics -- Determination of Charpy impact properties -- Part 1: Non-instrumented impact test. 2010.

25. Kister G, Cassanas G, Vert, M. Effects of morphology, conformation and configuration on the IR and Raman spectra of various poly(lactic acid)s. *Polymer* 1998; 39: 267-272.

26. 1628-1:2009, ISO. Determination of the viscosity of polymers in dilute solution using capillary viscometers -- Part 1: General principle.

27. Spinu M, Jackson C, Keating M Y, Gardner K H. Material Design in Poly(Lactic Acid) Systems: Block Copolymers, Star Homo- and Copolymers, and Stereocomplexes. *Journal of Macromolecular Science, Pure Applied Chemistry* 1996; 33: 1497-1530.

28. Levenberg K. A method for solution of certain non-linear problems in least squares. *Quarterly of Applied Mathematics* 1944; 2: 164-168.

29. Marquardt D. W. An algorithm for the least-squares estimation of non-linear parameters. *SIAM Journal of Applied Mathematics*, 1963; 11: 431-441.

30. Badía J.D., Strömberg E, Ribes-Greus A, Karlsson S. Assessing the MALDI-TOF MS sample preparation procedure to analyze the influence of thermo-oxidative ageing and thermo-mechanical degradation on poly (lactide). *European Polymer Journal*. In press.

31. ISO 11357-2 Plastics. Differential Scanning Calorimetry. Part 2- Determination of the glass transition. 1999.

32. Fox T.G., Flory P.J. Second-order transition temperatures and related properties of polystyrene, *Journal of Applied Physics* 1950; 21: 581-591

33. Pantani R, De Santis F, Sorrentino A, De Maio F, Titomanlio G. Crystallization kinetics of virgin and processed poly(lactic acid). *Polymer Degradation and Stability* 2010; 95: 1148-1159.

34. Yasuniwa M, Tsubakihara S, Sugimoto Y, Nakafuku C. Thermal analysis of the double-

- melting behavior of poly(l-lactic acid). *Journal of Polymer Science: Part B: Polymer Physics* 2004; 42: 25-32.
35. Pan P, Kai W, Zhu B, Dong T, Inoue Y. Polymorphous crystallization and multiple melting behavior of poly(L-lactide): Molecular weight dependence. *Macromolecules* 2007; 40: 6898-6905.
36. Yang S L, Wu Z H, Yang M B. Thermal and mechanical properties of chemical crosslinked polylactide (PLA). *Polymer testing* 2008; 27: 957-963.
37. Godard M.E., Saiter J.M. Fragility and non-linearity in polymethyl(α -n-alkyl)acrylates. *Journal of Non-Crystalline Solids* 1998; 23: 635-639.
38. Saiter A, Hess M, D'Souza NA, Saiter JM. Entropy and fragility in vitreous polymers. *Polymer* 2002; 43: 7497-7504.
39. Vogel H. The temperature dependence law of the viscosity of fluids. *Phys Z* 1921; 22: 645-646.
40. Fulcher G.S. Analysis of recent measurements of the viscosity of glasses. *Journal of the American Ceramic Society* 1925; 8: 339-355.
41. Tammann G, Hesse G. The dependence of viscosity upon temperature of supercooled liquids. *Z AnorgAllg Chem.* 1926; 156: 245-257.
42. Vilgis T.A.. Strong and fragile glasses: A powerful classification and its consequences. *Physical Review B* 1993; 47: 2882-2885.
43. Mijovic J, Sy J W. Molecular dynamics during crystallization of poly(l-lactic acid) as studied by broad-band dielectric relaxation spectroscopy. *Macromolecules* 2002; 35: 6370-6376.
44. Kunal K, Robertson C. G, Pawlus S, Hahn S. F, Sokolov A. P. Role of Chemical Structure in Fragility of Polymers: A Qualitative Picture. *Macromolecules* 2008; 41: 7232-7238.

8. REMARKABLE RESULTS

The application of mechanical recycling as a means of material valorization for both commercial poly(ethylene terephthalate) (PET) and polylactide (PLA) affected their structure in terms of oligomeric distribution and functional groups, and subsequently modified their thermal and mechanical performance. The application of several methodologies and analytical strategies was useful to determine degradation indicators that can be used as quality parameters for testing the suitability of reprocessed PET and PLA to be re-used several times. Several conclusions were drawn, concerning the following issues:

Application of methodologies and analytical strategies

The use of a design of Experiments DoE was useful to optimize the sample preparation for MALDI-TOF MS experiments with PET and PLA. Matrix, analyte-to-matrix proportion and use of cationization agent were suitable parameters to be considered as factors for the DoE analysis. As well, the analysis of quality parameters of the MALDI signal such as Signal-to-Noise ratio (S/N) and Resolution (RES) and the use of Main Effects and Interaction Effects Plots were to be useful for understanding the influence of all factors at different experimental settings. The best combination of levels and factors for the MALDI-TOF MS sample preparation of PET was: matrix (dithranol), proportion analyte/matrix/cationization agent (1/15/1 V/V/V), and concentration of cationization agent ($2\text{g}\cdot\text{L}^{-1}$). For the case of PLA: matrix (s-DHB), proportion analyte/matrix (1/5 V/V), without need of cationization agent.

The application of a three-fraction model, involving rigid amorphous (RAF) and crystalline (C) and mobile amorphous (MAF) fractions was useful to understand the effects of reprocessing on the performance of PET.

The monitoring of the crystallization during cooling in the case of PET and the cold-crystallization during heating in the case of PLA was helpful to monitor the occurrence of chain scissions during thermo-mechanical degradation. Onset and peak crystallization temperatures were appointed as suitable degradation indicators. Particularly for the case

of PLA, the monitoring of the mechanical recovery due to recrystallization during heating was also significant.

The use of a deconvolution procedure applied to the melting endotherm of both PET and PLA, along with a partial areas study permitted assessing the evolution of the newly formed crystalline phase. The partial crystallinity and the partial areas were appointed as reliable monitoring parameters, particularly those at the lowest temperatures, corresponding to the crystalline domains of lowest lamellar size.

The study of the segmental dynamics around the glass-rubber relaxation showed the relevance of the dynamic parameters, the apparent activation energy or the free-volume coefficient to explain the effects of reprocessing in terms of chain mobility and connectivity.

Structural changes

In the case of PET, MALDI-TOF-MS and FTIR showed that the ether links units acted as potential reaction sites, since they were mainly driven by the reduction of diethylene glycol to ethylene glycol units in the flexible part of the PET backbone ($[\text{GT}_\text{C}]_n\text{-G} \rightarrow [\text{GT}_\text{C}]_n$), and chain scission processes that produced -OH terminated species with shorter chain length, giving rise to hydroxyl and carboxyl terminated species ($\text{H-}[\text{GT}_\text{L}]_n\text{-GH}$ and $\text{H-}[\text{GT}_\text{L}]_n\text{-OH}$). In the case of PLA, the degradation primarily affected to initially predominant cyclic $[\text{LA}_\text{C}]_n$ and linear $\text{HO-}[\text{LA}_\text{L}]_n\text{-H}$ species. Thermo-mechanical degradation seemed to occur giving rise to a noticeable major abundance of $\text{CH}_3\text{-O-}[\text{LA}_\text{L}]_n\text{-H}$ groups after the second recycle.

General paths for thermo-mechanical degradation were proposed for both polymers, pointing out the action of intramolecular transesterifications and homolytic scissions.

Microstructural changes

According to a two-fraction model, considering amorphous and crystalline phases, multi-extruded PET showed a significant increase in crystallinity. Deeply, the new crystal populations started to segregate from the first recycle on.

Regarding multi-injected PET, according to a three-fraction model, an important increase in RAF after the second reprocessing was shown, connected to a loss of MAF. The crystalline fraction was formed earlier and steeper after each reprocessing step and towards the formation of domains with smaller lamellar thickness at lower temperatures.

Conversely, multi-injected PLA did not show formation of crystalline domains due to reprocessing. However, during the cold-crystallization of the DSC experiment, suggested the apparition of shorter chains after each processing cycle.

Effects on segmental dynamics

The packing behavior after rearrangement showed different effects for PET and PLA. The former presented a decoupling of mobile and rigid phases, with an increase in free volume and a decrease in dynamic fragility. The latter showed bigger resistance to changes due to its amorphous character, but after the second recycle, more packing defects (although in less extent than that shown by PET) were found.

Influence on the mechanical performance

In the case of PET, the rigid amorphous phase acted as initiator of crystallinity during the strain of the tensile testing, caused a significant decrease in the mechanical parameters (stress and strain at break), in comparison to those shown by PLA (inherently lowest than those of PET). The increase of crystalline fraction acted as a topological constraint for the impact of PET, while the amorphous PLA did not showed a critical drop of impact properties, being its properties at break reduced particularly after the second reprocessing step.

Recyclability of PET and PLA

Whereas PET experienced an overall loss of properties after the first reprocessing step, PLA maintained its properties up to two reprocessing cycles. Once achieved this sort of threshold, the properties of PET decayed in a higher extent than those of PLA, thus concluding the better recyclability of PET by means of material valorization.

CHAPTER IV

ENERGETIC VALORISATION

Modeling the behavior of PET and PLA for
pyrolysis and combustion systems

CHAPTER IV: ENERGETIC VALORISATION

CONTENTS

1. Chemical recycling with energetic valorisation	307
1.1. Pyrolysis	303
1.2. Gasification	305
1.3. Incineration	307
2. Thermolysis of PET and PLA	313
2.1. Thermal and thermo-oxidative decomposition mechanisms of PET	313
2.2. Thermal and thermo-oxidative decomposition mechanisms of PLA	319
2.3. Approaching pyrolysis and gasification of plastics by TGA.	321
3. References in this chapter	323
4. Contributions in this thesis	329
CONTRIBUTION IV-A: <i>Detailed methodology to assess the thermal stability and kinetics of thermal and thermo-oxidative decomposition behaviours of reprocessed poly(ethylene terephthalate)</i>	331
CONTRIBUTION IV-B: <i>Assessing the thermal stability, thermal and thermo-oxidative decomposition behaviours of reprocessed polylactide for the packaging industry</i>	369
5. Remarkable results	399

1. CHEMICAL RECYCLING AND ENERGETIC VALORISATION

Chemical (tertiary) recycling refers to advanced technological processes which convert plastic materials into smaller molecules, usually liquids or gases, which are suitable for being used as a feedstock for the production of new petrochemicals and plastics. The term *chemical* is used, due to the fact that an alteration is bound to occur to the chemical structure of the polymer. Products of chemical recycling have proven to be useful as fuel. The technology behind its success is the depolymerization process, that can result in a very profitable and sustainable industrial scheme, providing a high product yield and minimum waste ⁽¹⁾.

By definition, **energy recovery/valorisation** implies burning waste to produce energy in the form of heat, which may be converted into steam and electricity by a conventional thermoelectric plant. This is only considered a very sensible way of waste treatment, when material recovery processes fail due to economical constraints. Plastic materials possess a very high calorific value when burned; especially when considering that they are derived from crude oil. Table 4.1 illustrates the calorific value of a number of single-polymer plastics, compared to oil and household Plastic Solid Waste (PSW). Since the heating value of plastics is high, they make a convenient energy source such as heating oil and coal. Producing water and carbon-dioxide upon combustion make them similar to other petroleum based fuels ⁽²⁾.

The fraction of plastic waste from packaging treated by chemical recycling/energy recovery has increased up to twice the recovered amount registered a decade ago ⁽⁵⁾ in Europe, as can be seen at Fig 4.1. From the packaging fraction, those goods that come from domestic uses represent almost 90 % of the total rates, being the commercial and industrial packaging plastic waste recovered in fewer ratios. Despite the consciousness campaigns addressed to consumers, it is not transmitted to the industrial field. In addition, there is still some lack of waste management devoted to industrial plastic waste, and therefore it should be a sector to be enhanced.

Table 4. 1. Calorific value of some major plastics compared to common fuels. Adapted from refs (3-4)

Item	Calorific value (MJ·kg ⁻¹)
polyethylene	43.3-46.5
polypropylene	46.50
polystyrene	41.90
poly(ethylene terephthalate)	22.00
household PSW mixture	31.80
kerosene	46.50
gas oil	45.20
heavy oil	42.50
petroleum	42.30
coal	29.20

In comparison with other plastic fractions, chemical recycling is completely directed to packaging goods, while for energetic valorisation, it represents a 60 % of the total amount of plastic waste, as shown in Fig 4.2, followed by plastics coming from the building and demolition sector and from electric and electronic waste⁽⁵⁾.

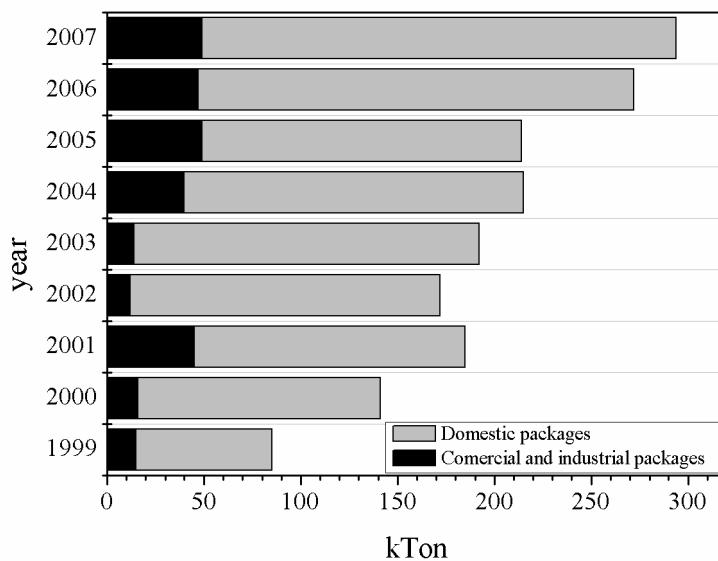


Figure 4. 1.Recovery ratio of packages in Europe by chemical recycling / energetic valorisation. Adapted from ref (5).

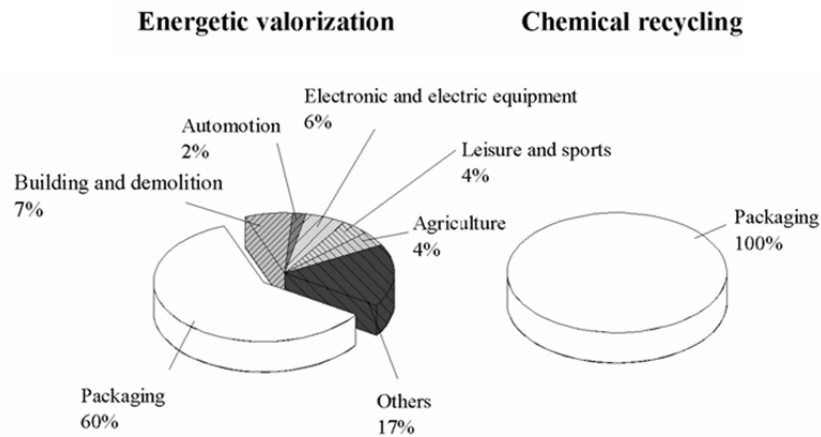


Figure 4. 2. Distribution of goods recovered by chemical recycling and energetic valorisation in Europe. Adapted from ref. (5).

In Spain, the energetic recovery represents a 13% of the total plastic waste management, which is far away from the values of other European countries, such as Norway and Sweden, with values close to 60 %, and further from more energetic recovering countries like Switzerland or Denmark, where it represents the main recovery option ⁽⁵⁾, as can be drawn from Fig 4.3. Therefore, this recovery procedures represent an established reality and efforts must be addressed for achieving the optimal figures, in both material and/or energy recovery terms.

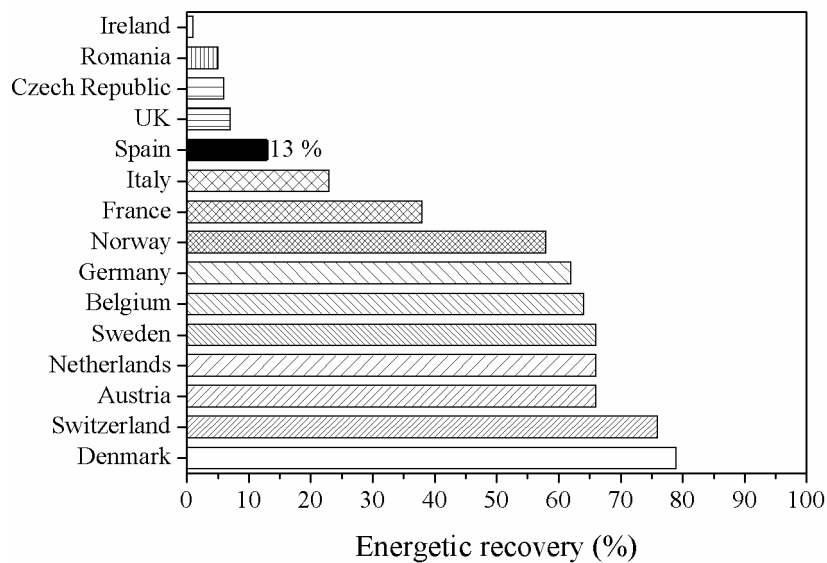


Figure 4. 3. Energetic recovery ration in European countries. Adapted from ref. (5).

In the field of plastics recovery, the terms chemical recycling and energy recovery are indiscriminately used to refer to the same processes and therefore lead to confusion. In general, the nomenclature could be distinguished more clearly if the recovery of the material could be assigned to **material valorisation** (if feedstock for further synthesis or polymerization is obtained) or **energetic valorisation** (if at the end of the process, energy in form of heat or electricity is achieved). Fig 4.4 comprises the chart-flow that plastic waste can follow through chemical/energetic recycling. This chapter focuses on the grey-shaded area, studying the thermal decomposition processes of plastic waste by means of **thermolytic processes**.

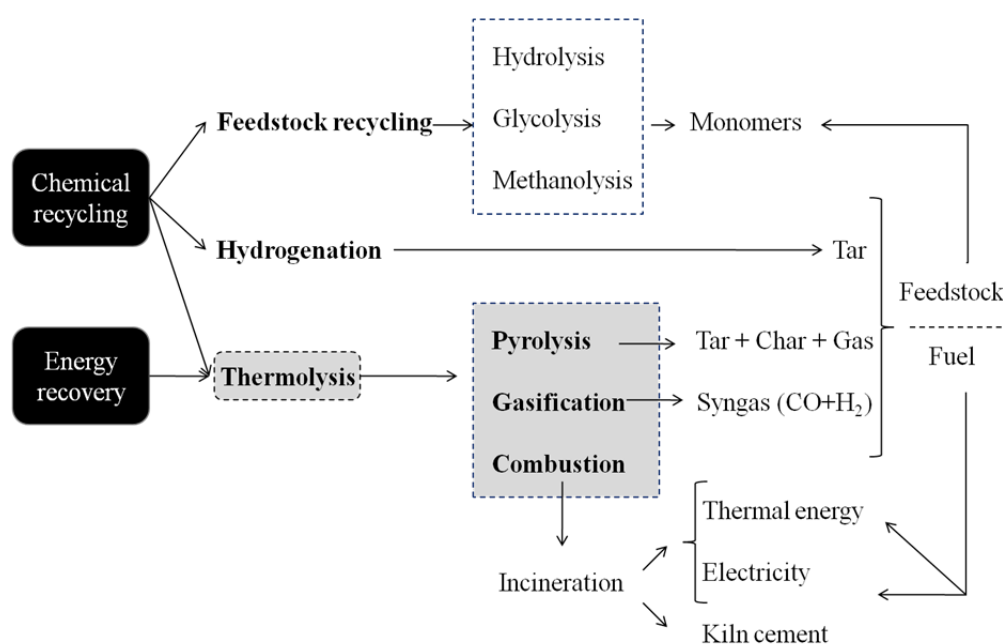


Figure 4. 4. Chemical recycling and energetic valorisation. Scheme of technologies.

Under the category of chemical recycling advanced processes, similar to those employed in the petrochemical industry, appear **pyrolysis**, gasification, **combustion**, liquid–gas hydrogenation, viscosity breaking, steam or catalytic cracking and the use of plastic solid waste as a reducing agent in blast furnaces ⁽⁶⁾. Much attention has been paid to chemical recycling (mainly non-catalytic thermal cracking - **thermolysis** -, catalytic cracking and steam degradation) as a method of producing various fuel fractions from Plastic Solid Waste (PSW). By their nature, a number of polymers are advantageous for such treatment. **Condensation polymers** such as poly (ethylene terephthalate) (PET) undergo degradation to produce monomer ⁽⁷⁾ units (which is termed as feedstock or monomer recycling), while **vinyl polymers** such as polyolefins produce a mixture containing

numerous components for use as a **fuel**. There is also a growing interest in developing value added products such as synthetic lubricants via PE thermal degradation ⁽¹⁾. Various degradation methods for obtaining petrochemicals are presently under investigation, and conditions suitable for pyrolysis and gasification are being researched extensively ⁽⁶⁾. Advanced thermo-chemical treatments of PSW in the presence of heat under controlled temperatures (thermolysis) provide a viable and an optimum engineering solution, with the **reduction of landfilling as an added advantage** ⁽⁶⁾. Not only healthy monomer fractions can be recovered up to 60% ⁽⁸⁾, but also valuable petrochemicals can be produced, which could be summarized as:

- **gases** (rich with low cut refinery products and hydrocarbons)
- **tars** (waxes and liquids very high in aromatic content)
- **char** (carbon black and/or activated carbon)

In general, post-consumer plastic waste consists of a variety of long chain polymer molecules, chemical contaminants and hetero-atoms such as chlorine, oxygen or nitrogen. Physical impurities like fillers, pigments or adhered dirt are present as well as larger inorganic material, arising from incomplete sorting, such as aluminium foil. In order to use this waste as feedstock for new plastics or fuel components, the following **problems need to be overcome** ⁽⁴⁾:

- Long polymer chains have to be cracked.
- Hetero-atoms need to be chemically separated.
- Inorganic particles have to be mechanically separated.
- Larger inorganic particles have to be discharged from the process in order to prevent the process to be blocked by, as well as to avoid the erosion of pipes and pumps.

If a recycler is considering a recycling scheme with 40% target or more, one should deal with materials that are very expensive to separate and treat. Actually, such recycling rates mean that the recyclers are dealing with more contaminated (commingled) material which is very costly to separate, thus promoting tertiary recycling technologies as viable solutions ^(9; 4). However, petrochemical plants are much greater in size (6–10 times) than plastic manufacturing plants. It is essential to utilize petrochemical plants in supplementing their usual feedstock by using PSW derived feedstock ⁽⁴⁾.

The development of value added recycling technologies is highly desirable as it would increase the **economic incentive to recycle polymers** ⁽¹⁰⁾. Several methods for chemical recycling are presently in use, such as direct chemical treatment involving gasification, smelting by blast furnace ⁽¹¹⁾ or coke oven ⁽¹²⁾. The main **advantage of chemical recycling/energetic valorisation** is the possibility of treating heterogeneous and contaminated polymers with limited use of pre-treatment. These technologies are predicted to grow worldwide by 30% until 2015 ^(13; 14). Generally, first products yielded are usually in the range of C₂₀ to C₅₀. These products are cracked in the gas phase to obtain lighter hydrocarbons, as ethene and propene, which are unstable at high temperatures and react to form aromatic compounds as benzene or toluene. If the residence time is long, coke, methane and hydrogen form ⁽¹⁵⁾. Long residence times of volatiles in reactors and high temperatures decrease tar production but increase char formation ⁽¹⁶⁾. The main disadvantage of plastic pyrolysis and gasification is that it is necessary to control the content of impurities and chloride, in case PVC is present in the feedstock, as well as the risk of bad fluidization because of particle agglomeration ⁽¹⁷⁾. It is reported that increasing temperatures above 500 °C and prolonging the gas residence time, result in a reduction in tar content of the gas product from both pyrolysis and gasification of PSW, and even mixtures of coal, biomass and PSW ⁽¹⁸⁾. In fact, at temperatures above 800 °C larger paraffins and olefins produced from decomposition of plastics are cracked into H₂, CO, CO₂, CH₄ and **lighter hydrocarbons** ⁽¹⁹⁾. As a result of methyl-group abstraction from aromatics and decomposition of paraffins, C₂H₄ and C₂H₂ are typically reported to increase with temperature ⁽²⁰⁾. The abstraction of methyl groups and hydroxyl groups from aromatic structures implies that the aromatic fraction does increase with temperature even though the total amount of tar decreases.

Both **pyrolysis** and gasification could be further utilized in industry in a more engineered and designed end-product fashion. Up till now, most pyrolysis and gasification processes applied on an industrial scale lack a designed end-product manner. Both processes could be improved by more appropriate scale-up and a detailed analysis of the products produced. **Many of the products yielded by pyrolysis and gasification are well marketed**. But a fact remains that an even larger market is now emerging for residual solids, to be utilized as carbon black or activated carbon. Although large industrial scale units do exist for both pyrolysis and gasification, a fact remains that most of them could perform more effectively targeting certain products depending on feedstock, market

performance and demand. All of such issues could be solved by end-product unit design⁽¹⁾.

Thermal decomposition schemes on the end-product (employing lumped product yield) are an essential step to develop and validate⁽⁶⁾. Advances in that area will aid in the improvement of pyrolysis and gasification reactors. Since, in this thesis, the pyrolysis and gasification processes are approached, a short description is detailed hereby. Afterwards, a short description on the incineration process is given, since this option is progressively being adopted as recovery system.

1.1. PYROLYSIS

The pyrolysis process is an advanced conversion technology that has the ability to produce a **clean, high calorific value gas** from a wide variety of waste and biomass streams, by thermal cracking of polymers in **inert atmospheres** at temperatures up to 800 °C. A detailed description of the technologies and experiences of PSW recycling via pyrolysis facilities can be found elsewhere⁽⁴⁾.

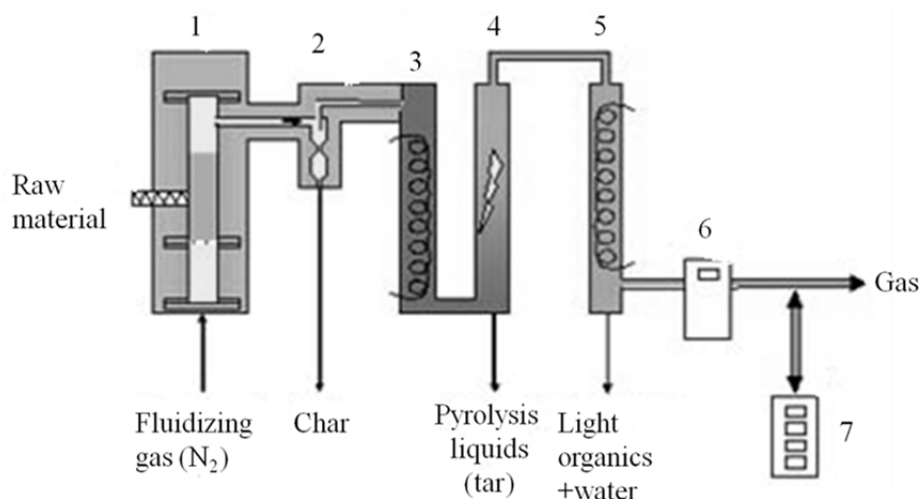


Figure 4. 5. Classic pyrolysis scheme in a fluidized bed reactor (1: reactor-screw feeding; 2: cyclones; 3: gas cooler; 4: electrostatic precipitator; 5: gas cooler; 6: dry gas meter; 7: gas analyzer for CO, CO₂, H₂, CH₄, C₂-C₅ hydrocarbons). Source: Bioenergy-NoE⁽²¹⁾

Fig 4.5 schematically shows a typical pyrolysis facility. The hydrocarbon content of the waste is mainly converted into a **gas**, which is suitable for utilization in either gas engines, with associated electricity generation, or in boiler applications without the need for flue gas treatment. This process is capable of treating many different solid hydrocarbon-based wastes while producing a clean fuel gas with a high calorific value. This gas will typically have a calorific value of **22–30 MJ·m⁻³** depending on the waste material being processed. The lower calorific value is associated with biomass waste, while higher calorific values are associated with other wastes such as sewage sludge. Gases can be produced with higher calorific values when the waste contains significant quantities of synthetic materials such as rubber and plastics.

The **solid char**, which contains both carbon and the mineral content of the original feed material, can either be further processed onsite to release the energy content of the carbon, or utilized offsite in other thermal processes.

Pyrolysis provides a number of **advantages** ⁽⁴⁻⁶⁾, such as

- **Operational advantages:**
 - The energy consumption of the pyrolysis process is very low. It is considered that a maximum of about 10 % of the energetic content of the plastic waste is used to convert the scrap into petrochemical products.
 - Utilisation of residual output of char used as a fuel or as a feedstock for other petrochemical processes.
 - The pyrolysis process operates without the need of air or admixtures of hydrogen.
 - It does not involve elevated pressures.
- **Environmental advantages:**
 - The process can handle plastic waste that cannot be efficiently recycled by alternative means.
 - Pyrolysis provides an alternative solution to landfilling and reduces greenhouse gases (GHGs) and CO₂ emissions.
- **Financial benefits:**
 - Pyrolysis produces a high calorific value fuel that could be easily marketed and used in gas engines to produce electricity and heat.

- If HCl from PVC is formed as by-product of the process, it can be recovered and used as raw material.
- **In comparison to incineration:**
 - There is a 5 to 20 times reduction in the volume of product gases, which is translated into a considerable reduction in gas conditioning facilities.
 - Pollutants and contaminants become concentrated in a coke-like matrix.
 - Since pyrolysis is a closed system, no pollutants can escape.

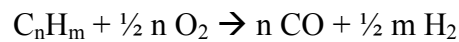
Several **obstacles and disadvantages** do exist for pyrolysis, mainly the handling of char produced ⁽²²⁾ and treatment of the final fuel produced if specific products are desired. Actually, mainly linear C₁₅-C₄₀ hydrocarbons are obtained, without a significant amount of calorific groups such as ramified, cyclic or aromatic compounds. Therefore, posterior catalytic cracking and reforming procedures have to be applied to obtain a valuable product. On the other hand, the char could be utilized in producing activated carbon with the application of steam, typically in an onsite Fluidized Bed Reactor. The derived oils maybe used as fuels or petroleum refinery feedstock after upgrading by means of processes such as steam or hydrogen cracking, quenching or middle cut distillation ⁽⁶⁾. In addition, there is not a sufficient understanding of the underlying reaction pathways, which has prevented a quantitative prediction of the full product distribution.

Pyrolysis has been investigated as a viable route of recycling by a number of researchers for the case of PSW treatment ⁽⁸⁾, or other waste including biomass ⁽²³⁾ and rubbers ⁽²⁴⁾. An updated review of the literature performed by *Al-Salem et al* ⁽⁶⁾, which refers to pyrolysis studies performed to PSW, is recommended for further information.

1.2. GASIFICATION

Declining landfill space and high incineration cost of Municipal Solid Waste (MSW) encourages research and development in thermolysis technologies, which gasification fall into, producing fuels or combustible gases from waste ⁽²⁵⁾. Gasification of waste is

performed at higher temperatures than pyrolysis (up to 1300 °C) and with the controlled addition of oxygen⁽⁴⁾. The basic gasification reaction is as follows:



Air in this process is used as a **gasification agent**, which demonstrates a number of advantages. The main advantage of using air instead of O₂ alone is to simplify the process and reduce the cost. But a disadvantage is the presence of inert N₂ in air which causes a reduction in the calorific value of resulting fuels due to the dilution effect on fuel gases. Hence, steam is introduced in a stoichiometric ratio to reduce the N₂ presence⁽¹⁾.

The primary product is a gaseous mixture of carbon monoxide and hydrogen. This gas mixture is known as **syngas**, and can be used as a substitute for natural gas. Additionally, a significant amount of **char** is always produced in gasification which needs to be further processed and/or burnt. This inorganic ash is bounded into a glassy matrix which can be used as a component in concrete or mortar due to its high acid resistance⁽⁴⁾.

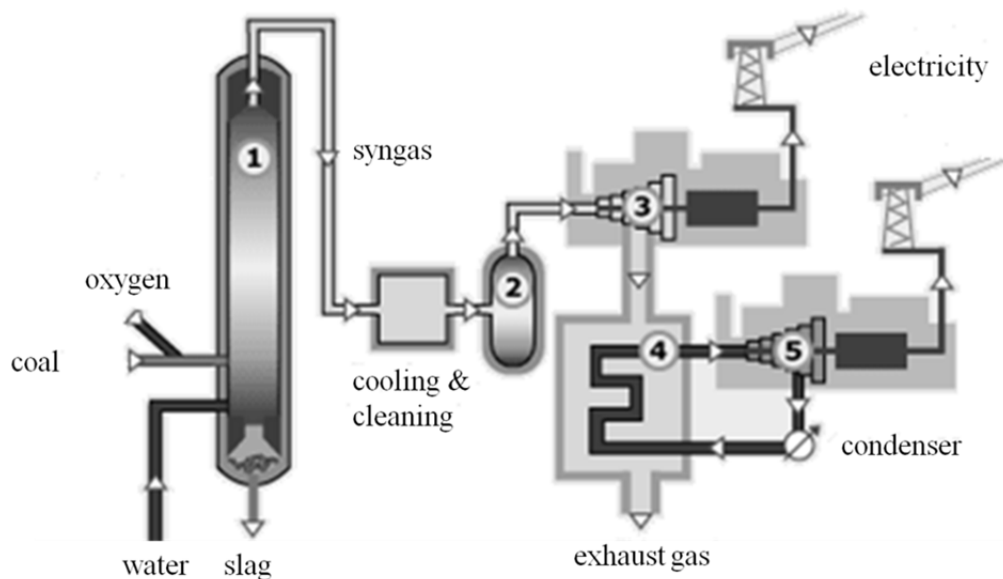


Figure 4. 6. Gasification process of coal (1: Gasification of feedstock into syngas; 2: Syngas burnt in combustor; 3: Hot gas drives into turbines; 4: Cooling gas heats water; 5: Steam drives steam turbines.)

Source: World coal institute⁽²⁶⁾

Fig 4.6 schematizes a classic gasification system in which coal is used as feedstock, as an example for gasification of other feedstocks as plastic waste. Several types of gasification processes have already been developed and reported⁽⁶⁾. Their practical performance data, however, have not necessarily been satisfactory for universal application. Pilot-scale

gasification schemes use a great deal of expensive pure oxygen, while others need considerable amounts of expensive materials such as coke and limestone, and deposit much sludge from which metals cannot be separated. **An ideal gasification process for PSW should:**

- produce high calorific value gas
- yield completely combusted char
- not require any additional installations for air/water pollution abatement

Gasification can be distinguished from incineration by its better environmental issues and more attractive economics. In addition, gasification does not yield pollutants such as dioxins or aromatic volatiles, due to the use of high temperatures and low oxygen partial pressure in its operational parameters ⁽⁴⁾.

Early gasification attempts of PSWs have been reported since the 1970s ^(27; 28). The gasification into high calorific value fuel gas obtained from PSW was demonstrated in research stages and results were reported and published in literature for PVC ⁽²⁹⁾, PP ⁽³⁰⁾ and PET ⁽³¹⁾. Also a need for utilizing as much waste as possible to treat in co-gasification is something that captured the attention of many researchers. The need for alternative fuels has lead for the **co-gasification of PSW** with other types of waste, mainly biomass. Further reading of common gasification technologies, described by *Scheirs* ⁽⁴⁾, is suggested for supplementary information.

1.3. INCINERATION

Incineration involves the burning of polymers, and therefore the knowledge of the thermal behaviour of plastics is remarkable. To perform incineration in an environmentally desirable way, the liberated energy should be captured and used, usually to generate electricity in a “trash-to-energy” facility. Polymers are an excellent fuel, with heating value comparable to oil and better than coal and most components of trash. The principal products of complete burning of most polymers are **water** and **carbon dioxide**, which are relatively environmentally benign (other than effects of CO₂ as a greenhouse gas). From a thermodynamic point of view, trash-to-energy procedures are superior in

that the energy content of the plastic is recovered, so beyond reuse and recycling, it is a viable approach, provided the polluting aspects can be eliminated ⁽¹⁾.

In general, it is considered that incineration of PSW results in a volume reduction of 90–99%, which reduces the dependence on landfilling. With the development of waste management assessment methods, such as Life Cycle Assessment (LCA), it is now easier to compare material recovery with energy recovery case-by-case ⁽⁶⁾. LCA is best defined as an objective process to evaluate the environmental impact associated with a product, process or activity, by identifying and quantifying energy and materials used and waste released to the environment. LCA evaluates and implements opportunities to allow environmental improvements ⁽³²⁾. Energy resources and their sustainable development require a supply of energy resources that are available at a reasonable cost and can cause no negative societal impacts. Thus, it is elementary to recognize high calorific value waste, namely PSW, as a valuable feedstock and an energy resource ⁽⁶⁾. Although polyesters like PET have aromatic structures in the polymer chain they are very combustible materials. The ease of release of highly combustible aliphatic gases, e.g. acetaldehyde, ethylene, dioxane, THF, butadiene, and the low tendency to crosslink and char are the main reasons for the high flammability ⁽³³⁾.

Fig 4.7 shows a typical scheme for an incineration facility. The PSW can be burned on its own or can be part of a mixed combustible fraction to be used in solid fuel fired boilers and power plants. An engineering approach to improve the waste incineration efficiency is to separate pyrolysis from actual combustion and burnout processes of the waste ⁽³⁴⁾. In industrial scale treatment schemes, external separation requires pyrolysis reactors with firing products (e.g. char, waxes, etc.). Incineration of PSW allows steam for heating or for electricity generation, as well as heat recovery from flue gases. Different facilities and technologies have been developed ⁽³⁵⁾. Essentially, energy recovery in incineration plants from plastic waste can be found in several forms, such as ⁽⁴⁾:

- Part of the incineration of municipal solid waste (MSW).
- Through mono-combustion.
- Through co-combustion with traditional fossil fuels.
- As a fuel in cement kilns, used as partial substitute for coal or coke.

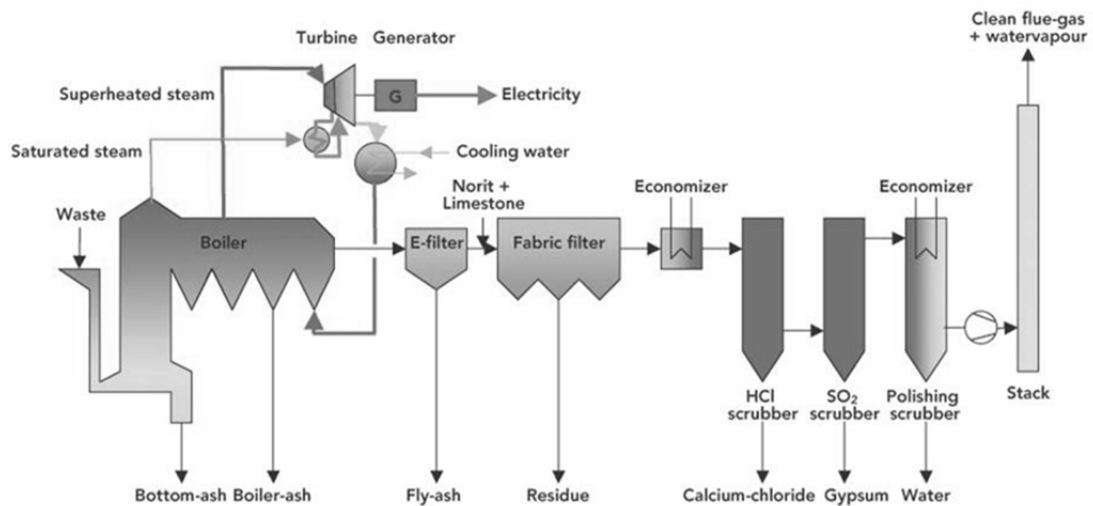


Figure 4. 7. Incineration scheme (plant in Amsterdam ⁽³⁶⁾)

In comparison to mechanical recycling, in the early 90s it became apparent that the recovery of small plastic packaging items (films, pouches, yoghurt cups, trays...) was both economically as well as environmentally costly ⁽⁴⁾. Due to the lightweight and diverse nature of these products, its collection, sorting and mechanical recycling was inviable. For example, in order to collect a ton of recycled plastic from yoghurt cups, approx. 200 000 cups were necessary ⁽³⁷⁾. Therefore, for this kind of plastics, the energy recovery stands out as an advisable recovery route.

Modern incinerators do not produce toxic fumes, regardless of the polymer content of their feedstock. The toxic fumes usually result from incomplete combustion, which can be avoided by operating the incinerator at a proper temperature with adequate oxygen supply. Furthermore, any toxic substances in the effluent that might result could be detected through proper monitoring of the effluent and eliminated by scrubbing the fumes. Capture and removal of flue gases in thermal (in general) and combustion processes (in particular) is a major issue dealt with by different pre-treatments ⁽¹⁾. In incineration processes, **temperature** is an essential parameter that leads to a reduction in CO and N₂O. Toxic materials in the ash are almost always not of polymer origin, but arise from other materials, usually containing heavy metals, that are mixed with the polymer feedstock. A desirable approach is to have a crude sorting of the feedstock so as to prevent their mixing with the polymer content. Emissions of heavy metals are in the same order of magnitude in coal or coal/PSW blends, and are lower than the limits imposed by

the EU directives ⁽³⁸⁾. In addition, the ash can be converted to a low-solubility slag through addition of materials like lime to the feedstock. In any case, incineration considerably reduces the volume of the waste so as to make its proper disposal more feasible. A consideration is what might happen to this possible content of toxic material if incineration had not been done. It would then probably enter into the landfill, probably in a more soluble form, and eventually leach out and enter the environment in an uncontrolled manner. Hence, **PSW could be considered as a renewable energy source under certain constrains of feed preparations.**

Advantages of plastic incineration for energy recovery include ⁽⁴⁾:

- Incineration destroys potentially harmful substances in the waste stream.
- The inorganic fraction of the waste, if any, is essentially mineralized by incineration to an inert slag that can be used as raw material in the construction of roads.
- It is recommendable for recovering products that are mixed, commingled, co-extruded, composited, bonded or laminated to other materials such as aluminium foil or paper, as well as for outdoor-exposed plastics, due to extensive weathering degradation.
- It is advisable for dealing with plastic waste used for medicals, drugs, hazardous-goods packaging, electronics or highly contaminated plastics, such as agricultural mulch films.

Nevertheless, there exist some **inconvenients** that have yet to be overcome ^(4,6,39):

- Inefficient incineration may produce some **unburnt material** (> 5% in weight)
- The destruction of foams and granules resulting from PSW also destroys **CFCs** and other harmful blowing agents present.
- Emission of certain **air pollutants** such as CO₂, NO_x and SO_x.
- **Generation of volatile organic** compounds (VOCs), smoke (particulate matter), particulate-bound heavy metals, polycyclic aromatic hydrocarbons (PAHs), polychlorinated dibenzofurans (PCDFs) and dioxins. Carcinogenic substances (PAHs, nitro-PAHs, dioxins, etc.) have been identified in airborne particles from incineration or combustion of

synthetic polymers such as PVC, PET, PS and PE. The presence of brominated flame retardants complicates the technical aspects of energy recovery receiving much of the attention nowadays.

- Incineration faces growing opposition due to the **low efficiency of electrical energy production** (four times fewer than thermal efficiency)
- Incineration remains **unpopular for the general public**, which does not allow the building of facilities in near locations, adopting the “not in my backyard” syndrome and therefore transportation costs increase. A societal problem in providing state-of-the-art incinerators is their cost. In the short run, the approach is often more expensive than alternative disposal means, but in the long run, it becomes cost-effective and environmentally desirable. However, this problem has been overcome, for example, by the Japanese, who combine the facilities with heated swimming pools and greenhouses, which win public acceptance.

2. THERMOLYSIS OF PET AND PLA

Chemical recycling of poly(ethylene terephthalate) and polylactide comprises both chemolysis (via glycolysis, methanolysis and hydrolysis) and **thermolysis** (via pyrolysis or gasification). Chemolysis technologies are already set for PET⁽⁴⁰⁾, while for PLA they are still under laboratory stage⁽⁴¹⁾.

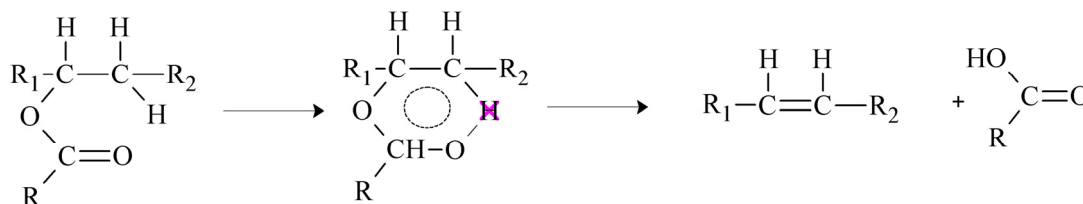
Despite thermal decomposition of PET is intensively reported in the literature⁽³³⁾, there still are ongoing disagreements over its mechanism. This chapter reviews different discussions regarding thermal and thermal oxidative decomposition of PET, as a first step to understand the reaction pathways undertaken during pyrolysis and gasification. In the case of PLA, energy recovery from PLA waste is covered in the waste treatment part by waste incineration⁽⁴²⁾ with electricity recovery. The thermolytic behaviour of PLA is well known under inert conditions. Otherwise, thermo-oxidative decomposition studies are still few.

The main decomposition routes for both PET and PLA under inert (thermal decomposition) and oxidative (thermo-oxidative decomposition) conditions are reviewed hereafter.

2.1. THERMAL AND THERMO-OXIDATIVE DECOMPOSITION OF PET

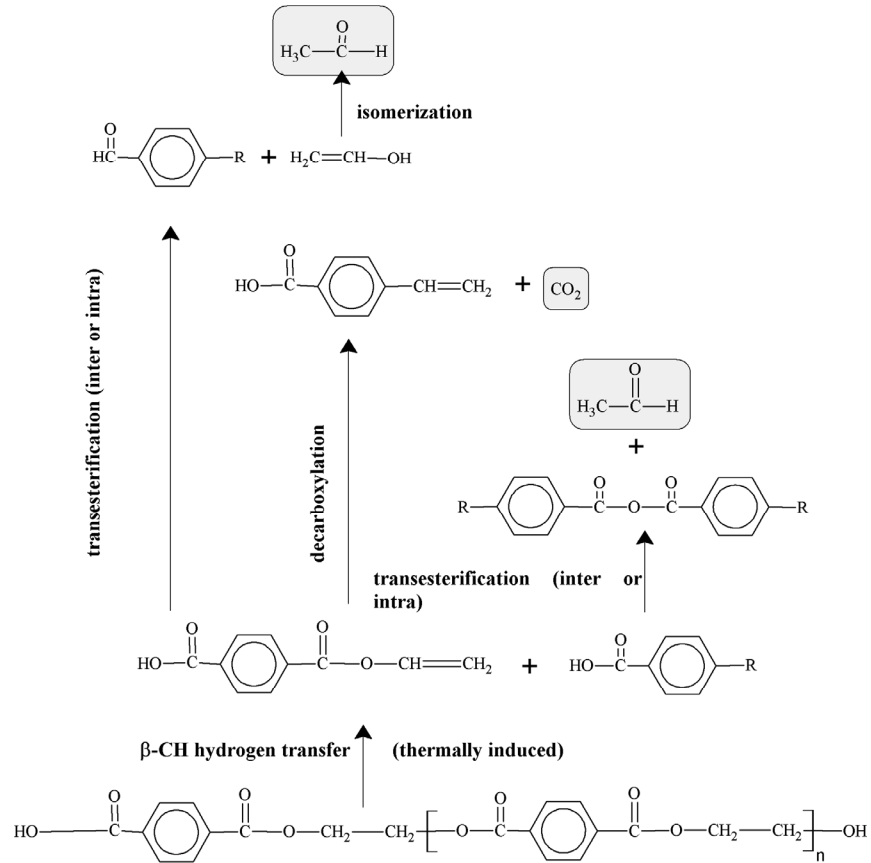
An early comprehensive overview of the thermal decomposition of PET was reported by *Buxbaum*⁽⁴³⁾. It was postulated that the primary scission of the ester linkage in the polymer is probably not a homolytic reaction, since thermal decomposition was not inhibited by free radical trapping agents. Based on the mechanism of thermal decomposition of model esters it was established that esters containing at least one β -hydrogen atom decompose to an olefin and acid through a cyclic transition state, as shown in Scheme 4.1. It has been shown that the C–O breakage is heterolytic and that the α -carbon atom develops some carbonium-ion character in the transition state. For a given ester at a fixed temperature, the rate of decomposition is determined more by the stability of the breaking alkoxy C–O bond than by the breaking C–H bond or the forming C = C

bond⁽⁴⁴⁾. Similar to ester compounds, **the principal point of weakness in PET chain is the β -methylene group**^(43; 45; 46; 47).



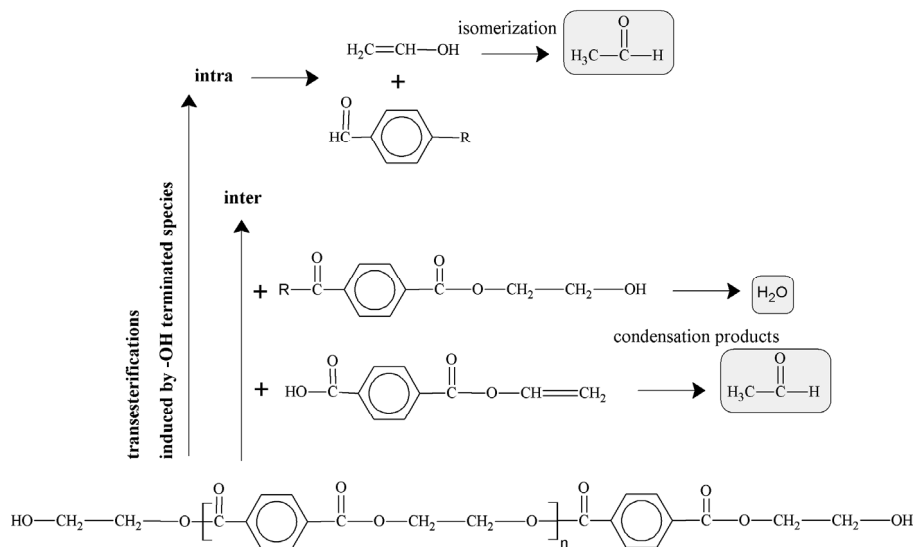
Scheme 4. 1. Model ester with β -methylene H decomposition (from ref. (43))

The main reactions in the thermal decomposition of PET occur due to **transesterification reactions**, both inter- or intra-molecular, taking place their initiations both in the middle (Scheme 4.2.) or in the end (Scheme 4.3.) of the chain⁽³³⁾. As long as free hydroxyl end groups exist in a PET melt, every broken polymer link can be reformed. When most of the hydroxyl end groups have been consumed, the molecular weight can start falling⁽³³⁾. *Edge et al.*⁽⁴⁸⁾ proposed that thermal cleavage of the ester bond initially results in the formation of a vinyl ester end-group and a carboxyl end-group. Because end-groups in PET are predominantly **hydroxyesters**, trans-esterification of the vinyl esters formed on degradation can take place to give vinyl alcohol which transforms into acetaldehyde. Essentially, hydroxyl end-groups would be replaced by carboxylic acid groups producing an equivalent quantity of **acetaldehyde**⁽⁴⁹⁾. *Vijaykumar et al*⁽⁵⁰⁾ suggested the formation of acetaldehyde, the major pyrolysis product of PET, through recombination of vinyl-terminated carboxylate and carboxylic acid-terminated units. This reaction may proceed by the intra- or intermolecular H shift to form vinyl alcohol, which isomerizes to give acetaldehyde. The **homolytic scission of ester bonds** was suggested by *Bounekhel and McNeill*⁽⁵¹⁾ based on their thermal decomposition study in vacuum of polyester made from poly(ethylene glycol) and terephthalic acid. They suggested that initial homolysis can occur in two possible ways, involving either alkyl-oxygen or acyl-oxygen scission, as shown in Scheme 4.4. These authors suggested that homolytic reactions can explain the whole range of observed degradation products. They argued that products such as CO and CO₂ are formed throughout the main temperature range of decomposition, whereas by a non-homolytic route, such products would only be found at the highest degradation temperatures (in the range up to 500°C).



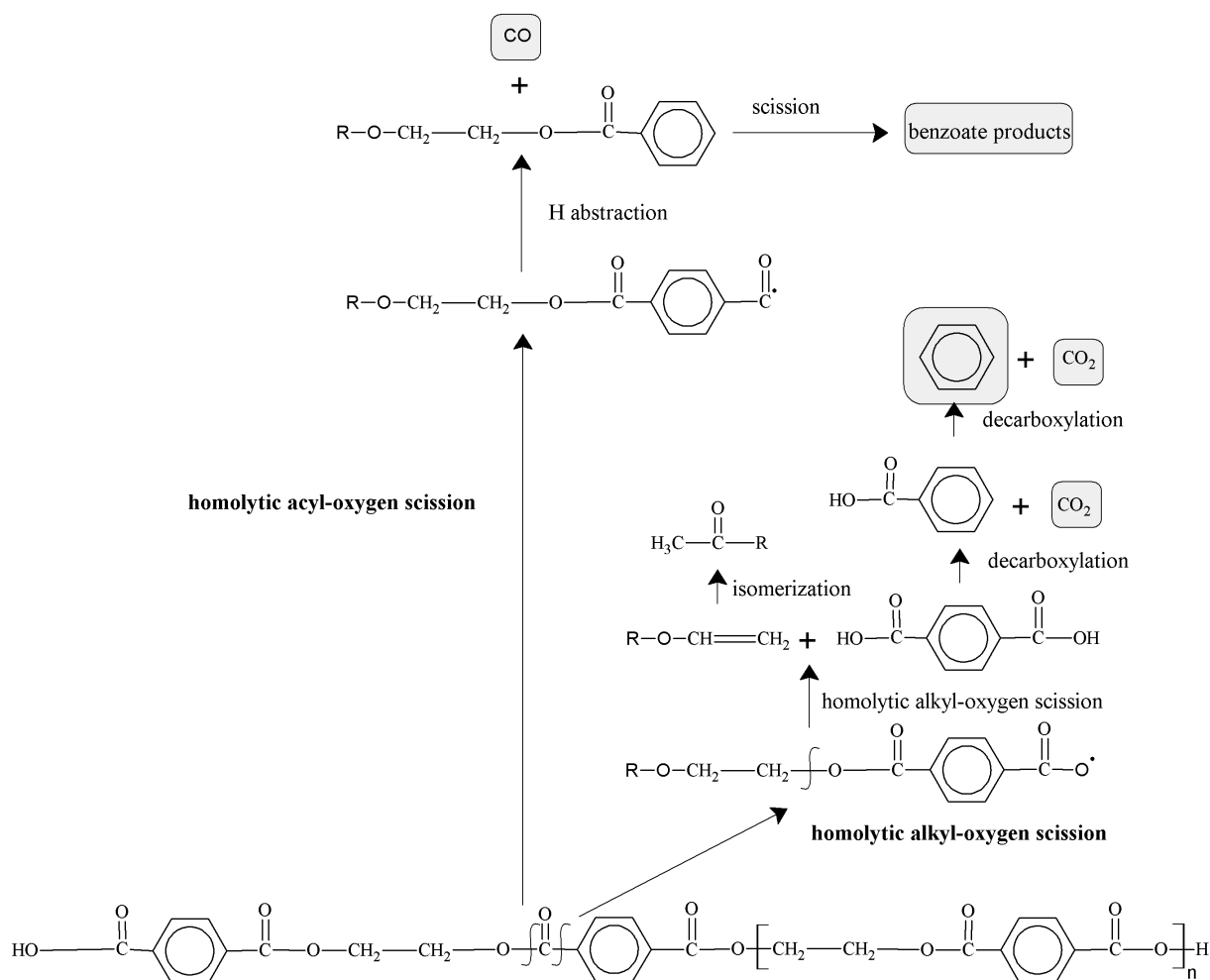
Scheme 4. 2. Transesterification reactions in the middle of the chain, as adapted from refs. in review (33) .

Note that R is an undefined PET chain fraction.



Scheme 4. 3. Transesterification reactions in the end of the chain, as adapted refs. in review (33). Note that

R is an undefined PET chain fraction.



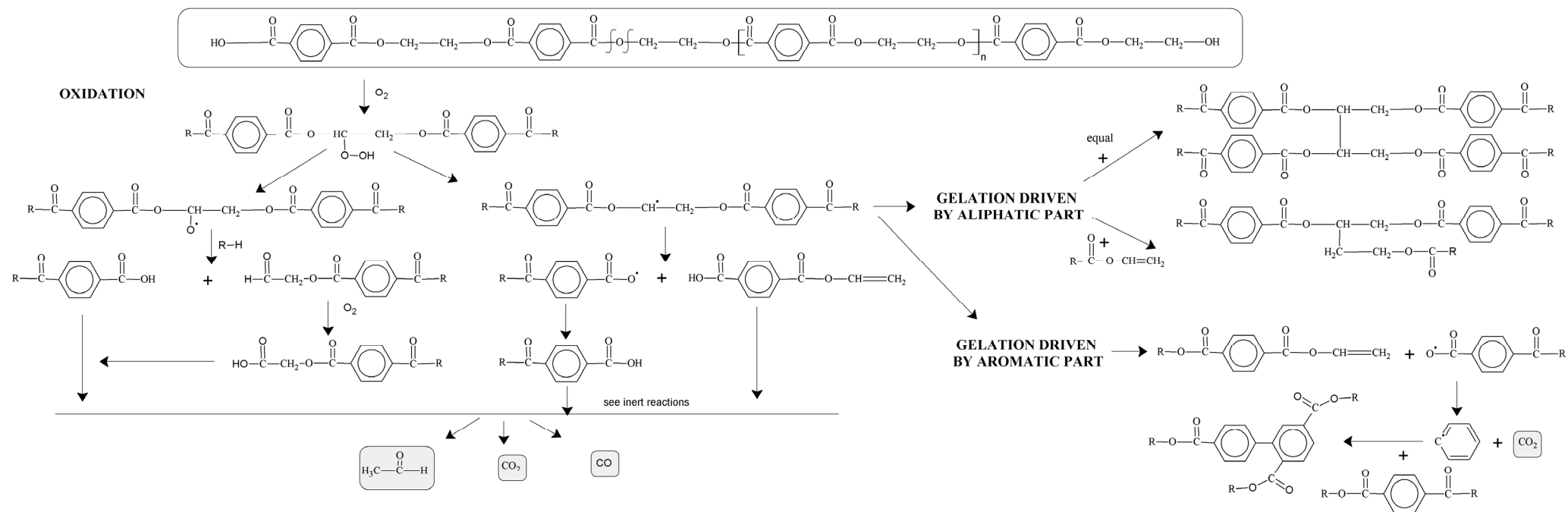
Scheme 4. 4. Homolytic thermal scissions, as adapted from refs. in review (33). Note that R is an undefined PET chain fraction.

Concerning the **thermo-oxidative decomposition behaviour** of PET, *Buxbaum*^(43,52) studied the degradation of PET in the presence of oxygen and proposed the mechanism shown in Scheme 4.5. It was suggested that the process starts with the formation of a **hydroperoxide** at the methylene group, followed by **homolytic chain scission**. In fact, *Allen et al.*⁽⁵³⁾ concluded that hydroperoxyde groups also take place not only as initiators but also as intermediates during thermo-oxidative decomposition.

In addition, it has been shown that PET undergoes **gelation**⁽⁵⁴⁻⁵⁶⁾ by heating at 230–300°C in air, whereas under nitrogen crosslinks are scarcely formed⁽⁵⁴⁾. Two different proposals have been given to explain gelation, according to the functional groups thought to be responsible, as shown in Scheme 4.5.

- On the one hand, it was proposed that the crosslinks are generated in the **aliphatic part** of the polyester ⁽⁵⁴⁾. In the first place, vinyl esters may be taken into consideration. First, random scission of polyester chains may take place, mainly forming carboxylic acids, vinyl esters, aldehydes and carbon dioxide. Afterwards, vinyl esters accumulate to some concentration, the vinyl esters react with the polymer chain, and network structures are formed.
- In contrast, *Nearly* ⁽⁵⁵⁾ and *Spanniger* ⁽⁵⁶⁾ believed that **aromatic fragments** are mostly responsible for the crosslinking and coloration. They had separated gelled PET from ungelled polymer and methanolized the gelled part. Based on the products found by gas chromatography in the filtrate, the mechanism leading to crosslinking was suggested. Such a mechanism depends on the generation of a phenyl radical which is probably formed after initial oxidation at a methylene position. After chain scission and decarboxylation, the phenyl radical arylates an adjacent benzene ring to form a crosslink.

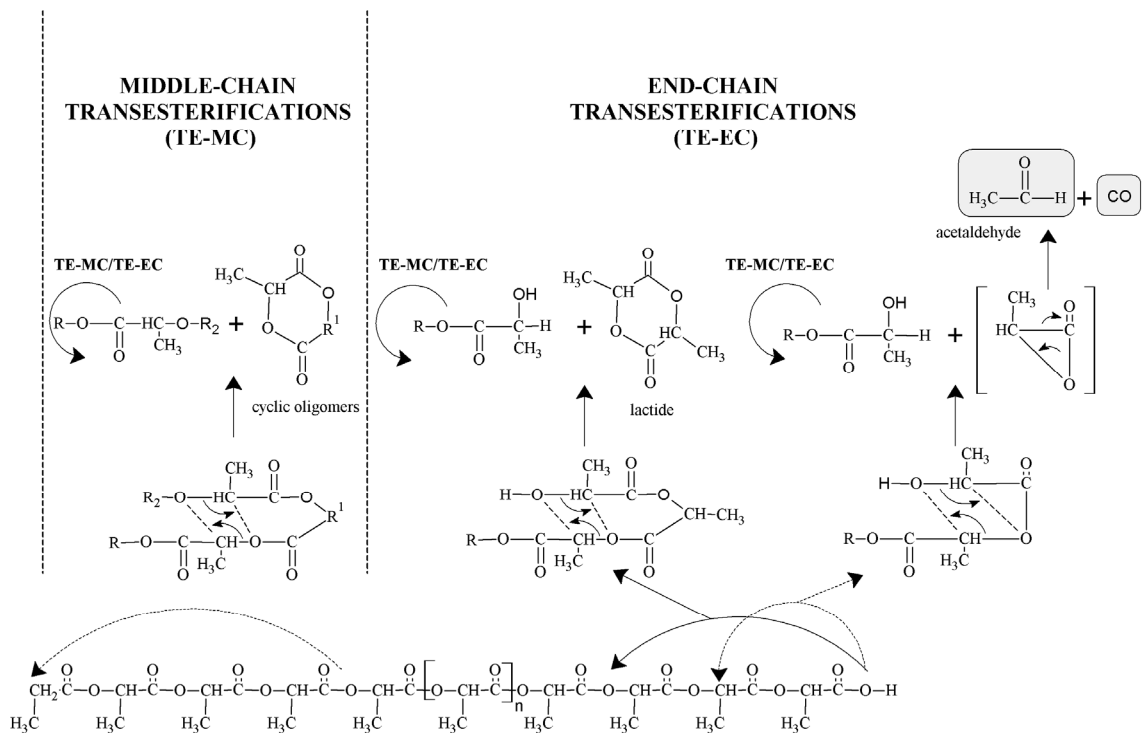
With regards to the study of the **evolved gases** from both thermal and thermo-oxidative decompositions, few reports have been published regarding the use of FT-IR as analytical technique ⁽⁵⁷⁾, being those analyses mainly performed by Gas Chromatography / Mass Spectrometry (GC-MS) ⁽⁵⁸⁻⁶¹⁾ or direct Mass Spectrometry from pyrolysis of PET ⁽⁶²⁾ more spread. The evolved gases from PET at its maximum **thermal decomposition** rate included acetaldehyde, benzoic acid, carbon dioxide, carbon monoxide and benzoic acid derivatives. It was believed that carbon dioxide, benzoic acid and aromatic esters were evolved in the initial stage of decomposition. Similarly, studies of the **thermal-oxidative decomposition of PET** in a tubular furnace with an air flow showed ⁽⁶⁰⁾ that the main evolved compounds are **carbon monoxide, acetaldehyde, formaldehyde, benzene, styrene, and aliphatic C₁-C₄ hydrocarbons**. The composition of the volatile products strongly depends on the degradation temperature. At lower temperatures, acetaldehyde, formaldehyde, and carbon monoxide are the main degradation products.



2.2. THERMAL AND THERMO-OXIDATIVE DECOMPOSITION OF PLA

Kopinke and Mackenzie ⁽⁶³⁻⁶⁴⁾ surveyed previous studies and concluded that the thermal decomposition of PLA is mainly driven by transesterification and homolytic reactions, and with minor participation, catalyzer (Sn)-based depolymerization or cis-elimination.

A detailed study of thermal PLA degradation was carried out by *McNeill and Leiper* ⁽⁶⁵⁾ According to their studies, the main reaction route is a non-radical, backbiting **transesterification** reaction involving -OH chain ends, as shown in Scheme 4.6. The same principal reaction mechanism can, depending upon the size of the cyclic transition state, produce lactide ($n = 0$), oligomers (R with $n \geq 1$), or **acetaldehyde** plus **carbon monoxide**. Middle-chain inter transesterifications are also shown.



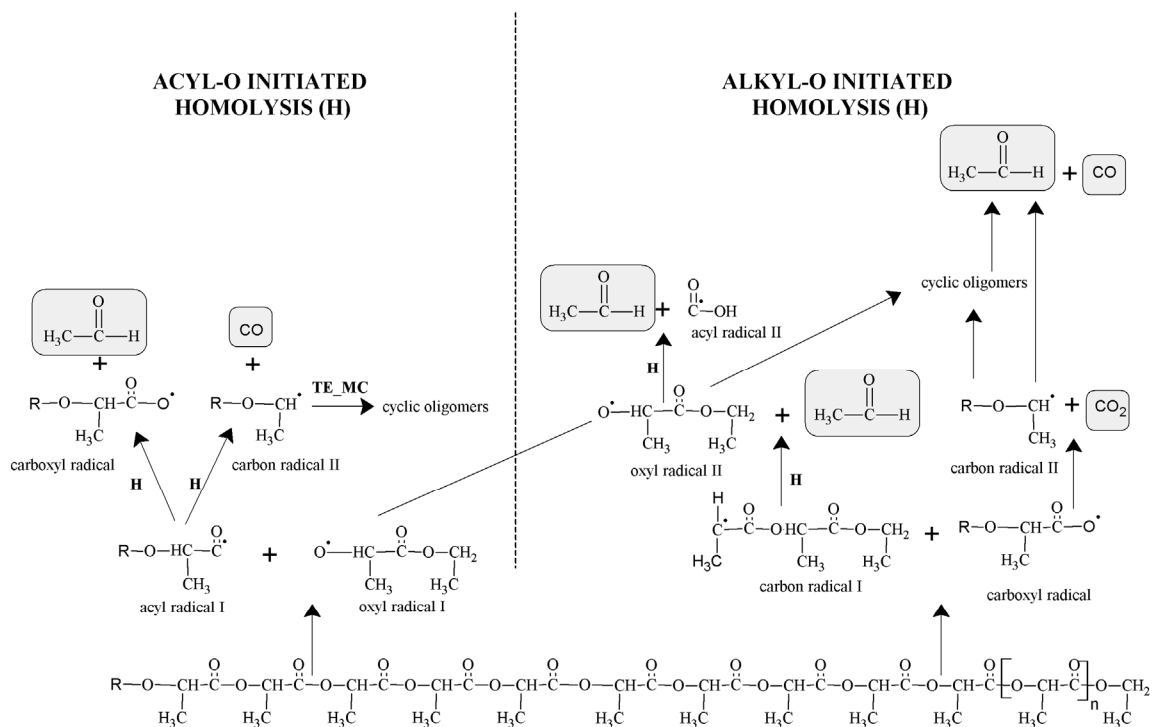
Scheme 4. 6. Transesterification reactions of thermal decomposition of PLA, as adapted from ref (65) .

Note that R is an undefined PLA chain fraction, unless contrarily indicated.

Lüderwald et al. ⁽⁶⁶⁻⁶⁷⁾ studied the thermal degradation of various polyesters, among them PLA, by preparative pyrolysis and in-source Py-MS. Their results gave clear evidence on

the prevailing pyrolysis mechanisms for various hydroxypolyesters. PLA produced mainly cyclic oligomers. Thus, the reaction mechanism is determined not by the position of the ester oxygen, but by the availability and reactivity of **β -C-H bonds** for **cis-elimination**. Although PLA has three primary C-H bonds available in the β -position to the ester oxygen, their reactivity is not high enough to let them successfully compete with transesterification reactions.

On the other hand, *Kopinke et al.*⁽⁶³⁾ showed that radical reactions can be assumed to start with either an alkyl-oxygen or an acyl-oxygen **homolysis**, as shown in Scheme 4.7. Several types of oxygen- and carbon-centred macroradicals may be formed. Starting with the cleavage of the two C-O bonds, various carbon- and oxygen-centred macroradicals can be generated. All these radicals can decompose further by splitting off smaller fragments (CO, CO₂, acetaldehyde, methylketene). Some of these are appropriate for cyclization by an addition-elimination mechanism, yielding lactide and other oligomers. The acyl- and the carboxyl-radical would mainly be expected to decompose, to release CO₂ which can be considered as a marker of radical reactions⁽⁶³⁾.



Scheme 4. 7. Homolytic reactions of thermal decomposition of PLA, as adapted from ref (63) . Note that R is an undefined PLA chain fraction.

Concerning, thermo-oxidative decomposition, few studies have been devoted to elucidate its mechanisms. **Random main-chain scission** was proposed by *Gupta and Deshmukh*⁽⁶⁸⁾ and therefore may promote radical compounds that may follow the reactions shown in Scheme 4.7.

Acetaldehyde, CO, CO₂, lactide and short-chain acids are the major **gases evolved** during both thermal and thermo-oxidative decompositions, as studied by FT-IR⁽⁶⁹⁾ and MS⁽⁷⁰⁾.

2.3. APPROACHING PYROLYSIS AND COMBUSTION BY THERMOGRAVIMETRY

Appropriate design and scale (of operation and economy) are of paramount importance when it comes to thermal treatment plants. **Thermolysis behaviour in laboratory scale** enables the assessment of a number of important parameters⁽⁶⁾, such as:

- thermal stability temperature of polymers
- thermal kinetics,
- activation energy assessment (energy required to degrade materials treated)
- product formation

To design a chemical reactor, the rate expression must be known. Assuming the reaction is known not to be elementary, the search for a mechanism that describes the reaction taking place or use experimental data directly must be aimed. Mechanisms can be hypothesized as the sum of a series of elementary reactions with intermediates. Using methods developed by physical chemists, whether the proposed mechanism fits the actual experimental evidence can be hypothesized. Systems kinetics will not only develop appropriate models that will predict systems products and their interaction, but through solving the derived mathematical expressions, they will predict the product interaction behaviour. This will assist in reducing side reactions and undesired by-products on an industrial scale. Developing rate expressions of the materials being treated will then be utilized in determining the optimum unit operation to be used and its required supply of

power and proper media of operation, in the case of pyrolysis, the sufficient amount of inert atmosphere in the pyrolyser or the ratio of steam to oxygen in a gasifier⁽⁷¹⁾.

In the attempt to develop a model for plastic thermal and thermo-oxidative decompositions in full-scale systems, the main purpose is to describe the behaviour of polymers in terms of an intrinsic kinetics, in which heat and mass transfer limitations are not included. General kinetic models are proposed in literature for plastics and biomasses. These models do not take into account the rigorous and exhaustive description of the chemistry of thermal decomposition of polymers and describe the process by means of a simplified reaction pathway. Each single reaction step considered is representative of a complex network of reactions⁽⁷²⁾.

Pyrolysis is usually the first process in a thermal plant, and is in need of appropriate end-product design. This could be achieved via the understanding of the systems kinetics on **Thermogravimetric Analyzers (TGA)** and pilot (bench scale unit) scales, using inert atmospheres such as Ar or N₂. Combustions/Gasification systems can also be approached by using O₂ or mixtures N₂/O₂ rich in the O₂ phase⁽⁶⁾. Therefore TGA stands out as fast, cost-effective and reliable characterization technique to ascertain a deeper knowledge about the ongoing thermal and thermo-oxidative decomposition of plastics. Completing this experimental technique with a proper theoretical model-fitting methodology is commonly used for the study of kinetic parameters such as the apparent activation energy E_a , the pre-exponential factor A and the reaction model $f(\alpha)$, which yield the so-called **kinetic triplet**.

Regarding theoretical approaches, literature reports indicate that different researchers use different kinetic models and diverse kinetic methodologies to perform their studies and come up to the kinetics of the thermal or thermo-oxidative decompositions, in an attempt to reach the description of pyrolysis and combustion of their polymers, respectively. This fact often provokes confusion concerning which model is more suitable and therefore should be used to best represent the system under study⁽⁷³⁻⁷⁴⁾. Even more, most reports over-simplify the kinetics of decomposition by assuming constant variables to explain the whole decomposition behaviour. In this thesis, a combination of different methods is used. In addition, the variation of the kinetic parameters along the decomposition range is considered.

3. REFERENCES IN THIS CHAPTER

1. Al-Salem S M, Lettieri P, Baeyens J. *Recycling and recovery routes of plastic solid waste (PSW): A review* Waste management 29 2625-2643 (2009)
2. Dirks E. *Energy recovery from plastic waste in waste incineration plants*. In: J Brandup J. Recycling and Recovery of Plastics. Hanser Verlag Publsh. 746-769 (1996)
3. Williams, E A y Williams, P T. *The pyrolysis of individual plastics and plastic mixture in a fixed bed reactor*. Journal of Chemical Technology and Biotechnology 70, 9-20 (1997)
4. Scheirs J. *Feedstock recycling - pyrolysis, hydrogenation and gasification*. In Scheirs J, Polymer recycling. Science, Technology and Applications. WileySeries in Polymer Science (1998)
5. PlasticsEurope, EuPC, EPRO, EuPR. Consolidated data. *The compelling facts about plastics. An analysis of European plastics production, demand and recovery for 2008*. (2009)
6. Al Salem S M, Lettieri P, Baeyens J. *The valorization of plastic solid waste (PSW) by primary to quaternary routes: from re-use to energy and chemicals*. Progress in Energy and Combustion Science 36, 103-129 (2010)
7. Yoshioka T, Grause G, Eger C, Kaminsky W, Okuwaki A. *Pyrolysis of poly(ethylene terephthalate) in a fluidized bed plant*. Polymer Degradation and Stability , 86, 499-504 (2004)
8. Smolders K, Baeyens J. *Thermal degradation of PMMA in fluidized beds*. Waste management 24, 849-857 (2004)
9. Mackey, G. *A review of advanced recycling technology*. American Chemical Society, ACS Symposium Ser. 95-609 (1995)
10. Horvat, N. *Tertiary polymer recycling: study of polyethylene thermolysis and polyethylene oil hydrogenation*. Chemical Engineering Department, University of Waterloo, Canada. Ph. D. Thesis. (1996)
11. Asanuma M, Ariyama T. *Recycling of waste plastics in blast furnace*. Journal of Japan Institute of Eenergy 83, 252-256 (2004)
12. Kato K, Fukuda K, Takamatsu N. *Waste plastics recycling technology using coke ovens*. Journal of Japan Institute of Eenergy 83, 248-251 (2004)
13. Chudzicki R. *The market has been hit hard but the future is not bleak*. Proceedings of the 9th European gasification conference. Düsseldorf

14. Griffiths J. *Gasification opportunities: where is the scope for developing the market or the use of gasification*. Proceedings of the 9th European gasification conference . Düsseldorf,
15. Westerhout, R W J. van Koningsbruggen, M P , Van der Ham A G J , Kuipers J.A.M., Swaaij van W.P.M. *Techno-economic evaluation of high temperature pyrolysis processes for mixed plastic waste*. Chemical Engineering Research and Design 76, 427-439 (1998)
16. Cozzani V, Tognotti L, Nicoletta C, Rovatti M. *Influence of gas phase reactions on the product yields obtained in the pyrolysis of polyethylene*. Industrial Engineering Research, 36, 342-348 (1997)
17. Kaminsky W, Schlesselmann B y Simon C. *Olefins from polyolefins and mixed plastics by pyrolysis*. Journal of Applied and Analytical Pyrolysis 32, 19-27 (1995)
18. Stiles H N, Kandiyoti R. *Secondary reactions of flash pyrolysis tars measured in a fluidized bed pyrolysis reactor with some novel design features*. Fuel 68, 275-282 (1989)
19. Ponzio A, Kalisz S, Blasiak W. *Effect of operating conditions on tar and gas composition in high temperature air/steam gasification (HTAG) of plastic containing waste*. Fuel Process Technology 87, 223-233 (2006)
20. Ledesma E B, Kalish M A, Nelson P F, Wornat M J, Mackie J C, *Formation and fate of PAH during pyrolysis of fuel-rich combustion of coal primary tar*. Fuel 79, 1801-1814 (2000)
21. Bioenergy Network of Excellence (NoE). Last visit: 2010-11-09. <http://www.bioenergy-noe.com>.
22. Ciliz N K, Ekinçi E, Snape C E, *Pyrolysis of virgin and waste polyethylene and its mixtures with waste polyethylene and polystyrene*. Waste management 2, 173-181 (2004)
23. Van der Welden M, Baeyens J, Boukins I. *Modelling CFB biomass pyrolysis reactors*. Biomass and Bioenergy 32, 128-139 (2008)
24. Wu S, Su M, Baeyens J. *The fluidized bed pyrolysis of shredded tyres: the influence of carbon particles, humidity and temperature on the hydrodynamics*. Powder Technology 93, 283-290 (1997)
25. China Plastics Processing Industry Association (CPPIA), *Chinese plastics industry goes from strength to strength*. Plastics, additives and compounding 3, 30-32 (2007)
26. World Coal Institute. Last visit 2010-11-09. <http://www.worldcoal.org>.
27. Buekens, A G. *Resource recovery and waste treatment in Japan*. Recovery and Conservation 3, 275-306 (1978)

28. Hasegawa M, Fukuda X, Kunii D. *Gasification of solid waste in a fluidized with circulating sand*. Conservation and recycling 3, 143-153 (1979)
29. Borgianni C, De Filippis P, Pochetti F, Paolucci M. *Gasification process of waste containing PVC*. Fuel 14, 1827-1833 (2002)
30. Xiao R, Jin B, Zhoub H, Zhonga Z, Zhanga M, *Air gasification of polypropylene plastic waste in fluidized bed gasifier*. Energy Conversion and management 48, 778-786 (2007)
31. Matsunami J, Yoshida S, Yokota O, Nezuka M, Tsuji M, Tamaura Y, *Gasification of waste tyre and plastic (PET) by solar thermochemical process for solar energy utilization*. Solar eenergy 65, 21-23 (1999)
32. Barton J R, Dalley D, Patel V S, *Life cycle assessment for waste management*. Waste management 16, 35-50 (1996)
33. Levchick S V, Weil, E D. *A review on thermal decomposition and combustion of thermoplastic polyesters*. Polymers for Advanced Technologies 15, 691-700 (2004)
34. *Novel and innovative pyrolysis and gasification technologies for energy efficient and environmentally sound MSW disposal*. Malkow, T. 2004, Waste management, Vol. 24, págs. 53-79.
35. Barrales-Rienda J M. Energy recovery from plastic materials. In: La Mantia F. *Handbook of plastics recycling*. Rapra Technology Limited (2002)
36. Tobias, C. What Can We Learn From Amsterdam About Waste to Energy? *Celsius: Climate change is not a spectator sport*. Last visit: 2010-11-07. <http://www.celsius.com/article/what-can-we-learn-amsterdam-about-waste-energy/>.
37. Bürke, Davos *Mandatory recycled plastic content - pros and cons*. Proceedings of the GLOBEC'96. Switzerland (1996)
38. Boavida D, Abelha P, Gulyurtlu I, Cabrita I. *Co-combustion of coal and non-recyclable paper and plastic waste in a fluidized bed reactor*. Fuel 82, 1931-1938 (2003)
39. Zia K M, Bhatti H N, Bhatti, I A. *Methods for polyurethane and polyurethane composites, recycling and recovery: a review*. Reactive and functional polymers 67, 675-692 (2007)
40. Scheirs J. Recycling of PET. *Polymer recycling. Science, technology and applicattions.*: Wiley series in polymer sciences (1998)
41. Dornburg V, Faaij A, Patel M, Turkenburg W C. *Economics and GHG emission reduction of a PLA bio-refinery system - Combining bottom-up analysis with price elasticity effects*. Resources, Conservation & recycling 46, 377-409 (2006)

42. Gruber P, O'Brien M. Natureworks TM PLA. In: Doi Y, Steinbüchel A. *Biopolymers. Vol 4. Polyestres III. Applications and commercial products*. Weinheim, Wiley-VCH Verlag GmbH (2002)
43. Buxbaum L H, *The Degradation of Poly(ethylene terephthalate)*. *Angewandte Chemie International Edition in English* 7, 182–190 (1968)
44. Macooll A, *Journal of Chemical Society*, 3398 (1958)
45. Pohl H A. *The thermal degradation of polyesters* *Journal of the American Chemical Society* 73, 5660 (1951)
46. Adams R. *Pyrolysis mass spectrometry of terephthalate polyesters using negative ionization* *Journal of Polymer Science, Polymer Chemistry* 20, 119-129 (1982)
47. Luderwald, I y Urrutia, H. *Strukturuntersuchung von polyestern durch direkten abbau im massenspektrometer, 1. Polyester der terephthalsäure*, *Die Makromolekulare Chemie* 177, 2079-2091 (1976)
48. Edge M, Wiles R, Allen N S, McDonald W A, Mortlock S V. *Characterisation of the species responsible for yellowing in melt degraded aromatic polyesters—I: Yellowing of poly(ethylene terephthalate)*, *Polymer Degradation and Stability*, 53, 141-151 (1996)
49. Khemani K C. *A novel approach for studying the thermal degradation, and for estimating the rate of acetaldehyde generation by the chain scission mechanism in ethylene glycol based polyesters and copolyesters*. *Polymer Degradation and Stability* 67, 91-99 (2000)
50. Vijayakumar C T, Ponnusamy E, Balakrishnan T, Kothandaraman H. *Thermal and pyrolysis studies of copolyesters*. *Journal of Polymer Science: Polymer Chemistry Edition* 20, 2715–2725 (1982)
51. Bounekhel M, Mc Neill I C. *Thermal degradation studies of terephthalate polyesters: 2. Poly(ether-esters)*. *Polymer degradation and stability*, 49, 347-352 (1995)
52. Buxbaum L.H. *Polym Prepr Am Chem Soc Div Polym Chem.* 8, 552 (1967)
53. Allen N S, Edge M, Mohammadian M, Jones K, *UV and thermal hydrolytic degradation of poly(ethylene terephthalate): importance of hydroperoxides and benzophenone end groups*, *Polymer Degradation and Stability* 41, 191-196 (1993)
54. Yoda K, Tsuboi A, Wada M, Yamadera R, *Network formation in poly(ethylene terephthalate) by thermooxidative degradation*. *Journal of Applied Polymer Science* 14, 2357–2376 (1970)
55. Nealy D L, Adams J L, *Oxidative crosslinking in poly(ethylene terephthalate) at elevated temperatures*. *Journal of Polymer Science Part A-1: Polymer Chemistry* 9, 2063–2070. (1971)

56. Spaninger P A, *Thermoxidative degradation leading to gel in poly(ethylene terephthalate)*, Journal of Polymer Science: Polymer Chemistry 14, 709-717 (1974)
57. Kinoshita R, Teramoto Y, Nakano T, Yoshida H *Thermal degradation of polyesters by simultaneous TGA-DTA/FT-IR analysis*. Journal of Thermal Analysis 38, 1891-1900. (1992)
58. Freire M T, Damant A P, Castle L., Reyes F G R, *Thermal stability of Polyethylene terephthalate (PET): Oligomer distribution and formation of volatiles*. Packaging Technology and Science 12, 29-36 (1999)
59. Botelho G, Queirós A, Liberal S, Gijsman P, *Studies on thermal and thermo-oxidative degradation of poly(ethylene terephthalate) and poly(butylene terephthalate)*. Polymer Degradation and Stability 74, 39-48 (2001)
60. Dzieciol M, Trzeszczynski J, *Studies of temperature influence on volatile thermal degradation products of poly(ethylene terephthalate)*, Journal of Applied Polymer Science 69, 2377-2381 (1998)
61. Dzieciol M, Trzeszczynski J. *Temperature and atmosphere influences on smoke composition during thermal degradation of poly(ethylene terephthalate)*. Journal of Applied Polymer Science 81, 3064-3068 (2001)
62. Montaudo G, Puglisi C, Samperi F , *Primary thermal degradation mechanisms of PET and PBT*. Polymer Degradation and Stability 42, 13-28 (1993)
63. Kopinke F D, Remmler M, Mackenzie K, Möder M, Waschen O, *Thermal decomposition of biodegradable polyesters - II: Poly(lactic acid)*. y otros. Polymer Degradation and Stability 53, 329-342 (1996)
64. Kopinke F D, Mackenzie K, *Mechanistic aspects of the thermal degradation of poly(lactic acid) and poly(beta-hydroxybutyric acid)*. Journal of Analytical and Applied Pyrolysis 40-41, 43-53 (1997)
65. McNeill I C, Leiper H A. *Degradation studies of some polyesters and polycarbonates - 2: Polylactide: degradation under isothermal conditions, thermal degradation mechanism and photolysis of the polymer*. Polymer Degradation and Stability 11, 309-326 (1985)
66. Kricheldorf H R, Lüderwald I, *Strukturuntersuchung von polyestern durch direkten abbau im massenspektrometer, 3. Poly- β -propiolacton, poly- β -pivalolacton und poly- δ -valerolacton*. Die Makromolekulare Chemie 179, 421-427 (1978)
67. Jacobi E, Lüderwald I, Schulz R C, *Strukturuntersuchung von polyestern durch direkten abbau im massenspektrometer, 4. Polyester und copolyester der milchsäure und glykolsäure*. Die Makromolekulare Chemie 179, 429-436 (1978)

68. Gupta M C, Deshmukh V G, *Thermal oxidative degradation of poly-lactic acid*. Colloid and Polymer Science 260, 308-311 (1982)
69. Vogel C, Siesler H W, *Thermal degradation of poly(ϵ -caprolactone), poly(L-lactic acid) and their blends with poly(3-hydroxy-butyrate) studied by TGA/FT-IR spectroscopy*. Macromolecular Symposia 265, 183-194 (2008)
70. Aoyagi Y, Yamashita K, Doi Y, *Thermal degradation of poly[(R)-3-hydroxybutyrate], poly[ϵ -caprolactone], and poly[(S)-lactide]*. Polymer Degradation and Stability 76, 53-59 (2002)
71. Tukker A, de Groot H, Simons L, Wiegersma S. *Chemical recycling of plastic waste: PVC and other resins*. European Commission, DG III, Final Report, STB-99-55 Final. Delft, the Netherlands (1999)
72. Wunderlich B. *Thermal analysis of polymeric materials*. Springer, Berlin, 2005.
73. Galwey A K, *What can we learn about the mechanisms of thermal decompositions of solids from kinetic measurements?* Journal of Thermal Analysis and Calorimetry 92, 967-983 (2008)
74. Galwey A K, Brown M E, *Solid-state decompositions - stagnation or progress?*. Journal of Thermal Analysis and Calorimetry 60, 863-877 (2000)
75. Khemani, K C. 1, 1990, Polym. Prep., Vol. 4, pág. 625.

CONTRIBUTION IV-A

Detailed methodology to assess the thermal stability and kinetics of thermal and thermo-oxidative decomposition behaviors of reprocessed poly (ethylene terephthalate)

J.D. Badia, A. Ribes-Greus

Manuscript

**DETAILED METHODOLOGY TO ASSESS THE THERMAL STABILITY AND KINETICS OF
THERMAL AND THERMO-OXIDATIVE DECOMPOSITION BEHAVIOURS OF
REPROCESSED POLY (ETHYLENE TEREPHTHALATE)**

J.D. Badía, A. Ribes-Greus*

Instituto Tecnológico de Materiales. Universidad Politécnica de Valencia.

Camino de Vera, s/n, 46022 Valencia (Spain)

*corresponding author: aribes@ter.upv.es

Keywords: Poly(ethylene terephthalate) (PET), Waste Management, Thermogravimetry coupled to Fourier-Transform Infra-Red Spectroscopy for Evolved-Gas Analysis (TGA/EGA-FTIR), thermal decomposition, thermo-oxidative decomposition, kinetic analysis, 2D-Correlation IR.

Abstract:

An exhaustive analysis to compare the behaviour of virgin or reprocessed poly (ethylene terephthalate) (PET) facing thermal and thermo-oxidative decomposition processes is presented in this work, as an approach for the waste management of post-consumer PET goods. Commercial PET was submitted to successive reprocessing cycles through multiple injection steps in order to simulate thermo-mechanical degradation induced to the polymer by mechanical recycling. Multi-rate linear-non-isothermal thermogravimetric (TGA) experiments under inert (Ar) and oxidative (O₂) conditions were performed to virgin PET and its recyclates in order to simulate the thermal behaviour of the materials facing pyrolysis and combustion processes. The release of gases has been monitored by Evolved Gas Analysis of the fumes of the TGA experiment, by in-line FT-IR analysis, with the aid of 2D-correlation IR spectra. A kinetic analysis methodology, consisting in the combination of six different methods (namely Flynn-Wall-Ozawa, Kissinger-Akashira-Sunose, Advanced IsoConversional method, Master-Curves and Perez-Maqueda Criterion along with Coats-Redfern equation) was thoroughly applied, and its validity for being used with both constant and variable kinetic parameters was proven. The kinetic model that mathematically describes both thermal and thermo-oxidative decompositions of PET and its recyclates is of the type A_n: nucleation and growth, which gives importance to the formation of gas bubbles in the melt. Different models and novel parameters are proposed to characterize the thermal stability along the reprocessing cycles, as well as the variation of the activation energy and the pre-exponential factor during thermal and thermo-oxidative decompositions. The reliability of a simplified kinetic triplet, where thermal activation parameters can be considered constant is validated only under thermal decomposition. The usability of PET after reprocessing showed a threshold in the thermal performance from the second recyclate on. During energetic valorisation processes, reprocessed PET behaves similarly to virgin PET, and thus current technologies can be assimilable for all materials.

1. Introduction

The extended use of poly(ethylene terephthalate) (PET) over the last two decades, mainly in the food packaging sector, is due to its excellent mechanical, chemical, processing and thermal properties. Consequently, the amount of post-consumed PET present in urban solid waste is high and has to be managed. Among all recovery methods, mechanical recycling represents one of the most successful processes and has received considerable attention due to its main advantages [1]. The application of protocols [2-7] to simulate the degradation subjected during mechanical recycling has stated that thermo-mechanical degradation induced by means of multiple reprocessing undergoes reactions among end-groups [8] at temperatures above the melting point, which provoke modifications in the oligomeric distribution of PET [6] thus diminishing its properties under mechanical, chemical, electrical or thermal solicitations [9]. Under this perspective, the application of technologies for energetic valorisation such as pyrolysis or controlled combustion can offer an added value to recycled plastics which service lives at good performance parameters have been overcome. With this processes, plastic waste breaks down due to the application of heat to mainly give out high calorific value gaseous products, from which energy can be obtained [1].

The behaviour of polymers submitted to pyrolysis and/or combustion must be kinetically assessed, in order to model the decomposition mechanism, the rate of the reaction and the rest of reaction parameters necessary to predict the product distribution. This knowledge will lead to the selection of the proper reactor, as well as to the optimization of the reactor design and operating conditions. In this sense,

Thermogravimetric analysis (*TGA*) stands out as fast, cost-effective and reliable characterization technique to ascertain a deeper knowledge about the ongoing thermal and thermo-oxidative decomposition of plastics. *TGA* can approach the experimental conditions of pyrolysis or combustion processes by using an inert or oxidative gas in the reactor, respectively. Coupling this experimental technique with a proper theoretical model-fitting methodology is commonly used for the study of kinetic parameters such as the apparent activation energy E_a , the pre-exponential factor A and the reaction model $f(\alpha)$, which yield the so-called kinetic triplet. Furthermore, the study of the evolved gases may complete the picture of the study and predict the major reaction pathways driven during both thermolytic processes. Fourier Transform Infra-Red (*FT-IR*) Spectroscopy is an effective hyphenated technique to monitor the release of gases. As well, the application of 2D-correlation IR spectroscopy [10] can help determine the sequence of gases released, as well to distinguish between overlapped bands to identify products evolved due to different reactions.

Mechanistically, it is widely known that thermal decomposition of PET may occur mainly via (i) intramolecular back-biting, leading to cyclic dimers or trimers, and (ii) via chain scission through a β -C-H hydrogen transfer reaction, leading to vinyl ester and acid end-groups [11-12]. Other reactions may occur, due to the high reactivity and variety of chemical groups present in PET. It has been reported how this reactions can be enhanced by the presence of aliphatic end-groups in PET oligomeric distribution [13] or by moieties due to deficient drying, even two-folding the hydrolytic reactions at temperatures

above the melting [14]. The presence of diethylene glycol in its formulation may promote thermal decomposition due to enhanced chain flexibility [15]. The complexity of the decomposition mechanisms is patent in the paper

reported by *Levchik and Weil* [11], where they review up to 9 different schemes for thermal decomposition and 5 for thermo-oxidative decomposition of PET. **Figure 1** shows the main thermolytic decomposition mechanisms proposed

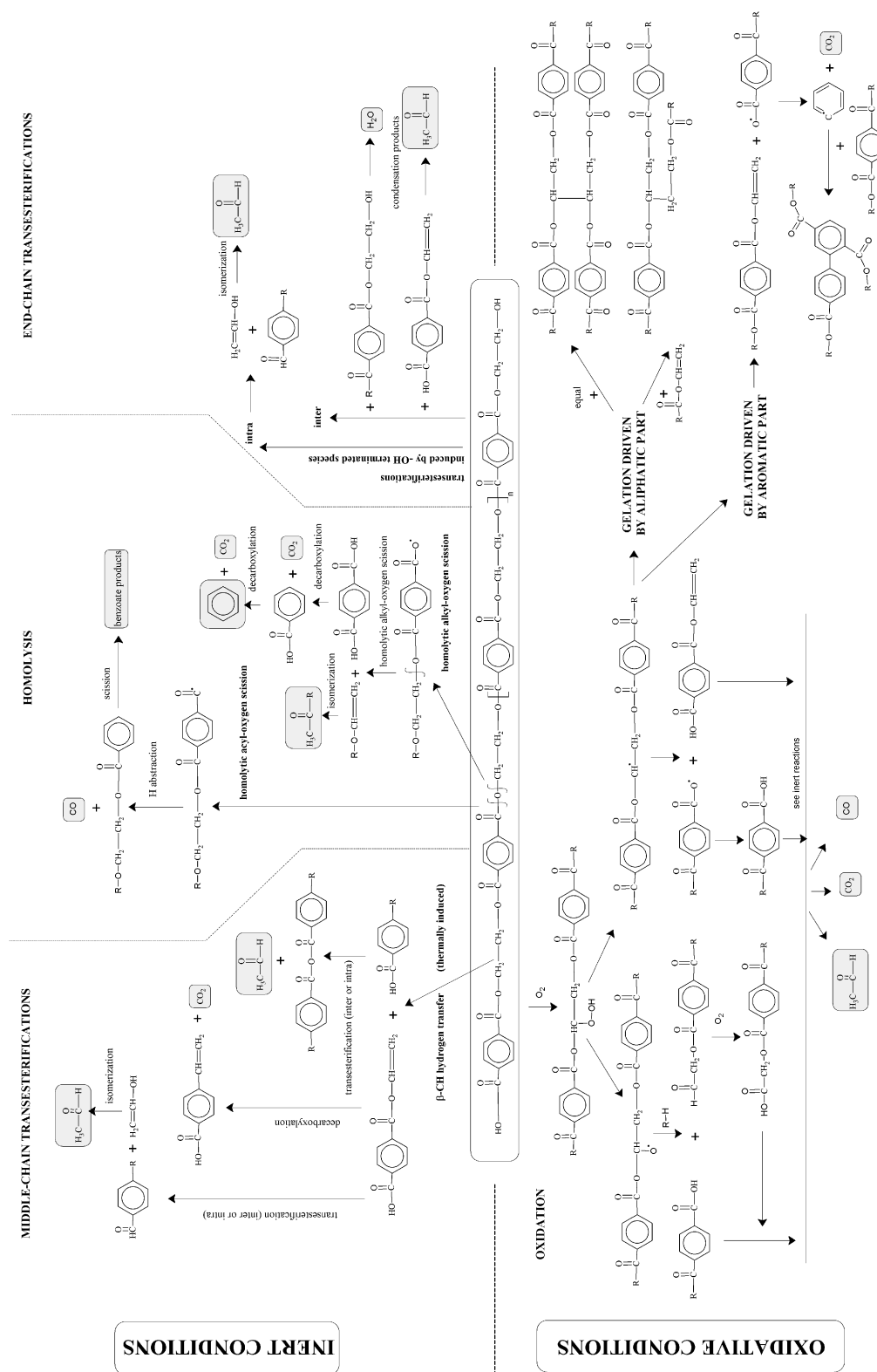


Figure 1. Thermolytic decomposition mechanisms of PET, as adapted from Ref. (11). Volatile compounds are grey-shadowed

for PET, which are mainly driven by transesterification and homolytic reactions. Regarding the gaseous compounds resulting from the thermal decomposition of PET, reported studies [15-16] show the release of main products such as carbon dioxide, acetaldehyde, benzaldehyde, vinyl benzoate, terephthalic acid, terephthaldehydic acid and linear dimers, and other products such as carbon monoxide, carbon monoxide, methane, ethylene, ketene, 1,4-dioxane, toluene, benzaldehyde, divinyl terephthalate, benzoic acid and cyclic dimers and trimers. The relative abundance of each compound depended on factors such as the grade of the polymer, the chemical modification, the sensitivity of each used technique, as well as the specific conditions of each experiment. Concerning thermo-oxidative decomposition [17], mainly yields acetaldehyde, formaldehyde and carbon monoxide at low temperatures and aliphatic and aromatic hydrocarbons, along with carbon monoxide at higher temperatures.

With regards to experimental procedures, common studies about the thermally-induced decomposition of PET have focused their interest in the characterization of the thermal stability, decomposition mechanisms and the emission of

volatile low molecular weight compounds [11], both in inert [18-19] and oxidative [20-21] atmospheres, also considering the influence of additives such as stabilizers or flame-retardants [22]. Concerning theoretical approaches, literature reports indicate that different researchers use different kinetic models and diverse kinetic methodologies to perform their studies and come up to the kinetics of the thermal or thermo-oxidative decompositions, in an attempt to reach the description of pyrolysis and combustion of their polymers, respectively. This fact often provokes confusion in ascertaining which model is more suitable and therefore should be used to best represent the system under study [23-24]. With the purpose of overcoming this confusion, a detailed methodology is presented in this work, as well as the suitability of using a simplified kinetic triplet is addressed.

Summing up, the aim of this work is to assess the combination of mechanical recycling and energetic valorisation procedures on a model polymer (i.e. PET) with the aim of obtaining a reliable methodology transferable to other polymeric materials. The study was focused in three aspects (**Figure 2**): (i) the control of gases emitted in relationship with the thermolytic

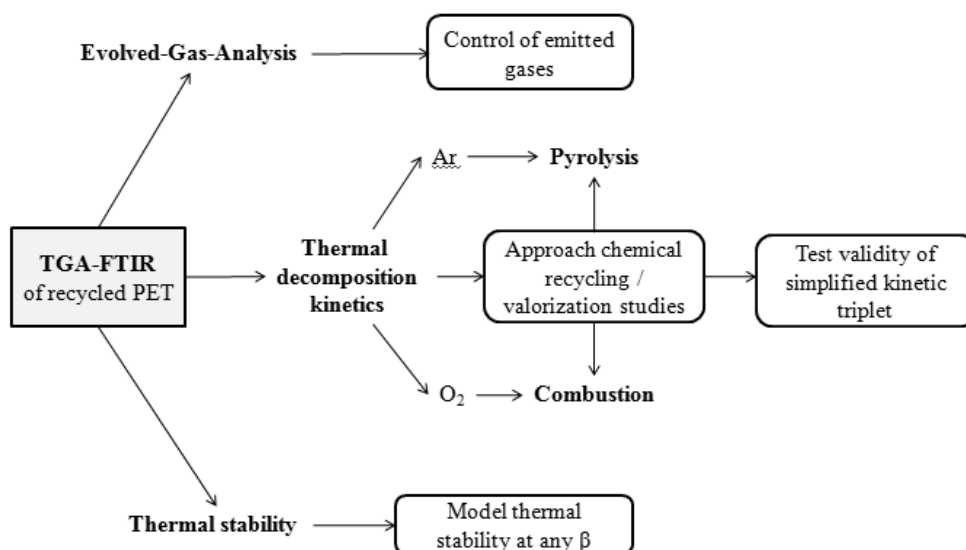


Figure 2. Combined strategy of assessment

mechanisms; (ii) the assessment of the influence of thermo-mechanical degradation induced by reprocessing on the thermal stability of PET under thermal and thermo-oxidative decomposition conditions; and (iii) the modelling of the energetic valorisation processes such as pyrolysis and combustion as a contribution to further plastic waste management solutions, when no more profit can be drawn from the polymer or the accumulation of plastic waste has to be reduced. In order to achieve the purposes, a simulation procedure consisting in five successive reprocessing cycles was used to induce the modifications that PET suffers through thermo-mechanical degradation during mechanical recycling. Afterwards, multi-linear non-isothermal thermogravimetric experiments were performed to model pyrolysis and combustion under different experimental conditions, in order to apply a detailed kinetic methodology that would furnish with the knowledge of the kinetic models that may explain the bulk thermal decomposition of PET at high temperatures, under different atmospheres.

2. Theoretical background

2.1. 2D-Correlation IR Spectroscopy

2D-Correlation IR Spectroscopy (hereafter *2D-IR*) has gained much attention since its introduction [10], as different reviews state [25]. Essentially, in *2D-IR*, a spectrum is collected as a function of two independent *IR* wavenumbers, due to the application of an external perturbation, and offers information that could not be obtained by conventional analysis of one-dimensional *IR* spectra. In this work, temperature is used as external input. A deep explanation of this

analytical procedure can be found elsewhere [10, 26-28]. However, a short description with the basics that help interpret the discussion of results of this study is given hereafter.

By applying the *Hilbert* transform method, the synchronous and asynchronous correlation spectra of two signals i and j at different wavenumbers ν can be described by Eq. (1) and Eq. (2), respectively:

$$\varphi(\nu_i, \nu_j) = (T_{max} - T_{min})^{-1} \cdot \int_{T_{min}}^{T_{max}} \tilde{y}(\nu_i, t) \cdot \tilde{y}(\nu_j, t) \cdot dt \quad (1)$$

$$\Psi(\nu_i, \nu_j) = (T_{max} - T_{min})^{-1} \cdot \int_{T_{min}}^{T_{max}} \tilde{y}(\nu_i, t) \cdot \tilde{z}(\nu_j, t) \cdot dt \quad (2)$$

where T_{min} and T_{max} are the limit temperatures of the *TGA* experiment, ν is the spectral variable (wavenumber in *IR* spectroscopy), \tilde{y} is the dynamic spectra and \tilde{z} its Hilbert transform, which expressions are shown in Eq. (3) and Eq. (4), respectively:

$$\tilde{y}(\nu, t) = \begin{cases} y(\nu, t) - \bar{y}(\nu), & t \in [T_{min}, T_{max}] \\ 0, & else \end{cases} \quad (3)$$

$$\tilde{z}(\nu, t) = \frac{1}{\pi} \cdot \int_{T_{min}}^{T_{max}} \tilde{y}(\nu, t') \cdot (t' - t)^{-1} \cdot dt' \quad (4)$$

being \bar{y} the reference spectrum usually time-averaged as:

$$\bar{y}(\nu, t) = \int_{T_{min}}^{T_{max}} y(\nu, t') \cdot dt \quad (5)$$

The synchronous spectra reflect the correlation of simultaneously varying of spectral intensity, while the asynchronous spectra reflect the non-comparability of spectral intensity variations, due to $\tilde{z}(\nu, t)$ is orthogonal to $\tilde{y}(\nu, t)$ and therefore appears when two signals are out-of-phase.

Therefore the synchronous and asynchronous spectra are symmetrical and anti-symmetrical with respect to their diagonal lines, respectively. The discussion of both types of graphs is given in terms of auto and cross peaks.

The auto-peaks (ν_i, ν_i) , (ν_j, ν_j) in synchronous spectra rely on the diagonal line and their intensity reflect the influence of the external perturbation on the molecular groups of wavenumbers ν_i and ν_j . Cross-peaks (ν_i, ν_j) , (ν_j, ν_i) off-diagonally located, represent the synchronicity of groups corresponding to wavenumbers ν_i and ν_j , stressing the strong cooperation or interaction between their different molecular groups. A positive cross-peak describes the increase or decrease of the intensities of both ν_i and ν_j , while a negative cross-peak indicates an increase in the intensity of ν_i during a decrease of ν_j .

The asynchronous spectrum has no auto-peaks by definition. The cross-peaks in this case represent the sequential changes of the spectral intensities ν_i and ν_j due to the asynchrony of the variations in their intensities. This characteristic is also very useful for distinguishing between overlapped bands that arise from different spectral variations. The rules for determination of the sequence of spectral intensity changes are shown as follows:

a) If intensity in the synchronous spectrum is positive: $\varphi(\nu_i, \nu_j) > 0$

a.1.) A positive cross-peak in the asynchronous spectrum $\Psi(\nu_i, \nu_j) > 0$ states that the change in intensity of ν_1 occurs before the change in ν_2 .

a.2.) A negative cross-peak in the asynchronous spectrum $\Psi(\nu_i, \nu_j) < 0$ states that the change in intensity of ν_2 occurs before the change in ν_1 .

b) If intensity in the synchronous spectrum is negative: $\varphi(\nu_i, \nu_j) < 0$, the rules above are reversed.

2.2. Kinetic methodology

In the attempt to develop a model for plastic thermal and thermo-oxidative decompositions in full-scale systems, the main purpose is to describe the behaviour of polymers in terms of an intrinsic kinetics, in which heat and mass transfer limitations are not included. General kinetic models are proposed in literature for plastics and biomasses. These models do not take into account the rigorous and exhaustive description of the chemistry of thermal decomposition of polymers and describe the process by means of a simplified reaction pathway. It is widely known that each single reaction step considered is representative of a complex network of reactions [29].

Recently, *Khawan* and *Flanagan* [30] have reviewed the relationship between the theoretical decomposition mechanisms and their mathematical models, the so-called kinetic functions $f(\alpha)$. The kinetic analysis of non-isothermal experiments is generally performed by using a single step kinetic equation:

$$\begin{aligned} \frac{d\alpha}{dt} &\equiv \beta \cdot \frac{d\alpha}{dT} = A \cdot f(\alpha) \cdot k(T) \\ &= A \cdot f(\alpha) \cdot e^{-\frac{E\alpha}{R \cdot T}} \end{aligned} \quad (6)$$

, where t is the time (t), T the temperature (K), α is the conversion degree, β is the heating rate

used in the thermogravimetric experiment ($\text{K}\cdot\text{s}^{-1}$), R is the ideal gas constant ($8.31 \text{ J}\cdot\text{mol}^{-1}\cdot\text{K}^{-1}$), A a pre-exponential factor (s^{-1}), $f(\alpha)$ the kinetic function and Ea is the activation energy ($\text{J}\cdot\text{mol}^{-1}$). For thermogravimetric experiments, $\alpha = (m_0 - m_t)/(m_0 - m_\infty)$, where m stands for mass (g), and subscripts 0 , ∞ and t respond to initial, final and actual thermogravimetric values. The obtaining of the so-called kinetic triplet ($f(\alpha)$ -model, Ea , A) may provide new knowledge regarding the kinetic model of thermal and thermo-oxidative decomposition for virgin PET and its recyclates, and offer new insights in further energetic valorisation processes for this polymer.

The integration of Eq. (6) after rearranging, leads to:

$$\begin{aligned} g(\alpha) &= \int_0^\alpha \frac{d\alpha}{f(\alpha)} = \frac{A \cdot Ea}{\beta \cdot R} \cdot \int_0^\infty \frac{e^{-x}}{x^2} \\ &= \frac{A \cdot Ea}{R \cdot T} \cdot p(x) \\ x &= \frac{Ea}{R \cdot T} \end{aligned} \quad (7)$$

Under linear heating rate program, Eq. (7) does not have an exact analytical solution to the temperature integral $p(x)$ and therefore some studies have reported different equations to approach the best values within the lower error margin [31]. In this work, the *Senum-Yang* [32] approximation (Eq. (8)) truncated at its fifth term was used, since it gives deviations from the exact value of the temperature integral lower than 10^{-8} % for $x > 10$ [33], which permits its application in solid-state decomposition reactions, where x is usually higher.

$$p(x) = \frac{e^{-x}}{x^2} \cdot \sum_n \frac{n \cdot (1 - n)}{x + 2 \cdot (n + 1)} \quad (8)$$

2.2.1. Determination of activation energy – isoconversional methods.

Solid-state kinetics were developed from reaction kinetics in homogeneous systems (i.e gases and liquids), and it has been generally assumed that the activation energy and the pre-exponential factor remain constant. However, it has been proved that these kinetic parameters may vary with the progress of the decomposition of solids. This variation can be detected by isoconversional methods, which use data from different multi-linear non-isothermal experiments and do not take modelistic assumptions for the analysis, main source of error of model-fitting methods. The most broadly used isoconversional methods are those integral linear methods developed by *Flynn-Wall-Ozawa (FWO)* [34-35] (supported on *Doyle's* integral approximation [36] and *Kissinger-Akahira-Sunose (KAS)* [37-38], which are represented at Eq. (9) and Eq. (10), respectively. These methods give rise to linear functions from which slopes the Ea at a fixed α is obtained.

$$[\log(\beta)]_y = \log\left(\frac{A_\alpha \cdot Ea_\alpha}{R \cdot g(\alpha)}\right) - 2.315 - \frac{0.457 \cdot Ea_\alpha}{R} \cdot \left[\frac{1}{T_\alpha}\right]_x \quad (9)$$

$$\left[\ln\left(\frac{\beta}{T^2}\right)\right]_y = \ln\left(\frac{A_\alpha \cdot R}{Ea_\alpha \cdot g(\alpha)}\right) - \frac{Ea_\alpha}{R} \cdot \left[\frac{1}{T_\alpha}\right]_x \quad (10)$$

, where $g(\alpha)$ is the inverse integral kinetic model, obtained as:

$$g(\alpha) = \int_0^\alpha (f(\alpha))^{-1} \cdot d\alpha \quad (11)$$

Vyazovkin and *Dollimore* [39] proposed a more accurate integral non-linear method (*IYZ*), which is based on the following expression:

$$\Omega = \left| \sum_{i=1}^h \sum_{j \neq i}^h \frac{\beta_j I(Ea_\alpha, T_\alpha^i)}{\beta_i I(Ea_\alpha, T_\alpha^j)} \right|, \quad (12)$$

$$I(Ea_\alpha, T_\alpha^{i,j}) = p_{i,j} \left(\frac{Ea_\alpha}{R \cdot T_\alpha} \right)$$

, where i and j are counters through the h experiments performed at different heating rates. The activation energy (Ea_α) is the value that minimizes Ω in Eq (12) for a particular α .

2.2.2. The use of Master-Plots

The reaction model may adopt various expressions, based on nucleation and nuclei growth, phase boundary reactions, diffusion or chemical reactions. The environmental gases, inert or reactive, have important roles regarding the selection of the decomposition models. A list of the most common $f(\alpha)$ applied to polymers is given at **Table 1**. Master Plots ($M-P$) are reference theoretical curves ($M-P_i$) depending on the kinetic model, but generally independent of the kinetic parameters of the process. Due to, in many cases, the experimental kinetic data can be easily transformed into experimental curves $M-P_e$, a comparison with the $M-P_i$ allows the selection of the appropriate kinetic model of the process under investigation or, at least, reducing the span of suitable kinetic models [40]. There exist three main types of $M-P_i$, those based on the differential form ($M-P_f$) of the generalized kinetic equation Eq (6); those based on the integral form ($M-P_g$), according to Eq. (7); and the most common one that combines both differential and integral forms ($M-P_{fg}$), that are usually reduced at $\alpha=0.5$ for better visualization. The mathematical description of each curve can be found elsewhere [40]. They are described after the introduction of the so-called generalized time θ , which denotes

the reaction time taken at a particular α at infinite temperature, defined as [41-42]:

$$\theta = \int_0^t e^{-\frac{Ea}{R \cdot T}} \cdot dt \quad (13)$$

, which differentiation in combination with Eq. (6), gives:

$$\frac{d\alpha}{d\theta} = A \cdot f(\alpha) = \frac{d\alpha}{dt} \cdot e^{\frac{Ea}{R \cdot T}} \quad (14)$$

Therefore, assuming A and Ea constant, due to interdependence of kinetic parameters, and using a reference point at $\alpha=0.5$, the theoretical $M-P_i$ and the expression for the reduced form of the experimental data can be drawn from Eq. (13) and Eq. (14) obtaining Eq. (15) and Eq. (16) for $M-P_f$ and $M-P_g$, respectively:

$$\frac{\frac{d\alpha}{d\theta}}{\frac{d\alpha}{d\theta}|_{0.5}} = \frac{f(\alpha)}{f(0.5)} = M-P_t \equiv M-P_e$$

$$= \frac{\frac{d\alpha}{dt} \cdot e^{\frac{Ea}{R \cdot T}}}{\frac{d\alpha}{dt}|_{0.5} \cdot e^{\frac{Ea}{R \cdot T}|_{0.5}}} \quad (15)$$

$$\frac{\theta}{\theta_{0.5}} = \frac{g(\alpha)}{g(0.5)} = M-P_t \equiv M-P_e = \frac{p(x)}{p(x_{0.5})} \quad (16)$$

To enhance the study given in this work, instead of using a constant Ea for all the process, the varying Ea_α obtained in the previous section was applied, calculating the $M-P_e$ points at each specific α . The advantage of using $M-P_f$ and $M-P_g$ in contrast to $M-P_{fg}$ is that the formers disperse clearly among different models in the ranges $\alpha < 0.5$ and $\alpha > 0.5$ respectively, therefore permitting a straightforward identification, whereas the latter tends to produce confusion due to the coincidence of lines from different kinetic models.

Table 1 Algebraic expressions for the kinetic functions of the most common models in solid-state reactions

Type	Model	Symbol	f(α)
NUCLEATION	random nucleation and growth of nuclei (Johnson-Mehl-Avrami)	A_n	$n \cdot (1 - \alpha) \cdot [-\ln(1 - \alpha)]^{1 - \frac{1}{n}}$
	n -order (instantaneous nucleation and n-dimensional growth)	F_n	$(1 - \alpha)^n$
REACTION	phase boundary controlled reaction (contracting n dimensions, n-dimensional shape)	R_n	$n \cdot (1 - \alpha)^{\frac{1}{n}}$
DIFFUSION	two-dimensional diffusion (bi-dimensional particle shape)	D_2	$[-\ln(1 - \alpha)]^{-1}$
	three-dimensional diffusion (tridimensional particle shape) (Jander equation)	D_3	$\frac{3 \cdot (1 - \alpha)^{\frac{2}{3}}}{2 \cdot (1 - \alpha)^{\frac{1}{3}}}$
	three-dimensional diffusion (tridimensional particle shape) (Ginstein-Brounshtein equation)	D_4	$\frac{3}{2 \cdot \left[-1 + (1 - \alpha)^{\frac{1}{3}}\right]}$

2.2.3. Independence of heating rate

In order to complete the kinetic triplet, the pre-exponential factor A has to be found. As well, the *Perez-Maqueda et al* criterion (*P-Mc*) [43] has to be accomplished; that is, the independence of the activation parameters E_a , A on the heating rate β . This criterion is usually employed with E_a and A invariable with the aid of the *Coats-Redfern* [44] equation written in the form:

$$\left[\ln \frac{\beta \cdot g(\alpha)}{T^2} \right]_y = \ln \frac{A \cdot R}{E_a} + \frac{E_a}{R} \cdot \left[\frac{1}{T} \right]_x \quad (17)$$

, the points $\{x, y\}$ should lie on the same straight line to all heating rates. In this work, the variation of A along the decomposition reaction A_α is evaluated along with the effective variation of E_{a_α} obtained by the isoconversional methods.

3. Experimental procedures

3.1. Reprocessing simulation and sample preparation

Poly (ethylene terephthalate) (PET) SEDAPET SP04 is a bottle-grade PET obtained from Catalana de Polimers S.A., Grup LaSeda (Barcelona, Spain) in the form of pellets. Prior to processing, virgin PET (VPET) pellets were dried during 5 h at 160 °C in a dehumidifier Conair Micro-D FCO 1500/3 (UK), in order to remove as much humidity as possible from the PET flakes. Afterwards, samples were processed by means of injection moulding employing an Arburg 420 C 1000-350 (Germany) injector, single-screw model (diameter $\Phi=35$ mm, length/ $\Phi=23$). Successive processing steps were

applied under the same conditions. Temperature gradient set from hopper to die was 270, 275, 280, 285 and 280 °C. Moulds were set at 15 °C. Cooling time residence was 40 s and total residence time ca. 60 s. Samples were dried before each processing cycle. After injection, a fraction of the samples was kept as test specimen and the rest was ground by means of a cutting mill Retsch SM2000 (UK), which provided pellets of size $\Phi < 20$ mm to be fed back into the recirculation process. Up to five processing cycles were applied to obtain the different testing specimens of reprocessed PET (RPET-i, with i: 1-5).

3.2. Thermogravimetric experiments.

Multi-linear non-isothermal thermogravimetric experiments were carried out in a Mettler-Toledo TGA/SDTA 851 (Columbus, OH). Samples weighing ca. 5 mg were heated in an alumina holder with capacity for 70 μ L. Experiments were performed from 25 to 900 °C at different heating rates ($\beta = 2, 5, 7, 10, 12, 15, 17, 20, 25, 30$ °C \cdot min $^{-1}$), under constant flow of 50 mL \cdot min $^{-1}$ of gas of analysis. An inert Ar atmosphere was used for assessing the thermal decomposition behaviour, whereas an O₂ reactive atmosphere was applied for characterizing the thermo-oxidative decomposition processes of PET and its recyclates. Experiments were repeated at least three times, and the averages were considered as representative values.

3.3. Evolved Gas Analysis

Evolved Gas Analysis (EGA) was applied to fumes released by both thermal and thermo-oxidative processes by means of coupled TGA/FT-IR. In this case, the TGA analysis was performed by means of a heating rate of 1 °C \cdot min $^{-1}$, according to the equipment

specifications. Samples weighing ca. 40 mg were heated in an alumina holder with capacity for 900 μ L. The flow rate of the carrier gas was set to 25 mL \cdot min $^{-1}$. FT-IR gas-phase spectra were collected by a Thermo Nicolet 5700 FT-IR Spectrometer (MA, USA), previously calibrated, from 4000 to 600 cm $^{-1}$ of wavenumber, at a resolution of 4 cm $^{-1}$. Both transfer line and gas cell were kept at 250 °C to prevent gas condensation. 16 coadded spectra were recorded every 30 s to assure the accuracy of the temperature scanning.

3.4. Analytical software and computational assumptions.

Thermogravimetric characterization was described with the aid of the software STAR^e 9.10 from Mettler-Toledo. FT-IR spectra were characterized by OMNIC 7.0 from Thermo Scientific. 2D IR was performed by means of the software 2Dshige [45]. Kinetic analyses were performed in the conversion degree α range from 0,1 to 0,8 since the main reaction took place in this region. All thermogravimetric data were analyzed using Microsoft® Excel software. Vyazovkin method required the tool Solver® of this mathematical package, by applying Newton method with progressive derivatives, setting an accuracy of 10 $^{-6}$ and a tolerance of 10 $^{-4}$. Fitting procedures were performed by means of OriginLab OriginPro 8.0, which uses the Levenberg-Marquardt algorithm [46-47] to adjust the parameter of the fitting values in the iterative procedure.

Values are plotted in terms of {average, dev_{max}, dev_{min}}, where dev_{max} = max(data)-average(data), and dev_{min} = average (data)-min(data). Tabulated errors were obtained by dividing the standard deviation by the average of data.

4. Discussion of results

The influence of multiple reprocessing on poly (ethylene terephthalate) was deeply characterized by Thermogravimetry (*TGA*), focusing on 3 types of analyses to offer a complete description of the thermally-induced decomposition processes that PET and its recyclates are submitted to at high temperatures in non-isothermal conditions, under inert and reactive atmospheres. Discussion is given in terms of the effects of thermo-mechanical degradation induced by multiple reprocessing on PET, as well as in terms of the suitability of *TGA* hyphenated with *FT-IR* to characterize the performance of polymers under thermal or thermo-oxidative decomposition conditions. In the first section, the study of the evolved gases (*EGA*) is studied by means of Fourier-Transform-Infra-Red (*FT-IR*) and 2D spectroscopic correlation (*2D-IR*). Afterwards, the thermal stability is evaluated and modelled in terms of characteristic temperatures. Finally, the kinetics of thermal and thermo-oxidative decomposition are evaluated by means of advanced kinetic methods that allow

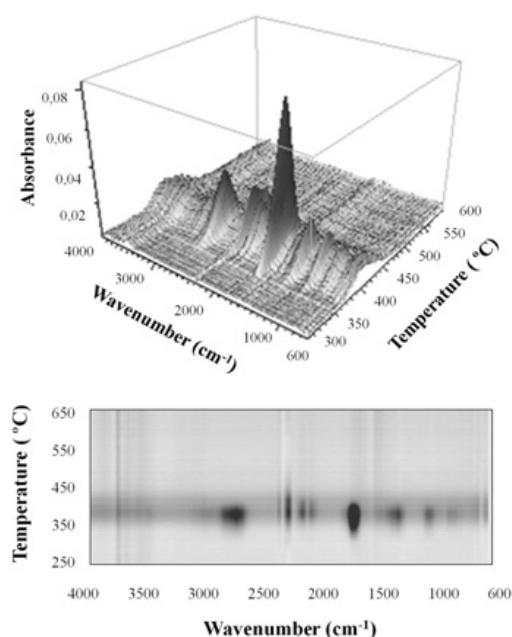


Figure 3. 3D/FT-IR and contour 2D/FT-IR plots of the thermal decomposition of virgin PET.

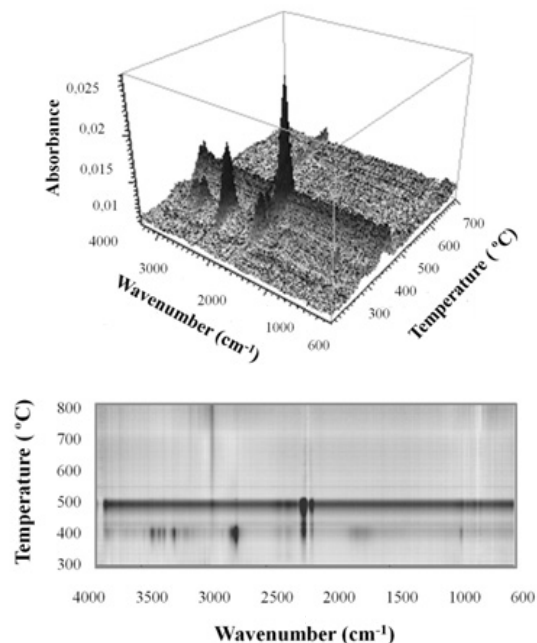


Figure 4. 3D/FT-IR and contour 2D/FT-IR plots of the thermo-oxidative decomposition of virgin PET.

modelling both pyrolysis and combustion processes with kinetic parameters expressed not only as a constant, but as a function depending on the conversion degree α . The suitability of using a simplified kinetic triplet, where activation parameters are considered constant, is assessed as well.

4.1. Evolved Gases Analysis: control of emission.

Before considering thermolytic procedures for the energetic recovery of plastics, the release of gaseous compounds has to be controlled, in order to establish proper facilities that reduce the emission of hazardous compounds to the environment. Owing to its cost-effectiveness, reliability to detect main evolved gases, and ease to be incorporated into in-line industrial processes, *FT-IR* was chosen for the analysis.

Due to the complexity of the oligomeric distribution of PET [6], different gaseous compounds can be released [15-17].

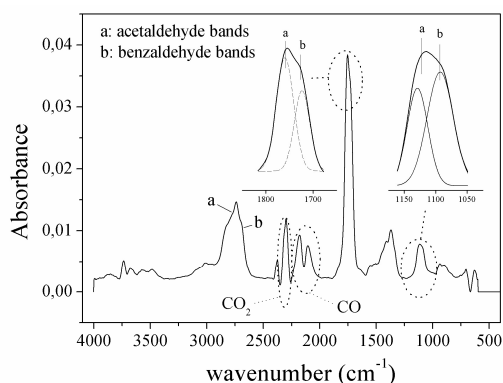


Figure 5. FT-IR spectra at the maximum decomposition rate of the thermal decomposition of virgin PET. Details of selected deconvolutions are given inserted.

Proper data analysis such as the use of *2D IR* correlation spectroscopy can help determine the main decomposition mechanisms taking place. **Figure 3** and **Figure 4** show the *3D/FT-IR* spectra and contour *2D/FT-IR* maps for the thermal decomposition (*TD*) and thermo-oxidative decomposition (*TOD*) of virgin PET, respectively. The pattern of gases released under inert atmosphere differed from that obtained under oxidative conditions. **Figure 5** and **Figure 6** represent the *FT-IR* spectra at the maximum

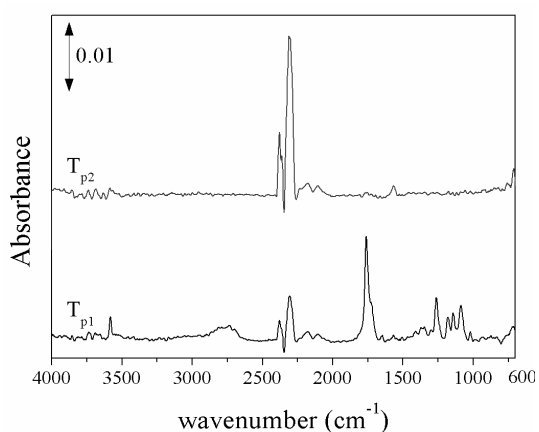


Figure 6. FT-IR spectra at the maximum decomposition rates of the thermo-oxidative decompositions of virgin PET. Tp1 and Tp2 stand for the first and second mass-loss peaks, respectively.

decomposition rates. PET decomposed in a progressive fashion under Ar, involving the common release of different compounds (**Figure 5**), while under O₂, PET decomposition was driven by two stages of decomposition (**Figure 6**). A list of the most significant gases is given in **Table 2**.

Table 2. Summary of major gases released during thermal and thermo-oxidative decompositions, as observed by FT-IR analysis.

Compound	Wavenumber (cm ⁻¹)	Vibrations *	Relative intensity in FTIR spectra	
			Ar	O ₂
Acetaldehyde	2968	ν (CH ₃)	↑↑	↑↑
	2740	ν (CHO)		
	1762	ν (C=O)		
	1414+1371	δ (CH ₃)		
	1127	ν (C-O)		
Benzaldehyde	2690	ν (CHO)	↑	↓
	1724	ν (C=O)		
	1081	ν (C-O)		
	936	δ_{oop} (C-H) _{arom}		
CO ₂	2356	ν_{as} (O=C=O)	↑↑	↑↑
CO	2174 + 2116	ν (C≡O)	↑↑	↓
* Notation on vibrations				
ν : stretching / δ : in-plane bending / ν_{as} : asymmetric / ν_{oop} : out-of-plane				

Under inert atmosphere, major observable gases by *FT-IR* were acetaldehyde, carbon monoxide, and carbon dioxide. The presence of peaks in the 1500-1600 cm⁻¹ and 800-950 cm⁻¹ regions, corresponding to aromatic species could be related to the release of compounds like benzene, benzoic acid or benzaldehyde, among other minor compounds. Due to the small presence of OH groups related to acids in the 3400-3800 cm⁻¹ region that may tend to decarboxylate giving rise

to CO₂, and according to the main decomposition mechanisms widely accepted for PET, the release of benzaldehyde was also considered. As well, small traces of water and methane could be taken into account.

The aldehydic peaks corresponding to acetaldehyde and benzaldehyde appeared overlapped, and therefore a deconvolution procedure by means of Lorentzian curves was applied in different characteristic stretching vibration regions (H-C=O; C=O and C-O). From each set of curves, benzaldehyde bands were those shifted to lower wavenumbers in comparison to those of acetaldehyde, due to the interaction with the aromatic group. Summing up, the following bands were assigned for further characterization : acetaldehyde [2968 cm⁻¹ ν (CH₃), 2740 cm⁻¹ ν (CHO), 1760 cm⁻¹ ν (C=O), 1414/1371 cm⁻¹ δ (CH₃) and 1127 cm⁻¹ ν (C-O)], benzaldehyde [2690 cm⁻¹ ν (CHO), 1724 cm⁻¹ ν (C=O), 1081 cm⁻¹ ν (C-O) and 936 cm⁻¹ δ_{oop} (C-H)_{arom}] carbon monoxide [2179/2106 cm⁻¹ ν (CO)]; and carbon dioxide [2356 cm⁻¹ ν_{as} (O=C=O)].

Under oxidative conditions, the first decomposition stage produced similar compounds to those obtained in inert conditions, and therefore can be assigned to the pyrolytic behaviour of PET, severely due to thermal conditions. As main differences attributable to the action of O₂, a major predominance of acetaldehyde to a detriment of benzaldehyde was observed, as well as a minor production of CO, being the release of CO₂ remarkably prevalent. In contrast to what happened under inert conditions, at higher temperatures, the thermo-oxidative decomposition of PET released CO₂, due to the combustion of the remaining char.

2D-Correlation Infra-Red Spectroscopy (2D-IR) was applied to the first stages of both thermal (TD) and thermo-oxidative (TOD) decompositions, which gave the same profile of results (Figure 7), thus confirming that the same mechanisms took place.

The synchronous spectrum (*S-2D*) in the 4000-600 cm⁻¹ region (Fig 7. (a)) shows the predominant auto-peaks of the main groups [ν (C=O), ν (CHO), ν (C-O), δ (CH₃), ν (C≡O) and ν_{as} (O=C=O)], with their corresponding positive cross-peaks which indicate the same behaviour of appearance for all bands. The asynchronous spectrum (*A-2D*) in the 2900-1600 cm⁻¹ region (Fig 7. (b)) shows four major negative cross peaks (*NCP*) at (2356, 1760), (2356, 1724), (2106, 1760), (2106, 1724) which indicate that both acetaldehyde and benzaldehyde were released before CO and CO₂. These results are in agreement with the general mechanism of thermal decomposition in which a first release of an aldehydic compound due to back-biting intramolecular esterification leaves an acid-terminated chain which may continue back-biting or decarboxylate to give out carbon oxides. Between these carbon oxides, the release of CO started before the appearance of CO₂, as shown by the *A-2D* in the 2400-2000 cm⁻¹ region (Fig 7. (c)). On the other hand, the *PCP* at (1760, 1724), (2740, 2690) and (1127, 1081) in the *A-2D* in the wavenumber regions (cm⁻¹) 1900-1700 (ν (C=O)), 2900-2400 (ν (CHO)) and 1600-800 (ν (C-O)), shown at Fig 7. (d), (e) and (f), respectively, clearly state that the first compound to evolve was acetaldehyde. As can be seen at the contour 2D/FT-IR map of thermal decomposition (Figure 3) when aldehydic compounds disappeared, CO and CO₂ still evolved at higher temperatures, being CO₂ the last released

compound. Summing up, in comparison with the general thermolytic mechanisms of PET given in **Figure 1**, one can figure out that both *TD* and

TOD were initiated by transesterification reactions, giving preference to the formation of acetaldehyde.

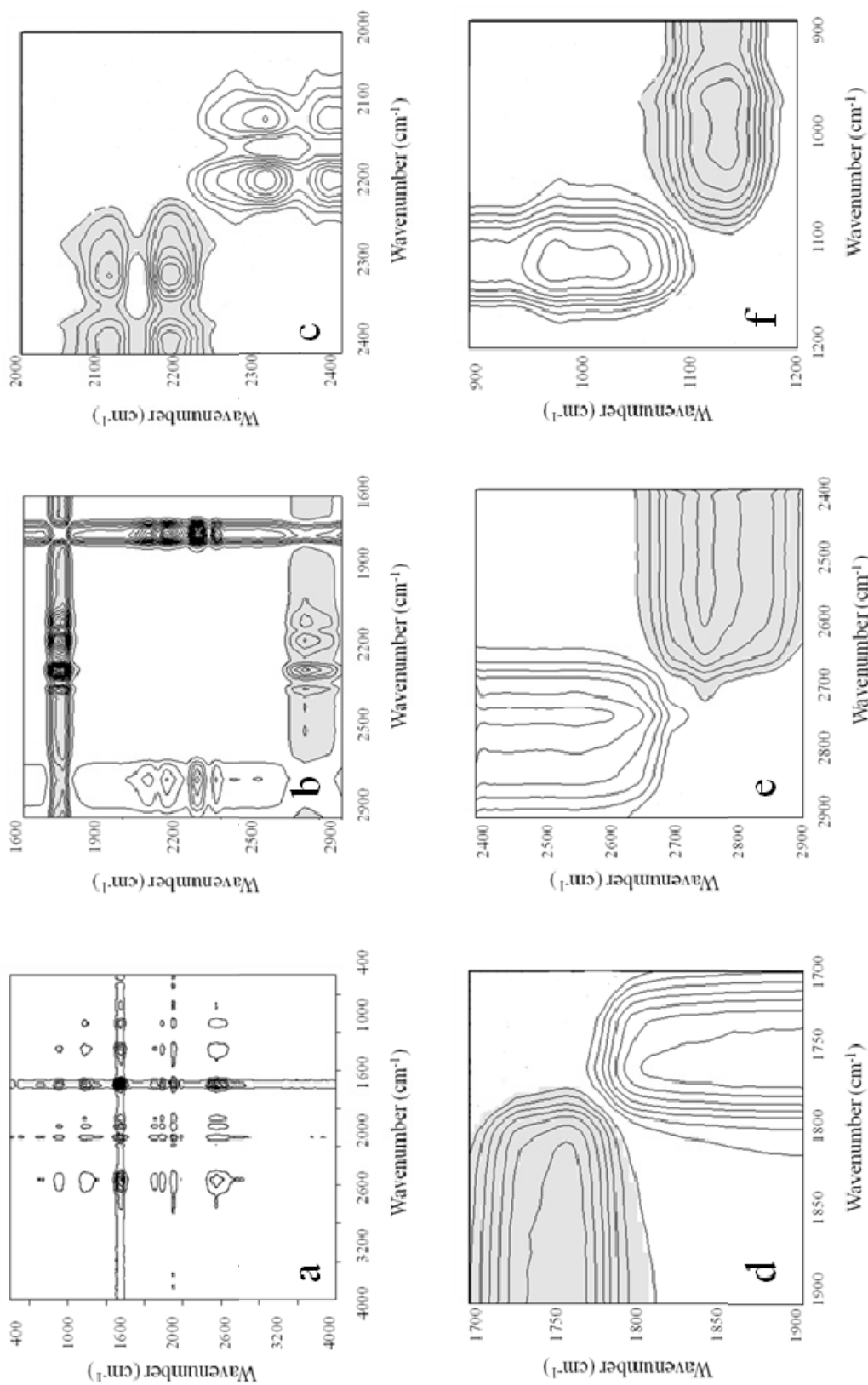


Figure 7. 2D-IR correlation spectra of the thermal decomposition of virgin PET at selected wavenumber regions (see text for details).

Homolytic scissions took place simultaneously during *TD* and continued at high temperatures. During *TOD*, homolysis disabled transesterification reactions at high temperatures, giving rise to the combustion of the material to mainly give CO_2 . Thus, the establishment of proper operation temperatures might control the nature of the gases released.

It is worth mentioning that the behaviour described is valid not only for virgin PET but also for the rest of reprocessed materials. Despite the material suffers chemical modifications in its structure and morphology due to thermo-mechanical degradation [6], at temperatures above the melting, the polymer decomposed in a similar fashion. Gram-Schmidt plots of evolved gases (not shown for conciseness) gave alike spectra under each atmosphere, only shifting the maximum decomposition regions, as shown in the next section. This fact is very important, since it means that the same facilities used to control the emission of gases for virgin PET could be adapted to its recyclates with no extra cost.

4.2. Thermal stability studies

In this section, the thermal performance of PET recyclates (RPET-*i*) was compared to that of virgin PET (VPET). A preliminary analysis of the differences observed in thermal stability temperatures was performed. For this purpose, the thermal decomposition curves (*TG*) and their first-order derivative curves (*DTG*) were analyzed after each reprocessing step at different heating rates β and compared to the *TG* and *DTG* curves of the virgin PET. **Figure 8** shows the influence of the thermal (*TD*) and thermo-oxidative (*TOD*) decomposition processes on the *TG* curve displayed for VPET and RPET-5; the

experiments of the other recyclates are omitted for the sake of clarity, but laid between those limiting lines. As usual, higher β lead to shift the thermograms to higher temperatures.

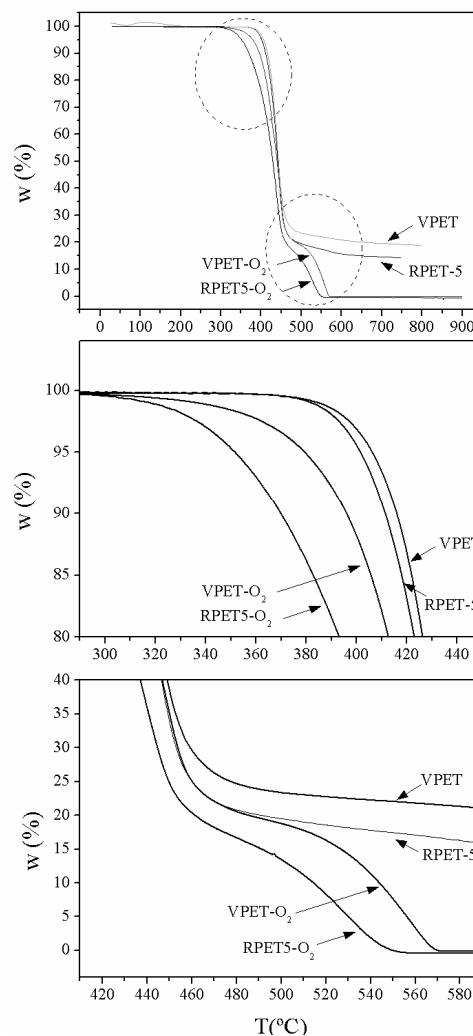


Figure 8. Thermogravimetric curves of virgin PET and its fifth recycle under both Ar and O₂ atmospheres (upper: full scale; middle: detail of onset of decompositions; lower: detail of endset of decomposition).

The *TD* of PET occurred through a single decay stage, regardless the reprocessing cycle and the β employed for the thermogravimetric analysis. After a long thermostability range, the material decomposes fast, consuming the majority of the mass. Afterwards, the remaining char

Table 3. Percentage of mass-loss for virgin PET and its recyclates after thermal and thermo-oxidative decomposition.

		VPET		RPET-1		RPET-2		RPET-3		RPET-4		RPET-5	
		Mass loss	e	Mass loss	e	Mass loss	e	Mass loss	e	Mass loss	e	Mass loss	e
Ar	Step 1 (%)	79,9	1,2	81,2	3,1	81,7	2,2	83,4	3,6	84,2	2,5	84,8	2,5
	Step 2 (%)	21,1	2,1	22	2,8	21,4	2,7	21	3,9	21,1	3,1	20	3,3

*Average and standard deviations (sd) taken from the analyses at different heating rates. Values given in percentages.

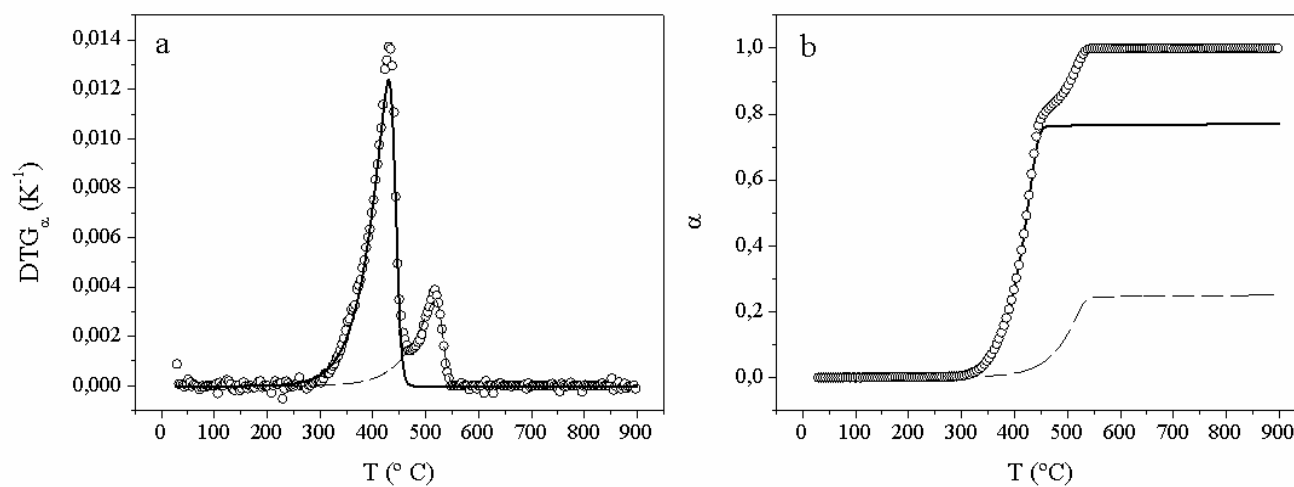


Figure 9. (a) Fitting-Deconvolution applied to virgin PET at experiment performed at 5 °C.min⁻¹. (b) Result on the evolution of the conversion degree α . (Hollow circles:experimental data; solid line: first mass-loss step; dashed line: secon mass-loss step.)

continuously smoothly decomposed until the end of the experiment, without showing any appreciable reaction, as was shown by *FT-IR* analysis of the evolved gases (*EGA/FT-IR*). The main mass-loss step slightly increased (from 80 to 85%) with each reprocessing step, as shown in **Table 3**, clear effect of a weakened material.

On the other hand, the *TOD* of PET followed a two-step mass-loss process. As expected, the use of an oxidative atmosphere fastened the decomposition of the material, shifting the *TG* curves to lower temperatures in comparison to those obtained by means of inert gas. Since the presence of oxygen did not significantly alter the beginning of the decomposition, it could be guessed that the chemical reaction that led the main mass-loss was of the same nature under both environments, as corroborated by the study of *EGA/FT-IR*. In contrast, the presence of O_2 enhanced the decomposition of the remaining char found in inert conditions, consuming therefore nearly the whole amount of material, since the remaining residue could be considered negligible ($\sim 0.5\%$).

The effect of reprocessing is patent comparing the *TOD* of VPET and RPET-5. Due to thermo-mechanical degradation, the reprocessed material had more potential sites liable to oxidation, as shown in previous studies [6], and therefore in presence of O_2 , the difference in thermal stability would be larger. For further analysis, the two-step thermo-oxidative decomposition was deconvoluted by means of Eq. (18) applied to the *DTG* curve, in order to characterize individually each of the contributions to the overall decomposition:

$$\frac{d\alpha}{dT}(T) = \frac{d\alpha}{dT}\Big|_{A=0} + \sum_i A_i \cdot \left(1 + e^{-\frac{T-T_i-w_{1i}/2}{w_{2i}}} \right)^{-1} \cdot \left(1 - \left(1 + e^{-\frac{T-T_i-w_{1i}/2}{w_{3i}}} \right)^{-1} \right) \quad (18)$$

, where A_i and T_i are the amplitude and peak temperature of each i peak; and w_{1i} , w_{2i} , w_{3i} are dispersion coefficients that adjust the width, asymmetry and skewness of the curves [48]. All fittings provided regression coefficients (R^2) higher than 98.5 %. **Figure 9** shows an example of the deconvolution procedure applied to virgin PET in terms of α vs. T and its first-derivative curve DTG_α . A posterior integration of the areas under each curve provided the relative importance of each mass-loss step to the overall decomposition. In contrast to studies under inert gas, the thermo-oxidative decomposition took place through a first step that consumed 77-80 % of mass, followed by a second step with a consumption of the resting 23-20 %, as showed in **Table 3**.

In order to assess the thermal stability under both inert and oxidative conditions, the corresponding decomposition onset and endset temperatures (T_{on} , T_{end}) were obtained by a tangential intercept method onto the *TG* curves for the whole process. Likewise, the temperature at the maximum decomposition rate $da \cdot dT^{-1}$, i.e. the peak temperature of the *DTG* curve, which is related to the inflection temperature of the *TG* curve (T_p) was also considered for both mass-loss processes. **Figure 10** shows the influence of the heating rate β on the aforementioned temperatures for the case of VPET, tested under Ar and O_2 . The same trend was shown by all PET recyclates. Technologist may be interested in finding the relationship between the influence of β and the characteristic *TGA* temperatures to

model the thermal stability behaviour of PET. That would be useful to predict the decomposition temperatures of PET under any β . At fast β , the relationship was almost linear, but it bended when β approached slower values. Other authors proposed linear dependences [49], but it was higher to nearly $15\text{ }^{\circ}\text{C}\cdot\text{min}^{-1}$ that the tendency got to a linear asymptote. It would be therefore interesting to apply functions to predict the thermal decomposition behaviour (*TDB*) of PET under any β . Eq. (19), where a , b and k are parameters of the fitting, was used in this study for this purpose, and its extension for the study of the *TDB* of other polymeric materials is proposed. The suitability of this expression can be checked at the regression coefficients shown in **Table 4** and **Table 5** for inert and oxidative conditions, respectively, along with the values of the fitting parameters.

$$TDB(\beta) = a \cdot (1 + b \cdot e^{-k \cdot \beta})^{-1} \quad (19)$$

With the aim of assessing the influence of thermo-mechanical degradation induced by multiple reprocessing on PET, the use of temperature parameters obtained for a single heating rate are not recommended, since they can be strongly dependent on the experimental

settings. In this work, the Zero-Decomposition Temperatures (*ZDT*), with subscripts 0 , p , e for onset, peak and endset, which are the temperatures at which *TDB* ($\beta \rightarrow 0$), are proposed, due to its use may attenuate the abovementioned experimental errors. On the other hand, one may be tempted to use the same expression and extrapolate to “infinite” β values, since *TDB* ($\beta \rightarrow \infty$) = a , and then perform *TGA* experiments at high β in order to ease the procedure, but it can be observed how a fluctuated within small ranges, and better tendency is shown by the *ZDT*.

Figure 11 displays the *ZDT* values for all materials under *TD* and *TOD*, along with the temperature range in which the decomposition would take place at β close to 0 ($ZDT_e - ZDT_0$), which results were quite useful for interpretation. *TD* started at higher temperatures up to RPET-2, recyclelate from which the ZDT_0 evolution became steady. It was shown in other studies by *MALDI-TOF-MS* [6] and *ATR/FT-IR* [50] that the oligomeric distribution of virgin PET was characterized by the presence of extra glycol units in the backbones of both cyclic and linear species, which disappear due to reprocessing.

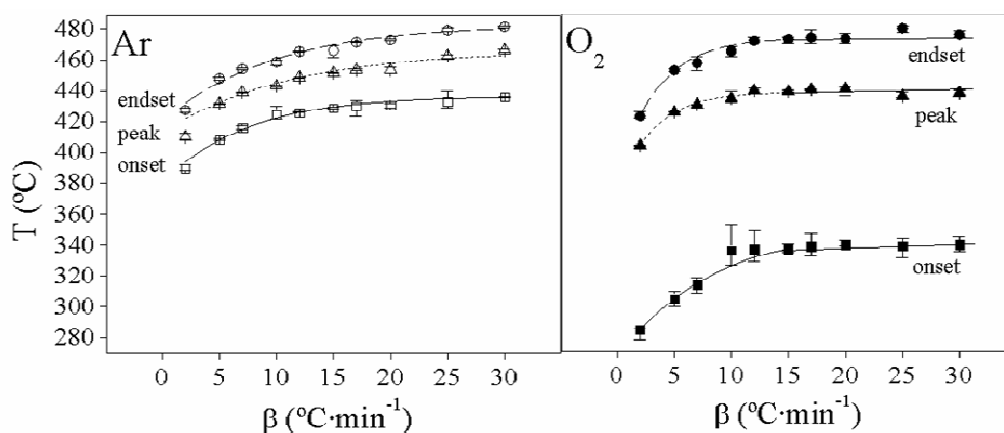


Figure 10. Thermal stability assessments. Fitting to equation *TDB* (Eq. 19).

Table 4. Fitting results obtained from modelling the evolution of the characteristic TGA temperatures to Eq.19 under inert conditions (0: onset / p: peak / e: endset)

Material	ZDT	Parameters						R ²
		a		b		k		
		value	e	value	e	value	e	
VPET	ZDT ₀	436,57	0,12 %	0,16	4,10 %	0,146	5,59 %	0,993
	ZDT _p	465,83	0,47 %	0,13	4,69 %	0,099	1,85 %	0,986
	ZDT _e	482,53	0,41 %	0,15	6,51 %	0,113	1,13 %	0,975
RPET-1	ZDT ₀	442,54	0,51 %	0,16	3,88 %	0,106	1,15 %	0,991
	ZDT _p	470,00	0,28 %	0,16	5,92 %	0,081	0,75 %	0,947
	ZDT _e	479,99	0,43 %	0,15	6,36 %	0,136	1,27 %	0,981
RPET-2	ZDT ₀	439,91	0,51 %	0,14	5,05 %	0,137	1,38 %	0,988
	ZDT _p	464,04	0,30 %	0,15	1,57 %	0,115	5,18 %	0,998
	ZDT _e	479,39	0,20 %	0,16	2,83 %	0,148	5,45 %	0,995
RPET-3	ZDT ₀	455,00	0,49 %	0,16	8,62 %	0,149	1,91 %	0,973
	ZDT _p	458,40	0,29 %	0,14	3,22 %	0,121	4,81 %	0,996
	ZDT _e	473,10	0,70 %	0,14	6,24 %	0,110	1,72 %	0,947
RPET-4	ZDT ₀	438,70	0,36 %	0,12	5,80 %	0,115	1,19 %	0,987
	ZDT _p	451,00	0,29 %	0,12	10,86 %	0,167	1,44 %	0,985
	ZDT _e	472,98	0,24 %	0,14	5,31 %	0,144	1,26 %	0,992
RPET-5	ZDT ₀	436,66	0,36 %	0,12	5,67 %	0,140	3,66 %	0,987
	ZDT _p	453,00	0,12 %	0,12	6,28 %	0,140	1,05 %	0,995
	ZDT _e	474,15	0,31 %	0,15	4,99 %	0,137	1,16 %	0,986

Table 5. Fitting results obtained from modeling the evolution of the characteristic TGA temperatures to Eq.19 , under oxidative conditions (0: onset / p: peak / e: endset) .

Material	ZDT	Parameters						R ²
		a		b		k		
		value	e	value	e	value	e	
VPET	ZDT ₀	347,67	1,38%	0,30	6,15%	0,149	1,44%	0,996
	ZDT _p	438,63	0,43%	0,17	3,15%	0,338	1,07%	0,997
	ZDT _e	473,87	0,32%	0,22	11,87%	0,308	4,38%	0,983
RPET-1	ZDT ₀	335,88	2,21%	0,29	18,23%	0,254	4,43%	0,932
	ZDT _p	435,88	0,39%	0,16	12,33%	0,424	3,81%	0,972
	ZDT _e	473,06	0,74%	0,15	0,87%	0,300	5,07%	0,951
RPET-2	ZDT ₀	332,63	0,45%	0,31	1,52%	0,230	5,29%	0,998
	ZDT _p	459,72	0,36%	0,27	5,50%	0,783	1,66%	0,961
	ZDT _e	471,86	0,48%	0,14	10,52%	0,270	5,28%	0,971
RPET-3	ZDT ₀	343,00	0,54%	0,25	24,77%	0,143	2,03%	0,994
	ZDT _p	449,21	2,23%	0,25	7,86%	0,168	4,86%	0,935
	ZDT _e	474,29	0,50%	0,15	4,02%	0,231	1,24%	0,993
RPET-4	ZDT ₀	343,30	0,33%	0,27	7,52%	0,179	5,09%	0,999
	ZDT _p	436,30	0,79%	0,24	15,98%	0,346	3,26%	0,931
	ZDT _e	479,17	0,27%	0,16	3,44%	0,238	6,02%	0,995
RPET-5	ZDT ₀	371,99	3,51%	0,40	10,90%	0,096	1,73%	0,996
	ZDT _p	444,90	0,53%	0,26	5,39%	0,236	1,37%	0,984
	ZDT _e	475,74	0,43%	0,17	2,30%	0,238	0,89%	0,997

This fact may leave fewer regions liable to decomposition and thus an increase of the ZDT_0 was registered. On the other hand, ZDT_p and ZDT_e slightly decreased also down to RPET-2, indicating that the remaining species were weakened by reprocessing, and therefore the maximum decomposition rate happened at lower temperatures. The reduction of the thermal decomposition range along the successive reprocessed materials also indicated the weakening of PET.

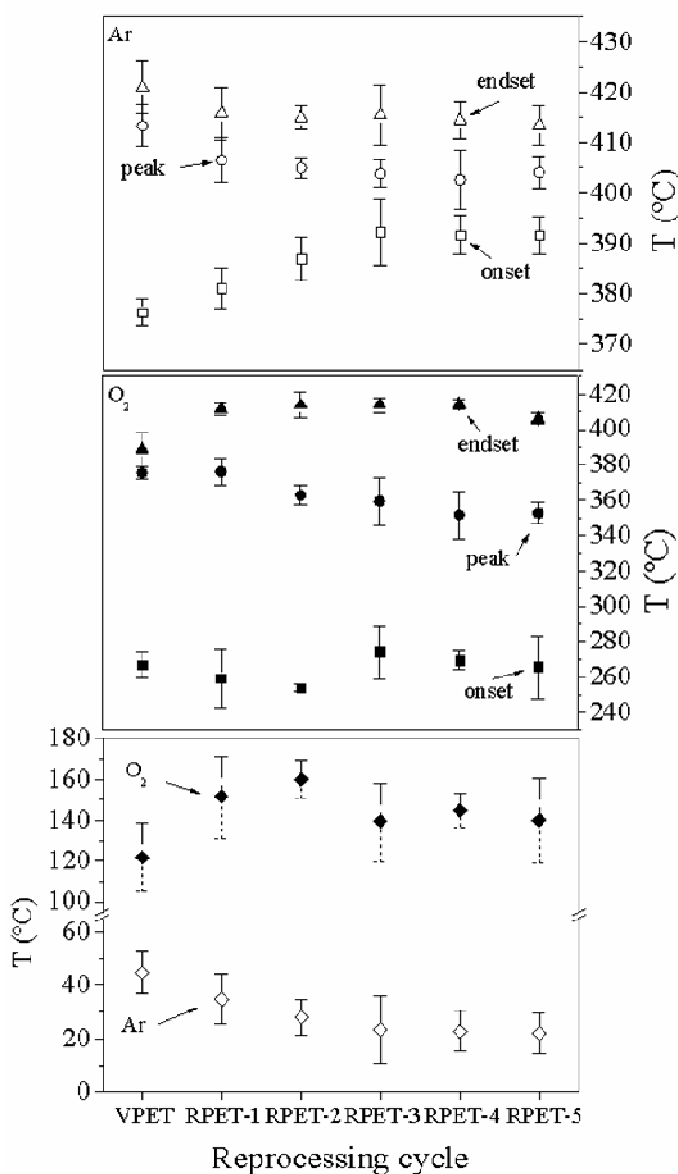


Figure 11. Thermal stability assessments. Evolution of ZDT at inert (upper) and oxidative (middle) conditions. The ZDT ranges at both atmospheres are given in the lower plot.

Concerning the TOD , the added action of O_2 initiated the decomposition ~ 100 °C lower tendency can be drawn from ZDT_0 , due to homolytic reactions might disable the predominant mechanism of transesterification under Ar. Nevertheless, ZDT_p showed a tendency similar to that shown by the same parameter in inert conditions, since it is more sensible to the strength of the backbone facing the decomposition. On the other hand, the second mass-loss process occurred in a wider temperature range with each reprocessing step, and thus it would enlarge the ZDT_e and the decomposition temperature range. However, it was strongly influenced by the first mass-loss step and therefore there were some temperature shifts that did not permit to apply Eq. (19) with high R^2 . This may be due to the difference in mass of the specimens, which could be higher to make the second step more reproducible. In this case, the peak temperature of the second process of the experiment performed at 5 °C·min⁻¹ is shown for interpretation at **Figure 12**. The evolution of this parameter also showed the decrease of the thermal stability of PET with the reprocessing cycles, since the decomposition of the remaining char demanded lower temperature.

Summing up, one may be careful when comparing the thermal stability of PET at different atmospheres, due to the underlying predominant decomposition mechanism might be different, and thus led to different interpretations, mainly at the beginning of the process. The use of the peak ZDT_p to monitor the weakening of the material against thermal and thermo-oxidative decompositions is remarkable. The change in tendency from VPET→RPET-2 to RPET-3→RPET-5 for all parameters may indicate the threshold of recycling for the

material in terms of thermal performance. These results were corroborated by those obtained from the kinetic study, which is shown as follows.

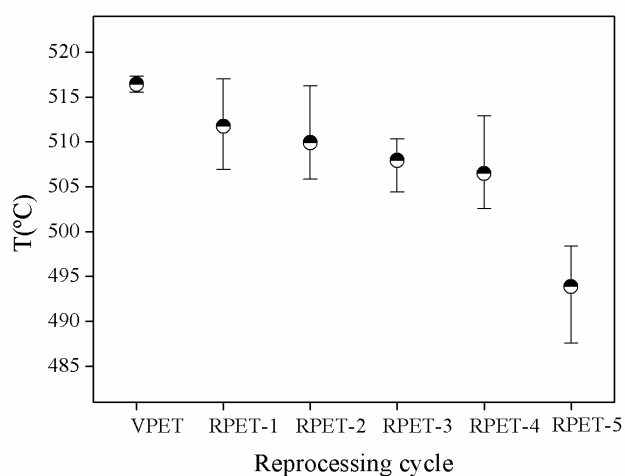


Figure 12. Thermal stability assessments. Evolution of the peak temperature of the second thermo-oxidative decomposition process of virgin PET.

4.3. Thermal and thermo-oxidative decomposition kinetics

Regardless the competitive chemical mechanisms involved in the thermal and thermo-oxidative decomposition of PET, the possibility of modelling its thermal performance in terms of an intrinsic kinetics will help technologists to approach the experimental settings of energetic valorisation processes such as pyrolysis or combustion. For this purpose, a methodology that combined (i) isoconversional methods, (ii) comparison of experimental data with theoretical Master-Plots, and (iii) *Perez-Maqueda et al.* criterion was carried out. It is common to establish a set of constant activation energy (E_a) and pre-exponential factors (A) to explain the behaviour throughout the whole decomposition process. In contrast, the variation of the kinetic parameters with the conversion degree was considered in this paper, with the aim of

modelling the TD and TOD processes with accurate precision. The possibility of using a simplified kinetic triplet (SKT) is addressed at the end of this analysis.

Flynn-Wall-Ozawa (FWO), *Kissinger-Akahira-Sunose (KAS)* and *Vyazovkin (VYZ)* methods were firstly applied to evaluate the dependence of the apparent activation energy (E_a) with the conversion degree α , avoiding the interference of an initial assumption of a specific kinetic model. **Figure 13** shows the results of the application of the isoconversional methods on virgin PET thermogravimetric data. **Fig.13 (a)** shows an example for the goodness of *FWO* method, since well-defined straight lines were obtained, from which slope the apparent activation energy was found for each conversion degree ($E_{a_{FWO}}$). The evolution of $E_{a_{FWO}}$ with α is shown in **Fig. 13 (b)**, along with the evolution of the apparent activation energies obtained by *KAS* ($E_{a_{KAS}}$) and *VYZ* ($E_{a_{VYZ}}$) methods. The regression coefficient of the linear *FWO* and *KAS* methods was far above the 95 % of confidence for experiments under Ar (as shown in inset at **Fig. 13 (b)**), whereas this coefficient dropped between an acceptable 92-96% range for experiments performed under O_2 . *VYZ* results accomplished the minimum tolerance set at 5%, as pointed out in the experimental section. It has to be stressed that for all materials at both tested environments, the results obtained by the three methods were pretty similar, but they are not shown for the sake of conciseness. The variation of the average apparent activation energy obtained by the isoconversional methods ($E_{a_{iso_\alpha}}$) is shown for virgin PET and its five successive recycles thermally decomposed in inert and oxidative atmospheres at **Fig. 13 (c)** and **(d)**, respectively. Two different behaviours could be

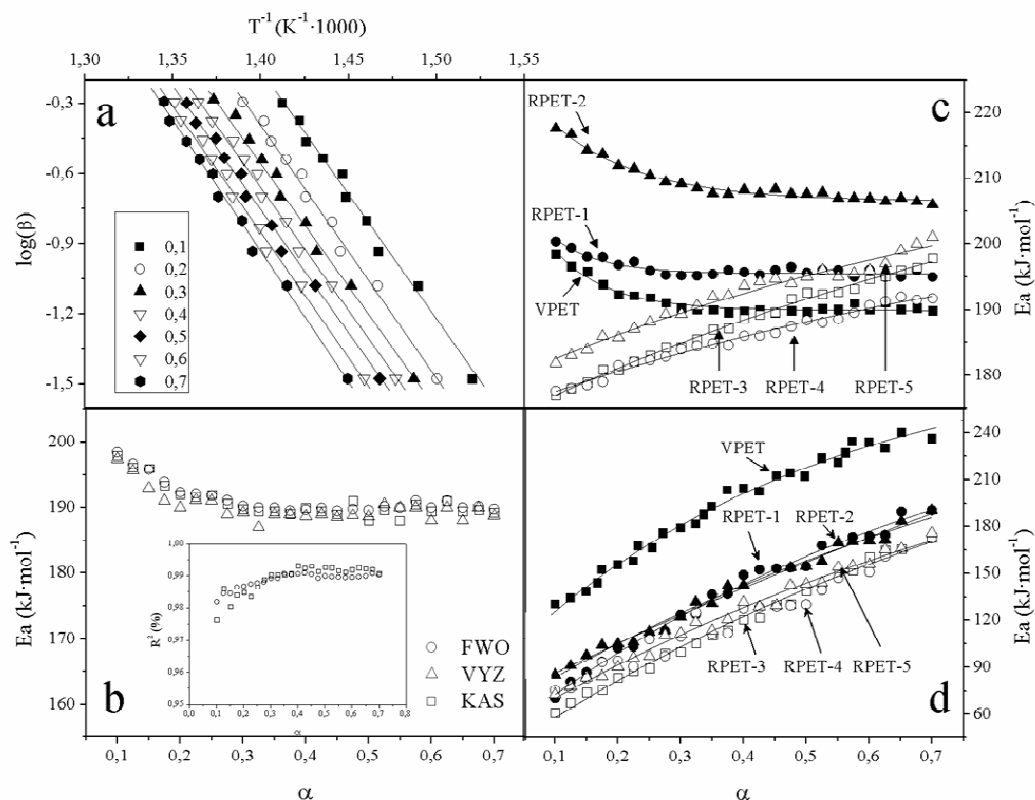


Figure 13. Application of isoconversional methods to virgin PET. (a) An example of FWO method for experiments under Ar; (b) E_a evolution with the conversion degree evaluated by FWO, KAS and VYZ methods (inset: regression coefficients of fittings); (c) Effect of recycling on the E_a evolution of PET under Ar atmosphere; (d) Idem to (c) but under O_2 atmosphere. Note: In (c) and (d) the solid lines represent the fitting of the proposed equation to the experimental E_a variation..

distinguished for TD , where VPET and RPET-1,2 showed an initial decrease approaching a constant value at $\alpha > 0.3$, whereas RPET-3,4-5 described an increasing slope from the beginning of the decomposition. On the other hand, during TOD , all materials showed the same increasing trend for $E_{a_{iso-\alpha}}$. According to the shape of the curves [51], the TD of VPET, RPET-1,2 has reversible stages, probably due to instantaneous reactions between short-chain acidic and alcoholic compounds to form esteric structures which immediately decomposed. Due to further thermo-mechanical degrading action, these reactions may be disabled for RPET-3, 4, 5, where now the parallel formation of aldehydic

compounds and carbon oxides may provoke the continuous increase of $E_{a\alpha}$. The presence of O_2 would also act promoting the volatilization reactions, without allowing recombination.

It was found that Eq. (20) fitted the experimental data with good correlation coefficients, as reflected in **Table 6**.

$$Ea(\alpha) = Ea^I + (Ea^{II} - Ea^I) \cdot e^{-\left(\frac{\alpha}{p}\right)} \quad (20)$$

, where Ea^I and Ea^{II} are parameters that can be obtained from the intercept at $\alpha = 0$ and in the asymptote, giving an idea of the amplitude of decomposition, and p is a power to correct the curvature of the function. This equation allows

Table 6. Results of fitting procedure to E_{aFWO} dependence with α .

Conditions	Material	Ea^I	e^I	Ea^{II}	e^{II}	p	e^p	R^2 (%)
Ar	VPET	189.88	0.08 %	218.94	1.84 %	0.0855	2.55 %	0.955
	RPET-1	195.52	0.06 %	216.04	1.44 %	0.0728	3.08 %	0.968
	RPET-2	206.58	0.10 %	230.18	0.70 %	0.1384	2.85 %	0.980
	RPET-3	229.26	0.26 %	172.49	0.14 %	1.2150	0.65 %	0.994
	RPET-4	209.34	0.30 %	174.12	0.17 %	0.9853	1.14 %	0.985
	RPET-5	219.25	0.42 %	178.44	0.27 %	0.9443	1.53 %	0.974
O ₂	VPET	293.91	1.37 %	88.76	3.52 %	0.5040	2.38 %	0.964
	RPET-1	289.85	1.07 %	42.11	3.17 %	0.7631	3.93 %	0.990
	RPET-2	320.00	1.27 %	60.57	3.05 %	1.0791	1.02 %	0.989
	RPET-3	307.63	1.18 %	31.51	3.17 %	1.0010	0.88 %	0.991
	RPET-4	266.53	3.19 %	45.76	4.43 %	1.0001	1.09 %	0.986
	RPET-5	296.91	1.38 %	53.96	4.00 %	1.0010	2.60 %	0.944

modelling both increasing and decreasing tendencies, also adapting to acceleration and deceleration phenomena. High regression coefficients obtained from the fitting ($R^2 > 95\%$), as well as the narrow confidence bands in which the nominal powers laid ($< 3.1\%$) were obtained. These parameters were useful for the characterization of the thermal behaviour of PET and its recyclates, where p values close to 0 indicated an Ea becoming almost constant, while higher p (close to 1) approached linear tendencies. Taking into account the whole α range, in inert conditions, an Ea increase was observed from VPET to RPET-1,2, therefore indicating higher energy to trigger the decomposition of the materials, probably due to the recombination of the chains scissored during reprocessing, as suggested in a previous study [6], where the formation of cyclic PET oligomers from the loss of an extra glycol unit in cyclic

oligomers was shown. These results were in agreement with the increase of temperature needed to trigger the decomposition (ZDT_0). Afterwards, a general decrease down to orders lower than those shown by VPET was obtained, as a weakening effect of the thermo-mechanical degradation induced to PET recyclates. The presence of more linear hydroxyl- and carboxyl-terminated linear species [6], more liable to temperature, could trigger and propagate the TD reactions in a faster fashion and therefore less energy would be needed. On the other hand, facing TOD , all recyclates showed a general decrease in their Ea , in two steps: from VPET to RPET-1,2; and then to RPET-3,4,5. As expected, the TOD of all materials would be initially achieved with less energy than the TD , due to the added influence of the oxidative ambient, as can be checked at **Figure 13**. The presence of O₂ attacks the structure of PET disabling the thermal

stability mechanisms of its recyclates and showing therefore a progressive degradation throughout the reprocessing cycles. From a cost-effective point of view, taking into account the energetic demand of each process, the combustion of reprocessed PET might result more interesting than its pyrolysis, specially bearing in mind that the thermal performance of PET is lost after the second recycle.

In order to continue with the kinetic methodology, the next step was the evaluation of the kinetic model. The Master Plots based on the differential form of the generalized kinetic equation were used, for the kinetic functions shown at **Table 1**. Eq. (21) was used to select the kinetic model that better fitted the experimental data, taking into account the experiments at all heating rates, where f_t and f_e are the theoretical and experimental kinetic functions in their differential form, which expressions can be obtained from **Table 1** and the right-hand of Eq. (15), respectively. The model that provided a minimum value of Φ was of the type A_n (Growth of previously formed nuclei) for virgin PET and all its recyclates under both environments. **Figure 14** shows the Master-Plots comparison as an example of the goodness of A_n to model the behaviour of both TD and TOD of VPET and RPET-1 along the studied α range for the experiment at $5\text{ }^\circ\text{C}\cdot\text{min}^{-1}$.

$$\Phi(f_t, \alpha) = \sum_{\beta} \left(\sum_{\alpha} [f_t(\alpha) - f_e(\alpha)]^2 \right), \quad (21)$$

$$\Delta\alpha = 0.025$$

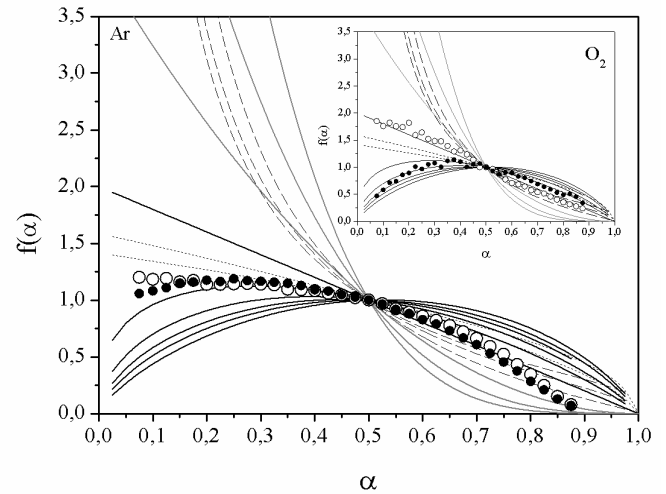


Figure 14. Master-Plots in the differential form for virgin (hollow) and first PET recycle (full) at $5\text{ }^\circ\text{C}\cdot\text{min}^{-1}$ for both environments. Kinetic models: An (Solid black lines), Fn (solid grey lines), Rn (pointed lines), Dn (dashed lines)

Taking into account that a suitable kinetic triplet should fulfil the *Perez-Maqueda et al* criterion (*P-Mc*); that is, the independence of the activation parameters Ea , A on the heating rate β , the minimization of ξ in Eq. (22) would provide the best n for the modelization, and thereafter provide the most accurate A , by averaging the A_β obtained from the intercept at $y=0$ of *Coats-Redfern* [44] expression (Eq. (23)), since among the different methods that calculate the Ea from a given $f(\alpha)$, this one was demonstrated to offer precise results [31]. The calculations were performed taking into account all h experiments with different β , and the integral form of the model A_n .

$$\xi(n, \alpha) = \sum_i^h \left| (-R) \cdot \frac{d}{dT} \left(\frac{\ln(\beta_i \cdot T^{-2} (-\ln(1-\alpha))^{\frac{1}{n}})}{T^{-1}} \right) - Ea_\alpha \right| \quad (22)$$

Table 7. Ranges of n for A_n kinetic model

		VPET		RPET-1		RPET-2		RPET-3		RPET-4		RPET-5	
method		n	e _{P-Mc}	n	e _{P-Mc}	n	e _{P-Mc}	n	e _{P-Mc}	n	e _{P-Mc}	n	e _{P-Mc}
Ar	M-P _f	1-1.5		1-1.5		1-1.5		1-1.5		1-1.5		1-1.5	
	P-M _C	1.380	1.45 %	1.365	1.52 %	1.223	1.11 %	1.384	1.12 %	1.371	1.31 %	1.375	1.21 %
O ₂	M-P _f	1		1.5-2		1-1.5		2-2.5		2-2.5		1.5-2	
	P-M _C	1.012	3.18 %	1.892	3.52 %	1.642	4.13 %	2.368	5.22 %	2.151	4.01 %	1.710	3.62 %

$$\left[\ln \frac{\beta \cdot (-\ln(1 - \alpha))^{\frac{1}{n}}}{T^2} \right]_y = \ln \frac{A_\beta \cdot R}{E a_\beta} + \frac{E a_\beta}{R} \cdot \left[\frac{1}{T} \right]_x \quad (23)$$

Table 7 reports the n values in which the experimental data laid, which range was approached by the application of the differential Master-Plots ($M-P_f$), in comparison with the averaged n value analytically obtained by the application of *Perez-Maqueda et al.* criterion ($P-M_C$), which offered nearly constant n values with a fairly small deviation for TD and acceptable values with error margins < 5.5 % for TOD . The consistency of the results given by both methods is remarkable.

Figure 15 shows the evolution of $\ln A_\alpha$ for virgin PET and its recyclates under inert and reactive atmospheres. Deviation among experiments performed at different heating rates was negligible therefore confirming the goodness of A_n as kinetic model. Finally, in order to mathematically describe the variation of the pre-exponential factor with α , the evolution of $\ln A_\alpha$ was also fitted to Eq. (20), by changing Ea into $\ln A$. **Table 8** shows the results of the fitting for all materials. Regression coefficients showed values above 95 %, strengthening the suitability of Eq. (20) as modeling function for the pre-exponential factor, as can be also checked at **Figure 15**.

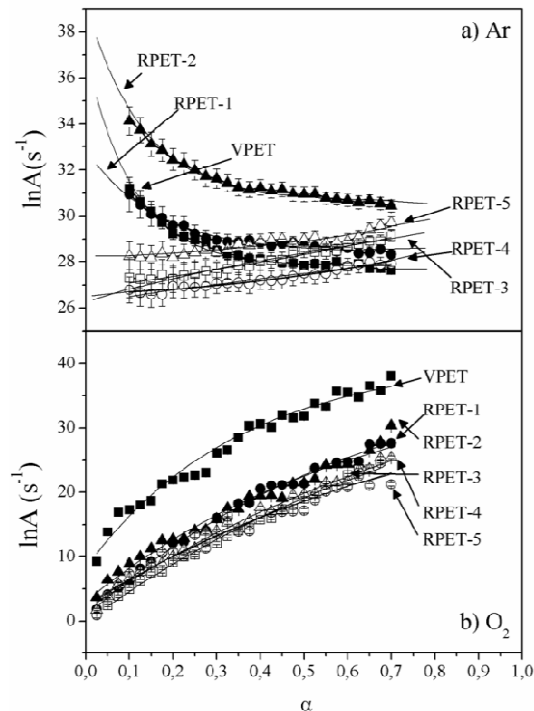


Figure 15. Variation of $\ln A$ for all materials under inert (a) and oxidative (b) conditions

This kinetic methodology therefore permitted to accurately describe the kinetic model for explaining the thermal and thermo-oxidative decomposition behaviours of virgin PET and successive recyclates, being the variation of the kinetic parameters specifically determined along the decomposition process. According to the results, the kinetic model that better explained both processes was a nucleation and growth model (A_n). Despite this kind of model is quite common in crystallization processes, for thermal and thermo-oxidative decompositions, it is scarcely reported [52-26]. However, in these studies, the controversy of the relationship between the mathematical models and the physical mechanisms was remarkable, as well as different assumptions such as constant Ea were taken. Even more, according to *Mamleev et al.* [57], the initial stage of polymer decomposition is often accompanied by the melting, where the control of the process is mainly run by the

formation of gas phase inside the molten polymer, and thus by nucleation and nuclei growth in an heterogeneous medium. Due to the low β used in the case of non-isothermal decompositions, low Ea_a values controlled the formation of nuclei, while a rapid increase in Ea_a controlled the nuclei growth [58]. This fact also pointed out the weakening of the material due to thermo-mechanical degradation induced by multiple processing, remarkably up to the second recycle, where the differences in behaviour among recycled materials were less noticeable. Therefore, under inert conditions, the formation of nuclei was important at the initial steps of decomposition for VPET, RPET-1,2, while the release of growing gas bubbles in the melt ruled the decomposition from the beginning for the rest of recyclates. Under an oxidative atmosphere, the decomposition of all materials was ridden by an increasing Ea_a throughout the process, since the liability of PET to react with O_2 induced potential sites where the reactions of gas formation could take place. The fact that the kinetic component inherent to the material, i.e. the kinetic model, did not change is very interesting, which means that technologists may transfer the procedures used for the pyrolysis and combustion of virgin PET to its recyclates, by only taking into account the kinetic components related to the temperature in relation with the variation in apparent activation energy throughout the decomposition processes.

4.4. Validity of a simplified kinetic triplet (SKT)

Most of the studies found in the literature report the parameters of the kinetic triplet (Ea , A) as constant values along the whole decomposition process. The possibility of approaching the behaviour of the thermal and thermo-oxidative decomposition processes by a simplified kinetic

Table 8. Results of fitting procedure to $\ln A_\alpha$ dependence with α to Eq 20.

Conditions	Material	$\ln A^I$	$e^{\ln A^I}$	$\ln A^{II}$	$e^{\ln A^{II}}$	$p_{\ln A}$	$e^{p_{\ln A}}$	R^2 (%)
Ar	VPET	27,81	0,17%	37,05	1,16%	0,1092	1,48%	0,955
	RPET-1	28,40	0,16%	32,81	1,30%	0,1630	2,18%	0,868
	RPET-2	30,64	0,21%	39,28	1,31%	0,1302	2,77%	0,980
	RPET-3	23,05	0,81%	26,83	0,21%	-1,4999	0,88%	0,994
	RPET-4	25,87	0,27%	26,55	0,15%	-0,6002	1,23%	0,985
	RPET-5	27,86	1,87%	28,19	0,55%	-0,4302	2,15%	0,974
O ₂	VPET	40,90	0,96%	8,26	1,03%	0,3532	2,24%	0,964
	RPET-1	41,75	6,56%	0,64	2,34%	0,6503	1,17%	0,990
	RPET-2	39,49	1,74%	3,03	4,92%	0,6529	1,94%	0,989
	RPET-3	45,18	1,23%	0,18	4,98%	0,9015	0,94%	0,991
	RPET-4	42,35	2,67%	2,56	2,25%	0,9688	2,17%	0,986
	RPET-5	47,00	1,36%	1,73	3,05%	0,9801	1,12%	0,944

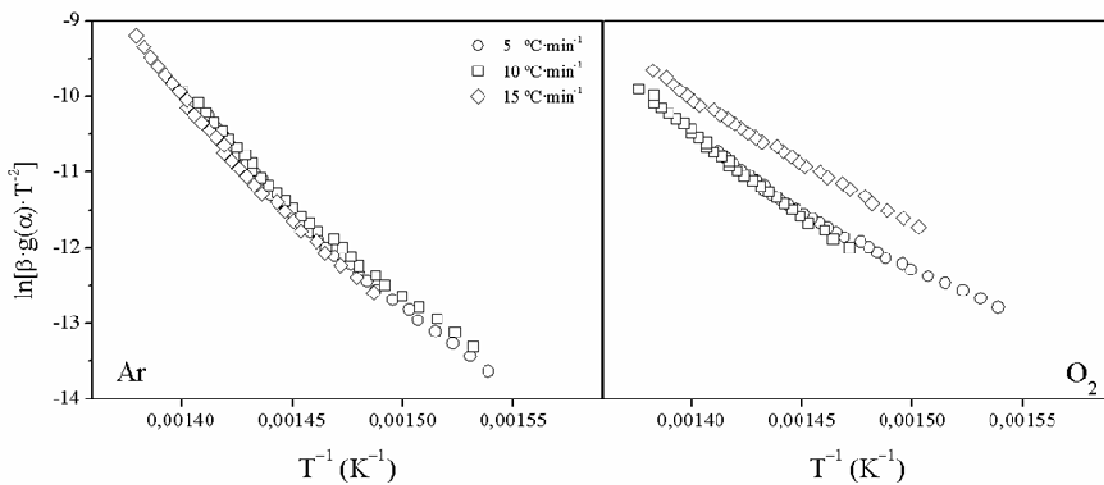


Figure 16. Application of Pérez-Maqueda *et al* criterion for the simplified kinetic triplets.

Table 9. Average values of activation energies obtained by Flynn-Wall-Ozawa (FWO), Kissinger-Akahira-Sunose (KAS) and Vyazovkin (VYZ) methods, and calculation of average activation energy for further analysis, at both testing environments.

Conditions	Material	$E_{a_{FWO}}$		$E_{a_{KAS}}$		$E_{a_{VYZ}}$		$E_{a_{iso}}$	
		(kJ·mol ⁻¹)	e_{FWO}	(kJ·mol ⁻¹)	e_{KAS}	(kJ·mol ⁻¹)	e_{VYZ}	(kJ·mol ⁻¹)	e_{iso}
Ar	VPET	194	3,1 %	193	3,6 %	191	3,3 %	192	3,3 %
	RPET-1	198	3,0 %	197	3,1 %	198	2,1 %	197	2,7 %
	RPET-2	210	3,2 %	212	3,7 %	211	2,8 %	221	3,2 %
	RPET-3	188	5,3 %	187	5,4 %	187	4,1 %	187	4,9 %
	RPET-4	186	5,0 %	184	5,1 %	185	4,2 %	185	4,7 %
	RPET-5	190	4,2 %	191	3,0 %	190	3,6 %	190	3,6 %
O ₂	VPET	196	20,3 %	195	22,0 %	192	17,3 %	194	19,8 %
	RPET-1	139	26,6 %	141	27,1 %	136	22,6 %	138	25,4 %
	RPET-2	140	23,6 %	141	22,2 %	137	20,4 %	139	22,1 %
	RPET-3	120	28,9 %	122	27,3 %	117	25,3 %	119	27,2 %
	RPET-4	115	22,9 %	118	23,2 %	113	19,8 %	115	21,9 %
	RPET-5	124	25,1 %	128	27,2 %	124	23,2 %	125	25,2 %

triplet (*SKT*) would fasten the calculations, and therefore ease the decision of the operational parameters for pyrolysis and combustion. In this section, the validity of using the *SKT* was assessed for the case of PET and its successive recyclates. **Table 9** shows the average apparent activation energies obtained by the aforementioned isoconversional methods ($E_{a_{FWO}}$, $E_{a_{KAS}}$ and $E_{a_{VYZ}}$), as well as the average activation energy ($E_{a_{iso}}$) susceptible for being used in further calculations. The $E_{a_{\alpha}}$ used along the previous sections may be therefore now

assumed constant along the α range of *TD*, since deviations were within a 5 %, whereas for *TOD*, the average values, though pretty similar among isoconversional methods, offered a big dispersion along the α range (17-29%). Care must be taken when interpreting E_a average data, since one could think that the same amount of energy would trigger the decomposition in both inert and reactive atmospheres, when actually, in the case of virgin PET, ca. 200 kJ·mol⁻¹ were needed under Ar, in contrast to ca. 140 kJ·mol⁻¹ under O₂ at lower α , as shown in **Fig. 13 (c) and (d)**.

Table 10. Simplified kinetic triplets of virgin PET and its recyclates under thermal and thermo-oxidative decomposition conditions.

	Material	E _{aP-Mc}		Model A _n	lnA _{P-Mc}	
		(kJ·mol ⁻¹)	e _{E_aP-Mc}	n _{P-Mc}	(s ⁻¹)	e _{lnA_{P-Mc}}
Ar	VPET	192	1,8 %	1,372	27,22	1,8 %
	RPET-1	197	1,6 %	1,375	28,13	1,8 %
	RPET-2	221	0,6 %	1,171	32,26	0,8 %
	RPET-3	187	1,4 %	1,384	26,32	1,6 %
	RPET-4	185	2,4 %	1,366	25,92	2,8 %
	RPET-5	190	1,3 %	1,359	26,89	1,5 %
O ₂	VPET	194	7,4 %	0,657	28,36	7,8 %
	RPET-1	138	16,3 %	1,038	18,15	18,3 %
	RPET-2	139	13,4 %	1,043	18,54	14,4 %
	RPET-3	119	21,6 %	1,011	14,87	25,1 %
	RPET-4	115	7,1 %	1,190	13,90	8,7 %
	RPET-5	125	11,1 %	0,960	15,76	13,5 %

Eq. (22) was applied to test the accuracy of the theoretical kinetic functions to fit to the experimental data, where now Ea_α is taken as constant parameter Ea_{iso} . The model that better fitted both *TD* and *TOD* was of the type A_n , in agreement with the previously obtained results with variable Ea . In order to complete the *SKT*, the Pérez-Maqueda *et al.* criterion ($P-M_C$) was considered in combination with Coats-Redfern expression ($C-R$). After the computation of n , the calculation of $\ln A$ was straightforward from the intercept at the origin of Eq. (23) for each β . The results of this procedure are reported at **Table 10** for virgin PET and its recyclates, at both tested atmospheres. While for the *TD*, all obtained values lay within a narrow experimental error and provide similar n to those obtained in the previous section, in the case of *TOD*, the deviation margins were wide and the n values quite different. This was due to the experimental error of assuming the Ea constant, which is transmitted along the rest of the calculations. **Figure 16** represents the application of the $P-M_C$ with $C-R$ method for RPET-2 as an example of the assessment of the suitability of the different *SKT* to be used in further analyses. It can be seen how for *TD* studies, all points laid on the same line, fact that occurred for the rest of materials, regardless the β employed. Contrarily, the points obtained for the *TOD* did not lie on the same line, thus confirming that the *SKT* shown was merely artifactual and therefore its use should be avoided. In this case, only the calculations shown in the previous section considering variation of kinetic parameters shall be operative.

5. Conclusions

The thermal and thermo-oxidative decompositions of reprocessed poly (ethylene terephthalate) (PET) were studied as an approach

to the combination of procedures for plastic waste management, that is, mechanical recycling and energetic valorisation. The emission of gases, the thermal performance and the kinetics of thermally-induced decomposition were investigated.

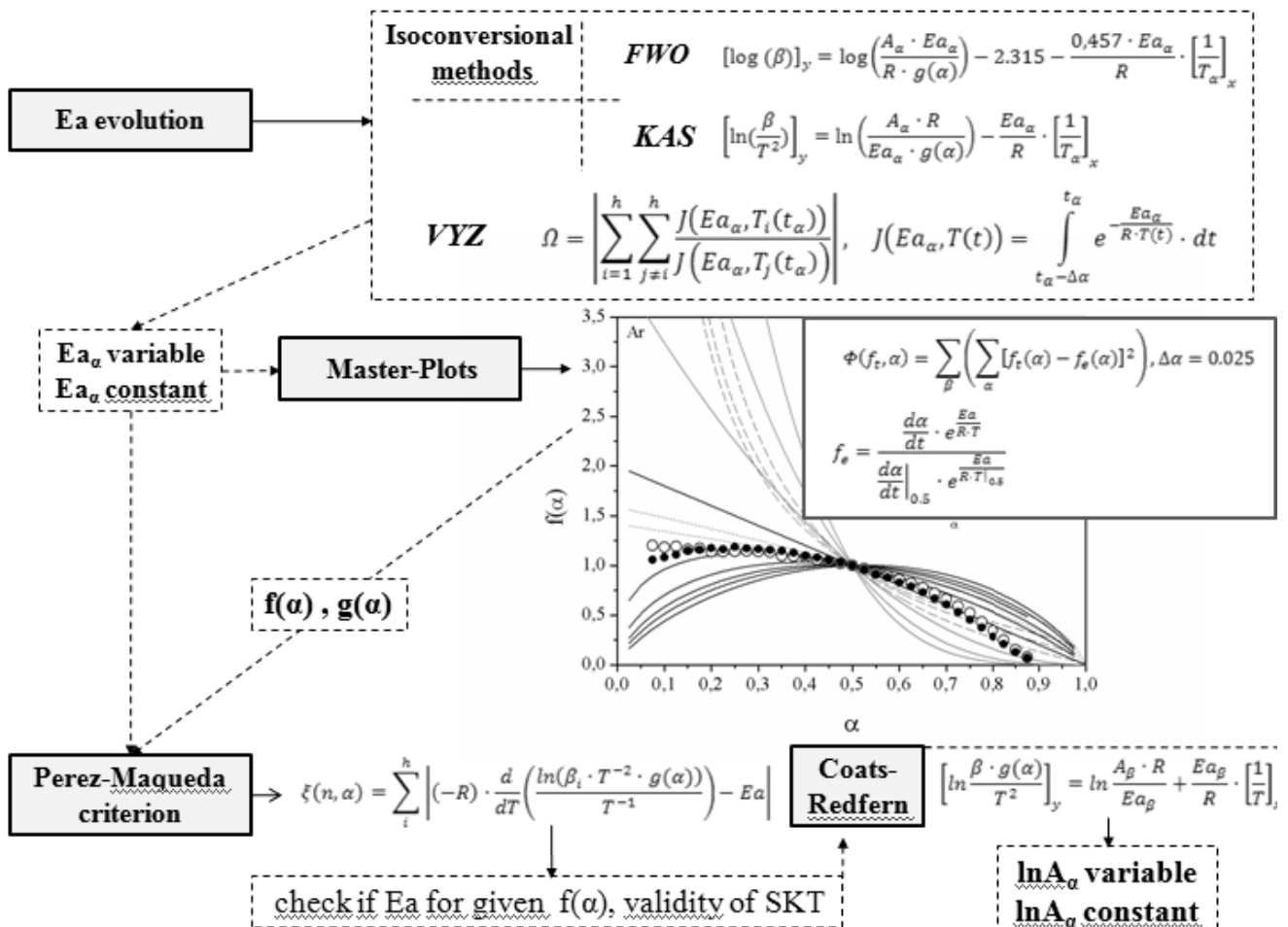
Under inert atmosphere, VPET and RPET-i mass-losses were driven by one stage of decomposition that mainly released acetaldehyde and, with less presence benzaldehyde, followed by a release of CO and CO₂, being the emission of the latter followed at higher temperatures. On the other hand, under oxidative atmosphere, the decomposition occurred through a double mass-loss profile. During the first stage, assignable to the bulk pyrolysis, mainly acetaldehyde was released, while throughout the second one, a noticeable production of CO₂ was assessed. The same gas emission profiles than those given by VPET were encountered for all recyclates, thus current gas control facilities used for VPET could be assimilated for all RPET.

A novel model (*TDB* (β), Eq.19) to estimate the characteristic decomposition temperatures under any linear heating profile and atmosphere was proposed. The effects of reprocessing on the thermal stability of PET were assessed by the use of the so-called Zero-Decomposition Temperatures (*ZDT*). Particularly, the use of the peak ZDT_p to monitor the weakening of the material against both thermal and thermo-oxidative decompositions stood out as a suitable indicator for thermo-mechanical degradation.

A kinetic analysis methodology, summarized at **Figure 17** consisting in the combination of six different methods (namely Flynn-Wall-Ozawa, Kissinger-Akashira-Sunose, Vyazovkin, Master-Curves and Pérez-Maqueda Criterion along with

Coats-Redfern equation) was applied. The kinetic methodology permitted the mathematical description of the thermal and thermo-oxidative decomposition of virgin PET and its successive recyclates throughout the whole α range. The kinetic model that mathematically described the thermal and thermo-oxidative decompositions of PET and its recyclates was of the type A_n : nucleation and growth, which gave importance to the formation of gas bubbles in the melt. The variation of Ea and A was taken into account and Eq. (20) was proposed to model their behaviour throughout the α range. The validity of a simplified kinetic triplet (SKT) was also assessed, being its use advisable when the activation energy could be considered constant within a narrow confidence interval.

Regarding the usability of PET recyclates after reprocessing, a change in tendency shown by thermal stability and thermal activation parameters from the second to the third recyclate may indicate the threshold of reprocessing cycles achievable by PET within a certain thermal performance. These results are in agreement to previous studies in which the mechanical, viscoelastic and morphological properties were assessed, showing a remarkable loss once applied the second reprocessing step [50]. In general, lower temperatures and energies were necessary to run thermo-oxidative decomposition of PET. Focusing on each process, under Ar, RPET-1 and RPET-2 needed more energy to decompose than VPET, being then reduced for the rest of recyclates; whereas under O_2 , the decomposition



of all recyclates was overcome at lower E_a than that of VPET. All the considerations shown in the work may provide technologists with plausible indicators for the selection of the adequate recovery option of poly(ethylene terephthalate). The applicability of the methodology presented may be transferred to the plastic waste management of other polymeric materials.

References

1. S.M. Al-Salem, P. Lettieri, J. Baeyens, Recycling and recovery routes of plastic solid waste (PSW): A review, *Waste management*, 29 (2009) 2625-2643.
2. E. Strömberg, S. Karlsson, The design of a test protocol to model the degradation of polyolefins during recycling and service life, *Journal of Applied Polymer Science*, 112 (2009) 1835-1844.
3. F. Vilaplana, A. Ribes-Greus, S. Karlsson, Degradation of recycled high-impact polystyrene. Simulation by reprocessing and thermo-oxidation. *Polymer Degradation and Stability*, 91 (2006) 2163-2170.
4. F. Vilaplana, A. Ribes-Greus, S. Karlsson, Changes in the micro-structure and morphology of high-impact polystyrene subjected to multiple processing and thermo-oxidative degradation. *European Polymer Journal*, 43 (2007) 4371-4381.
5. J.D. Badia, F. Vilaplana, S. Karlsson, A. Ribes-Greus, Thermal analysis as a quality tool for assessing the influence of thermo-mechanical degradation on recycled poly(ethylene terephthalate), *Polymer Testing*, 28 (2009) 169-175.
6. J.D. Badia, E. Strömberg, A. Ribes-Greus, S. Karlsson, Optimizing the MALDI-TOF-MS sample preparation procedure to determine the thermo-mechanical degradation mechanisms of poly(ethylene terephthalate). *Analytica Chimica Acta* 692 (2011) 85-95
7. J.D. Badia, E. Strömberg, A. Ribes-Greus, S. Karlsson, Assessing the MALDI-TOF MS sample preparation procedure to analyze the influence of thermo-oxidative ageing and thermo-mechanical degradation on poly(lactide). *European Polymer Journal*, 47 (2011) 1416-1428
8. F. Samperi, C. Puglisi, R. Alicata, G. Montaudo, Thermal degradation of poly(ethylene terephthalate) at the processing temperature. *Polymer Degradation and Stability*, 83 (2004) 3-10.
9. F. Awaja, D. Pavel, Recycling of PET. *European Polymer Journal*, 41 (2005) 1453-1477.
10. I. Noda, Two-Dimensional Infrared (2D IR) Spectroscopy: Theory and Applications, *Applied Spectroscopy*, 44 (1990) 550-561.
11. S. V. Levchick, E. D. Weil, A review on thermal decomposition and combustion of thermoplastic polyesters. *Polymers for Advanced Technologies*, 15 (2004) 691-700.
12. G. Montaudo, C. Puglisi, F. Samperi, Primary thermal degradation mechanisms of PET and PBT. *Polymer Degradation and Stability*, 42 (1993) 13-28.
13. F. Villain, J. Coudane, M. Vert, Thermal degradation of poly(ethylene terephthalate) and the estimation of volatile degradation products, *Polymer Degradation and Stability*, 43 (1994) 431-440.

14. K. S. Seo, J.D. Cloyd, Kinetics of hydrolysis and thermal degradation of polyester melts, *Journal of Applied Polymer Science*, 42 (1991) 845-850.
15. B.J. Holland, J.N. Hay, The thermal degradation of PET and analogous polyesters measured by thermal analysis–Fourier transform infrared spectroscopy. *Polymer*, 43 (2002) 1835-1847.
16. R. Kinoshita, Y. Teramoto, T. Nakano, H. Yoshida, Thermal degradation of polyesters by simultaneous TGA-DTA/FT-IR analysis. *Journal of Thermal Analysis*, 38 (1992) 1891-1900.
17. M. Dzieciol, J. Trzeczynski, Studies of temperature influence on volatile thermal degradation products of poly(ethylene terephthalate), *Journal of Applied Polymer Science*, 69 (1998) 2377-2381.
18. B. Saha, A.K. Ghoshal, Thermal degradation kinetics of poly(ethylene terephthalate) from waste soft drink bottles. *Chemical Engineering Journal*, 111 (2005) 39-43.
19. B. Saha, A. K. Maiti, A. K. Ghoshal, Model-free method for isothermal and non-isothermal decomposition kinetics analysis of PET sample, *Thermochimica Acta*, 444 (2006) 46-52.
20. I. Martín-Gullón, M. Esperanza, R. Font, Kinetic model for the pyrolysis and combustion of poly-(ethylene terephthalate) (PET). *Journal of Analytical and Applied Pyrolysis*, 58-59 (2001) 635-650.
21. J. Moltó, R. Font, J.A. Conesa, Kinetic model of the decomposition of a PET fibre cloth in an inert and air environment, *Journal of Analytical and Applied Pyrolysis*, 79 (2007) 289-296.
22. S. V. Levchik, E.D. weil, Flame retardancy of thermoplastic polyesters—a review of the recent literature, *Polymer International*, 54 (2004) 11-35.
23. A.K. Galwey, What can we learn about the mechanisms of thermal decompositions of solids from kinetic measurements? *Journal of Thermal Analysis and Calorimetry*, 92 (2008) 967-983.
24. A. K. Galwey, M. E. Brown, Solid-state decompositions - stagnation or progress? *Journal of Thermal Analysis and Calorimetry*, 60 (2000) 863-877.
25. I. Noda, Recent advancement in the field of two-dimensional correlation spectroscopy. *Journal of Molecular Structure*, 883-884 (2008) 2-26.
26. I. Noda, Generalized Two-Dimensional Correlation Method applicable to Infrared, Raman, and other types of Spectroscopy. *Applied Spectroscopy*, 47 (1993) 1329-1336.
27. I. Noda, Recent developments in two-dimensional infrared (2D IR) correlation spectroscopy. *Applied Spectroscopy*, 47 (1993) 1317-1323.
28. X. Dou, B. Yuan, H. Zhao, G. Yin, Generalized two-dimensional correlation spectroscopy - Theory and applications in analytical field. *Science in China Serie B: Chemistry*, 47 (2004) 257-266.
29. B. Wunderlich, *Thermal analysis of polymeric materials*. Springer, Berlin, 2005.
30. A. Khawan, D. R. Flanagan, Solid-State Kinetic Models: Basics and Mathematical Fundamentals. *Journal of Physical Chemistry B*, 110 (2006) 17315-17328.

31. L. A. Pérez-Maqueda, P. E. Sánchez-Jiménez, J.M. Criado, Kinetic analysis of solid-state reactions: precision of the activation of the activation energy calculated by integral methods. *International Journal of Chemical Kinetics*, 37 (2005) 658-666.
32. G. I. Senum, R. T. Yang, Rational approximations of the integral of the Arrhenius function, *Journal of Thermal Analysis and Calorimetry*, 11 (1977) 446.
33. L. A. Pérez-Maqueda, J. M. Criado, The accuracy of Senum and Yang's approximations to the Arrhenius Integral. *Journal of Thermal Analysis and Calorimetry*, 60 (2000) 909-915.
34. J. H. Flynn, L. A. Wall, A quick, direct method for the determination of activation energy from thermogravimetric data. *Journal of Polymer Science*, 4 (1966) 323-342.
35. T. Ozawa, Kinetic analysis of derivative curves in thermal analysis. *Journal of Thermal Analysis*, 2 (1970) 301.
36. C. D. Doyle, Series approximations to the equation of thermogravimetric data., *Nature*, 207 (1965) 209.
37. H. E. Kissinger, Reaction kinetics in differential thermal analysis. *Analytical Chemistry*, 29 (1957) 1702-1706.
38. T. Akahira, T. Sunose, *Trans. Joint Convention of Four Electrical Institutes*, Paper No. 246 Research Report/ Chiba Institute of Technology, *Scientific Technology*, 16 (1971) 22-31.
39. S. Vyazovkin, D. Dollimore, Linear and non-linear procedures in isoconversional computations of the activation energy of non-isothermal reactions in solids. *Journal of Chemical Information and Modelling*, 36 (1996) 42-45.
40. F.J. Gotor, J.M. Criado, J. Málek, N. Koga, Kinetic Analysis of Solid-State Reactions: The universality of Master Plots for Analyzing Isothermal and Non-Isothermal Experiments., *Journal of Physical Chemistry A*, 104 (2000) 10777-10782.
41. T. Ozawa, A New Method of Analyzing Thermogravimetric Data. *Bulletin of the Chemical Society of Japan*, 38 (1965) 1881.
42. T. Ozawa, Non-isothermal kinetics and generalized time. *Thermochemica Acta*, 100 (1986) 109.
43. L. A. Pérez-Maqueda, J. M. Criado, F. J. Gotor, J. Málek Advantages of Combined Kinetic Analysis of Experimental Data Obtained under Any Heating Profile. *Journal of Physical Chemistry A*, 106 (2002) 2862-2868.
44. A. W. Coats, J. P. Redfern, Kinetic analysis from thermogravimetric data. *Nature*, 68 (1964) 4914.
45. S. Morita, 2D Shige (c). Kwansai-Gakuin University, 2004-2005.
46. K. Levenberg, A method for solution of certain non-linear problems in least squares, *Quarterly of Applied Mathematics*, 2 (1944) 164-168.
47. D. W. Marquardt, An algorithm for the least-squares estimation of non-linear parameters. *SIAM Journal of Applied Mathematics*, 11 (1963) 431-441.
48. L. Santonja-Blasco, R. Moriana, J.D. Badía, A. Ribes-Greus, Thermal analysis applied to the

- characterization of degradation in soil of polylactide: I. Calorimetric and viscoelastic analyses. *Polymer Degradation and Stability*, 95 (2010) 2185-2191.
49. B. Liu, X. Zhao, X. Wang, F. Wang, Thermal degradation kinetics of poly(propylene carbonate) obtained from the copolymerization of carbon dioxide and propylene oxide. *Journal of Applied Polymer Science*, 90 (2003) 947-953.
50. J.D. Badia, E. Strömberg, S. Karlsson, A. Ribes-Greus. Unpublished results.
51. S. Vyazovkin, A. Lesnikovich, An approach to the solution of the inverse kinetic problem in the case of complex processes: Part 1. Methods employing a series of thermoanalytical curves, *Thermochimica Acta*, 165 (1990) 239-280.
52. S. T. Stoeva, K. Gjurova, M. Zagorcheva, Thermal analysis study on the degradation of the solid state chlorinated poly(ethylene). *Polymer Degradation and Stability*, 67 (2010) 117-128.
53. L. Li, C. Guan, A. Zhang, D. Chen, Z. Qing, Thermal stabilities and the thermal degradation kinetics of polyimides. *Polymer Degradation and Stability*, 84 (2004) 369-373.
54. J.T. Sun, Y.D. Huang, G.F. Gong, H.L. Cao, Thermal degradation kinetics of poly(methylphenylsiloxane) obtaining methacryloyl groups., *Polymer Degradation and Stability*, 91 (2005) 339-346.
55. G.Grausea, J. Ishibashia, T. Kamedaa, T.Bhaskarb ,T. Yoshioka, Kinetic studies of the decomposition of flame retardants containing high-impact polystyrene. *Polymer Degradation and Stability*, 95 (2010) 1129-1137.
56. J.D. Badía, L. Santonja-Blasco, R. Moriana, A. Ribes-Greus, Thermal analysis applied to the characterization of degradation in soil of polylactide: II. On the thermal stability and thermal decomposition kinetics. *Polymer Degradation and Stability*,95 (2010) 2192-2199.
57. V. Mamleev, S. Bourbigot, M. L. Bras, S. Duquesne, J. Sesták, Modelling of nonisothermal kinetics in thermogravimetry. *Physical Chemistry Chemical Physics*, 2 (2000) 4708-4716.
58. S. Vyazovkin, C. A. Wight, Kinetics of Thermal Decomposition of Cubic Ammonium Perchlorate. *Chemistry of Materials*, 11 (1999) 3386.

CONTRIBUTION IV-B

Assessing the thermal stability and kinetics of thermal and thermo-oxidative decompositions of reprocessed poly(lactide)

J.D. Badia, A. Ribes-Greus.

Manuscript

**ASSESSING THE THERMAL STABILITY AND KINETICS OF THERMAL AND THERMO-
OXIDATIVE DECOMPOSITIONS OF REPROCESSED POLYLACTIDE**

J.D. Badía, A. Ribes-Greus*

Instituto Tecnológico de Materiales. Universidad Politécnica de Valencia.

Camino de Vera, s/n, 46022 Valencia (Spain)

*corresponding author: aribes@ter.upv.es

Keywords: polylactide (PLA), Thermogravimetry coupled to Fourier-Transform Infra-Red Spectroscopy for Evolved-Gas Analysis (TGA/EGA-FTIR), thermal decomposition, thermo-oxidative decomposition, kinetic analysis, 2D-Correlation IR.

Abstract:

This work was devoted for the assessment of the individual and synergic effect of both mechanical recycling and energetic valorisation processes on the thermal performance of polylactide (PLA), both in terms of thermal stability and kinetics of decomposition. Commercial PLA was submitted to successive reprocessing cycles through multiple injection steps in order to simulate thermo-mechanical degradation induced to the polymer by mechanical recycling. Multi-rate linear-non-isothermal thermogravimetric (TGA) experiments under inert (Ar) and oxidative (O₂) conditions were performed to virgin PLA and its recyclates in order to simulate the thermal behaviour of the materials facing processes of pyrolysis and combustion. A novel model to establish the thermal stability of PLA under any heating profile was proposed. The release of gases was monitored by Evolved Gas Analysis of the fumes of the TGA experiment, by in-line FT-IR analysis, with the aid of 2D-correlation IR spectra. A kinetic analysis methodology, consisting in the combination of six different methods (namely Flynn-Wall-Ozawa, Kissinger-Akashira-Sunose, Advanced IsoConversional method, Master-Curves and Perez-Maqueda Criterion along with Coats-Redfern equation) was methodically applied, and its validity for being used with both constant and variable kinetic parameters was proven.

1. Introduction

The packaging industry is a highly important economic sector that involves big quantities of plastic materials. One-use applications critically reduce the service life of these products, being rapidly drawn to their disposal with all their properties almost intact. Packages made of commodities such as poly (ethylene) (PE), poly (propylene) (PP), poly (styrene) (PS) or poly (ethylene terephthalate) (PET) are usually immediately discarded after the first use, and their elimination and reintegration into the life cycle can require hundreds or even thousands of years. Therefore, the interest on plastic materials that accomplish the two-fold benefit of coming from renewable resources and being biodegradable within a reasonable period once discarded has gained much attention. One of the most popular biodegradable polymers with a currently well-established industry is the poly (lactic acid) or poly (lactide) (PLA). Polylactides are thermoplastic polyesters derived from the ring-opening polymerization of the monomer lactide, which is obtained from the fermentation of sugar feedstocks [1], at a price considerably cheaper than that previously achievable from petrochemical-derived products. PLAs have numerous interesting properties including good processability, mechanical properties, thermal stability and low environmental impact [2], which enhances their performance as suitable candidates for replacing commodities at the packaging sector. This solution will therefore imply the increase of a new source of polymeric waste, which will have to be managed. Moreover, with the aim of enlarging the usability of PLAs before finally discarding them, it would be advisable to explore the possibilities of recovering, as well as extending their use during service life. Among all recovery methods,

mechanical recycling represents one of the most successful processes and has received considerable attention due to its main advantages, since it is environmentally friendly, relatively simple, requires low investment, and its technological parameters are controlled [3]. Simulation of mechanical recycling by multiple processing to assess the effects of thermo-mechanical degradation has been successfully performed for commodities [4-11] such as PE [4], PP [4], PS [5-6], PVC [7] or PET [8-11]. It has been pointed out that several degradation processes may modify the structure and morphology of these polymers and consequently change the thermal, rheological and mechanical properties of its recyclates [8]. The assessment of the degradation mechanism is therefore necessary to determine the quality of recycled PLA and guarantee its further performance in second-market applications. In a previous study, the influence of mechanical recycling on the oligomeric distribution of PLA was characterized by MALDI-TOF-MS [12], showing the chemical changes induced on the polymer that resulted in a decrease of its mechanical, morphological and viscoelastic properties [13].

Focusing on the avoidance of landfilling, a viable solution to manage plastics waste when no more performance at good properties can be guaranteed by mechanical recycling is the application of thermally-induced energetic recovery technologies, such as pyrolysis, gasification or combustion. Several technologies are developed to optimize the energetic balance of the valorisation processes by means of different facilities [14]. In the selection of the operational parameters for the correct performance of the valorisation, the knowledge of the thermal behaviour of the materials is primary. Thermogravimetric analysis (TGA) is a

R) permits the identification of the main evolved species at both inert [29,35] and oxidative conditions [35]. The analysis of 2D-IR correlation spectroscopy [36, 37] permits to distinguish between overlapped peaks and identify the order of released compounds.

Macroscopic solid-state kinetics are complex, since they might give information about multiple steps taking place simultaneously, and therefore induce to misleading results [38]. In the attempt to develop a model for plastic thermal behaviour in full-scale systems, the main purpose is to describe the thermal decomposition in terms of an intrinsic kinetics, without taking into account the rigorous description of the chemistry of the decomposition, describing the process by means of a simplified reaction pathway, representative of a complex network of reactions [39]. Literature indicates that different researchers use different kinetic models and diverse kinetic methodologies to perform their studies. This fact often provokes confusion concerning which model is more suitable and therefore should be used to best represent the system under study. With the aim of shedding light on this matter, a comprehensive analysis is presented in this work, taking into consideration both variable and constant thermal activation parameters.

Summing up, the aim of this work was to assess the combination of mechanical recycling and energetic valorisation procedures on PLA, in order to (i) control the gases evolved from thermal processes under Ar and O₂; (ii) model the thermal stability behaviour of PLA and its recyclates with the aim of assuring their processability and performance conditions; and (iii) model energetic valorisation processes such as pyrolysis and combustion as a contribution to further plastic waste management solutions. To

achieve these purposes, a simulation procedure consisting in successive reprocessing cycles was used to induce the modifications that PLA suffers through thermo-mechanical degradation during mechanical recycling.

Multi-linear non-isothermal thermogravimetric experiments were carried out, in order to apply an advanced kinetic methodology that will furnish with the knowledge of the kinetic models that may explain the bulk decomposition of PLA at high temperatures, under both inert and oxidative atmospheres. Evolved Gas Analysis (EGA) by means of coupling TGA to an Infrared Spectrometer with Fourier Transform (TGA/FT-IR) permitted to identify the main gases released during the decompositions.

2. Experimental procedure

2.1. Reprocessing simulation

Poly lactide (PLA) 2002D is a thermo-forming grade PLA obtained from Natureworks LLC (Minnetonka, MN) in the form of pellets. Prior to processing, virgin PLA pellets were dried during 2 h at 80 °C in a dehumidifier Conair Micro-D FCO 1500/3 (UK), in order to remove as much humidity as possible from PLA flakes. Afterwards, samples were processed by means of injection moulding by means of an Arburg 420 C 1000-350 (Germany) injector, single-screw model (diameter $\Phi=35$ mm, length/ $\Phi=23$). Successive processing steps were applied under the same conditions (temperature gradient set from hopper to die: 160, 170, 190, 200 and 190°C; moulds set at 15 °C; cooling time residence ~ 40 s and total residence time ~60s). Samples were dried before each processing cycle. After injection, a fraction of the samples

were kept as test specimens and the rest was ground by means of a cutting mill Retsch SM2000 (UK), which provide pellets of size $d < 20$ mm to be fed back into the recirculation process. Up to five processing cycles were applied to obtain the different testing specimens of reprocessed PLA (RPLA-i, with i: 1-5).

2.2. Thermogravimetric experiments

Multi-linear non-isothermal thermogravimetric experiments were carried out in a Mettler-Toledo TGA/SDTA 851 (Columbus, OH). Samples weighing ca. 5 mg were heated in an alumina holder with capacity for 70 μL . Experiments were performed from 25 to 750 $^{\circ}\text{C}$ at different heating rates ($\beta = 2, 5, 7, 10, 12, 15$ $^{\circ}\text{C}\cdot\text{min}^{-1}$), under constant flow of 50 $\text{mL}\cdot\text{min}^{-1}$ of gas of analysis. An inert Ar atmosphere was used for assessing the thermal decomposition behaviour, whereas an O_2 reactive atmosphere was applied for characterizing the thermo-oxidative decomposition processes of PLA and its recyclates. Experiments were repeated at least three times, and the averages were considered as representative values.

2.3. Evolved Gas Analysis

Evolved Gas Analysis (EGA) was applied to fumes released by both thermal and thermo-oxidative processes by means of coupled TGA/FT-IR. In this case, the TGA analysis was focused on a temperature range in which the main decomposition range of PLA occurred, from 180 to 500 $^{\circ}\text{C}$, by means of a heating rate of $1^{\circ}\text{C}\cdot\text{min}^{-1}$, according to the equipment specifications. Samples weighing ~ 40 mg were heated in an alumina holder with capacity for 900 μL . The flow rate of the carrier gas was set to 25 $\text{mL}\cdot\text{min}^{-1}$, according to technical specifications. FT-IR gas-phase spectra were collected by a

previously calibrated Thermo Nicolet 5700 FT-IR Spectrometer (MA, USA), from 4000 to 600 cm^{-1} of wavenumber, at a resolution of 4 cm^{-1} . Both transfer line and gas cell were kept at 250 $^{\circ}\text{C}$ to prevent gas condensation. 16 coadded spectra were recorded every 30 s to assure accuracy of the temperature scanning. The Gram-Schmidt plots as well as its corresponding 3D and individual spectra at different constant temperatures were analyzed.

2.4. Analytical software and computational assumptions.

Thermogravimetric characterization was assessed with the aid of the software STAR[®] 9.10 from Mettler-Toledo. FT-IR spectra were characterized by OMNIC 7.0 from Thermo Scientific. 2D spectroscopic correlation was performed by means of the software 2Dshige [40]. Kinetic analyses were carried out in the conversion degree α range from 0,1 to 0,8 since the main reaction took place in this region. All thermogravimetric data were analyzed using Microsoft Excel software. Advanced Isoconversional method required the tool Solver of this mathematical package, by applying Newton method with progressive derivatives, setting an accuracy of 10^{-6} and a tolerance of 10^{-4} . Fitting procedures were performed by means of OriginLab OriginPro 8.0, which uses the Levenberg-Marquardt [41,42] algorithm to adjust the parameters of the fitting values in the iterative procedure.

Values are plotted in terms of {average, dev_{max} , dev_{min} }, where $\text{dev}_{\text{max}} = \max(\text{data}) - \text{average}(\text{data})$, and $\text{dev}_{\text{min}} = \text{average}(\text{data}) - \min(\text{data})$. Tabulated errors were obtained by dividing the standard deviation by the average of data.

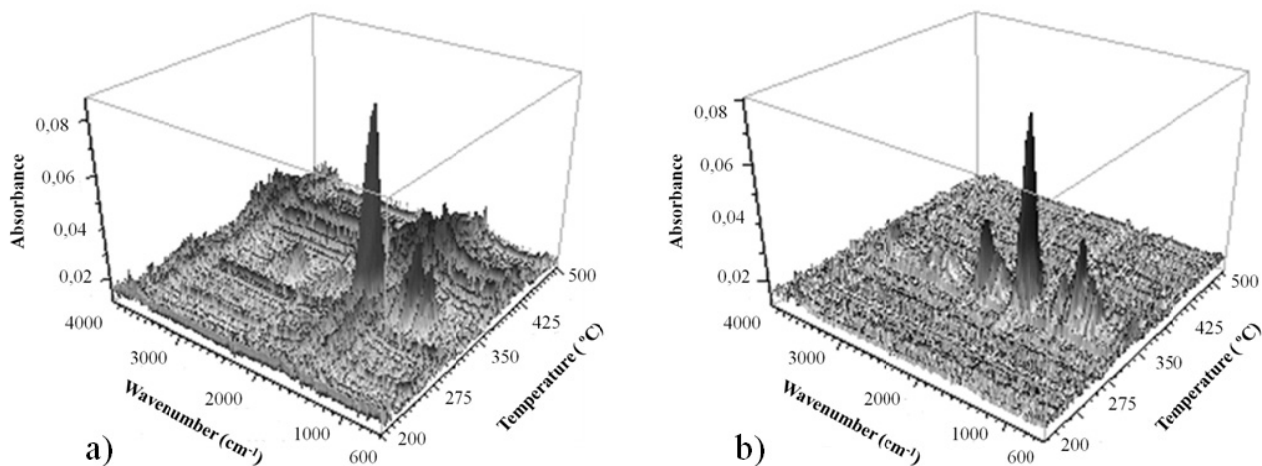


Figure 2. 3D-FTIR spectra of VPLA evolved gases from TGA experiment under (a) inert and (b) oxidative conditions

3. Discussion of results

3.1. Evolved Gases Analysis

Figure 2 shows the 3D-FTIR spectra of (a) thermal decomposition (*TD*) and (b) thermo-oxidative decomposition (*TOD*) of virgin PLA. **Figure 3** shows the characteristic spectra recorded at their decomposition maxima for both *TD* and *TOD*. Main decomposition products are listed in **Table 1**. Discussion is given hereby:

Under inert atmosphere, main evolved species were: lactide [43] [$3008\text{ cm}^{-1}\nu(\text{CH})$, $2952\text{ cm}^{-1}\nu_{\text{as}}(\text{CH}_3)$, $2893\text{ cm}^{-1}\nu_{\text{s}}(\text{CH}_3)$, $1796\text{ cm}^{-1}\nu(\text{C}=\text{O})$, $1365\text{ cm}^{-1}\delta(\text{CH}_3)$, $1248/1108\text{ cm}^{-1}\nu(\text{C}-\text{O}-\text{C})$ and 932 cm^{-1} corresponding to the ring skeletal vibration], acetaldehyde [$2968\text{ cm}^{-1}\nu(\text{CH}_3)$, 2740

$\text{cm}^{-1}\nu(\text{CHO})$, $1762\text{ cm}^{-1}\nu(\text{C}=\text{O})$, $1414/1371\text{ cm}^{-1}\delta(\text{CH}_3)$ and $1127\text{ cm}^{-1}\nu(\text{C}-\text{O})$], carbon monoxide [$2174/2116\text{ cm}^{-1}\nu(\text{C}\equiv\text{O})$]; and, in traces: carbon dioxide [$2349\text{ cm}^{-1}\nu_{\text{as}}(\text{O}=\text{C}=\text{O})$], water [$3900\text{--}3400\text{ cm}^{-1}\nu(\text{H}-\text{O})$, $1800\text{--}1300\text{ cm}^{-1}\delta(\text{H}-\text{O})$], and acetic acid [$3586\text{ cm}^{-1}\nu(\text{H}-\text{O})$, $1778\text{ cm}^{-1}\nu(\text{C}=\text{O})$, highly overlapped]. Different mechanisms are taking place in the formation of each compound [34]: acetaldehyde may be formed by homolysis reactions, along with CO, as may happen also to CO₂, which release may be enhanced by the O₂ presence; lactide may be formed by transesterification and/or by chain

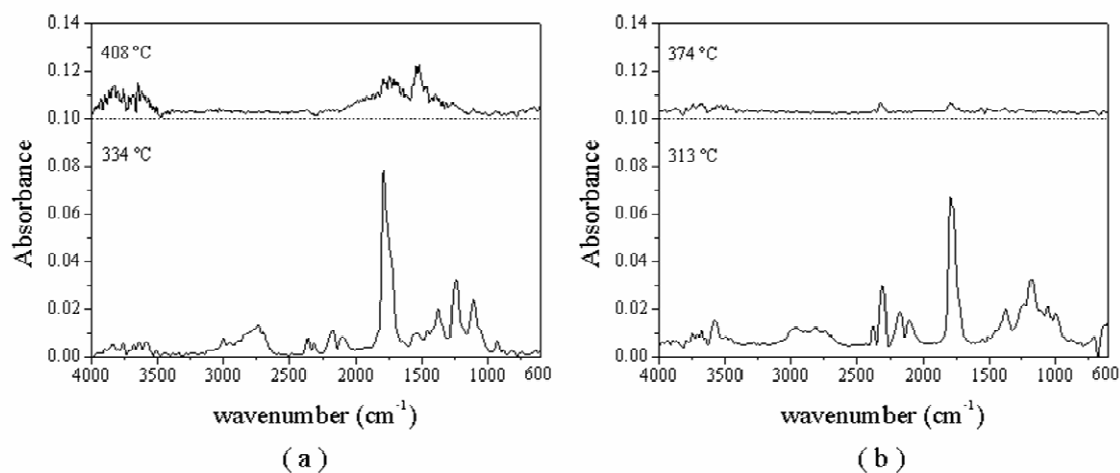


Figure 3. FTIR spectra of main decomposition products of VPLA under (a) inert and (b) oxidative conditions. Note that spectra at higher temperatures have been displaced for better visualization, but scale has not been changed.

Table 1. IR absorption bands of evolved gases from thermal and thermo-oxidative decomposition of PLA

Compound	Wavenumber (cm ⁻¹)	Vibrations
Acetaldehyde	3475	2 X ν (C=O)
	2968	ν (CH ₃)
	2740	ν (CHO)
	1762	ν (C=O)
	1414+1371	δ (CH ₃)
	1127	ν (C-O)
Lactide	3008	ν (CH ₃)
	2952	ν_{as} (CH ₃)
	2893	ν_s (CH ₃)
	1795	ν (C=O)
	1365	δ (CH ₃)
	1248+1108	ν (C-O-C)
Short-chain acids + their dimers and trimers	3589	ν (H-O)
	2952	ν (CH ₂)
	2816	ν (CH)
	1778	ν (C=O)
	1164 + 1107	ν (C-O)
CO ₂	2349	ν_{as} (O=C=O)
CO	2174 + 2116	ν (C≡O)
H ₂ O	3900-3400 + 1800-1300	ν (H-O) + δ (H-O)
ν : stretching / δ : in-plane bending / s : symmetric / as : asymmetric		

homolysis of PLA; acetic acid and other short-chain acids may be formed by oxidation of acetaldehyde and other oligomers. In order to offer more information, 2D-correlation spectroscopy (see *Appendix A*) was performed to the FT-IR spectral data in the temperature range from 200 to 450 °C, considering a spectrum every 2 °C for calculations. **Figure 4** shows the synchronous (*S-2D*) and asynchronous (*A-2D*) spectra at different infrared regions, for the study of the *TD* of PLA under inert conditions. In the 2400-1600 cm⁻¹ region, the *S-2D* shows (**Fig 4 a**) a wide auto-peak (*AP*) corresponding to the ν (C=O) region, which reflects the strong influence of the temperature on this spectral vibration. In the 1600-800 cm⁻¹ region (**Fig 4 c**), 2 strong *AP* (1376 |1127) which correspond to

acetaldehyde and an *AP* (1248) which corresponds to lactide, along with their related positive cross-peaks, which indicate that both compounds evolve together. *A-2D* (**Fig 4 b, d, e**) provided more information, taking into account positive and negative cross-peaks (*PCP* and *NCP*, respectively). Lactide evolved before acetaldehyde, as can be guessed from *PCP* (1248,1127), *PCP* (1796, 1762), *NCP* (1414, 1248), and *NCP* (1376, 1248). Carbon dioxide evolved before acetaldehyde and lactide, as drawn from *PCP* (2378, 1796), *PCP* (2316, 1796), *PCP* (2378, 1762), and *PCP* (2316, 1762). Carbon monoxide evolved before lactide but after acetaldehyde, as shown by *PCP* (2116, 1762) and *NCP* (2116, 1796). Under oxidative atmosphere, the gaseous decomposition products were essentially the same, as can be seen at **Figure 3 b**, where similar IR bands were obtained. As main differences, carbon mono- and dioxide evolved with bigger intensity, due to the combustion processes were enhanced; the bands of acetaldehyde decreased, and those related to acetic acid slightly increased, due to the oxidation effect of O₂; as well, lactide still appeared, but its bands were overlapped along with those corresponding to short-chain acids and their dimers and trimers [35] [3589 cm⁻¹ ν (OH), 2952 cm⁻¹ ν (CH₂), 2816 cm⁻¹ ν (CH), 1778 cm⁻¹ ν (C=O), and 1164/1107 cm⁻¹ ν (C-O)] and thus a finer identification was complicated. 2D-correlation spectra are similar to those offered for the studies under Ar. The main results obtained from *A-2D* were *PCP* (2378, 1796), *PCP* (2316, 1796) and *NCP* (2116, 1796), which exposed that CO₂ was evolved before the main decomposition product (ν (C=O) region), while CO was released afterwards. At higher temperatures, whereas for inert conditions the disappearance of formed oligomers during main decomposition took place,

in presence of oxygen the whole material was consumed at lower temperatures. Further description is given in the next section. After reprocessing, the chemical nature of polylactide is essentially the same, though shorter chains can

be obtained, and thus when it comes to the evolved gases, no differences are likely to be found. Similar IR spectra were consequently obtained, only displaced to lower temperatures due to weakening of thermal stability in the recyclates, as it is shown in the next section.

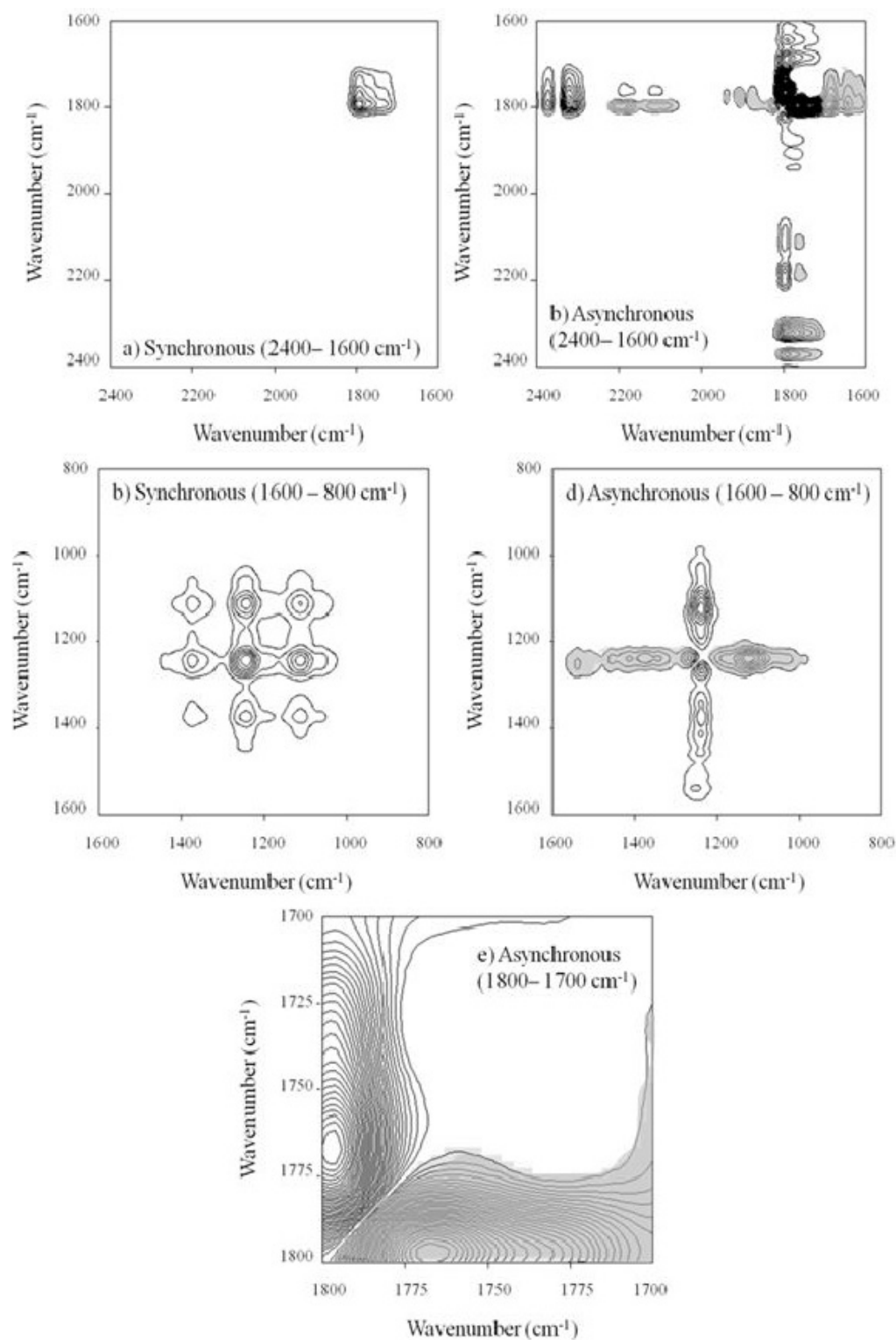


Figure 4. 2D correlation spectra of VPLA under inert conditions at different wavenumber ranges .

Negative cross-points are grey-shadowed.

3.2. Thermal stability

Figure 5 shows the thermogravimetric (*TG*) curves for both virgin and fifth reprocessed poly lactides analyzed under inert and oxidative atmospheres (VPLA, RPLA5, VPLA-O₂ and RPLA5-O₂, respectively) at the heating rate $\beta = 5 \text{ }^\circ\text{C}\cdot\text{min}^{-1}$. The region for the induction of thermal (*TD*) and thermo-oxidative (*TOD*) decompositions is zoomed in the upper-right region. As expected, the oxidizing environment forced the decomposition at lower temperatures than those needed in inert conditions. PLA *TD* occurred through a single-step process between 250 °C and 370 °C, consuming nearly 98-99 % of mass when the polymeric chains broke down to evolve to the gaseous phase. The rest of oligomers decomposed in a low-sloped fashion, until the rest of material was completely pyrolysed. On the other hand, the *TOD* of PLA occurred via a two-step process, since the main decompositions mechanisms to lactide and short-chain acids are overlapped. The first one took place from 250 °C to 370 °C as in inert atmosphere, consuming nearly 96-98 % of the material. Immediately afterwards, the second step appeared from 370 °C to 400 °C, eliminating 4-2 % of the polymer, as can be observed in the lower-left zoomed graph. Note that given temperatures do not match with those shown at Figure 2, due to different β were employed. For further calculations, the second step under O₂ was considered negligible if compared to the main decomposition under O₂ and therefore the study was focused on the first decomposition step at both inert and oxidative conditions. As usual, higher β led to shift the thermograms to higher temperatures, but have not been shown for the sake of clarity. Likewise, *TG* curves of all recyclates are not shown, since they behave in a similar fashion than that presented by VPLA and

RPLA-5 in both testing environments. The residue content that may indicate the presence of inorganic compounds in the polymeric sample was in all cases, both for *TD* and *TOD*, nearly 0%.

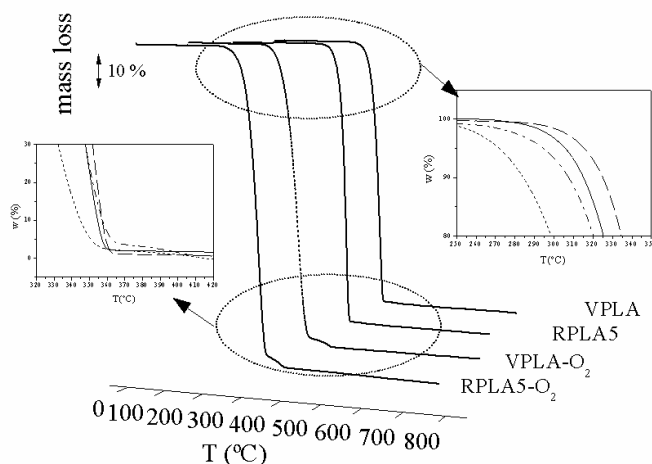


Figure 5. *TG* curves of virgin and fifth-reprocessed PLA under inert (VPLA, RPLA5) and oxidative (VPLA-O₂, RPLA5-O₂) conditions. Upper-right inset: detail of the onset of decomposition. Lower-left inset: detail of endset of decomposition.

In order to assess the thermal stability under both inert and oxidative conditions, the corresponding decomposition onset and endset temperatures were obtained by a tangential intercept method onto the *TG* curves for the whole process. Likewise, the temperature at the maximum decomposition rate da/dT^{-1} , i.e. the peak temperature of the differential thermogravimetric curve (*DTG*), which is related to the inflection temperature of the *TG* curve, was also considered for both mass-loss processes. Technologist may be interested in finding the relationship between the influence of the heating rate β and the characteristic TGA temperatures to model the thermal stability behaviour of plastics. It has been shown that at high β , the relationship is almost linear. Thus, several linear regressions can be found in the literature for different plastics (see for example [44]). However, in the case of

PLA, as β decreases, the linearity was lost. Therefore, other functions must be used in order to predict the thermal decomposition behaviour (*TDB*) of PLA under any β . This procedure is shown with more detail in a previous contribution, in which the thermal stability of poly (ethylene terephthalate) (PET) is assessed [45]. As proposed in that work, Eq. (1), where a , b and k are parameters of the fitting, is suitable for this purpose.

$$TDB(\beta) = a \cdot (1 + b \cdot e^{-k\beta})^{-1} \quad (1)$$

The results of the fitting to onset, peak and endset temperatures (subscripts, θ , p and e , respectively) are shown at **Table 2** for all materials and both inert and oxidative atmospheres. Despite other authors have proposed linear relationships between the thermogravimetric characteristic temperatures with β [44], **Figure 6** clearly shows for VPLA that when considering lower β , the linear assumption may not be operative.

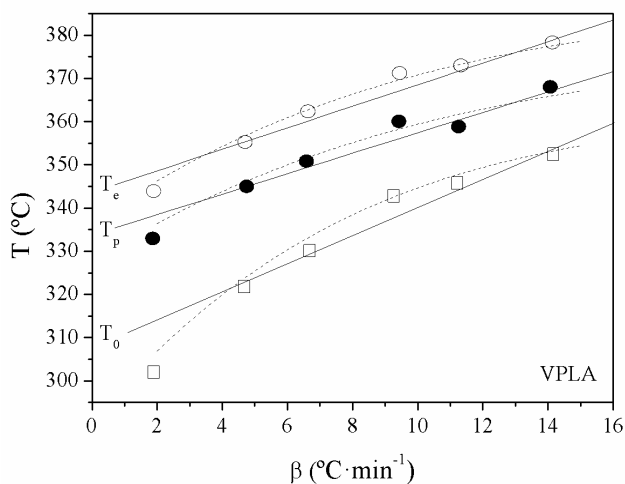


Figure 6. Fittings applied to the evolution of the characteristic TGA temperatures for VPLA (solid line: linear regression; dashed line: regression applied according to Eq. (1))

In order to evaluate the influence of thermo-mechanical degradation induced to PLA by

means of multiple reprocessing to its thermal stability, instead of choosing the experimental temperatures obtained at a specific β , which can be locally affected by both experimental errors and misleading calculation assumptions (i.e., the tangent slope is strongly dependent on the points chosen for drawing), the so-called [45] Zero-Decomposition Temperatures (*ZDT*) were used ($TDB(\beta \rightarrow 0)$), due to the fitting smoothens the possible variations in local temperatures, with excellent R^2 in this study ($> 95\%$ in most cases).

Figure 7 shows the evolution of the *ZDTs* along the reprocessing cycles at both inert and oxidative atmospheres. The onset *ZDT* slightly increased up to the third recycle in inert conditions (**Fig 7 a**), whereas the peak and endset *ZDTs* showed a small decrease. Afterwards, all *ZDTs* followed the same steady trend, slightly decreasing the *ZDT* range (**Fig 7 c**), as clear effect of diminution of PLA thermal stability. On the other hand, under oxidative conditions (**Fig 7 b**) the results may provide more information regarding the degradative influence of recycling on the thermal behaviour of PLA in real conditions. Actually, after the second reprocessing, a sharp decay of nearly $40\text{ }^\circ\text{C}$ of the onset *ZDT* occurred, while peak and endset *ZDTs* practically did not change, thus widening the *ZDT* range (**Fig 7 c**). In a previous study [12] in which the influence of multiple reprocessing on the oligomeric distribution of PLA was assessed by means of MALDI-TOF-MS, the increase of carboxy-methyl terminated linear species was specially remarkable after the second recycle, accompanied by a decrease of initially predominant both cyclic and methyl/carboxyl terminated linear species, and aided by intermolecular transesterification reactions among other low abundant species. These variations in the oligomeric distribution affect to

Table 1. Fitting results obtained from modeling the evolution of the characteristic TGA temperatures to Eq. (1)

Material	ZDT	Thermal decomposition (Ar)						R ²	Thermo-oxidative decomposition (O ₂)						R ²
		a		b		k			a		b		k		
		value	e	value	e	value	e		value	e	value	e	value	e	
VPLA	ZDT ₀	363,91	0,05 %	0,25	0,84 %	0,15	1,31 %	0,993	340,98	1,45 %	0,34	0,53 %	0,22	2,76 %	0,997
	ZDT _p	378,63	0,95 %	0,16	0,48 %	0,12	2,17 %	0,986	358,74	0,76 %	0,18	0,83 %	0,28	2,56 %	0,998
	ZDT _e	389,14	0,59 %	0,16	1,35 %	0,11	1,59 %	0,975	374,44	0,72 %	0,17	3,09 %	0,24	2,72 %	0,989
RPLA-1	ZDT ₀	345,39	0,28 %	0,19	0,58 %	0,28	1,77 %	0,991	345,40	0,63 %	0,35	0,34 %	0,19	0,10 %	0,993
	ZDT _p	368,35	0,74 %	0,15	1,38 %	0,19	1,23 %	0,947	371,16	0,60 %	0,22	0,31 %	0,14	1,06 %	0,997
	ZDT _e	387,75	0,80 %	0,19	1,66 %	0,17	1,56 %	0,981	391,38	2,25 %	0,20	1,09 %	0,10	3,04 %	0,996
RPLA-2	ZDT ₀	348,73	0,46 %	0,17	1,27 %	0,31	1,51 %	0,988	362,52	2,89 %	0,26	0,35 %	0,09	3,17 %	0,998
	ZDT _p	370,00	1,16 %	0,14	0,89 %	0,18	0,88 %	0,998	370,00	2,35 %	0,20	5,00 %	0,16	0,63 %	0,964
	ZDT _e	378,91	0,48 %	0,15	0,66 %	0,23	3,58 %	0,995	386,05	1,09 %	0,13	7,55 %	0,09	1,89 %	0,999
RPLA-3	ZDT ₀	367,97	1,14 %	0,17	0,70 %	0,06	1,61 %	0,973	337,33	0,08 %	0,45	1,02 %	0,49	0,99 %	0,998
	ZDT _p	367,31	0,74 %	0,13	0,80 %	0,19	1,04 %	0,996	380,00	1,38 %	0,21	2,43 %	0,10	1,00 %	0,949
	ZDT _e	379,59	0,71 %	0,13	0,72 %	0,18	0,65 %	0,947	392,00	0,82 %	0,18	1,11 %	0,09	2,75 %	0,971
RPLA-4	ZDT ₀	360,33	0,04 %	0,15	0,53 %	0,13	1,66 %	0,987	340,17	0,92 %	0,36	1,38 %	0,31	2,36 %	0,929
	ZDT _p	378,29	0,66 %	0,16	1,09 %	0,13	1,36 %	0,985	361,05	0,61 %	0,12	0,65 %	0,20	1,87 %	0,998
	ZDT _e	390,00	0,29 %	0,17	3,04 %	0,21	2,57 %	0,992	394,00	0,34 %	0,16	3,25 %	0,08	1,25 %	0,957
RPLA-5	ZDT ₀	365,35	0,60 %	0,16	1,63 %	0,10	2,12 %	0,987	339,20	1,12 %	0,40	2,03 %	0,26	2,07 %	0,965
	ZDT _p	374,96	0,64 %	0,15	1,03 %	0,15	1,38 %	0,995	358,87	0,20 %	0,21	1,87 %	0,23	4,58 %	0,991
	ZDT _e	390,14	0,44 %	0,17	3,75 %	0,13	1,64 %	0,986	374,81	0,89 %	0,10	0,55 %	0,19	3,89 %	0,958

the heterogeneity and polydispersity of the material, weakening its polymeric structure and producing species with more decomposition sites more liable to O₂.

The changes in thermal stability were governed by modifications in its thermal and thermo-oxidative decomposition behaviours. Subsequent analysis was therefore needed to establish a suitable methodology to model the pyrolysis and combustion processes for further full-scale energetic valorisation facilities.

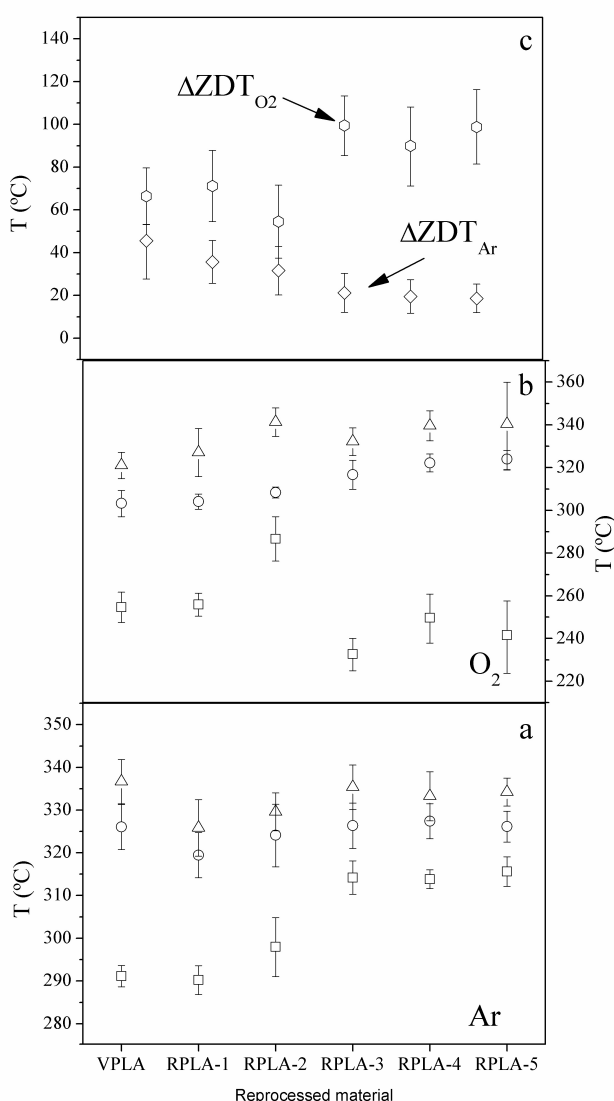


Figure 7. (a) Evolution of ZDT under inert (8a) and oxidative (b) conditions (squares: onsets, circles: peaks, triangles: endsets); (c) ZDT ranges of decomposition at both environments.

3.3. Assessment of the apparent activation energy

The first step in the study of decomposition kinetics is the assessment of the evolution of the apparent activation energy (Ea). Solid-state kinetics (See *Appendix B*) were developed from reaction kinetics in homogeneous systems (i.e gases and liquids), and it is generally assumed that the Ea and the pre-exponential factor (A) remain constant. However, it has been proved that these kinetic parameters may vary with the progress of the decomposition. This variation can be detected by isoconversional methods, which use data from different multi-linear non-isothermal experiments and do not take modelistic assumptions for the analysis, main source of error of model-fitting methods. The most broadly used isoconversional methods are those integral linear methods developed by Flynn-Wall-Ozawa (*FWO*) [46,47] (supported on Doyle's integral approximation [48] and Kissinger-Akahira-Sunose (*KAS*) [49,50], which are represented at Eqs. (3) and (4), respectively. These methods give rise to linear functions from which slopes the Ea at a fixed decomposition degree α are obtained. Good linear regressions within > 95% of confidence resulted from the application of *FWO* and *KAS* methods to both thermal and thermo-oxidative decompositions.

$$[\log(\beta)]_y = \log\left(\frac{A_\alpha \cdot Ea_\alpha}{R \cdot g(\alpha)}\right) - 2.315 - \frac{0.457 \cdot Ea_\alpha}{R} \cdot \left[\frac{1}{T_\alpha}\right]_x \quad (2)$$

$$\left[\ln\left(\frac{\beta}{T^2}\right)\right]_y = \ln\left(\frac{A_\alpha \cdot R}{Ea_\alpha \cdot g(\alpha)}\right) - \frac{Ea_\alpha}{R} \cdot \left[\frac{1}{T_\alpha}\right]_x \quad (3)$$

The results were compared to those obtained by the non-linear Advanced Isoconversional (*AIC*) method developed by Vyazovkin [51], in order to test the consistency of the results. This

method, which accounts for variable heating rates and systematic errors in the activation energy, is given at Eq. (4)

$$\Omega = \left| \frac{\sum_{i=1}^h \sum_{j \neq i}^h \frac{J(Ea_\alpha, T_i(t_\alpha))}{J(Ea_\alpha, T_j(t_\alpha))} \right| \quad (4)$$

$$J(Ea_\alpha, T(t)) = \int_{t_\alpha - \Delta\alpha}^{t_\alpha} e^{-\frac{Ea_\alpha}{R \cdot T(t)}} \cdot dt$$

, where i and j are counters through the h experiments performed at different heating rates β . $T(t) = T_0 + \beta \cdot t$, where T_0 is the initial temperature. $\Delta\alpha = (m^{-1})$, with m being the number of α segments chosen for integration (40 in this work). The integral $J(Ea_\alpha, T(t))$ was numerically evaluated by the Simpson 1/3 method. The apparent activation energy (Ea_α) was the value that minimized Ω at Eq. (4) for a particular α .

The averages of the apparent activation energy obtained by *FWO*, *KAS* and *AIC* methods are gathered at **Table 3**, at both inert and oxidative conditions for the whole decomposition processes. For the thermal decomposition, the average values lay within coincident values among all methods, with very low dispersion values. Therefore, it was assumed that the average isoconversional energy may be used as constant throughout the decomposition process for the following calculations, as suggested in a previous work [45]. Thus, a simplified kinetic triplet (*SKT*) which considers constant Ea and A , along with a proper kinetic model $f(\alpha)$ would fulfil the behaviour of PLA and its recyclates in inert conditions. Contrarily, the Ea drastically changed along the thermo-oxidative decomposition, thus avoiding the use of a constant activation energy for the resolution of

the kinetic triplet, and therefore its variation was taken into account.

3.4. Thermal decomposition simplified kinetic triplet

Figure 8 shows the evolution of the isoconversional activation energy \overline{Ea}_{iso} , taking into account the average of the results given by *FWO*, *KAS* and *AIC* methods, summarized at **Table 4**. Virgin PLA gave an average value of $152 \text{ kJ}\cdot\text{mol}^{-1}$, which is comparable to values reported in different studies for PLA grades in the same molecular weight order and analyzed by the same isoconversional methods [52,53]. After the first reprocessing step, a sharp 26.5 % increase was registered up to $207 \text{ kJ}\cdot\text{mol}^{-1}$, keeping this order of value within a 5 % along

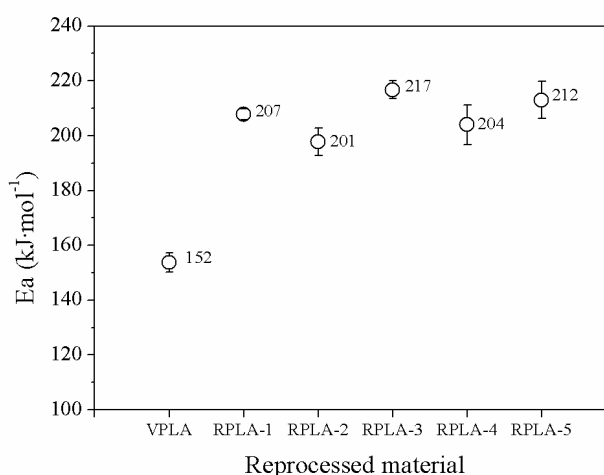


Figure 8. Evolution through reprocessing cycles of the average isoconversional activation energy of thermal decomposition

This change could be related to the presence of more linear hydroxyl- and carboxy-methyl terminated species in the oligomeric distribution of PLA recyclates, to a detriment of mainly predominant cyclic species in virgin PLA [12], which may vary the principal thermal decomposition mechanisms. As well, provided

the mechanism does not change, it might occur that linear species need more energy to depolymerize through backbiting intramolecular transesterification than cyclic species, which already possess ring tension. In any case, to achieve the mathematical decomposition model, regardless the decomposition mechanisms will help design the proper pyrolysis/combustion systems. Thus, in the next step of the kinetic characterization of the thermal decomposition of PLA and its recyclates, the kinetic function $f(\alpha)$ could be approached by the use of reduced Master-Plots. The reaction model may adopt various expressions, based on nucleation and nuclei growth, phase boundary reactions, diffusion or order reactions [54]. The environmental gases, inert or reactive, have important roles regarding the selection of the decomposition models. A list of the most common $f(\alpha)$ applied to polymers is given at **Table 4**. Master Plots ($M-P$) are reference theoretical curves ($M-P_i$) dependent on the kinetic model, but generally independent of the kinetic parameters of the process. Due to in many cases, the experimental kinetic data can easily be transformed into experimental curves ($M-P_e$), a comparison with the theoretical $M-P_i$ allows the selection of the appropriate kinetic model of the process under investigation or, at least, reducing the span of suitable kinetic models [55]. There exist three main types of $M-P_i$, those based on the differential form ($M-P_f$) of the generalized kinetic equation Eq. (7); those based on the integral form ($M-P_g$), according to Eq. (8); and the most common one that combines both differential and integral forms ($M-P_{fg}$), that are usually reduced at $\alpha = 0.5$ for better visualization. The mathematical description of each curve can be found elsewhere [55]. They are described after the introduction of the so-called generalized time θ , which denotes

the reaction time taken at a particular α at infinite temperature, defined as [47, 56-57]:

$$\theta = \int_0^t e^{-\frac{Ea}{R \cdot T}} \cdot dt \quad (5)$$

, which differentiation in combination with Eq. (20) (see *Appendix B*), one obtains:

$$\frac{d\alpha}{d\theta} = A \cdot f(\alpha) = \frac{d\alpha}{dt} \cdot e^{\frac{Ea}{R \cdot T}} \quad (6)$$

Therefore, assuming A and Ea constant, due to interdependence of kinetic parameters, and using a reference point at $\alpha=0.5$, the theoretical $M-P_f$ and the expression for the reduced form of the experimental data can be drawn from the following expression:

$$\frac{\frac{d\alpha}{d\theta}}{\left.\frac{d\alpha}{d\theta}\right|_{0.5}} = \frac{f(\alpha)}{f(0.5)} = M-P_t \equiv M-P_e = \frac{\frac{d\alpha}{dt} \cdot e^x}{\left.\frac{d\alpha}{dt}\right|_{0.5} \cdot e^{x_{0.5}}} \quad (7)$$

As well, the theoretical $M-P_g$ is defined as follows:

$$\frac{\theta}{\theta_{0.5}} = \frac{g(\alpha)}{g(0.5)} = M-P_t \equiv M-P_e = \frac{p(x)}{p(x_{0.5})} \quad (8)$$

, where $p(x)$ is the temperature integral given at the *Appendix B*, and x is $Ea \cdot R^{-1} \cdot T^{-1}$, being R the ideal gas constant ($8.31 \text{ J} \cdot \text{mol}^{-1} \cdot \text{K}^{-1}$) and calculated by using \overline{Ea}_{iso} . The advantage of using $M-P_f$ and $M-P_g$ is that the former clearly disperse among different $f(\alpha)$ in the range $\alpha < 0.5$ and the latter disperse for $\alpha > 0.5$ and therefore permits a straightforward identification. In contrast, the use of the common $M-P_{fg}$ tends to produce confusion due to the coincidence of different kinetic models under the same line. In order to select the best kinetic model, the condition of minimization of Φ in Eq. (9) was applied, taking into account experiments performed at all heating rates.

Table 2. Ea averages of thermal and thermo-oxidative decompositions obtained by isoconversional methods.

	Thermal decomposition (Ar)						Thermo-oxidative decomposition (O ₂)					
	FWO		KAS		AIC		FWO		KAS		AIC	
Material	Ea (kJ·mol ⁻¹)	e (%)	Ea (kJ·mol ⁻¹)	e (%)	Ea (kJ·mol ⁻¹)	e (%)	Ea (kJ·mol ⁻¹)	e (%)	Ea (kJ·mol ⁻¹)	e (%)	Ea (kJ·mol ⁻¹)	e (%)
VPLA	153	6.3	151	6.9	152	7.1	101	30.7	96	31.2	112	25.0
RPLA-1	208	1.2	208	1.3	205	1.9	106	19.8	102	21.5	97	23.7
RPLA-2	202	2.9	202	3.1	198	6.0	127	30.6	123	33.3	120	31.0
RPLA-3	219	6.1	220	6.3	213	8.4	114	29.8	116	28.4	103	27.3
RPLA-4	205	4.7	207	4.9	202	5.8	121	21.8	119	19.6	114	18.5
RPLA-5	216	1.1	216	1.2	205	2.1	97	27.8	92	30.4	89	39.3

Table 3. Algebraic expressions for the kinetic functions of the most common models in solid-state reactions

type	model	symbol	f(α)
NUCLEATION	random nucleation and growth of nuclei (Johnson-Mehl-Avrami)	A _n	$n \cdot (1 - \alpha) \cdot [-\ln(1 - \alpha)]^{1 - \frac{1}{n}}$
	n-order (instantaneous nucleation and n-dimensional growth)	F _n	$(1 - \alpha)^n$
REACTION	phase boundary controlled reaction (contracting n dimensions, n-dimensional shape)	R _n	$n \cdot (1 - \alpha)^{\frac{1}{n}}$
DIFFUSION	two-dimensional diffusion (bi-dimensional particle shape)	D ₂	$[-\ln(1 - \alpha)]^{-1}$
	three-dimensional diffusion (tridimensional particle shape) (Jander equation)	D ₃	$\frac{3 \cdot (1 - \alpha)^{\frac{2}{3}}}{2 \cdot (1 - \alpha)^{\frac{1}{3}}}$
	three-dimensional diffusion (tridimensional particle shape) (Ginstein-Bronshtein equation)	D ₄	$\frac{3}{2 \cdot [-1 + (1 - \alpha)^{-\frac{1}{3}}]}$

$$(f_t, g_t, \alpha) = \sum_{\beta} (\sum_{\alpha=0}^{0.5} [f_t(\alpha) - f_e(\alpha)]^2 + \sum_{\alpha=0.5}^1 [g_t(\alpha) - g_e(\alpha)]^2); \quad (9)$$

$$\Delta\alpha = 0.025; \forall f_t, g_t$$

, where f_t and g_t are the differential and integral forms of the kinetic models represented at **Table 4**, and f_e and g_e the experimental form of the reduced curves given by the right-hand part of Eq. (7) and (8), respectively. **Figure 9** shows as an example the comparison of the experimental master curves of RPLA-2 at $\beta = 5 \text{ }^\circ\text{C}\cdot\text{min}^{-1}$ with the differential (**Fig 9a**) and integral (**Fig 9b**) abaci. Results conclude that virgin PLA and its recyclates follow an A_n kinetic model (growth of previously formed nuclei) with n close to 1.5. This kind of kinetic model is quite common in crystallization processes, though scarcely reported in studies dealing with thermal decomposition processes of polymers [28, 58-62], where the controversy of the relationship between the mathematical models and the physical mechanisms is evident. Nevertheless, the model A_n indicates the presence of active zones more chemically liable to thermal decomposition [63], which activate the formation and growth of gas bubbles in the polymer melt [62].

In order to complete the kinetic triplet, the pre-exponential factor A has to be found, along with the n of the kinetic model, and thus obtain a full mathematical description of the kinetic model. Taking into account that a suitable *SKT* should fulfill the *Perez-Maqueda et al* criterion (*P-MC*) [64]; that is, the independence of the activation parameters Ea , A on the heating rate β , the minimization of ξ in Eq. (10) will provide the best n for the modelization, and thereafter endow with the most accurate A , by averaging the A_β obtained from the intercept at $y=0$ of Coats-

Redfern [65] equation (Eq. (11)) at each experiment with different heating rates β , as proposed in a previous study for the characterization of the thermal decomposition of poly(ethylene terephthalate) (PET) [45].

$$\xi(n, \alpha) = \sum_i^h \left| (-R) \cdot \frac{d}{dT} \left(\frac{\ln\left(\beta_i \cdot T^{-2} (-\ln(1-\alpha))^{\frac{1}{n}}\right)}{T^{-1}} \right) - \overline{Ea}_{iso} \right| \quad (10)$$

$$\left[\ln \frac{\beta \cdot (-\ln(1-\alpha))^{\frac{1}{n}}}{T^2} \right]_y = \ln \frac{A_\beta \cdot R}{Ea_\beta} + \frac{Ea_\beta}{R} \cdot \left[\frac{1}{T} \right]_x \quad (11)$$

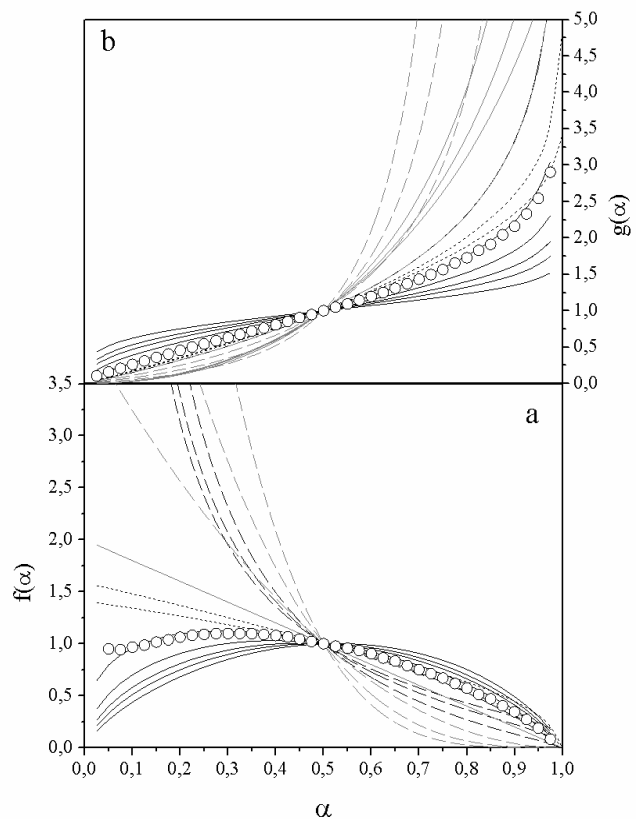


Figure 9. Master plots based on the (a) differential and (b) integral forms of the general kinetic law compared to experimental data obtained for thermal decomposition of RPLA-2 (hollow circles). (Black solid lines: A_n ; Grey solid lines: F_n ; Dashed grey lines: D_n ; Pointed black lines: R_n)

Table 4. Simplified kinetic triplets for the thermal decomposition of PLA and its recyclates.

Material	SIMPLIFIED KINETIC TRIPLET					
	MODEL		ACTIVATION ENERGY		PRE-EXPONENTIAL FACTOR	
	Function	n	Ea (kJ·mol ⁻¹)	e (%)	lnA (s ⁻¹)	e (%)
VPLA	A _n	1.611	153	6.1	24.41	5.2
RPLA-1		1.354	207	2.5	34.72	2.7
RPLA-2		1.510	201	4.3	32.59	4.1
RPLA-3		1.231	217	1.5	40.08	6.1
RPLA-4		1.529	204	6.0	33.70	5.6
RPLA-5		1.346	212	3.9	35.72	4.1

Table 5 shows the results obtained by this methodology completing the *SKT* of thermal decomposition of PLA and its recyclates. Figure 10 shows the fulfilment of the *P-M_C* by VPLA and RPLA-1 as an example of the goodness of the results. It is important to notice that technologist may use the same experimental settings for the pyrolysis of PLA to the rest of its recyclates, by only smoothly adjusting 3 parameters, since the thermal behaviour under inert atmosphere of the materials was essentially the same after the first recycle. The thermal

behaviour of PLA in presence of an oxidative ambient is different and calculations therefore followed a different path, as it is shown in the next section.

3.5. Thermo-oxidative decomposition kinetics

Figure 11 shows the results of the evaluation of the apparent activation energy ($E_{a\alpha}$) under oxidative conditions. Fig 11a depicts the evolution of $E_{a\alpha}$ obtained by *FWO*, *KAS* and *AIC* methods, showing a good coincidence along the decomposition reaction, as also obtained for the

Table 5. Results of fitting of Ea and lnA to Eq. (15)

Material	ACTIVATION ENERGY / Ea					PRE-EXPONENTIAL FACTOR / lnA				
	P1		P2		R ² (%)	P1		P2		R ² (%)
	value	e (%)	value	e (%)		value	e (%)	value	e (%)	
VPLA	0.791	2.61	---	---	99.82	0.746	2.82	---	---	99.64
RPLA-1	0.591	6.39	9.352	7.81	99.85	0.672	7.99	9.467	8.30	99.80
RPLA-2	0.413	2.46	11.783	2.89	99.06	0.399	7.22	10.63	4.11	99.64
RPLA-3	0.746	6.55	5.737	8.40	99.82	0.712	7.86	5.732	8.51	99.79
RPLA-4	0.357	8.40	8.294	3.96	99.81	0.342	7.08	10.47	4.23	99.68
RPLA-5	0.807	6.93	7.545	6.10	99.79	0.775	7.65	7.377	6.52	99.69

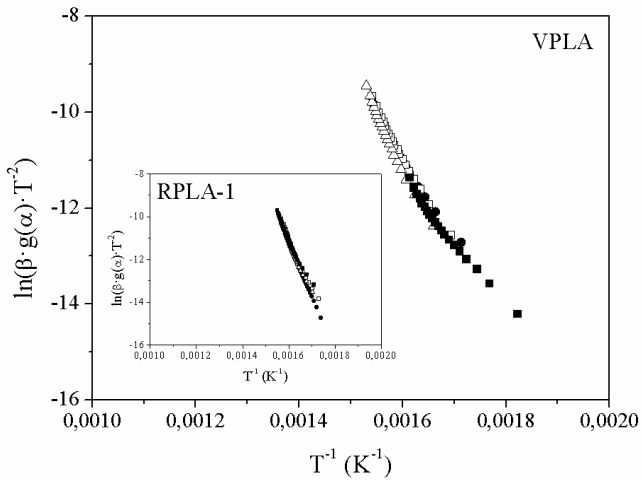


Figure 10. Application of *Perez-Maqueda et al.* criterion to virgin PLA and first reprocessed material (inset)

reprocessed materials. **Fig 11b** and **11c** show the evolution of Ea_α for all materials, split into two plots for simplicity. For comparison between virgin material and recyclates facing the thermo-oxidative decomposition, the Ea_α at a conversion rate of 0.2 is taken (that is, $Ea_{0,2}$). An increase up to the second recyclate was registered, which was not followed by the successive reprocessed materials, which kept their $Ea_{0,2}$ in similar values. In comparison to the behaviour shown under inert atmosphere, as expected, the Ea_α needed to trigger the decomposition under oxygen was lower, since the reactions were enhanced by oxidation processes which led to the formation of radical species such as carboxylic-ended species that accelerated the decomposition [63, 66-67]. In order to mathematically describe the evolution of Ea_α throughout the decomposition process, a powered equation was chosen, based on the *Freundlich* model [68] for growing behaviours, according to Eq.(12):

$$Ea(\alpha) = Ea_0^* + \sum_i b_i \cdot \alpha^{p_i} \quad (11)$$

,where i is the number of slope changes in the curve, Ea_0^* is a fictive activation energy at $\alpha = 0$, b is a fitting parameter and p is a power that accounts for the shape of the curve; whether $p <$

1, the increase is decelerative, and if $p > 1$, the increase is accelerative. **Table 6** shows the powers resulted from the fitting of Eq. (12) to the Ea evolution of all materials. High regression coefficients from the fitting ($R^2 > 99\%$), as well as narrow confidence bands in which the nominal powers laid ($< 10\%$), were obtained. These parameters were useful for the characterization of the thermal behaviour of PLA and its recyclates.

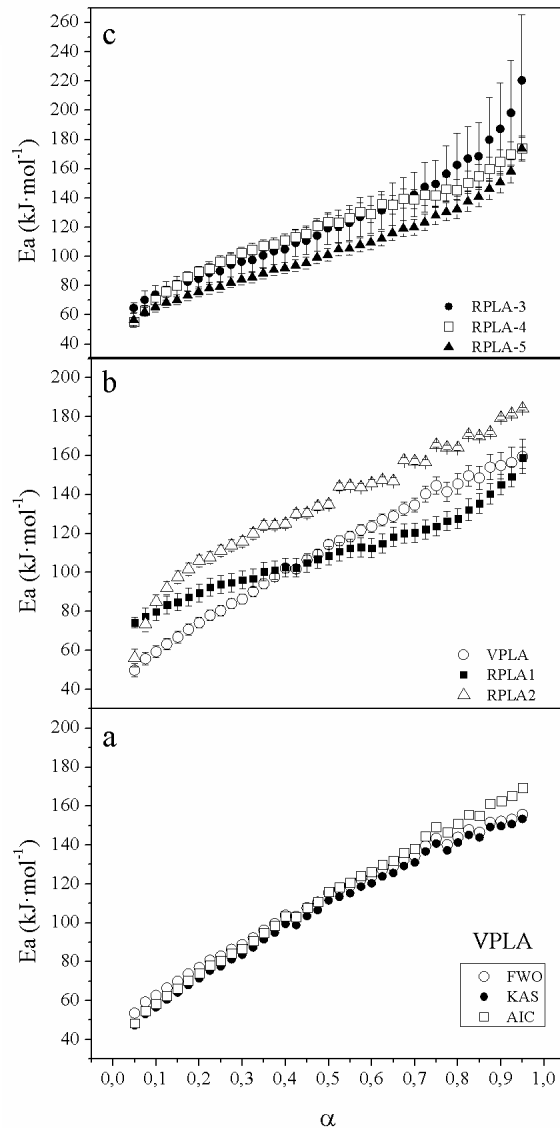


Figure 11. (a) Apparent Ea obtained for VPLA by means of FWO, KAS and AIC methods; (b) Average isoconversional activation energy of VPLA, RPLA-1 and RPLA-2; (c) Evolution of average isoconversional activation energy for RPLA-3, RPLA-4 and RPLA-5

As can be seen, virgin PLA only showed a decelerative curve, while the rest of materials presented a change in tendency at advanced conversions, rapidly increasing its Ea_α in an accelerative fashion. It can be also observed how smaller p_1 indicate a faster initial increase and vice versa, as clearly happened from VPLA to RPLA-2; on the other hand, smaller p_2 also indicate more brusque changes in tendency to faster Ea_α which increases along the decomposition reaction, as shown for RPLA-3 to 5. The presence of shorter chains due to reprocessing may enhance the intramolecular transesterifications to produce intermediate lactide and cyclic oligomers, which decomposition into smaller volatiles would need higher energy to evolve.

Provided that Ea_α is not constant, its variation was considered in Eq. (10), and Eq. (9) was modified into Eq (12), since the application of Eq. (11) did not work, due to the increase of thermal energies ($R \cdot T_\alpha$) in x were overcome by the increase of Ea_α , and therefore x increased with T_α , changing the tendency of the fraction $p(x) \cdot p(x_{0,5})^{-1}$. Note that for Ea constant, x decreases with T , and $p(x) \cdot p(x_{0,5})^{-1}$ increases.

$$\Phi(f_t, \alpha) = \sum_{\beta} \left(\sum_{\alpha=0}^1 [f_t(\alpha) - f_e(\alpha)]^2 \right); \Delta\alpha \quad (12)$$

$$= 0.025; \forall f_t$$

The minimization of Φ in Eq. (13) was achieved for virgin PLA and its successive recyclates facing thermo-oxidative decomposition by the model A_n , with n ranging from 2 to 4, as shown in Table 7. Figure 12 shows the $M-P_f$ of VPLA and RPLA-1 as an example of the goodness of this technique to predict the model of decomposition. In order to assure the value of n for each α that accounted for the variation of Ea_α

along the thermo-oxidative decomposition, the minimization of ξ in Eq. (10) was accomplished, considering Ea_α instead of \overline{Ea}_{iso} in its formulation and therefore performing an isoconversional analysis of the data. Figure 13 shows the evolution of n along the α range, which could be assumed to be almost constant within a confidence margin lower than 7%, as shown by n'' in Table 7. Therefore, the suitability of model A_n was strengthened. In addition, the possibility of using n' (average of n_β in Table 7) is remarked, since closer values to those given by the analytical procedure (n'') were obtained, thus permitting to continue the calculations with less time-consuming computations.

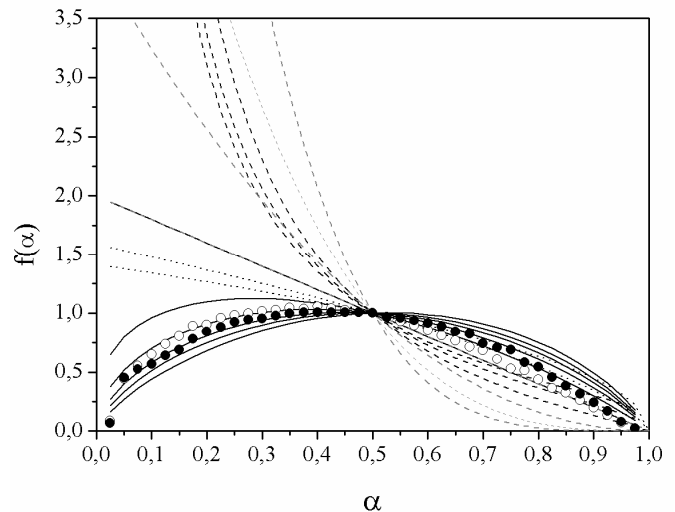


Figure 12. Master plots based on the differential form of the general kinetic law compared to experimental data obtained for thermo-oxidative decomposition of VPLA (hollow circles) and RPLA-1 (full circle). Models according to Table 1 (Black solid lines: A_n ; Grey solid lines: F_n ; Dashed grey lines)

Finally, the evolution of the pre-exponential factor along the α decomposition range ($\ln A_\alpha$) was obtained from the intercept at the origin in Eq. (11), considering Ea_α and n' in its calculation. Figure 13 shows the evolution of $\ln A_\alpha$ for VPLA and RPLA-2. The rest are not

Table 6. n_{β} : Values of n of the A_n model found for the thermo-oxidative decomposition of PLA and its recyclates at different β ; n' : average of n_{β} ; n'' : values obtained from the minimization method (results at fixed α shown in Fig. 13)

Material	n_{β}						n'	n''	
	β ($^{\circ}\text{C}\cdot\text{min}^{-1}$)							average	e (%)
	2	5	7	10	12	15			
VPLA	2.0	2.5	2.5	2.5	3.0	3.0	2.58	2.65	6.2
RPLA-1	2.0	2.0	2.5	2.5	3.0	3.0	2.50	2.41	6.9
RPLA-2	2.0	2.0	2.5	2.5	2.5	3.0	2.41	2.26	6.5
RPLA-3	2.0	2.5	2.5	2.5	3.0	4.0	2.76	2.76	5.3
RPLA-4	3.0	3.0	3.0	4.0	3.5	4.0	3.40	3.49	6.8
RPLA-5	2.5	2.5	3.0	4.0	4.0	4.0	3.33	3.38	6.4

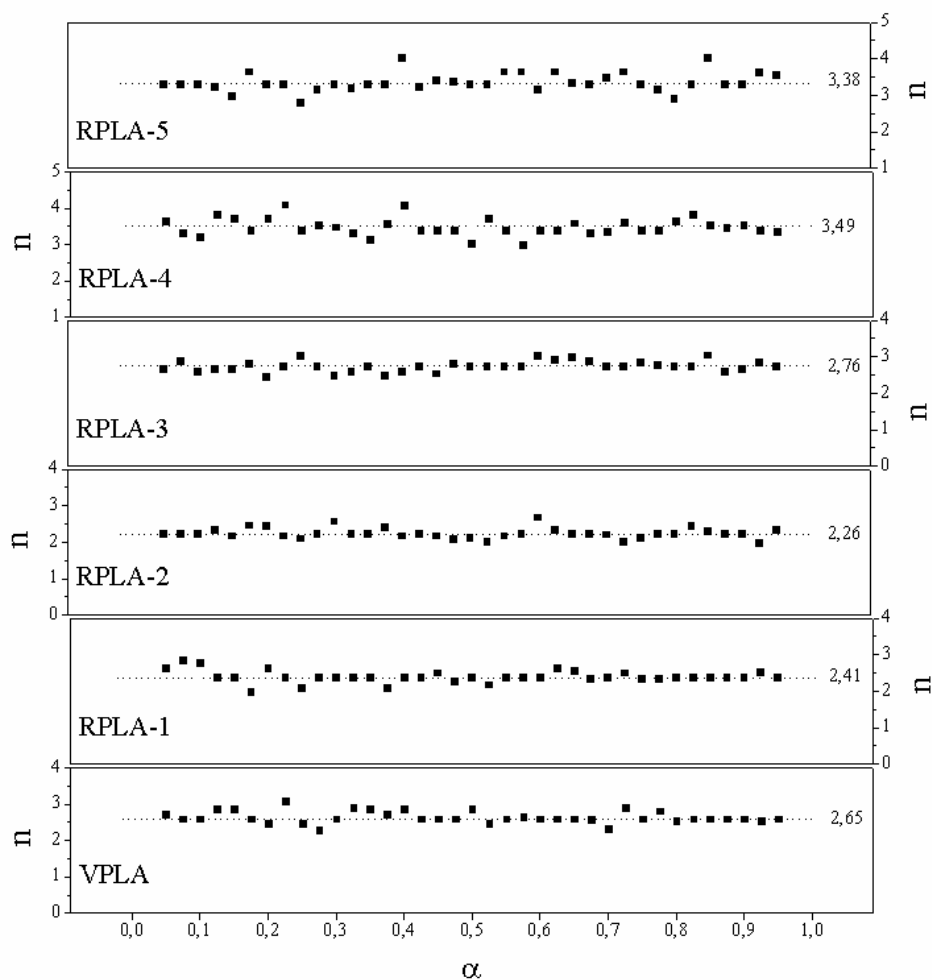


Figure 13. n evolution for A_n model of thermo-oxidative decomposition of virgin PLA and its successive recyclates. The number is the average of data (n'' in Table 7)

presented to prevent overlapping of curves. It can be seen how $\ln A_\alpha$ was strongly connected to the behaviour of Ea_α , since both presented similar shapes along the α range. Therefore, one may suggest that the application of Eq. (12) might also be suitable for fitting the experimental data and thus provide a mathematical description of $\ln A_\alpha$ evolution. The goodness of the fitting can be seen at **Figure 14** and assessed at **Table 6**, since the obtained R^2 values were $>99.5\%$. In addition, the powers p_1 and p_2 were of the same order than those obtained for Ea_α , thus permitting the use of the powers previously obtained for Ea_α as initialization values in the iteration of the fitting of $\ln A_\alpha$.

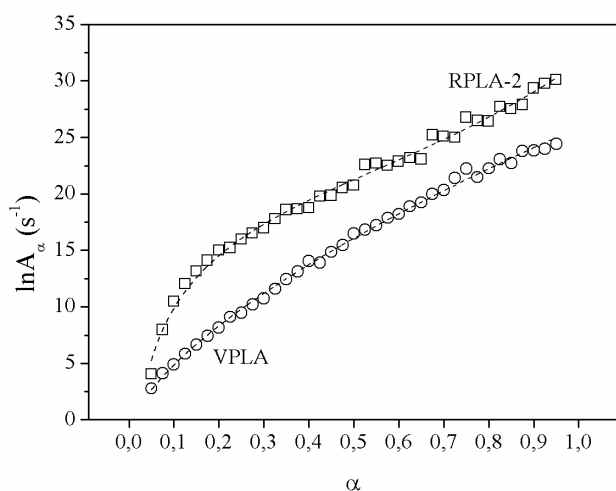


Figure 14. $\ln A_\alpha$ evolution given for VPLA and RPLA-2 as an example of the goodness of fitting of Eq. (12) to explain its behavior along the α range. Hollow symbols: obtained $\ln A_\alpha$ values; dashed lines: computed fittings.

5. Conclusions

Commercial polylactide was submitted to 5 successive reprocessing cycles through multiple injection steps in order to simulate thermo-mechanical degradation induced to the polymer by mechanical recycling. Multi-rate linear-non-isothermal thermogravimetric (TGA)

experiments under inert (Ar) and oxidative (O_2) conditions were performed to virgin PLA and its recyclates in order to simulate the thermal behaviour of the materials facing pyrolysis and combustion processes.

The release of gases was monitored by Evolved Gas Analysis of the fumes of the TGA experiment, by in-line FT-IR analysis, with the aid of 2D-correlation spectra. Main evolved gases were acetaldehyde, lactide and short-chain acids, as well as CO , CO_2 and H_2O . Reprocessed PLA did not modify the profile of evolved gases, and thus the transfer of technologies for the control of emitted gases is straightforward.

The thermal stability was studied in terms of the Thermal Decomposition Behaviour (TDB), which permitted to predict the thermal performance of the materials under any linear heating profile. The Zero-Decomposition Temperatures (ZDT) were also proposed as proper indicators of degradation, showing the decrease of thermal endurance from the second recycle on.

A kinetic analysis methodology, consisting in the combination of six different methods (namely Flynn-Wall-Ozawa, Kissinger-Akashira-Sunose, Advanced IsoConversional method, Master-Curves and Perez-Maqueda Criterion along with Coats-Redfern equation) was methodically applied, and its validity for being used with both constant and variable kinetic parameters was proven. A powered equation was used to explain the variations of the activation energies and the pre-exponential factors along the decomposition processes. The kinetic methodology provided the mathematical description of the thermal and thermo-oxidative decomposition of virgin PLA and its successive recyclates throughout the whole α range, as shown in **Figure 15** as an

example. A nucleation and growth model (A_n) which gave importance to the formation of gas bubbles in the polymer melt was valid for all materials.

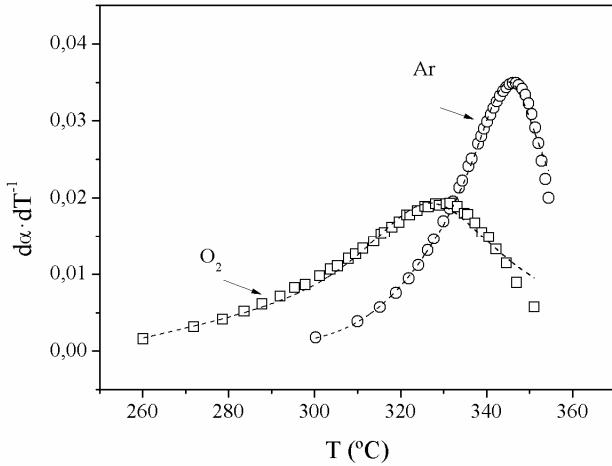


Figure 15. Comparison of experimental DTG curves (symbols) to computed kinetic functions (dashed lines) obtained from the kinetic methodology for VPLA at both studied atmospheres.

APPENDIXES

APPENDIX A: 2D-Correlation IR Spectroscopy

2D-Correlation IR Spectroscopy (hereafter 2D-IR) has gained much attention since its introduction [36]. Basically, in 2D-IR, a spectrum is obtained as a function of two independent IR wavenumbers, due to the application of an external perturbation, such as temperature, and provides information that cannot be drawn from conventional one-dimensional IR spectra. Although a deep description of this analytical procedure can be found elsewhere [36-37, 69-70], a short description with the basics to understand the discussion of results, is given hereafter.

By applying the Hilbert transform method, the synchronous and asynchronous correlation spectra of two signals I and 2 at different

wavenumbers ν can be described by Eq. (14) and Eq. (15), respectively:

$$\varphi(\nu_1, \nu_2) = \quad (16)$$

$$(T_{max} - T_{min})^{-1} \cdot \int_{T_{min}}^{T_{max}} \tilde{y}(\nu_1, t) \cdot \tilde{y}(\nu_2, t) \cdot dt$$

$$\Psi(\nu_1, \nu_2) = (T_{max} - T_{min})^{-1}$$

$$\cdot \int_{T_{min}}^{T_{max}} \tilde{y}(\nu_1, t) \cdot \tilde{z}(\nu_2, t) \cdot dt \quad (17)$$

where T_{min} and T_{max} are the limit temperatures of the TGA experiment, ν is the spectral variable (wavenumber in IR spectroscopy), \tilde{y} is the dynamic spectra and \tilde{z} its Hilbert transform, which expressions are shown in Eq. (16) and Eq. (17), respectively:

$$\tilde{y}(\nu, t) = \begin{cases} y(\nu, t) - \bar{y}(\nu), & t \in [T_{min}, T_{max}] \\ 0, & else \end{cases} \quad (18)$$

$$\tilde{z}(\nu, t) = \frac{1}{\pi} \cdot \int_{T_{min}}^{T_{max}} \tilde{y}(\nu, t') \cdot (t' - t)^{-1} \cdot dt' \quad (19)$$

being \bar{y} the reference spectrum usually time-averaged as:

$$\bar{y}(\nu, t) = \int_{T_{min}}^{T_{max}} y(\nu, t') \cdot dt \quad (20)$$

The synchronous spectra reflect the correlation of simultaneously varying of spectral intensity, while the asynchronous spectra reflect the non-comparability of spectral intensity variations, due to $\tilde{z}(\nu, t)$ is orthogonal to $\tilde{y}(\nu, t)$ and therefore appears when two signals are out-of-phase. Therefore the synchronous and asynchronous spectra are symmetrical and anti-symmetrical with respect to their diagonal lines, respectively. The discussion of both types of graphs is given in terms of auto and cross peaks.

The auto-peaks (ν_1, ν_1) , (ν_2, ν_2) in synchronous spectra rely on the diagonal line and their intensity reflect the influence of the external

perturbation on the molecular groups of wavenumbers ν_1 and ν_2 . Cross-peaks (ν_1, ν_2) , (ν_2, ν_1) are located off-diagonal, and represent the synchronicity of groups corresponding to wavenumbers ν_1 and ν_2 , highlighting the strong cooperation or interaction between their different molecular groups. A positive cross-peak describes the increase or decrease of the intensities of both ν_1 and ν_2 , while a negative cross-peak indicates an increase in the intensity of ν_1 during a decrease of ν_2 .

The asynchronous spectrum has no auto-peaks by definition. The cross-peaks in this case represent the sequential changes of the spectral intensities ν_1 and ν_2 due to the asynchrony of the variations in their intensities. This characteristic is also very useful for distinguishing between overlapped bands that arise from different spectral variations. The rules for determination of the sequence of spectral intensity changes are shown as follows:

1) If intensity in the synchronous spectrum is positive: $\varphi(\nu_1, \nu_2) > 0$

1.1.) A positive cross-peak in the asynchronous spectrum $\Psi(\nu_1, \nu_2) > 0$ states the change in intensity of ν_1 occurs before the change in ν_2 .

1.2.) A negative cross-peak in the asynchronous spectrum $\Psi(\nu_1, \nu_2) < 0$ states the change in intensity of ν_2 occurs before the change in ν_1 .

2) If intensity in the synchronous spectrum is negative: $\varphi(\nu_1, \nu_2) < 0$, the rules above are reversed.

APPENDIX B: Solid-state kinetics

The intrinsic kinetics of solid-state decompositions are usually described by three parameters: activation energy (Ea), pre-

exponential factor (A or $\ln A$) and kinetic function $f(\alpha)$, conforming the so-called kinetic triplet. These kinetic functions mathematically express different physical kinetic models. General kinetic models are proposed in literature for plastics and biomasses, which do not take into account the rigorous and exhaustive description of the chemistry of thermal decomposition of polymers and describe the process by means of a simplified reaction pathway. Each single reaction step considered is representative of a complex network of reactions [39]. Recently, *Khawan* and *Flanagan* [71] reviewed the relationship between the theoretical decomposition mechanisms and their mathematical models. Kinetic analysis of non-isothermal experiments is generally performed by using a single step kinetic equation:

$$\begin{aligned} \frac{d\alpha}{dt} &\equiv \beta \cdot \frac{d\alpha}{dT} = A \cdot f(\alpha) \cdot k(T) \\ &= A \cdot f(\alpha) \cdot e^{-\frac{Ea}{R \cdot T}} \end{aligned} \quad (21)$$

, where t is the time (s), T the temperature (K), α is the conversion degree, β the heating rate used in the TGA ($K \cdot s^{-1}$), R is the ideal gas constant ($8.31 J \cdot mol^{-1} \cdot K^{-1}$), A a pre-exponential factor (s^{-1}), $f(\alpha)$ the kinetic function and Ea is the activation energy ($J \cdot mol^{-1}$). For thermogravimetric experiments, $\alpha = (m_0 - m_t) / (m_0 - m_\infty)$, where m stands for mass (g), and subscripts 0 , ∞ and t respond to initial, final and actual thermogravimetric values. The integration of Eq. (19), after rearranging, leads to:

$$\begin{aligned} g(\alpha) &= \int_0^\alpha \frac{d\alpha}{f(\alpha)} = \frac{A \cdot Ea}{\beta \cdot R} \cdot \int_0^\infty \frac{e^{-x}}{x^2} \\ &= \frac{A \cdot Ea}{R \cdot T} \cdot p(x) \quad , \quad x \\ &= \frac{Ea}{R \cdot T} \end{aligned} \quad (22)$$

, where $g(\alpha)$ is the inverse integral kinetic function.

Under linear heating rate program, Eq. (20) does not have an exact analytical solution to the temperature integral $p(x)$ and therefore a vast number of publications have performed approximated equations to approach the best values within the lower error margin [72]. In this work, the Senum-Yang [73] approximation shown at Eq. (21) truncated at its fifth term has been used, since it gives deviations from the exact value of the temperature integral lower than 10^{-8} % for $x > 10$ [74], which permits its application in solid-state decomposition reactions, where x is usually higher.

$$p(x) = \frac{e^{-x}}{x^2} \cdot \sum_n \frac{n \cdot (1 - n)}{x + 2 \cdot (n + 1)} \quad (23)$$

References

1. J. Lunt, Large-scale production, properties and commercial applications of polylactic acid polymers, *Polymer Degradation and Stability*, 59 (1998) 145-152.
2. A. P. Gupta, V. Kumar, New emerging trends in synthetic biodegradable polymers - Polylactide: a critique, *European Polymer Journal*, 43 (2007) 4053-4074.
3. F. Vilaplana, S. Karlsson, Quality concepts for the improved use of recycled polymeric materials: a review. *Macromolecular Materials and Engineering*, 293 (2008) 274-297.
4. E. Strömberg, S. Karlsson, The design of a test protocol to model the degradation of polyolefins during recycling and service life, *Journal of Applied Polymer Science*, 112 (2009) 1835-1844.
5. F. Vilaplana, A. Ribes-Greus, S. Karlsson, Degradation of recycled high-impact polystyrene. Simulation by reprocessing and thermo-oxidation. *Polymer Degradation and Stability*, 91 (2006) 2163-2170.
6. F. Vilaplana, A. Ribes-Greus, S. Karlsson, Changes in the micro-structure and morphology of high-impact polystyrene subjected to multiple processing and thermo-oxidative degradation. *European Polymer Journal*, 43 (2007) 4371-4381.
7. N. Yarahmadi, I. Jakubowicz, T. Gevert, Effects of repeated extrusion on the properties and durability of rigid PVC scrap. *Polymer Degradation and Stability*, 73 (2001) 93-99.
8. J.D. Badia, F. Vilaplana, S. Karlsson, A. Ribes-Greus, Thermal analysis as a quality tool for assessing the influence of thermo-mechanical degradation on recycled poly(ethylene terephthalate), *Polymer Testing*, 28 (2009) 169-175.
9. F. La Mantia, M. Vinci, Recycling poly(ethylene terephthalate), *Polymer Degradation and Stability*, 45 (1994) 121-125.
10. N. Torres, J. J. Robin, B. Boutevin, Study of thermal and mechanical properties of virgin and recycled poly(ethylene terephthalate) before and after injection molding, *European Polymer Journal*, 36 (2000) 2075-2080.
11. J.D. Badia, E. Strömberg, A. Ribes-Greus, S. Karlsson, Optimizing the MALDI-TOF-MS sample preparation procedure to determine the thermo-mechanical degradation mechanisms of poly (ethylene terephthalate). *Analytica Chimica Acta* 692 (2011) 85-95
12. J.D. Badia, E. Strömberg, A. Ribes-Greus, S. Karlsson, Assessing the MALDI-TOF MS sample preparation procedure to analyze the influence of thermo-oxidative ageing and thermo-mechanical degradation on poly (lactide). *European Polymer Journal* 47 (2011) 1416-1428
13. J.D. Badia, E. Strömberg, A. Ribes-Greus, S. Karlsson. Personal communication.
14. S.M. Al-Salem, P. Lettieri, J. Baeyens, Recycling and recovery routes of plastic solid waste (PSW): A review, *Waste management*, 29 (2009) 2625-2643.
15. M. Grigante, M. Ischia, M. Baratieri, R. Dal Maschio, M. Ragazzi, Pyrolysis analysis and solid residue stabilization of polymers, waste tyres, spruce sawdust and sewage sludge, *Waste and Biomass Valorization*, 1 (2010) 381-393.
16. R. Moriana, J.D. Badía, L. Santonja-Blasco, A. Ribes-Greus, Assessing the mechanical enhancement and the thermostabilising effect of adding cotton fibres to a starch-based matrix using thermal analysis. Unpublished results.

17. P. T. Williams, S. Besler, Pyrolysis-thermogravimetric analysis of tyres and tyre components, *Fuel*, 74 (1995) 1277-1283.
18. D. K. Seo, S. S. Park, J. Hwang, T.U. Yu, Study of the pyrolysis of biomass using thermogravimetric analysis (TGA) and concentration measurements of evolved species, *Journal of Analytical and Applied Pyrolysis*, 89 (2010) 66-73
19. P. Fu, S. Hu, J. Xiang, P.Li, D. Huang, L. Jiang, A. Zhang, J. Zhang, FTIR study of pyrolysis products evolving from typical agricultural residues, *Journal of Analytical and Applied Pyrolysis*, 88 (2010) 117-123.
20. L. Yanfen, M. Xiaoqian, Thermogravimetric analysis of the co-combustion of coal and paper mill sludge, *Applied Energy*, 87 (2010) 3526-3532.
21. K. Liu, X. Q. Ma, H. M. Xiao, Experimental and kinetic modeling of oxygen-enriched air combustion of paper mill sludge, *Waste Management*, 30 (2010) 1206-1211.
22. M. Otero, X. Gómez, A. I. García, A. Morán, Effects of sewage sludge blending on the coal combustion: A thermogravimetric analysis, *Chemosphere*, 69 (2007) 1740-1750.
23. I. Martín-Gullón, M. Esperanza, R. Font, Kinetic model for the pyrolysis and combustion of poly-(ethylene terephthalate)(PET). *Journal of Analytical and Applied Pyrolysis*, 58-59 (2001) 635-650.
24. R. Aguado, M. Olazar, B. Gaisán, R. Prieto, J. Bilbao, Kinetics of polystyrene pyrolysis in a conical spouted bed reactor. *Chemical Engineering Journal*, 92 (2003) 91-99.
25. H. Bockhorn, A. Hornung, D. Schawaller, Kinetic study on the thermal degradation of polypropylene and polyethylene, *Journal of Analytical and Applied Pyrolysis*, 48 (1999) 93-109.
26. I. E. Yuzay, R. Auras, H. Soto-Valdez, S. Selke, Effects of synthetic and natural zeolites on morphology and thermal degradation of poly(lactic acid) composites. *Polymer Degradation and Stability*, 95 (2010) 1769-1777.
27. X. Liu, S. Khor, E. petinakis, L. Yu, G. Simon, K. Dean, S. Bateman, Effects of hydrophilic fillers on the thermal degradation of poly(lactic acid), *Thermochimica Acta*, 509 (2010) 147-151.
28. J.D. Badía, L. Santonja-Blasco, R. Moriana, A. Ribes-Greus, Thermal analysis applied to the characterization of degradation in soil of polylactide: II. On the thermal stability and thermal decomposition kinetics. *Polymer Degradation and Stability*, 95 (2010) 2192-2199
29. H. Zou, C. Yi, L.Wang, H. Liu, W. Xu, Thermal degradation of poly(lactic acid) measured by thermogravimetry coupled to Fourier transform infrared spectroscopy. *Journal of Thermal Analysis and Calorimetry*, 97 (2009) 929-935.
30. M. Żenkiewicz, J. Richert, P. Rytlewski, K. Moraczewski, M. Stepczyńska, T. Karasiewicz, Characterisation of multi-extruded poly(lactic acid). *Polymer Testing*, 28 (2009) 412-418.
31. F. Carrasco, P. Pagès, J. Gámez-Pérez, O.O. Santana, M. L. Maspocho, Kinetics of the thermal decomposition of processed poly(lactic acid). *Polymer Degradation and Stability*, 95 (2010) 2508-2514.
32. F. D. Kopinke, K. Mackencie, Mechanistic aspects of the thermal degradation of poly(lactic acid) and poly(beta-hydroxybutyric acid), *Journal of Analytical and Applied Pyrolysis*, 40-41 (1997) 43-53.
33. F. D. Kopinke, M. Remmler, K. Mackenzie, M. Möder, O. Wachsen, Thermal decomposition of biodegradable polyesters - II: Poly(lactic acid), *Polymer Degradation and Stability*, 53 (1996) 329-342.
34. I. C. Mc Neill, H. A. Leiper, Degradation studies of some polyesters and polycarbonates - 2: Polylactide: Degradation under isothermal conditions, thermal degradation mechanisms and photolysis of the polymer. *Polymer Degradation and Stability*, 11 (1985) 309-326.
35. C. Vogel, H. W. Siesler, Thermal degradation of poly(e-caprolactone), poly(L-lactic acid) and their blends with poly(3-hydroxy-butyrato) studied by TGA/FT-IR spectroscopy, *Macromolecular Symposia*, 265 (2008) 183-194.
36. I. Noda, Two-Dimensional Infrared (2D IR) Spectroscopy: Theory and Applications. , *Applied Spectroscopy*, 44 (1990) 550-561.
37. I. Noda, Generalized Two-Dimensional Correlation Method applicable to Infrared, Raman, and other types of Spectroscopy. *Applied Spectroscopy*, 47 (1993) 1329-1336.

38. M Brown (ed.), *Techniques and Applications. Introduction to Thermal Analysis*. 2nd. Edition, Kluwer Academic Publishers (2001).
39. B. Wunderlich, *Thermal analysis of polymeric materials*. Springer, Berlin, 2005..
40. S. Morita, 2D Shige (c). Kwansai-Gakuin University, 2004-2005.
41. K. Levenberg, A method for solution of certain non-linear problems in least squares, *Quarterly of Applied Mathematics*, 2 (1944) 164-168.
42. D. W. Marquardt, An algorithm for the least-squares estimation of non-linear parameters. *SIAM Journal of Applied Mathematics*, 11 (1963) 431-441.
43. C. N. Tam, P. Bour, T.A. Keiderling, Vibrational Optical Activity of (3S, 6S)-3,6-Dimethyl-1,4-dioxane-2,5-dione, *Journal of the American Chemical Society*, 118 (1996) 10285.
44. B. Liu, X. Zhao, X. Wang, F. Wang, Thermal degradation kinetics of poly(propylene carbonate) obtained from the copolymerization of carbon dioxide and propylene oxide. *Journal of Applied Polymer Science*, 90 (2003) 947-953.
45. J.D. Badía, A. Ribes-Greus, Detailed methodology to assess the thermal stability and kinetics of thermal and thermo-oxidative decomposition behaviours of reprocessed poly(ethylene terephthalate). Unpublished results.
46. J. H. Flynn, L. A. Wall, A quick, direct method for the determination of activation energy from thermogravimetric data. *Journal of Polymer Science*, 4 (1966) 323-342.
47. T. Ozawa, Kinetic analysis of derivative curves in thermal analysis. *Journal of Thermal Analysis*, 2 (1970) 301.
48. C. D. Doyle, Series approximations to the equation of thermogravimetric data., *Nature*, 207 (1965) 209.
49. H. E. Kissinger, Reaction kinetics in differential thermal analysis. *Analytical Chemistry*, 29 (1957) 1702-1706.
50. T. Akahira, T. Sunose, *Trans. Joint Convention of Four Electrical Institutes*, Paper No. 246 Research Report/ Chiba Institute of Technology, *Scientific Technology*, 16 (1971) 22-31.
51. S. Vyazovkin, Advanced Isoconversional Method, *Journal of Thermal Analysis*, 49 (1997) 1493-1499.
52. J. Li, W. Zheng, L. Li, Y. Zheng, X. Lou, Thermal degradation kinetics of g-HA/PLA *Thermochimica Acta*, 493 (2009) 90-95.
53. Q. Zhou, M. Xanthos, Nanosize and microsize clay effects on the kinetics of the thermal degradation of polylactides, *Polymer Degradation and Stability*, 94 (2009) 327-338.
54. A. K., Galwey, M. E. Brown, *Thermal decomposition of ionic solids. Studies in physical and theoretical chemistry*. Amsterdam, Elsevier (1999)
55. F.J. Gotor, J.M. Criado, J. Málek, N. Koga, Kinetic Analysis of Solid-State Reactions: The universality of Master Plots for Analyzing Isothermal and Non-Isothermal Experiments., *Journal of Physical Chemistry A*, 104 (2000) 10777-10782
56. T. Ozawa, A New Method of Analyzing Thermogravimetric Data. *Bulletin of the Chemical Society of Japan*, 38 (1965) 1881
57. T. Ozawa, Non-isothermal kinetics and generalized time. *Thermochimica Acta*, 100 (1986) 109.
58. S. T. Stoeva, K. Gjurova, M. Zagorcheva, Thermal analysis study on the degradation of the solid state chlorinated poly(ethylene). *Polymer Degradation and Stability*, 67 (2010) 117-128
59. L. Li, C. Guan, A. Zhang, D. Chen, Z. Qing, Thermal stabilities and the thermal degradation kinetics of polyimides. *Polymer Degradation and Stability*, 84 (2004) 369-373.
60. J.T. Sun, Y.D. Huang, G.F. Gong, H.L. Cao, Thermal degradation kinetics of poly(methylphenylsiloxane) obtaining methacryloyl groups., *Polymer Degradation and Stability*, 91 (2005) 339-346.
61. X. Meng, Y. Huang, H. Yu, Z. Lu, Thermal degradation kinetics of polyimide containing 2,6-benzobisoxazole units, *Polymer Degradation and Stability*, 92 (2007) 962-967.
62. G. Grausea, J. Ishibashia, T. Kameda, T. Bhaskarb, T. Yoshioka, Kinetic studies of the decomposition of flame retardants containing high-impact polystyrene. *Polymer Degradation and Stability*, 95 (2010) 1129-1137
63. X. Liu, Y. Zou, W. Li, G. Cao, W. Chen, Kinetics of thermo-oxidative and thermal

degradation of poly(D,L- Lactide) (PDLLA) at processing temperature. *Polymer Degradation and Stability*, 91 (2006) 3259-3265.

64. L. A. Pérez-Maqueda, J. M. Criado, F. J. Gotor, J. Málek Advantages of Combined Kinetic Analysis of Experimental Data Obtained under Any Heating Profile. *Journal of Physical Chemistry A*, 106 (2002) 2862-2868

65. A. W. Coats, J. P. Redfern, Kinetic analysis from thermogravimetric data. *Nature*, 68 (1964) 4914.

66. W. C. Lai and W. B. Liao, "Thermo-oxidative Degradation of Poly(ethylene glycol)/Poly(L-lactic acid) Blends", *Polymer* 44, (2003) 8103

67. D. N. Bikiaris, G. P. Karayannidis, Effect of carboxylic end groups on thermooxidative stability of PET and PBT, *Polymer Degradation and Stability*, 66 (1999) 213-218.

68. Freundlich, H. *Colloid and Capillary Chemistry*. New York : E P Dutton & Co, (1928).

69. I. Noda, Recent developments in two-dimensional infrared (2D IR) correlation spectroscopy. *Applied Spectroscopy*, 47 (1993) 1317-1323.

70. X. Dou, B. Yuan, H. Zhao, G. Yin, Generalized two-dimensional correlation spectroscopy - Theory and applications in

analytical field. *Science in China Serie B: Chemistry*, 47 (2004) 257-266

71. A. Khawan, D. R. Flanagan, Solid-State Kinetic Models: Basics and Mathematical Fundamentals. *Journal of Physical Chemistry B*, 110 (2006) 17315-17328.

72. L. A. Pérez-Maqueda, P. E. Sánchez-Jiménez, J.M. Criado, Kinetic analysis of solid-state reactions: precision of the activation of the activation energy calculated by integral methods. *International Journal of Chemical Kinetics*, 37 (2005) 658-666.

73. G. I. Senum, R. T. Yang, Rational approximations of the integral of the Arrhenius function, *Journal of Thermal Analysis and Calorimetry*, 11 (1977) 446.

74. L. A. Pérez-Maqueda, J. M. Criado, The accuracy of Senum and Yang's approximations to the Arrhenius Integral. *Journal of Thermal Analysis and Calorimetry*, 60 (2000) 909-915.

5. REMARKABLE RESULTS

Thermogravimetric analysis was useful for modelling energetic valorisation processes such as pyrolysis and combustion of virgin and reprocessed PET and PLA. The study of the evolved gases, the changes in thermal stability and the kinetics of decomposition pictured the behaviour of both polymers under both thermolytic processes. Several remarks could be concluded, regarding the following matters:

Profiles of decomposition

Both virgin PET and PLA, as well as their successive 5 recyclates, described a mass-loss driven by one decomposition stage in inert conditions and two in oxidizing conditions. In both cases, the first step could be ascribed to the pyrolysis of the backbone. The second mass-loss step under O₂ was related to the decomposition of the remaining char, more present in PET (~20%) than in PLA (~2%).

Evolved-gas analysis

In the case of PET, a release of acetaldehyde and, with less presence benzaldehyde, followed by a release of CO and CO₂, being the emission of the latter followed at higher temperatures, was found in inert conditions. However, the decomposition occurred firstly releasing mainly acetaldehyde, being followed by a noticeable production of CO₂ under oxidative atmosphere.

In the case of PLA, similar profiles were encountered except for the presence of benzene-containing species. Thus, main evolved gases were acetaldehyde, lactide and short-chain acids, as well as CO, CO₂ and H₂O.

The gas emission profiles given by virgin PET and PLA were also shown by all respective recyclates, thus the transfer of technologies for the control of emitted gases could be straightforward.

Thermal stability

The thermal performance of the materials under any linear heating profile was predicted by means of the proposed Thermal Decomposition Behaviour (TDB) model. The Zero-

Decomposition Temperatures (ZDT) and particularly the use of the peak ZDT_p were also used as proper indicators of thermo-mechanical degradation to monitor the weakening of the material against both thermal and thermo-oxidative decompositions.

Kinetic analysis

The combination of six different methods (namely Flynn-Wall-Ozawa, Kissinger-Akahira-Sunose, Advanced IsoConversional method or Vyazovkin, Master-Curves and Perez-Maqueda Criterion along with Coats-Redfern equation) was methodically applied. Its validity for being used with both constant and variable kinetic parameters was confirmed. The variation of the kinetic parameters Ea and A was taken into account and their behaviours were modelled as well throughout the thermal decomposition range.

The kinetic model that mathematically described the thermal and thermo-oxidative decompositions of PET, PLA and their recyclates was of the type A_n : nucleation and growth, which gave importance to the formation of gas bubbles in the melt.

Effects of reprocessing

From the second to the third reprocessing cycle, a change in tendency was shown by thermal stability and thermal activation parameters for both PET and PLA recyclates. Focusing on each process, under Ar the recyclates needed more energy and temperatures to decompose than virgin materials, whereas under O_2 the decomposition of all recyclates was overcome at lower Ea than that of virgin materials. Thus controlled combustion could be an option to valorise both materials energetically. All the considerations shown in the work may provide technologist with plausible indicators for the selection of the adequate energetic recovery option of recycled PET and PLA.

CHAPTER V

BIOLOGICAL VALORISATION

Performance of Thermal Analysis Techniques
for monitoring the biodegradation in soil process
of PLA

CHAPTER V: BIOLOGICAL VALORISATION

CONTENTS

1. Biodegradation: general aspects	405
1.1. Degradation after service life	406
1.2. Biodegradation processes	408
1.2.1. Biodeterioration	408
1.2.2. Biofragmentation	409
1.2.3. Bioassimilation	412
2. Testing procedures for assessing biodegradation	415
2.1. Analytical strategies	415
2.2. Relevant ISO standards for the measurement of biodegradation	417
2.3. Standardisation and certification	418
3. Biodegradation of PLA	421
4. References in this chapter	425
5. Contributions in this thesis	429
CONTRIBUTION V-A: <i>Thermal analysis applied to the characterization of degradation in soil of polylactide: I. Calorimetric and viscoelastic analyses</i>	431
CONTRIBUTION V-B: <i>Thermal analysis applied to the characterization of degradation in soil of polylactide: II. On the thermal stability and thermal decomposition kinetics</i>	441
6. Remarkable results	451

1. BIODEGRADATION: GENERAL ASPECTS

The design of polymeric materials moves towards the preparation of sustainable polymers with controlled degradability and enhanced bio-reintegration, or what is termed, from cradle to cradle. From a more open point of view, **cradle-to-cradle design** (C²D) enables the establishment of completely beneficial industrial systems driven by the synergistic search of positive economic, environmental and social goals. The practical, strategic expression of the eco-effective philosophy, C²D defines a framework for designing products and industrial processes that turn materials into nutrients by enabling their perpetual flow within both biological and technical metabolisms⁽¹⁾. Thus the understanding of the degradation mechanisms of both natural and synthetic polymers by microorganisms and enzymes should open new prospects in the field of biodegradable plastics.

The biodegradation mechanisms of the polymeric materials should contribute to further developments of the next generation of materials having a high environmental acceptability and recyclability. Polymer degradation and transformation technologies are essential for polymer production and recycling. Nature-based polymers such as polylactides, bio-polyesters and microbial poly(amino acid)s may become the most promising commodity bio-based plastics because they can be produced from renewable resources, and thus they should be recycled by various routes, such as bio-recycling, bio-refining, chemical recycling and material recycling. In order to develop technologies for the design of sustainable biodegradable and bio-recyclable polymers, the understanding of the biodegradation mechanism for each polymer would become a powerful tool⁽²⁾.

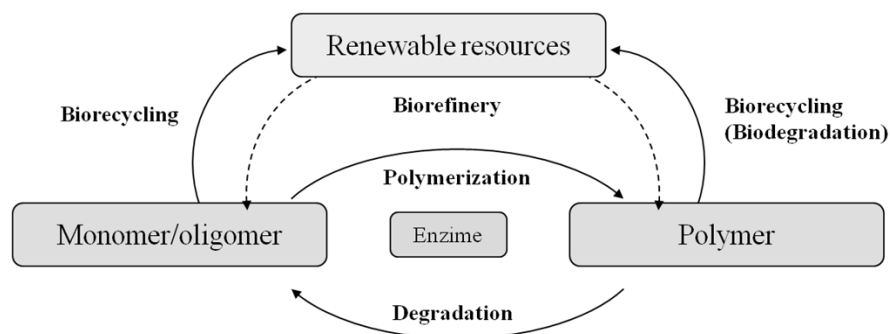


Figure 5. 1. Sustainable polymer production and recycling, as adapted from Ref (2).

Indeed, **biodegradation** is a natural complex phenomenon. Due to the great number of parameters synergically occurring during the biogeochemical valorisation of nature-based polymers, nature-like experiments are difficult to perform in laboratory conditions. Nevertheless, the biodegradability tests are necessary to estimate the environmental impact of industrial materials and to find solutions to avoid the disturbing accumulation of polymers. Several derived biodegradability tests have been developed by different research groups (see as example those works by *Pagga*⁽³⁾, *Rizarrelli*⁽⁴⁾, *Wallström*⁽⁵⁾ and co-workers) which have conducted to different interpretations about the biodegradation mechanisms taking place. To compensate for this problem, it is necessary to explain the different phenomena involved in biodegradation, such as **biodeterioration**, **biofragmentation** and **assimilation**, in connection to the required estimation techniques⁽⁶⁾.

1.1. DEGRADATION AFTER SERVICE LIFE

Many polymers that are claimed to be *biodegradable* are in fact *bioerodable*, *hydrobiodegradable* or *photodegradable*, or just partially biodegradable⁽⁷⁾. These different polymer classes are grouped by some authors under the broader category of **environmentally degradable polymers** (EDP). EDP can be considered a group of natural-based and synthetic polymeric materials that undergo chemical changes under the influence of environmental factors. The chemical changes must be followed by complete microbial assimilation of degradation products resulting in carbon dioxide and water.

When polymers fulfil their service life, most still possess their abilities intact during the disposal stage. The landfill has served mankind for much longer than any alternative disposal option. **Landfilling** is defined as the disposal, compression and embankment fill of waste at appropriate sites⁽⁸⁾. More advanced options for biodegradable polymers include the composting plants, which operate at temperature and humidity conditions more favourable for the polymer degradation. Important factors that need to be taken into account for the correct function of the disposal sites are the selection of the site, the design and organization of the site, the operating performance and the life cycle and biodegradability of the wastes⁽⁹⁾. The environmental impact of waste landfilling depends on the design and operational mode of the landfill facility and the nature of the waste

deposited⁽¹⁰⁾. In both cases of landfilling or composting, the degradation of plastic waste should not result in contamination of the soil and pollution of the environment (including aesthetic pollution). The rate of disintegration and integration into the carbon cycle is driven by the degradation paths characteristics of each plastic. Describing plastics degradation, measuring it, and controlling it are all complicated by three major factors⁽⁷⁾:

Polymer composition

Regardless the environment, the mechanism and rate of degradation depend on the chemical composition of the polymer. The rate of possible biodegradation in particular, depends on the polymers characteristics because the polymer is the substrate for the microorganisms or enzymes. One factor that determines the degradability or biodegradability of a polymer is the nature of the **chemical bonds** that are present. As well, the features of **chain branching** and even **stereochemistry** (the detailed spatial arrangement of atoms and bonds) are also important, because enzymes are often specific for attacking one particular type of chain branching and one particular stereochemistry. Other remarkable aspects to take into account are the **molar mass** of the polymer, **chain flexibility**, or morphology, including the extent of surface and the degree of crystallinity.

Mechanisms

Plastics can and do degrade by many routes, consecutively or simultaneously. Fragmentation often plays an important role in the early stages of degradation and can be brought about by physical forces of mechanical nature. Chemical changes within the plastic can occur and may begin with **abiotic degradation**, by interaction with chemicals and substances liable to react with the plastic. It generally involves chain scission within the polymeric backbones. For instance, the surface erosion can be the result of chain scission resulting from chemical hydrolysis. At some point, some specific plastics may be attacked effectively by microorganisms, which point out the induction of the **biotic degradation**, or biodegradation.

Environmental conditions

The degradation of plastics in particular conditions depends on the environment the plastics are exposed to, during their useful lifetime and the environment the polymer wastes are disposed to, afterwards. Concretely, the rates of degradation depend on

whether the environment is dry air, humid air, soil, a landfill, a composting environment, sewage, freshwater or a marine environment. Each environment has its own characteristic concentration profile of important **factors** such as oxygen, water, other chemicals, daylight or degrading microorganisms⁽¹¹⁾.

- The **environmental** factors affecting the rate of degradation that is due to microorganisms include temperature, moisture level, atmospheric pressure, and pressure of oxygen, concentrations of acids and metals, and the degree of exposure to light.
- Factors relating to **microorganisms** include their concentration, whether or not they have enzymes for which the polymer is substrate, the concentration of enzymes, the presence of trace nutrients for the microorganisms and the presence of inhibitors or predators⁽¹²⁾.

1.2. BIODEGRADATION PROCESSES

The degradation process of EDP comprises two phases, **disintegration** and **mineralization**⁽¹³⁾. During the initial phase, disintegration is significantly associated with the deterioration in physical properties, such as discoloration, embrittlement and fragmentation. The second phase, mineralization, is assumed to be the ultimate conversion of plastic fragments, after being broken down to molecular sizes, to CO₂, water, cell biomass (aerobic conditions), and CH₄, CO₂ and cell biomass in the case of anaerobic conditions. The EDP degradation and assimilation must be complete and occur at a sufficiently rapid rate so as to avoid accumulation of materials in the environment⁽¹⁴⁾.

The different stages throughout biodegradable polymers degrade are exposed hereafter:

1.2.1. BIODETERIORATION⁽⁶⁾

The biodeterioration of thermoplastic polymers could proceed by two different mechanisms, those are, bulk and surface erosion⁽¹⁵⁾. In the case of **bulk erosion**, fragments are lost from the entire polymer mass and the molar mass changes due to bond cleavage. This breakage is provoked by chemicals such as H₂O, acids, bases, transition

metals and radicals, but not by enzymes, since they are too large to penetrate throughout the matrix framework. In the case of **surface erosion**, matter is lost but there is not change in the molar mass of polymers of the matrix.

If the diffusion of chemicals throughout the material is faster than the cleavage of polymer bonds, the polymer undergoes bulk erosion. If the cleavage of bonds is faster than the diffusion of chemicals, the process occurs mainly at the surface of the matrix. A schematic representation of both erosion processes is shown in Figure 5. 2.

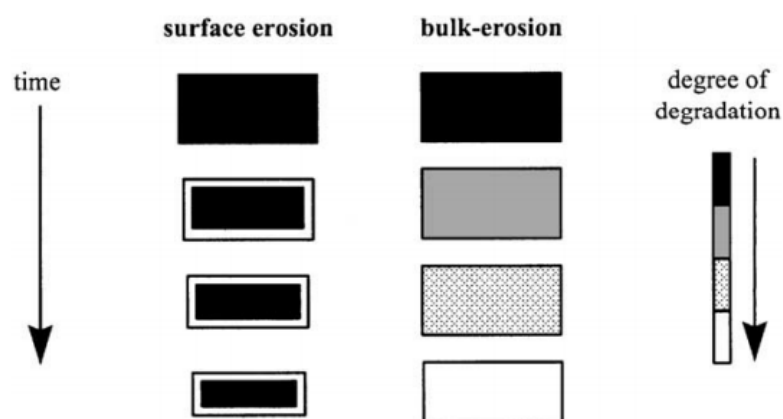


Figure 5. 2. Schematic illustration of the changes in a polymer matrix undergone by surface and bulk erosion (adapted from Ref. (15))

1.2.2. BIOFRAGMENTATION^{(6) (7)}

A polymer is considered as fragmented when low molecular weight molecules are found within the media. The fragmentation is a lytic phenomenon necessary for the subsequent assimilation of the broken up polymeric chains into the surrounding environment. Due to the high molar mass of a polymer, the macromolecules are unable to cross the cell wall and/or cytoplasmic membrane of microorganisms. It is therefore indispensable to cleave several bonds to obtain a mixture of oligomers and/or monomers. The energy to accomplish scissions may be of different origins: **abiotic** (thermal, light, mechanical, and chemical) and/or **biotic** (biological).

Concerning biotic biofragmentation, microorganisms cleave polymers by different means, secreting specific enzymes or generating free radicals. Actually, the biodegradation is

generally considered as consisting of both enzyme-catalyzed hydrolysis and non-enzymatic hydrolysis ⁽¹⁶⁾.

A. Enzymatic degradation

Enzymes are catalytic proteins that decrease the level of activation energy of molecules favouring chemical reactions. According to the IUPAC nomenclature, several enzymes can be found depending on the class of groups preferred during a given chemical reaction: *oxidoreductases*, *transferases*, *hydrolases*, *lyases*, *isomerases* or *ligases*. Enzymatic degradation can be carried out either by extracellular enzymes present in the microorganisms' environment or by intracellular enzymes. Both result in chain scission whereby the polymer chains are cleaved into smaller segments. The enzymes may be either exoenzymes, which cleave terminal monomer units sequentially; or endoenzymes (such as *endopeptidases* and *endoesterases*) which cleave internal linkages randomly resulting in a more rapid decrease in molar mass. Under some conditions, microorganisms contribute to degradation of polymers through ingestion, mastication and excretion ⁽⁷⁾.

The enzymes have a wide **diversity** and a remarkable **specificity**, but they are easily denatured by heat, radiations or surfactants ⁽¹⁷⁾. **Constitutive** enzymes are synthesised during all the cellular life, independently of the presence of specific substrates. **Inducible** enzymes are produced when a molecular signal due to the presence of a specific substrate is recognised by the cell. In this case, the enzymes are not synthesised instantaneously but a latent period is necessary to establish the cell machinery. The concentration of inducible enzymes increases as a function of time and stops at substrate exhaustion. When released into the extracellular environment, enzymes can be found as free catalysts (i.e. soluble within aqueous or lipophilic media) or fixed on particles such as soil organic matter, clays or sand. Fixed enzymes are stabilised and their catalytic activity is often increased. The activity of secreted enzymes can continue even if the producer cells are dead.

Biodegradation is fundamentally an **electron transfer process** ⁽¹²⁾. Biological energy is obtained through the oxidation of reduced materials, where the enzymes catalyze the electron transfer. Electrons are removed from organic substrates to capture the energy that is available through the oxidation process. The electrons are moved through respiratory or electron transfer chains (metabolic pathways) composed of a series of compounds to terminal electron acceptors. A large proportion of the microbial population in soil

depends upon oxygen as the terminal electron acceptor for metabolism. Loss of oxygen induces a change in the activity and composition of the soil microbial population. Facultative anaerobic organisms, which can use oxygen when it is present or can switch to alternative electron acceptors, such as nitrates and sulphates, in the absence of oxygen, and obligate anaerobic organisms become dominant when oxygen is not available ⁽¹²⁾, but aerobic biodegradation is typically more efficient.

Enzymatic hydrolysis

The enzymatic hydrolysis is mainly concerned by enzymes that belong to hydrolases. *Cellulases*, *amylases* and *cutinases* are hydrolases readily synthesised by soil microorganisms to hydrolyse natural abundant polymers like cellulose, starch or cutin. Regarding polyesters, *lipases* and *esterases* attack specifically carboxylic linkages.

Enzymatic oxidation

When the scission reactions by specific enzymes are difficult (i.e. crystalline area, hydrophobic zones and steric hindrances), other enzymes are implicated in the transformation of the molecular edifices. For instance, *mono-oxygenases* and *di-oxygenases* (like *oxidoreductases*) incorporate, respectively, one and two oxygen atoms, forming alcohol or peroxy groups that are more easily fragmentable. Other transformations are catalysed by peroxidases leading to smaller molecules. They are *hemoproteins*, enzymes containing a prosthetic group with an iron atom that can be electron donor or acceptor (i.e. reduced or oxidative form). Peroxidases catalyse reactions between a peroxy molecule (e.g. H_2O_2 and organic peroxide) and an electron acceptor group as phenol, phenyl, amino, carboxyl, thiol or aliphatic unsaturation ⁽⁶⁾.

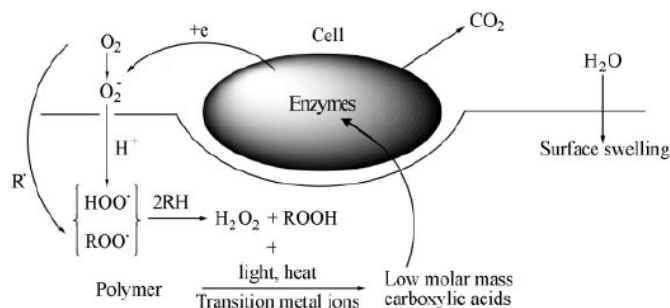


Figure 5. 3. Assimilation of biodegradable plastics, as adapted from Ref. (18)

B. Radicalar oxidation

The addition of a hydroxyl function, the formation of carbonyl or carboxyl groups increases the polarity of the molecule. The increase of the hygroscopic character of the compound favours biological attack. Moreover, some oxidation reactions catalysed by various enzymes produce free radicals conducing to chain reactions that accelerate polymer transformations. However, crystalline structures and highly organised molecular networks are not favourable to the enzymatic attack, since the access to the internal part of these structures is extremely constrictive. Several soil decomposers, particularly fungi, are able to produce H_2O_2 that is an oxidative molecule very reactive allowing the enzymatic biodegradation of cellulose molecules ⁽⁶⁾.

1.2.3. BIOASSIMILATION^{(6) (7)}

The assimilation is the unique event in which there is a real integration of atoms from fragments of polymeric materials inside microbial cells. This integration brings to microorganisms the necessary sources of energy, electrons and elements such as carbon, nitrogen, oxygen, phosphorus, or sulphur, among others, for the formation of the cell structure. Assimilation allows microorganisms to growth and to reproduce while consuming nutrient substrate (that is, polymeric materials) from the environment. Monomers surrounding the microbial cells must go through the cellular membranes to be assimilated. Inside the cells, the transported molecules are oxidised through catabolic pathways conducing to the production of *adenosine triphosphate* (ATP) and constitutive elements of cells structure.

Depending on the microbial abilities to grow in aerobic or anaerobic conditions, there exist three essential catabolic pathways to produce the energy to maintain cellular activity, structure and reproduction:

- **Aerobic respiration:** numerous microorganisms are able to use oxygen as the final electron acceptor. These microorganisms need substrates that are oxidised into the cell. Firstly, basic catabolic pathways (e.g. glycolysis, β -oxidation, aminoacids catabolic reactions, and purine and pyrimidine catabolism) produce a limited quantity of energy. Secondly, more energy is then produced by

the oxidative phosphorylations performed by electron transport systems that reduce oxygen to water ⁽¹⁹⁾.

- **Anaerobic respiration:** several microorganisms are unable to use oxygen as the final electron acceptor. However, they can perform complete oxidation by adapted electron transport in membrane systems. They use final electron acceptors other than oxygen (like NO_3^- , SO_4^{2-} , S, CO_2 , Fe^{3+} or fumarate). The result is also the synthesis of larger quantities of ATP molecules than in an incomplete oxidation.
- **Fermentation:** some microorganisms lack of electron transport systems. They are unsuitable to use oxygen or other exogenous mineral molecules as final electron acceptors. Fermentation, an incomplete oxidation pathway, is their sole possibility to produce energy. Endogenous organic molecules synthesised by the cell itself are used as final electron acceptors. The products of fermentation can be mineral and/or organic molecules excreted into the environment (e.g. CO_2 , ethanol, lactate, acetate and butanediol). Frequently, these molecules can be used as carbon sources by other organisms, since they have still a reduction power.

Generally, mineral molecules released by microorganisms do not represent **ecotoxicity** risk, since they follow the biogeochemical cycles. On the contrary, microbial organic molecules excreted or transformed could present ecotoxic hazards in some conditions and at different levels ⁽⁶⁾.

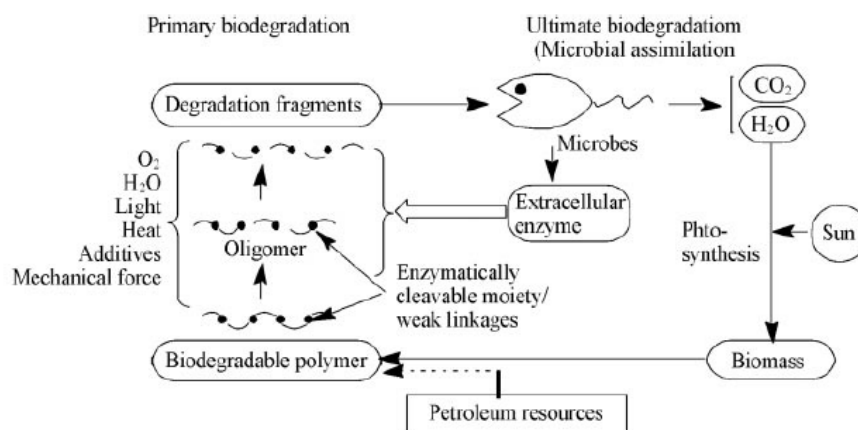


Figure 5. 4. Summary of degradation processes of biodegradable polymers

2. TESTING PROCEDURES FOR ASSESSING BIODEGRADATION

Studies aimed to enhance the suitability and the reproducibility of laboratory methods to assess the biodegradation of Environmentally Degradable Polymers (EDPs) are in continuous progression. This is due to the fact that some operative difficulties can arise during the performance of the tests, thus affecting the accuracy of the measurements as based on the monitoring of suited parameters of choice, as well as the outstanding number of new and structurally different EDP-based materials⁽¹³⁾.

A relatively large number of specific problems might be encountered during the performance of tests designed to assess the extent of biodegradation as CO₂ release or O₂ uptake especially under solid-state conditions and in the presence of organic rich incubation media such as mature compost. On the contrary, the tests carried out in aqueous medium are considered easier to set up and generally more reproducible, but are not significant for burying conditions. In particular, the biodegradation kinetics of a test material under solid state conditions can be influenced by the concentration of the material in the solid medium, as well as by the nature of the microbial populations; whereas the test results might vary significantly depending upon the test duration and the reference (positive) material designed in the standard test specifications⁽¹³⁾.

2.1. ANALYTICAL STRATEGIES

Polymer biodeterioration can be tested by several methods:

- The evaluation of **macroscopic modifications in the materials**, such as roughening of the surface, formation of holes and cracks, changes in colour or development of microorganisms over the surface^{(20) (21) (22) (23)}. There exist normalised tests to estimate the biodeterioration by the colonisation of microorganisms on Petri dishes⁽²⁴⁾. A positive result of the test is considered as an argument indicating the consumption of the polymer by the microbial species.

Notwithstanding, since microorganisms are able to use reserve substances and other molecules as impurities; this result cannot be accepted as an irrefutable conclusion. In this way, different microscopic techniques are used to refine the analysis: photonic microscopy ⁽²⁵⁾, electronic microscopy ⁽²⁶⁾, polarisation microscopy ⁽²⁷⁾, and/or atomic force microscopy ⁽²⁸⁾.

- The **measure of the weight loss** is frequently used for the estimation of biodegradability, but actually the measure of the weight loss of samples even from buried materials is not really representative of a material biodegradability, since this loss of weight can be due to the vanishing of volatile and soluble impurities.
- **Internal biodeterioration** can be evaluated by change of mechanical, rheological or thermal properties ⁽²⁹⁾ ⁽³⁰⁾.
- **Product formation** can also be used as an indicator of biodeterioration. For instance the production of glucose can be followed to assert the degradation of polymeric materials containing cellulose ⁽³¹⁾.

On the other hand, **polymer bioassimilation** is generally estimated by standardised respirometric methods ⁽³²⁾, which mainly consist in measuring the consumption of oxygen or the evolution of carbon dioxide). The decrease of oxygen is detected by the diminution of the pressure and may be fully automated. The experiment can be conducted with oxygen limitation or not. In anaerobic conditions, gases are released and the augmentation of the pressure is then measured. The identification of the evolved gases is realised by GC. This technique is also used to estimate the evolution of carbon dioxide, but in most cases, FTIR is preferred ⁽³³⁾. The quantity of carbon dioxide may be also determined by titration. Carbon dioxide is trapped in an alkaline solution to form a precipitate. The excess of hydroxide is titrated by an acid solution with a colour indicator ⁽³⁴⁾ ⁽³⁵⁾. The durability of degradable plastics before the end of their useful life is of great importance to manufacturers of packaging and agricultural products such as mulching films. Provided the same standard procedures are used to simulate the effects of the

environment on degradable plastics in the pre-biodegradation stage (service life), it must be pointed out that they have no direct relevance to the rate of bioassimilation⁽³⁶⁾.

2.2. STANDARDS FOR THE MEASUREMENT OF BIODEGRADATION

The most common ISO standards used for determining the biodegradation of plastics have set the criteria by which biodegradable plastics are currently assessed:

- **Degradation in soil conditions:** ISO 846: Action of microorganisms⁽³⁷⁾. This norm is used to determine and evaluate the effect of fungi and bacteria on polymeric materials. The ISO 846 test proposes visual examination along with the measurement of mass and physical properties changes. This is the standard followed in this thesis, since it approaches non-controlled disposal conditions.
- **Composting conditions:** ISO 14855: aerobic biodegradation under controlled conditions⁽³⁸⁾⁽³⁹⁾. These norms specify a method for the determination of the ultimate aerobic biodegradability of plastics, based on organic compounds, under controlled composting conditions by measurement of the amount of carbon dioxide evolved and the degree of disintegration of the plastic at the end of the test. This method is designed to simulate typical aerobic composting conditions for the organic fraction of solid mixed municipal waste. The test material is exposed to an inoculum which is derived from compost. The composting takes place in an environment wherein temperature, aeration and humidity are closely monitored and controlled. The test method is designed to yield the percentage of conversion of the carbon in the test material to evolved carbon dioxide as well as the rate of conversion. Also specified is a variant of the method, using a mineral bed (vermiculite) inoculated with thermophilic microorganisms obtained from compost with a specific activation phase, instead of mature compost. This variant is designed to yield the percentage of carbon in the test substance converted to carbon dioxide and the rate of conversion.

A more detailed review of biodegradation laboratory tests, international standards and applications to EDPs is gathered in the papers by *Eubeler et al* ⁽⁴⁰⁾⁽⁴¹⁾.

2.3. STANDARIZATION AND CERTIFICATION

The main critical parameters proposed by the International Standards Organisation (ISO) are either oxygen absorption or carbon dioxide evolution in the presence of microorganisms, as introduced above. The ISO14855 procedure is taken over directly by the European Standards Organisation (CEN) in EN 13432 ⁽⁴²⁾. In this standard, the compostability is assessed by the following criteria, all of which must be satisfied.

- Identification of **packaging constituents**, dry solid content, ignition residues, and hazardous metal residues.
- **Biodegradability**: 90% of the total theoretical CO₂ evolution in compost or simulated compost in six months.
- **Disintegration**: not more than 10% shall fail to pass through a < 2 m⁻³ sieve.
- **Compost quality**: no negative effects on density, total dry solids, volatile solids, salt content, pH, total nitrogen, ammonium nitrogen, phosphorus, magnesium and potassium eco-toxicity effects on two crop plants.

Labelling serves to identify and verify the compostability of a product. The compostable logos are designed to address the confusion that has existed by building credibility and recognition for products that meet the compostability standards among consumers, waste management regulators and others ⁽⁴³⁾. Labelling systems for compostable polymer materials exist in Europe, the USA and Japan.

- **European labelling organizations**: DIN CERTCO (Germany), AIB Vinçotte (Belgium) and Finnish Solid Waste Association, FSWA (Finland)
- **American labelling organizations**: Biodegradable Products Institute/US Composting Council.

- **Asiatic labelling organizations:** Biodegradable Products Institute/US Composting Council

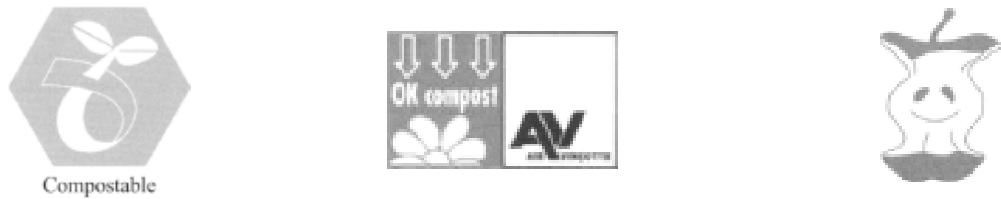


Figure 5. 5. Certified labels of compostability in Europe: (left) DIN CERTCO; (middle) AIB Vinçotte; (right) FSWA



Figure 5. 6. Certified labels of compostability in USA (left) and Japan (right)

The **worldwide cooperation of certification systems** and the mutual recognition of certificates among institutions are of extreme importance. A cooperative network of certification institutions is set (see Table 5.10 in Ref (43)) at a global level to facilitate trade and the application of certified products by mutual recognition of composting methods and legislation.

3. BIODEGRADATION OF PLA

It is known that the biodegradation of PLA proceeds via a **two-stage mechanism**⁽⁴⁴⁾. In the first step, after several months exposure to moisture, random non-enzymatic scission of ester linkage occurs, which can be accelerated by acid or bases and is affected by both temperature and moisture levels⁽⁴⁵⁾. In the primary degradation phase, no microorganisms are involved. Here, the PLA degradability is driven by the hydrolysis and cleavage of the ester linkages in the polymer backbone, which can be auto-catalyzed by the carboxylic acid end groups. In a second stage, as the molar mass diminishes, microorganisms present in the soil can begin to digest the low molecular weight PLA diffused out of the bulk polymer and, producing carbon dioxide and water. This two-stage mechanism of degradation is a distinct advantage of PLA over other biodegradable polymers, which typically degrade by a single-step process involving bacterial attack on the polymer itself. This is a useful attribute, particularly for product storage and in applications requiring food contact. PLA degrades rapidly in the composting atmosphere of high humidity and temperature but at lower temperatures and/or lower humidity, the storage stability of PLA products is considered to be acceptable⁽⁴⁶⁾.

Factors affecting PLA biodegradation

Although the degradation process in PLA is a simple hydrolysis, the degradation rate can be affected, as explained above, by many factors due to the complexity of the solid-liquid reaction system. The polymer degradation rate is mainly determined by polymer reactivity with water and catalysts. The effect of factors which affect the reactivity and the accessibility, such as particle size and shape, temperature, moisture, crystallinity, % isomer, residual lactic acid concentration, molar mass, molar mass distribution, water diffusion and metal impurities from the catalyst, are reported elsewhere (see references given by *Auras et al* in their review⁽⁴⁵⁾).

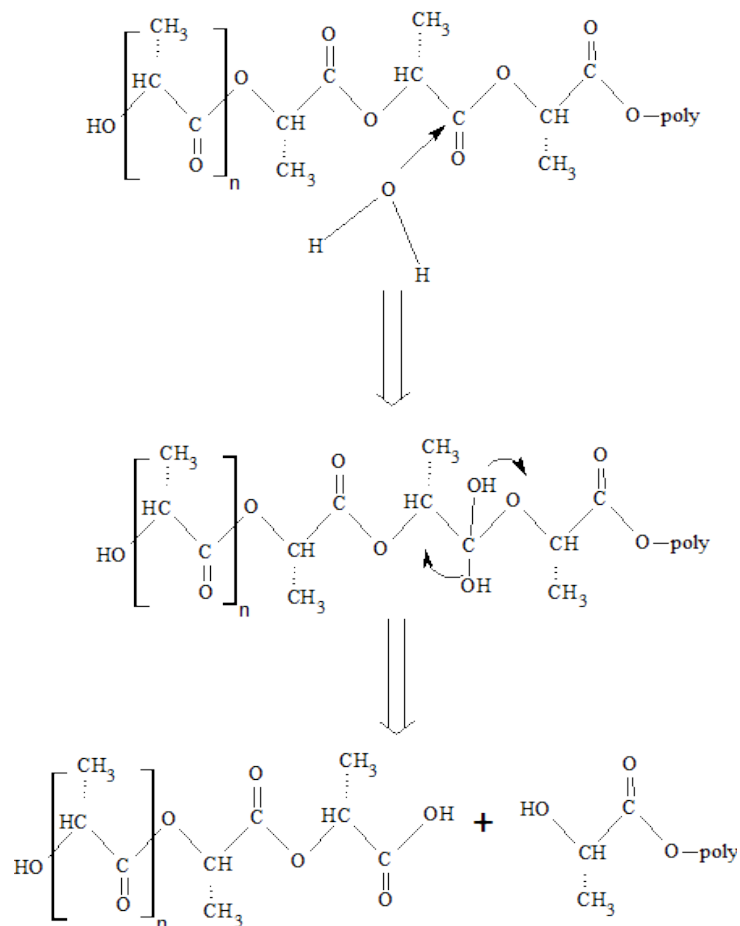


Figure 5. 7. PLA hydrolysis and molecular weight loss

Degradation of PLA in composting facilities

PLA is largely resistant to the attack of microorganisms in soil or sewage under ambient conditions. The polymer must first be hydrolysed at elevated temperatures to reduce the molar mass before biodegradation can be initiated. Thus, PLA will not degrade in typical garden compost in a reasonable time period ⁽⁴⁶⁾.

On the other hand, PLA is fully biodegradable when composted in a large-scale operation with temperatures of 60 °C and above. The studies ⁽⁴⁶⁾ indicate that PLA can be considered as a compostable material, being stable during use at mesophilic temperatures, but degrading rapidly during waste disposal in compost or anaerobic treatment facilities. The first stage of degradation of PLA takes about two weeks, and then the metabolization by microorganisms into carbon dioxide, water and biomass proceeds.

Enzymes such as *proteinase K*, *pronase* and *bromelain* have been used to bring about hydrolysis of polylactide *in vivo*. However, enzymes are large molecules and are unable to diffuse through the crystalline regions. As expected, little enzymatic degradation occurs at the beginning of the degradation process. Enzymatic involvement can produce pores and fragmentation, making more polymer regions accessible to the enzymes⁽⁴⁵⁾.

An extended summary of studies and reports can be found in literature. Further readings are recommended in remarked books^{(2) (46)} and journal reviews^{(45) (47)}.

4. REFERENCES IN THIS CHAPTER

1. Braungart M, McDonough W, Bollinger A, *Cradle-to-cradle design: creating healthy emissions - a strategy for eco-effective product and system design*. Journal of Cleaner Production 15, 1337-1348 (2007)
2. Matsumura S. *Mechanism of biodegradation*. In: Smith R. *Biodegradable polymers for industrial applications*. London : Queen Mary University (2005)
3. Pagga U, Schafer A, Muller R J, Pantke M. *Determination of the aerobic biodegradability of polymeric material in aquatic batch tests*. Chemosphere 42, 319-331 (2001)
4. Rizzarelli P, Puglisi C, Montaudo G. *Soil burial and enzymatic degradation in solution of aliphatic co-polyester*. Polymer Degradation and Stability 85, 855-863 (2004)
5. Wallström S, Strömberg E, Karlsson S. *Microbiological growth testing of polymeric materials: an evaluation of new methods*. Polymer testing 24, 557-563 (2005)
6. Lucas N, Bienaime C, Belloy C, Queneudec M, Silvestre F, Nava-Saucedo J E, *Polymer biodegradation: Mechanisms and estimation techniques – A review*. Chemosphere 73, 429-442 (2008)
7. Kyrikou I, Briassoulis D. *Biodegradation of agricultural plastic films: a critical review*. Journal of Polymers and the Environment 15, 125-150 (2007)
8. Arvanitoyannis I S. *Waste Management in food packaging industries*. Elsevier Inc, (2008)
9. Karakasidis N G. *Recovery raw materials and energy from aseptic paperboards*. Food Drinks 2, 58-62 (1997)
10. Dascalopoulos E, Badr E, Probert S D. *An integrated approach to municipal solid waste management*. Resources Conservation and Recycling 24, 33-50 (1998)
11. Albertsson A C, Karlsson S, *The influence of biotic and abiotic environments on the degradation of polyethylene*. Progress in Polymer Science 15, 177-192 (1990)
12. Stevens E S. *Green Plastics: An introduction to the new science of biodegradable plastics*. Princeton University Press (2002)
13. Krzan A, Hemjinda S, Miertus S, Corti A, Chiellini E. *Standardization and certification in the area of environmentally degradable plastics*. Polymer Degradation and Stability 91, 2819-2833
14. Agamuthu P, Faizura P N. *Biodegradability of degradable plastic waste*, Waste Management and Research 23 , 95–100 (2005)

15. Von-Burkersroda F, Schedl L, Göpferich A *Why degradable polymers undergo surface erosion or bulk erosion*. *Biomaterials* 23, 4221-4231 (2002)
16. Wackett L, Hershberger D C. *Biocatalysis and biodegradation. Microbial transformation of organic compounds*. ASM Press. Washington DC (2001)
17. Garret R H, Grisham C M. *Biochemistry*. Boston : Brooks/Cole C engage learning, (2010)
18. Scott G. *Polymers and the environment*. Royal Society Chemistry (1999)
19. Moussard. *Biochimie Structurale et Métabolique (3ème ed.)*, De Boeck & Larcier, Bruxelles (2006)
20. Lugauskas A, Levinskaite L, Peciulyte D. *Micromycetes as deterioration agents of polymeric materials*, *International Biodeterioration and Biodegradation* 52, 233–242. (2003)
21. Rosa D S, Lotto N T, Lopes D R, Guedes C G F. *The use of roughness for evaluating the biodegradation of poly- β -(hydroxybutyrate) and poly- β -(hydroxybutyrate-co- β -valerate)*, *Polymer Testing* 23, 3–8. (2004)
22. Bikiaris D N, Papageorgiou G Z, Achilias D S. *Synthesis and comparative biodegradability studies of three poly(alkylene succinate)s*, *Polymer Degradation and Stability* 91, 31–43 (2006)
23. Kim H S, Kim H J, Lee J W, Choi I G. *Biodegradability of bio-flour filled biodegradable poly(butylene succinate) bio-composites in natural and compost soil*, *Polymer Degradation and Stability* 91, 1117–1127. (2006)
24. ISO 11266: *Soil quality—guidance on laboratory testing for biodegradation of organic chemicals in soil under aerobic conditions*. (1994)
25. Hakkarainen M, Karlsson S, Albertsson A C. *Rapid (bio)degradation of polylactide by mixed culture of compost microorganisms – low molecular weight products and matrix changes*, *Polymer* 41, 2331–2338 (2000)
26. Marqués-Calvo M S, Cerda-Cuellar M, Kint D R P, Bou J J, Muñoz-Guerra S. *Enzymatic and microbial biodegradability of poly(ethylene terephthalate) copolymers containing nitrated units*, *Polymer Degradation and Stability* 91, 663–671 (2006)
27. Tsuji H, Echizen Y, Nishimura Y. *Photodegradation of biodegradable polyesters: a comprehensive study on poly(l-lactide) and poly(ϵ -caprolactone)*, *Polymer Degradation and Stability* 91, 1128–1137 (2006)
28. Chanprateep S, Shimizu H, Shioya S. *Characterization and enzymatic degradation of microbial copolyester P(3HB-co-3HV)s produced by metabolic reaction model-based system*, *Polymer Degradation and Stability* 91, 2941–295 (2006)

29. Van de Velde K, Kiekens P. *Biopolymers: overview of several properties and consequences on their applications*, Polymer Testing 21, 433–442 (2002)
30. Morancho J M, Ramis X, Fernandez X, Cadenato A, Salla J M, Vallès A, Contat L, Ribes-Greus A. *Calorimetric and thermogravimetric studies of UV-irradiated polypropylene/starch-based materials aged in soil*, Polymer Degradation and Stability 91, 44-51 (2002)
31. Aburto J, Alric I, Thiebaud S, Borredon E, Bikiaris D, Prinós J, Panayiotou C. *Synthesis, characterization, and biodegradability of fatty-acid esters of amylose and starch*, Journal of Applied Polymer Science 74, 1440–1451 (1999)
32. ISO 14852: *Determination of the ultimate aerobic biodegradability of plastic materials in an aqueous medium – method by analysis of evolved carbon dioxide* (1999)
33. Itavaara M, Vikman M. *A simple screening test for studying the biodegradability of insoluble polymers*, Chemosphere 31, 4359–4373 (1995)
34. Calmon A, Duserre-Bresson L, Bellon-Maurel V, Feuilloley P, Silvestre F. *An automated test for measuring polymer biodegradation*, Chemosphere 41, 645–65 (2000)
35. Peltola J S P, Juhanoja J, Salkinoja-Salonen M S. *Biodegradability and waste behaviour of industrial wood-based construction materials*, Journal of Industrial Microbiology and Biotechnology 24, 210-218 (2000)
36. Scott G. *Standards for environmentally biodegradable plastics*. In: Smith R, Biodegradable polymers for industrial applications. Queen Mary University, London, UK (2005)
37. ISO 846: *Plastics -- Evaluation of the action of microorganism*. (1998)
38. ISO 14855-1: *Determination of the ultimate aerobic biodegradability of plastic materials under controlled composting conditions -- Method by analysis of evolved carbon dioxide -- Part 1: General method* (2005)
39. ISO 14855-2: *Determination of the ultimate aerobic biodegradability of plastic materials under controlled composting conditions -- Method by analysis of evolved carbon dioxide -- Part 2 Gravimetric measurement of carbon dioxide evolved in a laboratory-scale test*. (2007)
40. Eubeler J, Zok S, Bernhard M, Knepper T P. *Environmental biodegradation of synthetic polymers - I. Tests methodologies and procedures*. Trends in Analytical Chemistry 28, 1057-1072 (2009)
41. Eubeler J, Zok S, Bernhard M, Knepper T P. *Environmental biodegradation of synthetic polymers II. Biodegradation of different polymer groups*. Trends in Analytical Chemistry 29, 84-100 (2010)

42. EN 13432: *Requirements of packaging recoverable through composting and biodegradation-Test scheme and evaluation criteria for the final acceptance of packaging*. (2000)
43. Rudnik E. *Composting methods and legislation*. In: Rudnik E. *Compostable polymer materials*. Elsevier Ltd (2007)
44. Lunt J. *Large-scale production, properties and commercial applications of polylactic acid polymers*. *Polymer Degradation and Stability* 59, 145-152 (1998)
45. Auras R, Harte B, Selke S. *An overview of polylactides as packaging materials*. *Macromolecular Bioscience* 4, 835-864 (2004)
46. Rudnik E. *Biodegradability testing of compostable polymer*. In: Rudnik E. *Compostable polymer materials*. Elsevier Ltd (2007)
47. Kale G, Kijchavengkul T, Auras R, Rubino M, Selke S E, Singh S P, *Compostability of bioplastic packaging materials: an overview*. *Macromolecular bioscience* 7, 255-277 (2007)

5. CONTRIBUTIONS IN THIS THESIS

It has been shown that PLA is mainly biodegraded in composting conditions, when temperatures are fairly above the glass transition and high humidity grades. Both factors can favour the hydrolysis of the macromolecular chains. On the other hand, to obtain noticeable results in the case of biodegradation after burial in soil, long times of exposure are necessary, and thus few reports are published. In this thesis, with the aim of simulating the behaviour of PLA packaging goods under non-controlled disposal, the samples were buried during 450 days at 28 °C in order to induce a low rate of degradation.

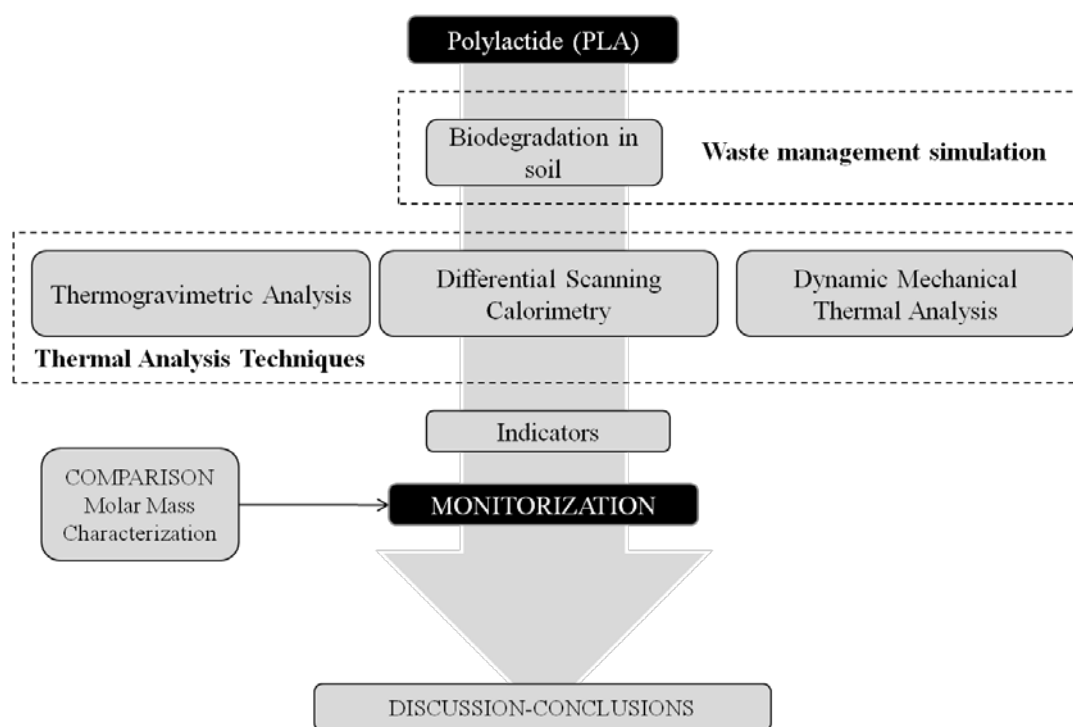


Figure 5. 8. Diagram of contributions in the field of biological valorisation of PLA

In addition, common measurements of biodegradation mainly involved the use of respirometric techniques, capable of identifying gases such as O₂ and CO₂, which may be interpreted as a way to test the biodegradation on the environment. However, the studies of the effects of biodegradation on the polymers themselves are reported with less frequency, and mainly tested on films. In this thesis, thicker plates (1 mm) were used. As

well, the measurement of the mechanical and thermal properties was proposed for the monitoring of biodegradation on the sample. Particularly, the use of Thermal Analysis techniques (namely, Differential Scanning Calorimetry DSC, Dynamical-Mechanical Thermal Analysis DMTA and Thermogravimetric Analysis TGA) was stressed as suitable analytical strategies to monitor the changes induced by the polymer even at low degradation rates.

The results of the study were reported in two contributions, as follows:

CONTRIBUTION V-A: L. Santonja-Blasco, Rosana Moriana, J.D. Badia, A. Ribes-Greus. Thermal analysis applied to the characterization of degradation in soil of polylactide: I. Calorimetric and viscoelastic analyses. *Polymer Degradation and Stability* 2010, 95; 2185-2191.

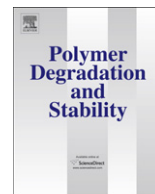
CONTRIBUTION V-B: J.D. Badia, L. Santonja-Blasco, Rosana Moriana, A. Ribes-Greus. Thermal analysis applied to the characterization of degradation in soil of polylactide: II. On the thermal stability and thermal decomposition kinetics. *Polymer Degradation and Stability* 2010, 95; 2192-2199.

CONTRIBUTION V-A

Thermal analysis applied to the characterization of degradation in soil of
polylactide: I. Calorimetric and viscoelastic analyses

L. Santonja-Blasco, Rosana Moriana, J.D. Badia, A. Ribes-Greus

Polymer Degradation and Stability 2010, 95; 2185-2191



Thermal analysis applied to the characterization of degradation in soil of polylactide: I. Calorimetric and viscoelastic analyses

L. Santonja-Blasco, Rosana Moriana, J.D. Badía, A. Ribes-Greus*

Instituto de Investigación en Tecnología de Materiales, Universidad Politécnica de Valencia, Camino de Vera s/n 46071 Valencia, Spain

ARTICLE INFO

Article history:

Received 30 November 2009
Received in revised form
26 July 2010
Accepted 6 August 2010
Available online 14 August 2010

Keywords:

Poly(lactide) (PLA)
Degradation in soil
Differential Scanning Calorimetry (DSC)
Dynamic-Mechanical-Thermal Analysis (DMTA)
Free volume
Lamellar thickness distribution

ABSTRACT

An accelerated soil burial test has been performed on a commercial polylactide (PLA) for simulating non-controlled disposal. Degradation in soil promotes physical and chemical changes in polylactide properties, which can be characterized by Thermal Analysis techniques. Physical changes occurred in polylactide due to the degradation in soil were evaluated by correlating their calorimetric and viscoelastic properties. It is highly remarkable that each calorimetric scan offers specific and enlightening information. Degradation in soil affects the polylactide chains reorganization. A multimodal melting behavior is observed for buried PLA, degradation in soil also promotes the enlarging the lamellar thickness distribution of the population with bigger average size. Morphological changes due to degradation in soil lead to an increase in the free volume of the polylactide chains in the amorphous phase that highly affected the bulk properties. Thermal Analysis techniques provide reliable indicators of the degradation stage of polylactide induced by degradation in soil, as corroborated by molecular weight analysis.

© 2010 Elsevier Ltd. All rights reserved.

1. Introduction

Poly(lactide) (PLA) is an aliphatic, biodegradable, and compostable polyester which can be easily processed with standard equipment to yield articles that can be used in many applications such as in industrial packaging, in the building area, in medical, agriculture and textile field, etc [1–3]. Initially, polylactide products were produced for biomedical purposes and thus their hydrolysis processes captured the whole research attention [4,5]. Studies performed in neutral media such as phosphate-buffered solution, in vivo solution and water, have been extensively analyzed in order to determine the hydrolytic degradation mechanism [6–10]. Nowadays PLA stands out as a reliable alternative to commodities in packaging applications. This solution will therefore imply an increase of a new source of plastic waste. Hence, to correctly manage the PLA disposal, its biodegradability performance has been studied in several environmental conditions, such as composting, microbiological cultures, biological degradation and disposal in soil [11–14].

Extensive work has been performed by several researchers for understanding the degradation in soil of polymers. Former PLA

biodegradation studies stated that hydrolytic reactions seem to act in the initial stage of the overall PLA biodegradation, proceeding by chain-end scission in the PLA matrix, which eases the successive biotic assimilation [11,15–17]. A biotic environment implies chain scissions and the physical and chemical properties of the polymer can be severely modified. Thus, the common characterization is mainly carried out by means of the measurement of the molecular weight or the weight loss changes. Ho et al. found that about 20% of a PLA film was mineralised to CO₂ after 182 days in a laboratory respirometer charged with soil at 28 °C [18]. Calmon et al. found that PLA films had weight losses varying from 0 to 100% after burial in soil for 24 months depending on PLA type and location [19]; in contrast Urayama et al. only found a decrease of a 20% in molecular weight of PLA (100% L) plates after 20 months in soil [14]. In addition, it has been suggested that traditional techniques as the measurement of the weight loss changes for studying polymer biodegradation have some limitations especially after 3 months, because of the adhesion of soil and fungi to the polymer, which can mask real results and thus induce misleading information [14,20,21]. Fast, cost-effective and reliable characterization procedures for testing the biodegradation effects on polymers should be developed and implemented. Thermal Analysis techniques have been successfully applied in our research group to monitor and control the degradation effects on the macroscopic properties of polymers submitted to different degradative environments since

* Corresponding author. Fax: +34963879817.

E-mail address: aribes@ter.upv.es (A. Ribes-Greus).

they offer a huge amount of parameters that can act as indicators of the extent of degradation [22–26]. Fig. 1 summarizes the Thermal Analysis techniques proposed for the study of the extent of degradation on PLA: Thermogravimetry (TGA), Differential Scanning Calorimetry (DSC) and Dynamic-Mechanical-Thermal Analysis (DMTA), as well as the principal parameters selected for the study. The first paper is focused on the DSC and DMTA study, whereas a forthcoming second paper will report on TGA data.

The aim of this work is to simulate the degradation in the environmental conditions that PLA is subjected during non-controlled disposal. In this set of papers, the physical changes occurred to polylactide properties throughout the degradation in soil process are analyzed by Thermal Analysis, making efforts on establishing new insights in studying the degradation in soil process on polymers. The study is complemented with the analysis of the evolution of the average molecular weight in number and weight by Gel Permeation Chromatography, aiming to test the reliability and consistency of the techniques proposed in the assessment of degradation in soil effects on PLA.

2. Experimental section

2.1. Material and sample preparation

A commercial polylactide (PLA), obtained from renewable resources by ring opening polymerization supplied by Natureworks (Minnetonka, USA) was used in this study. This PLA is a commercial resin with 3.8% meso-lactide and with a number-average molecular weight of 102.230 g/mol, as measured by Gel Permeation Chromatography.

PLA pellets were previously dried with demineralized air at 80 °C during 4 h. Rectangular plates were prepared by melt compression in a Collin PCS-GA Type Press 800 (GA, USA) at an initial temperature of the hot plates of 195 °C and a final temperature of 60 °C. Five pressure steps were performed as follows starting with an 5 min at 6 bar, 8 min at 75 bar, 8 min at 155 bar, 4 min at 215 bar, and 11 min at 45 bar. Specimens of 145 × 10 × 2 mm were cut from the melt-pressed plates for the degradation in soil tests. Since this work approaches the degradation in soil of non-controlled landfilling of consumer goods, which are obtained by means of, at least, one processing step, “non-buried PLA” has been considered the reference material of the study.

2.2. Accelerated soil burial test

PLA plates were subjected to a controlled degradation in soil test under controlled conditions (temperature, water content and pH), following the ISO 846-1997 International Norm, method D [27]. Samples were buried in biologically active soil and kept in a Heraeus B12 (Hanau, Germany) culture oven at 28 °C. The soil used in these tests was a red soil extract taken from a culture field in Alginet (Valencia). Microbial activity of soil was monitored with cotton along the extension of the experiment. The soil was maintained at approximately pH 7 and a relative humidity of 0.87 g water/g wet soil. To ensure the oxygenation of the soil, a protocol of periodical air oxygen supply was followed. Test specimens were extracted at 30, 150, 300 and 450 days, cleaned and kept in a desiccator during 4 days in order to ensure water desorption before being analyzed.

2.3. Analytic procedures

Samples were thermally characterized by means of Differential Scanning Calorimetry (Mettler Toledo DSC822, Columbus, OH, USA). The calibration of the DSC was previously checked by In and Zn standards. Three calorimetric scans were performed to each sample at a heating/cooling rate of 10 °C/min. Samples of around 4 mg were introduced in a pierced aluminium crucible, with capacity for 40 µL. The first heating scan, in which the thermal history is suppressed, was performed from 0 to 200 °C; the cooling scan went from 200 °C to 0° and the third heating scan from 0 to 200 °C. All experiments were performed under N₂ dry gas as protective gas (50 ml/min) to avoid the water condensation in the equipment and purged with N₂ (200 ml/min) in the furnace.

The mechanical and viscoelastic properties were assessed by means of a Rheometric Scientifics Dynamic-Mechanical-Thermal Analyser Mark IV (USA). The deformation force was set at 0.01 N. The displacement was checked before each experiment. Experiments were performed by using dual cantilever clamping in bending mode. Specimens of 40 × 10 × 2 mm were heated from 35 to 150 °C in iso-step mode every 2 °C in the frequency (*f*) range from 0.1 to 39 Hz measuring 5 points per decade.

In order to correlate the results obtained by Thermal Analysis with the molecular weight changes, the number and weight average molecular weights (\bar{M}_n and \bar{M}_w respectively) of the

		THERMAL ANALYSIS			
		Technique	Experiment	Direct observation	Further data analysis
ANALYSIS OF CHEMICAL AND PHYSICAL PROPERTIES	1 st Paper	Differential Scanning Calorimetry (DSC)	Heating/ Cooling/ Heating	→ Glass transition temperature → Crystallization temperatures and enthalpies → Melting temperatures and enthalpies → Crystallinity degree	→ Structural relaxation / physical ageing → Lamellar thickness distribution → Multi-modal melting behaviour characterisation
		Dynamical-Mechanical Thermal Analysis (DMTA)	Multi-frequency	→ Storage and Loss Moduli → Loss tangent	→ Activation energies of relaxations → Free-volume ratio (thermal expansion coefficient)
	2 nd Paper	Thermogravimetry (TGA)	Non-isothermal analysis Multi-heating rates	→ Decomposition temperatures (thermal stability) → Percentage of mass loss and residue	→ Safety decomposition temperatures → Activation energies evolution → Kinetic models

Fig. 1. Summary of parameters used to assess the extent of degradation in soil on polylactide.

samples were evaluated in tetrahydrofuran (THF) at 25 °C by means of a GPC Agilent 1100 Series, using a PL Gel 5 μm 104 Å column, of 300 \times 7.5 mm, from Polymer Laboratories.

3. Results and discussion

The extent of biodegradation of polylactide (PLA) has been deeply characterized by means of Differential Scanning Calorimetry (DSC) and Dynamic-Mechanical-Thermal Analysis (DMTA) experiments. A parallel DSC/DMTA results interpretation along the study will thus provide specific indicators to monitor the extent of degradation, by understanding the role of both amorphous and crystalline fractions of PLA. Furthermore, these results have been associated with the average molecular weight evolution in order to validate the suitability of Thermal Analysis techniques for monitoring degradation in soil on PLA.

Fig. 2a and b show the calorimetric thermogram and the mechanical relaxation spectrum of non-buried PLA, respectively. In the Fig. 2a, the three calorimetric (heating, cooling, and second heating) scans are plotted. From the first heating scan, the degradation in soil effect on PLA was assessed, since it represents the current status of the buried polymer and because the second cooling scan does not offer information. The following transitions are observed along the increasing temperature-axis: glass transition (between 40 °C and 75 °C), cold crystallization (between 90 °C and 140 °C) and melting process (between 140 °C and 160 °C). From each calorimetric transition, sensitive indicators were studied to evaluate degradation. The cooling DSC scan only shows the glass transition and the second DSC heating scan shows the glass transition, overlapped with the structural relaxation. In the second heating scan, the PLA amorphous phase does not crystallize at 10 °C/min.

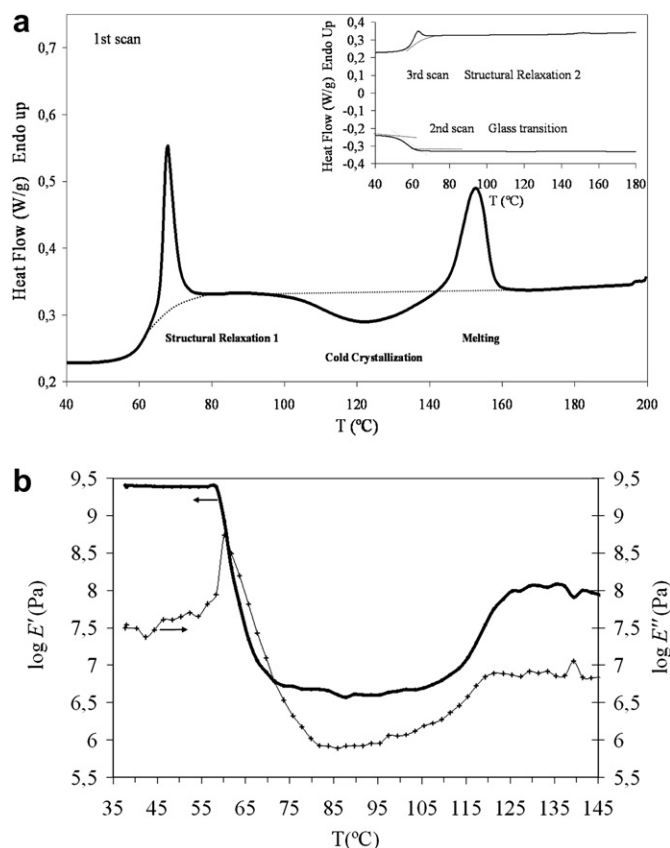


Fig. 2. Calorimetric and viscoelastic behavior of non-buried polylactide (a) calorimetric thermogram and (b) $\log(E')$ and $\log(E'')$ versus temperature.

In the Fig. 2b the storage (E') and loss (E'') moduli versus temperature at the commonly used frequency of 1 Hz are plotted. Similar curves are obtained for all the other frequencies between 0.1 and 39 Hz, but are not displayed for the sake of clarity. The mechanical relaxation spectra show different relaxation zones which can be assigned to the calorimetric transitions along the increasing temperature-axis: glass/rubber transition (55–75 °C), rubbery plateau (75–90 °C), crystallization (90–140 °C).

Fig. 3 shows the effect of degradation in soil on the first DSC heating scan. The effect of the degradation in soil is basically appreciate in the changes on the crystallization transition and consequently in the melting. The degradation in soil modifies the storage and loss moduli spectra as can be seen at Fig. 4a and b, respectively. Taking into account that the first calorimetric thermogram (first DSC scan) and the mechanical relaxation spectrum (DMTA scan) are directly related; the discussion of the results is focused in the three important transitions observed in the first calorimetric thermogram and the corresponding mechanical relaxation spectrum.

3.1. Glass transition assessment

The study of the glass transition region from the calorimetric and the mechanical techniques enables analyzing the effect of degradation on the amorphous molecular chains. At the first calorimetric scan (Fig. 2) an endothermic phenomenon, the structural relaxation, overlapped to the glass transition relaxation, is observed

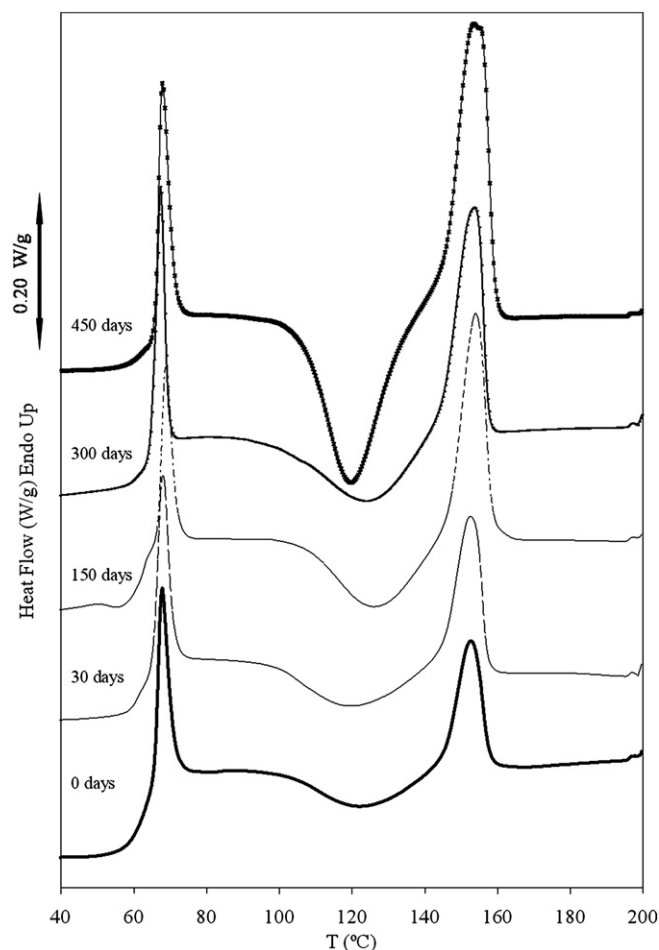


Fig. 3. Comparative first scan of the calorimetric thermograms at different degradation times.

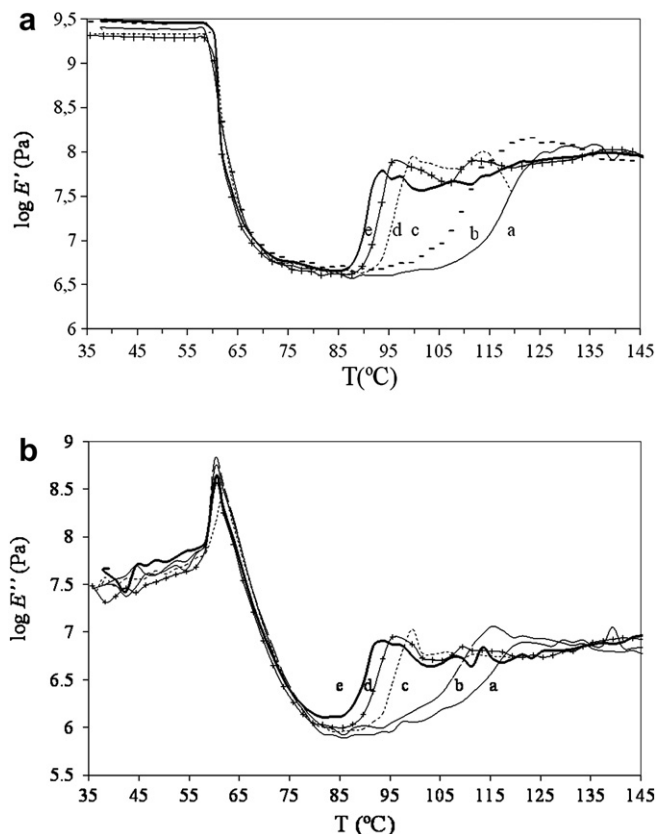


Fig. 4. (a) Effect of degradation in soil on $\log E'$ vs. temperature. (b) Effect of degradation in soil of polylactide on $\log E''$ vs. temperature. (a. 0 days; b. 30 days; c. 150 days; d. 300 days; e. 450 days).

at 61 °C. In order to assess this phenomenon, the relative structural relaxation enthalpy (ΔH_R) is proposed as indicator. The enthalpies were calculated by the specific area (J/g) of the consequent endotherm using a spline baseline. The relative structural relaxation enthalpy (ΔH_R) is obtained by the subtraction of the structural relaxation enthalpy of the first scan (ΔH_{R1}) to the one related obtained in the second heating scan (ΔH_{R3}). It is provided in relative terms with regards to the non-buried sample (sample "o") to study the "i" times of degradation in soil $\Delta H_{Ri} = (\Delta H_{R1i} - \Delta H_{R3i}) / (\Delta H_{R1o} - \Delta H_{R3o})$. Table 1 shows the changes of ΔH_R . It can be seen that when the soil burial test advances, there is an increasing tendency of this indicator reaching a 70% increase at 450 days.

The glass transition temperature (T_g) is obtained from the second heating DSC scan in which this is the only phenomenon shown, due to the applied cooling rate does not allow crystallization. The T_g is calculated as the temperature at the inflection point of the phenomenon, and for non-buried PLA it is located around 56 °C.

The glass-rubber relaxation of PLA appears in DMTA as a drop of E' to very low values. The peak temperature (T_{max}) taken from the

Table 1
Calorimetric and viscoelastic parameters related to the glass transition relaxation.

Time in soil (days)	DSC			DMTA
	T_g (°C)	ΔH_{R1} (J/g) - ΔH_{R3} (J/g)	ΔH_R (J/g)	T_{max} (°C)
0	56.5 ± 1.0	4.3 ± 0.1	1.0 ± 0.02	60.9 ± 0.5
30	56.1 ± 0.8	4.7 ± 0.1	1.1 ± 0.02	60.9 ± 0.3
150	56.7 ± 1.0	5.2 ± 0.2	1.2 ± 0.04	62.0 ± 0.7
300	55.7 ± 0.7	6.0 ± 0.3	1.4 ± 0.07	60.7 ± 0.2
450	55.9 ± 0.6	7.3 ± 0.3	1.7 ± 0.04	60.8 ± 0.7

maximum of E'' related to the glass transition gives a value of approx. 60 °C at the frequency of 1 Hz. As was expected, the temperature related to the glass-rubber relaxation is higher than the calorimetric glass transition temperature.

The values of T_g and T_{max} obtained for PLA submitted to degradation in soil are shown at Table 1. These parameters do not offer significant changes with burial, because are sensitive to large-scale morphological changes. With the aim of assessing the morphological rearrangements of PLA amorphous chains, a closer inspection has been carried out.

The calculation of the Arrhenius maps has thus been performed (Fig. 5) in order to predict the influence of the degradation in soil on the viscoelastic performance of PLA. As expected, the relationship of $\ln(f)$ and T_{max}^{-1} can be fitted to the Vogel-Fulcher-Tamman-Hesse (VFTH) equation (1) for obtaining the thermal expansion coefficient [28]:

$$\ln f = A - m_v \cdot \frac{1}{T_{max} - T_\infty} \quad (1)$$

where f represent the selected frequencies in Hz, T_{max} in K, is the temperature obtained at the maximum value of E'' , $m_v = B/\alpha_f$, being α_f the thermal expansion coefficient and $B \cong 1$, T_∞ , is the temperature at which the free volume would be zero and A is a pre-exponential factor. The thermal expansion coefficient trend during the degradation in soil for all samples is shown in Fig. 6. The thermal expansion coefficient presents an increasing tendency when degradation time becomes longer. The increase is more noticeable from 300 days on.

Therefore, the free volume existing among the amorphous chains is higher as the extent of degradation rises up. This may be a direct consequence of chain cleavages in the amorphous phase, caused by degradation in soil agents (water and microorganisms) on the PLA matrix. Specifically in the presence of water it has been found to proceed through two alternative mechanisms: surface or heterogeneous, and bulky or homogeneous erosion [29]. The free volume of the studied PLA arises with degradation in soil strengthening the suggestion of easy molecular motions as degradation in soil advances.

3.2. Cold-crystallization evaluation

When the glass transition relaxation is overcome other phenomenon very significant presented by PLA is the cold crystallization. In the first heating DSC scan, the cold crystallization is observed in an onset (T_{on}) around 85 °C (Fig. 2 and Table 2), since the chains which were constrained have the condition to freely

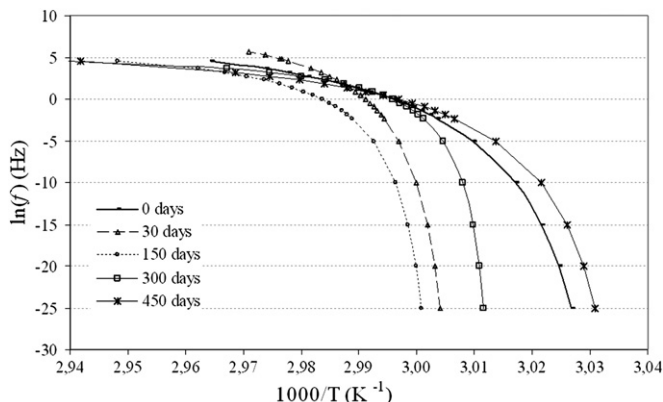


Fig. 5. Arrhenius Maps obtained from multi-frequency DMTA analysis.

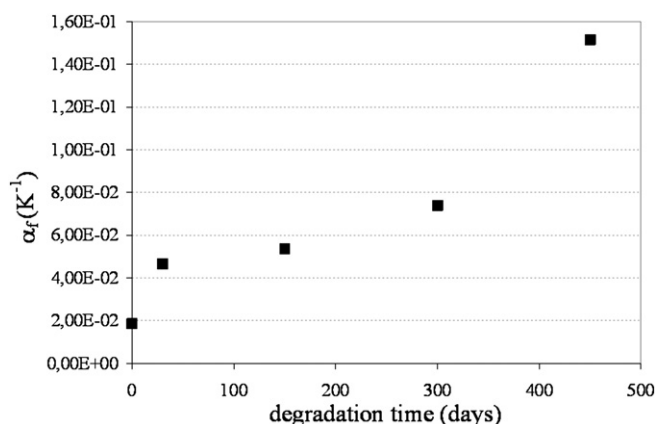


Fig. 6. Thermal expansion coefficient vs. degradation time.

crystallize and at around 123 °C the exothermic peak (T_c) is situated. The mechanical relaxation spectrum shows that the storage modulus increases again after the glass transition, at a determined temperature named onset crystallization temperature (T_0), around 85 °C (Fig. 4 and Table 2), which is in good agreement with the DSC results. The endset temperature (T_e) of the crystallization phenomenon is taken as the temperature reached when the increase in both viscoelastic modulus achieve a second plateau, being for the non-buried sample around 125 °C. This increase in the storage modulus indicates an increase of the rigidity of the material. The slow heating rate enhances the crystallization process during the DMTA measurement and the development of spherulites as other authors have confirmed using Thermal Optical Analysis and X-Ray Diffraction methods [30].

Significant changes due to the degradation in soil are observed by both techniques. The principal parameters evaluated for the analysis of the cold crystallization are listed in Table 2. Degradation in soil principally modifies the magnitude of the cold crystallization exotherm (ΔH_c), especially from 300 days of burying in soil on. The increase of this parameter indicates the presence of more polymeric chains involved in the crystallization process as the degradation time is higher, thus strengthening the hypothesis of morphological changes previously drawn from the glass transition assessment.

Changes are also observed in the mechanical spectra; the rubbery plateau is narrower as samples are more degraded, since the crystallization ends at lower temperatures. These results may suggest that the effect of degradation in soil on the amorphous regions is forming shorter chains that easily rearrange in spherulites, since the mobility is enhanced by the availability of more free volume.

3.3. Melting characterization

The study of the PLA melting process allows the determination of new parameters that will reinforce the knowledge of the

Table 2
Calorimetric and viscoelastic parameters related to the cold crystallization.

Cold Crystallization					
Time in soil (days)	DSC		DMTA		
	T_{0n} (°C)	T_c (°C)	$\log E'$ (Pa)	T_0 (°C)	T_e (°C)
0	84.9 ± 1.5	123.0 ± 1.0	7.9 ± 0.2	85.5 ± 1.0	125.3 ± 1.0
30	84.3 ± 1.0	119.0 ± 1.3	7.8 ± 0.3	85.1 ± 1.0	125.4 ± 1.4
150	86.6 ± 1.8	125.2 ± 1.6	7.9 ± 0.2	85.0 ± 0.8	99.5 ± 1.0
300	84.3 ± 1.6	123.2 ± 1.1	7.8 ± 0.3	85.1 ± 0.9	95.6 ± 0.6
450	89.9 ± 1.3	119.7 ± 1.2	7.7 ± 0.1	85.0 ± 0.7	93.6 ± 1.2

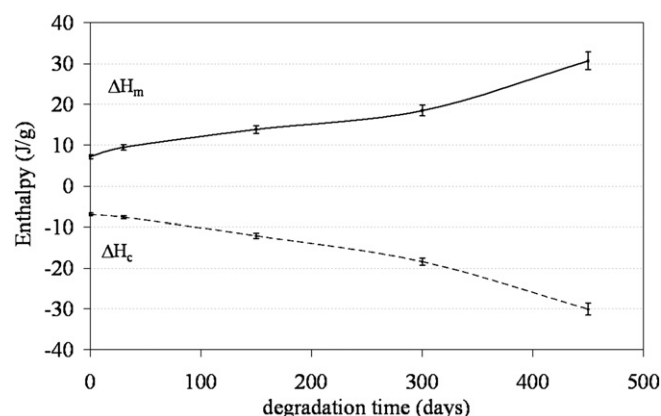


Fig. 7. Crystallization and melting enthalpies vs. degradation time.

degradation in soil effects on PLA morphology and thermal properties. The melting process of non-buried PLA has been analyzed by the deconvolution of the melting endotherms that represent two different crystalline distributions. The lowest melting temperature peak, corresponding to the population with lower size (peak 1) is located at 151 °C and the highest, corresponding to crystalline conformations with larger size (peak 2), appears at 155 °C, (T_{m1}) and (T_{m2}) respectively. Fig. 7 represents the evolution of both melting (ΔH_m) and cold crystallization (ΔH_c) enthalpies along the degradation test. It is obtained that the melting enthalpy slightly differs from the immediately previous cold-crystallization enthalpy regardless the time of the experiment, confirming that PLA is initially amorphous. Higher degradation time leads to equally increase both enthalpies: as can be seen, the initially melting enthalpy was around 7 J/g and at 300 days it reached 18 J/g but it is up to this time when the increase is more significant, achieving at 450 days, 30 J/g.

Nonetheless, it has been considered interesting to perform an accurate study of the morphology of the coldly obtained crystallites. Hence, from the obtained results of the melting process during the first scan, the lamellar thickness distribution " l_c " in Åströngs ($1 \text{ \AA} = 10^{-10} \text{ m}$) of the newly grown crystallites was calculated by means of Thompson equation.

$$l_c = \frac{2 \cdot \sigma_e}{\Delta h_m^\infty \left(1 - \frac{T}{T_m^0}\right)} \quad (2)$$

where: T = observed melting temperature (K), T_m^0 = equilibrium melting temperature (K), σ_e = free surface energy of the basal plane (J m^{-2}) and Δh_m^∞ = melting enthalpy per volume unit for a crystalline phase (J m^{-3}). For PLA the values used for calculating the lamellar thickness are, $T_m^0 = 480 \text{ K}$, $\sigma_e = 60.89 \cdot 10^{-3} \text{ J m}^{-2}$, and $\Delta h_m^\infty = 111.083 \times 10^8 \text{ J m}^{-3}$ [31]. According to the Thompson equation, Eder assumes that at a given temperature for a sample of molten polymer, the rate of heat consumption is proportional to the fraction of lamellar which thickness is l_c [32]. The plot has been done subtracting the baseline of the endotherm and normalized to the maximum value of the enthalpy. For the non-buried material, l_c relays between 75 and 115 Å. The influence of degradation in soil on the lamellar thickness of the crystallites is shown at Fig. 8. The plots slightly shift to higher l_c values with longer degradation in soil, showing the continuous formation of crystalline zones with higher lamellar size. The lamellar thickness distribution is splitting into two different shoulders. A multimodal endothermic behavior, attributed to segregation into two main populations can be observed. A deconvolution procedure was applied to the melting thermograms in order to individually characterize the behavior of each population and their contribution to the overall effect using

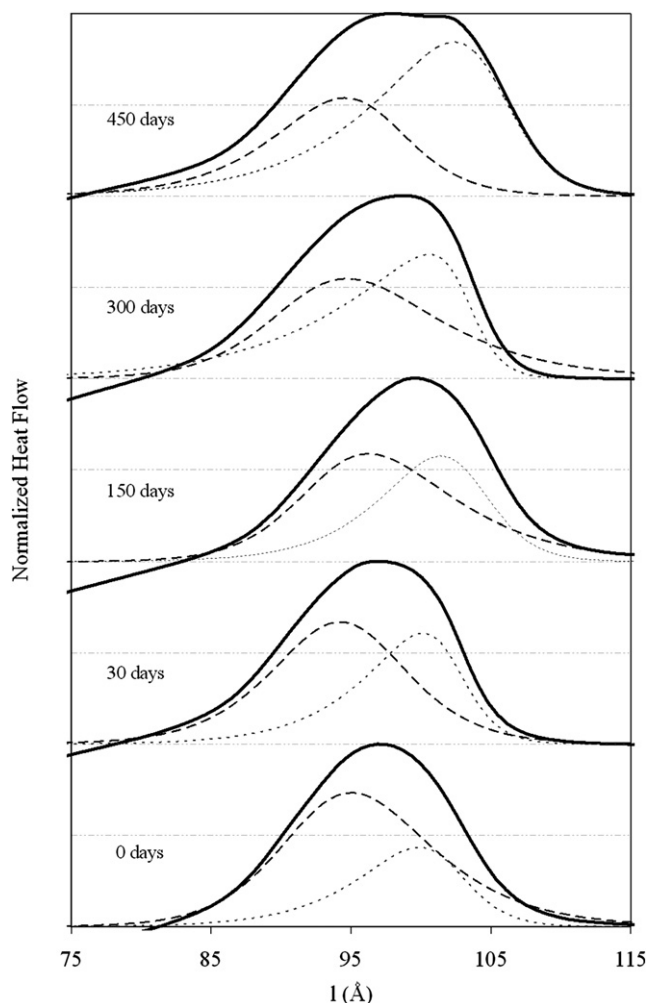


Fig. 8. Influence of degradation in soil on the lamellar thickness distribution of polylactide. (—) overall endotherm, (---) 1st deconvoluted lamellar thickness distribution with lower crystalline sizes and (···) 2nd deconvoluted lamellar thickness distribution with higher crystalline sizes.

a partial areas study [33]. The following expression was employed as deconvolution.

$$y_i = y_0 + A \cdot \left(\frac{1}{1 + \exp\left(\frac{-(x-x_c+w_1/z)}{w_2}\right)} \right) \cdot \left(1 - \frac{1}{1 + \exp\left(\frac{-(x-x_c+w_1/z)}{w_3}\right)} \right) \quad (3)$$

where y_i is the normalized heat flow for each deconvoluted curve, x are the l_c values, x_c is a position parameter related to maximum value of the curve ($l_{c \max}$), A is an amplification parameter and w_1 , w_2 , w_3 describe the dispersion and symmetry of the curve.

Table 3
Calorimetric parameters related to the melting transition.

Melting parameters						
Time in soil (days)	T_{m1} (°C)	$l_{c \max 1}$ (Å)	$Area_1$ (% $Area_{total}$)	T_{m2} (°C)	$l_{c \max 2}$ (Å)	$Area_2$ (% $Area_{total}$)
0	151.6 ± 2.0	93.7 ± 1.2	61	154.9 ± 2.0	101.3 ± 1.4	39
30	151.7 ± 1.8	94.5 ± 0.8	56	155.1 ± 1.4	101.6 ± 1.2	44
150	151.8 ± 1.6	94.4 ± 1.0	49	155.6 ± 1.7	102.7 ± 1.1	51
300	151.4 ± 1.2	92.8 ± 1.2	46	154.9 ± 2.0	102.6 ± 0.8	54
450	151.8 ± 1.3	95.9 ± 0.8	37	156.9 ± 1.3	104.5 ± 0.9	63

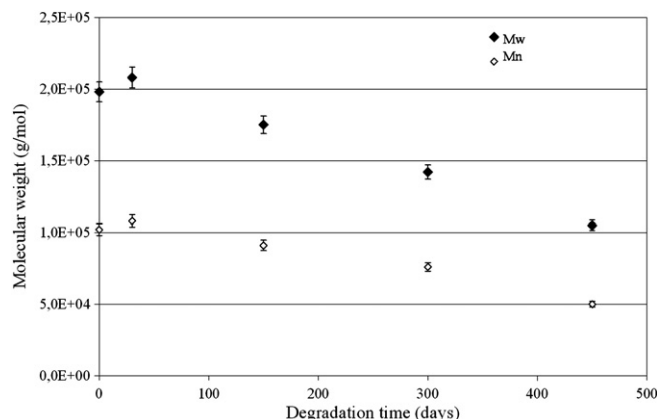


Fig. 9. \bar{M}_n and \bar{M}_w evolution calculated by GPC.

The curve of the normalized heat flow is expressed as $y = y_0 + \sum_{i=1}^n y_i$ where y_0 is the y value of the baseline of the curve and n is the number of deconvoluted curves. Deconvoluted peak temperatures, as well as the lamellar thickness at the maximum of both populations are gathered at Table 3. As can be seen, T_{m1} remains almost constant and T_{m2} slightly increases with degradation. The integration of the individual curves have been calculated from $l_c = 75$ to 115 Å (Fig. 8) and the values obtained are named $Area_1$ and $Area_2$, corresponding to the curves with a maximum in T_{m1} and T_{m2} respectively. The values are expressed in % percentage respect the total integration value ($Area_{total}$) and are listed at Table 3, indicating that degradation in soil promotes the growing of the lamellar distribution with higher crystalline sizes. These results indicate that as a consequence of the degradation, the heterogeneity of this material increase. Both techniques indicate that the crystallization process as an important indicator of the samples degradation.

Summing up, the increase of the relative structural relaxation enthalpy and the thermal expansion coefficient manifest the chain cleavages induced by degradation in soil of PLA. The increased free volume between the molecular chains that form the amorphous phase allows a major mobility of the free chains. The apparition of shorter chains is monitored by the continuous increase in the cold-crystallization enthalpy, especially after 300 days of burying. The raise of crystallization is confirmed by the increase of the relative area of the melting endotherm related to the coldly-formed crystalline population with higher lamellar thickness.

Results provided by Thermal Analysis have been correlated with the obtained by directly measuring the molecular weight. Fig. 9 shows the behavior of average molecular weight in number and weight (\bar{M}_n and \bar{M}_w , respectively) as a function of the days in soil. A slight increase in the molecular weight after 30 days due to the rearrangements that PLA underwent in contact with water and soil is shown [34]. The molecular weight continuously decreases from 30 days on and it specially drops after 300 days, reaching a 50% decrease of the initial molecular weight of PLA at 450 days.

The correlation of Thermal Analysis assessment with the molecular weight characterization has been therefore shown to be complementary and interesting, since the stage of degradation can be effectively examined by both types of analysis. DSC and DMTA techniques are very sensitive to study the molecular rearrangements occurring before large-scale degradation processes, and therefore capable of explaining the morphological changes induced during degradation in soil. Likewise, Thermal Analysis techniques have effectively monitored the effects of burial when the molecular weight experiences a remarkable decrease, thus confirming the suitability of these techniques for understanding the influence of degradation in soil on polylactide.

4. Conclusions

Polylactide was buried in active soil in order to simulate its disposal stage following an international standard, and the changes in their physical properties were assessed by Differential Scanning Calorimetry and Dynamic Mechanical Thermal Analysis.

Along the degradation in soil process, indicators such as the relative structural relaxation enthalpy and the thermal expansion coefficient have given an idea about the free volume generated within the amorphous matrix. Onset, endset and peak cold crystallization temperatures and enthalpies showed the variation of the crystalline phase, due to the liability of shorter chains to rearrange in spherulites after cleavages induced by degradation in soil. The melting behavior of the crystalline fraction formed, especially after 300 days of burial, show that the lamellar thickness distribution experiences a change towards higher sizes, coinciding with the molecular weight decrease. These facts stress the relation between the heterogeneity acquired by PLA after chain scissions and the notable change of properties, also corroborated by molecular weight reduction.

The combination of both Thermal Analysis and Molecular Weight Characterization stands out as a very interesting option for assessing not only the macroscopic changes on PLA structure induced by degradation in soil, but also for establishing new insights on the morphological rearrangements involved during the whole process.

Acknowledgements

Partial funding of this work by Ministerio de Educación y Ciencia, Project ENE2007-67584-C03-02 and for a pre-doctoral grant scholarship FPU to J.D. Badía, and by the Ministerio de Ciencia e Innovación for a pre-doctoral grant scholarships FPI to L. Santonja Blasco and Rosana Moriana, is gratefully acknowledged.

References

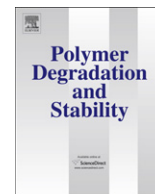
- [1] Doi Y, Fukuda K, editors. Biodegradable plastic and polymers. Amsterdam, The Netherlands: Elsevier; 1994.
- [2] Scott G, editor. Biodegradable polymers. Principles and applications. 2nd ed. Dordrecht, The Netherlands: Kluwer Academic Publishers; 2002.
- [3] Vert M, Schwach G, Coudane J. Present and future of PLA polymers. *J Macromol Sci Pure Appl Chem* 1995;A32:787–96.
- [4] De Jong SJ, Arias ER, Rijkers DTS, van Nostrum CF, Kettenes-van den Bosch JJ, Hennink WE. New insights into the hydrolytic degradation of poly(lactic acid): articulation of the alcohol terminus. *Polymer* 2001;42:2795–802.
- [5] Kronenthal RL, Oser Z, Martin E, editors. Polymers in medicine and surgery. New York, NY: Plenum Press; 1975. p. 119–37.
- [6] Li S, Garreau H, Vert M. Structure-property relationships in the case of the degradation of massive aliphatic poly-(α -hydroxy acids) in aqueous media. *J Mater Sci Mater Med* 1990;1:123–30.
- [7] Migliaresi C, Fambri L, Cohn D. A study on the *in vitro* degradation of poly (lactic acid). *J Biomater Sci Polym Ed* 1994;4:591–606.
- [8] Södergård A, Selin J-F, Näsman JH. Hydrolytic degradation of the peroxide modified poly (L-lactide). *Polym Degrad Stab* 1996;51:351–9.
- [9] Tsuji H, Mizuno A, Ikada Y. Properties and morphology of poly(L-lactide). III. Effects of initial crystallinity on long-term *in vitro* hydrolysis of high molecular weight poly(L-lactide) film in phosphate-buffered solution. *J Appl Polym Sci* 2000;77:1452–64.
- [10] Tsuji H, Ikada Y. Properties and morphology of poly(L-lactide) 4. Effects of structural parameters on long-term hydrolysis of poly(L-lactide) in phosphate-buffered solution. *Polym Degrad Stab* 2000;67:179–89.
- [11] Hakkarainen M. Aliphatic polyesters: abiotic and biotic degradation and degradation products. *Adv Polym Sci* 2002;157:113–38.
- [12] Shogren RL, Doane WM, Garlotta D, Lawton JW, Willett JL. Biodegradation of starch/polylactic acid/poly(hydroxyester-ether) composite bars in soil. *Polym Degrad Stab* 2003;79:405–11.
- [13] Torres A, Li SM, Roussos S, Vert M. Poly(lactic acid) degradation in soil or under controlled conditions. *J Appl Polym Sci* 1996;62:2295–302.
- [14] Urayama H, Kanamori T, Kimura Y. Properties and biodegradability of polymer blends of poly(L-lactide)s with different optical purity of the lactate units. *Macromol Mater Eng* 2002;287:116–21.
- [15] Siepmann J, Göpferich A. Mathematical modeling of bioerodible, polymeric drug delivery systems. *Adv Drug Deliv Rev* 2001;48(2–3):229–47.
- [16] Schliecker G, Schmidt C, Fuchs S, Kissel T. Characterization of a homologous series of D, L-lactic acid oligomers; a mechanistic study on the degradation kinetics *in vitro*. *Biomaterials* 2003;24:3835–44.
- [17] Aso Y, Yoshioka S, Li Wan Po A, Terao T. Effect of temperature on mechanisms of drug release and matrix degradation of poly(DL-lactide) microspheres. *J Control Release* 1994;31(1):33–9.
- [18] Ho KLG, Pometto III AL, Hinz PN. Effects of temperature and relative humidity on polylactic acid plastic degradation. *J Environ Polym Degrad* 1999;7: 83–92.
- [19] Calmon A, Guillaume S, Bellon-Maurel V, Feuilloloy P, Silvestre F. Evaluation of material biodegradability in real conditions-development of a burial test and an analysis methodology based on numerical vision. *J Environ Polym Degrad* 1999;7:157–66.
- [20] Iman HS. Adhesive properties of a symbiotic bacterium from a wood-boring shipworm. *Appl Environ Microbiol* 1990;56:1317–22.
- [21] Goheen RP, Wool RP. Degradation of polyethylene-starch blends in soil. *J Environ Polym Degr* 1991;42:2691–701.
- [22] Santonja-Blasco L, Contat-Rodrigo L, Moriana-Torro R, Ribes-Greus A. Thermal characterization of polyethylene blends with a biodegradable masterbatch subjected to thermo-oxidative treatment and subsequent soil burial test. *J Appl Polym Sci* 2007;106:2218–30.
- [23] Badía JD, Vilaplana F, Karlsson S, Ribes-Greus A. Thermal analysis as a quality tool for assessing the influence of thermo-mechanical degradation on recycled poly(ethylene terephthalate). *Polym Test* 2009;28:169–75.
- [24] Contat-Rodrigo L, Ribes-Greus A, Diaz-Calleja R. Characterization by thermal analysis of PP with enhanced biodegradability. *J Appl Polym Sci* 2001;82: 2174–84.
- [25] Vallés-Lluch A, Contat-Rodrigo L, Ribes-Greus A. Influence of previous annealing on the first stage of degradation of LDPE-Mater-Bi blends aged in soil. Comparative study by thermal analysis. *J Appl Polym Sci* 2003;90: 3359–73.
- [26] Contat-Rodrigo L, Ribes-Greus A. Viscoelastic behavior of degradable polyolefins aged in soil. *J Appl Polym Sci* 2000;78:1707–20.
- [27] ISO 846, 1997. Plastics—determination of behaviour under the action of microorganisms. Evaluation by visual examination or measurement of changes in mass or physical properties.
- [28] Vogel H. The temperature dependence law of the viscosity of fluids. *Phys Z* 1921;22:645–6.
- [29] Heya T, Okada H, Ogawa Y, Toguchi H. *In-vitro* and *in-vivo* evaluation of thyrotropin-releasing-hormone release from copoly(DL-lactic/glycolic acid) microspheres. *J Pharm Sci* 1994;83(5):636–40.
- [30] Pluta M. Morphology and properties of polylactide modified by thermal treatment, filling with layered silicates and plasticization. *Polymer* 2004;45: 8239–51.
- [31] Vasanthakumari R, Pennings AJ. Crystallization kinetics of poly(L-lactic acid). *Polymer* 1983;24:175–8.
- [32] Wlochowicz A, Eder M. Distribution of lamella thicknesses in isothermally crystallized polypropylene and polyethylene by differential scanning calorimetry. *Polymer* 1984;25:1268.
- [33] Moriana-Torró R, Contat-Rodrigo L, Santonja-Blasco L, Ribes-Greus A. Thermal characterisation of photo-oxidized HDPE/Mater-Bi and LDPE/Mater-Bi blends buried in soil. *J Appl Polym Sci* 2008;109:1177–88.
- [34] Liua X, Zoub Y, Lia W, Cao G, Chen W. Kinetics of thermo-oxidative and thermal degradation of poly(DL-lactide) (PDLA) at processing temperature. *Polym Degrad Stab* 2006;91(12):3259–65.

CONTRIBUTION V-B

Thermal analysis applied to the characterization of degradation in soil of polylactide: II. On the thermal stability and thermal decomposition kinetics

J.D. Badia, L. Santonja-Blasco, Rosana Moriana, A. Ribes-Greus

Polymer Degradation and Stability 2010, 95; 2192-2199



Thermal analysis applied to the characterization of degradation in soil of polylactide: II. On the thermal stability and thermal decomposition kinetics

J.D. Badía, L. Santonja-Blasco, Rosana Moriana, A. Ribes-Greus*

Instituto de Tecnología de Materiales, Universidad Politécnica de Valencia, Camino de Vera, s/n, 46071, Valencia, Spain

ARTICLE INFO

Article history:

Received 1 December 2009

Received in revised form

19 April 2010

Accepted 3 June 2010

Available online 12 June 2010

Keywords:

Poly lactide

Degradation in soil

Thermal decomposition kinetic analysis

Isoconversional methods

ABSTRACT

The disposal stage of polylactide (PLA) was assessed by burying it in active soil following an international standard. Degradation in soil promotes physical and chemical changes in the polylactide properties. The characterization of the extent of degradation underwent by PLA was carried out by using Thermal Analysis techniques. In this paper, studies on the thermal stability and the thermal decomposition kinetics were performed in order to assess the degradation process of a commercial PLA submitted to an accelerated soil burial test by means of multi-linear-non-isothermal thermogravimetric analyses. Results have been correlated to changes in molecular weight, showing the same evolution as that described by the parameters of thermal stability temperatures and apparent activation energies. The decomposition reactions can be described by two competitive different mechanisms: Nucleation model (A2) and Reaction Contracting Volume model (R3). The changes in the kinetic parameters and kinetic models are in agreement with the calorimetric and dynamic–mechanical–thermal results, presented in the Part I of the study [1].

© 2010 Elsevier Ltd. All rights reserved.

1. Introduction

Due to the significant impact of plastic waste on the environment, to find eco-friendly solutions to manage the disposal of synthetic plastics is a key challenge. A promising solution is the use of biodegradable polymers for packaging, as well as many other applications. Due to its good thermal, mechanical and processing properties, economic and environmental advantages [2–12], one of the most potential candidates is polylactide (PLA), which is being currently established at the polymer industry. However, the use of new materials would also imply the generation of a new and huge source of polymeric materials waste in the near future, which should be carefully managed. Therefore, the degradation process involved the disposal stage of PLA must be assessed, with the aim of ensuring the completion of its life cycle.

The necessity of developing and implementing fast, cost-effective and reliable characterization testing procedures has been stated in order to ascertain a deeper knowledge about the ongoing interaction of the polymer with its disposal environment [1]. Thermal Analysis techniques have demonstrated to be very appropriate and reliable methodologies to monitor and control the influence of several degradation phenomena on biodegradable

polymers, such as hydrolysis, photo-oxidation, swelling, or degradation in soil [13–15]. Chain cleavage processes induce morphological and mechanical changes, as observed by Differential Scanning Calorimetry and Dynamical Mechanical Thermal Analysis [1]. These morphological changes may alter the thermal decomposition process of the bulk PLA and thus its characterization would also provide a complementary interpretation on the macroscopic effects of degradation in soil on PLA. As discussed in previous studies [16,17], the decomposition of PLA during thermal treatment is mainly caused by intramolecular transesterification reactions leading to cyclic oligomers of lactic acid and lactide. Simultaneously, there is a recombination of the cyclic oligomers with linear polyesters through insertion reactions, whereas molecules with longer chains lengths are favoured. Evolved gases in inert atmosphere also contain acetaldehyde, carbon monoxide, carbon dioxide and methylketene, among others [18].

Due to its applicability in the macroscopic scale, the modeling of the thermal decomposition processes in inert or reactive conditions has been broadly applied by using isoconversional and non-isoconversional methods proposed by different authors with good acceptance because of its versatility in different materials [19,20]. The completion of the kinetic triplet, consisting in kinetic model function $f(\alpha)$, apparent activation energy (E_a), and pre-exponential factor (A) can furnish with the knowledge of the polymer thermal decomposition behaviour, and thus be related to the ongoing degradation stage.

* Corresponding author. Tel.: +34 963879817.

E-mail address: aribes@ter.upv.es (A. Ribes-Greus).

The aim of this work is to test by thermal Analysis techniques the thermal changes that PLA suffers through degradation in soil. To mimic the environmental conditions at which PLA is subjected in non-controlled disposals, PLA is submitted to a standardized accelerated degradation in soil test. Physical and chemical changes occurred to the polylactide properties, throughout the degradation in soil process are analyzed, making efforts on establishing new insights in studying the degradation in soil process on polymers by other accurate methods; alternative and complementary to the chemical analytical techniques. The current paper is focused on the influence of degradation in soil on the thermal stability and the thermal decomposition kinetics of PLA. Once assessed the effect of degradation in soil on PLA molecular weight (MW), parameters such as the characteristic thermal stability temperatures (T_{on} , T_{end} , T_p) and the components of the kinetic triplet ($f(\alpha)$, A and E_a) have been correlated to MW evolution and consequently evaluated as indicators of degradation.

2. Theoretical background

The primary purpose of the kinetic analysis is to obtain the aforementioned kinetic triplet. Recently, Khawan and Flanagan [21,22] have reviewed the relationship between the theoretical decomposition mechanisms and their mathematical models, the so-called kinetic functions $f(\alpha)$. A list of the most common $f(\alpha)$ applied to polymers is given at Table 1.

Macroscopic kinetics are complex since they might give information about multiple steps simultaneously occurring, and therefore induce to misleading results [23]. Some investigations have been hence carried out in order to focus on the challenge of clarifying the interpretation of macroscopic kinetics; and have settled isoconversional methods as suitable analysis procedures to evaluate the apparent activation energy (E_a) [23,24]. These methods, which require experiments at several linear heating rates, are based on the assumption that at a constant extent of conversion α , the decomposition rate $d\alpha/dt$ is a function only of the temperature, and do not need any conversion model assumption at the initial stages of the analysis. The most broadly used isoconversional methods are those developed by Friedman [25] and Flynn-Wall-Ozawa [26,27] (supported on Doyle's integral approximation [28]). These methods give rise to linear functions from which slopes the E_a at a constant α is obtained. Likewise, the model free kinetic method established by Kissinger [29] is widely employed by many authors in order to check their results. This method calculates the activation energy from the slope of a linear function which takes into account the relationship between the peak temperature of the first-derivative thermogravimetric curve and the heating rate employed in the experiment.

Table 1
List of common kinetic functions to explain the thermal decomposition mechanisms in bulk polymers.

model	Differential form $f(\alpha) = 1/k \cdot d\alpha/dt$	Integral form $g(\alpha) = k \cdot t$
Nucleation models		
Avrami–Erofeyev (A2)	$2 \cdot (1 - \alpha) [-\ln(1 - \alpha)]^{1/2}$	$[-\ln(1 - \alpha)]^{1/2}$
Avrami–Erofeyev (A3)	$3 \cdot (1 - \alpha) [-\ln(1 - \alpha)]^{2/3}$	$[-\ln(1 - \alpha)]^{1/3}$
Avrami–Erofeyev (A4)	$4 \cdot (1 - \alpha) [-\ln(1 - \alpha)]^{3/4}$	$[-\ln(1 - \alpha)]^{1/4}$
Geometrical contraction models		
Contracting area (R2)	$2 \cdot (1 - \alpha)^{1/2}$	$1 - (1 - \alpha)^{1/2}$
Contracting volume (R3)	$3 \cdot (1 - \alpha)^{1/3}$	$1 - (1 - \alpha)^{1/3}$
Reaction-order models		
Zero-order (F0/R1/ $n = 0$)	1	α
First-order (F1, $n = 1$)	$(1 - \alpha)$	$-\ln(1 - \alpha)$
Second-order (F2, $n = 2$)	$(1 - \alpha)^2$	$\frac{1}{1 - \alpha} - 1$
Third-order (F3, $n = 3$)	$(1 - \alpha)^3$	$\frac{1}{2} \cdot \left[\frac{1}{(1 - \alpha)^2} - 1 \right]$

Regarding the kinetic function $f(\alpha)$ evaluation, the most common methodologies are those proposed by Criado [30], which allows the comparison of the experimental data to theoretical reduced master-curves, and Coats-Redfern [31], which gives a linear fitting for a given kinetic model function. By combining both methods, Coats-Redfern method is applied to those theoretical kinetic functions $f(\alpha)$ that better fit the experimental behaviour according to the results drawn from the Criado method. A comparison of the apparent activation energy E_a obtained from the slope for each $f(\alpha)$ with the average apparent activation energy given by the Friedman, Flynn-Wall-Ozawa and Kissinger methods $E_{a,iso}$ will be deciding in the selection of the $f(\alpha)$. The pre-exponential (A) is also obtained from this method, and the kinetic triplet is thus achieved, which is automatically related to the physical decomposition mechanism. An extended explanation of these methods can be found elsewhere [32]. To summarize, Fig. 1 schematically represents the theoretical description of these methods and the kinetic strategy followed at this paper.

3. Experimental procedures

3.1. Material and sample preparation

A commercial polylactide with 3.8% content of meso-lactide, obtained from renewable resources by ring opening polymerization supplied by Natureworks (Minnetonka, USA) was used in this study. This PLA is a commercial resin with a number-average molecular weight of 102.130 g/mol, as measured by Gel Permeation Chromatography.

Pellets of PLA were dried with demineralized air at 80 °C during 4 h. Rectangular bars were prepared by compression moulding in a Collin PCS-GA Type Press 800 (GA, USA) at an initial temperature of the hot plates of 195 °C and final temperature of 60 °C. Five pressure steps were performed as follows: 5 min at 6 bar, 8 min at 75 bar, 8 min at 155 bar, 4 min at 215 bar, and 11 min at 45 bar. Test specimens were presented as bars of (145 × 10 × 2 mm). Since this work approaches the degradation in soil of discarded consumer goods, which are obtained by means of, at least, one processing step, “non-buried PLA” has been considered the starting material of the study.

3.2. Accelerated soil burial test

PLA plates were subjected to a controlled degradation in soil test under controlled conditions (temperature, water content and pH), following the ISO 846-1997 International Norm [33], according to method D. Samples were buried in biologically active soil and kept in a Heraeus B12 (Hanau, Germany) culture oven at 28 °C. The soil used in these tests was a red soil extract taken from a culture field in Alginet (Valencia). To ensure the oxygenation of the soil, a protocol of periodical air oxygen supply was followed. Microbial activity of soil was monitored with cotton along the extension of the experiment. According to norm, if the activity of the cellulose-degrading micro-organisms is in order, the case is also applicable to the rest of flora. The soil was maintained at approximately pH 7 and a relative humidity of 0.87 g water/g wet soil. Test specimens were extracted at 30, 150, 300 and 450 days, cleaned and kept in a desiccator during 4 days in order to ensure water desorption before being analyzed.

3.3. Thermogravimetric analysis

Experiments were carried out in a Mettler-Toledo TGA/SDTA 851 (Columbus, OH), from 25 to 750 °C at different heating rates ($\beta = 5, 10, 15, 20, 25, 30$ °C/min), under constant flow of 50 mL/min of Argon atmosphere.

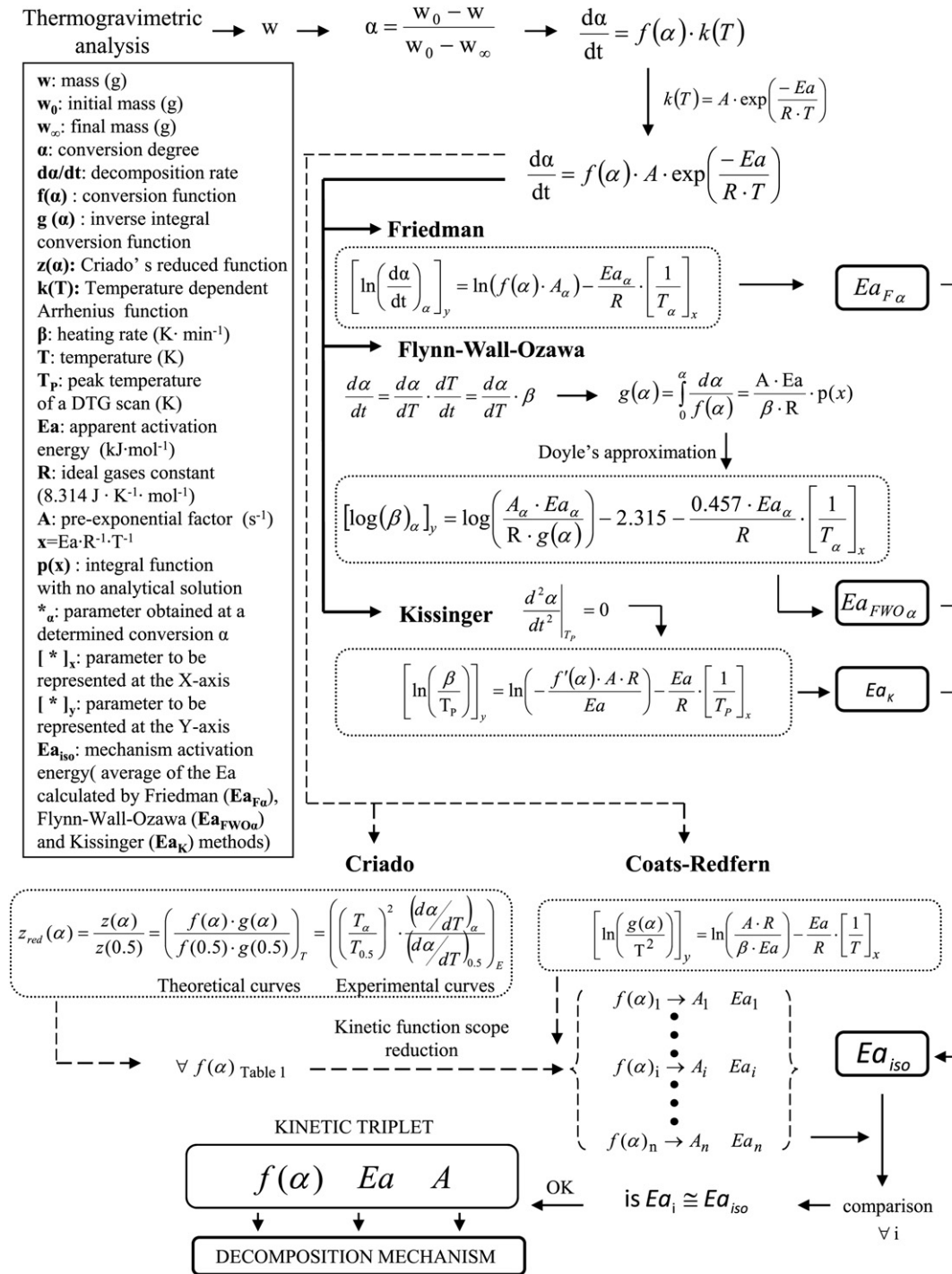


Fig. 1. Methodology applied for the characterisation of the thermal decomposition kinetics of PLA submitted to degradation in soil.

4. Results and discussion

The influence of degradation in soil on polylactide has been deeply characterized by Thermogravimetry (TGA). The changes in the thermal stability have been firstly studied. A further assessment of the thermal decomposition behaviour in the bulk PLA is performed. Results are related to those showed by Differential Scanning Calorimetry (DSC) and Dynamical Mechanical Thermal Analysis (DMTA), reported in the Part I of the study [1]. Discussion is given in terms of both the effects of degradation in soil on the

physical–chemical properties of PLA, and the reliability of these thermal analysis techniques to offer reliable indicators of the degradation extent.

4.1. Thermal stability

A preliminary analysis of the differences observed in thermal stability temperatures for non-buried PLA and samples submitted to the accelerated soil burial test was performed. For this purpose, the thermal decomposition (TG) curves and their first-order

derivative (DTG) curves for samples extracted at 30, 150, 300 and 450 of burying have been analyzed at different heating rates and compared to the TG and DTG curves of the non-buried PLA. Fig. 2 shows the influence of the degradation process on the TG and DTG curves in terms of the conversion degree evolution displayed for non-buried and 450-days-buried PLA samples; the other soil burial experiments were omitted for the sake of clarity.

As usual, higher heating rates (β) lead to shift the thermograms to higher temperatures. PLA thermal decomposition occurs through a single decay stage, regardless the degradation in soil time and the β employed for the thermogravimetric analysis. The mass loss was around 98–99% in all cases. The corresponding decomposition onset and endset temperatures (T_{on} , T_{end}) were obtained by a tangential intercept method onto the TG curve. Likewise, the peak temperature of the DTG curve, which is related to the inflection temperature of the TG curve (T_p) was also considered. Fig. 3 displays the T_{on} , T_{end} and T_p evolution along the degradation in soil process at the experiment of lower β (5°C min^{-1}), since it is supposed to offer the best accuracy and the major independence with the experimental TGA conditions [23]. All thermal stability temperatures describe the same behaviour, clearly differentiated in two stages: firstly, an overall increase of around 5°C is stated; afterwards, the decomposition temperatures continuously diminish, describing an attenuated decreasing tendency. These results suggest modifications in the arrangement of chains in the bulk PLA matrix. Initial hydrolytic reactions might give out smaller free chains able to react or reorganize, thus offering a slightly higher resistance to the thermal decomposition [34]. Later on, the degradation weakens the structure of the bulk polymer, and thus lower temperatures are capable of overcoming its thermal stability. The results from thermogravimetric analysis lead to guess that degradation in soil produces small changes in the bulk polymer, since the interaction of the polymer and the testing environment takes place slowly, as it has been shown in other studies [13,14]. However, these small variations might indicate modifications in the thermal decomposition kinetic model. Further analysis is therefore carried out to establish good indicators which correlate the thermal decomposition behaviour of PLA with its degradation in soil stage.

4.2. Thermal decomposition kinetic model

In the attempt to develop a model for plastic thermal behaviour in full scale systems, the main purpose is to describe the thermal decomposition of polymers in terms of an intrinsic kinetics, in which heat and mass transfer limitations are not included. Generally, kinetic models are proposed in literature for plastics and biomasses.

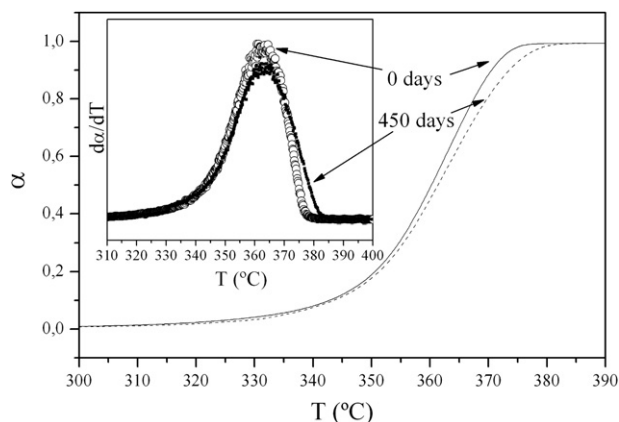


Fig. 2. Comparison of the conversion degree evolution and its first-derivative thermogravimetric curve plot for non-degraded PLA and PLA buried during 450 days.

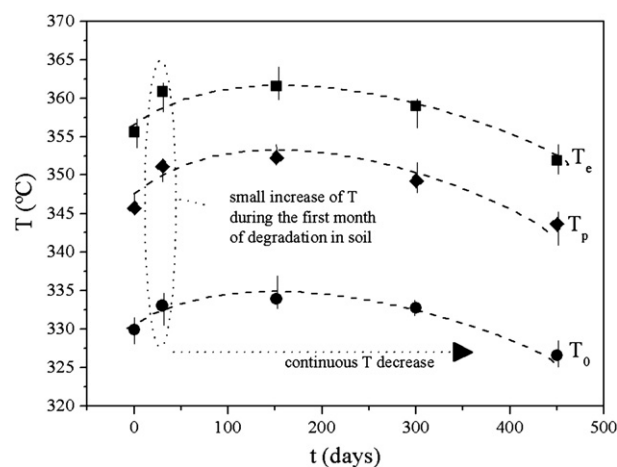


Fig. 3. Effect of degradation in soil on the thermal stability temperatures obtained from TGA experiments at 5°C/min .

These models do not take into account the rigorous and exhaustive description of the chemistry of thermal decomposition of polymers and describe the process by means of a simplified reaction pathway. Each single reaction step considered is representative of a complex network of reactions [21]. The obtaining of the aforementioned kinetic triplet may provide new knowledge regarding the kinetic model of PLA thermal decomposition. A deep kinetic analysis according to the kinetic methodology formerly proposed in Fig. 1 has been performed. The Friedman, Flynn-Wall-Ozawa and Kissinger methods have been initially applied to evaluate the degradation in soil effect on the apparent activation energy (E_a) of the PLA thermal decomposition. These three methods offer good experimental data fittings to straight lines, for all degradation in soil times studied. Fig. 4 (a, b, c) shows the application of these methods to the non-buried PLA.

The E_a for every constant conversion degree α value has been obtained from the slope of each line. Since the main mass loss decomposition process occurs in the α domain comprised between 0.2 and 0.7 for all samples, the analyses have been focused in that range. Table 2 shows the isoconversional apparent activation energy $E_{a,\alpha}$ values for all samples submitted to the soil burial test. In order to investigate the degradation consequences on the PLA thermal decomposition kinetics, the average apparent activation energy $E_{a,iso}$ value has been taken. Fig. 5 represents the $E_{a,iso}$ evolution with the soil burial time for the three employed methods. As can be seen, a consistent behaviour in a small confidence range has been given by all of them. The $E_{a,iso}$ tendency is similar to the evolution described by all the characteristic thermal stability temperatures and molecular weights [1]. In a first stage, a slight increase in molecular weight ($M_n = 1.02 \times 10^5 \text{ g mol}^{-1}$ at 0 days and $1.08 \times 10^5 \text{ g mol}^{-1}$ at 30 days) strengthens the suggestion previously drawn on molecular recombinations of smaller chains into the polymeric backbone for the action of the humidity of the soil [34], which is further supported by the increase of the $E_{a,iso}$, since more energy is needed to trigger the thermal decomposition. Later on, the $E_{a,iso}$ continuously decreases, which indicates a progressive weakening of the PLA structure, related to a continuous decrease in molecular weight ($M_n = 9.1 \times 10^4 \text{ g mol}^{-1}$ at 150 days, $7.6 \times 10^4 \text{ g mol}^{-1}$ at 300 days, and $5 \times 10^4 \text{ g mol}^{-1}$ at 450 days) as a consequence of the degradation in soil subjected, as it was shown [1]. These changes support the hypothesis previously drawn, which considered modifications on the thermal decomposition mechanism as a degradation in soil effect, as it is shown as follows.

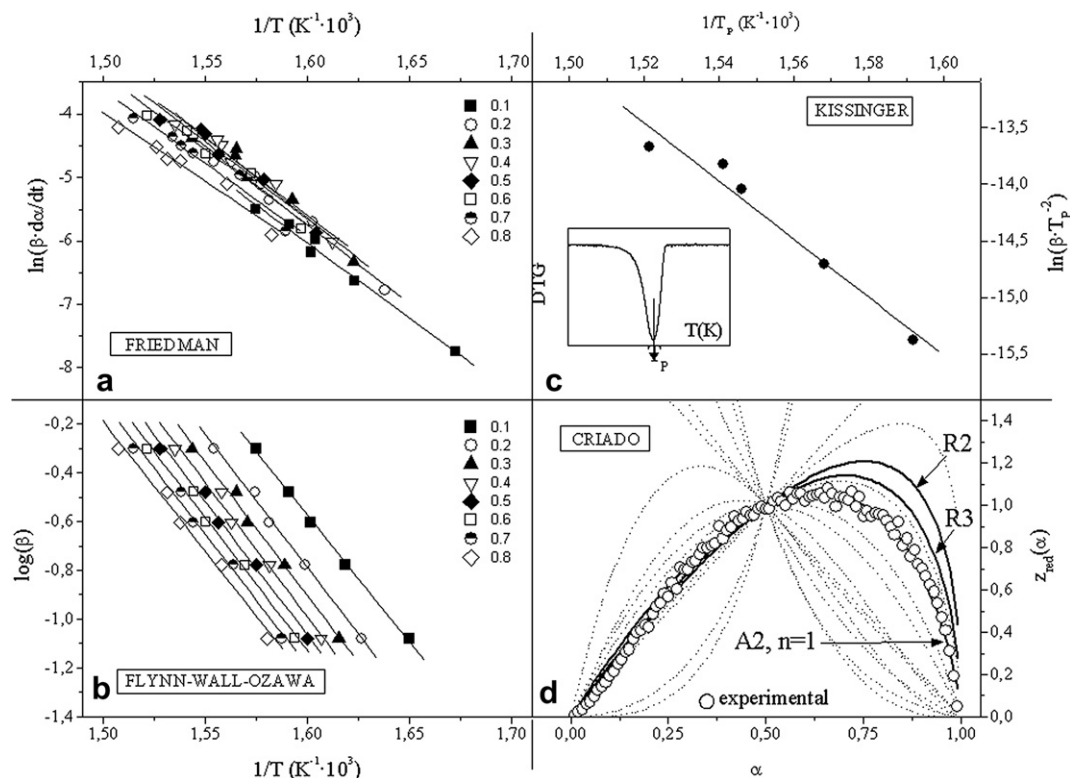


Fig. 4. Kinetic methods applied to non-degraded PLA. a) Friedman method; b) Flynn-Wall-Ozawa method. c) Kissinger method. d) Criado method.

Concerning the completion of the kinetic triplet, the kinetic model function $f(\alpha)$, and the pre-exponential factor (A) should be obtained. Criado method has been applied for all the theoretical $f(\alpha)$ related at Table 1. Fig. 4 (d) shows the comparison of the reduced Criado functions of non-buried PLA to the master-curves for the experiments carried out at the slower heating rate ($5\text{ }^\circ\text{C}\cdot\text{min}^{-1}$), which are supposed to offer more accurate results [23]. This method allows for the discrimination of the most possible kinetic models which can explain the thermal decomposition behaviour of polymers. Nevertheless, a parallel evaluation of the apparent activation energies E_a is required to verify the chosen kinetic function $f(\alpha)$. Among the different methods that calculate the E_a from a given $f(\alpha)$, Coats-Redfern method has been demonstrated to offer the most precise results [35]. In that way, the results of the combination of the analyses performed by means of the application of Criado, Coats-Redfern and the isoconversional methods are shown at Table 3, together with the kinetic triplet obtained and the corresponding physical thermal decomposition model for each soil burial time. The knowledge of the complete kinetic triplet allows mathematically describing the thermal

degradation process at any time of the soil burial experiment. As can be seen at Fig. 6, the theoretical kinetic models drawn from the analysis to all samples perfectly fit to the thermogravimetric experimental data.

The kinetic analysis methodology has permitted to accurately model the thermal decomposition process along the degradation in soil test. The kinetic triplet interpretation eases the complexity of the decomposition processes taking place, and permits to relate the changes induced by degradation in soil to the changes in the morphology of the bulk PLA. The non-buried PLA thermal decomposition mechanism is described by a Nucleation model (A2). This kind of kinetic model is quite common in crystallization processes, but have only been observed in few studies dealing with thermal decomposition processes of polymers [36–42]. In these studies, the controversy of the relationship between the mathematical models and the physical mechanisms is patent. Even being aware of the limitations of these studies, a physical approach of the influence of degradation in soil on the bulk PLA have been drawn from our kinetic analysis. Therefore, the A2 model indicates the presence of active zones (nuclei), more

Table 2
Apparent activation energies values obtained by the Friedman (E_{aF}), Flynn-Wall-Ozawa (E_{aFWO}) and Kissinger (E_{aK}) methods.

α	PLA_0 days			PLA_30 days			PLA_150 days			PLA_300 days			PLA_450 days		
	E_{aF} (kJ mol^{-1})	E_{aFWO} (kJ mol^{-1})	E_{aK} (kJ mol^{-1})	E_{aF} (kJ mol^{-1})	E_{aFWO} (kJ mol^{-1})	E_{aK} (kJ mol^{-1})	E_{aF} (kJ mol^{-1})	E_{aFWO} (kJ mol^{-1})	E_{aK} (kJ mol^{-1})	E_{aF} (kJ mol^{-1})	E_{aFWO} (kJ mol^{-1})	E_{aK} (kJ mol^{-1})	E_{aF} (kJ mol^{-1})	E_{aFWO} (kJ mol^{-1})	E_{aK} (kJ mol^{-1})
0.2	205.5	206.0		235.7	260.9		217.7	233.0		180.5	215.3		195.2	222.6	
0.3	207.6	212.4		259.8	261.3		224.3	241.7		201.7	218.8		199.2	214.3	
0.4	208.0	202.5	206.7	271.8	265.9	259.7	229.1	238.9	239.0	211.7	217.2	214.3	201.7	203.3	199.7
0.5	206.1	202.7		283.9	272.0		231.6	237.4		219.8	207.1		199.3	193.2	
0.6	205.4	197.0		274.8	263.9		233.9	240.3		222.5	202.5		194.8	179.7	
0.7	204.1	191.8		252.7	261.7		235.7	235.7		222.9	186.0		193.6	176.4	

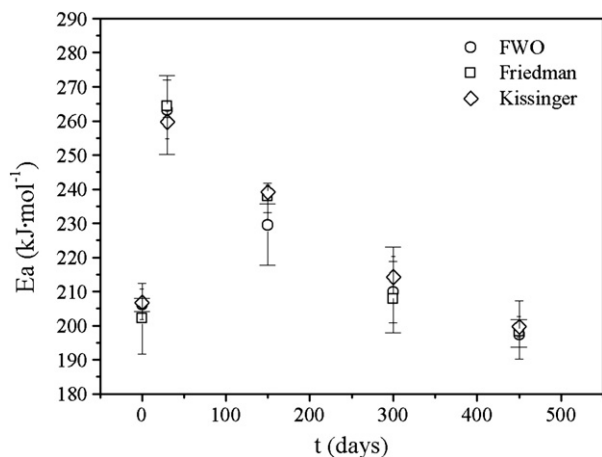


Fig. 5. Evolution of the apparent activation energy throughout the degradation in soil process.

chemically liable to thermal decomposition [34], which activate the formation and growth of gas bubbles in the polymer melt [42]. However, the degradation in soil process alters the thermal decomposition behaviour of PLA. When PLA samples are submitted to the accelerated soil burial test, changes in the kinetic triplet are involved, due to the humidity and the presence of micro-organisms, which mainly induce chemical changes in the polymeric structure [43–46]. In this first stage, humidity may affect the PLA structure and the effect of ingestion and coalescence nuclei processes could difficult the molecules release and produce a change in the thermal decomposition mechanism, which may be primarily controlled by a Reaction Contracting model (R3). This model explains the thermal decomposition in a generalized fashion throughout the bulk PLA, where the gas release is controlled in the phase boundaries. After this first stage, the thermal decomposition mechanism remains being described by an R3 model but, due to the continuous interaction between the polymer and the degrading environment, low molecular

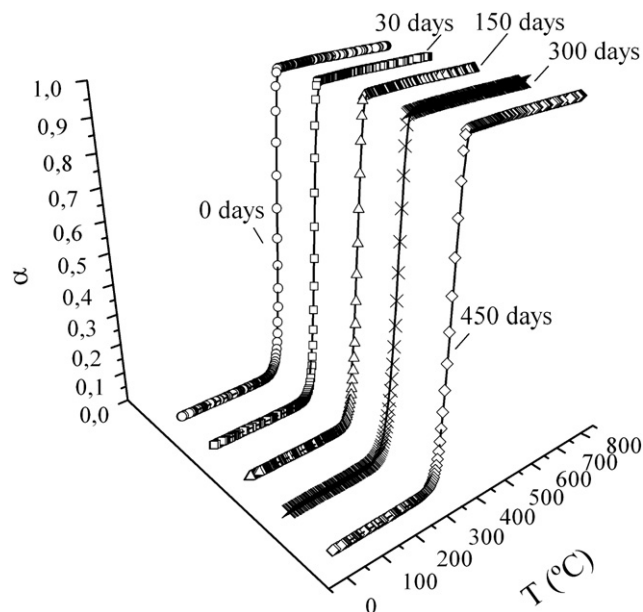


Fig. 6. Comparison of experimental TG curves (symbols) to fitted kinetic functions (solid lines) obtained from the kinetic methodology.

weight compounds might be released. Hence, the characteristic temperatures and the $E_{a_{iso}}$ of the thermal decomposition process show a decrease, which is a sign of the progressive weakening of PLA structure, since it requires lower energy to activate its thermal decomposition process as longer is PLA submitted to degradation in soil. The R3 kinetic model is maintained during almost 300 days but after this time, in agreement with the morphological variations stated by the DSC and DMTA results [1], a rearrangement of chains into weaker conformations is produced and the generalized decomposition may be therefore disabled, giving relevance to the decomposition in specific sites (nuclei) and thus the thermal decomposition process is again governed by an A2 Nucleation model.

Table 3

Results of kinetic methodology. Evolution of kinetic triplet of PLA thermal decomposition throughout the degradation in soil process.

PLA degradation in soil									
Burial in soil	Criado analysis	Coats-Redfern analysis			Isoconversional analysis	Kinetic triplet Decomposition mechanism			
Time (days)	$f(\alpha)$ scope reduction	E_a (kJ mol ⁻¹)	$\ln A$ (s ⁻¹)	R2	Average E_a (kJ mol ⁻¹)	$f(\alpha)$	E_a (kJ mol ⁻¹)	$\ln A$ (s ⁻¹)	
0	$n = 1$	378.7	67.4	0.998	205.0	A2	205.0	46.1	Nucleation
	A2	205.1	46.1	0.999					
	R2	318.9	55.0	0.997					
	R3	337.7	58.3	0.998					
30	$n = 1$	300.3	50.3	0.998	262.4	R3	262.4	43.0	Reaction Contracting volume
	A2	161.1	37.4	0.995					
	R2	244.9	40.6	0.998					
	R3	259.3	43.0	0.999					
150	$n = 1$	240.4	40.2	0.956	232.5	R3	232.5	36.9	Reaction Contracting volume
	A2	135.7	32.2	0.949					
	R2	224.7	36.3	0.969					
	R3	229.8	36.9	0.975					
300	$n = 1$	253.9	43.5	0.985	210.7	R3	210.7	34.8	Reaction Contracting volume
	A2	142.4	33.6	0.987					
	R2	227.0	36.9	0.993					
	R3	214.6	34.8	0.996					
450	$n = 1$	354.7	62.1	0.997	198.4	A2	198.4	43.1	Nucleation
	A2	193.2	43.1	0.997					

5. Conclusions

Commercial polylactide was buried in active soil in order to mimic its disposal stage following an international standard, and the changes in their physical and chemical properties were assessed by Thermal Analysis techniques. The research in this second paper focuses on the thermal stability and thermal decomposition kinetics of PLA. Multi-rate linear-non-isothermal thermogravimetric experiments have been performed and indicators for monitoring the influence of degradation in soil on the bulk PLA have been proposed.

A single thermal decomposition stage has been stated for all PLA degraded in soil samples, regardless the burial time and the heating rate employed. The effect of degradation in soil on PLA thermal stability has been evaluated in terms of onset, endset and the peak decomposition temperatures. All temperature indicators follow the same double-stage behaviour: a first increase related to the major degrading activity in the polymer; and a continuous attenuated decay along the degradation in soil process. These changes have been also assessed by the evolution of the apparent activation energy, being in this case the difference between both stages more noticeable. The correlation of these parameters to the evolution observed for the molecular weight strengthens the usefulness of thermogravimetry as a means for monitoring the influence of degradation on polymers.

A kinetic analysis methodology, consisting in the combination of five different methods (namely Friedman, Flynn-Wall-Ozawa, Kissinger, Criado and Coats-Redfern) has been successfully applied and has allowed the determination of the PLA kinetic triplet evolution throughout the degradation in soil process. The PLA thermal decomposition mechanism is influenced, since it can be described by two competitive different decomposition models: on the one hand, a Nucleation model (A2), which gives importance to specific decomposition sites; and on the other hand, a Reaction Contracting model (R3), which represents a particles release generalized on the whole polymer surface. Therefore, the knowledge of the thermal decomposition model at each degradation stage has permitted to interpret from a macroscopic point of view the degradation in soil consequences on PLA bulk morphology.

Acknowledgements

The authors would like to acknowledge the Ministerio de Educación y Ciencia (Spanish Government) and the European Regional Development Fund for the economical support through the Project ENE2007/67584/C03-02 and the research position granted through the FPU pre-doctoral program to J.D. Badía. The Ministerio de Ciencia e Innovación is acknowledged by L.Santonja-Blasco and Rosana Moriana for the research position by means of the FPI pre-doctoral programme.

References

- [1] Santonja-Blasco L, Moriana R, Badía JD, Ribes-Greus A. Thermal analysis applied to the characterization of degradation in soil of polylactide: I. Calorimetric and viscoelastic analyses. *Polymer Degradation and Stability* 2010;95:2185–91.
- [2] Tsuji H, Doi Y, Steinbüchel A, editors. *Biopolymers. Polyesters III. Applications and commercial products*. Weinheim: Wiley-VCH Verlag GmbH; 2002.
- [3] Auras R, Harte B, Selke S. An overview of polylactides as packaging materials. *Macromolecular Bioscience* 2004;4:835–64.
- [4] Gupta AP, Kumar V. New emerging trends in synthetic biodegradable polymers-polylactide: a critique. *European Polymer Journal* 2007;43(10):4053–74.
- [5] Holland SJ, Tighe BJ. *Biodegradable polymers in advances in pharmaceutical sciences*. London: Academic Press London; 1992.
- [6] Bogaert JC, Coszach P. Poly(lactic acids): a potential solution to plastic waste dilemma. *Macromolecular Symposia* 2000;153:287.
- [7] Dorgan JR, Lehermeier HJ, Palade LI, Cicero J. Thermal and rheological properties of commercial-grade poly(lactic acid)s. *Macromolecular Symposia* 2001;175:55.
- [8] Tsuji H, Ikada Y. Crystallization from the melt of poly(lactide)s with different optical purities and their blends. *Macromolecular Chemistry and Physics* 1996;197:3483.
- [9] Sarasua JR, Prud'homme RE, Wisniewski M, Le Borgne A, Spassky N. Crystallization and melting behavior of polylactides. *Macromolecules* 1998;31:3895.
- [10] Miyata T, Masuko T. Crystallization behaviour of poly(L-lactide). *Polymer* 1998;39:5515.
- [11] Dattaa R, Tsaia SP, Bonsignorea P, Moona SH, Frank JR. Technological and economical potential of poly(lactic acid) and lactic acid derivatives. *FEMS Microbiology Reviews* 1995;16:221.
- [12] Vink ETH, Rabago KR, Glassner DA, Gruber PR. Applications of life cycle assessment to nature works polylactide (PLA) production. *Polymer Degradation and Stability* 2003;80(3):403–19.
- [13] Santonja-Blasco L, Contat-Rodrigo L, Moriana-Torró R, Ribes-Greus A. Thermal characterization of polyethylene blends with a biodegradable masterbatch subjected to thermo-oxidative treatment and subsequent soil burial test. *Journal of Applied Polymer Science* 2007;106:2218–30.
- [14] Moriana-Torró R, Contat-Rodrigo L, Santonja-Blasco L, Ribes-Greus A. Thermal characterization of photo-oxidized HDPE/Mater-Bi and LDPE/Mater-Bi blends buried in soil. *Journal of Applied Polymer Science* 2008;109:1177–88.
- [15] Torres A, Li SM, Roussos S, Vert M. Poly(lactic acid) degradation in soil or under controlled conditions. *Journal of Applied Polymer Science* 1998;62(13):2295–302.
- [16] Hakkarainen M. Aliphatic polyesters: abiotic and biotic degradation and degradation products. *Advances in Polymer Science* 2002;157:113–38.
- [17] Ho KGL, Pometto AL, Hinz PN. Effects of temperature and relative humidity on polylactide acid plastic degradation. *Journal of Environmental Polymer Degradation* 1999;7:83–92.
- [18] Mc Neill IC, Leiper HA. Degradation studies of some polyesters and polycarbonates. II: polylactide: degradation under isothermal conditions, thermal degradation mechanism and photolysis of the polymer. *Polymer Degradation and Stability* 1985;11(4):309–26.
- [19] Ramis XC, Salla JM, Morancho JM, Vallés A, Contat L, Ribes A. Thermal degradation of polypropylene/starch-based materials with enhanced biodegradability. *Polymer Degradation and Stability* 2004;86:483–91.
- [20] Alvarez VA, Vázquez A. Thermal degradation of cellulose derivatives/starch blends and sisal fibre biocomposites. *Polymer Degradation and Stability* 2004;84:13–21.
- [21] Wunderlich B, editor. *Thermal analysis of polymeric materials*. Berlin: Springer; 2005.
- [22] Khawam A, Flanagan DR. Solid-state kinetic models: basics and mathematical fundamentals. *Journal of Physical Chemistry Part B* 2006;110:17315–28.
- [23] *Techniques and Applications*. In: Brown M, editor. Introduction to thermal analysis. 2nd ed. Secaucus, NJ, USA: Kluwer Academic Publishers; 2001.
- [24] Brown ME, Vyazovkin S, Nomen R, Sempere J, Burnham A, Opfermann J, et al. Computational aspects of kinetic analysis. Part A: the ICTAC kinetics project-data, methods and results. *Thermochimica Acta* 2000;355:125–43.
- [25] Friedman HL. Kinetics and gaseous products of thermal decomposition of polymers. *Journal of Macromolecular Science Part A* 1967;1(1):57–79.
- [26] Flynn JH, Wall LA. A quick, direct method for the determination of activation energy from thermogravimetric data. *Journal of Polymer Science* 1966;4:323–42.
- [27] Ozawa T. Kinetic analysis of derivative curves in thermal analysis. *Journal of Thermal Analysis* 1970;2:301.
- [28] Doyle CD. Series approximations to the equation of thermogravimetric data. *Nature* 1965;207:290.
- [29] Kissinger HE. Reaction kinetics in differential thermal analysis. *Analytical Chemistry* 1957;29(11):1702–6.
- [30] Criado JM. Kinetic analysis of DTG data from master curves. *Thermochimica Acta* 1978;24:186–9.
- [31] Coats AW, Redfern JP. Kinetic parameters from thermogravimetric data. *Nature* 1964;68(201):4914.
- [32] Moriana Rosana, Badía JD, Santonja-Blasco L, Ribes-Greus A. Assessing the mechanical enhancement and the thermostabilising effect of adding cotton fibres to a starch-based matrix using thermal analysis, in preparation.
- [33] ISO 846, 1997. *Plastics – determination of behaviour under the action of microorganisms. Evaluation by visual examination or measurement of changes in mass or physical properties*.
- [34] Liua X, Zoub Y, Lia W, Caoa G, Chen W. Kinetics of thermo-oxidative and thermal degradation of poly(D, L-lactide) (PDLLA) at processing temperature. *Polymer Degradation and Stability* 2006;91(12):3259–65.
- [35] Pérez-Maqueda LA, Sánchez-Jiménez PE, Criado JM. Kinetic analysis of solid-state reactions: precision of the activation energy calculated by integral methods. *International Journal of Chemical Kinetics* 2005;37:658–66.
- [36] Stoeva St, Gjurova K, Zagorcheva M. Thermal analysis study on the degradation of the solid-state chlorinated poly(ethylene). *Polymer Degradation and Stability* 2000;67:117–28.
- [37] Li L, Guan C, Zhang A, Chen D, Qing Z. Thermal stabilities and the thermal degradation kinetics of polyimides. *Polymer Degradation and Stability* 2004;84:369–73.
- [38] Sun JT, Huang YD, Gong GF, Cao HL. Thermal degradation kinetics of poly(methylphenylsiloxane) containing methacryloyl groups. *Polymer Degradation and Stability* 2005;91:339–46.
- [39] Meng X, Huang Y, Yu H, Lu M. Thermal degradation kinetics of polyimide containing 2,6-benzobisoxazole units. *Polymer Degradation and Stability* 2007;92:962–7.

- [40] Chen Y, Wang Q. Thermal oxidative degradation kinetics of flame-retarded polypropylene with intumescent flame-retardant master batches in situ prepared in twin-screw extruder. *Polymer Degradation and Stability* 2007;92:280–91.
- [41] Budrugaec P, Segal E, Pérez-Maqueda LA, Criado JM. The use of the IKP method for evaluating the kinetic parameters and the conversion function of the thermal dehydrochlorination of PVC from non-isothermal data. *Polymer Degradation and Stability* 2004;84(2):311–20.
- [42] Grausea G, Ishibashia J, Kamedaa T, Bhaskarb T, Yoshioka T. Kinetic studies of the decomposition of flame retardant containing high-impact polystyrene. *Polymer Degradation and Stability* 2010;95:1129–37.
- [43] Proikakis CS, Mamouzelos NJ, Tarantili PA, Andreopoulos AG. Swelling and hydrolytic degradation of poly(D, L-lactic acid) in aqueous solutions. *Polymer Degradation and Stability* 2006;91(3):614–9.
- [44] Zhang X, Wyss UP, Pichora D, Goosen MFA. An investigation of poly (lactic acid) degradation. *Journal of Bioactive and Compatible Polymers* 1994;9:80.
- [45] Gupta AP, Deshmukh VG. Thermal oxidative degradation of poly-lactic Acid; Part I: activation energy of thermal degradation in air. *Colloid and Polymer Science* 1982;260:11.
- [46] Kopinke FD, Remmler M, Mackenzie K, Möder M, Wachsen O. Thermal decomposition of biodegradable polyesters—II. Poly(lactic acid). *Polymer Degradation and Stability* 1996;53(3):329–42.

6. REMARKABLE RESULTS

Burial in soil was an effective degradation method to simulate the environmental conditions subjected by PLA goods under non-controlled disposal. The changes in its physical and chemical properties could effectively be assessed by Thermal Analysis Techniques, in comparison with Molar Mass Characterization. The analytical methodology stood out as an interesting option for characterizing the macroscopic changes on PLA structure, as well as for establishing new insights on the morphological rearrangements involved during the biodegradation process. The main significant remarks are listed as follows, according to the next issues:

Selection of indicators

Different degradation indicators were highlighted: relative structural relaxation enthalpy; thermal expansion coefficient; onset, endset and peak cold crystallization and melting temperatures and enthalpies, as well as decomposition temperatures and kinetic parameters such as the apparent activation energy and the kinetic model.

A kinetic analysis methodology, consisting in the combination of five different methods (namely Friedman, Flynn-Wall-Ozawa, Kissinger, Criado and Coats-Redfern) allowed the determination of the evolution for the kinetic triplet of thermal decomposition of PLA throughout the degradation in soil process.

Effects of degradation in soil

The PLA thermal decomposition mechanism was influenced by the biodegradation in soil. Two competitive different decomposition models: a Nucleation model (A2), which gave importance to specific decomposition sites; and a Reaction Contracting model (R3), which represented a particles release generalized on the whole polymer surface, ruled the thermal decomposition.

After 300 days of burial, an increasing crystalline fraction (during the DSC run, due to the presence of shorter PLA chains) experienced a change from a uni-modal towards a multi-modal melting behaviour, coinciding with the macroscopic molar mass decrease. These facts stress the relation between the heterogeneity acquired by PLA after chain scissions and the notable loss of properties due to a remarkable reduction in molar mass.

CHAPTER VI

CONCLUSIONS

1. CONCLUSIONS

The waste management processes such as material, energetic and biological valorisations on two key polyesters of the packaging industry, poly (ethylene terephthalate) (PET) and polylactide (PLA) require a rigorous assessment of the material properties along the whole life cycle.

Several analytical strategies were used to propose the reliability of specific indicators of degradation to monitor the variations in the physico-chemical properties of the polymers, in correlation with the performance of PET and PLA.

The control and monitoring of the proposed quality indicators may be a useful tool for ascertaining a suitable waste management, in terms of optimizing the successive service lives of the materials and reducing the amount of plastic wastes in the packaging sector.

The conclusions obtained in this thesis were classified according to the following issues:

Effects of material valorisation

The DoE analysis on MALDI-TOF MS sample preparation

The quality of the experimental sample preparation in MALDI-TOF MS measurements was improved by the application of a statistical Design of Experiments (DoE).

The choice of matrix, analyte-to-matrix proportion and use of cationization agent were suitable parameters to be considered as factors for the DoE analysis.

Quality parameters of the MALDI signal such as signal-to-noise ratio (S/N) and resolution (RES) were shown to be appropriate for data interpretation.

The application of DoE for the improvement of the MALDI measure of PET stated that the best combination of levels and factors was the following: matrix (dithranol), proportion analyte/matrix/cationization agent (1/15/1 V/V/V), and concentration of cationization agent ($2\text{g}\cdot\text{L}^{-1}$).

The application of DoE for the enhancement of the MALDI measure of PLA showed that the best combination of factors and levels was: matrix (s-DHB), proportion analyte/matrix (1/5/1 V/V/V), and use of cationization agent (NO).

Combination of techniques for the analysis of PET and PLA performance after material valorisation

The synergetic application of structural (Mass Spectrometry *MALDI-TOF MS*, Fourier-Transform Infrared Analysis *FTIR*, viscosimetry), thermal (Differential Scanning Calorimetry *DSC*) and thermomechanical (Dynamic Mechanical Thermal Analysis *DMTA*) analytical techniques showed to be a powerful combination to assess the effects of material valorisation on PET and PLA, in comparison with other techniques traditionally used in the industry such as Melt-Flow Rate *MFR*, tensile or impact tests.

Structural changes

General paths for thermo-mechanical degradation were proposed for both polymers, pointing out the action of intramolecular transesterifications and homolytic scissions.

The ether links units of PET acted as potential degradation sites, since they suffered the reduction of diethylene glycol to ethylene glycol units in the flexible part of the PET backbone. Degradation primarily affected to initially predominant cyclic species, by dramatically decreasing the abundance of $[\text{GT}_\text{C}]_n\text{-G}$ species, which was mainly transformed into $[\text{GT}_\text{C}]_n$, $\text{H-}[\text{GT}_\text{L}]_n\text{-GH}$ and $\text{H-}[\text{GT}_\text{L}]_n\text{-OH}$.

In the case of PLA, the thermo-mechanical degradation primarily affected to initially predominant cyclic $[LA_C]_n$ and linear $HO-[LA_L]_n-H$ species, giving rise to a major abundance of $CH_3-O-[LA_L]_n-H$ species.

The occurrence of chain scissions in PET and PLA could be monitored by:

- the study of the promotion of $-OH$ terminated species and reduction of initially cyclic oligomers by *FTIR* and *MS*.
- the evolution of the intrinsic viscosity,
- the progress of the crystallization exotherm -in terms of specific enthalpy Δh_C and temperatures T_{C0} , T_C , and the melting endotherm in terms of partial areas or partial crystallinity degrees, or
- the variation of the dynamic fragility parameters by DMTA.

Microstructural changes

The use of a three-fraction model, which involves the interaction between crystalline (C) and mobile (MAF) and rigid amorphous fractions (RAF), was significant to correlate the microstructural changes to the thermal and mechanical performance of mechanically reprocessed PET.

Successive extrusion or injection operations modified the microstructure of PET, with the earlier and steeper formation of crystalline fractions of small lamellar thickness with each processing cycles. The extrusion was more aggressive giving higher crystallinity and more extended crystal segregation than during injection moulding, since the operational parameters during the latter were better controlled.

According to a three-fraction model, the rearrangement of chains of PET after cleavage of the MAF due to multi-injection cycles, was promoted towards the formation of RAF, which ruled the further thermal and mechanical performance of PET recyclates.

Conversely, multi-injected PLA did not show formation of crystalline domains due to reprocessing, and thus remained amorphous for all recyclates. However, the cold-crystallization during the 2nd DSC heating suggested the apparition of shorter chains after each processing cycle, as also suggested by the reduction of the partial area at low melting temperatures.

Effects on chain mobility

The packing behavior after rearrangement showed different effects for PET and PLA. The former presented a drop in chain connectivity, due to decoupling of mobile (MAF) and rigid (C, RAF) phases, with an increase in free volume and a decrease in dynamic fragility. PLA showed bigger resistance to changes due to its amorphous character, but after the second recyclate, more packing defects (although in less extent than that shown by PET) were found.

Influence on the mechanical performance

The role of the RAF in PET, which acted as initiator of crystallinity during the strain of the tensile testing, caused a significant decrease in the mechanical parameters (stress and strain at break), in comparison to those shown by PLA (inherently lower than those of PET). The increase of crystalline fraction acted as a topological constraint for the impact of PET, while the amorphous PLA did not showed a critical drop of impact properties.

Suitability of material valorisation for PET and PLA

It was shown that PET suffered a general loss of properties after the second reprocessing step, arriving to a ground viscosity, and it should be considered its threshold for mechanical recycling. On the other hand, PLA could be considered more appropriate for material valorisation than PET since the changes after the second injection cycle were

less abrupt with no ground viscosity value, and only significant in terms of segmental dynamics.

Effects of energetic valorisation

A complete description of the energetic valorisation options

An exhaustive analysis by means of Thermogravimetric Analysis *TGA* to compare the thermal and thermo-oxidative decomposition processes of virgin and reprocessed PET and PLA was given, as an approach for the application of pyrolysis and combustion in full-scale systems.

The thermal stability was studied in terms of the Thermal Decomposition Behavior (*TDB*), which permitted to predict the thermal performance of the materials under any linear heating profile. The Zero-Decomposition Temperatures (*ZDT*) and particularly the use of the peak ZDT_p were proposed as proper indicators of thermo-mechanical degradation to monitor the weakening of the material against both thermal and thermo-oxidative decompositions.

The suitability of the use of 2D-correlation IR spectra to monitor the release of gases from pyrolytic and combustion decompositions was proven.

A kinetic analysis methodology, consisting in the combination of six different methods (namely Flynn-Wall-Ozawa, Kissinger-Akashira-Sunose, Vyazovkin or Advanced Isoconversional method, Master-Curves/Criado and Perez-Maqueda Criterion along with Coats-Redfern equation) was thoroughly applied, and its validity for being used with both constant and variable kinetic parameters was demonstrated. The reliability of a simplified kinetic triplet, where thermal activation parameters can be considered constant was guaranteed under thermal decomposition.

Profiles of decomposition

Under inert atmosphere, both virgin PET and PLA, as well as their successive 5 recyclates, described a mass-loss process driven by one stage of thermal decomposition. On the contrary, under oxidizing conditions, they were driven by two thermo-oxidative decomposition stages. The first step could be ascribed to the pyrolysis of the backbone in both cases, while the second mass-loss step was related to the decomposition of the remaining char, more present in PET (~20%) than in PLA (~2%).

Evolved-gas analysis

Under inert atmosphere, VPET mainly released acetaldehyde and, with less presence benzaldehyde, followed by a release of CO and CO₂, being the emission of the latter followed at higher temperatures. Under oxidative atmosphere, the decomposition occurred firstly releasing mainly acetaldehyde, followed by a noticeable production of CO₂. In the case of PLA, similar profiles were encountered except for the presence of benzene-containing species. Thus, main evolved gases were acetaldehyde, lactide and short-chain acids, as well as CO, CO₂ and H₂O.

The gas emission profiles given by virgin PET and PLA were also showed by all respective recyclates, thus the transfer of technologies for the control of emitted gases could be straightforward.

Kinetic analysis

The kinetic model that mathematically described the thermal and thermo-oxidative decompositions of PET, PLA and their recyclates was of the type A_n: nucleation and growth, which gave importance to the formation of gas bubbles in the melt.

Energetic valorization of mechanically recycled PET and PLA

Focusing on each process, under Argon, the recyclates needed more energy and temperatures to decompose than virgin materials whereas under O₂, the decomposition of all recyclates was overcome at lower E_a than that of virgin materials. Thus controlled combustion could be an option to valorise both materials energetically.

Effects of biological valorisation

The use of thermal analysis for the characterisation of degradation in soil

The application of *DSC*, *DMTA* and *TGA*, proposed as suitable techniques alternative to traditional methods for monitoring the effects of degradation in soil on PLA, showed that indicators such as the relative structural relaxation enthalpy, the thermal expansion coefficient, the cold-crystallization parameters, the decomposition temperatures and kinetic parameters were relevant for the evaluation.

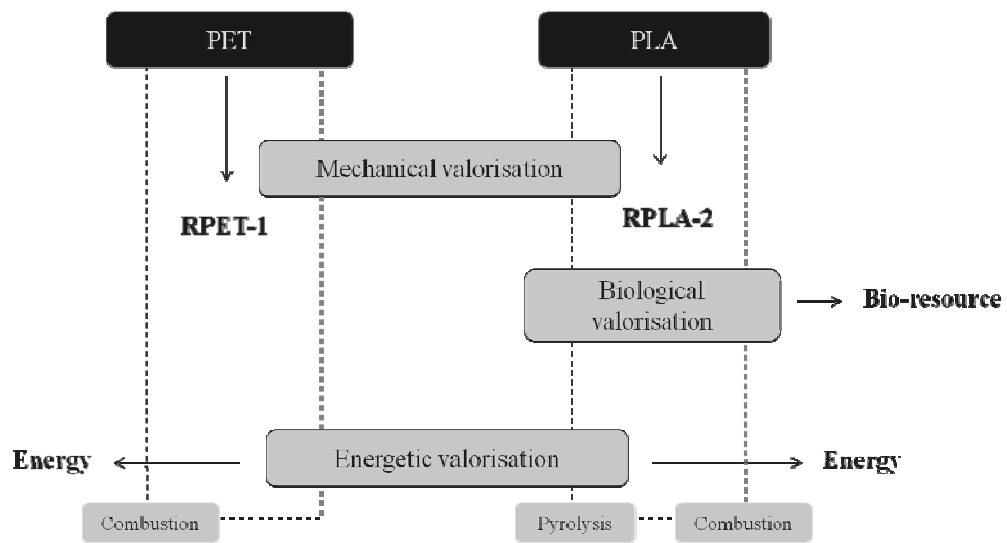
Effects of biodegradation

Particularly after 300 days of burial, an increasing formation of crystalline domains during the DSC-heating run was indicative of chain scission, coinciding with the macroscopic molar mass decrease.

A sustainable plastic waste management

A brief summary of the suitable valorisation processes for a sustainable plastic waste management of PET and PLA is discussed. The mechanical recycling of both polymers should be promoted in order to obtain as much profit as possible from the materials themselves. One cycle of injection is advised in the case of PET, while up to 2 cycles could be applied for PLA without a dramatic loss of performance. Afterwards, in the case of PLA, as bio-based product, the optimal management option would be the biological valorisation, but if the rates of plastic waste increased to levels at which the facilities

could not cover the demand, the energetic valorisation would be recommendable. Both pyrolysis and controlled combustion could be applied, although combustion is less energy-demanding. In the case of PET, the energetic valorisation by controlled combustion could be the optimal procedure for treating its wastes, since applying pyrolysis would require further treatment of char. In any case, the disposal option is discarded. A summary of this discussion can be followed in the figure below.



2. CONCLUSIONES

Los procesos de gestión de residuos plásticos, tales como las valorizaciones material, energética y biológica en dos poliésteres clave de la industria del embalaje, el poli (tereftalato de etileno) (PET) y polilactida (PLA), requieren una evaluación rigurosa de sus propiedades a lo largo del ciclo de vida.

En este trabajo se emplearon diversas estrategias de análisis para proponer indicadores específicos fiables que permitan monitorizar las variaciones en las propiedades físico-químicas de los polímeros PET y PLA durante su uso y su consecuente degradación.

El control y seguimiento de los indicadores de calidad propuestos pueden ser una herramienta útil para favorecer una adecuada gestión de los residuos, en términos de optimización de la vida en servicio de los materiales y de reducción de la cantidad de residuos plásticos en el sector del embalaje.

Las conclusiones obtenidas en esta tesis se clasificaron en base a las siguientes temáticas:

Efectos de la valorización material

Análisis DoE de la preparación de muestras de ensayos MALDI-TOF MS

La aplicación de un diseño estadístico de experimentos (DoE) permitió mejorar la calidad de la señal de ensayos de espectrometría de masas MALDI-TOF MS a partir de una correcta preparación experimental de muestras.

La elección de la matriz, la proporción analito/matriz y el uso de agentes de cationización fueron los parámetros adecuados para ser considerados como factores para el análisis del DoE.

Se mostró la idoneidad de los parámetros de calidad de las medidas de MALDI-TOF MS como la relación señal/ruido (S/N) y resolución de pico (RES) para ser empleados como efectos en el DoE.

La aplicación de DoE para la mejora de la medida de MALDI para PET estableció que la mejor combinación de los niveles y los factores fue la siguiente: la matriz (dithranol), la proporción de analito/ matriz /agente de cationización (1/15/1 V /V/ V), y la concentración del agente de cationización ($2 \text{ g} \cdot \text{L}^{-1}$).

La aplicación de DoE para la mejora de la medida de MALDI para PLA mostró que la mejor combinación de factores y niveles fue: la matriz (s-DHB), la proporción de analito / matriz (1/5 V/V), sin necesidad de agente cationización (NO).

Combinación de técnicas para el análisis del rendimiento de PET y PLA tras la valorización material

La aplicación sinérgica de técnicas analíticas estructurales (espectrometría de masas MALDI-TOF MS, Análisis infrarrojo con Transformada de Fourier FTIR, viscosimetría), térmicas (Calorimetría Diferencial de Barrido DSC) y termo-mecánicas (Análisis Dinamo-Mecánico-Térmico DMTA) es una combinación eficaz para evaluar los efectos de la valorización material de PET y PLA, en comparación con otras técnicas utilizadas tradicionalmente en la industria como índice de masa fluida MFR o los ensayos mecánicos de tracción o de impacto.

Cambios estructurales

Se han propuesto los mecanismos de degradación termo-mecánica para ambos polímeros.

Las reacciones más frecuentes son las transesterificaciones intramoleculares y las escisiones homolíticas.

Los enlaces éter de PET son los puntos lábiles de las cadenas en el proceso de degradación, ya que potencian la reducción de dietilenglicol a etilenglicol en la parte flexible de la cadena principal de PET. La degradación afecta principalmente a las especies cíclicas, inicialmente predominantes, reduciendo drásticamente la abundancia de especies $[GT_C]_n-G$, que se transforman principalmente en $[GT_C]_n$, $H-[GT_L]_n-GH$ y $H-[GT_L]_n-OH$.

En el caso de PLA, la degradación termo-mecánica afecta principalmente a las especies inicialmente predominantes cíclica $[LA_C]_n$ y lineal $HO-[LA_L]_n-H$, dando lugar a una mayor abundancia de especies $CH_3-O-[LA_L]_n-H$.

Las escisiones de cadenas en PET y PLA se pudieron monitorizar por:

- El estudio mediante FTIR y MS de la aparición de especies $-OH$ y la desaparición de grupos cíclicos,
- la evolución de la viscosidad intrínseca,
- la evolución de las exotermas de cristalización, en términos de entalpía específica y temperaturas de inicio y pico de la cristalización, así como de las endotermas de fusión, en términos de áreas parciales o grados parciales de cristalinidad,
- la variación de los parámetros de fragilidad dinámica obtenidos mediante DMTA.

Cambios microestructurales

El uso de un modelo de tres fracciones, que implica la interacción entre las fracciones cristalina (C) y amorfas móvil (MAF) y rígida (RAF), fue significativa para correlacionar los cambios microestructurales con las prestaciones térmicas y mecánicas del PET reprocesado mecánicamente.

La aplicación de operaciones sucesivas de extrusión o inyección modificaron la microestructura del PET, con una formación de fracciones cristalinas de pequeño espesor lamelar, a temperaturas más bajas y más pronunciada con cada ciclo de procesado. La extrusión fue más agresiva que el moldeo por inyección, obteniéndose una mayor cristalinidad y mayor segregación de los tamaños cristalinos.

De acuerdo con un modelo microestructural de tres fracciones, la reordenación de las cadenas de PET después de la escisión de la MAF debido a los ciclos de inyección, favorece la formación de la RAF, lo que modifica el comportamiento térmico y mecánico del PET reciclado.

Por el contrario, tras sucesivas inyecciones de PLA, éste no muestra la formación de dominios cristalinos debido al reprocesado, de modo que permanece amorfo durante todos los reciclados. Sin embargo, la cristalización en frío durante el segundo calentamiento de DSC sugiere la aparición de cadenas más cortas después de cada ciclo de procesado, lo que también apunta la reducción del área parcial del pico de fusión a baja temperatura.

Efectos sobre la movilidad de cadenas

El comportamiento de empaquetado y reordenamiento de las cadenas tiene efectos diferentes para PET y PLA.

El PET muestra una caída de la conectividad de las cadenas, debido a la disociación de la fracción móvil (MAF) y rígida (C, RAF), con un incremento en el volumen libre y una disminución en la fragilidad dinámica.

El PLA presenta una mayor resistencia a los cambios debido a su carácter amorfo, pero después de que el material fuera reciclado dos veces, se encontraron mayores defectos de empaquetamiento, aunque en menor medida a los mostrados por PET.

Influencia en el comportamiento mecánico

El papel de la RAF en PET, que actúa como iniciador de la cristalinidad durante el ensayo a tracción, provoca una disminución significativa en los parámetros mecánicos (tensión y deformación a la rotura), en comparación con los mostrados por PLA (inherentemente inferiores a los de PET). El aumento de la fracción cristalina actúa como una restricción topológica para el impacto del PET, mientras que el PLA amorfo no muestra una caída importante en las propiedades de impacto.

Eficacia de la valorización material de PET y PLA

Se ha demostrado que el PET sufre una pérdida general de las propiedades después de dos ciclos de reprocesado, llegándose a una viscosidad baja tope, pudiéndose considerar un umbral para el reciclado mecánico. Por otro lado, el PLA puede ser más apropiado para la valorización material que el PET ya que los cambios después del segundo ciclo de inyección fueron menos abruptos, sin valor límite de viscosidad, y sólo significativos en términos de fragilidad dinámica.

Efectos de la valorización energética

Descripción de la valorización energética

Se aplicó un análisis exhaustivo por medio de análisis termogravimétrico TGA para comparar los procesos de descomposición térmica y termo-oxidativa de PET virgen y reprocesado y PLA, como una primera aproximación a la aplicación de la pirólisis y combustión en sistemas a gran escala.

La estabilidad térmica se estudió en términos de comportamiento de descomposición térmica (TDB), que permite predecir el comportamiento térmico de los materiales correspondientes a cualquier perfil lineal de calentamiento. Las temperaturas de descomposición cero (ZDT) y en particular el uso de la ZDT pico (ZDT_p) se tomaron como indicadores de degradación termo-mecánica, para así controlar el debilitamiento del material frente a las descomposiciones térmica y térmico-oxidativa.

Se probó la idoneidad de la utilización de la espectroscopia IR con correlación 2D (2D-IR) para controlar la emisión de gases de combustión y descomposición pirolítica. Asimismo, se propuso una metodología de análisis cinético, que consiste en la combinación de seis métodos diferentes (Flynn-Wall-Ozawa, Kissinger-Akashira-Sunose, Vyazovkin o el método Isoconversional avanzado, Master-Curves/Criado, Criterio Pérez-Maqueda, junto con la ecuación de Coats-Redfern) y se demostró su validez para su uso con los parámetros cinéticos constantes y variables. La fiabilidad de una tripleta cinética simplificada, donde los parámetros de activación térmica pueden considerarse constantes se garantiza en el caso de la descomposición térmica.

Perfiles de descomposición

Bajo atmósfera inerte, tanto el PET como el PLA vírgenes, así como sus sucesivos reciclados, se describe un proceso de pérdida de masa en una única etapa de descomposición térmica. Por el contrario, bajo condiciones oxidativas, la descomposición térmica se produce mediante dos etapas. La primera etapa se atribuye a la pirólisis de la cadena principal en ambos casos, mientras que la segunda etapa está asociada a la descomposición del residuo restante, más presente en el PET (20%) que en el PLA (~2%).

Análisis de gases emitidos

Bajo atmósfera inerte, VPET principalmente emite acetaldehído y, con menor presencia, benzaldehído, seguida de una liberación de CO y CO₂, siendo la emisión de este último continuada a temperaturas más altas. Bajo atmósfera oxidante, la descomposición produjo en primer lugar la liberación de acetaldehído, seguido por una notable producción de CO₂. En el caso de PLA, se encontraron perfiles similares, con excepción de la presencia de compuestos bencénicos. Por lo tanto, los principales gases desprendidos fueron acetaldehído, ácidos lácticos de cadena corta, así como CO, CO₂ y H₂O.

Los perfiles de las emisiones de gases definidos para PET y PLA vírgenes se encontró también para todos sus respectivos materiales reciclados, y por tanto la transferencia de tecnologías para el control de los gases de misión es viable.

El análisis cinético

El modelo cinético que describe matemáticamente la descomposición térmica y termo-oxidativa de PET, PLA y sus materiales reciclados es del tipo A_n: nucleación y crecimiento, lo que da importancia a la formación de burbujas de gas en la masa fundida.

Valorización energética de la PET y PLA reciclados

Centrándose en cada proceso, en atmósfera de argón, los productos reciclados necesitan más energía y temperaturas más altas para descomponerse que los vírgenes, mientras que bajo O₂, la descomposición de todos los materiales reciclados ocurre a menor *E_a* que los materiales vírgenes. Así, la combustión controlada puede ser una opción factible para valorar energéticamente ambos materiales.

Efectos de la valorización biológica

El uso del análisis térmico para la caracterización de la degradación en el suelo

La aplicación de DSC, TGA y DMTA, propuestas como técnicas analíticas alternativas a los métodos tradicionales para controlar los efectos de la degradación del suelo en el PLA, demostró que indicadores tales como la entalpía de la relajación estructural, el coeficiente de expansión térmica, los parámetros de cristalización en frío, las temperaturas de descomposición y los parámetros cinéticos fueron relevantes para la evaluación.

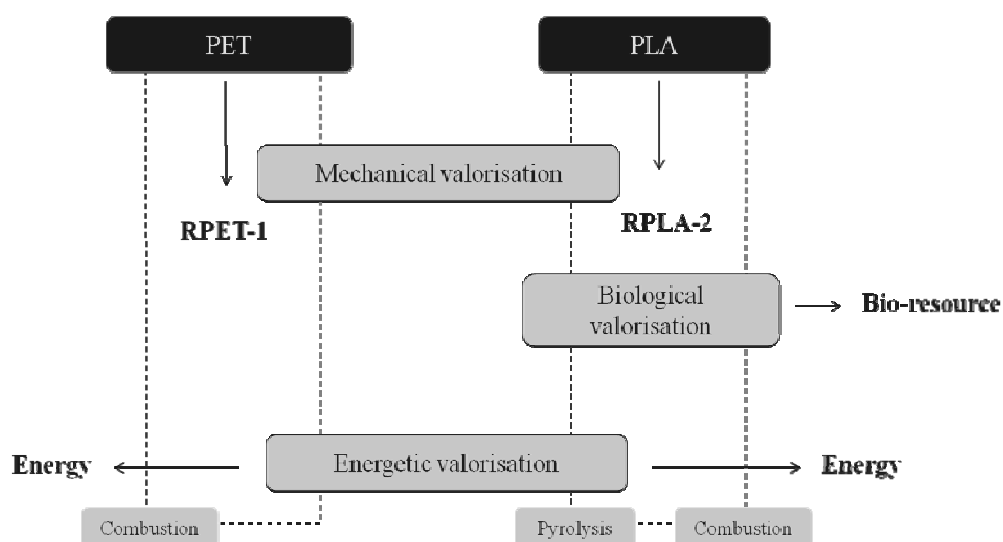
Efectos de la biodegradación

Después de 300 días de degradación en tierra, la formación cada vez mayor de dominios cristalinos durante la ejecución del ensayo de calentamiento en DSC fue indicativo de procesos de escisión de cadena, coincidiendo con la disminución de la masa molar.

Un modelo de gestión sostenible de residuos plásticos

Los procesos de valorización adecuados para una gestión sostenible de los residuos de plástico de PET y PLA deben entenderse de forma integrada. El reciclado mecánico de los polímeros se debe favorecer con el fin de obtener las mayores prestaciones posibles de los propios materiales en servicio. Un ciclo de inyección se recomienda en el caso de PET, mientras que más de 2 ciclos se podrían aplicar para PLA, sin pérdida considerable de rendimiento. Posteriormente, en el caso de PLA, como bio-producto, la opción de gestión óptima sería su gestión mediante valorización biológica, pero si las tasas de residuos plásticos aumentaran a niveles en los que las instalaciones no pueden cubrir la demanda, la valorización energética sería recomendable. Tanto la

pirólisis como la combustión controlada se podrían aplicar, aunque la combustión demanda menor energía. En el caso del PET, la valorización energética por combustión controlada podría ser el procedimiento más adecuado para el tratamiento de sus residuos, ya que la aplicación de la pirólisis requeriría el tratamiento posterior del residuo. En cualquier caso, la opción de vertido se descarta. Un resumen de la combinación eficaz de procesos de valorización puede seguirse en la figura siguiente:



3. FUTURE RESEARCH LINES

In order to promote the studies performed in this thesis and to widen the studies in the framework of bio-based polymers for the packaging industry, the following research lines could be implemented in several directions:

- To upgrade mechanically-recycled PLA in order to enlarge its service life before further management.
- To study the energetic valorisation of PET and PLA in medium-scale systems for pyrolysis, combustion or gasification, with the aim of optimizing the energetic rates.
- To explore the microbiological world in search for specific microorganisms capable of biodegrading both PET and PLA, in order to tailor the bio-disposal processes and transfer them to full systems for biological valorisation.
- To study the use of composting for the biological valorisation of reprocessed PLA. It is worth remarking that currently the pilot plant is designed and ready to start the study.
- To widen the span of analytical techniques, mainly those focused on the microstructure of the materials, i.e. X-ray scattering or Modulated DSC. As well, to implement analytical methodologies to test the release of low molecular weight compounds by recycled PET and PLA.
- To extent the study of the material, energetic and biological valorisations to PLA blends and composites.

GLOSSARIES

LIST OF TABLES

Table 1. 1. Comparison of typical biodegradable polymer properties with commodities	48
Table 2. 1. Summary of main kinetic models for the analysis of thermal decompositions	127
Table 3.1 . Collection figures of Spanish companies	190
Table IIIA. 1. Fuoss–Kirkwood parameters for virgin and reprocessed PET after loss modulus fitting as a function of temperature	212
Table IIIA. 2. Calorimetric parameters for virgin and reprocessed PET:	213
Table IIIA. 3. Individual melting parameters and partial crystallinity for each population after deconvolution of the melting calorimetric thermograms for virgin and reprocessed PET	214
Table IIIB. 1. Summary of factors, levels and general characteristics of the design of experiments applied in this study.	221
Table IIIB. 2. Results of analysis of variance in terms of p -value ($\alpha=0.05$) after application of the design of experiments to MALDI-TOF-MS spectra of virgin PET	222
Table IIIB. 3. Structures and m/z values for cyclic oligomeric species assigned in the MALDI-TOF MS spectra of virgin and reprocessed PET (for $n = 10, 11$).	226
Table IIIB. 4. Structures and m/z values for linear oligomeric species assigned in the MALDI-TOF MS spectra of virgin and reprocessed PET (for $n = 10, 11$).	226
Table IIIC. 1. Calorimetric parameters	241
Table IIIC. 2. Calorimetric parameters after deconvolution	243
Table IIIC. 3. Results from the assessment of the segmental dynamics	246
Table IIID. 1. Summary of factors, levels and general characteristics of the Design of Experiments applied in this study.	259
Table IIID. 2. Results of Analysis of Variance after application of the Design of Experiments to MALDI-TOF MS spectra of virgin PLA.	261

Table IIID. 3. Relative variations in S/N and RES means taking as reference run (s-DHB, 1/5, NO)	262
Table IIID. 4. Oligomeric species found for PLA by means of MALDI analysis	266
Table IIIE. 1. Results from DSC characterization	290
Table IIIE. 2. Evolution of parameters drawn from DMTA characterization	294
Table IIIE. 1. Results of fitting the viscoelastic behaviour to VFTH model. Fragility parameters: D , B , m .	295
Table 4. 1. Calorific value of some major plastics compared to common fuels	308
Table IVA.1 Algebraic expressions for the kinetic functions of the most common models in solid-state reactions	351
Table IVA.2. Summary of major gases released during thermal and thermo-oxidative decompositions, as observed by FT-IR analysis	354
Table IVA.3. Percentage of mass-loss for virgin PET and its recyclates after thermal and thermo-oxidative decomposition	358
Table IVA.2. Fitting results obtained from modelling the evolution of the characteristic TGA temperatures under inert conditions to TDB equation	361
Table IVA.3. Fitting results obtained from modelling the evolution of the characteristic TGA temperatures to TDB , under oxidative conditions	362
Table IVA.4. Results of fitting procedure to $Ea_{\alpha FWO}$ dependence with α	366
Table IVA.7. Ranges of n for A_n kinetic model	358
Table IVA.5. Results of fitting procedure to $\ln A_{\alpha}$ dependence	370
Table IVA.6. Average values of activation energies obtained by Flynn-Wall-Ozawa (FWO), Kissinger-Akahira-Sunose (KAS) and Vyazovkin (VYZ) methods, and calculation of average activation energy for further analysis, at both testing environments	371
Table IVA.7. Simplified kinetic triplets of virgin PET and its recyclates under thermal and thermo-oxidative decomposition conditions	372
Table IVB. 1. IR absorption bands of evolved gases from thermal and thermo-oxidative decomposition of PLA	387
Table IVB. 2. Fitting results obtained from modelling the evolution of the characteristic TGA temperatures to TDB	390
Table IVB. 3. Ea averages of thermal and thermo-oxidative decompositions obtained by isoconversional methods	395
Table IVB. 4. Algebraic expressions for the kinetic functions of the most common models in solid-state reactions	395
Table IVB. 5. Simplified kinetic triplets for the thermal decomposition of PLA and its recyclates	397
Table IVB 6. Results of fitting of Ea and $\ln A$	397

Table IVB 7. n_{β} :Values of n of the A_n model found for the thermo-oxidative decomposition of PLA and its recyclates at different β ; n' : average of n_{β} ; n'' : values obtained from the minimization method	400
Table VA.1. Calorimetric and viscoelastic parameters related to the glass transition relaxation	446
Table VA.2. Calorimetric and viscoelastic parameters related to the cold crystallization	447
Table VA.3. Calorimetric parameters related to the melting transition	448
Table VB.1. List of common kinetic functions to explain the thermal decomposition mechanisms in bulk polymers	454
Table VB.2. Apparent activation energies values obtained by the Friedman (E_{aF}), Flynn-Wall-Ozawa (E_{aFWO}) and Kissinger (E_{aK}) methods	457
Table VB.3. Results of kinetic methodology. Evolution of kinetic triplet of PLA thermal decomposition throughout the degradation in soil process	458

LIST OF FIGURES

Figure 1. 1. World plastics production in 2009	37
Figure 1. 2. Percentages of European plastic demand in 2009 by segments (commodities + technical polymers)	40
Figure 1. 3. Worldwide production of biomass and use of mankind	42
Figure 1. 4. Development stage of main emerging bio-based material types.	44
Figure 1. 5. Capacity of emerging bio-based plastics by regions, 2003 and 2007	45
Figure 1. 6. Current and emerging (partially) bio-based plastics and their biodegradability	48
Figure 1. 7. General scheme of plastics life-recover-disposal cycle	52
Figure 1. 8. Total recovery ration of post-consumer plastic waste in Europe in 2009	54
Figure 1. 9. Chemical routes for the polymerization of PET	59
Figure 1. 10. World and European supplies and demands of PET	61
Figure 1. 11. Worldwide applications of PET in 2004	62
Figure 1. 12. Stereoisomers of lactic acid.	63
Figure 1. 13. Industrial obtaining of lactic acid	64
Figure 1. 14. Different structures of lactide	65
Figure 1. 15. Synthesis methods for obtaining high molecular weight PLA	66
Figure 1. 16. Synthesis methods for obtaining high molecular weight PLA	67
Figure 2. 1. Raw pellets of PET and PLA	79
Figure 2. 2. Schematic relation between valorisation techniques, degradation induced and pilot plants needed and applied for simulation	81
Figure 2. 3. Extrusion machine and “one-hole mouth”,	82
Figure 2. 4. Schematic reprocessing simulation cycle	83

Figure 2. 5. Machinery employed for simulation of reprocessing for both PET and PLA. D	
ehumidifier, injector, cutting mill	83
Figure 2. 6. Tubular reactor of the thermogravimetric analyze	85
Figure 2. 7. Bio-degradation in soil test	85
Figure 2. 8. Summary of techniques applied, in connection with the analyzed properties	87
Figure 2. 9. A liquid moving at shear rate under an applied stress τ	88
Figure 2. 10. Schematic plots of Newtonian and Non-Newtonian behaviours	89
Figure 2. 10. Comparison of molar masses	92
Figure 2. 11. Cannon-Fenske type capillary viscosimeter	92
Figure 2. 12. Experimental results of viscosimetric experiments for virgin PLA	94
Figure 2. 13. Pictures of experimental test for measuring capillary viscosimetry	95
Figure 2. 15. Desorption/ionization process induced by laser to an analyte embedded in a matrix	97
Figure 2. 14. Schematic representation of a MALDI equipment with reflector	98
Figure 2. 15. MALDI analysis	100
Figure 2. 16. MALDI matrixes used in this thesis	101
Figure 2. 17. MALDI-TOF-MS Bruker Daltonics	105
Figure 2. 18. The electromagnetic spectrum	106
Figure 2. 19. The IR regions in the electromagnetic spectrum	107
Figure 2. 20. Typical beam path configuration of FTIR-ATR	109
Figure 2. 21. Stretching modes of vibration	109
Figure 2. 22. Bending mode of vibration of water (scissoring)	109
Figure 2. 25. Vibrations of the group $-\text{CH}_2-$	110
Figure 2. 23. Picture of used IR spectrometer with ATR accessory	111
Figure 2. 24. Schematic diagram of a scanning electron microscope	112
Figure 2. 25. SEM (left) and sputter coater (right) used for analysis in this thesis	114
Figure 2. 26. Picture of MFR indexer used	115

Figure 2. 27. Stress-strain curve	116
Figure 2. 28. Universal testing machine used for analysis	118
Figure 2. 29. Schematic impact test	119
Figure 2. 30. TG curves of virgin PET and its fifth recycle under inert and oxidative conditions.	122
Figure 2. 31. Application of isoconversional methods to virgin PET	126
Figure 2. 32. Application of Pérez-Maqueda et al. criterion for thermal decomposition of PET	129
Figure 2. 36. Kinetic methodology applied for recycled PET and PLA	129
Figure 2. 37. Kinetic methodology applied for bio-degraded PLA	130
Figure 2. 38. Picture of TGA used in this thesis	131
Figure 2. 39. 3D-IR fishnet representation	133
Figure 2. 40. Schematic representation of external dynamic perturbation for 2D-IR correlation analysis	134
Figure 2. 41. Synchronous 2D-IR correlation spectrum	135
Figure 2.42. Asynchronous 2D-IR correlation spectrum	137
Figure 2. 43. FTIR spectrometer coupled to thermo-balance for analysis of fumes	139
Figure 2. 44. Geometrical disposition of sample and reference holders in the DSC	140
Figure 2. 45. DSC of virgin PLA	141
Figure 2.46. Example of deconvolution applied to melting endotherms of multi-extruded PET	144
Figure 2. 47 Picture of DSC analyzer used in this thesis	144
Figure 2. 48. Electric-like schemes of Maxwell and Voigt-Kelvin models for viscoelasticity of polymers	147
Figure 2. 49. Electric-like scheme to approach the real viscoelastic behaviour of a polymer	149
Figure 2. 50. Phase-lag between stress and strain	149
Figure 2. 51. Schematic representation of a DMTA instrument	151
Figure 2. 52. DMTA devices used in this thesis: MarK IV, DMA/SDTA861°	154

Figure 3. 1. General scheme of material valorisation	166
Figure 3. 2. Material cycle of a plastic package	169
Figure 3. 3. PSW management options in Spain in comparison with the European countries with highest and lowest mechanical recycling percentages	171
Figure 3. 4. Mechanical recycling steps	173
Figure 3. 5. SPI identification code for PET	180
Figure 3. 6. Usage of recycled PET in USA	184
Figure 3. 7. Comparison of energy used for producing Virgin PET to varying levels of recycled PET	186
Figure 3. 8. Comparison of gases released during production of Virgin PET to varying levels of recycled PET	186
Figure 3. 9. Percentages of PET collection of European countries in 2006	189
Figure 3. 10. Distribution of Spanish recycled PET	190
Figure 3. 11. PET production capabilities	190
Figure 3. 12. Scheme of hydrolysis of PET	192
Figure 3. 13. Scheme of esterification of PET	192
Figure 3. 14. Scheme of intramolecular transesterification of PET	193
Figure 3. 15. Scheme of intermolecular transesterification of PET	194
Figure 3. 16. Scheme of hydrolysis of PLA	196
Figure 3. 17. Scheme of esterification of PLA	196
Figure 3. 18. Scheme of intramolecular transesterifications of PLA	196
Figure 3. 19. Scheme of intermolecular transesterifications of PLA.	197
Figure 3. 20. Scheme of chain scission of PLA	197
Figure 3.22. Schematic description of the contributions of this thesis in the field of material valorisation of plastic materials	203
Figure IIIA. 1. Schematic representation of the mechanical recycling simulation procedure by multiple processing and analysis techniques employed	210
Figure IIIA. 2. Evolution of melt-mass flow rate (MFR) through reprocessing simulation	211
Figure IIIA. 3. Effect of reprocessing on the oxidation temperature (T_{Ox}) of PET.	211

Figure IIIA. 4. Reprocessing influence on the dynamic-mechanical behavior of PET	211
Figure IIIA. 5. Loss modulus experimental data fitting to Fuoss–Kirkwood model for virgin PET	211
Figure IIIA. 6. DSC thermograms for virgin and reprocessed PET	212
Figure IIIA. 7. Lamellar thickness distribution evolution for virgin and reprocessed PET	213
Figure IIIA. 8. Deconvolution of the melting calorimetric thermogram into crystalline populations I, II, and III for PET reprocessed 4 times.	214
Figure IIIB. 1. Main effects plot for the analysis of the signal-to-noise (S/N) ratio	223
Figure IIIB. 2. Main effects plot for the analysis of the resolution (RES)	223
Figure IIIB. 3. Interaction plot for the analysis of the signal-to-noise (S/N) ratio	224
Figure IIIB. 4. Interaction plot for the analysis of the resolution (RES)	224
Figure IIIB. . 5. MALDI-TOF MS spectra in the m/z 2300–2400 range to check the applicability of the design of experiments applied	225
Figure IIIB. 6. MALDI-TOF MS spectrum of virgin PET. Inset: zoomed area in the m/z range 1900–2300 for identification of predominant oligomers	225
Figure IIIB. 7. MALDI-TOF MS spectra in the m/z 1900–2100 range to characterize the appearance of oligomeric species due to thermo-mechanical degradation. Zoomed areas represent low abundant oligomeric species	227
Figure IIIB. 8. Normalized ion abundances of PET oligomeric species through the multiple reprocessing cycle	227
Figure IIIB. 9. Proposed mechanisms of thermo-mechanical degradation of PET	228
Figure IIIC. 1. FT-IR analysis of the C-H stretching region	238
Figure IIIC. 2. O-H stretching vibration study	238
Figure IIIC. 3. Evolution of intrinsic viscosity, molar masses and polydispersity index	239
	487

Figure IIIC. 4. Surface analysis by SEM. (upper: VPET, lower: RPET-5)	239
Figure IIIC. 5. Evolution of the balance between crystalline and mobile and rigid amorphous fractions	240
Figure IIIC. 6. C-H vibrations study	240
Figure IIIC. 7. Evolution of DSC cooling thermograms	242
Figure IIIC. 8. Lamellar thickness distributions of virgin and reprocessed PETs.	242
Figure IIIC. 9. Evolution of relative partial crystallinity degrees	243
Figure IIIC. 10. Evolution of loss moduli. Inset: variation of the peak temperatures and the full widths at medium height.	244
Figure IIIC. 11. Angell's plot. Evolution of the fragility index m .	246
Figure IIIC. 12. Variation of mechanical properties as analyzed by tensile and impact testing.	247
Figure IIIC. 13. Evolution of storage moduli at 1 Hz. Inset: variation of mechanical stresses through the reprocessing cycles	248
Figure IIID. 1. Experimental procedure followed for the simulation of degradation induced by PLA due to mechanical recycling and service life	259
Figure IIID. 2. Chemical structures of the matrixes used for the MALDI analysis	260
Figure IIID. 3. Schematic summary of the purpose of combining DOE with MALDI analysis	261
Figure IIID. 4. Main effects plot for the analysis of the signal-to-noise ratio (S/N)	262
Figure IIID. 5. Main effects plot for the analysis of the Resolution (RES)	263
Figure IIID. 6. Interaction Plot for the analysis of the signal-to-noise ratio (S/N)	263
Figure IIID. 7. Interaction Plot for the analysis of the Resolution (RES)	264
Figure IIID. 8. MALDI-TOF MS spectra of PLA at different MALDI sample preparations to check the applicability of the Design of Experiments applied.	265

Figure IIID. 9. Identification of oligomeric species that compose PLA	266
Figure IIID. 10. Proposed degradation mechanism map for polylactide	267
Figure IIID. 11. Influence of thermo-oxidative ageing on the relative abundances of PLA oligomeric species	268
Figure IIID. 12. Influence of thermo-mechanical cycles on the relative abundances of PLA oligomeric species	268
Figure IIIE. 1. SEM pictures of VPLA and RPLA-5.	277
Figure IIIE. 2. Results from tensile and impact testing: (a) Young Modulus and Impact value; (b) Stress and strain at break.	278
Figure IIIE. 3. FT-IR analysis: (a) FT-IR spectra of virgin and fifth reprocessed PLA; (b) evolution of the carbonyl region; (c) variation of the hydroxyl region; (d) changes in functional indexes	278
Figure IIIE. 4. Variation of intrinsic viscosity and molar mass throughout the injection steps. Insert: Detail of calculation of Huggins and Kraemer plots for the case of VPLA	279
Figure IIIE. 5. Evolution of the heating DSC thermograms for VPLA and RPLA-i (i:1-5)	281
Figure IIIE. 6. Results of partial area study after deconvolution of the melting region of the DSC scans	281
Figure IIIE. 7. DMTA spectra of VPLA at 1Hz: (upper) loss modulus; (lower) storage modulus	282
Figure IIIE. 8. Evolution of storage (lower) and loss (upper) moduli at 1 Hz	283
Figure IIIE. 9. Evolution of apparent activation energy associated to the glass-rubber relaxation and coefficient of free volume	284
Figure 4. 1. Recovery ratio of packages in Europe by chemical recycling / energetic valorisation	297
Figure 4. 2. Distribution of goods recovered by chemical recycling and energetic valorisation in Europe	298
Figure 4. 3. Energetic recovery ration in European countries	299
	489

Figure 4. 4. Chemical recycling and energetic valorisation.		
Scheme of technologies	300
Figure 4. 5. Classic pyrolysis scheme in a fluidized bed reactor	303
Figure 4. 6. Gasification process of coal	306
Figure 4. 7. Incineration scheme	309
Scheme 4. 1. Model ester with β -methylene H decomposition	314
Scheme 4. 2. Transesterification reactions in the middle of the chain	315
Scheme 4. 3. Homolytic thermal scissions	316
Scheme 4. 4. Homolytic thermal scissions,	318
Scheme 4. 5. Transesterification reactions of thermal decomposition of PLA	319
Scheme 4. 6. Homolytic reactions of thermal decomposition of PLA	320
Figure IVA. 1. Thermolytic decomposition mechanisms of PET	335
Figure IVA. 2. Combined strategy of assessment	336
Figure IVA. 3. 3D/FT-IR and contour 2D/FT-IR plots of the thermal decomposition of virgin PET	343
Figure IVA. 4. 3D/FT-IR and contour 2D/FT-IR plots of the thermo-oxidative decomposition of virgin PET	343
Figure IVA. 5. FT-IR spectra at the maximum decomposition rate of the thermal decomposition of virgin PET. Details of selected deconvolutions are given inserted	344
Figure IVA. 6. FT-IR spectra at the maximum decomposition rates of the thermo-oxidative decompositions of virgin PET	344
Figure IVA. 7. 2D-IR correlation spectra of the thermal decomposition of virgin PET at selected wavenumber regions	346
Figure IVA. 8. Thermogravimetric curves of virgin PET and its fifth recyclate under both Ar and O ₂ atmospheres	347
Figure IVA. 9. (a) Fitting-Deconvolution applied to virgin PET at experiment performed at 5 °C.min ⁻¹ . (b) Result on the evolution of the conversion degree α	348

Figure IVA. 10. Thermal stability assessments	350
Figure IVA. 11. Thermal stability assessments. Evolution of ZDT at inert (upper) and oxidative (middle) conditions	353
Figure IVA. 12. Thermal stability assessments. Evolution of the peak temperature of the second thermo-oxidative decomposition process of virgin PET	354
Figure IVA. 13. Application of isoconversional methods to virgin PET	355
Figure IVA. 14. Master-Plots in the differential form for virgin and first PET recycle at $5\text{ }^{\circ}\text{C}\cdot\text{min}^{-1}$ for both environments	357
Figure IVA. 15. Variation of $\ln A$ for all materials under inert and oxidative conditions	359
Figure IVA. 16. Application of <i>Pérez-Maqueda et al</i> criterion for the simplified kinetic triplets	360
Figure IVA. 17. Kinetic methodology summary	364
Figure IVB. 1. Summary of thermally-induced decomposition reactions of polylactide	373
Figure IVB. 2. 3D-FTIR spectra of VPLA evolved gases from TGA experiment under inert and oxidative conditions	376
Figure IVB. 3. FTIR spectra of main decomposition products of VPLA under inert and oxidative conditions	376
Figure IVB. 4. 2D correlation spectra of VPLA under inert conditions at different wavenumber ranges	378
Figure IVB. 5. TG curves of virgin and fifth-reprocessed PLA under inert (VPLA, RPLA5) and oxidative (VPLA-O ₂ , RPLA5-O ₂) conditions	379
Figure IVB. 6. Fittings applied to the evolution of the characteristic TGA temperatures for VPLA	380
Figure IVB. 7. Evolution of ZDT under inert and oxidative conditions, ZDT ranges of decomposition at both environments	382
Figure IVB. 8. Evolution through reprocessing cycles of the average isoconversional activation energy of thermal decomposition	383
Figure IVB. 9. Master plots based on the differential and integral forms of the general kinetic law compared to experimental data obtained for thermal decomposition of RPLA-2	386
	491

Figure IVB. 10. Application of Perez-Maqueda et al. criterion to virgin PLA and first reprocessed material	388
Figure IVB. 11. (a) Apparent E_a obtained for VPLA by means of FWO, KAS and AIC methods; (b) Average isoconversional activation energy of VPLA, RPLA-1 and RPLA-2; (c) Evolution of average isoconversional activation energy for RPLA-3, RPLA-4 and RPLA-5	388
Figure IVB. 12. Master plots based on the differential form of the general kinetic law compared to experimental data obtained for thermo-oxidative decomposition of VPLA (hollow circles) and RPLA-1	389
Figure IVB. 13. n evolution for A_n model of thermo-oxidative decomposition of virgin PLA and its successive recyclates	390
Figure IVB. 14. $\ln A$ evolution given for VPLA and RPLA-2	391
Figure IVB. 15. Comparison of experimental DTG curves to computed kinetic functions obtained from the kinetic methodology for VPLA at both studied atmospheres	392
Figure 5. 1. Sustainable polymer production and recycling,	405
Figure 5. 2. Schematic illustration of the changes in a polymer matrix undergone by surface and bulk erosion	409
Figure 5. 3. Assimilation of biodegradable plastics	411
Figure 5. 4. Summary of degradation processes of biodegradable polymers	413
Figure 5. 5. Certified labels of compostability in Europe: DIN CERTCO; AIB Vinçotte; FSWA	417
Figure 5. 6. Certified labels of compostability in USA and Japan	417
Figure 5. 7. PLA hydrolysis and molecular weight loss	422
Figure 5. 8. Diagram of contributions in the field of biological valorisation of PLA	429
Figure VA.1. Summary of parameters used to assess the extent of degradation in soil on polylactide	434
Figure VA.2. Calorimetric and viscoelastic behavior of non-buried polylactide (a) calorimetric thermogram and (b) $\log(E')$ and $\log(E'')$ versus temperature	435
Figure VA.3. Comparative first scan of the calorimetric thermograms at different degradation times	435

Figure VA.4.(a) Effect of degradation in soil on $\log E'$ vs. temperature. (b) Effect of degradation in soil of polylactide on $\log E''$ vs. temperature	436
Figure VA. 5. Arrhenius Maps obtained from multi-frequency DMTA analysis	436
Figure VA.6. Thermal expansion coefficient vs. degradation time	437
Figure VA.7.Crystallization and melting enthalpies vs. degradation time	437
Figure VA.8. Influence of degradation in soil on the lamellar thickness distribution of polylactide	438
Figure VA. 9 . M_n and M_w evolution calculated by GPC	438
Figure VB.1. Methodology applied for the characterisation of the thermal decomposition kinetics of PLA submitted to degradation in soil	445
Figure VB.2. Comparison of the conversion degree evolution and its first-derivative thermogravimetric curve plot for non-degraded PLA and PLA buried during 450 days	446
Figure VB. 4. Kinetic methods applied to non-degraded PLA. a) Friedman method; b) Flynn-Wall-Ozawa method. c) Kissinger method. d) Criado method	446
Figure VB.5. Evolution of the apparent activation energy throughout the degradation in soil process	447
Figure VB.6. Comparison of experimental TG curves (symbols) to fitted kinetic functions (solid lines) obtained from the kinetic methodology	448

GLOSSARY OF TERMS

Acronymous	Meaning
2D-IR	Infrared Correlation in 2 Dimensions
A-2D	Asynchronous 2D-IR EGA Spectra
AIC	Advanced Isoconversional Method
AIMPLAS	Instituto Tecnológico del Plástico
An	Avrami-Erofeyev Model
AP	Autopeak (EGA)
ATR	Attenuated Total Reflection
C	Crystalline
C (Subscript)	Cyclic
C ² D	Cradle-to-Cradle Design
C-R	Coats-Redfern
DEG	Diethylene Glycol
DHB	2,5-dihydroxybenzoic Acid
DMT	Dimethyl terephthalate
DMTA	Dynamic-Mechanical-Thermal Analysis
DoE	Design of Experiments
DSC	Differential Scanning Calorimetry
DTG	Differential Thermogravimetric Curve
ECOEMBES	Ecoembalajes España S.A. (Spanish Integrated MSW Management System)
EDP	Environmentally-Degradable Polymers
EG	Ethylene Glycol
EGA	Evolved-Gas Analysis
EGD	End-Groups Distribution
F	Factors (MALDI analysis)
FA	Ferulic acid
FDA	Food and Drugs Organization
Fn	n-Order Model
FT-IR	Fourier-Transform Infrared Analysis
FWO	Flynn-Wall-Ozawa
G	Glycol Unit
GLM	General Linear Model
GT	PET repeating unit
HABA	2-(4-hydroxyphenylazo) Benzoic Acid
HDPE	High-Density Polyethylene
HFIP	1,1,1,3,3,3-hexafluoro-2-propanol
I	Intensity
IAA	Trans-3-indoleacrylic Acid
IEP	Interaction Effects Plot
ISO	International Standard Organization

IWM	Integrated Waste Management
KAS	Kissinger-Akahira-Sunose
L	Levels (MALDI analysis)
L (subscript)	Linear
L/D	Length to Diameter Ratio in an extruder
LA	Lactic Acid Unit
LCA	Life-Cycle Analysis
LDPE	Low-Density Polyethylene
MAC	Matrix-Analyte-Cationization Agent MALDI set
MAF	Mobile Amorphous Fraction
MALDI	Matrix-Assisted Laser Desorption/Ionization
MEP	Main Effects Plot
MFR	Melt Flow Rate
MMD	Molar Mass Distribution
M-P	Master Plot
M-P _e	Experimental Master-Plots
M-P _f	Master plots based on the differential form of the general kinetic equation
M-P _{fg}	Master plots based on the differential and integral form of the general kinetic equation
M-P _g	Master plots based on the integral form of the general kinetic equation
M-Pt	Theoretical Master Plots
MRF	Municipal Reclamation Facility
MS	Mass Spectrometry
MSW	Municipal Solid Waste
NAPCOR	National Association for PET Container Resources
NaTFA	Sodium Trifluoroacetate
NCP	Negative Cross-Peak (EGA)
NGO	Non-Governmental Organization
NOL	Non-Objection Letter
OECD	Organisation for Economic Cooperation and Development
PCP	Positive Cross-Peak (EGA)
PE	Polyethylene
PET	Poly(ethylene terephthalate)
PFR	Plastic Reclamation Facility
PGA	Polyglycolic Acid
PLA	Poly lactide
P-M _c	Perez-Maqueda et al Criterion
PP	Polypropylene
PPP	People, Planet, Profit or Prosperity
PS	Polystyrene
PSW	Plastic Solid Waste
PVC	Poly(vinyl chloride)
R&D	Research and Development
RAF	Rigid Amorphous Fraction
RES	Resolution
Rn	Contracting Area/Volume Model
ROP	Ring Opening Polymerization

RPET	Reprocessed PET
RPLA	Reprocessed PLA
S/N	Signal-to-Noise Ratio
S-2D	Synchronous 2D-IR EGA Spectra
SA	Sample Analysis
SD	Sustainable Development
SEM	Scanning Electron Microscopy
SKT	Simplified Kinetic Triplet
SP	Sample Preparation
SPI	Society of Plastics Industry
T	Terephthalate Unit
TD	Thermal Decomposition
TDB	Thermal Decomposition Behaviour
TEM	Transmission Electron Microscopy
TG	Thermogravimetric Curve
TGA	Thermogravimetric Analysis
THA	2,4,6-trihydroxy Acetophenone
THF	Tetrahydrofuran
TOD	Thermo-Oxidative Decomposition
TOF	Time-Of-Flight
TPA	Terephthalic Acid
VPET	Virgin PET
VPLA	Virgin PLA
VYZ	Vyazovkin
ZDT	Zero-Decomposition Temperature

MAIN SIMBOLOGY

Symbol	Meaning
α	Conversion degree
A	Pre-exponential Arrhenius Factor
A_M^i	Partial melting area
β	Heating/Cooling rate
C_p	Heat capacity
Δ	Increment
D	Dynamic fragility
E'	Storage modulus
E''	Loss modulus
E_a	Apparent activation energy
ϵ	Elongation at break
$f(\alpha)$	Differential kinetic function
FWMH	Full-Width Medium-High
$g(\alpha)$	Integral kinetic function
h_M	Melting specific enthalpy
h_C	Crystallization specific enthalpy
h_{CC}	Cold-crystallization specific enthalpy
l_C	Lamellar thickness
m/z	Mass-to-charge ratio
η	Viscosity
M_V	Viscous molar-mass
M_n	Number molar-mass
M_w	Weight molar-mass
ϕ	Free-volume coefficient
PDI	Polydispersity index
R^2	Linear regression coefficient
τ	Relaxation time
T_g	Glass-Transition temperature
T_M	Melting temperature
T_C	Crystallization temperature
T_{CC}	Cold-Crystallization temperature
T_P	Peak temperature
T_0	Onset temperature
T_e	Endset temperature
T_K	Kauzmann temperature
T_M^i	Partial melting temperature
X^i	Partial crystallinity degree
X_C	Crystallinity degree

X_{RAF}

Rigid amorphous fraction degree

X_{MAF}

Mobile amorphous fraction degree

EPILOGUE

Pensaments, dedicatòries, agraïments

PENSAMENTS, AGRAÏMENTS, DEDICATÒRIES

No m'ho crec... per fi done punt i...seguit? a esta tesi doctoral... Tal volta una de les aventures més enriquidores que he emprés fins a estos moments... Una de les etapes de creixement personal i professional que segur em marcarà i em definirà durant tota la vida. És emocionant tindre un moment de calma i tranquil·litat per fer memòria del que han significat i signifiquen tots estos anys de dedicació, esforç, lluita i goig per una forma de vida que va més enllà d' un ofici. Perquè tant la investigació com la docència calen d' una forma vocacional que sempre et du a plantejar-te nous reptes, nous projectes, nous desafiaments...

Sense dubte, esta aventura no haguera estat possible sense eixe meravellós grup de persones en el que vaig recalar. Perquè amb ells es va més lluny del companyerisme professional, son un GRUP amb majúscules, en totes les seues conseqüències, amb un esperit familiar del que desitge mai s' oblidem.

Tal volta la principal causant d' açò siga la nostra directora, Amparo Ribes, a la que he d' agrair especialment que m' impliqués en el mon investigador des de fa ja més de 10 anys, quan en segon de carrera comencí a fer treballs dirigits, beques associades amb mil programes, un Erasmus, la FPU, els màsters, les estàncies... Amparo, mil gràcies per eixe esperit emprenedor i lluitador, per donar-nos l' oportunitat d' investigar, d' innovar, d' experimentar, d' ensenyar... en definitiva d' aprendre. Gràcies per l' esforç i dedicació posats en esta tesi, així com en la resta de treballs al llarg d' estos anys. Gràcies per les lliçons purament professionals i especialment per les vitals. Gràcies per ser fidel als teus principis, perquè això ens dona molta força per créixer. En definitiva, mil gràcies....

Tanmateix, voldria donar les gràcies als que han estat durant tota esta aventura al meu costat... literalment... qüestions d' economia d' espai, clar... Mil gràcies a Alf, Lau i Ros (qüestions d' economia de vocabulari, clar també...), pels grans moments, viatges (grans JIP i italian road trip!), anècdotes, sopars, dinars, moments estel·lars (l'esglai a la ministra, les famílies índies, la font, les santonjaes....), berenars, rassocons, cafenets, xarradetes... pare ací a vore si ara no es creuran que treballem... Mai oblidaré que s' hem

fet grans junts, i que hem après a ser professionals junts. Gràcies pel vostre recolzament en moments durs. És fàcil estar i convidaure amb temps de bonances, però és a les temporades de baixó i dificultats quan els grans amics es fan valdre, i no dubteu que vos tinc en un pedestal. No soles a nivell personal, sinó també a nivell professional, sou uns cracks i uns treballadors de 10, ja que es deixeu la pell en cada nou desafiament. Simplement, vos estime.

A la generació que ja es una realitat, els grans Tito Rober i Marta. Pels bons moments viscuts, les rialles, la harmonia que despreneu... perquè sou els valors de futur d' este grup, el vostre treball vos precedeix. De cor desitge el millor per vosaltres. Per molts anys junts...

A Cris, pels grans moments de diversió i bogeria al grup i en especial en la nostra tasca en comú... Et desitge el millor dels futurs... i recorda... sempre ens quedarà Gramolita...

A Fran, per la seua dedicació en la meua primera etapa de la tesi, perquè es nota la seua herència en la meua forma de treballar, pels consells d' anar pas a pas... No tinc cap dubte que aconseguiràs el que et proposes. Espere que els nostres camins es tornen a creuar en un futur.

A tots els meus estudiants de Projecte Final de Carrera: Peter, Irene, Neus, Pepi, Alfredo, Ana, Luís i Òscar. Per fer-me sentir orgullós dels vostres treballs. Per ajudar-me en el meu procés docent a ser millor professor, perquè he crescut amb cada dubte plantejat. Per la vostra dedicació i ganes d' aprendre, mil gràcies i molta sort a les vostres vides. Una menció especial per a Òscar: tens esperit d' investigador, t' animes a seguir l' aventura?

A tots els que han passat per laboratori, per sumar vida i il·lusions als nostres projectes. Menció especial per a Linda, a qui trobem a faltar; per a Soraia, amb qui volem continuar col·laborant; i per a Gökhan, un altra gran persona i de gran valor professional al qual desitgem que continue amb nosaltres.

Vull agrair a la Professora Sigbritt Karlsson i a la doctora Emma Strömberg, per acceptar-me a realitzar diverses estades d' investigació a la Kungliga Tekniska Högskolan d' Estocolm, Suècia. Per donar-me l' oportunitat de conèixer una cultura molt interessant, una ciutat increïble i altre grup de gent que sempre guardaré al cor. Gràcies en especial a Jonas, Sara, Åsa, Peter, Thorshak, Kristin, Mathilda and Sevil.

Thanks Sigbritt for your kind and always warming welcome into your group and for giving me the chance of getting involved in such a great Swedish experience. Tack så mycket! Special thanks to Emma, for becoming my supervisor, colleague and friend. For those long talks about present and future! Just for being there...

Voldria agrair a D. Carlos Ferrer la seua labor al capdavant de la creació i primers passos de l' Institut de Tecnologia de Materials. Li desitge a D. Vicent Amigó, nou director de l' institut, que la seua etapa done els seus fruits i que tinga el suport favorable per aconseguir que el mon dels materials es faça un lloc a la comunitat universitària. Tanmateix agrair a D. Marcos Signes pel seu magnífic treball com a gestor i la seua continua predisposició per tirar una mà.

També voldria agrair a D. Francisco Payri, director del Departament de Màquines i Motors Tèrmics, per permetre'm impartir docència, ja que ha sigut una de les experiències més enriquidores de tot punt insuperable. En eixe sentit, voldria recordar als "meus" alumnes, en especial als xicons i xicones de l' assignatura *Thermal characterisation for polymeric materials*. Per fer-me passar de la por a l' eufòria. Per fer-me gaudir de la docència. Bona sort a tots i totes.

Finalment, gràcies a D. Alfonso Cárcel, director del Departament d' Enginyeria Mecànica i Materials, per haver accedit a tutoritzar este treball dins del Programa de Postgrau d' Enginyeria i Producció Industrial.

Com en tota història, tal volta no es poden apreciar les alegries sense que hi hagen penes a la balança. Però on hi ha obscuritat, potser la llum incideix en més força... i es pot aprendre a botar les pedres que altres deixen al teu camí... Tal volta això també siga creixement personal...

En quant a dedicatòries, no tinc cap dubte en dirigir-les a família i amics, perquè son els patidors a l' ombra... Que si hui no puc... Que si demà no puc... Que si a l' altre...potser... Per no deixar d' estirar-me i estar sempre que es necessita. Part d' esta tesi és per vosaltres.

A la meua mare, a la que mai deixaré d' admirar, per traure endavant una família amb molt d' esforç i treball, sense perdre una mica d' estima en les seues accions i mirant al futur sempre de manera positiva. Per tot el que m' has inculcat, molta part d' esta tesi es teua. Al meu pare, m' haguera agradat que estigueres físicament ací per celebra-ho, però amb la teua presència soc feliç. A Lorena, la meua xicoteta i peça fonamental a la meua vida. Perquè em feu sentir especial al vostre costat. Vos estime.

A la meua família política, per haver-me considerat sempre com un fill més des de que vaig entrar en casa. Potser pareix senzill, però jo ho trobe molt gran. Perquè sempre esteu per ajudar i donar ànims. Mil gràcies.

I per a Mireia...

perquè la seua ànima està en cada línia escrita... sense tú este treball no haguera estat possible...

per estar sempre al meu costat en cada repte, en cada projecte, en cada dificultat, en cada alegria, en cada aventura...

per alçar-me quan he caigut...

per fer-me sentir la persona més afortunada d' este mon... no m' imagine el futur sense tú...

per donar-me el regal de ser amic...

per donar-me el regal de ser parella...

per donar-me el regal de ser pare...